

**Photocatalysis with Cu(II)- and Cu(I)-complexes:
Cu(II)-photocatalyzed Decarboxylative
Oxygenation of Carboxylic Acids and Cu(I)-
photocatalyzed Bromonitroalkylation of Olefins**

Dissertation

Zur Erlangung des Doktorgrades der Naturwissenschaften

Dr. rer. nat.

der Fakultät für Chemie und Pharmazie

der Universität Regensburg



vorgelegt von

Alexander Reichle

aus Kardorf

Regensburg 2023

Die Arbeit wurde angeleitet von : Prof. Dr. Oliver Reiser

Promotionsgesuch eingereicht am : 06.07.2023

Promotionskolloquium am : 29.09.2023

Prüfungsausschuss: Vorsitz : Prof. Dr. Rainer Müller

1. Gutachter : Prof. Dr. Oliver Reiser

2. Gutachter : Prof. Dr. Julia Rehbein

3. Prüfer : Prof. Dr. Frank-Michael Matysik

Der experimentelle Teil der vorliegenden Arbeit wurde in der Zeit von Juni 2019 bis Dezember 2022 unter der Leitung von Herrn Prof. Dr. Oliver Reiser am Institut für Organische Chemie der Universität Regensburg angefertigt.

Besonders bedanken möchte ich mich an dieser Stelle bei Herrn Prof. Dr. Oliver Reiser für die Aufnahme in seinen Arbeitskreis, die Überlassung des interessanten Themas, die anregenden Diskussionen und die stete umfangreiche Unterstützung

Für meine Frau Maria und meine Familie

Soli Deo Gloria

Table of Contents

Chapter 1 Light-induced Homolysis of Copper(II)-complexes	1
1.1 Abstract.....	1
1.2 Introduction	1
1.3 LIH of Copper(II) chloride-complexes	5
1.3.1 LIH of CuCl_2 – chlorine radical addition to alkenes / alkynes	7
1.3.2 LIH of CuCl_2 – chlorine radicals as HAT catalyst	10
1.4 LIH of Copper(II)- N_3 – azide radicals	12
1.5 LIH of Copper(II)- CH_2R – benzyl radicals	13
1.6 LIH of Copper(II)-enolates – enolate radicals	14
1.7 LIH of Copper(II)-amine-complexes – amino radicals	16
1.8 LIH of Copper(II)-carboxylates.....	18
1.9 LIH of Cu(II)-sulfoximines – <i>N</i> -centered sulfoximiny radical	25
1.10 Outlook: Transformations involving $\text{Cu}^{n+}/\text{Cu}^{n-1}$ transitions.....	26
1.11 Summary and Perspectives.....	30
1.12 References	32
Chapter 2 Copper(II)-photocatalyzed Decarboxylative Oxygenation of Carboxylic Acids.....	35
2.1 Outline of this Study.....	36
2.2 Coordination Modes of Copper(II)-carboxylates	36
2.3 Synthesis of Copper(II)-carboxylates.....	38
2.3.1 Crystal Structures of Copper(II)-carboxylates.....	39
2.3.2 Electronic Properties of Copper(II)-carboxylates	42
2.4 Evaluation of Paddle-Wheel vs. Monodentate Coordination	44
2.5 Further Optimization Studies	45
2.6 Substrate Scope of the Cu(II)-photocatalyzed Decarboxylative Oxygenation	46
2.7 Upscaling and Synthetic Utility	48
2.8 Mechanistic Investigations.....	49
2.8.1 UV-vis, Solution phase IR- and NMR Studies.....	49
2.8.2 Water Titration Experiment	51
2.8.3 Radical Trapping Experiment and Reaction under N_2 Atmosphere	52
2.8.4 EPR-Analysis	52
2.8.5 Photostability Test of Decarboxylation Products.....	54

2.8.6 Investigations on Selective Product Formation	55
2.9 Proposed Reaction Mechanism	57
2.10 Attempts towards Decarboxylative Coupling Reactions	59
2.11 Conclusion	61
2.12 References	62
Chapter 3 Cu(I)-photocatalyzed Bromonitroalkylation of Olefins	65
3.1 Introduction and Outline of the Study	66
3.2 Reaction Optimization.....	68
3.3 Comparison with other Photocatalysts.....	70
3.4 Substrate Scope	71
3.5 Upscaling and Synthetic Utility	74
3.5.1 Nucleophilic Substitutions and Eliminations.....	75
3.5.2 Hydrogenation and Reduction.....	77
3.5.3 Nitro- and Aminocyclopropane Synthesis	78
3.6 Mechanistic Investigations.....	81
3.6.1 UV-vis Studies.....	81
3.6.2 Stern-Volmer Interaction Analysis.....	82
3.6.3 Investigation on Radical Character/ Determination of the Quantum Yield.....	84
3.6.4 Investigations on the Homolysis of [Cu ^I (dap) ₂]Cl	84
3.6.5 Experiments on Product Formation with different Bromonitroalkanes	86
3.6.6 EPR Studies.....	88
3.7 Proposed Reaction Mechanism.....	94
3.8 Studies with Chiral Ligands	96
3.9 Studies on Three-Component Type ATRA Reactions	97
3.10 Conclusion and Outlook.....	100
3.11 References	101
Chapter 4 Summary/ Zusammenfassung.....	104
4.1 Summary	104
4.2 Zusammenfassung	106
Chapter 5 Experimental Part	109
5.1 General Information	109

5.2 Photochemical Setup.....	111
5.2.1 Schlenk Tube Setup.....	111
5.2.2 Upscaling Reactors	113
5.3 Experimental Part for Chapter 2	115
5.3.1 UV-vis Absorption Measurements.....	115
5.3.2 Radical Trap Experiment and Reaction under N ₂ -Atmosphere.....	116
5.3.3 Synthesis of Copper(II)-carboxylates	118
5.3.4 Synthesis of Compounds via Photocatalytic Decarboxylation	120
5.4 Experimental Part for Chapter 3	130
5.4.1 Selected Olefins Photocatalyst Comparison	130
5.4.2 UV-vis Absorption Measurements.....	130
5.4.3 Quantum Yield Measurement	130
5.4.4 Fluorescence Quenching Interactions (Stern-Volmer)	133
5.4.5 Investigations on Homolysis of [CuI(dap) ₂]Cl.....	135
5.4.6 Synthesis of Compounds	137
5.5 References for Experimental Part.....	192
Chapter 6 Scientific Appendix	194
6.1 NMR Spectra for Chapter 2	195
6.2 Crystallographic Data for Chapter 2	213
6.3 NMR Spectra for Chapter 3	214
6.4 Crystallographic Data for Chapter 3	303
Chapter 7 Personal Appendix	304
Chapter 8 Acknowledgements	306
Chapter 9 Declaration/ Eidesstattliche Erklärung.....	309

List of Abbreviations

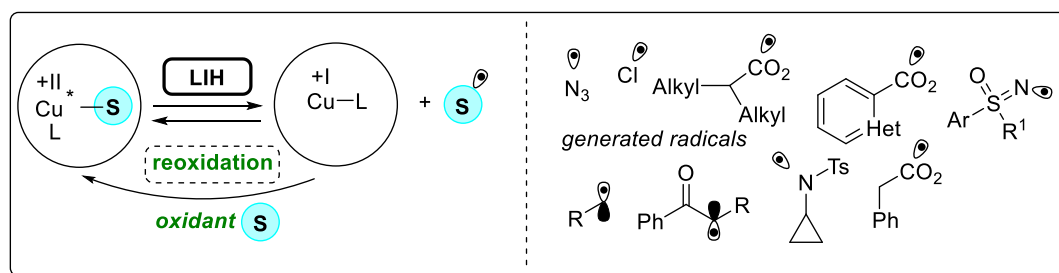
Acc.	according	DMC	dimethyl carbonate
Ac	acetyl	DMF	<i>N,N</i> -dimethylformamide
AIBN	2,2'-azobis(isobutyronitrile)	dmp	2,9-dimethyl-1,10-phenanthroline
Ampl.	Amplitude	d.r.	diastereomeric ratio
anh.	anhydrous	dtbbpy	4,4'-di- <i>tert</i> -butyl-2,2'-bipyridine
APCI	atmospheric pressure Chemical ionization	$E/E_{1/2}/E_{red}$	Standard reduction potential
aq.	aqueous	ϵ	Extinction coefficient
Ar	aryl	EDG	electron donating group
AT	atom transfer	<i>e.g.</i>	<i>exempli gratia</i>
ATRA	atom transfer radical addition	EI	Electric ionization
BET	back electron transfer	EPR	Electron paramagnetic resonance
BINAP	2,2'-bis(diphenylphosphonio)-1,1'-binaphthyl	equiv	equivalents
BINOL	1,1'-bi-2-naphthol	ESI	electrospray ionization
Bn	benzyl	<i>etc.</i>	<i>et cetera</i>
Boc	<i>tert</i> -butyloxycarbonyl	Et	ethyl
bpy	2,2'-bipyridine	EtOAc	ethyl acetate
bpz	2,2'-bipyrazine	EWG	Electron-withdrawing group
^t Bu	<i>tert</i> -butyl	f	Correction factor
°C	Degree celsius	<i>fac</i>	facial
c	centi / speed of light	fs	femto seconds
CCDC	Cambridge Crystallographic Data Centre	FT-IR	Fourier-transformation infrared spectroscopy
CDCl ₃	chloroform	G	gauss
CFL	Compact fluorescence lamp	g	gram
CF ₃	trifluoromethyl	GP	general procedure
cm	centimeter	h	Hour(s)
CN	cyano	<i>h</i>	Planck constant
conc.	concentrated	HAT	Hydrogen atom transfer
crm	complex reaction mixture	HPLC	High pressure liquid chromatography
CT	charge transfer	HRMS	high resolution mass
CW	continuous wave	Hz	Hertz
4-CzIPN	1,2,3,5-tetrakis(carbazol-9-yl)-4,6-dicyanobenzene	IR	infrared
δ	chemical shift	<i>i.e.</i>	<i>id est</i>
dap	2,9-bis(para-anisyl)-1,10-phenanthroline	<i>J</i>	Coupling constant
dba	dibenzylideneacetone	<i>J</i> _s	Joule-second
DBU	1,8-diazabicyclo- [5.4.0]undec-7-ene	K	Kelvin
DCC	dicyclohexylcarbodiimide	kcal	Kilo calorie
DCM	dichloromethane	L	Ligand, liter
DE	diethyl ether	λ	wavelength
dF(CF ₃)ppy	2-(2,4-difluorophenyl)-5-(trifluoromethyl)pyridine	λ_{ex}	excitation wavelength
DFT	density functional theory	λ_{max}	wavelength of maxima
DIPEA	<i>N,N</i> -diisopropylethylamine	LED	Light emitting diode
DMAP	4-dimethylaminopyridine	LMCT	Ligand-to-metal charge transfer
		M	molar, mega, metal
		m	meter, milli
		<i>m</i>	meta
		mA	Milli ampere
		Me	methyl

MeCN	acetonitrile	ref.	reference
MeOH	methanol	rt	room temperature (25 °C)
MeO	methoxy	RuPhos	2-dicyclohexylphosphino-2',6'-diisopropoxybiphenyl
mg	milligram		
MHz	mega hertz	s	second
min	minutes	sat.	saturated
mL	Milli liter	SCE	standard calomel electrode
μL	micro liter	SET	single electron transfer
MLCT	metal-to-ligand charge transfer	T	temperature
		TBAF	Tetra- <i>n</i> -butylammonium fluoride
mm	milli meter		
mM	milli molar	TC	thiophene carboxylate
mmol	Milli mole	TDDFT	time-dependent density functional theory
μmol	micro mole	TEMPO	(2,2,6,6-tetramethyl-piperidin-1-yl)oxyl
mol	mole		
mol%	mole percent	Tf	triflyl
mp	melting point	THF	tetrahydrofuran
μs	microseconds	TLC	thin layer chromatography
mT	megatesla	TMS	trimethyl silyl
mW	milli Watt	Ts	tosyl
m/z	mass-to-charge ratio	UV	ultraviolet
N ₃	azide	V	Volt
nd	not detected	LIH	light-induced homolysis
NFTPT	1-fluoro-2,4,6-trimethylpyridinium tetrafluoroborate	vs.	<i>versus</i>
		W	Watt
NFSI	<i>N</i> -fluorobenzene-sulfonimide	X	arbitrary halogen
		Xantphos	4,5-bis(diphenylphosphino)9,9-dimethylxanthene
NIS	<i>N</i> -iodosuccinimide		
nm	nano meter		
NMR	Nuclear magnetic resonance		
NO ₂	nitro		
nr	no reaction		
ns	nanoseconds		
NSAIDs	Non-steroidal anti-inflammatory drugs		
Nu	nucleophile		
<i>o</i>	<i>ortho</i>		
<i>p</i>	<i>para</i>		
PBN	<i>C</i> -phenyl- <i>N</i> - <i>tert</i> -butylnitrone		
PC	photocatalyst		
Ph	phenyl		
pH	power of hydration		
phen	phenanthroline		
phth	phthalimide		
ppm	Parts per million		
ppy	2-phenylpyridine		
ⁱ Pr	<i>iso</i> -propyl		
ps	pico seconds		
Φ	quantum yield		
Q-TOF	Quadrupole time-of-flight		
R _f	retardation factor		
<i>rac</i>	racemic		
redox	reduction-oxidation		

Chapter 1 Light-induced Homolysis of Copper(II)-complexes

1.1 Abstract

In the past ten years powerful strategies have been developed in the field of photocatalysis regarding the functionalization of compounds *via* radical intermediaries in a selective manner. The shift towards earth-abundant metal-based photocatalysts is currently less explored, in comparison to the well-established iridium- or ruthenium-based photocatalysts, which fulfil the requirements of a photocatalyst, such as long excited-state lifetimes and photostability. Although only having excited-state lifetimes in the low millisecond range or below, the idea of light-induced homolysis (LIH) for producing radicals has recently attracted significant interest as a potential platform for initiating photoreactions using earth-abundant 3d-metal complexes. Exploiting this idea involves the use of Cu(II)-complexes, which will be presented by demonstrating current advancements in organic synthesis with an eye toward the field's future.



This chapter is based on: [A. Reichle[†]](#) and [O. Reiser[†]](#), *Chem. Sci.*, **2023**, *14*, 4449. ([†]A.R. and O.R. jointly wrote the manuscript).

1.2 Introduction

One of the main goals of synthetic chemistry is to discover novel strategies for creating and destructing chemical bonds in straightforward procedures. Thus, there is great interest in developing catalytic techniques for the activation of tiny molecules in order to use resources and feedstocks sustainably. Visible light photocatalysis has developed into a potent technology to permit synthetic transformations in recent years.^[1] One of the newest fields in organic chemistry, synthetic green chemistry was first envisioned by Italian chemist G. Ciamicin in 1912, and its success and growth have since been predicted.^[2] The simplest scenario for forming a classical chemical bond involves an ionic path connecting electrophiles and nucleophiles. The lack of selectivity associated with the relatively harsh conditions required to generate such species, despite the background knowledge about how to synthesize new chemical bonds using radical species, hindered the development of sustainable radical pathways for organic synthesis^[3], despite impressive breakthroughs in this field.^[4] Radicals of

many different types have become available with recent advancements in using light as an alternative to temperature conditions, opening up new avenues for designing organic syntheses. The heavy transition-metal polypyridinyl complexes based on iridium and ruthenium were undoubtedly the most frequently used as the major photocatalysts for this purpose. These metal-based complexes have excellent characteristics, such long excited-state lifetimes, high visible-light absorption coefficients, and strong oxidation and reduction potentials that are necessary to activate substrates through single electron transfer events (SET). However, they are disadvantageous in terms of sustainability and abundance.^[5] As a result, there is an increased strive to create a paradigm shift from expensive Ir- and Ru-based photocatalysts to more environmentally benign and abundant 3D metals like Cu, Fe, Co, Ni, or Mn.^{[6],[7]} Nevertheless, due to the typical ultrashort excited-state lifetimes of such metal complexes in the pico- or at most in the low nanosecond range,^[8] bimolecular processes *via* an outer-sphere mechanism are unlikely.

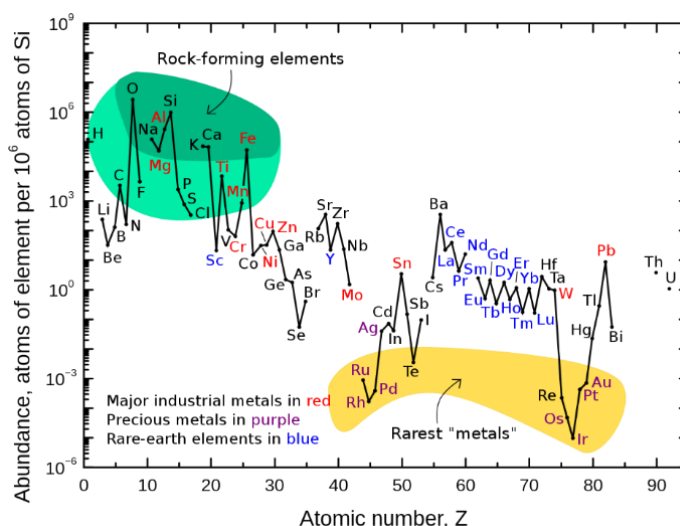
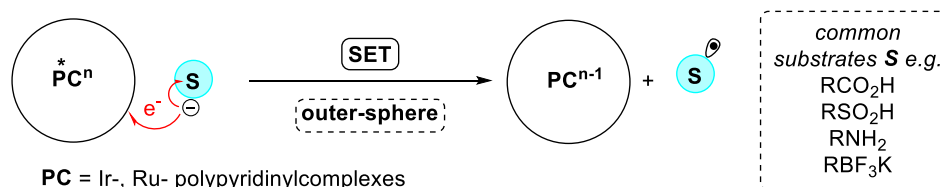


Figure 1. Abundance (atom fraction) of the chemical elements in Earth's upper continental crust as a function of atomic number. (Figure adapted from Ref. [5], Creative Commons, public domain).

Notwithstanding, it is possible to create homo- and heteroleptic copper(I)-complexes with excited-state lifetimes in the high nano- and even microsecond range. Mimicking the chemical behavior of Ru(II)- or Ir(III)-complexes in oxidative quenching cycles, they can be successfully used in synthetic transformations that include the reduction of a substrate and a single electron transfer (SET) from Cu(I)* to Cu(II).^{[9],[10]} In turn, comparable reductive quenching cycles (Scheme 1) that are common for ruthenium (Ru(II)* to Ru(I) or iridium (Ir(III)* to Ir(II)) are rare for copper(I) complexes (Cu(I)* to Cu(0)).^{[11],[12]} Similarly, Cu(II)-complexes that undergo photoinduced outer-sphere SET to generate Cu(I) and an oxidized substrate have not been investigated due to the low oxidation potential of Cu(II). The concept of light-induced homolysis (LIH), typically triggered by a ligand-to-metal charge transfer (LMCT) transition, is one alternative approach for the utilization of Cu(II) as a photocatalyst:

If a Cu(II)-substrate complex Cu(II)-S is excited by light, a homolytic dissociation to Cu(I) and a substrate radical S^\bullet can occur. The radical S^\bullet can then be applied in future synthetic transformations. A simple ligand exchange reaction with a nucleophilic substrate and a sufficient Cu(II)-precursor can create the required Cu(II)-substrate complex. As a result, the whole process is comparable to the nucleophile's one-electron oxidation. While precoordination of the substrate is necessary, such activation is favorable due to the strong chemoselectivity of the photochemical process. The ability of 3d metals to coordinate various nucleophiles effectively and there are manifold possibilities to create molecular assemblies by the choice of ligand and metal combinations. Copper(II) has been the most widely used 3d-metal for this reaction mode,^[13] which most likely is acting in thermal oxidation of substrates.^[14] So far, this concept has been successfully extended to various 3d-metals such as Mn, Fe, Co, and Ni, and rare earth metals such as Ce.^{[15],[16]}

Traditional Photoredox Activation with a Photocatalyst

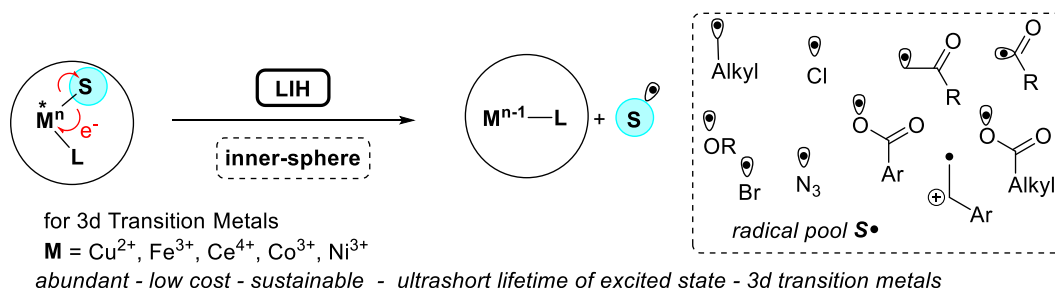


not abundant - high cost - unsustainable - long lifetime of excited state - heavy transition metal

Common Electronic Transitions of Transition Metals



Activation via (Visible) Light-Induced Homolysis (LIH)



Scheme 1. Traditional Photoredox Activation and the Concept of LIH.

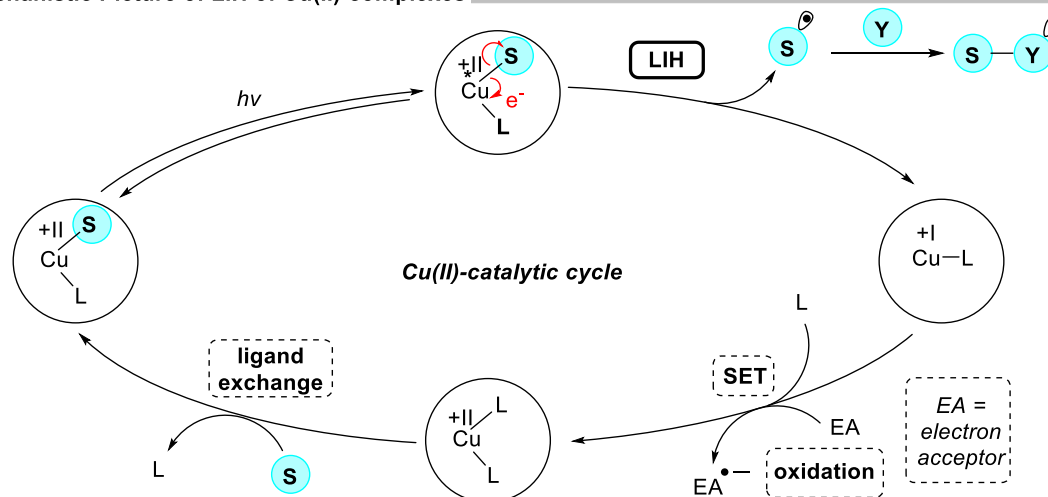
Kochi's pioneering work in the 1960s demonstrated that metal complexes can undergo photolysis processes, specifically for $CuCl_2$ that under UV-irradiation forms $CuCl + Cl^\bullet$.^[17] Nevertheless, until recently, the use of metal-substrate homolysis for synthetic purposes had received little attention. Now, due to the development of synthetic applications and insightful mechanical investigations, several fundamental aspects are involved.

Thus a coherent picture is emerging, which might serve as a toolbox for novel applications. The following issues need to be considered:

- The types of metal-(ligand)-substrate complexes that are appropriate for light-induced homolysis processes to create substrate radicals.
- The time scale of the homolysis process needs to be investigated. 3d-metal complexes have short excited-state lifetimes in the low nanosecond or even picosecond range and it needs to be clarified if they are appropriate to start synthetic transformations.
- The effectiveness of the homolysis process and in particular, if the potential recombination of the formed substrate radical with the reduced metal prohibits the ensemble from participating in subsequent transformations.
- The reduced metal complex formed during homolysis must be reoxidized for reactions to be catalytic. If this is not achievable, synthetic transformations may still be viable and beneficial, but stoichiometric quantities of the metal complexes must be used.

Hence, a design concept (Scheme 2) for Cu(II)-photocatalyzed reactions *via* LIH may be provided to guide future developments: To begin, a Cu(II)-substrate complex must be generated, which is most typically accomplished by ligand exchange of Cu(II)L₂ species with a nucleophilic substrate **S**. If exposed to light, this complex undergoes light-induced homolysis, yielding Cu(I) and the radical **S**[•]. In order to launch a successful synthetic transformation rather than unproductive recombination with the reduced metal complex, the radical **S**[•] has to be combined with a second substrate **Y**. To complete the catalytic cycle, the latter must be oxidized *via* an appropriate electron acceptor.

Mechanistic Picture of LIH of Cu(II)-complexes



Scheme 2. The general concept of LIH of Cu(II)-intermediates.

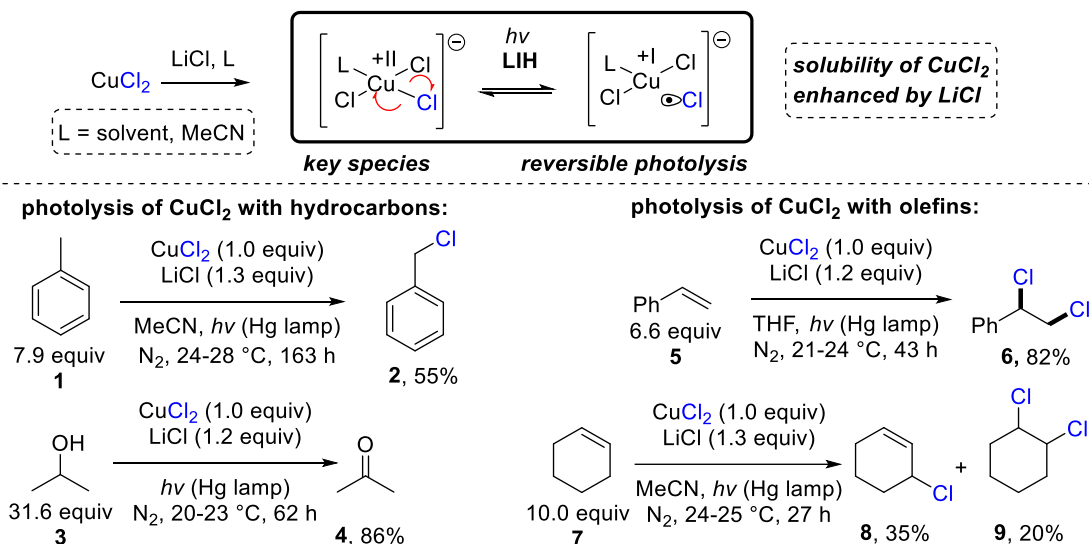
Notably, external ligands are not required in most of the described processes involving LIH steps of Cu(II)-substrate species. Nevertheless, near UV-light (365 nm) or violet light (427 nm) irradiation is required in such scenarios because the LMCT transition of copper(II)-substrate

species requires higher energies to reach the dissociative states.^[18] Up to date, only a few Cu(II)-intermediates have been reported to undergo light-induced homolysis (LIH). An overview of the transformations that have been developed employing copper as a radical promoter *via* the LIH mechanism will be shown in the following chapters.

1.3 LIH of Copper(II) chloride-complexes

Given the significant potential for the oxidation $\text{Cl}^- \rightarrow \text{Cl}^\bullet$ ($E_{\text{ox}} > +1.21$ V vs. saturated calomel electrode (SCE)),^[19] the formation of chlorine radicals needs harsh conditions. However it is still feasible using weakly oxidizing Cu(II) ($\text{Cu(II)} \rightarrow \text{Cu(I)}$, $E_{\text{red}} = +0.50$ V vs. SCE).^[20,21] Kochi pioneered the field of light-induced homolysis in 1962 as he reported the reversible homolysis of Cu(II)Cl_2 to Cu(I)Cl and a chlorine radical when irradiated with a low-pressure mercury lamp.^[17] Adding lithium salts such as lithium chloride was advantageous, explaining that greater solubility of anhydrous cupric chloride (CuCl_2) leads to improved activity. Mereshchenko and colleagues improved these discoveries by using spectroscopic techniques to investigate the formation of several extreme labile copper(II) chloride complexes more than 50 years later.^[22] It was found that the anionic complex $[\text{Cu}^{\text{II}}(\text{MeCN})\text{Cl}_3]^-$ is formed in acetonitrile (MeCN) and undergoes reversible photolysis at a significantly faster rate (Scheme 3).

Kochi (1962)



Scheme 3. Pioneering work of Kochi in 1962; photolysis of cupric chloride (CuCl_2).

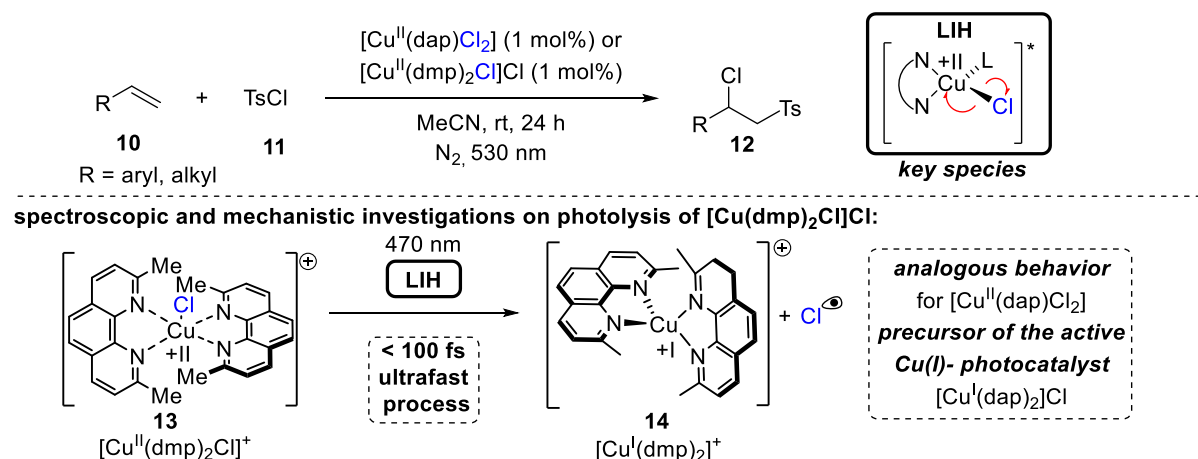
This observation corresponds to Kochi's investigations: Due to the poor reactivity of the chlorine radicals towards solvents such as acetic acid and MeCN, competing with a quick rebound with Cu(I) to regenerate the initial Cu(II)Cl_2 , essentially no reaction occurred. Solvents with structural motifs, such as secondary or tertiary C-H bonds or olefins, on the other hand, undergo transformations induced by chlorine radicals: The production of benzyl chloride (**2**) was reported with saturated hydrocarbons such as toluene (**1**). Similarly, isopropyl alcohol (**3**)

was converted to acetone (**4**). Both reactions are initiated by hydrogen atom transfer (HAT) of a chlorine radical from a mechanistic point of view. The photolysis of cupric chloride (CuCl_2) in the presence of olefins such as styrene (**5**) or cyclohexene (**7**) yielded the corresponding dichlorination products **6** and **8**, as well as **9**, in good to moderate yield, which may be explained by the chlorine radical addition to the double bond. CuCl_2 is used in stoichiometric levels in these reactions, indicating the problem in reoxidizing Cu(I) generated during photolysis back to Cu(II) .

According to Kochi's proposal, copper(II)-complexes such as $[\text{Cu}^{\text{II}}(\text{dap})\text{Cl}_2]$ (dap = 2,9-bis(4-methoxyphenyl)-1,10-phenanthroline) or $[\text{Cu}^{\text{II}}(\text{dmp})_2\text{Cl}]\text{Cl}$ (dmp = 2,9-dimethyl-1,10-phenanthroline) (**13**) as a convenient and more inexpensive precursor for the active Cu(I) -photocatalyst and be successfully utilized in photocatalytic ATRA reactions (Scheme 4). Following the mechanistic concept established for Cu(I) -photocatalyzed reactions,^[9,10] Cu(II) -complexes undergo homolytic cleavage of the Cu-Cl bond to form *in situ* the catalytically active Cu(I) -species, which can promote a variety of ATRA reactions such as chlorosulfonylation, bromoalkylations, or iodoperfluoroalkylations of alkenes.^[23]

As a representative example shown for complex **13**, transient spectroscopy revealed that the homolysis of the Cu-Cl bond is an ultrafast process, occurring in less than 100 fs,^[24] indicating that photoinitiation of transformations *via* such bond homolysis is feasible with metal complexes with excited state lifetimes only in the picosecond range, *e.g.* accessing options for iron being the most abundant transition metal on earth, to participate in photocatalytic processes.^[7]

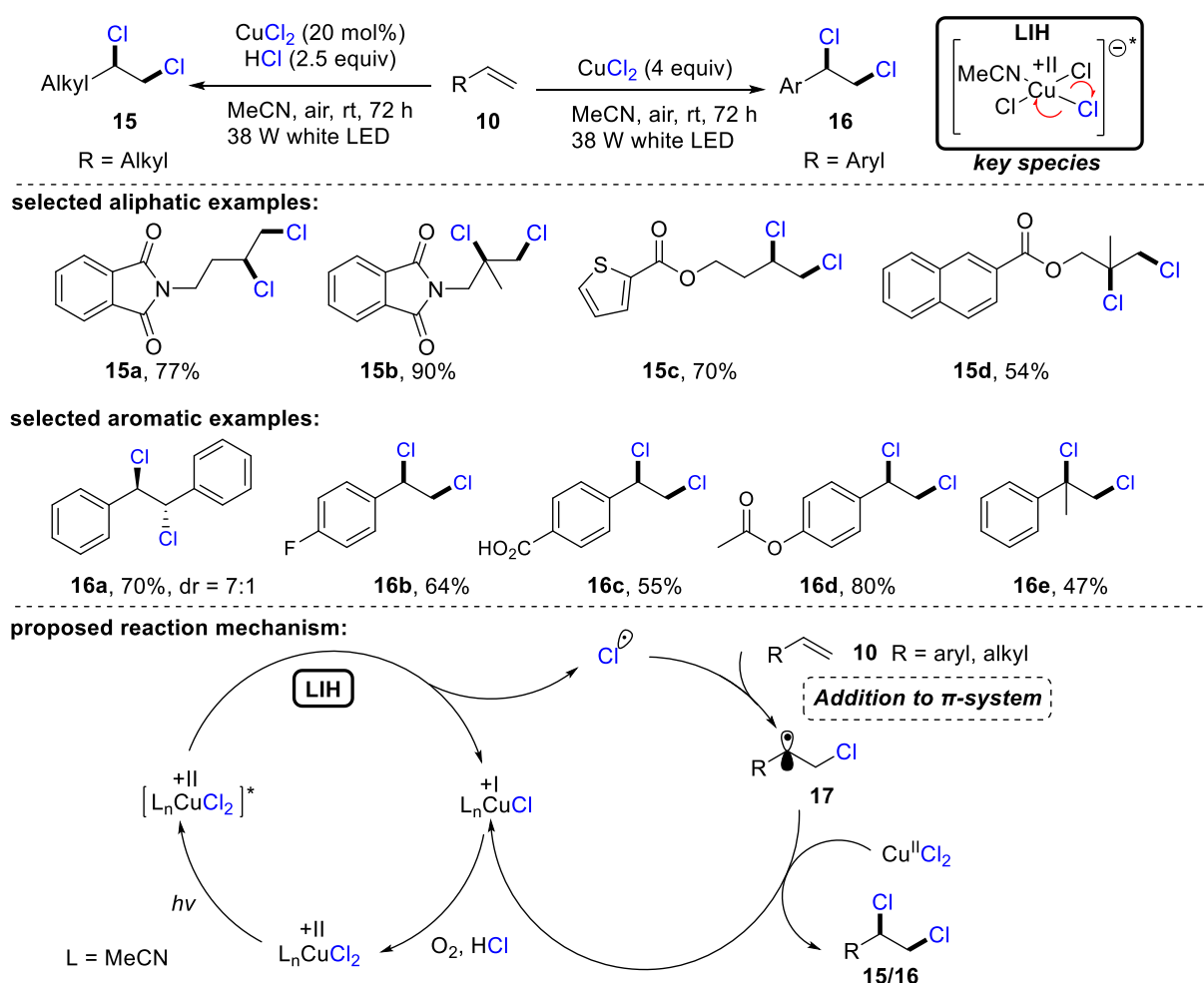
Reiser *et al.* (2019, 2020) Castellano, Reiser *et al.* (2020)



Scheme 4. Cu(II) -complexes as catalyst precursor: LIH of defined complexes.

1.3.1 LIH of CuCl_2 – chlorine radical addition to alkenes / alkynes

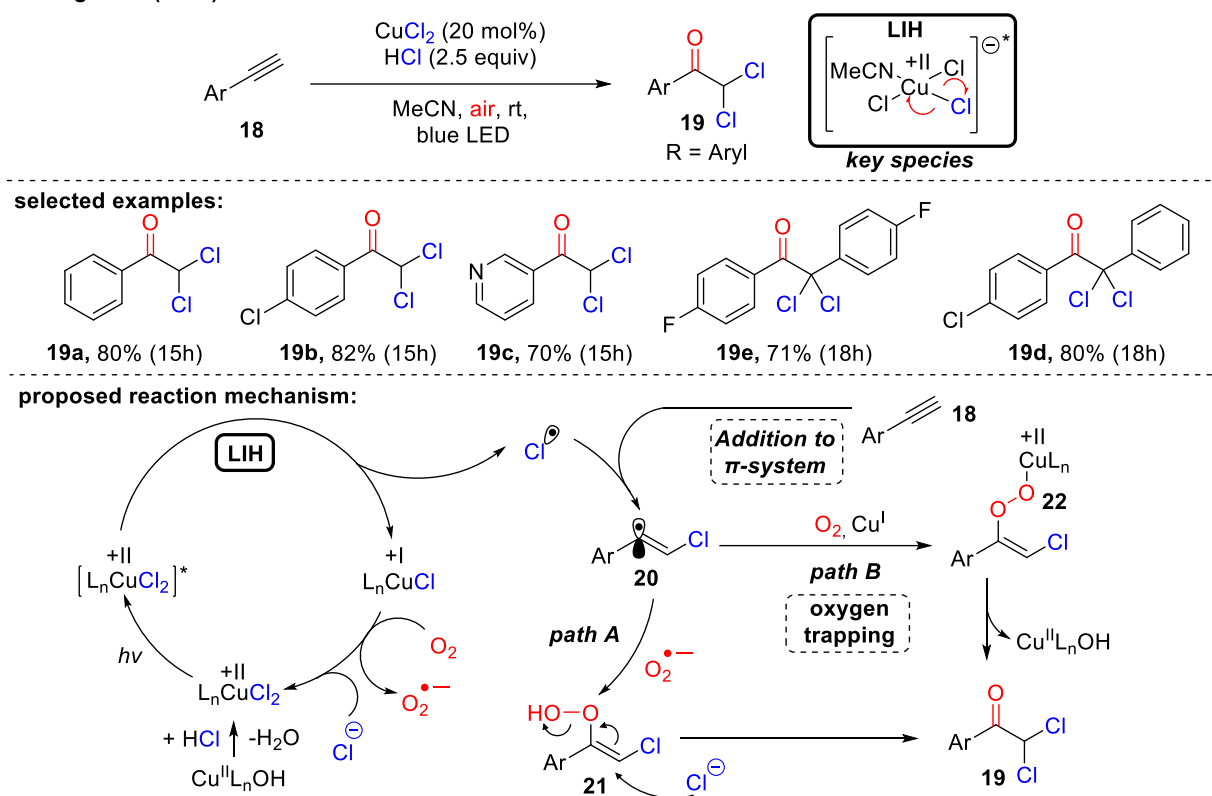
Wan *et al.* established the vicinal dichlorination of olefins **10** to get products **15** and **16** by capitalizing on Kochi's discovery (Scheme 5).^[25] Under aerobic conditions, a combination of substoichiometric quantities of copper(II)-chloride (0.2 equiv) and hydrochloric acid (2.5 equiv) was shown to be successful as an inexpensive and easily accessible chlorine source, yielding compounds of type **15**. The reoxidation of Cu(I) generated through homolysis of CuCl_2 was postulated to take place *via* oxygen and thus, making the process catalytic. Following this logic, it is unexpected that activated alkenes, *i.e.* vinyl arenes, required a significant excess of CuCl_2 (4.0 equiv) to accomplish the reaction. It could be rationalized by the fact that benzylic radicals **17** (R = aryl) could be trapped by oxygen, as established *e.g.* in the Cu(II)-catalyzed azido-ketonization (*vide infra*, Scheme 11).

Wan *et al.* (2020)

Scheme 5. Vicinal dichlorination of activated and unactivated olefins.

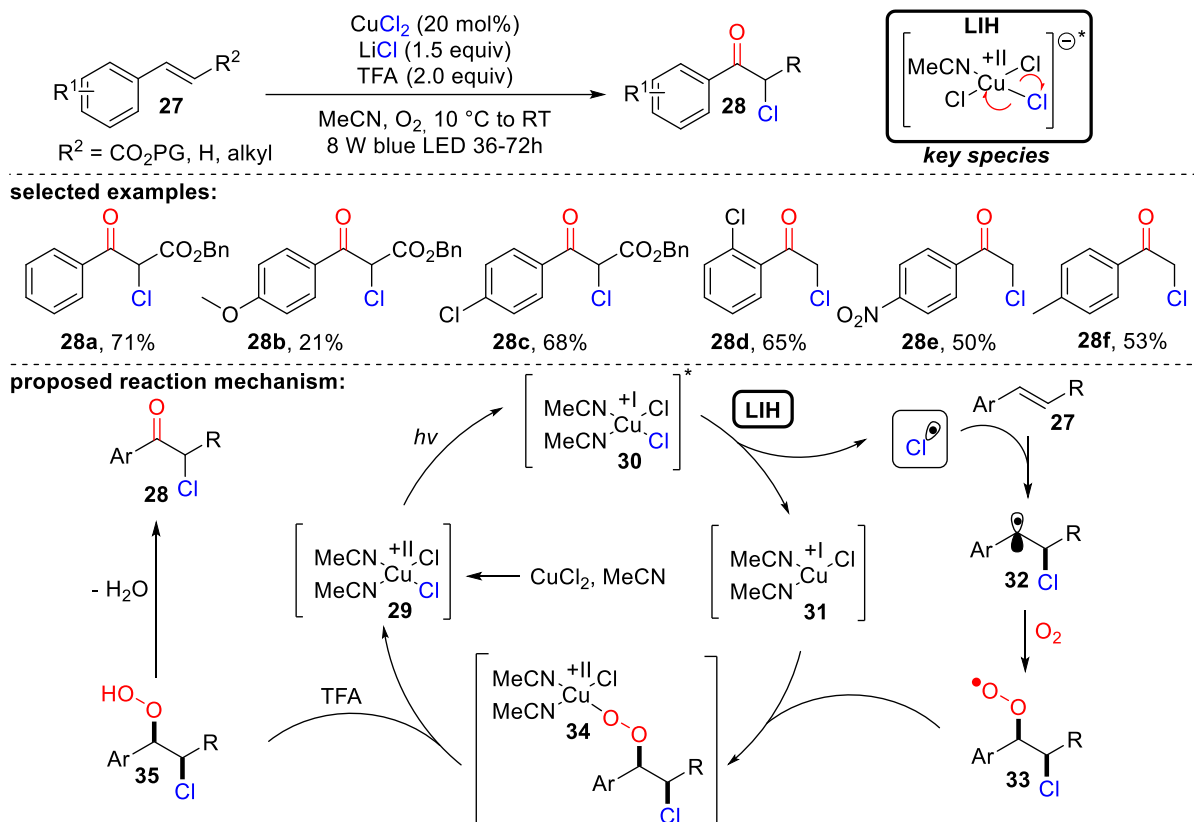
In 2022, the Hwang group reported visible-light-induced oxidative α -keto-dichlorination of arylalkynes **18** enhanced by CuCl_2 at ambient temperature (Scheme 6).^[26] The reoxidation of Cu(I) by oxygen with the concurrent generation of $\text{O}_2^{\cdot-}$ through path A is also suggested, which should recombine with **20** to yield the product **19**. Although EPR investigations detected $\text{O}_2^{\cdot-}$, trapping it with **20** would result in the recombination of two short-lived species existing in low concentrations. Path B allows for the direct trapping of **20** with O_2 , followed by recombination of the resultant peroxy radical with Cu(I) to intermediate **22**, regenerating Cu(II) (*cf.* Scheme 11).

Hwang *et al.* (2022)



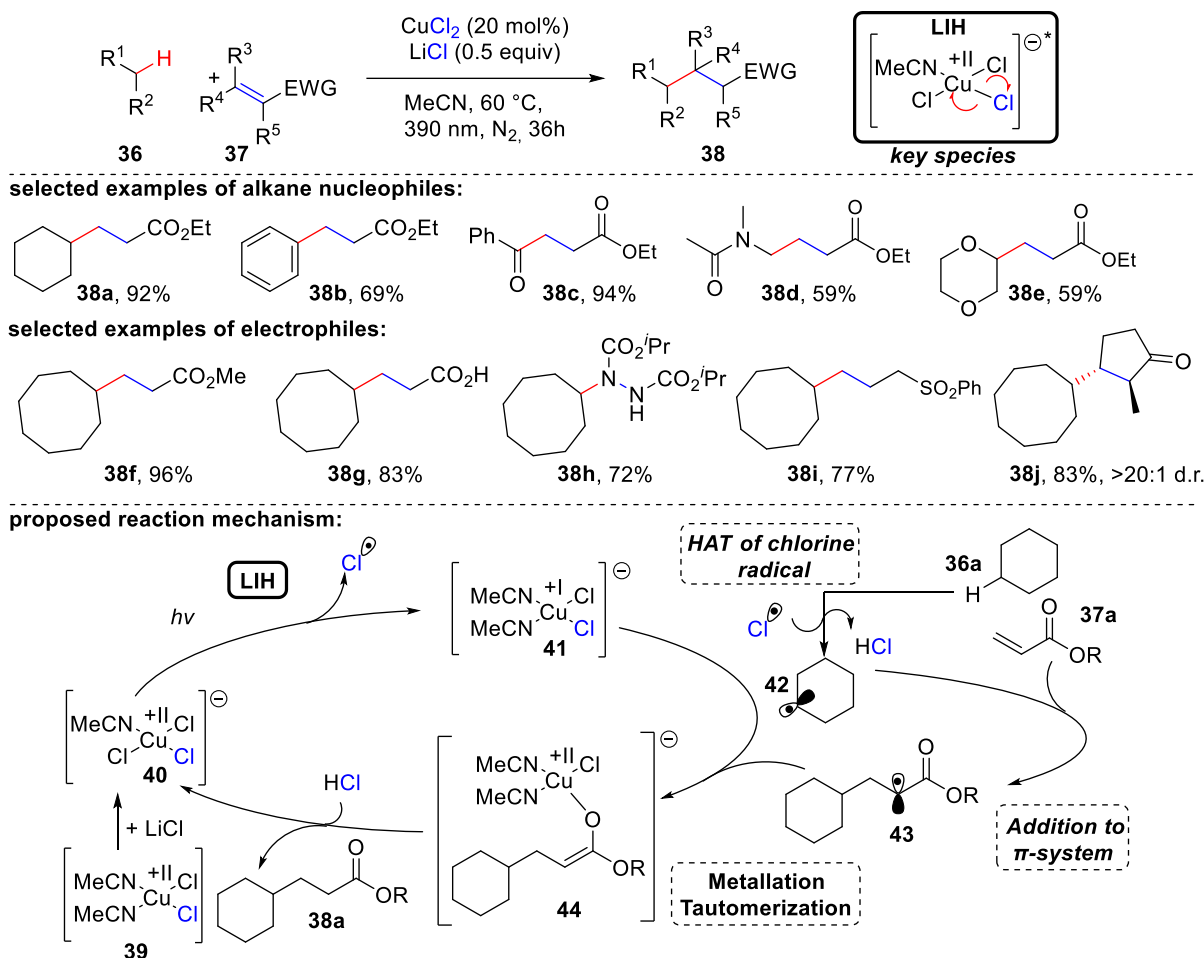
Scheme 6. Synthesis of α -keto-dichlorination of arylalkynes.

LIH of CuCl_2 was successfully applied by Zhang's group in a synthetic method for the effective regioselective chlorination of coumarins **22**, as shown in Scheme 7.^[27] The direct regioselective addition of Cl^\cdot to the 3-position of coumarin **23a** results in the formation of a stable benzylic radical **25**. (path A). The chlorinated product **24a** is created by SET oxidation of the benzylic radical with either oxygen or CuCl_2 , followed by deprotonation. The authors also suggest that the chlorine radicals may recombine to produce Cl_2 . A further reaction with water yields hypochlorite as a positive chlorine source. Thus, the chlorinated products **24** might be obtained by selective electrophilic addition of Cl^+ to the coumarin's double bond at the 3-position (path B) and subsequent deprotonation. Due to the fact that CuCl_2 was applied in overstoichiometric amounts, rather than catalytic amounts, it can be assumed that the reoxidation of Cu(I) to Cu(II) by oxygen is inefficient.

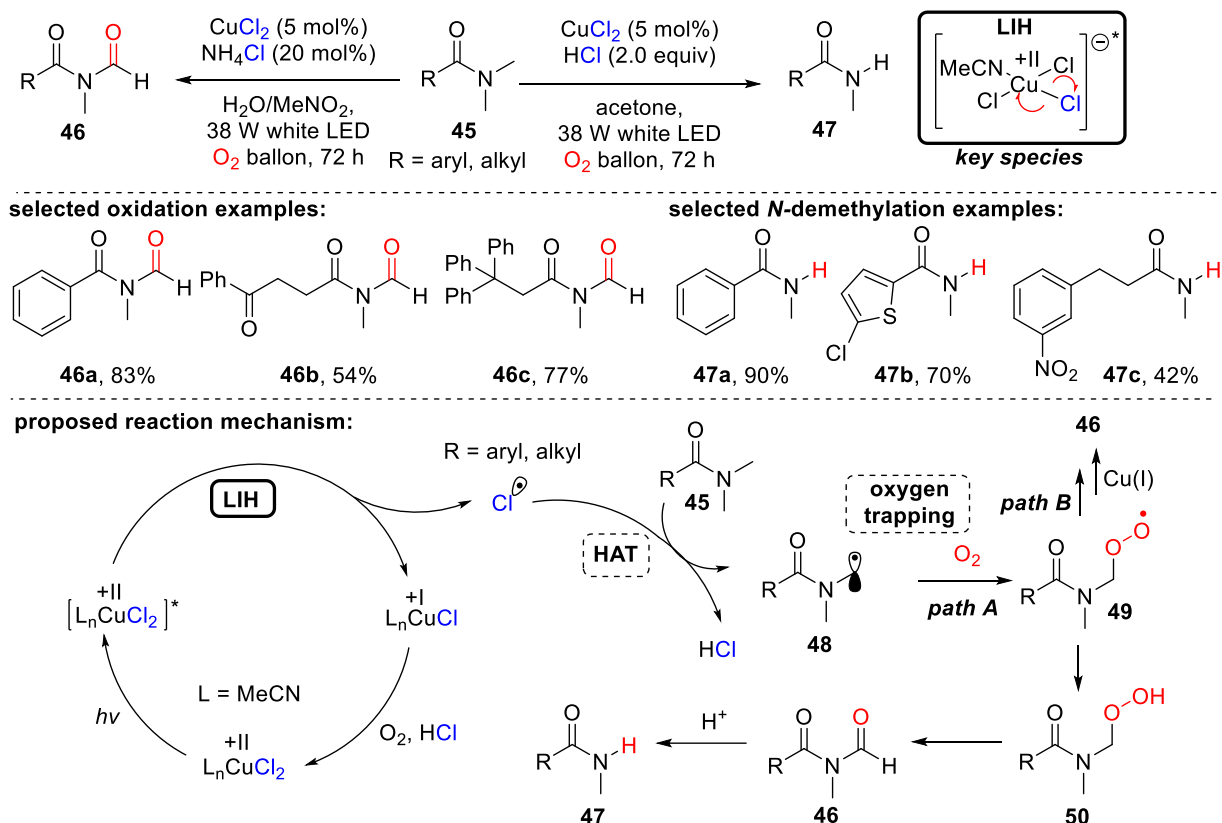
Cai *et al.* (2022)Scheme 8. α -Chloroketone synthesis of aromatic alkenes.

1.3.2 LIH of CuCl_2 – chlorine radicals as HAT catalyst

In addition to the creation of C-C double bonds, the chlorine radicals produced by light-induced homolysis of $\text{Cu}^{\text{II}}\text{Cl}_2$ are effective hydrogen atom transfer (HAT) reagents. Rovis *et al.* successfully demonstrated the activation of $\text{C}(\text{sp}^3)\text{-H}$ bonds in alkanes **36** by forming a strong H-Cl bond (BDE = 103 kcal mol⁻¹) through chlorine radicals (Scheme 9).^[29] Nucleophilic alkyl radicals formed as a result can be coupled with electron-deficient olefins **37** to form hydroalkylation products **38**. Despite the use of a comparably high loading of CuCl_2 (20 mol%), the total process is catalytic in Cu(II) without the necessity for an additional oxidant such as oxygen (cf. Schemes 7 and 8). The crucial reoxidation to Cu(II) is afforded by the combination of radical **43** with Cu(I), *i.e.* reversing the known one-electron oxidation of enolates by Cu(II).

Rovis *et al.* (2021)Scheme 9. CuCl₂-mediated activation of aliphatic feedstock chemicals.

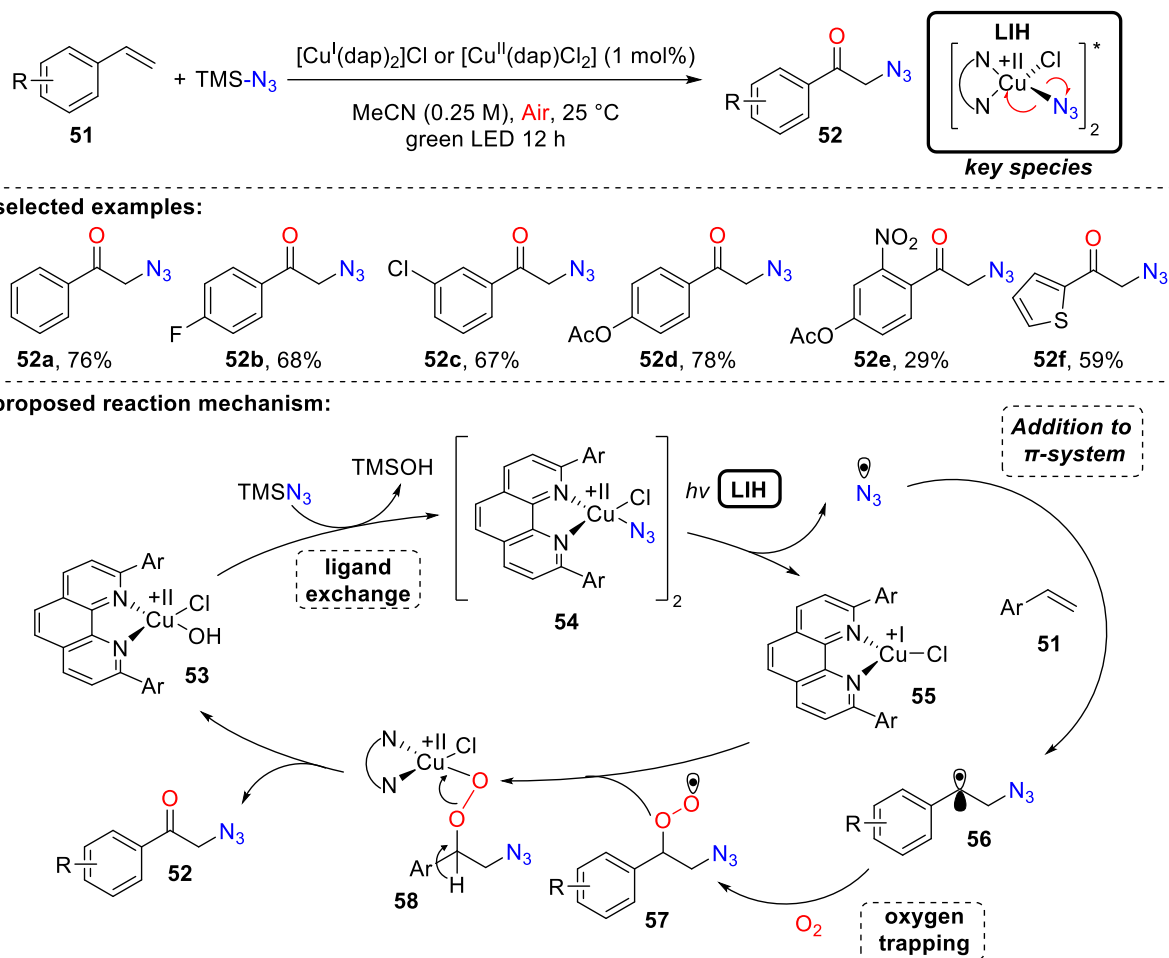
In an analogous manner, amino radicals can be generated by H-abstraction from amine derivatives **45**, such as secondary and tertiary amines, sulfonamides, carbamates, and ketoamides.^[30] Subsequently, oxidation through O₂ with concurrent Cu(II) regeneration occurs, as previously stated (cf. Scheme 6–8). The final result of this process is either oxidation to *N*-formyl derivatives **46** or demethylated adducts **47** under a more acidic environment through further deformylation (Scheme 10). According to the authors, the essential reoxidation of Cu(I) to Cu(II) occurs directly by oxygen, which would require an extra hydrogen abstraction step of peroxide **49** to **50**. A feasible alternative here would be the oxidation of Cu^I by peroxide **49** followed by the formal elimination of Cu^{II}-OH, as discussed previously.

Wan *et al.* (2022)

Scheme 10. Photocatalytic derivatization of amine derivatives.

1.4 LIH of Copper(II)-N₃ – azide radicals

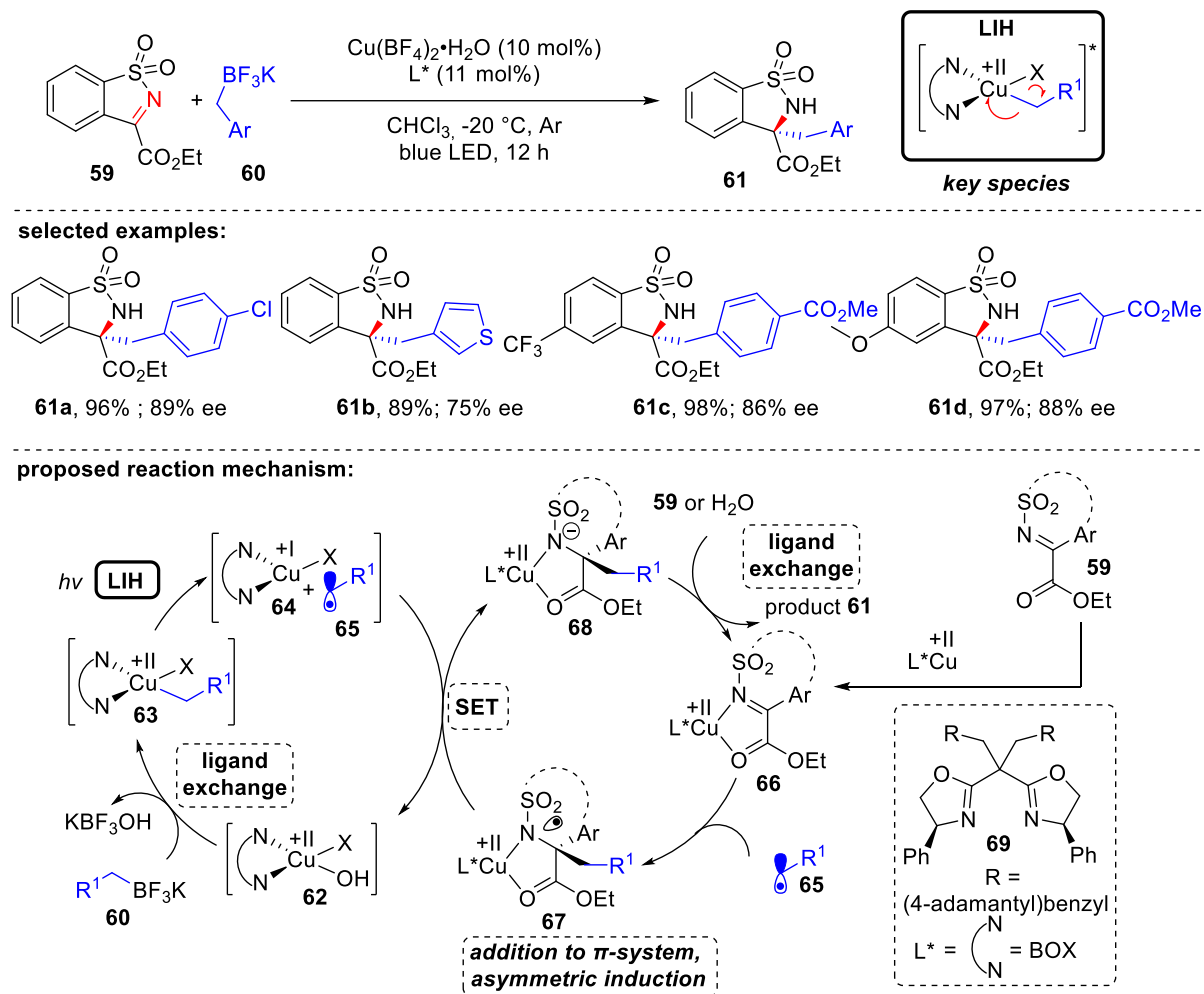
The first example demonstrating that complexes susceptible to LIH may be produced *in situ*, permitting the use of a Cu(II)-complex in catalytic levels, was successfully demonstrated in 2018 by Reiser and co-workers (Scheme 11).^[31] Utilizing TMS-N₃ as a stoichiometric azide source, azide/chloride substitution with [Cu^{II}(dap)X₂] generated the essential Cu(II)-azide intermediate **54**. Azide radicals generated upon LIH were added to a large variety of vinyl arenes to finally obtain products **62**. Termination of the transformation was successfully achieved with concurrent regeneration of the Cu(II)-catalyst through **57** and **58** following the lines previously mentioned.

Reiser *et al.* (2018)

Scheme 11. Copper(II)-photocatalyzed oxo-azidation of styrenes

1.5 LIH of Copper(II)-CH₂R – benzyl radicals

Gong and colleagues revealed that another ligand exchange process, particularly the *in situ* transmetalation of benzyl trifluoroborate salts, can result in the formation of benzyl radicals **65** through LIH soon after the report of Reiser *et al.* (Scheme 12).^[32] Because of the insufficient reduction potential ($\text{Cu(II)} \rightarrow \text{Cu(I)}$, $E_{\text{red}} = +0.50 \text{ V vs. SCE}$)^[20,21], the alternative formation of **65** via direct oxidation of the trifluoroborate ($E_{\text{ox}} = +1.34 \text{ V vs. SCE}$)^[32] salts by Cu(II) was ruled out. Benzyl radicals **65** were trapped enantioselectively by sulfonylimines **59** that were activated by a chiral bis(oxazoline)-Cu(II) complex **66**. Interestingly, the intermediate **67** generated following the addition of **65** was shown to undergo Cu(I) reduction, releasing the alkylated product **61** while simultaneously regenerating the Cu(II)-catalyst **62**. No external oxidant was necessary, thus resulting in an overall catalytic process.

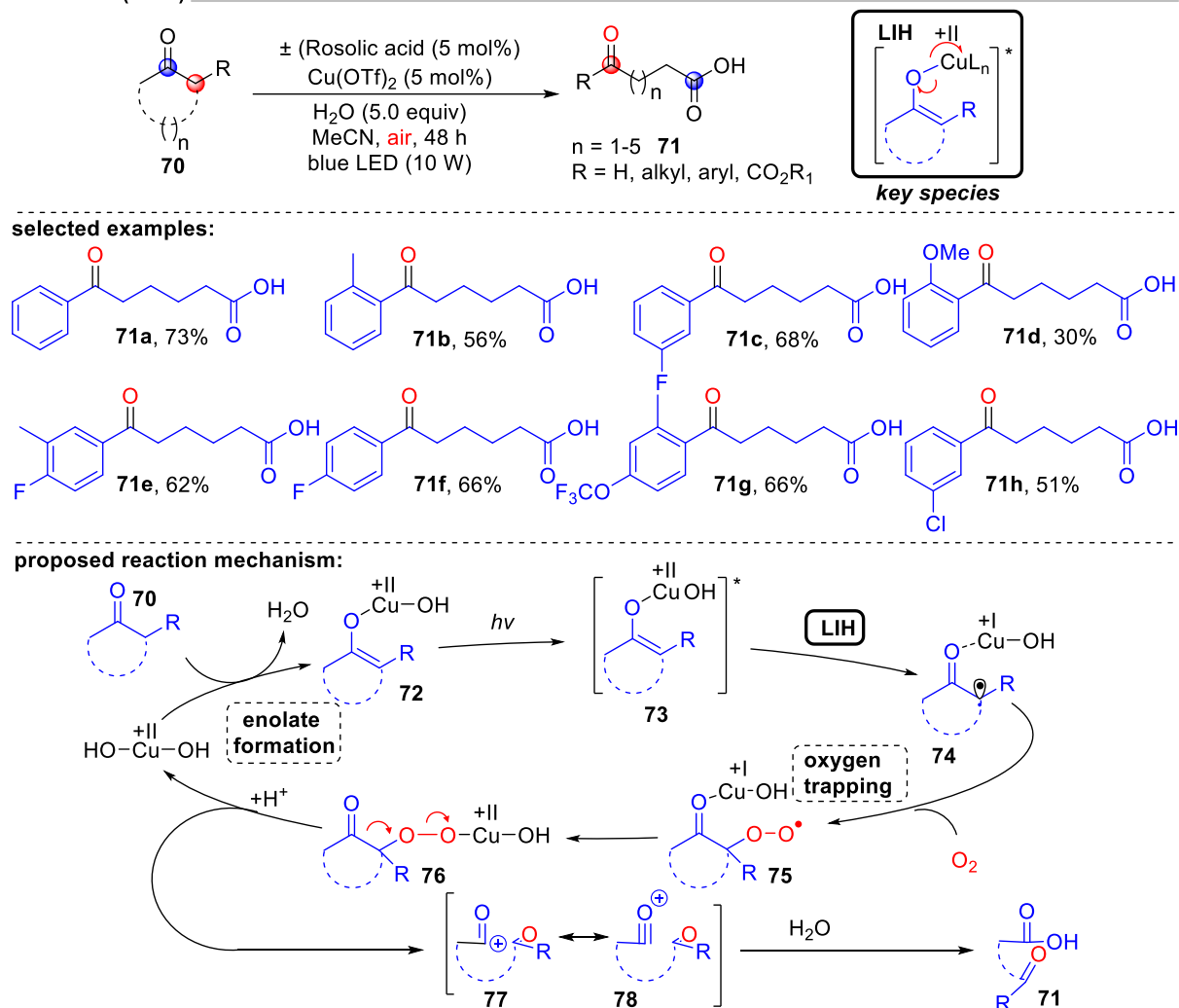
Gong *et al.* (2018)

Scheme 12. Enantioselective alkylation of imines.

1.6 LIH of Copper(II)-enolates – enolate radicals

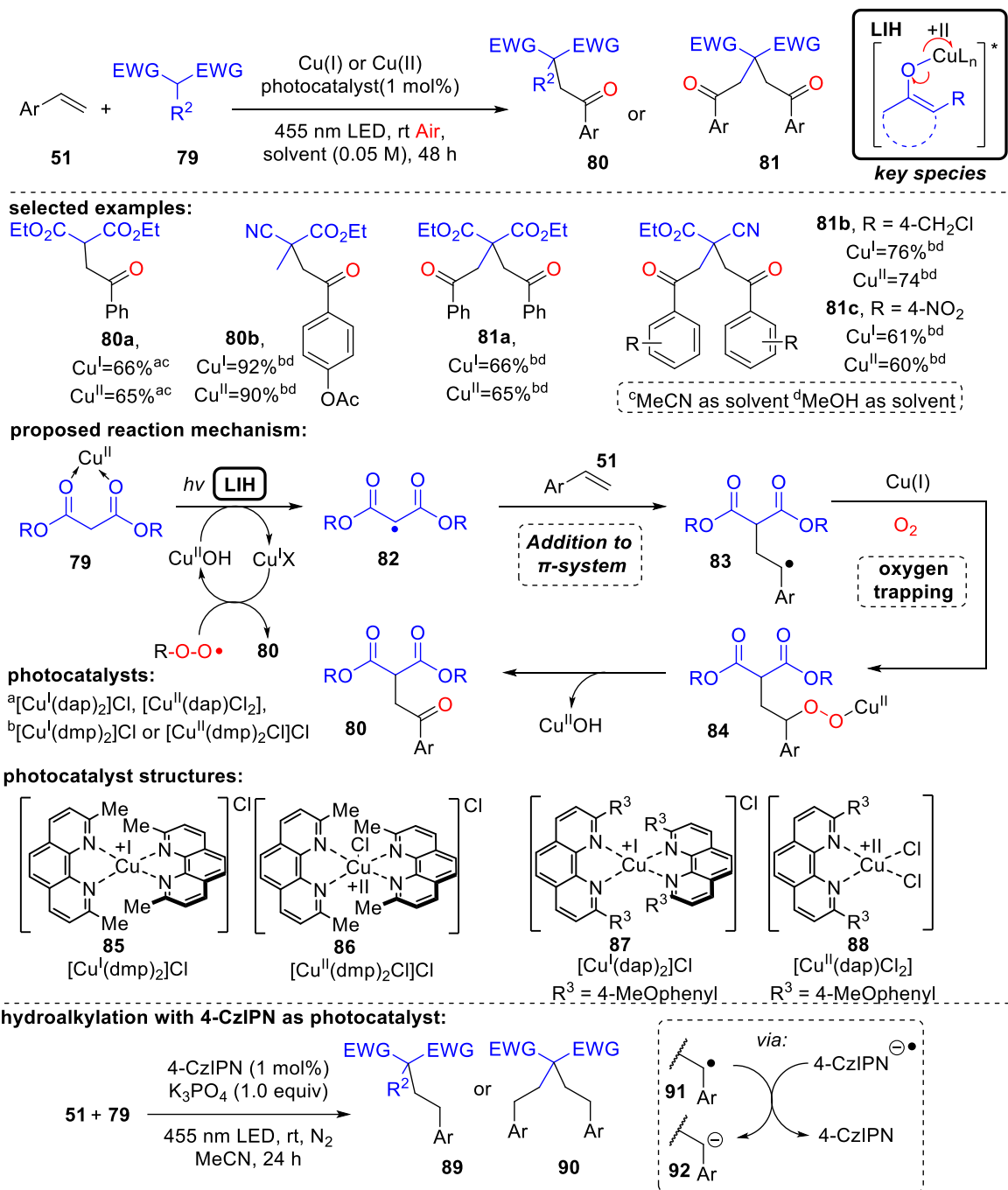
Guo and colleagues achieved the oxidative cleavage of α -phenyl-substituted cycloalkanones **70** to ketoacids **71** by relying on the known oxidation of enolates by Cu(II) under thermal conditions.^[33] Under 10 W blue light irradiation, Cu(OTf)₂ in catalytic dose in aqueous MeCN is sufficient for achieving the transformation, as depicted in Scheme 13.^[34] Also in this case, oxygen is required to capture the enolate radical **65** generated by LIH of the excited copper(II)-enolate **73**, which, in the absence of a α -hydrogen, causes a carbon elimination to the acylation **77**, giving rise to **71** after the addition of water.

Guo et al. (2021)



Scheme 13. Aerobic oxidative cleavage of cycloalkanones.

Reiser and coworkers demonstrated that analogously radicals formed from 1,3-dicarbonyl compounds **79** could be obtained using Copper(II)-induced LIH (Scheme 14). The radicals are employed to synthesize oxoalkylated viny arenes **80/81**.^[35] Again Oxygen is required as a terminal oxidant to regenerate the Cu(II)-photocatalyst, probably via **84**, *i.e.* creating a peroxoradical trapped by Cu(I). The fact that when 1,2,3,5-tetrakis(carbazol-9-yl)-4,6-dicyanobenzene (4-CzIPN) is employed instead of Cu(II), the reduced photocatalyst 4-CzIPN⁻ may change **91** to its corresponding anion **92**, resulting in hydroalkylated products **89/90** underlines the importance of this step. Hereby a divergent photocatalytic reaction is achievable; on the one hand oxoalkylation is only achievable with Cu(II), whereas on the other hand hydroalkylation is only possible with 4-CzIPN.

Reiser *et al.* (2022)

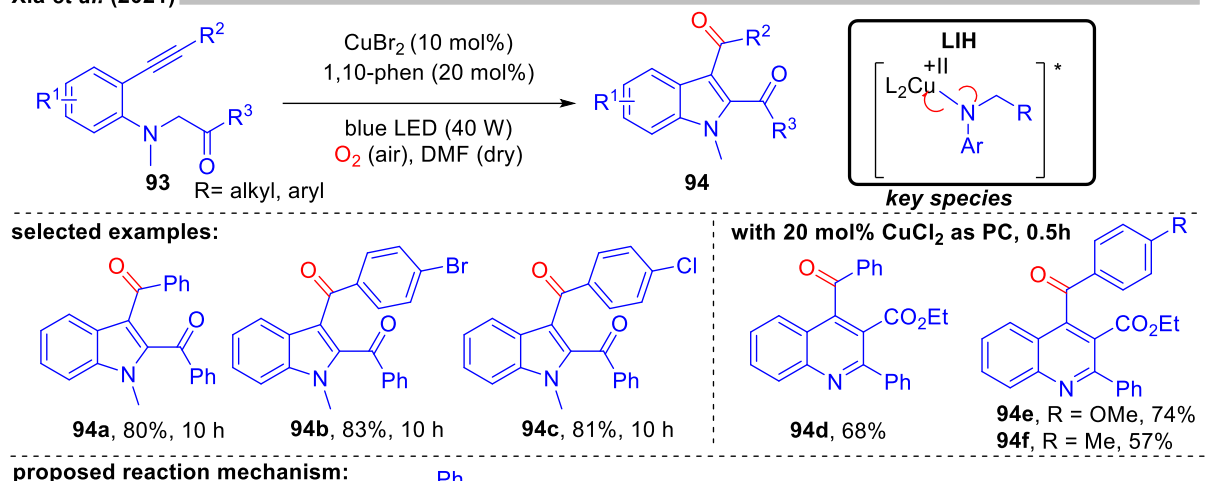
Scheme 14. Cu(II)-photocatalyzed oxo-alkylation of vinylarenes.

1.7 LIH of Copper(II)-amine-complexes – amino radicals

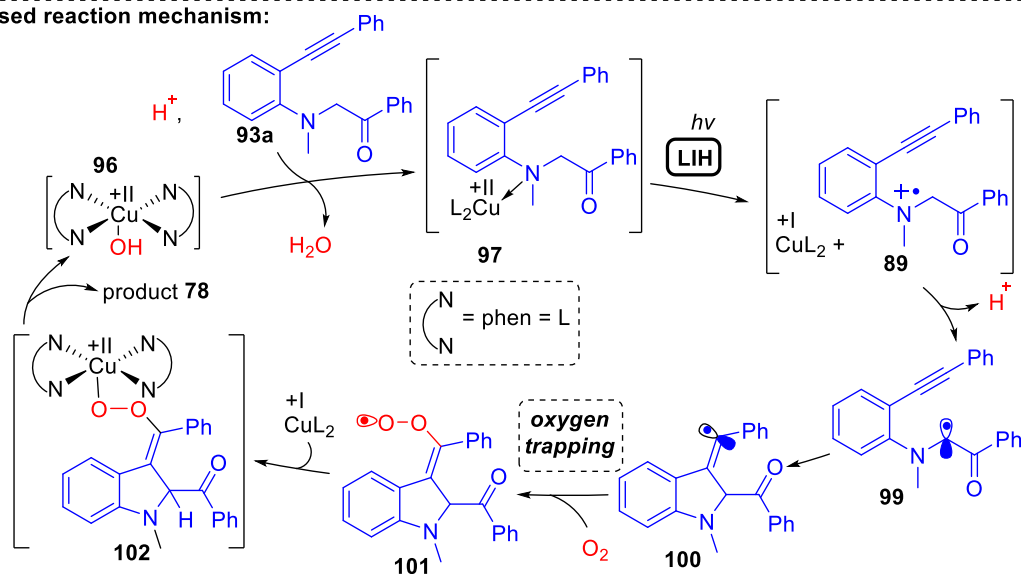
In 2021, Xia *et al.* reported a Cu(II)-photocatalyzed intramolecular oxidative cyclization process of substituted aromatic amines **93** and the C(sp³)-H bond next to nitrogen with alkynes or alkenes, yielding multi-substituted indoles **94** and quinolines **95** employing dioxygen as terminal oxidant (Scheme 15).^[36] It was assumed that copper(II) first oxidizes **93a** to the radical cation **98**.

UV investigations indicate the formation of an *N*-coordinated species with Cu(II) of type **97**. Therefore, it seems reasonable that LIH of the Cu(II)-*N* bond occurs, yielding following proton loss amino radical **99**, which promptly undergoes cyclization to carbon-centered radical **100**. Trapping of the latter by oxygen, along with reoxidation of Cu(I), finally results in product **94a**. From a mechanistic point of view, we argue that this may occur *via* **101** and **102** as previously stated for oxo-azidation (Scheme 11) or oxo-alkylation (Scheme 14).

Xia *et al.* (2021)



proposed reaction mechanism:

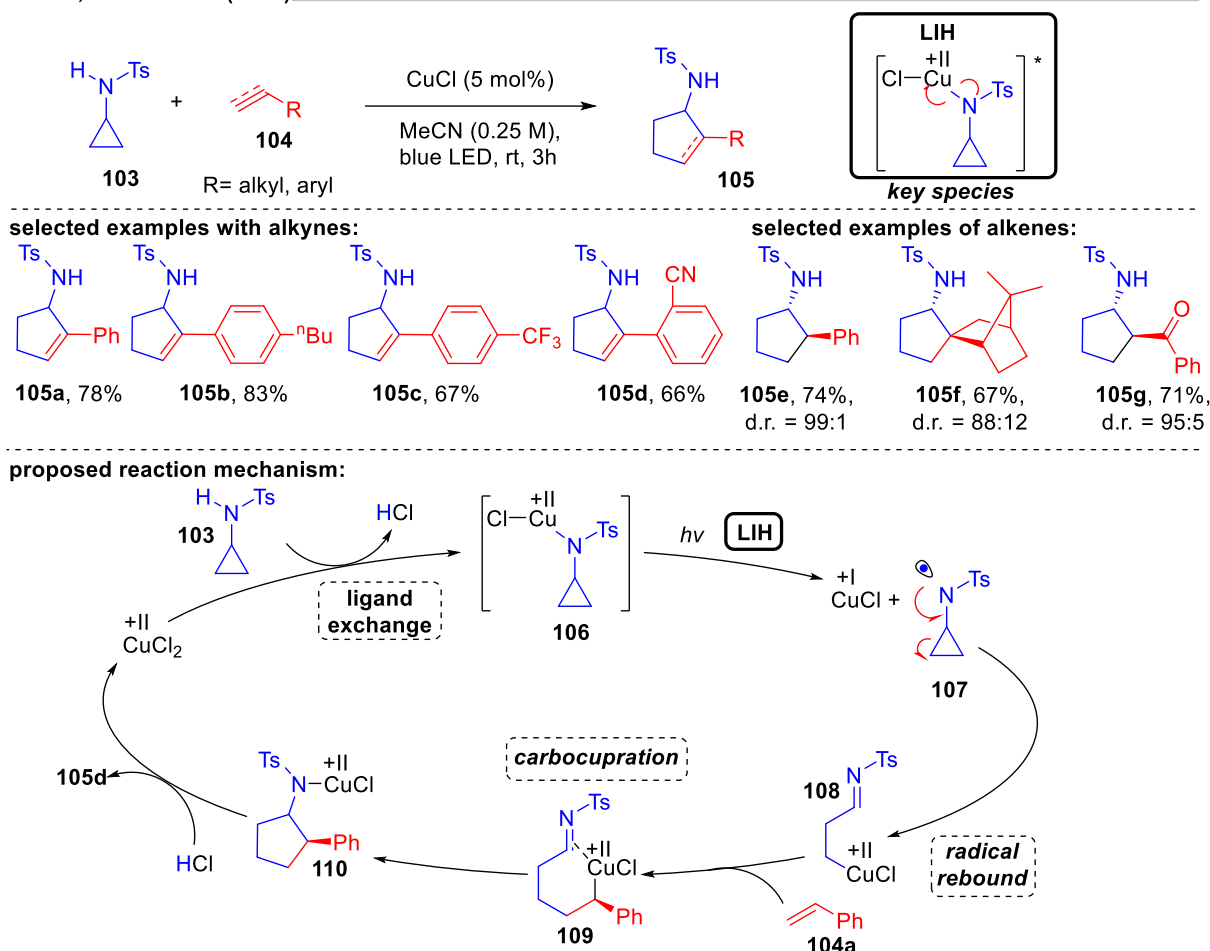


Scheme 15. Cu(II)-photocatalyzed oxidative cyclization reaction of aromatic amines.

Similarly, Verma, Reiser *et al.* showed that *N*-centered radicals can indeed be created from Cu(II)-amide complexes applying the principle of LIH, as depicted in Scheme 16.^[37] The authors discovered that an aryl-sulfonyl group on nitrogen is critical for a successful transformation, providing enough stability for the resultant nitrogen in contrasting *N*-benzoyl protective groups. Furthermore, an *N*-cyclopropyl substituent enabled the rapid transformation of the cyclopropyl-*N*-radical **107** at its inception by an irreversible ring opening. As a final outcome, [3+2] cycloaddition of *N*-tosylcyclopropane **103** with various alkynes and alkenes **104** yielded aminocyclopentanes and aminocyclopentenenes **105** with excellent regio- and

diastereoselectivity. The last feature was linked to the ability of Cu(I) to interact with the radicals created, for example, in intermediates **108** or **109**, in contrast to analogous transformations triggered by Ru(bpz)₃(BF₄)^[38] or 4-CzIPN.^[39] No external oxidant is required for these transformations, raising the question of whether Cu(II) behaved as a Lewis acid rather than a photoredox catalyst or whether the reaction could be activated thermally in the absence of the copper-catalyst. However, other mechanistic paths were ruled out by control studies: no reaction occurred in the absence of light, as well as the absence of copper.

Verma, Reiser *et al.* (2022)

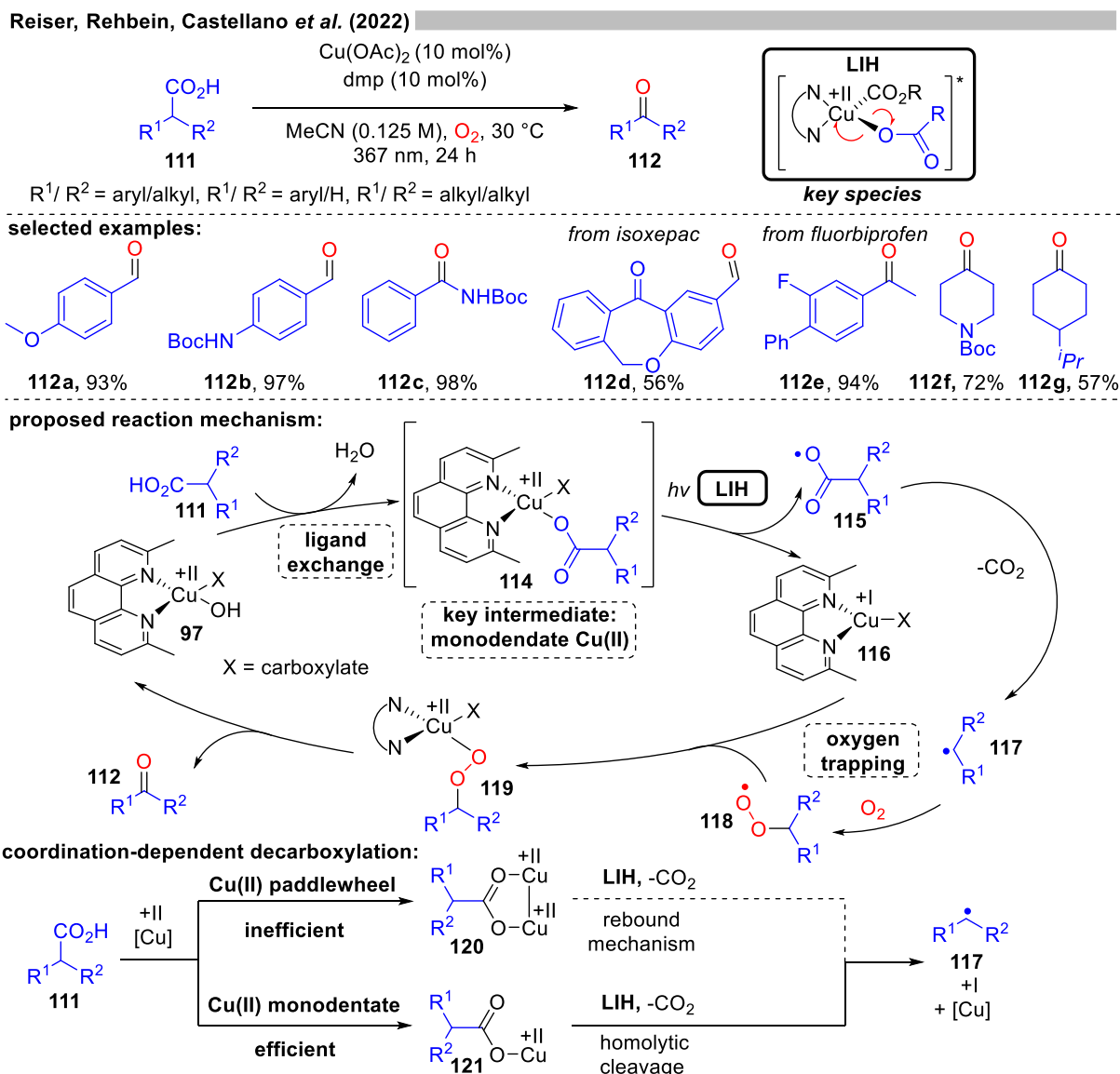


Scheme 16. Visible-light-accelerated copper-catalyzed [3 + 2] cycloaddition of *N*-tosylcyclopropylamines with alkynes/alkenes.

1.8 LIH of Copper(II)-carboxylates

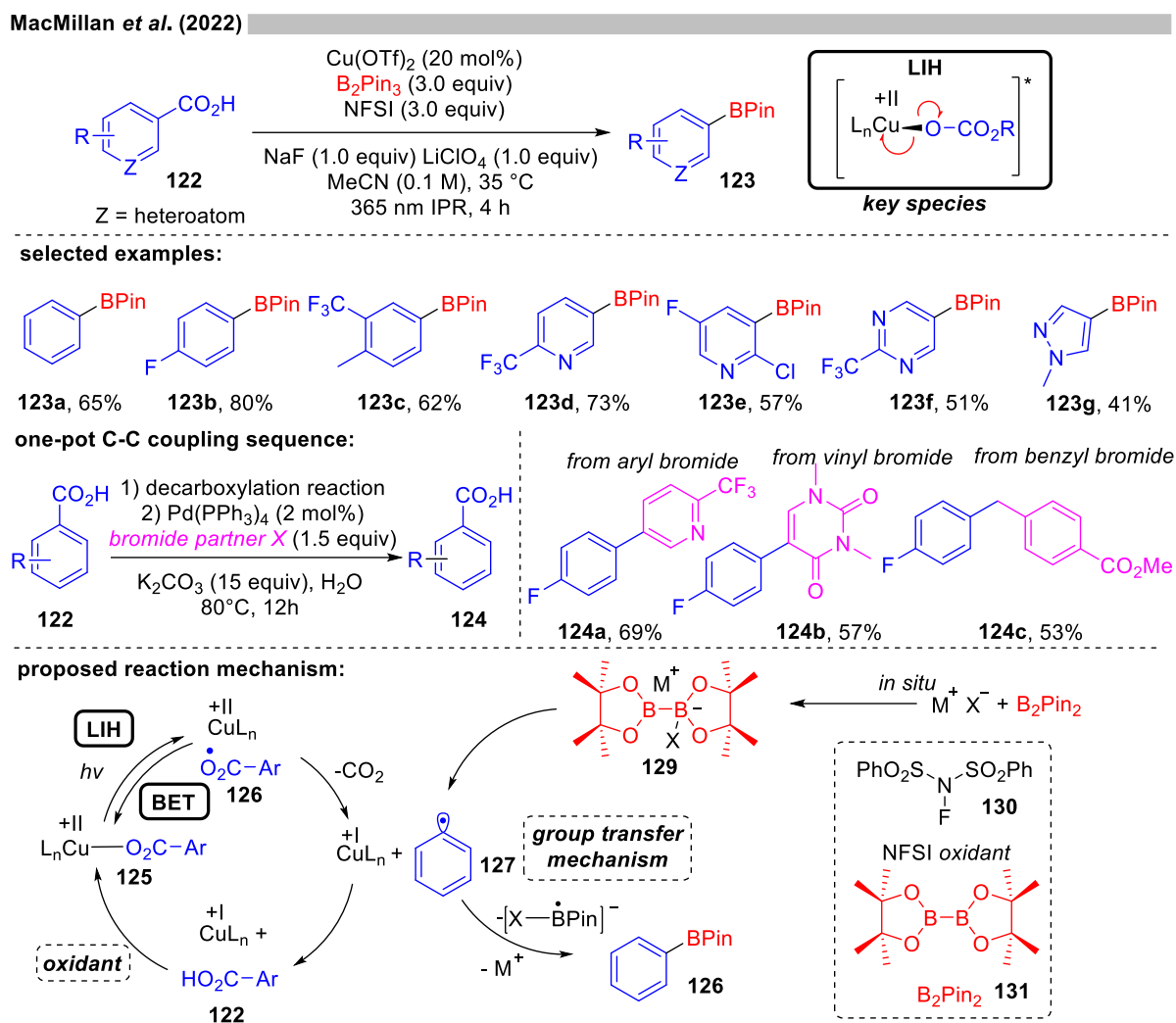
While the decarboxylation of carboxylic acids in the presence of Cu(II)-salts has been known for a long time,^[40] it has not been utilized in synthetic processes. At first sight, this is surprising, considering the capacity to create alkyl and aryl radicals from widely accessible feedstock, which should hold promise for converting renewable resources to value-added building blocks. Nevertheless, the critical issue in this scenario is achieving catalytic turnover, *i.e.* returning the

resultant Cu(I) to Cu(II), after LIH of the Cu(II)-carboxylate. One probable explanation is the generated radicals' significant reactivity to oxidants, especially oxygen.



Scheme 17. Decarboxylative oxygenation of carboxylic acids.

A recent study by Reiser, Rehbein, Castellano *et al.* on the photocatalytic decarboxylation of phenylacetic or secondary carboxylic acids **111** revealed that a catalytic Cu(II)/Cu(I)-cycle could be accomplished in the presence of oxygen as the terminal oxidant (*vide supra*, Scheme 17).^[41] However, the radicals **117** created by decarboxylation could only be trapped by oxygen; all attempts to intercept them by other radicalophils, *e.g.*, such as alkenes, which was successful with malonyl radicals (*cf.* Scheme 14), were unsuccessful. This investigation also indicated that monodentate coordination of a carboxylate to copper(II), *i.e.* **114/121**, is far superior to the commonly found bidentate paddle-wheel type coordination **120** for establishing LIH.



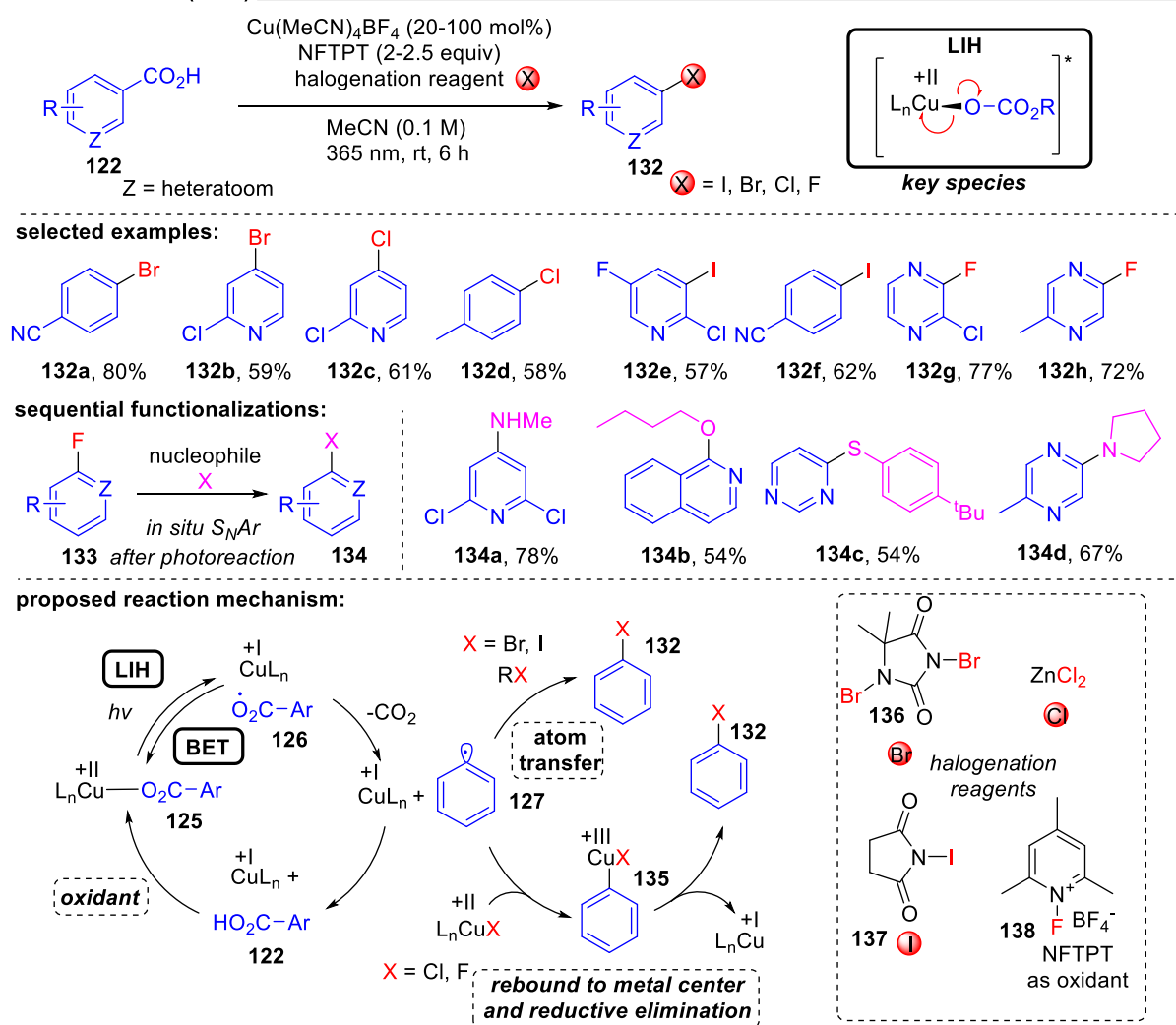
Scheme 18. Decarboxylative borylation of (hetero)arylcarboxylic acids.

As shown in Scheme 18 (*vide supra*), MacMillan and colleagues successfully established an alternative cooxidant that enabled catalytic turnover in copper(II).^[42] The decarboxylative borylation of (hetero)arylcarboxylic acids **122** was accomplished by using a combination of $\text{Cu}(\text{OTf})_2$ (20 mol%) and *N*-fluorobenzenesulfonimide **130** (NFSI, 3.0 equiv). Thereby the authors discovered a method to regenerate $\text{Cu}(\text{II})$ -carboxylate **125** from $\text{Cu}(\text{I})$ and carboxylic acid **122**, thus achieving the process catalytic in $\text{Cu}(\text{II})$. Additionally, the procedure was also suitable for further developments. One-pot couplings in Suzuki-Miyaura arylation, vinylation, alkylation, or coupling of heteroaryl boronic ester were developed, highlighting the synthetic value of the boronic ester products generated.

Furthermore, the same group developed the decarboxylative halogenation of (hetero)aryl carboxylic acids.^[43] It was found that as terminal oxidant 1-fluoro-2,4,6-trimethylpyridinium tetrafluoroborate (NFTPT) (**138**), which finally accomplishes the reoxidation of $\text{Cu}(\text{I})$ to $\text{Cu}(\text{II})$, enables the utilization of sub-stoichiometric levels of $\text{Cu}(\text{II})$. Two distinct strategies for introducing the halide nucleophile were explored (Scheme 19):

On the one hand, atom transfer (AT) was utilized to achieve bromination with the reagent 1,3-dibromo-5,5-dimethylhydantoin (**136**) and iodination with NIS (N-Iodosuccinimide) (**137**) to obtain products **132**. Fluorination and chlorination, on the other hand, became possible with NFTPT or ZnCl_2 as halogenating agent, which occurs by a rebound mechanism *via* a Cu(III)-intermediate **117**, according to the proposed mechanism. However, It must be mentioned that the fluorination protocol still needed stoichiometric amount of the copper salt as already observed by Ritter *et al.* (*vide infra*, Scheme 20). Why the catalytic cycle is not closed in this case remains unclear.

MacMillan *et al.* (2022)



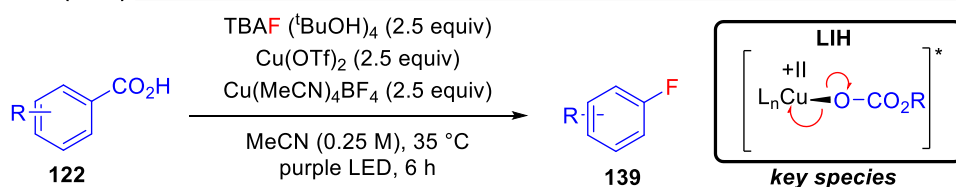
Scheme 19. Decarboxylative halogenation of (hetero)arylcaboxylic acids.

So far, the photooxidation of carboxylic acids by Cu(II) as a starting point for alkyl and aryl radicals is highly promising, making the (over)stoichiometric usage of Cu(II)-salts an acceptable compromise for the synthetic transformations that may be accomplished through this process. This method has been implemented in a series of elegant investigations for various transformations that are challenging to carry out otherwise. As depicted in Scheme 20, Ritter and co-workers demonstrated that copper(II)-benzoates can be the starting point for

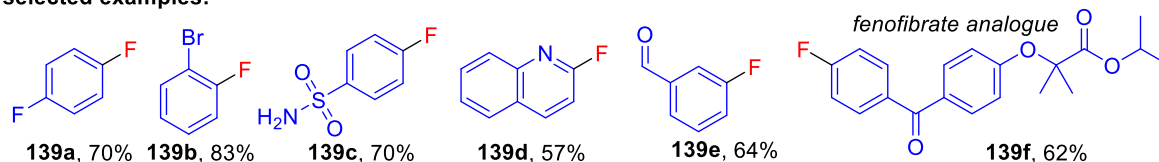
obtaining fluorinated arenes by employing TBAF·(*t*BuOH)₄ as the fluorine source.^[44] Notably, functional groups that are susceptible to oxidation, such as aldehydes, are tolerated in the process, and the protocol can also be applied to derivatize bioactive molecules. According to the proposed mechanism, Cu(II) is involved in two processes: In each step, Cu(II) is converted to Cu(I). That indicates why a minimum of two equiv of Cu(OTf)₂ is required for this transformation. LIH of a copper(II)-arylcarboxylate **125** generates **126** and after decarboxylation an arylradical **127** and Cu(I).

The decarboxylation of aryl carboxyl radicals ($k \approx 10^6 \text{ s}^{-1}$)^[45] is about 1000 times slower than decarboxylation of alkyl carboxyl radicals ($k \approx 10^9 \text{ s}^{-1}$)^[46] and therefore, it is assumed that the LIH step is reversible. The aryl radical **127** is subsequently transformed to the arylcopper(III)-species **141**, either *via* direct trapping with Cu(II) or trapping by Cu(I) accompanied by a one-electron oxidation by Cu(II) (path B). It does not make any difference which pathway is occurring. Thus, both pathways require the employment of another equivalent of Cu(II).

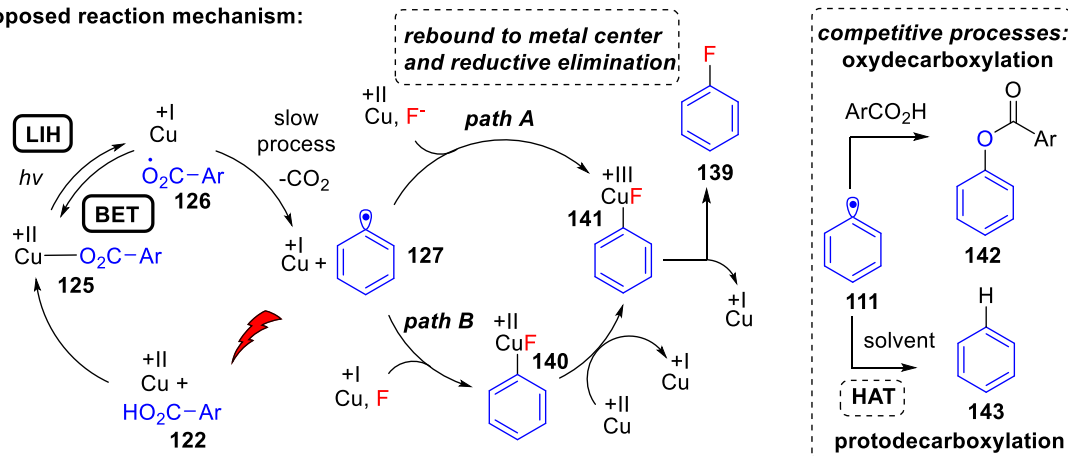
Ritter *et al.* (2021)



selected examples:



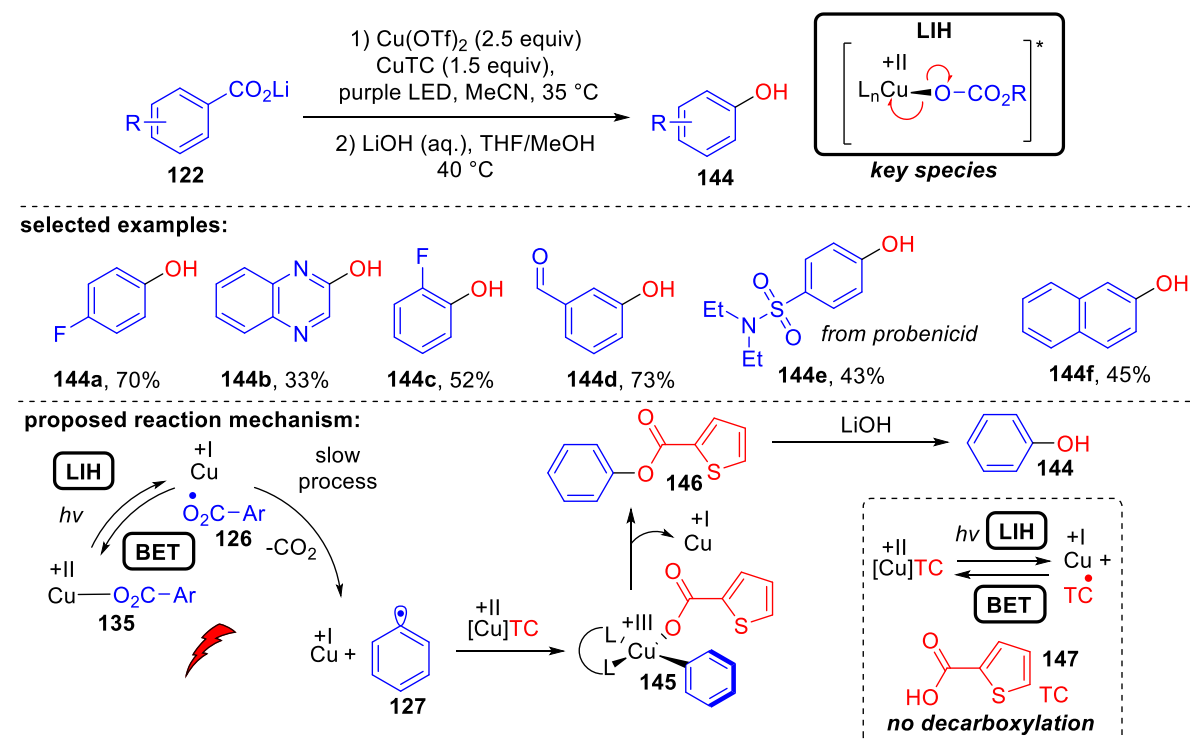
proposed reaction mechanism:



Scheme 20. Cu(II)-photocatalyzed decarboxylative fluorination of benzoic acids.

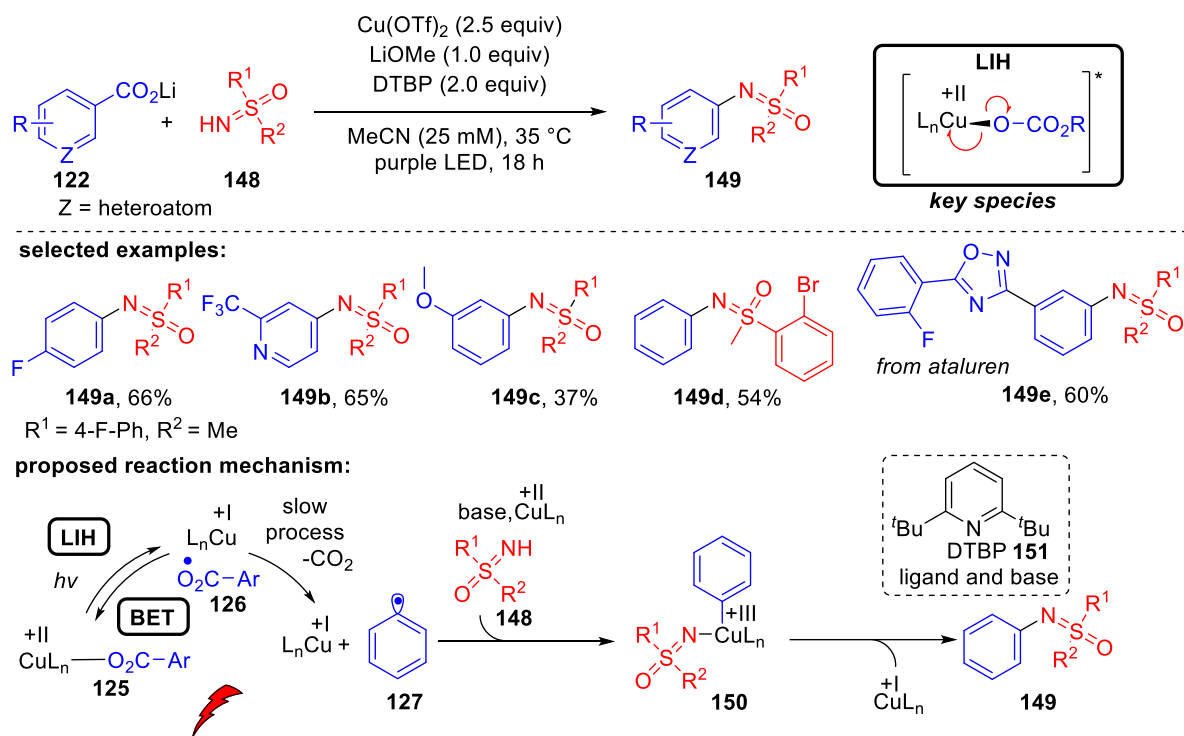
Apart from fluoride, it was shown in a subsequent investigation that the carboxylate itself might function as the nucleophile, producing benzoates **146**, which upon hydrolysis produce valuable phenols **144** as depicted in Scheme 21. However, for this purpose, one equivalent of the carboxylic acid is sacrificed, resulting in a maximum yield of just 50%. Ritter and colleagues

discovered a solution to this challenge by utilizing thiophene-2-carboxylic acid (TC) **147** as the nucleophile: it was recognized that Cu(II)-TC may undergo LIH to give Cu(I) and the corresponding thiophene-2-carboxyl radical, the latter cannot be decarboxylated.^[47] As a consequence, thiophene-2-carboxylate can be regenerated via back electron transfer (BET) with Cu(I). Therefore Cu(II)-TC is available for trapping of the aryl radical **127** to the Cu(III)-intermediate **145**. Subsequent reductive elimination produces oxygenated arene **146** and Cu(I). However, the catalytic cycle is also disrupted at this step, which explains why an excess of Cu(II)-salts is required to achieve a successful overall process.

Ritter *et al.* (2021)

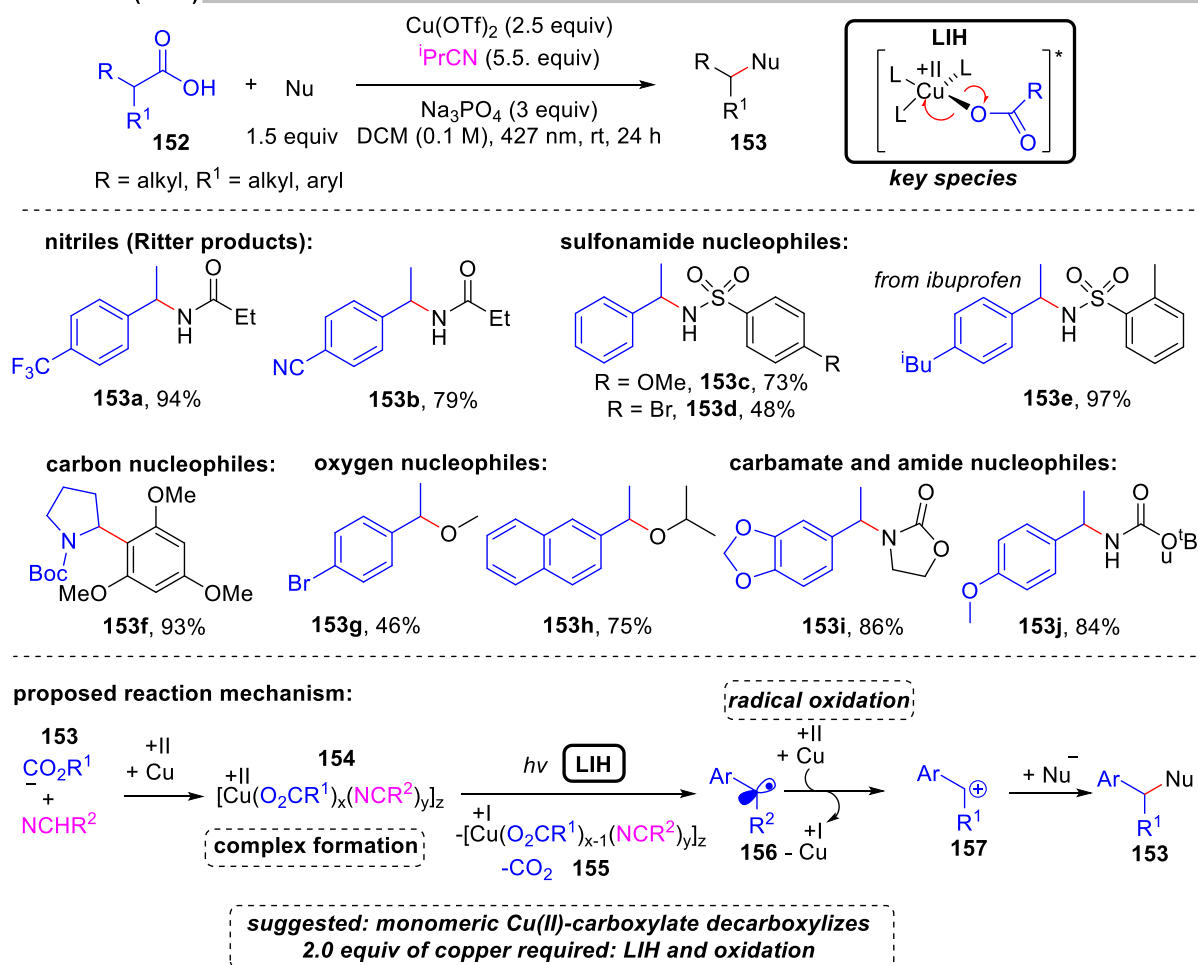
Scheme 21. Decarboxylative hydroxylation of benzoic acids.

In the same way, Ritter and co-workers reported a method for the decarboxylative sulfoximination of benzoic acids **122** (Scheme 22).^[48] To obtain high reaction efficiency, lithium carboxylates with 2,6-di-*tert*-butylpyridine (DTBP) (**151**) and LiOMe as additive were necessary. To enable the transformation, it was necessary to overcome the formation of undesired sulfoximine-ligated Cu(II)-species and to suppress undesired oxidecarboxylation to phenols. It was assumed, that the weak coordination of the ligand DTBP to Cu(II) might favor C–N over C–O reductive elimination or aid the generation of photoactive Cu(II)-carboxylate species. The function of LiOMe is unknown. However, it was assumed that it could reduce the concentration of free sulfoximines by forming weakly soluble lithium salts of sulfoximine. Oxidizable groups, as well as strong coordinating groups, e.g. amines inhibited the transformation, according to the authors.

Ritter *et al.* (2022)

Scheme 22. Decarboxylative sulfoximation of benzoic acids.

Yoon *et al.* developed a copper-mediated decarboxylative coupling of arylacetic- and aliphatic carboxylic acids **152** and nucleophiles under irradiation at 427 nm (Scheme 23), which was reported at the end of 2021.^[49] The established process has an extensive scope, including various nucleophiles, such as nitrogen-, oxygen- and carbon-based ones. The copper(II) salt performs two tasks in the protocol: the radical formation through LIH of Cu(II)-carboxylate **154** and the subsequent oxidation of the benzylic radical **156** to the corresponding benzylic cation **157**. As a result, two equivalents of copper(II) must be utilized (stoichiometric amount), as it was the case in similar work of this group.^[50] *t*PrCN was found to serve as an essential ligand for Cu(II) to form active monomeric copper(II)-carboxylates. Dimeric copper(II)-carboxylates were suggested to be photocatalytically inactive, which indeed was demonstrated by Reiser *et al.* (*cf.* Scheme 17).^[41]

Yoon *et al.* (2022)

Scheme 23. Decarboxylative cross-coupling reaction with different nucleophiles.

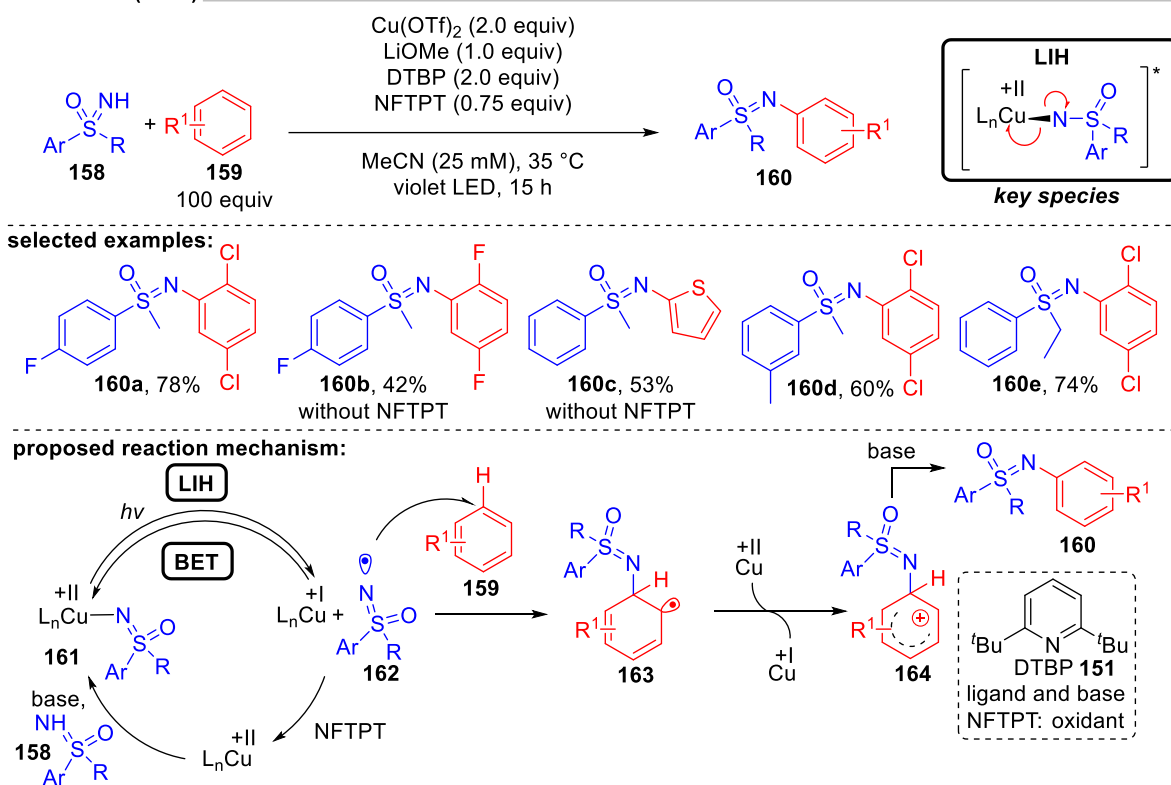
1.9 LIH of Cu(II)-sulfoximines – N-centered sulfoximiny radicals

Furthermore, the Ritter group developed C-H-sulfoximation protocol of arenes **159** (Scheme 24).^[51] Because of the high oxidation potential ($E_{\text{ox}} = +1.92$ to $+2.00$ V vs SCE)^[52] as well as the high bond dissociation energy (BDE, $\text{BDE}_{\text{N-H}} = 104$ – 106 kcal/mol, by DFT calculation),^[51] the direct generation of sulfoximiny radicals from *NH*-sulfoximines **158** (e.g. through HAT or SET) is difficult.

Nevertheless, as previously demonstrated by Verma and Reiser *et al.* for *N*-tosylamines (*cf.* Scheme 16), *N*-centered radicals are accessible from *NH*-sulfoximines **158** using the LIH principle. It was shown that LiOMe served to be the optimum base for deprotonating **158**, thus resulting in more efficiently formed Cu(II)-sulfoximine complexes. DTBP (**151**) was discovered to be a critical ligand in preventing undesirable BET by stabilizing Cu(II)-sulfoximine complex **161**. The elaborated protocol involved a wide variety of electron-neutral and rich arenes: Electron-deficient arenes were less reactive, leading to the unfavorable HAT of sulfoximiny

radicals with unproductive Cu(II) consumption as a competing process. Consequently, the use of NFTPT as an oxidant was shown to be advantageous to Cu(II) regeneration.

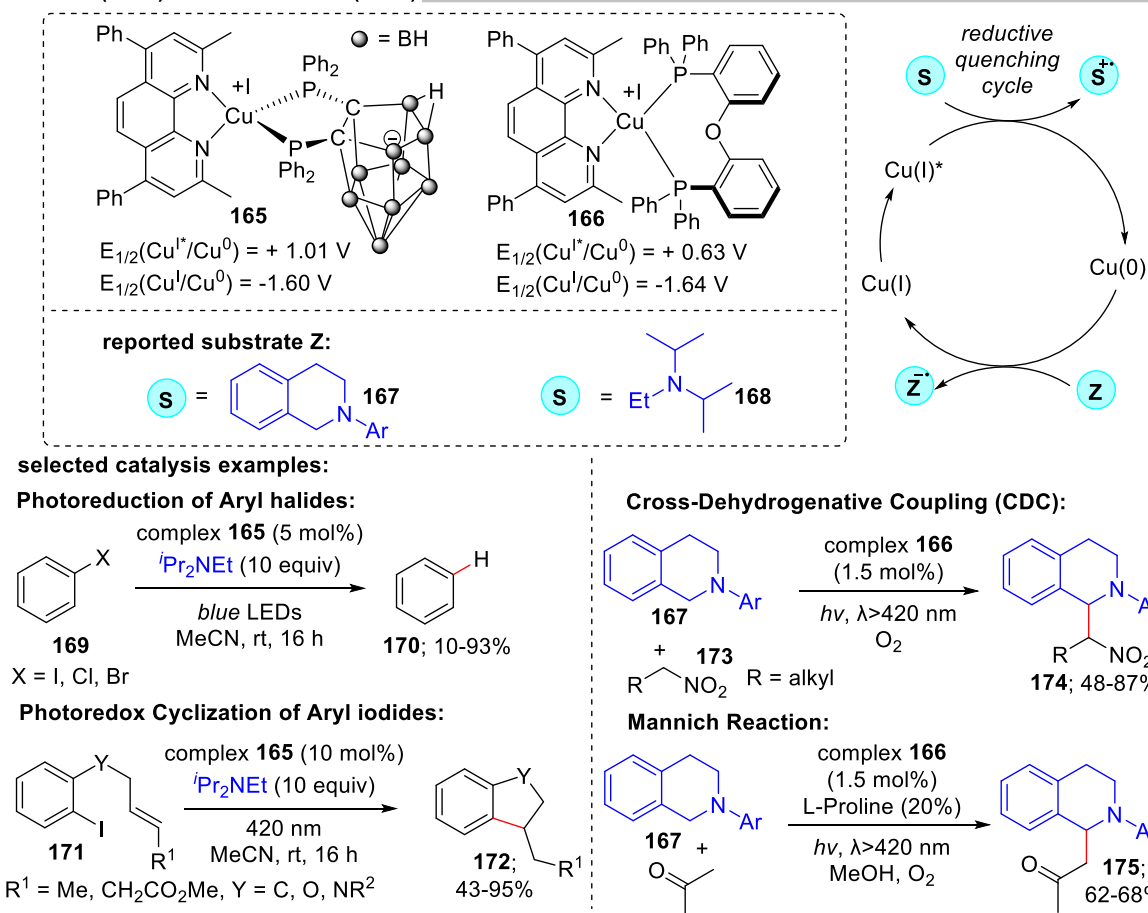
Ritter *et al.* (2022)



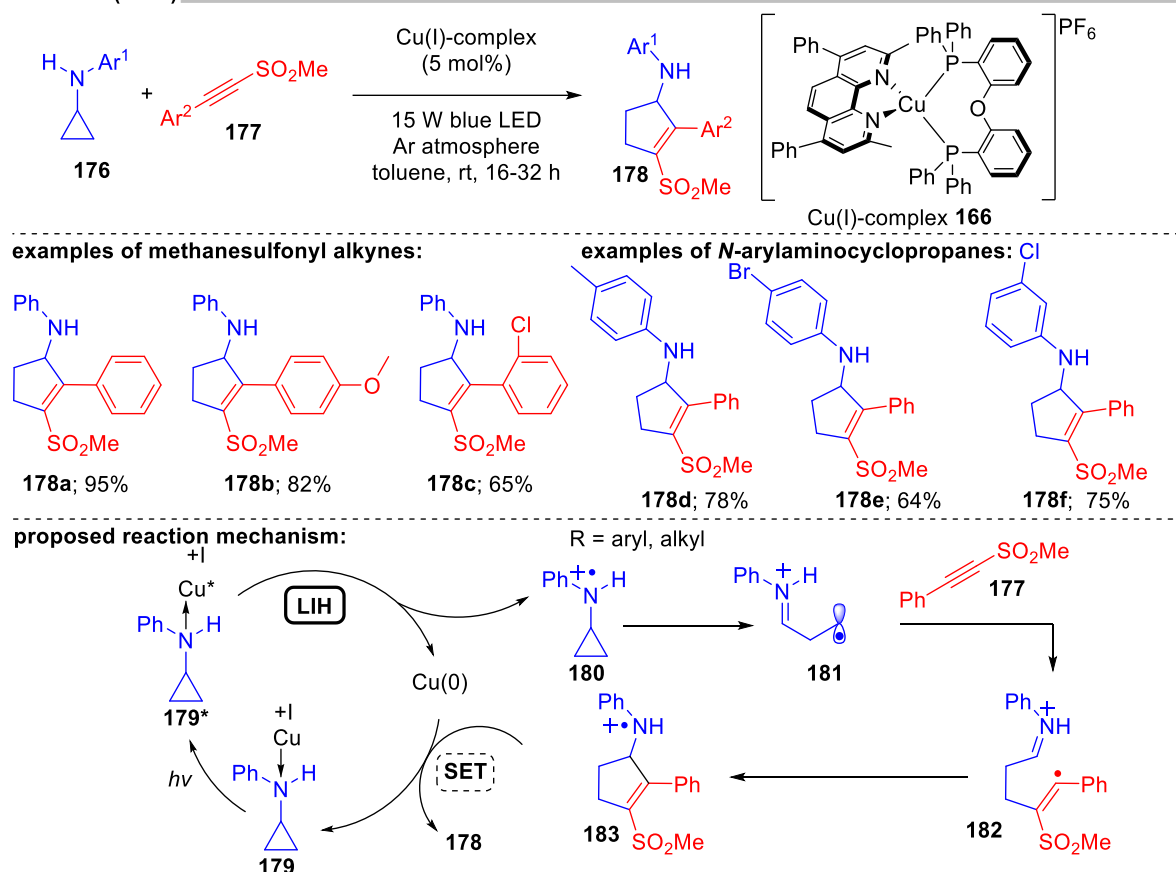
Scheme 24. C–H sulfoximation of arenes.

1.10 Outlook: Transformations involving Cu^{n*}/Cuⁿ⁻¹ transitions

Apart from depending on Cu(II)* to Cu(I) for the dissociative LMCT process, another possible copper transition for such transformation might be initiated by Cu(I)* → Cu(0). However, there are only a few examples of this mode available. The photostable zwitterionic copper(I)-complex **165** was employed by Che and co-workers^[11] in a reductive quenching cycle involving a Cu(0) intermediate for the oxidation of amines (Scheme 25). Furthermore, Evano *et al.*^[12] reported a heteroleptic copper-based photocatalyst **166** in the same way. Nonetheless, these oxidations may be attributed to outer-sphere processes.

Che *et al.* (2014) and Evano *et al.* (2017)Scheme 25. Heteroleptic complexes acting in $\text{Cu}(\text{I})^* \rightarrow \text{Cu}(\text{0})$ cycle.

Liu and co-workers^[53] proposed evidence for LIH via a dissociate LMCT involving a $\text{Cu}(\text{I}) \rightarrow \text{Cu}(\text{0})$ transition for the [3+2]-cycloaddition of *N*-arylamino cyclopropanes **176** with alkynes **177**, mirroring the transformation reported by Verma, Reiser and co-workers^[37] via $\text{Cu}(\text{II})/\text{Cu}(\text{I})$ cycles (*cf.* Scheme 16) as shown in Scheme 26. Stern-Volmer experiments show that the excited $\text{Cu}(\text{I})$ -photocatalyst interacts with *N*-arylamino cyclopropanes, implying that a precoordination of $\text{Cu}(\text{I})$ with aminocyclopropane **176** is plausible. Subsequent SET from **179** to $\text{Cu}(\text{I})^*$ affords cyclopropyl radical cation **180**. After that, ring opening delivers **181** followed by cycloaddition to yield the products **178** and back electron transfer to renew the $\text{Cu}(\text{I})$ -photocatalyst.

Liu *et al.* (2022)Scheme 26. Copper-catalyzed [3 + 2] cycloaddition involving a Cu(I)*⁺/Cu(0) cycle.

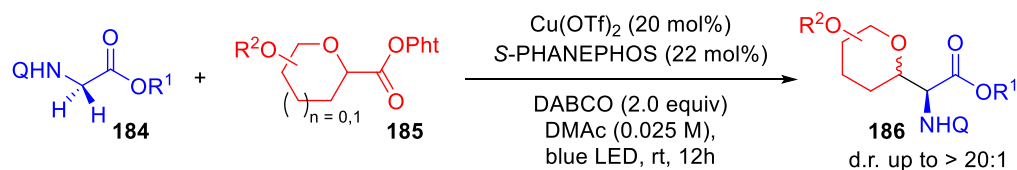
Cu(III)*⁺ → Cu(II) could be another potential transition. Cu(III)-intermediates are generally challenging to isolate,^[54] but they were successfully applied in photocatalytic transformations *via* trapping of transient radicals by Cu(II), which can be considered to be a persistent radical, thus generating an efficient process. Reductive elimination results in Cu(I), which accounts for the short-lived Cu(III)-species.

Nonetheless, the visible-light promoted, stereoselective C(sp³)-H glycosylation for the synthesis of C-glycoamino acids and C-glycopeptides was reported by Xu *et al.* in 2022 (Scheme 27).^[55] It was assumed that Cu(I) being generated *in situ* from Cu(II). The catalytic cycle starts with well-established elemental steps, such as SET of the Cu(I)-substrate complex **189** to the second substrate **185**. This process generates radical intermediate **191**, which affords after a rebound to Cu(II) the critical Cu(III)-intermediate **193**.

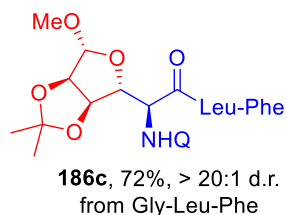
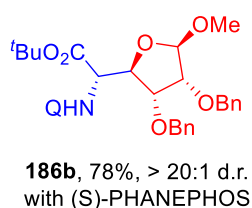
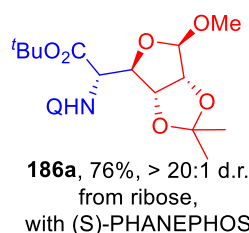
For the two organic moieties that need to be connected to afford overall the final product **186**, the intermediate **196** appears to be plausible. According to the authors, **196** can be obtained from **193** by deprotonation and MLCT via a Cu(II)-species of type **195**. For this purpose, UV-spectroscopy provides evidence for the presence of Cu(III). Instead, it could be assumed that a glycine moiety might undergo direct ligand exchange to **194** to obtain **195**, which could be in

equilibrium with **196** through LIH to adopt the most advantageous geometry guided by the chiral ligand **187** for the final reductive elimination.

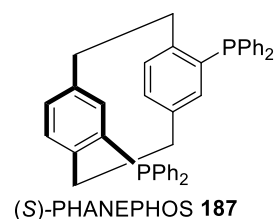
Wang, Xu *et al.* (2022)



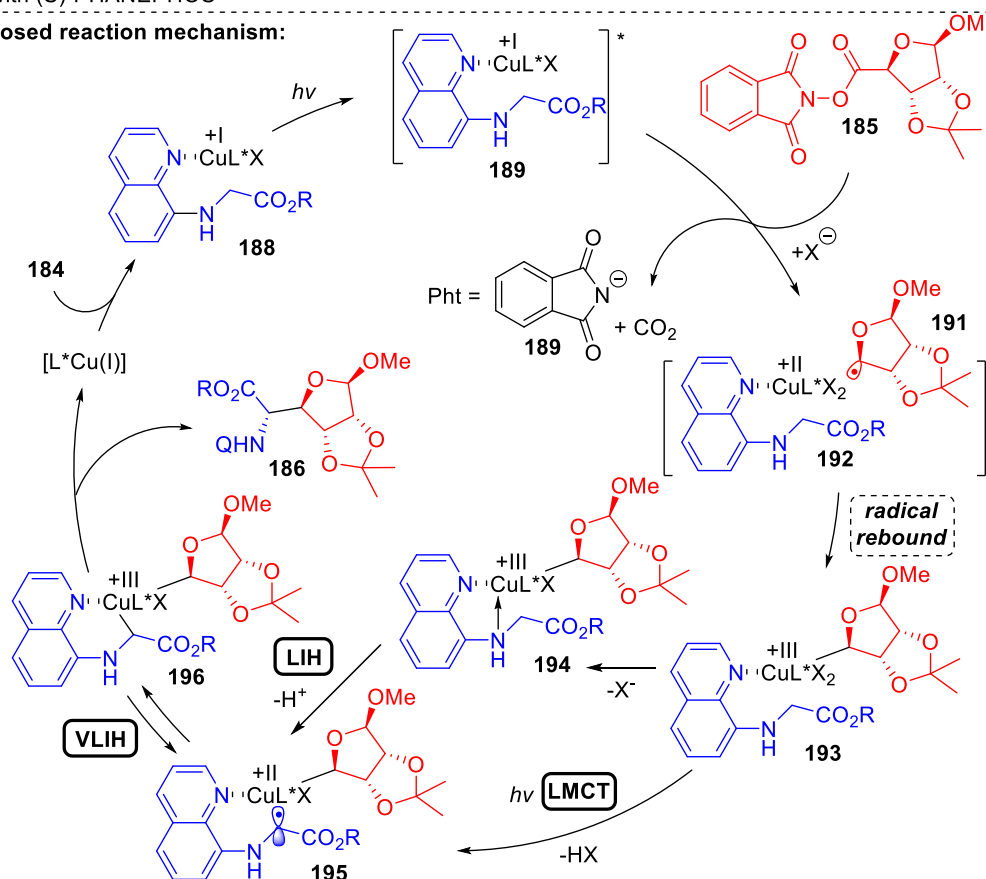
selected examples:



chiral ligand L:



proposed reaction mechanism:



Scheme 27. Copper-promoted C(sp³)-H glycosylation involving a Cu(III)^{*}/Cu(II) cycle.

1.11 Summary and Perspectives

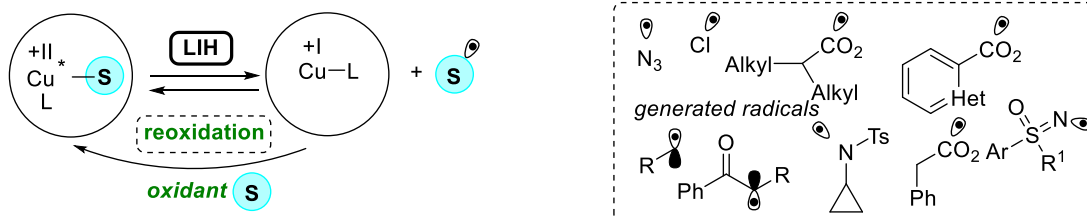
Because of the readily accessible nature of 3d-transition metals, replacing them with their valuable 4d- and 5d-congeners is an important but demanding research area. To address the issue of ultrashort excited-state lifetimes in 3d-metal complexes, precoordination of substrates that undergo light-induced homolysis (LIH, which is typically dissociative LMCT) seems to be an attractive solution, as depicted in Scheme 28A.

The importance of excited-state lifetimes for radical production via SET has been pushed back by spectroscopic data which suggest that such homolysis events are ultra-fast (< 1 ps). Up to date, copper(II)-complexes containing azide, amine, sulfoximine, carboxylate, enolate, or alkyl substituents have been successfully demonstrated as promising substrates for LIH due to the flexible coordination chemistry of Cu(II). Radicals \mathbf{S}^{\bullet} may be produced under mild circumstances, along with the ability of the copper catalyst to interact and hence stabilize intermediates formed within a catalytic cycle. Overall, this enabled the development of unique reaction pathways, as depicted in Scheme 28B:

ATRA or ATRA-like processes have been proven to initiate with addition to π -systems (pathway A). Hydrogen atom abstraction (HAT, route B) has been demonstrated as an effective method for functionalizing feedstock hydrocarbons. Rapid fragmentation of the radical \mathbf{S}^{\bullet} to afford a new radical \mathbf{S}'^{\bullet} might occur. This is best known for carboxyl radicals. Manifold atom transfer reactions (XAT) have been demonstrated to be feasible from here (pathway C), which may be preceded by the rebound of \mathbf{S}^{\bullet} to Cu(I) or Cu(II) (pathway D).

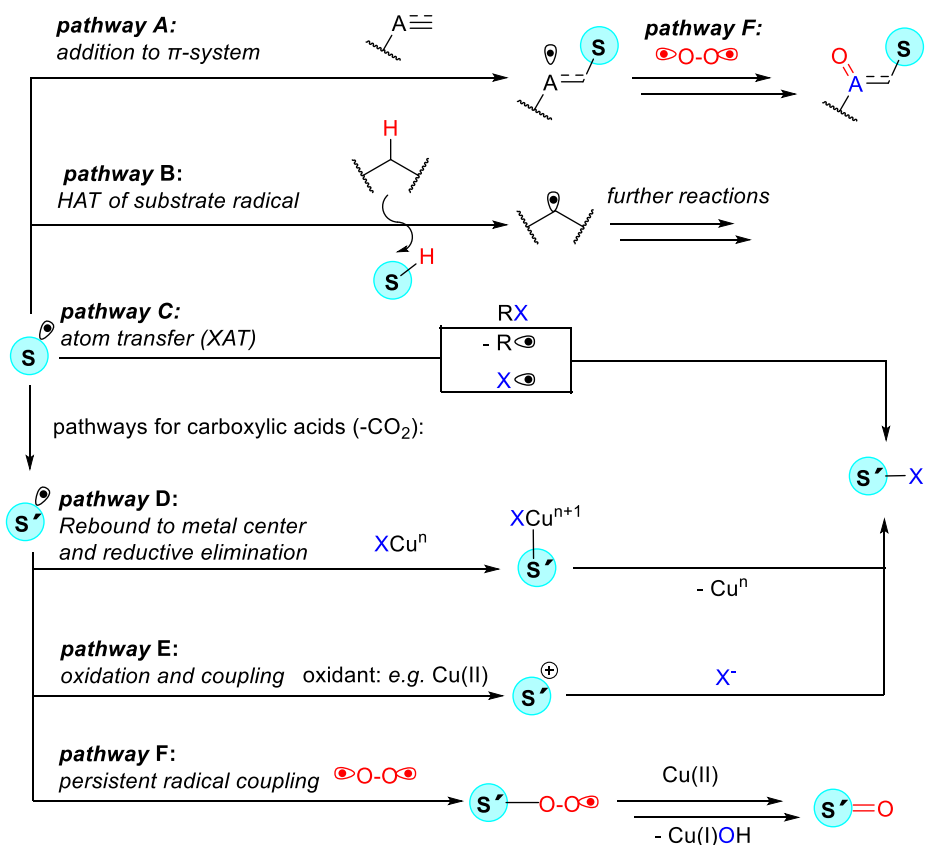
The oxidation of \mathbf{S}^{\bullet} to the corresponding cation $\mathbf{S}^{+\bullet}$ in the presence of a suitable oxidant, often achieved by applying overstoichiometric amounts of Cu(II), establishes the conditions for the coupling with nucleophiles (pathway E). Another option is a radical-radical coupling between the transient radical \mathbf{S}^{\bullet} or \mathbf{S}'^{\bullet} and a persistent radical, most commonly molecular oxygen, which accesses ketones or aldehydes (pathway F).

(A) LIH of Copper(II)-Substrate-Complexes and Radical Pool



to render Cu(II) catalytic: reoxidation with suitable oxidant (O_2 , NFSI, NFTPT) is required

(B) Possible Reaction Pathways for the Generated Radical



Scheme 28. Perspectives: achieving a platform for synthetic transformations.

1.12 References

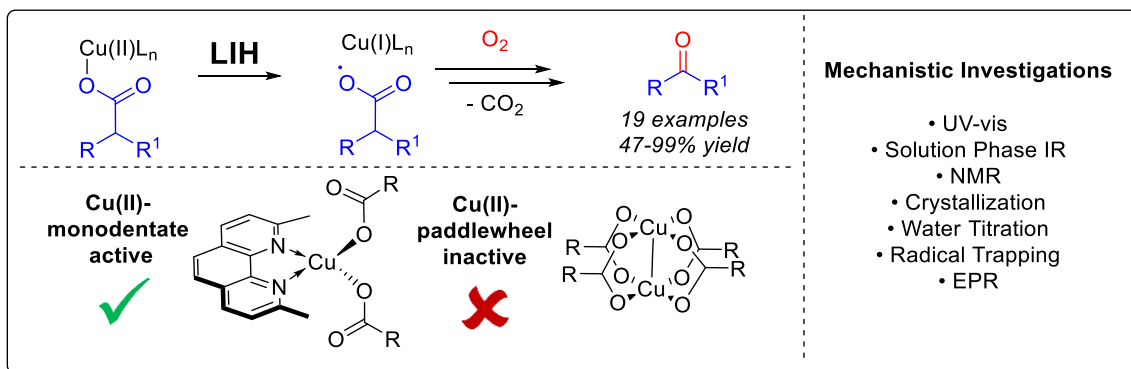
- [1] a) M. H. Shaw, J. Twilton, D. W. C. MacMillan, *J. Org. Chem.* **2016**, *81*, 6898; b) L. Marzo, S. K. Pagire, O. Reiser, B. König, *Angew. Chem. Int. Ed.* **2018**, *57*, 10034.
- [2] G. Ciamician, *Science* **1912**, *36*, 385.
- [3] M. Ramaiah, *Tetrahedron* **1987**, *43*, 3541.
- [4] a) D. P. Curran, N. A. Porter, B. Giese, *Stereochemistry of Radical Reactions. Concepts, Guidelines, and Synthetic Applications With a Foreword by Ernest L. Eliel*, Wiley-VCH, Weinheim, **2008**; b) C. P. Jasperse, D. P. Curran, T. L. Fevig, *Chem. Rev.* **1991**, *91*, 1237; c) A. Studer, D. P. Curran, *Angew. Chem. Int. Ed.* **2016**, *55*, 58.
- [5] G. B. Haxel, J. B. Hedrick, G. J. Orris, *Rare Earth Elements-Critical Resources for High Technology*, **2002**.
- [6] A. Hossain, A. Bhattacharyya, O. Reiser, *Science* **2019**, 364.
- [7] B. M. Hockin, C. Li, N. Robertson, E. Zysman-Colman, *Catal. Sci. Technol.* **2019**, *9*, 889.
- [8] O. S. Wenger, *J. Am. Chem. Soc.* **2018**, *140*, 13522.
- [9] J. Beaudelot, S. Oger, S. Peruško, T.-A. Phan, T. Teunens, C. Moucheron, G. Evano, *Chem. Rev.* **2022**, *122*, 16365.
- [10] S. Engl, O. Reiser, *Chem. Soc. Rev.* **2022**, *51*, 5287.
- [11] B. Wang, D. P. Shelar, X.-Z. Han, T.-T. Li, X. Guan, W. Lu, K. Liu, Y. Chen, W.-F. Fu, C.-M. Che, *Chem. Eur. J.* **2015**, *21*, 1184.
- [12] B. Michelet, C. Deldaele, S. Kajouj, C. Moucheron, G. Evano, *Org. Lett.* **2017**, *19*, 3576.
- [13] a) J. He, C. Chen, G. C. Fu, J. C. Peters, *ACS Catal.* **2018**, *8*, 11741; b) C. Uyeda, Y. Tan, G. C. Fu, J. C. Peters, *J. Am. Chem. Soc.* **2013**, *135*, 9548; c) Y. Tan, J. M. Muñoz-Molina, G. C. Fu, J. C. Peters, *Chem. Sci.* **2014**, *5*, 2831.
- [14] a) S. D. McCann, S. S. Stahl, *Acc. Chem. Res.* **2015**, *48*, 1756; b) S. E. Allen, R. R. Walvoord, R. Padilla-Salinas, M. C. Kozlowski, *Chem. Rev.* **2013**, *113*, 6234; c) R. Trammell, K. Rajabimoghadam, I. Garcia-Bosch, *Chem. Rev.* **2019**, *119*, 2954.
- [15] Y. Abderrazak, A. Bhattacharyya, O. Reiser, *Angew. Chem. Int. Ed.* **2021**, *60*, 21100.
- [16] R. Zhao, L. Shi, *Org. Chem. Front.* **2018**, *5*, 3018.
- [17] J. K. Kochi, *J. Am. Chem. Soc.* **1962**, *84*, 2121.
- [18] A. S. Mereshchenko, P. K. Olshin, A. M. Karimov, M. Y. Skripkin, K. A. Burkov, Y. S. Tveryanovich, A. N. Tarnovsky, *Chem. Phys. Lett.* **2014**, *615*, 105.

- [19] S. Rohe, A. O. Morris, T. McCallum, L. Barriault, *Angew. Chem. Int. Ed.* **2018**, *57*, 15664.
- [20] S. E. Manahan, R. T. Iwamoto, *Inorg. Chem.* **1965**, *4*, 1409.
- [21] H. Roth, N. Romero, D. Nicewicz, *Synlett* **2016**, *27*, 714.
- [22] A. S. Mereshchenko, P. K. Olshin, K. E. Karabaeva, M. S. Panov, R. M. Wilson, V. A. Kochemirovsky, M. Y. Skripkin, Y. S. Tveryanovich, A. N. Tarnovsky, *J. Phys. Chem.* **2015**, *119*, 8754.
- [23] A. Hossain, S. Engl, E. Lutsker, O. Reiser, *ACS Catal.* **2019**, *9*, 1103.
- [24] R. Fayad, S. Engl, E. O. Danilov, C. E. Hauke, O. Reiser, F. N. Castellano, *J. Phys. Chem. Lett.* **2020**, *11*, 5345.
- [25] P. Lian, W. Long, J. Li, Y. Zheng, X. Wan, *Angew. Chem. Int. Ed.* **2020**, *59*, 23603.
- [26] V. Pramod Charpe, M. Gupta, K. Chu Hwang, *ChemSusChem* **2022**, *15*, e202200957.
- [27] W. Li, J. Liu, M. Zhou, L. Ma, M. Zhang, *Org. Biomol. Chem.* **2022**, *20*, 6667.
- [28] X.-X. He, H.-H. Chang, Y.-X. Zhao, X.-J. Li, S.-A. Liu, Z.-L. Zang, C.-H. Zhou, G.-X. Cai, *Chem. Asian. J.* **2023**, *18*, e202200954.
- [29] S. M. Treacy, T. Rovis, *J. Am. Chem. Soc.* **2021**, *143*, 2729.
- [30] P. Lian, R. Li, L. Wang, X. Wan, Z. Xiang, X. Wan, *Org. Chem. Front.* **2022**, *9*, 4924.
- [31] A. Hossain, A. Vidyasagar, C. Eichinger, C. Lankes, J. Phan, J. Rehbein, O. Reiser, *Angew. Chem. Int. Ed.* **2018**, *57*, 8288.
- [32] Y. Li, K. Zhou, Z. Wen, S. Cao, X. Shen, M. Lei, L. Gong, *J. Am. Chem. Soc.* **2018**, *140*, 15850.
- [33] J.-M. Brégeault, F. Launay, A. Atlamsani, *C. R. Acad. Sci., Ser. Ilc: Chim.* **2001**, *4*, 11.
- [34] H. Xin, X.-H. Duan, M. Yang, Y. Zhang, L.-N. Guo, *J. Org. Chem.* **2021**, *86*, 8263.
- [35] N. Katta, Q.-Q. Zhao, T. Mandal, O. Reiser, *ACS Catal.* **2022**, *12*, 14398.
- [36] Q. Huang, M. Zhao, Y. Yang, Y.-N. Niu, X.-F. Xia, *Org. Chem. Front.* **2021**, *8*, 5988.
- [37] M. Kumar, S. Verma, V. Mishra, O. Reiser, A. K. Verma, *J. Org. Chem.* **2022**, *87*, 6263.
- [38] S. Maity, M. Zhu, R. S. Shinabery, N. Zheng, *Angew. Chem. Int. Ed.* **2012**, *51*, 222.
- [39] D. H. White, A. Noble, K. I. Booker-Milburn, V. K. Aggarwal, *Org. Lett.* **2021**, *23*, 3038.
- [40] a) J. Y. Morimoto, B. A. DeGraff, *J. Phys. Chem.* **1972**, *76*, 1387; b) J. Y. Morimoto, B. A. DeGraff, *J. Phys. Chem.* **1975**, *79*, 326; c) P. Natarajan, G. Ferraudi, *Inorg. Chem.* **1981**, *20*, 3708; d) G. Ferraudi, S. Muralidharan, *Coord. Chem. Rev.* **1981**, *36*, 45; e) R. Matsushima, Y. Ichikawa, K. Kuwabara, *Bull. Chem. Soc. Jpn.* **1980**, *53*, 1902.

- [41] A. Reichle, H. Sterzel, P. Kreitmeier, R. Fayad, F. N. Castellano, J. Rehbein, O. Reiser, *Chem. Commun.* **2022**, 58, 4456.
- [42] N. W. Dow, P. S. Pedersen, T. Q. Chen, D. C. Blakemore, A.-M. Dechert-Schmitt, T. Knauber, D. W. C. MacMillan, *J. Am. Chem. Soc.* **2022**, 144, 6163.
- [43] T. Q. Chen, P. S. Pedersen, N. W. Dow, R. Fayad, C. E. Hauke, M. C. Rosko, E. O. Danilov, D. C. Blakemore, A.-M. Dechert-Schmitt, T. Knauber et al., *J. Am. Chem. Soc.* **2022**, 144, 8296.
- [44] P. Xu, P. López-Rojas, T. Ritter, *J. Am. Chem. Soc.* **2021**, 143, 5349.
- [45] a) J. Chateaufneuf, J. Luszytk, K. U. Ingold, *J. Am. Chem. Soc.* **1988**, 110, 2877; b) J. Chateaufneuf, J. Luszytk, K. U. Ingold, *J. Am. Chem. Soc.* **1988**, 110, 2886.
- [46] J. W. Hilborn, J. A. Pincock, *J. Am. Chem. Soc.* **1991**, 113, 2683.
- [47] W. Su, P. Xu, T. Ritter, *Angew. Chem. Int. Ed.* **2021**, 60, 24012.
- [48] P. Xu, W. Su, T. Ritter, *Chem. Sci.* **2022**, 13, 13611.
- [49] Q. Y. Li, S. N. Gockel, G. A. Lutovsky, K. S. DeGlopper, N. J. Baldwin, M. W. Bundesmann, J. W. Tucker, S. W. Bagley, T. P. Yoon, *Nat. Chem.* **2022**, 14, 94.
- [50] a) N. L. Reed, M. I. Herman, V. P. Miltchev, T. P. Yoon, *Org. Lett.* **2018**, 20, 7345; b) B. J. Lee, K. S. DeGlopper, T. P. Yoon, *Angew. Chem. Int. Ed.* **2020**, 59, 197.
- [51] W. Su, P. Xu, R. Petzold, J. Yan, T. Ritter, *Org. Lett.* **2023**, 25, 1025.
- [52] A. Wimmer, B. König, *Adv. Synth. Catal.* **2018**, 360, 3277.
- [53] L. Chen, Y. Li, M. Han, Y. Peng, X. Chen, S. Xiang, H. Gao, T. Lu, S.-P. Luo, B. Zhou et al., *J. Org. Chem.* **2022**, 87, 15571.
- [54] L. M. Huffman, S. S. Stahl, *J. Am. Chem. Soc.* **2008**, 130, 9196.
- [55] R. Qi, C. Wang, Z. Ma, H. Wang, Q. Chen, L. Liu, Da Pan, X. Ren, R. Wang, Z. Xu, *Angew. Chem. Int. Ed.* **2022**, 61, e202200822.

Chapter 2 Copper(II)-photocatalyzed Decarboxylative Oxygenation of Carboxylic Acids

Abstract



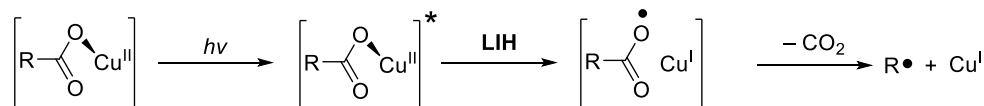
Demonstrating the concept of light-induced homolysis (LIH) for the generation of radicals, the Cu(II)-photocatalyzed decarboxylative oxygenation of carboxylic acids with molecular oxygen as the terminal oxidant is described. Two Cu(II)-carboxylate complexes, different in their coordination geometries, were synthesized and characterized by X-ray analysis. Mechanistic investigations were carried out, such as correlating their structure with their ability to undergo light-induced homolysis. Based on mechanistic investigations, e.g., UV-vis absorption spectra, solution-phase IR spectra, and EPR studies, it was found that the light-induced homolysis of monodentate Cu(II)-carboxylate, rather than paddle-wheel type chelation occurs. The synthetic method can be successfully applied to nonsteroidal anti-inflammatory drugs (NSAIDs) such as felbinac, ibuprofen, or naproxen, delivering the corresponding decarboxylated products in high yields. Also, cyclohexyl-substituted carboxylic acids could be converted to corresponding cyclohexanones.

This chapter is based on: [A. Reichle](#), H. Sterzel, P. Kreitmeier, R. Fayad, F. N. Castellano, J. Rehbein, O. Reiser, *Chem. Commun.* **2022**, 58, 4456.

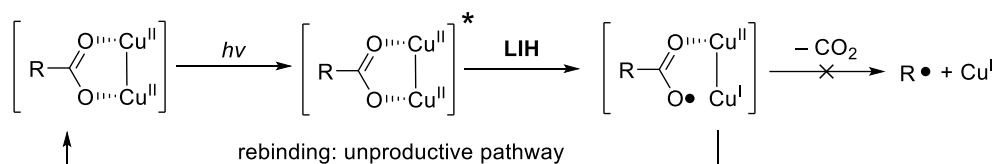
2.1 Outline of this Study

This work utilizes UV-vis, FT-IR, EPR, NMR-spectroscopy and computational studies to demonstrate Cu(II)-carboxylates generally undergo a light-induced homolysis. It was discovered that the specific coordination geometry of copper-carboxylate plays a pivotal role in the decarboxylation process. Monodentate carboxylates are shown to be decisive for the success of subsequent synthetic transformations, whereas bidentate carboxylates are less effective. For a long time, thermal oxidative Cu(II)-catalyzed decarboxylation reactions of carboxylic acids have been established, and many synthetic transformations have been developed.^[1] In comparison, there were fewer reports of photochemical variants available.^[2] The underlying mechanism for such decarboxylations was based on light-induced homolysis (LIH) as the critical step of a Cu(II)-carboxylate species. Given the plentiful and varied options for Cu(II)-carboxylates in coordination geometry, the present project aimed to expand knowledge of the process requirements to develop more effective catalysts. Decarboxylation of copper(II)-carboxylates is achieved *via* two main mechanistic scenarios, as depicted in Scheme 1: After LIH, Monodentate Cu(II)-carboxylate produces radicals through a homolytic cleavage mechanism, whereas bidentate Cu(II)-carboxylates of the paddle-wheel type lead to an unproductive rebinding pathway after LIH.

(A) Monodentate Cu(II)-carboxylates: Homolytic cleavage mechanism



(B) Dinuclear paddle-wheel type Cu(II)-carboxylates: Rebound mechanism



Scheme 1. Mechanistic proposal for the Cu(II)-mediated oxidation of carboxylic acids.

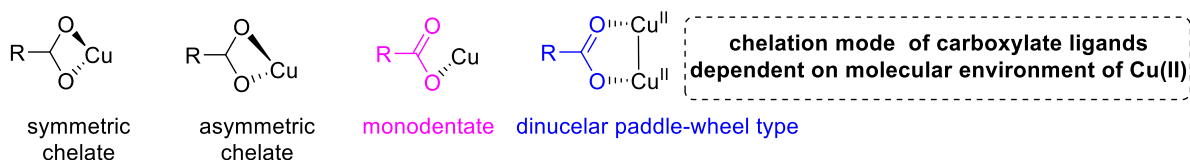
2.2 Coordination Modes of Copper(II)-carboxylates

Since the 1970s, copper(II)-carboxylates have been the subject of intense research due to their various structural properties and a broad range of applications, e.g. in the field of molecular magnetism.^[3] Further, polymeric copper(II) paddle-wheel carboxylates have been used as model substances for DNA binding and display antifungal properties.^[4] The carboxylate group can adopt various coordination modes, *i.e.* symmetric and asymmetric chelation *en route* to monodentate complexation. Nevertheless, the dinuclear paddle-wheel-type **A** coordination mode is very frequent (Scheme 2).^[5] This type of coordination has previously been suggested to be the active species in the thermal decarboxylation of carboxylic

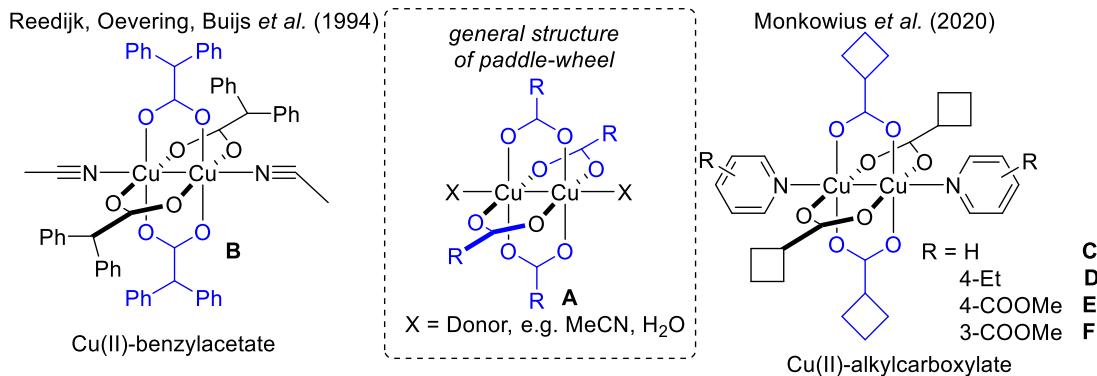
acids, e.g. investigated by Reedijk, Oevering and Buijs in 1994 (complex **B**).^[6] Other examples of dinuclear paddle-wheel type Cu(II)-complexes **C–F** were, e.g. successfully characterized by Monkowius *et al.*^[7] in 2020.

As demonstrated by Belfaitha (complex **G**)^[8], or Dege *et al.* (complex **H**)^[9] the paddle-wheel coordination can be converted into a monodentate one by way of modification of the coordination sphere, e.g. by using sterically bulky ligands. Further, the coordination of water to copper complexes can shift an equilibrium from a paddle-wheel coordination complex towards a monodentate one. Cu(II)-aqua complexes are generated, as Tsuboi and co-workers demonstrated (complex **I**).^[10] These could be considered to be part of the “monodentate type” class.

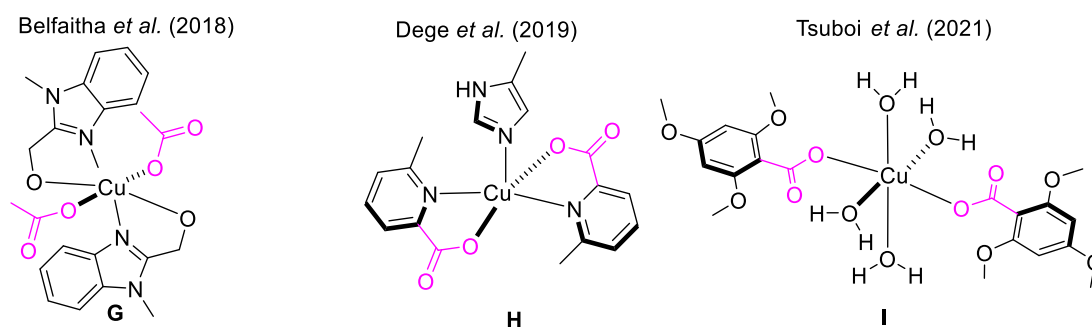
Selected Examples for Chelation of Cu(II)-carboxylates



Selected Examples of dinuclear paddle-wheel type Cu(II)-carboxylates



Selected Examples of monodentate Cu(II)-carboxylates

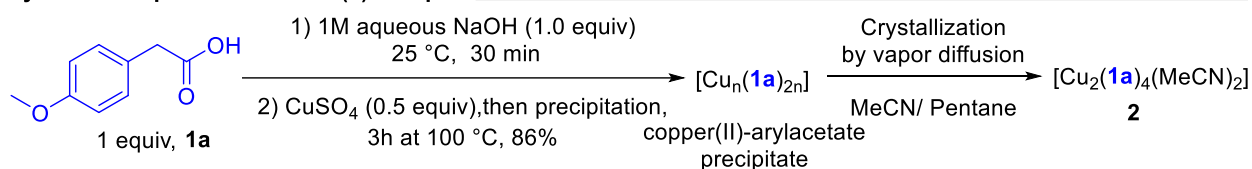


Scheme 2. Common coordination modes in Cu(II) carboxylates and representative examples: Reedijk, Oevering, Buijs *et al.*,^[11] Monkowius *et al.*,^[7] Belfaitha *et al.*,^[8] Dege *et al.*,^[9] Tsuboi *et al.*^[10].

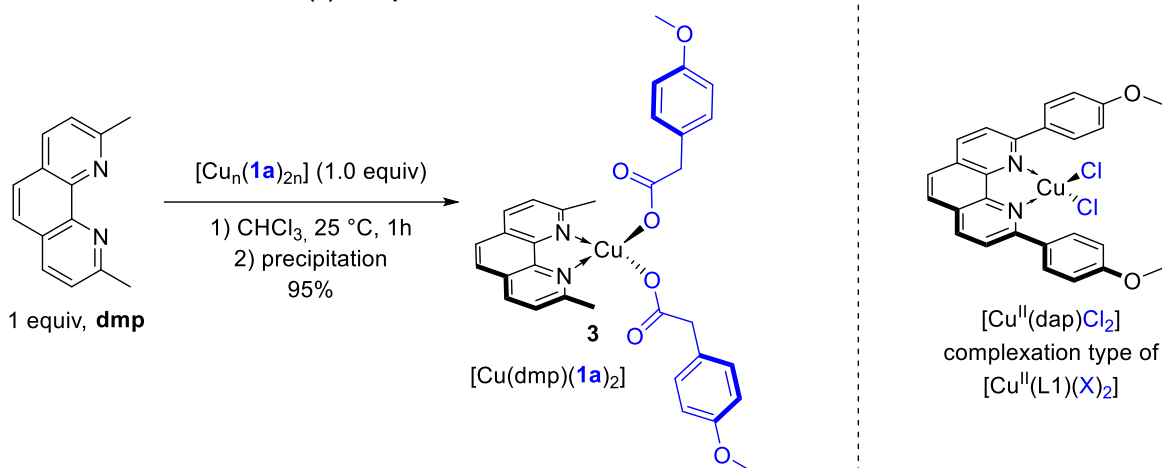
2.3 Synthesis of Copper(II)-carboxylates

It was attempted to synthesize and crystallize copper(II)-carboxylates to study the influence of the coordination mode of copper(II)-carboxylate complexes in photocatalytic decarboxylation reactions. A straightforward method for generating copper(II)-carboxylates is complexation. To this end, generally, two different methods are used. Complexation of carboxylic acid in basic media with a copper(II)-salt, or the reaction of a copper(II)-salt with the sodium salt of the carboxylic acid.^[12] Based on a report from Lundgren and co-workers,^[13] we started our investigations by deprotonating carboxylic acid **1a** with aqueous NaOH and subsequent complexing with CuSO₄. The precipitate was directly obtained from the reaction mixture and dried *in vacuo* to provide a water-free copper(II)-carboxylate.

Synthesis of paddle-wheel Cu(II)-complex



Synthesis of monodentate Cu(II)-complex



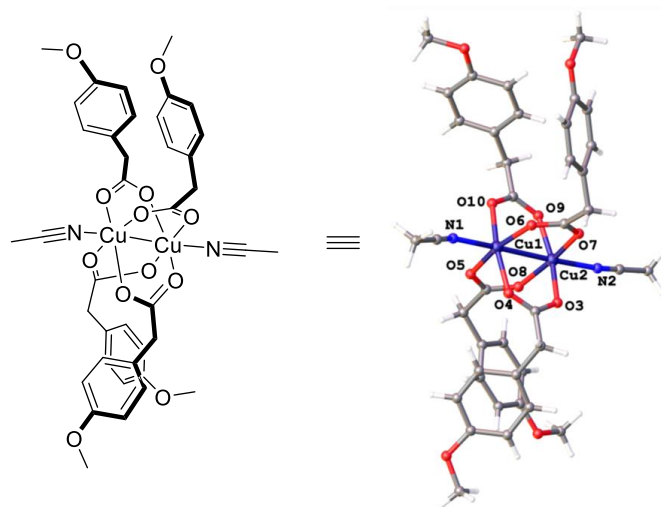
Scheme 3. Synthesis of $[\text{Cu}(\mathbf{1a})_4(\text{MeCN})_2]$ and complex $[\text{Cu}(\text{dmp})(\mathbf{1a})_2]$.

Successful recrystallization from MeCN afforded dinuclear paddle-wheel type complex $[\text{Cu}(\mathbf{1a})_4(\text{MeCN})_2]$ (**2**). Previous work^[14] inspired us to utilize dmp (dmp = 2,9-dimethyl-1,10-phenanthroline) over dap (dap = 2,9-bis(para-anisyl)-1,10-phenanthroline) as a bulky ligand to obtain monodentate coordination, due to its structural similarity, commercial availability and low costs compared to dap. To obtain copper(II) complexes of the general structure $[\text{Cu}(\text{L1})(\text{X})_2]$ (ligands = X, L1), one equivalent of copper(II)-salt CuX_2 has to be complexed with one equivalent of the ligand L1. For example, Wu, Yang and co-workers reported the synthesis and characterization of similar phenanthroline-based complexes^[15] and Lankes^[16] described the synthesis of complex $[\text{Cu}(\text{dap})\text{Cl}_2]$. Following this principle, we obtained after precipitation $[\text{Cu}(\text{dmp})(\mathbf{1a})_2]$ (**3**) as a bright greenish solid (*vide supra*, Scheme 3).

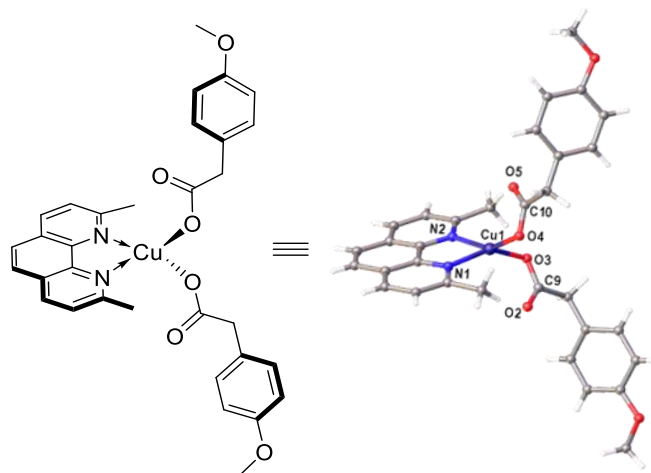
2.3.1 Crystal Structures of Copper(II)-carboxylates

From the uniform precipitates of Cu(II)-carboxylate complexes, single crystals suitable for X-ray analysis were afforded by vapor diffusion (pentane/MeCN for paddle-wheel complex **2**; CHCl₃/pentane for monodentate complex **3**). The crystal structures gave valuable insight into the different coordination modes of Cu(II) in both compounds. The paddle-wheel complex [Cu₂(**1a**)₄(MeCN)₂] (**2**) reveals a coordination mode that is generally expected for comparable dinuclear copper(II)-carboxylates.^[17] As expected, the crystal structures revealed two copper(II)-metal centers surrounded by four carboxylate ligands (Table 1). The solvent ligands acetonitrile (MeCN) are bound at the axial positions. A distorted octahedral geometry is accomplished through Cu–Cu interactions. The Cu–Cu distance of 2.6206(6) Å is in agreement with analogous copper(II)-paddle-wheel complexes.^[18] The four carboxylates are tightly bound in a bidentate fashion (Cu–O_{carboxy} 197 pm). This syn-syn coordination mode and bond length are typical for such complexes.^[19]

Unexpectedly, the Cu(II)-complex [Cu(dmp)(**1a**)₂] (**3**) displays two monodentate coordinated carboxylates and one molecule of 2,9-dimethylphenanthroline (dmp) as ligand coordinated *via* the two nitrogen atoms (Cu–O 193 pm, interatomic distance Cu–O 272 pm). The copper-center has a pseudo-tetrahedral geometry with a pronounced flatter distortion (Table 2). The dihedral angle between the planes of the complex (N–Cu–N / O–Cu–O) is significantly increased (for monodentate **3**: 44.96(7) deg). This coordination geometry is unusual because the pseudo-tetrahedral geometry is more comparable to the phenanthroline complex [Cu(dap)Cl₂].^[16] As expected, the methyl groups in complex **3** have a significant steric influence since the carboxylate anions inhibit interactions with the methyl groups in positions 1 and 10 of the dmp ligand, which profoundly influences the overall coordination sphere.

Table 1. X-ray structure of $[\text{Cu}(\mathbf{1a})_4(\text{MeCN})_2] \cdot (\mathbf{2})$.

$[\text{Cu}(\mathbf{1a})_4(\text{MeCN})_2] \cdot (\mathbf{2})$		
Bond Angle [deg]		
O10-Cu1-O6		91.35(10)
O5-Cu1-O10		91.00(10)
O3-Cu2-O8		87.82(10)
O7-Cu2-Cu1		84.96(7)
O10-Cu1-Cu2		85.16(7)
O3-Cu2-Cu1		84.59(7)
N1-Cu1-Cu2		174.59(7)
N2-Cu2-Cu1		176.89(7)
O9-Cu2-Cu1		83.90(6)
O7-Cu2-Cu1		84.96(7)
Bond Length [Å]		
Cu1-O10		1.972(2)
Cu1-O4		1.969(2)
Cu2-O7		1.967(2)
Cu2-O3		1.967(2)
Cu1-Cu2		2.6206(6)
Cu1-N1		2.204(3)
Cu2-N2		2.189(3)

Table 2. X-ray structure of [Cu(dmp)(1a)₂] (3).

[Cu(dmp)(1a) ₂] (3)	
Bond Angle [deg]	
N1-Cu1-N2	82.59(6)
N2-Cu1-O4	148.71(27)
O4-Cu1-O3	96.82(7)
O3-Cu1-N1	147.27(7)
Cu1-O4-C10	107.73(13)
Cu1-O3-C9	109.89(14)
Dihedral Angle [deg]	
N2-Cu1-N1 / O4-Cu1-O3	44.96(7)
Bond Length [Å]	
Cu1-N2	2.0213(16)
Cu1-N1	2.0256(16)
Cu1-O3	1.9267(15)
Cu1-O4	1.9323(15)
Interatomic Distance [Å]	
Cu1...O5	2.6956(17)
Cu1...O2	2.7534(17)

2.3.2 Electronic Properties of Copper(II)-carboxylates

UV-vis absorption properties of copper(II)-carboxylate complexes were investigated in spectroscopic grade MeCN and recorded at 25 °C. The acquired spectra of compounds **2** and **3** are depicted in Figure 1.

The wavelengths and extinction coefficients are shown in Table 3. The complexes show next to no absorption in the spectral range of green wavelengths (530 nm) being shifted to the blue (455 nm) and red part of the spectrum (680 nm). Both complexes show enhanced absorption at 367 nm. Both absorption shoulder bands of the complexes around 340 to 470 nm can be assigned to metal-to-ligand charge-transfer transitions (LMCT). Around 450 nm, the monodentate compound **3** exhibits a distinctive absorption attributed to the dmp-ligand.^[20] Paddle-wheel complex **2** displays the typical d-d transitions of Cu(II) around 550–900 nm, a characteristic feature for Cu(II) coordination compounds.^[21] Similarly, these absorptions can be found for complex **3**, but more red-shifted and very weak due to its chemical environment on the copper(II)-center.^[22] The visible bands are characteristic metal-to-ligand or ligand-to-metal charge transfer (MLCT or LMCT) transitions and are considerably weaker than the UV bands.^[23] Theoretically, both complexes can be excited *via* LMCT around 360 to 450 nm and should therefore undergo desired LIH.

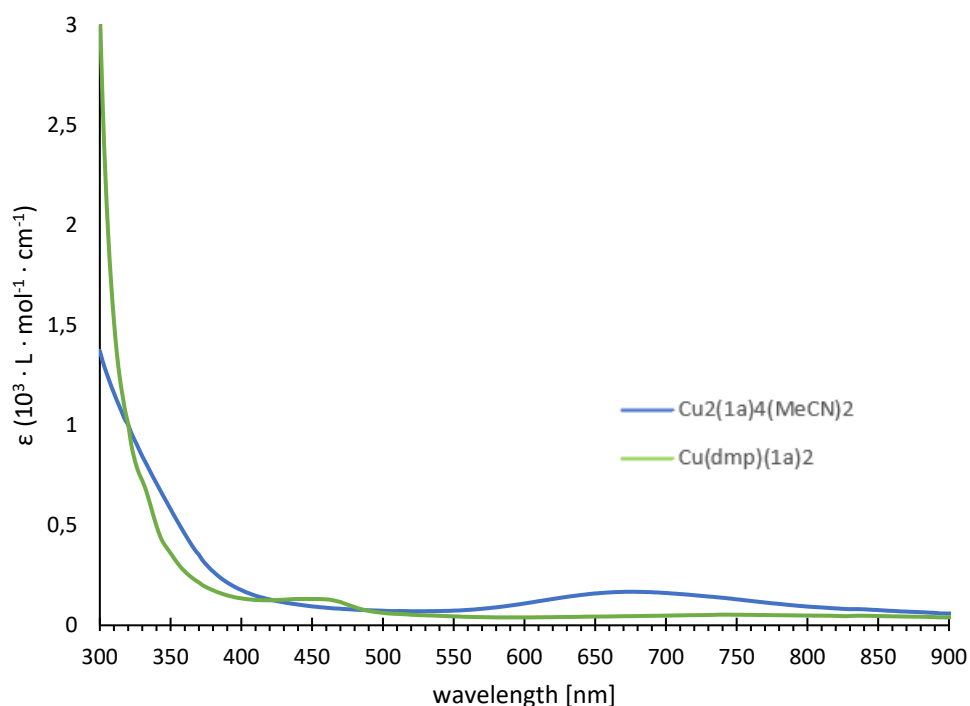


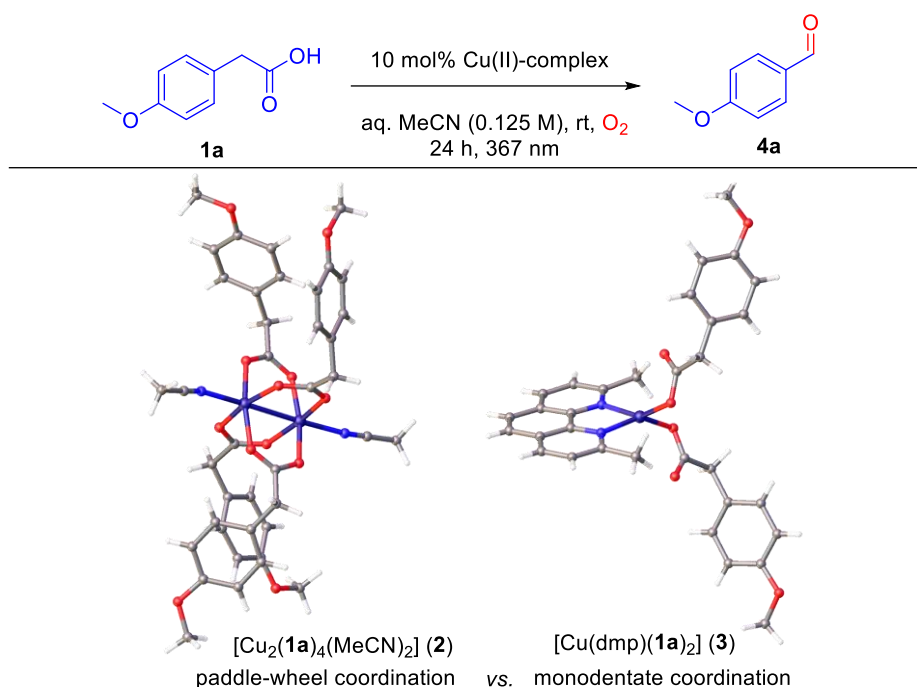
Figure 1. Absorption spectra of Cu(II)-complexes at ambient temperature (25 °C) (blue line: paddle-wheel **2**, green line monodentate complex **3**).

Both complexes have allowed molecular extinction coefficients. Characteristics are for the paddle-wheel complex **2** the charge-transfer (CT) transitions in the range of $\epsilon \approx 1.3 \cdot 10^2 \cdot \text{L} \cdot \text{mol}^{-1} \cdot \text{cm}^{-1}$ and d-d transitions in the range of $\epsilon \approx 1.6 \cdot 10^2 \cdot \text{L} \cdot \text{mol}^{-1} \cdot \text{cm}^{-1}$, which are in agreement with other literature reports.^{[24][25]}

Table 3. Photophysical properties of copper(II)-carboxylates.

Complex	Absorption λ_{max} [nm]	Molar Extinction Coefficient ϵ [$10^3 \cdot \text{L} \cdot \text{mol}^{-1} \cdot \text{cm}^{-1}$]
[Cu ₂ (1a) ₄ (MeCN) ₂] (2)	300	$1.4 \cdot 10^3$
	320	$1.0 \cdot 10^3$
	350	$5.8 \cdot 10^2$
	370	$3.5 \cdot 10^2$
	400	$1.7 \cdot 10^2$
	430	$1.1 \cdot 10^2$
	450	$0.9 \cdot 10^2$
	550	$0.7 \cdot 10^2$
	650	$1.6 \cdot 10^2$
[Cu(dmp)(1a) ₂] (3)	750	$1.3 \cdot 10^2$
	850	$0.7 \cdot 10^2$
	300	$3.0 \cdot 10^3$
	320	$1.0 \cdot 10^3$
	350	$3.6 \cdot 10^2$
	370	$2.1 \cdot 10^2$
	400	$1.3 \cdot 10^2$
	430	$1.3 \cdot 10^2$
	450	$1.3 \cdot 10^2$
550	$0.4 \cdot 10^2$	
650	$0.4 \cdot 10^2$	
750	$0.5 \cdot 10^2$	
850	$0.4 \cdot 10^2$	

2.4 Evaluation of Paddle-Wheel vs. Monodentate Coordination

Table 4. Evaluation of Paddle-wheel (**2**) vs. monodentate Cu(II) complex (**3**) in the oxidative decarboxylation of carboxylic acid **1a**.^a

Entry	Cu(II)-complex	Irradiation Power [mW]	Water Content [Vol%]	λ_{\max} [nm]	Yield ^b (%)
1	[Cu ₂ (1a) ₄ (MeCN) ₂] (2)	160	-	367	11
2	[Cu ₂ (1a) ₄ (MeCN) ₂] (2)	160	2.2	367	21
3	[Cu(dmp)(1a) ₂] (3)	160	-	367	86
4	[Cu(dmp)(1a) ₂] (3)	160	2.2	367	91
5	No	160	-	367	10
6	Cu(OAc) ₂ + dmp (<i>in situ</i>)	160	2.2	367	60
7	Cu(OAc) ₂ + dmp (<i>in situ</i>)	400	2.2	367	95 (93 ^d)
8	Cu(dmp)(1a) ₂ (3)	400	2.2	367	95
9 ^c	Cu(OAc) ₂ + dmp (<i>in situ</i>)	400	2.2	367	33
10 ^c	No	400	2.2	367	nr

^aStandard conditions: **1a** (0.25 mmol, 1.0 equiv), 10 mol% Cu(II) (12.5 μ mol, for complex **2** (Dimer) or 25 μ mol, for complex **3**) in MeCN (2.0 mL, 0.125 M), water (45 μ L, 2.2 Vol%), Irradiation at 367 nm with a radiant power of 160 mW under O₂ atmosphere for 24 h at room temperature (30 °C). ^bNMR yield using 1,1,2,2-tetrachloroethane as internal standard. ^cReaction time was 2.5 h. ^disolated yield on a 0.5 mmol scale.

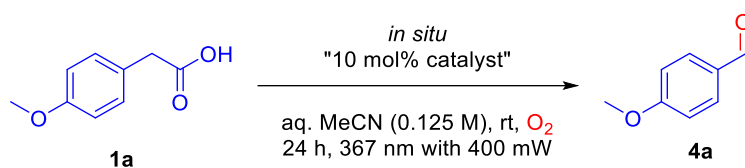
We examined the Cu(II)-complexes (paddle-wheel and monodentate) for their potential as catalysts to promote decarboxylation reactions by irradiating **1a** at 367 nm in an oxygen atmosphere for 24 h (Table 4). While complex **2** produced *p*-methoxy benzaldehyde (**4a**) in a low yield (entry 1), complex **3** had outstanding efficiency by creating **4a** in 86% yield (entry 3). The reaction was also conducted in aqueous solvents, following the example of Schröder *et al.*^[26], who previously demonstrated that water breaks up the copper complex clusters,

following the hypothesis that the paddle-wheel coordination might be the root cause for the low efficiency of **2**. The yield of **4a** increased to 21%, as shown in entry 2, but it still pales compared to complex **3**, which also saw a benefit from adding water (entry 4). Further, it was discovered that a background reaction (entry 5) was equally effective in the presence and absence of copper complex **2**. Additionally, we tested the combination of $\text{Cu}(\text{OAc})_2$, *i.e.* having an innocent carboxylate ligand present together with the free dmp ligand, with an emphasis on creating a generally applicable catalyst system. To our delight, converting **1a** to **4a** (entry 6) with this reagent combination gave 60% of product **4a**. A more intense light source successfully increased the yield to 95% (entry 7). Applying the defined complex **3** in combination with a stronger light source afforded **4a** also in high yield (entry 8). To further investigate the background reaction, the reaction mixture was irradiated in the presence and absence of the photocatalyst for a period over 2.5 h (entries 9–10), showing that the product was only generated in the presence of the photocatalyst.

2.5 Further Optimization Studies

To increase the synthetic applicability of the discovered copper-mediated decarboxylation reaction, we performed optimization studies using the *in situ* combination of 10 mol% of $\text{Cu}(\text{OAc})_2$ and dmp (Table 5). As described above, increasing the irradiation power to 400 mW afforded 95% of **4a** (entry 1). The reaction also worked well if $\text{Cu}(\text{I})(\text{OAc})$ was used instead of $\text{Cu}(\text{II})(\text{OAc})_2$, suggesting that after oxidation by molecular oxygen^[27] to $\text{Cu}(\text{II})$, the decarboxylation reaction can be initiated (entry 2). Considering the use of higher wavelengths, such as 400 nm and 455 nm, we observed a decrease in product formation (entries 3–4). A possible explanation for this observation could be that the corresponding dissociative LMCT transitions, which lead to LIH, are located exclusively at lower wavelengths. When the reaction was performed open under air, a high yield of 90% was obtained (entry 5). Under a nitrogen atmosphere, only traces of the product could be detected (entry 6).

Further, we recognized that the water content of the reaction solution plays an essential role since a drastic increase in the amount of water led to a decrease in product formation (entries 7–10). However, a small water amount was necessary to obtain the best yield (entry 1). Corresponding EPR investigations on the copper(II)-carboxylates present in the solution are described in Chapter 2.8.2 Water Titration Experiment. Screening the solution concentration showed an increased product formation in diluted solutions (entries 11–12), most likely because of the solubility effects of the photoactive complex.

Table 5. Additional Parameter Screening.^a

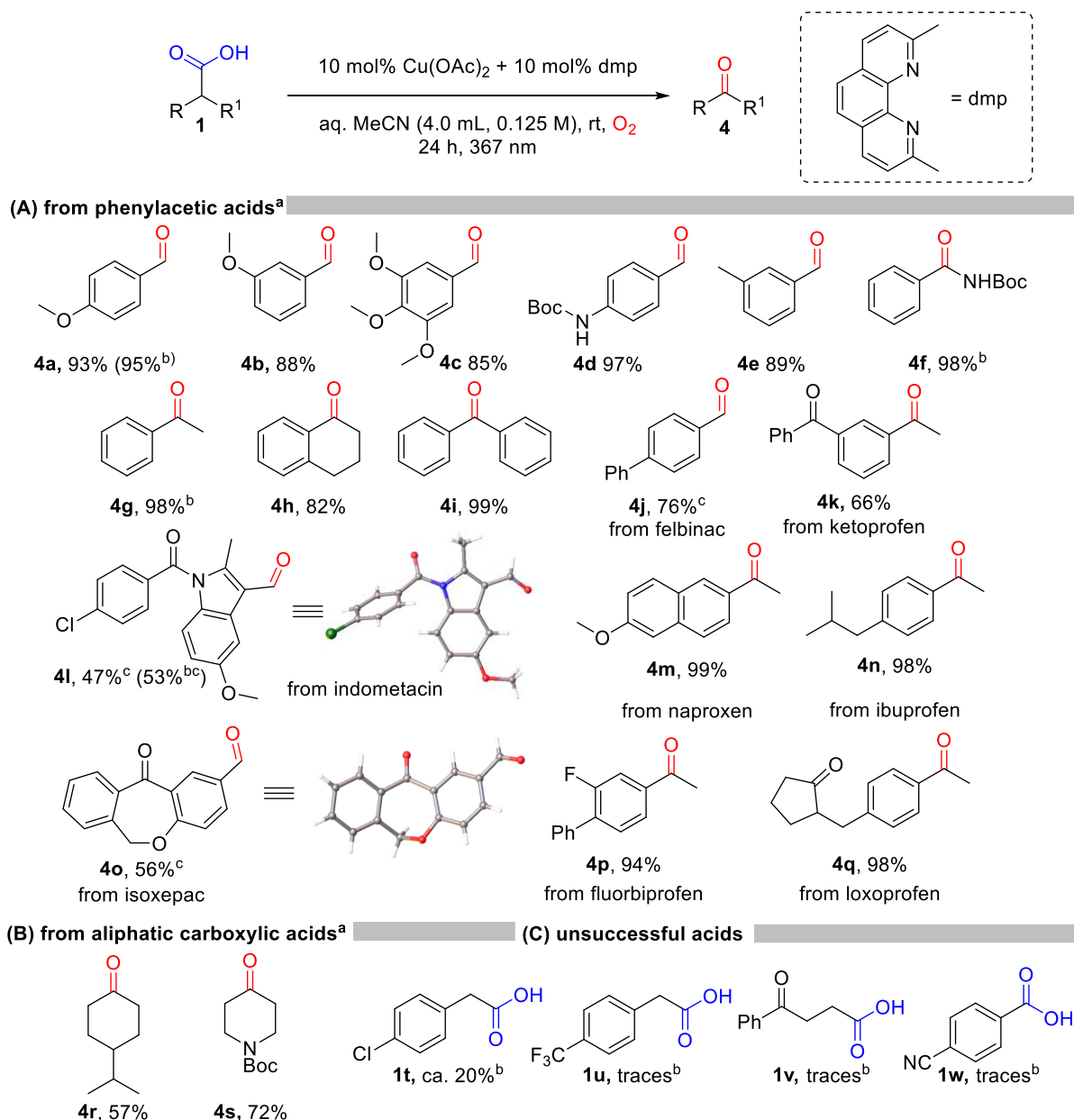
Entry	Change from "standard conditions"	λ_{max} [nm]	Yield ^b (%)
1	No changes	367	95 (93 ^c)
2	With 10 mol% of Cu(OAc) instead of Cu(OAc) ₂	367	94
3	Irradiation at 400 nm (irradiation power = 440 mW)	400	28
4	Irradiation at 455 nm (irradiation power = 550 mW)	455	23
5	Open to air	367	90
6	Under N ₂ atmosphere	367	traces
7	Without water	367	83
8	Water content of 0.2 Vol%	367	88
9	Water content of 10.3 Vol%	367	34
10	Water content of 18.7 Vol%	367	44
11	MeCN (0.250 M)	367	88
12	MeCN (0.083 M)	367	95

^aStandard conditions: 4-methoxyphenylacetic acid (**1a**) (0.25 mmol, 1.0 equiv), Cu(OAc)₂ (25 μ mol, 10 mol%), dmp (2,9-dimethyl-1,10-phenanthroline) (25 μ mol, 10 mol%) in MeCN (2.0 mL, 0.125 M), water (45 μ L, 2.2 Vol%). Irradiation at 367 nm with a radiant power of 400 mW under an O₂ atmosphere for 24 h at room temperature (30°C).

^bNMR yield using 1,1,2,2-tetrachloroethane as internal standard. ^cIsolated yield (0.5 mmol scale).

2.6 Substrate Scope of the Cu(II)-photocatalyzed Decarboxylative Oxygenation

To our delight, various electron-rich primary phenylacetic acids delivered the corresponding aldehydes in high yield. Furthermore, secondary phenylacetic acids provided corresponding ketones in high to quantitative yield (Scheme 4). With the intent to identify possible degradation pathways of non-steroidal anti-inflammatory drugs (NSAIDs) applicable in pollution abatement, widely used agents such as felbinac, ibuprofen, or naproxen gave rise to the corresponding decarboxylated products **4j–4q** in high yields. In addition, cyclohexyl-substituted carboxylic acids could be converted to the corresponding cyclohexanones **4r** and **4s**.



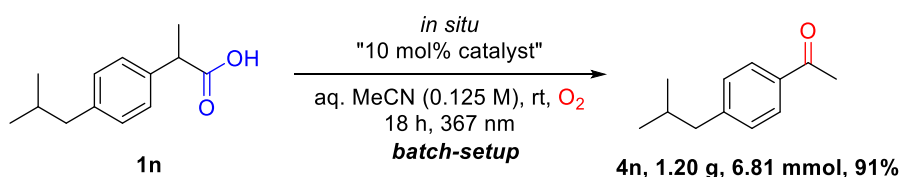
Scheme 4. Substrate scope for the decarboxylative oxygenation of carboxylic acids. Standard conditions^a: phenylacetic acid (0.5 mmol, 1.0 equiv), Cu(OAc)₂ (50 μmol, 10 mol%), dmp (50 μmol, 10 mol%) in MeCN (4.0 mL), water (95 μL, 2.2 Vol%), distributed over two Schlenk tubes. Irradiation at indicated λ_{max} with a radiant power of 400 mW under an O₂ atmosphere for 24 h at room temperature (25°C). ^bNMR yield using 1,1,2,2-tetrachloroethane as internal standard (on an 0.250 mmol scale). ^cWith a radiant power of 160 mW.

Low amounts of product were detected for chlorine-substituted carboxylic acid (**1t**) and only product traces could be detected if an electron-deficient carboxylic acid such as 4-CF₃-phenylacetic acid (**1u**) was used. This led us to the concluding assumption that the decarboxylation process is inefficient for these types of electron-poor substrates. Further, primary alkyl carboxylic acid (**1v**) was not an appropriate substrate: Because of the low stability of the resulting unstabilized primary alkyl radical, it appears that CO₂-extrusion upon homolysis of the carboxylate ligand from Cu(II) is not accessible to the current methodology. Nonetheless, the carboxyl radical recombining with Cu(I) may reverse the first homolysis.^[28] It was also found that an aryl carboxylic acid (**1w**), undergoing decarboxylation following the protocol by

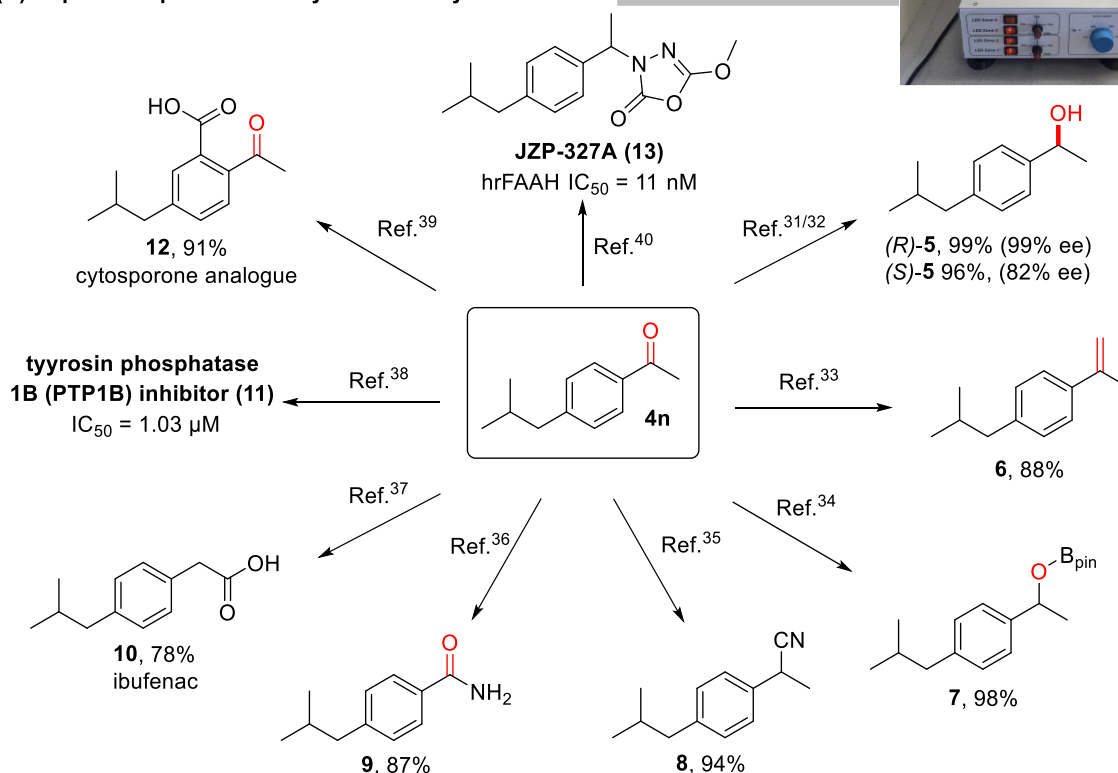
MacMillan and co-workers^[29], was no suitable substrate for the reported copper-mediated method. It is assumed that the highly unstable phenyl radical resulting from a hypothetical initial light-induced homolysis makes this pathway unfavorable. Further, the decarboxylation of aryl carboxylic acids is reportedly a very slow process ($k \approx 10^6 \text{ s}^{-1}$)^[30], about 1000 times slower than the decarboxylation of alkyl carboxyl radicals ($k \approx 10^9 \text{ s}^{-1}$)^[28]. It is currently believed that the back electron transfer (BET) between the aryl radical and Cu(I)-photocatalyst is the main competing pathway.

2.7 Upscaling and Synthetic Utility

(A) Gram-scale decarboxylative oxygenation



(B) Reported representative synthetic utility of the ketone



Scheme 5. Gram-scale functionalization of aryl carboxylic acid with upscaling reactor on 7.5 mmol scale. Standard conditions: carboxylic acid (**1n**) (1.0 equiv, 7.5 mmol), $\text{Cu}(\text{OAc})_2$ (10 mol%, 0.75 mmol), dmp (10 mol%, 0.75 mmol) in MeCN/water (0.125 M); Irradiation at indicated wavelength $\lambda = 367 \text{ nm}$ under O_2 atmosphere for given time at room temperature (25°C).

An upscaling reaction was performed to demonstrate the synthetic utility (Scheme 5). Therefore, irradiation took place in a photoreactor, where irradiation was achieved with 367 nm 3 W LEDs. Cooling of the LEDs was accomplished *via* water cooling of the outer mantle of the reaction vessel, providing irradiation at room temperature (25 °C). The reaction solution was additionally cooled with a cooling glass finger (for details of the reaction apparatus, see the experimental part). We were pleased to see that decarboxylation of ibuprofen (**1n**) as model substrate afforded the desired ketone **4n** in 91% yield after column chromatography on a 7.5 mmol scale, and the reaction time could be decreased from 24 h to 18 h. The tremendous synthetic utility of the synthesized ketone **4n** is amply documented in the literature as shown in Scheme 5: Representative transformations of the ketone are enantioselective reduction to the alcohols (*R*)-**5**^[31] and (*S*)-**5**,^[32] the Wittig reaction to obtain olefin **6**,^[33] hydroboration to **7**,^[34] conversion to nitrile **8**^[35] or primary amide **9**,^[36] ibuprofen derivative ibufenac **10**,^[37] the synthesis of a tyrosine phosphatase inhibitor (**11**)^[38] or cytosporone analog (**12**).^[39] Especially, ketone **4n** has been used as a key intermediate in synthesizing the fatty acid amide hydrolase (FAAH) inhibitor **JZP-327A (13)**,^[40] a highly potent drug candidate.

2.8 Mechanistic Investigations

With our collaboration partners in the groups of Professor Rehbein and Professor Castellano, various experiments were conducted to acquire insight into the mechanistic pathway. Please take note that while we synthesized the relevant copper(II)-complexes, the Rehbein group conducted mechanistic calculations and electron paramagnetic resonance (EPR) experiments and the Castellano group additional spectroscopic investigations. A plausible mechanistic picture for the decarboxylative oxygenation was successfully achieved by combining all the results.

2.8.1 UV-vis, Solution phase IR- and NMR Studies

The Castellano group recorded time-resolved UV-vis absorption spectra, revealing the formation of $[\text{Cu}(\text{dmp})_2]^+$ after irradiation at 427 nm into the LMCT transition. A control experiment of independently prepared $[\text{Cu}(\text{dmp})_2]^+$ successfully allowed the designation of the UV-vis band (Figure 2 *Left*). As seen in the UV-vis spectra, the photochemical reduction is consistent with the proposed LMCT excitation, leading to LIH of the Cu(II) carboxylate bond in $[\text{Cu}(\text{dmp})(\mathbf{1a})_2]$ (**3**). Additionally, changes can be recognized for the ligand field d-d transition absorption band,^[21] which is a characteristic feature for Cu(II) coordination compounds and not observed in Cu(I) d^{10} species.^[41,42]

The band of the Cu(II) carboxylate during irradiation gradually shifted to 800 nm. Eventually, it decreased, agreeing with indicated photoreduction of Cu(II) to Cu(I) *via* LIH, over the course of the reaction. Moreover, the extrusion of CO₂ was followed with solution-phase IR spectra of fresh and irradiated [Cu(dmp)(**1a**)₂] (**3**) showing the emergence of the carbon dioxide absorbance band at 2335 cm⁻¹ growing with irradiation time (Figure 2 *Right*). The proposed CO₂ release upon decarboxylation of the 4-methoxyphenyl acetoxy radical species **I** is assigned to the absorbance band (*vide infra*, Scheme 6).

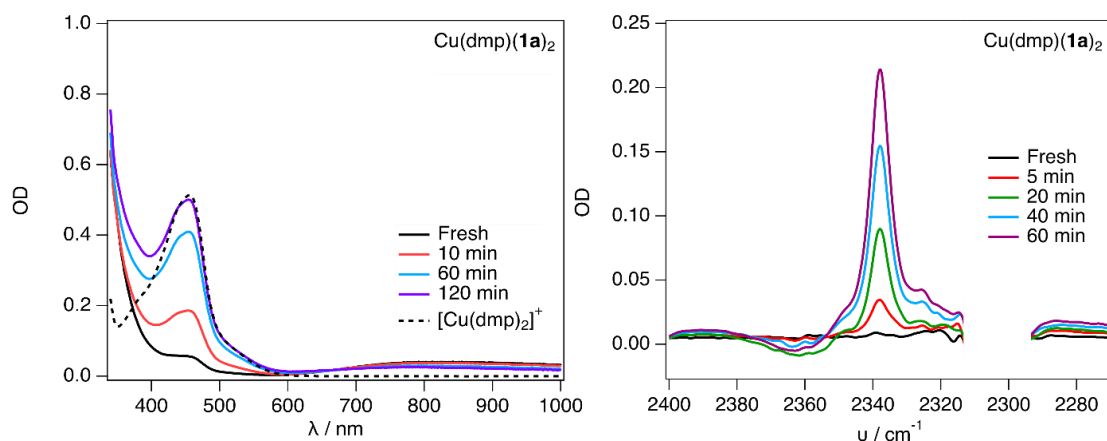


Figure 2. *Left*: Time-resolved UV-vis absorption spectra of fresh and 427 nm photolyzed [Cu(dmp)(**1a**)₂] (**3**) in acetonitrile. Irradiation times are indicated in the legend. The spectrum of independently prepared [Cu(dmp)₂]⁺ (dashed line) is overlaid for comparison. *Right*: Solution-phase IR spectra of fresh and 427 nm photolyzed [Cu(dmp)(**1a**)₂] (**3**) in dichloromethane. Irradiation times are indicated in the legend. Experiments were carried out by the Castellano group and the shown graphics were kindly provided by them.

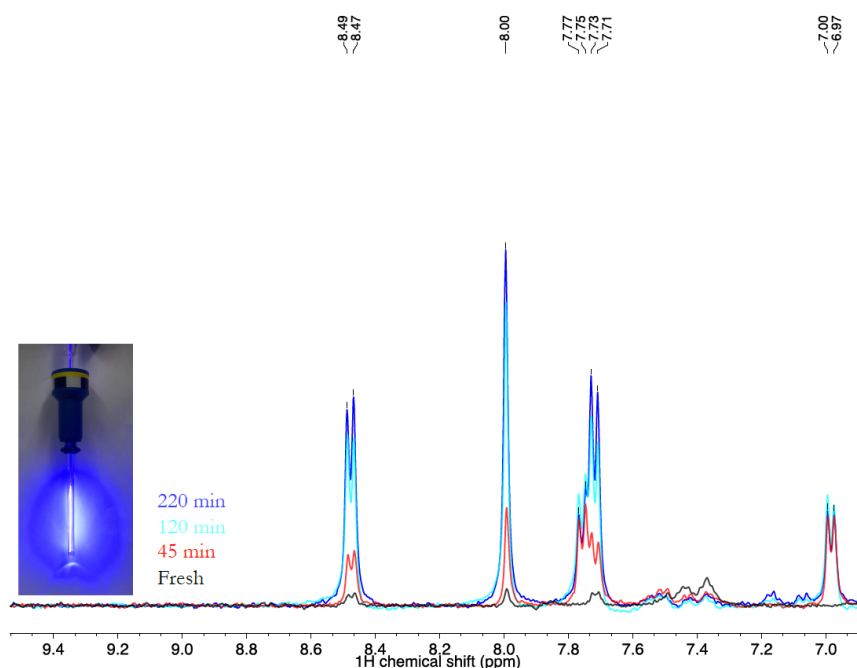
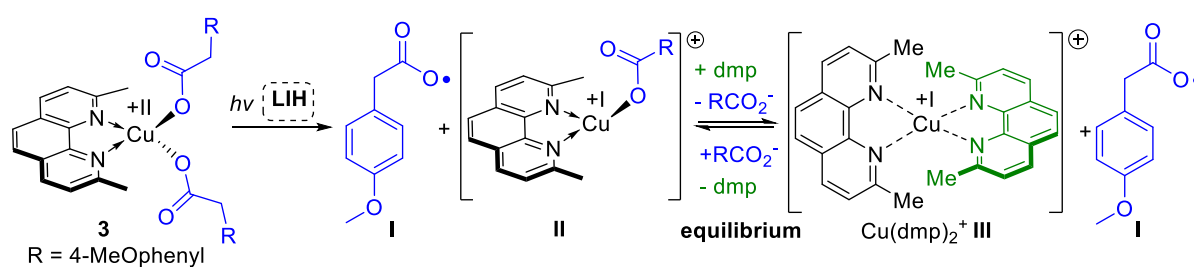


Figure 3. ¹H NMR spectra (400 MHz) of fresh and 420 nm photolyzed Cu(dmp)(**1a**)₂ (**3**) in MeCN. The photolysis was carried out *in situ* using a 420 nm LED fiber optic coupled to a capillary jacket within the 5 mm NMR tube. Irradiation times are indicated in the legend. Experiments were carried out by the Castellano group and the shown graphics were kindly provided by them.

Additionally, the reaction was monitored by $^1\text{H-NMR}$ analysis following the formation of the photolysis product at 420 nm (*vide supra*, Figure 3). Here 4-methoxy benzaldehyde (**4a**) (6.95 ppm (doublet), 7.75 ppm (doublet)) and the Cu(I)-coordinated dmp proton peaks (8.47 ppm (doublet), 8.00 ppm (singlet) and 7.71 ppm (doublet)), were observable. The $[\text{Cu(I)(dmp)}_2]^+$ species **III**, observed by $^1\text{H NMR}$, can be considered to be in equilibrium with a $[\text{Cu(I)(dmp)(1a)}]^+$ species **II**, as shown in Scheme 6. This result further supports the mechanistic proposal of light-induced homolysis of $[\text{Cu(dmp)(1a)}_2]$ (**3**) and corresponds to the recorded UV-vis spectra.



Scheme 6. Proposed LIH and formation of Cu(I)-species **II** and 4-MeO-phenylacetoxo radical species **I**.

2.8.2 Water Titration Experiment

A water titration study was carried out to investigate the copper(II)-species formed in the presence of water. The study was conducted with substrate-catalyst complexes **2** (paddle-wheel) and **3** (monodentate) (Figure 4). Since **2** showed diminished performance in catalysis, we were interested if monomeric Cu(II) complexes are the key to good turn-over rates.

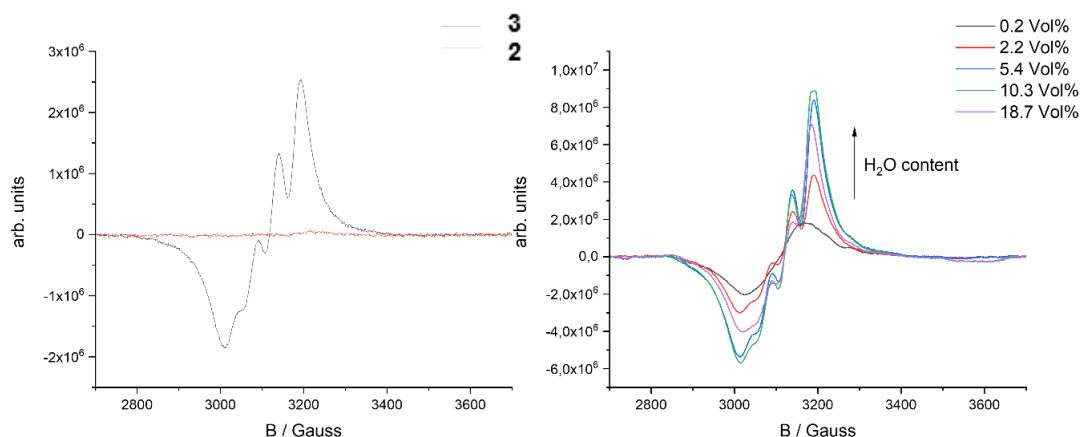


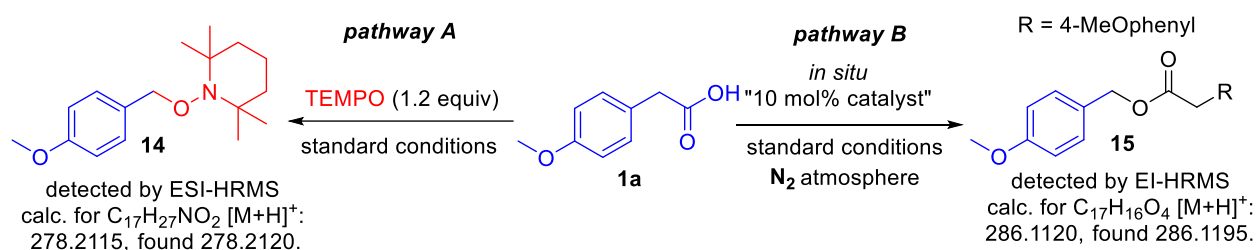
Figure 4. Water titration experiment of Cu(II)-complex. *Left*: Cu(II)-complex **2** (12.5 mmol/L) or **3** (6.25 mmol/L) formed *in situ* in MeCN (2.0 mL), water (45 μL , 2.2 Vol%) from Copper(II)-carboxylate at room temperature (25 $^{\circ}\text{C}$). *Right*: Cu(II)-complex **3** (12.5 mmol/L) formed *in situ* in MeCN (2.0 mL at room temperature (25 $^{\circ}\text{C}$). Water: 0.2 Vol% (4.5 μL), 2.2 Vol% (45 μL), 5.4 Vol% (115 μL), 10.3 Vol% (230 μL), 18.7 Vol% (461 μL). (Experiments were carried out by the Rehbein group and the shown graphics were kindly provided by them).

EPR-spectral analysis of the two complexes in MeCN with 2 Vol% of water indicated that a significantly higher proportion of monomeric Cu(II) species is present for complex **3** compared to **2**, as shown in Figure 4. Additional titration studies of water to complex **3** further support that in MeCN solutions, clustering of Cu(II) to an overall diamagnetic species is enhanced in case of low water amount. Related studies by Schröder and co-workers on copper(II) acetate in acetonitrile revealed that complex species in solution are strongly dependent on the water content within the solvent. By way of example, 5.0 Vol% of water resulted in the dominance of monomeric copper(II) complexes.^[26] It was shown that monomeric Cu(II) species are essential for achieving good conversion rates in the decarboxylation step.

2.8.3 Radical Trapping Experiment and Reaction under N₂ Atmosphere

Complementary radical trapping experiments with TEMPO under standard conditions revealed a complete shutdown of the decarboxylation, and the formation of TEMPO-adduct **14** was confirmed by mass-spectrometric analysis (Scheme 7, pathway A).

Performing the reaction under a nitrogen atmosphere (pathway B), we observed the coupling product **15** that forms by trapping 4-methoxyphenylacetoxy radical species with carboxylic acid **1a**. However, in the absence of an oxidant, the necessary back oxidation to Cu(II) cannot occur, thus making such processes stoichiometric^[43] rather than catalytic in copper. Thus, identifying oxidative reaction conditions that won't obstruct the early coupling of radicals or nucleophiles should be considered in future investigations.



Scheme 7. Mechanistic investigations under standard reaction conditions: *Pathway A*: reaction in the presence of TEMPO. *Pathway B*: reaction under N₂ atmosphere. Standard conditions: see experimental part for details.

2.8.4 EPR-Analysis

The Rehbein group successfully monitored the photolysis process by recording the electron paramagnetic resonance (EPR). Spin trapping experiments of [Cu(dmp)(**1a**)₂] (**3**) and C-phenyl-*N-tert*-butylnitrone (PBN) in aqueous acetonitrile revealed the existence of 4-methoxybenzyl radicals as adducts, agreeing with the TEMPO-trapping experiment (*vide supra*, Scheme 7). As demonstrated by Figure 5A, the PBN signal forms after irradiation and further allows the characterization of the organic radical PBN-R by its hyperfine coupling constants (Figure 5B). Through these data, it was possible to visualize the decrease of complex [Cu(dmp)(**1a**)₂] (**3**) upon irradiation at 367 nm (with $k_{\text{initial}} = 0.015 \pm 0.004 \text{ s}^{-1}$) and the increase in the formation of the spin trap signal of PBN-R (with $k_{\text{initial}} = 0.013 \pm 0.002 \text{ s}^{-1}$) (Figure 5C).

Both initial rate constants match up. By following the time course, the (initial) photolysis seems to be an extremely fast process. The concentration of Cu(II) decreases upon irradiation, agreeing with e.g. the photolysis study of complex $[\text{Cu}(\text{dmp})_2\text{Cl}]\text{Cl}$ reported by Castellano, Reiser and co-workers.^[42]

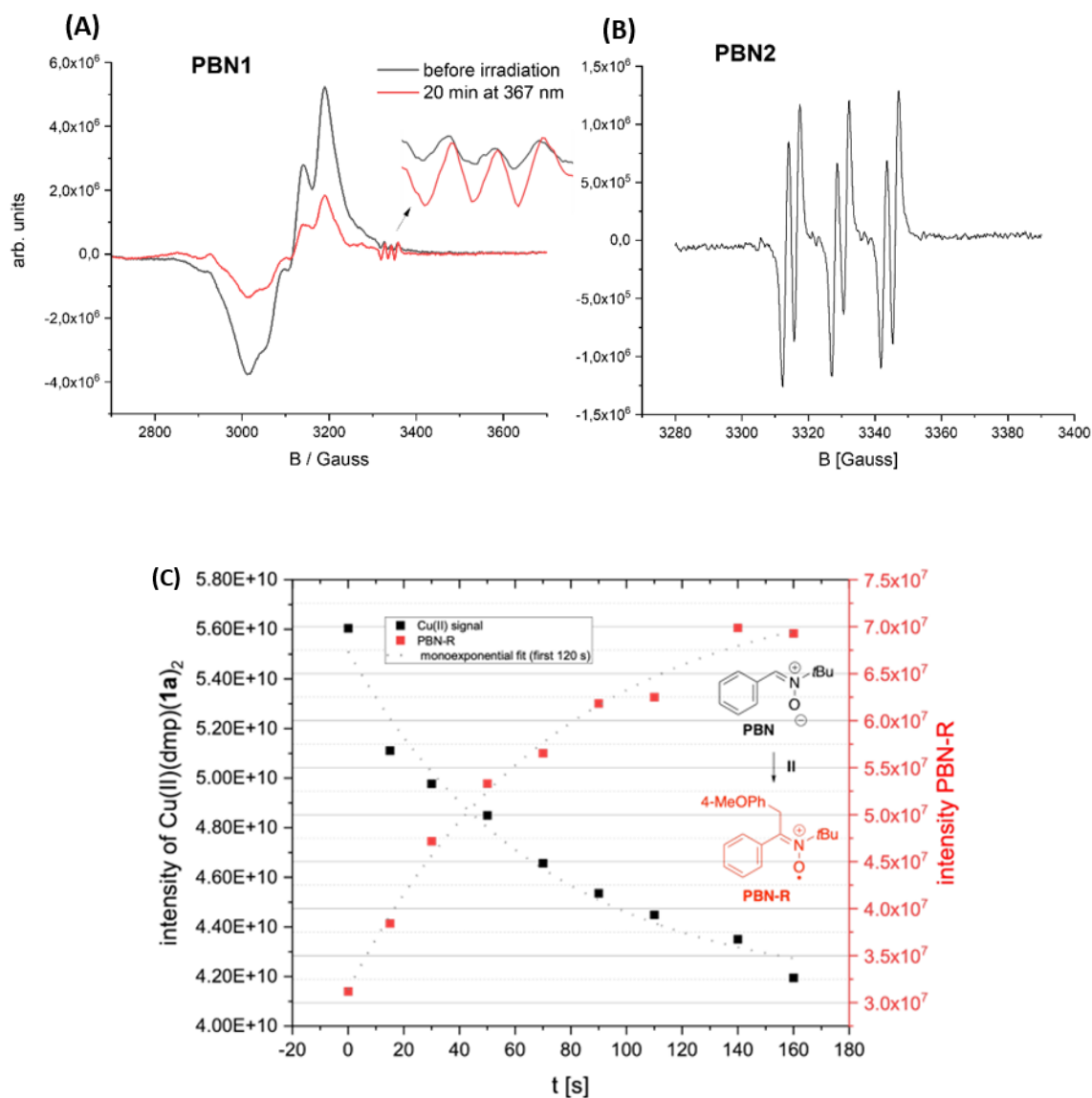


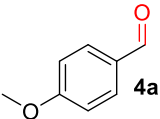
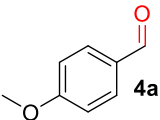
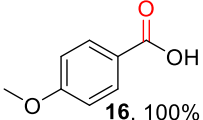
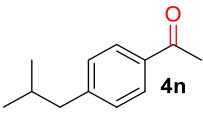
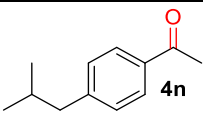
Figure 5. (A) EPR Spectra before and after irradiation. (B) Trapping signal of PBN-R. (C) Kinetic traces of Cu(II)-signal (black squares) with $k_{\text{initial}} = 0.015 \pm 0.004 \text{ s}^{-1}$ and of the growth of the PBN-R signals (red squares) with $k_{\text{initial}} = 0.013 \pm 0.002 \text{ s}^{-1}$. Fitted at early times with a single exponential function and assuming pseudo-first order conditions for the PBN-R formation (Experiments were carried out by the Rehbein group and the shown graphics were kindly provided by them)

2.8.5 Photostability Test of Decarboxylation Products

In principle, the decarboxylated product could undergo a further oxidation process under oxidative conditions to afford the corresponding benzoic acids. Regarding ketones, e.g. the photolysis of ibuprofen under UV-light irradiation initiated by hydroxyl-radicals in an aqueous solution was investigated. However, this method led to no selective oxygenation, and a mixture of oxygenation products was obtained.^[44] To investigate the product stability and presence of possible side reactions for the Cu(II)-photocatalyzed process, irradiation experiments were performed as shown in Table 6.

The product of the photoreaction 4-methoxybenzaldehyde (**4a**) was irradiated in the presence of 10 mol% of the „*in situ*“ photocatalyst (Cu(OAc)₂ + dmp). After 24 h of irradiation, no overoxidation product (benzoic acid) or other oxygenation products were observed (entry 1). If solely dmp was applied as a photocatalyst (entry 2), quantitative overoxidation to benzoic acid (**16**) was observed.

Table 6. Experiments on the photostability of decarboxylated products (**4a** and **4n** as model substrates).^a

Entry	Photocatalyst	Decarboxylation Product (Product of the photoreaction)	Outcome / Yield ^b
1	Cu(OAc) ₂ (10 mol%) + dmp (10 mol%)		Starting material recovered (100%)
2	dmp (10 mol%)		 16 , 100%
3	Cu(OAc) ₂ (10 mol%) + dmp (10 mol%)		Starting material recovered (94%)
4	dmp (10 mol%)		Starting material recovered (58%)

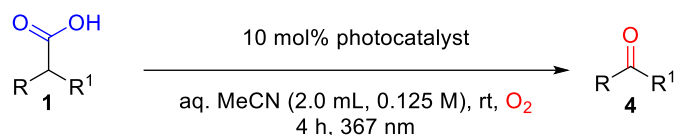
^aStandard conditions: product **4** (0.25 mmol, 1.0 equiv), 10 mol% catalyst: (Cu(OAc)₂ + dmp) or (dmp) in MeCN (2.0 mL), water (45 μL, 2.2 Vol%). Irradiation at indicated λ_{max} with a radiant power of 400 mW under an O₂ atmosphere for 24 h at room temperature (25°C). ^bNMR yield using 1,1,2,2-tetrachloroethane as internal standard (on a 0.250 mmol scale).

The same experiment was carried out with product **4n** as the model substrate. After 24 h, **4n** was recovered in 94% yield revealing that no undesired oxidation process occurred under the reaction conditions (entry 3). If the ligand dmp solely was applied as a photocatalyst, only 58% of the starting material (**4n**) was obtained, and several unidentified degradation products were formed (entry 4). Thus, it can be concluded that the reaction stops for benzylic carboxylic acids at the aldehyde oxidation stage or for secondary carboxylic acids at the ketone oxidation state and no overoxidation occurs.

2.8.6 Investigations on Selective Product Formation

Additionally, we performed corresponding ¹H-NMR investigations on the decarboxylation reaction of ibuprofen (**4n**) and an aliphatic carboxylic acid (**4r**), as depicted in Table 7:

Table 7. Experiments on the decarboxylation of carboxylic acids (**1n** and **1s** as model substrates)^a



Entry	Photocatalyst	Acid	Outcome / Yield ^b
1	Cu(OAc) ₂ (10 mol%) + dmp (10 mol%)		 4n , 27%
2	dmp (10 mol%)		50% 4n , but no selective product formation, several side products
3	Cu(OAc) ₂ (10 mol%) + dmp (10 mol%)		 4s , ca. 10%
4	dmp (10 mol%)		crm

^aStandard conditions: acid **1** (0.25 mmol, 1.0 equiv), 10 mol% catalyst: Cu(OAc)₂ + dmp or solely dmp in acetonitrile (2.0 mL), water (45 μL, 2.2 Vol%). Irradiation at indicated λ_{max} with a radiant power of 400 mW under an O₂ atmosphere for 4 h at room temperature (25°C). ^bNMR yield using 1,1,2,2-tetrachloroethane as internal standard (on a 0.250 mmol scale).

These experiments were designed to clarify whether the defined oxidation process requires the photoactive complex consisting of Cu(II) and dmp as the ligand. We irradiated the corresponding acids in the presence of 10 mol% Cu(OAc)₂ and dmp or the presence of solely 10 mol% dmp. As result, exclusive product formation was observable, if a combination of Cu(OAc)₂ and dmp was used (entry 1 and 3). For ibuprofen (**1n**), ¹H-NMR analysis clearly indicated selective product formation if the combination of 10 mol% Cu(OAc)₂ and dmp as a photocatalyst was employed (*vide infra*, Figure 6).

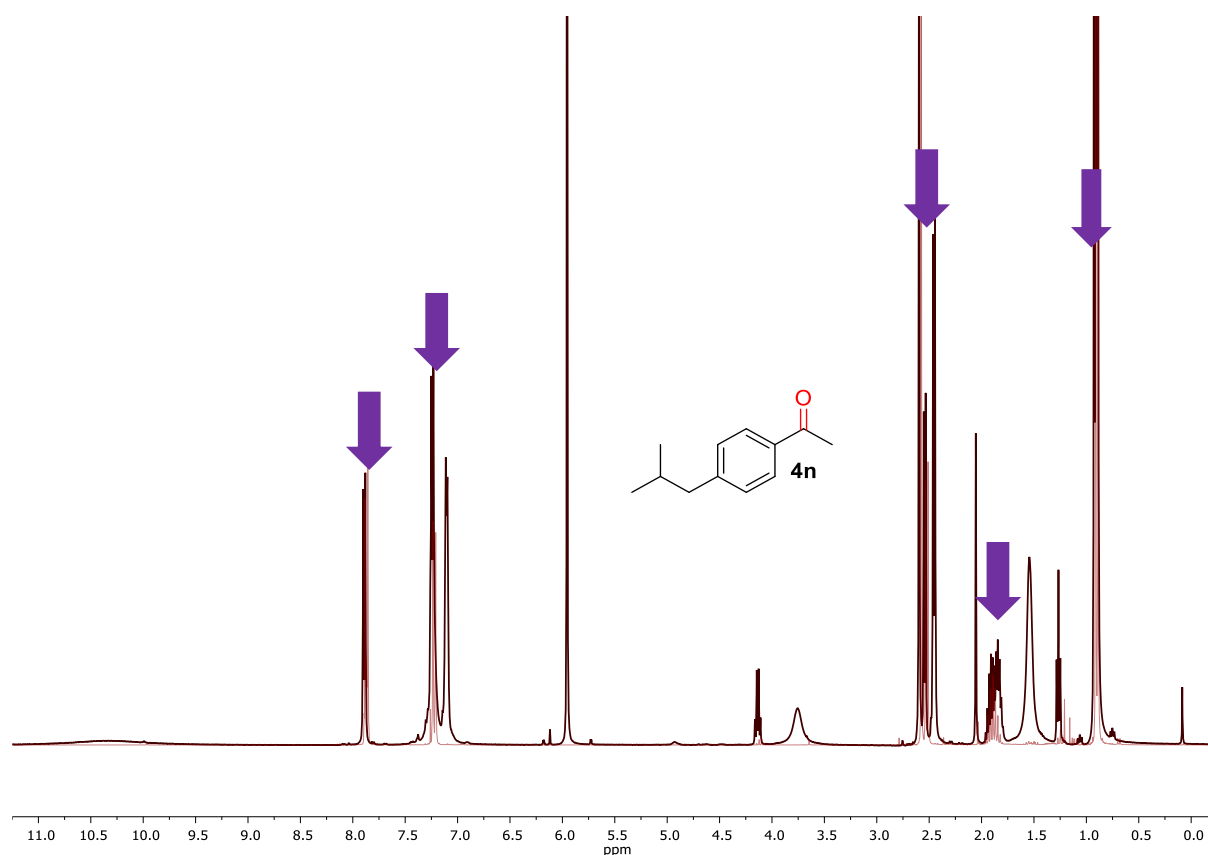


Figure 6. Crude ¹H-NMR in CDCl₃ of photolysis of ibuprofen (**1n**) in presence of 10 mol% Cu(OAc)₂ + dmp as photocatalyst showing the selective product formation (**4n**) (violet arrows); NMR of pure product **4n** is shown for comparison (red line); 5.95 ppm = signal of the internal standard 1,1,2,2-tetrachloroethane.

Contrary to this, unselective product formation was observed if 10 mol% of dmp was subjected to the photocatalytic reaction conditions (*vide infra*, Figure 7). In the case of the aliphatic carboxylic acid (**1s**), product formation (**4s**) was observed only in the presence of the *in situ* formed Cu(II)-complex (entry 3). In contrast, no product was detectable if just 10 mol% of dmp was used as a photocatalyst (entry 4). The experiments confirm that the active photocatalytic complex consisting of dmp and copper(II) has to be formed to initiate successful transformations. Thereby, the high efficiency of the photolysis *via* LIH goes hand in hand with selective product formation.

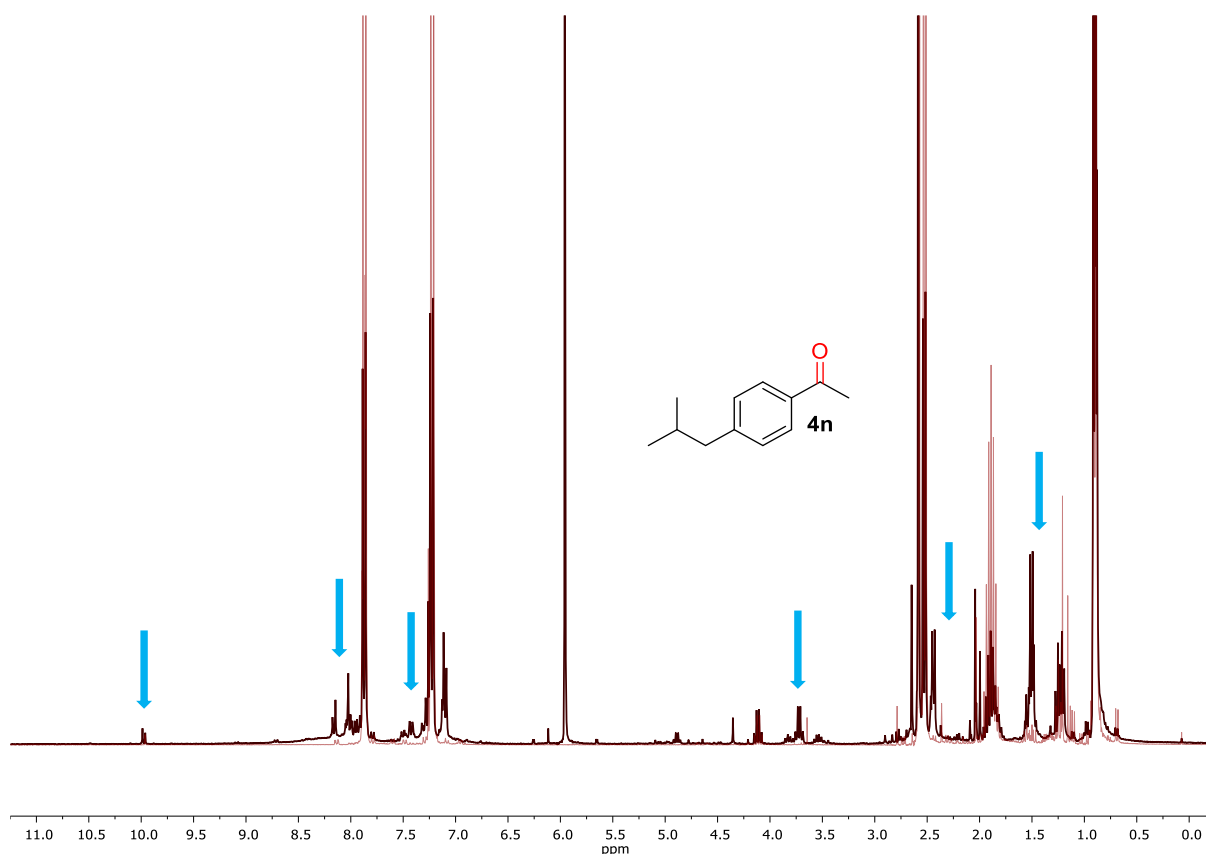


Figure 7. Crude ¹H-NMR in CDCl₃ of photolysis of ibuprofen (**1n**) in presence of 10 mol% dmp as photocatalyst showing unclean reaction mixture (blue arrows); NMR of pure product **4n** is shown for comparison (red line); 5.95 ppm = signal of the internal standard 1,1,2,2-tetrachloroethane.

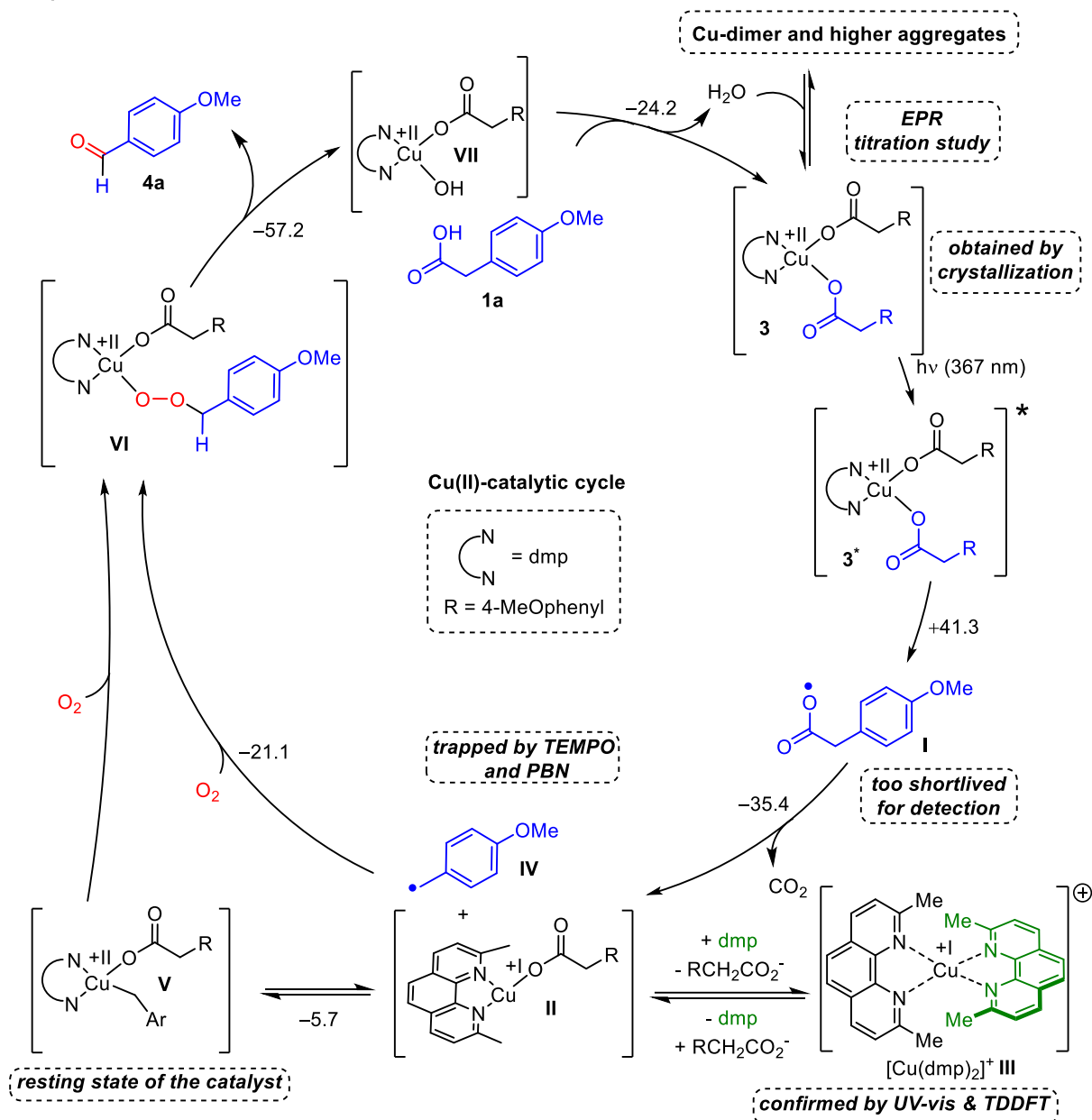
2.9 Proposed Reaction Mechanism

By combining all mechanistic investigations (UV/vis monitoring, trapping experiments, EPR) as well as DFT calculations (as conducted and kindly provided by the Rehbein group), a feasible proposal for a catalytic cycle for the oxidative decarboxylation, driven by the monomeric Cu(II)-dmp complex **3**, is as shown in Scheme 8:

Complex **3** is excited by light to **3***. Subsequently, radical **I** is generated upon homolytic Cu-O bond cleavage. This key step was calculated to be a significant up-hill process ($\Delta_R G = 41.3$ kcal/mol) but is still feasible through irradiation at the wavelength at which **3** absorbs most strongly, *i.e.* $\lambda_{\max} = 367$ nm delivering approximately 78 kcal/mol per photon. Arylcarboxyl radical **I** is too short-lived for direct observation or trapping, given that the release of CO₂, which was monitored by solution phase IR, giving rise to benzyl radical **IV** (trapped by TEMPO as well as *N*-tert-butyl- α -phenylnitron (PBN)), which is a strongly exothermic process by -35.4 kcal/mol.

Concurrently, a species of type Cu(I)dmp (**II**) is formed, which was confirmed by detecting $[\text{Cu(I)dmp}_2]^+$ (**III**) by UV-Vis, TDDFT and NMR. In line with recent mechanistic studies of oxygenase-catalyzed transformations,^[45] coordination of O_2 and back-binding of **IV** to **II** would lead to the peroxy-complex **VI**, being again highly exothermic by -21.1 kcal/mol. The catalytic cycle is closed by the extrusion of product **4a** and the formation of intermediate **VII**. Finally, after ligand exchange, complex **3** is regenerated.

Proposed Reaction Mechanism

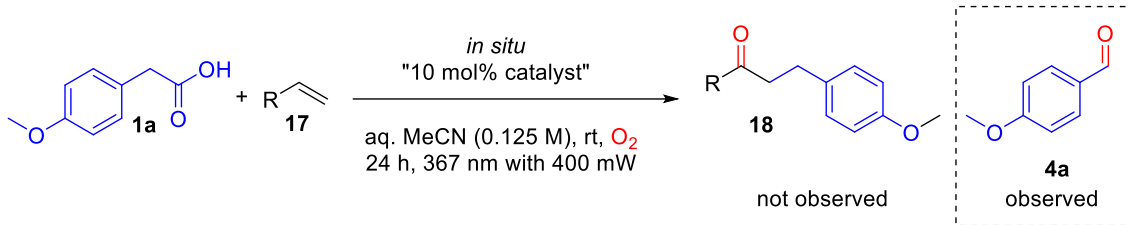


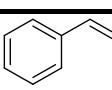
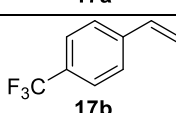
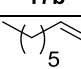
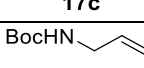
Scheme 8. Proposed Reaction mechanism based on mechanistic experiments and DFT-calculations.

2.10 Attempts towards Decarboxylative Coupling Reactions

We started our investigations inspired by the oxo-azidation of styrenes^[46] (*vide* chapter 1.4 for reaction and mechanism) and aimed towards a decarboxylative oxo-alkylation. Therefore, we changed the decarboxylation protocol by adding 2.0 equiv of a radical acceptor **17**, as shown in Table 8. With styrene (**17a**), no additional product (**18**) was observed, but benzaldehyde (**4a**) was formed in high yield (entry 1). Next, considering the vast nucleophilicity of 4-methoxybenzyl radical, electron-deficient 4-CF₃-styrene (**17b**) was used to trap the radical, but only decarboxylative aldehyde formation was observed (entry 2). Similarly, unactivated olefins (**17c** and **17d**) did not deliver any corresponding oxo-alkylated product (entries 3–4). As a result of this observation, we concluded that radical trapping with oxygen is a highly efficient process that is preferable to adding an acceptor in the presence of an oxygen atmosphere.

Table 8. Attempts towards decarboxylative oxo-alkylation of olefins.^a



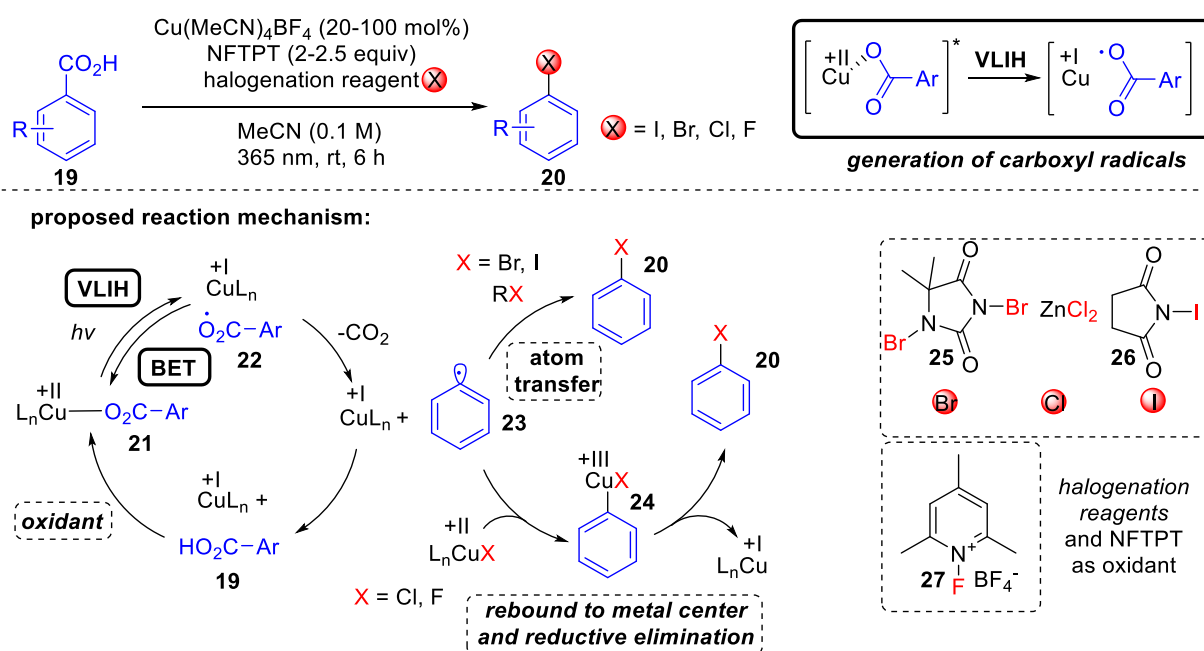
Entry	Olefin	Yield ^b
1	 17a	91% 4a
2	 17b	95% 4a
3	 17c	94% 4a
4	 17d	66% 4a

^aStandard conditions: 4-methoxyphenylacetic acid (**1a**) (0.25 mmol, 1.0 equiv), olefin **17** (0.5 mmol, 1.0 equiv), Cu(OAc)₂ (25 μmol, 10 mol%), dmp (2,9-dimethyl-1,10-phenanthroline) (25 μmol, 10 mol%) in MeCN (2.0 mL, 0.125 M), water (45 μL, 2.2 Vol%). Irradiation at 367 nm with a radiant power of 400 mW under an O₂ atmosphere for 24 h at room temperature (30°C). ^bNMR yield using 1,1,2,2-tetrachloroethane as internal standard.

After these initial results, it was considered to achieve decarboxylative addition under a nitrogen atmosphere to prevent the radical trapping with oxygen. Recently, MacMillan *et al.*^[29] reported the decarboxylative halogenation of aryl carboxylic acids. From a mechanistic point of view, as shown in Scheme 9, after light-induced homolysis of the copper(II)-arylcarboxylate **21** followed by decarboxylation of **22**, radical trapping was achieved by a copper(II)-species to afford copper(III)-intermediate **24**. The products **20** were released upon reductive elimination from Cu(III), affording Cu(I). To complete the catalytic cycle, the group identified NFTPT (**27**) and other oxidants, such as NFSI as suitable oxidants regenerating Cu(II).

Motivated by this impressive literature, we tried to develop similar decarboxylative coupling reactions by applying different reagents, such as TMSCN, TMSCF₃, TMSN₃ *etc.*, which are well known to undergo ligand exchange with copper(II) in three-component atom transfer radical addition (ATRA) reactions.^[47] As a result, reaction pathways *via* Cu(III)-intermediates should be feasible to investigate a new type of decarboxylative couplings, and the use of a stoichiometric amount of an oxidant, for example NFSI, is thought to regenerate Cu(II) to achieve catalytic transformation.

MacMillan *et al.* (2022)



Scheme 9. Decarboxylative Halogenation protocol of MacMillan and co-workers^[29].

As the model substrate, we used 4-cyano benzoic acid (**21**), 20 mol% of Cu(MeCN)₄BF₄ as a copper source for initial screening 1.0 equiv NFSI (which was reported by MacMillan and co-workers also to be suitable oxidant)^[29] in combination with several reagents X. Unfortunately, only low amounts of a homocoupling side product (**22**) as well as more unidentified side products in trace amount were observed (Table 9, entries 1–6). The formation of a homocoupling product was described as a side reaction in similar reports on photocatalytic decarboxylation of arylcarboxylic acids by Ritter and co-workers.^[48] Although the reaction solutions displayed a color change from blue to red, indicating a change in the corresponding oxidation state of Cu(II) to Cu(I), it appears that the catalytic cycle was not closed under the given conditions. Hence, it was concluded that the overall success of a photocatalytic decarboxylative coupling reaction seems highly dependent on the nature of the reagent X. At the current point of time, it remains unsolved why no corresponding Cu(II)-X species was formed under the chosen reaction conditions. Due to that reason, further investigations were stopped at this point.

Table 9. Attempts on the two-component decarboxylative coupling reaction under N₂-atmosphere.^a

Entry	Reagent X	Expected Product	Yield ^b
1	TMS-CN	20a	2% 23 + crm
2	TMS-CF ₃	20b	9% 23 + crm
3	TMS-N ₃	20c	9% 23 + crm
4	Br-CH ₂ -NO ₂	20d	8% 23 + crm
5 ^c	24	20e	nd ^c
6 ^c	25	20f	nd ^c

^aStandard conditions: benzoic acid (**21**) (0.25 mmol, 1.0 equiv), Cu(MeCN)₄BF₄ (50 μmol, 20 mol%), NFTPT (0.25 mmol, 1.0 equiv), reagent X (0.25 mmol, 1.0 equiv) in MeCN (2.5 mL, 0.1 M), Irradiation at 367 nm under N₂ atmosphere for 4.5 h at room temperature (30°C). ^bNMR yield using 1,1,2,2-tetrachloroethane as internal standard. ^cnd: not detected via thin layer chromatography (TLC). crm = complex reaction mixture.

2.11 Conclusion

In conclusion, we have developed a practical methodology for the oxidative decarboxylation of phenylacetic acids to access the corresponding aldehydes or ketones using oxygen as the terminal oxidant. The crucial step in the process was identified as the light-induced homolysis of a Cu(II)-carboxylate, which appears to require monodentate coordination rather than chelation of the paddle-wheel type. This desired type of coordination can be successfully accessed by employing the sterically demanding 2,9-dimethyl-1,10-phenanthroline (dmp) as a ligand. After Cu(II)-carboxylate is homolyzed and then decarboxylated, the resulting radical is effectively trapped by oxygen and the reduced copper(I) species, which delivers the aldehydes/ketones and copper in its initial Cu(II) oxidation state, completing the catalytic cycle.

2.12 References

- [1] a) N. Rodríguez, L. J. Goossen, *Chem. Soc. Rev.* **2011**, *40*, 5030; b) T. Patra, D. Maiti, *Chem. Eur. J.* **2017**, *23*, 7382; c) Q. Feng, Q. Song, *J. Org. Chem.* **2014**, *79*, 1867.
- [2] J. Y. Morimoto, B. A. DeGraff, *J. Phys. Chem.* **1975**, *79*, 326.
- [3] a) N. R. de Campos, M. A. Ribeiro, W. X. C. Oliveira, D. O. Reis, H. O. Stumpf, A. C. Doriguetto, F. C. Machado, C. B. Pinheiro, F. Lloret, M. Julve et al., *Dalton Trans.* **2016**, *45*, 172; b) P. J. Hay, J. C. Thibeault, R. Hoffmann, *J. Am. Chem. Soc.* **1975**, *97*, 4884.
- [4] M. Iqbal, S. Ali, M. N. Tahir, *Z. Anorg. Allg. Chem.* **2018**, *644*, 172.
- [5] B. Kozlevcar, P. Segedin, *Croat. Chem. Acta* **2008**, *81*, 369.
- [6] a) F. Agterberg, H. Provó Kluit, W. L. Driessen, J. Reedijk, H. Oevering, W. Buijs, N. Veldman, M. T. Lakin, A. L. Spek, *Inorganica Chim. Acta* **1998**, *267*, 183; b) F. P. W. Agterberg, H. A. J. Provó Kluit, W. L. Driessen, H. Oevering, W. Buijs, M. T. Lakin, A. L. Spek, J. Reedijk, *Inorg. Chem.* **1997**, *36*, 4321.
- [7] P. Edelsbacher, G. Redhammer, U. Monkowius, *Monatsh. Chem.* **2020**, *151*, 543.
- [8] A. Benhassine, H. Boulebd, B. Anak, A. Bouraiou, S. Bouacida, M. Bencharif, A. Belfaitah, *J. Mol. Struct.* **2018**, *1160*, 406.
- [9] D. Avci, S. Altürk, F. Sönmez, Ö. Tamer, A. Başoğlu, Y. Atalay, B. Zengin Kurt, N. Dege, *Appl. Organometal. Chem.* **2019**, *33*.
- [10] M. Mikuriya, C. Yamakawa, K. Tanabe, R. Nukita, Y. Amabe, D. Yoshioka, R. Mitsuhashi, R. Tatehata, H. Tanaka, M. Handa et al., *Magnetochemistry* **2021**, *7*, 35.
- [11] F. Agterberg, W. L. Driessen, J. Reedijk, H. Oeveringb, W. Buijs, *Stud. Surf. Sci. Catal.* **1994**, 639–646.
- [12] F. Hamza, G. Kickelbick, *Macromolecules* **2009**, *42*, 7762.
- [13] P. J. Moon, A. Fahandej-Sadi, W. Qian, R. J. Lundgren, *Angew. Chem. Int. Ed.* **2018**, *57*, 4612.
- [14] S. Engl, O. Reiser, *Eur. J. Org. Chem.* **2020**, *2020*, 1523.
- [15] P. Yang, X.-J. Yang, B. Wu, *Eur. J. Inorg. Chem.* **2009**, *2009*, 2951.
- [16] C. Lankes, *Photoredox Catalysis Using Copper Complexes*. PhD thesis, University of Regensburg, **2017**.
- [17] A. N. Wein, R. Cordeiro, N. Owens, H. Olivier, K. I. Hardcastle, J. F. Eichler, *J. Fluor. Chem.* **2009**, *130*, 197.
- [18] N. Politeo, M. Pisačić, M. Đaković, V. Sokol, B.-M. Kukovec, *Acta Cryst.* **2020**, *76*, 225.

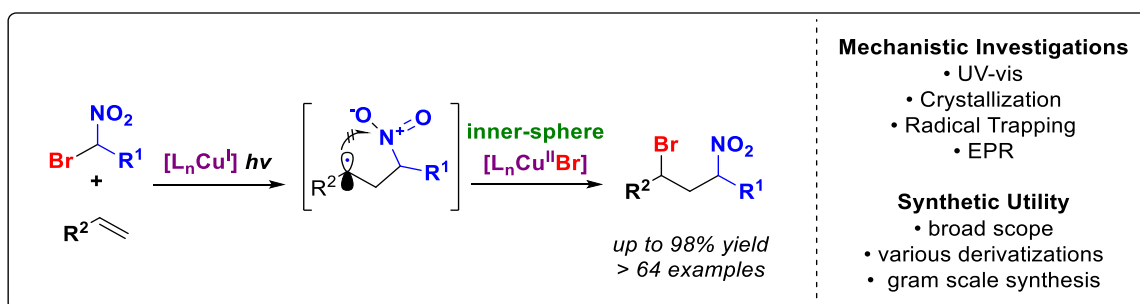
- [19] H. Phetmung, A. Nucharoen, *Polyhedron* **2019**, *173*, 114121.
- [20] A. A. Gouda, A. S. Amin, *Arab. J. Chem.* **2010**, *3*, 159.
- [21] R. Cao, Q. Shi, D. Sun, M. Hong, W. Bi, Y. Zhao, *Inorg. Chem.* **2002**, *41*, 6161.
- [22] E. Prenesti, P. G. Daniele, S. Berto, S. Toso, *Polyhedron* **2006**, *25*, 2815.
- [23] M. T. Miller, P. K. Gantzel, T. B. Karpishin, *Inorg. Chem.* **1998**, *37*, 2285.
- [24] Z. Staszak, A. Krojcer, M. Kubiak, A. Puszko, G. Maciejewska, M. Cieślak-Golonka, *Struct. Chem.* **2010**, *21*, 305.
- [25] M. Mikuriya, R. Indrawati, R. Hashido, S. Matsubara, C. Nakamura, D. Yoshioka, K. Yokota, M. Fukuzaki, M. Handa, *Magnetochemistry* **2018**, *4*, 22.
- [26] A. Tsybizova, B. L. Ryland, N. Tsierkezos, S. S. Stahl, J. Roithová, D. Schröder, *Eur. J. Inorg. Chem.* **2014**, *2014*, 1407.
- [27] S. D. McCann, S. S. Stahl, *Acc. Chem. Res.* **2015**, *48*, 1756.
- [28] J. W. Hilborn, J. A. Pincock, *J. Am. Chem. Soc.* **1991**, *113*, 2683.
- [29] T. Q. Chen, P. S. Pedersen, N. W. Dow, R. Fayad, C. E. Hauke, M. C. Rosko, E. O. Danilov, D. C. Blakemore, A.-M. Dechert-Schmitt, T. Knauber et al., *J. Am. Chem. Soc.* **2022**, *144*, 8296.
- [30] a) J. Chateaufneuf, J. Luszytk, K. U. Ingold, *J. Am. Chem. Soc.* **1988**, *110*, 2877; b) J. Chateaufneuf, J. Luszytk, K. U. Ingold, *J. Am. Chem. Soc.* **1988**, *110*, 2886.
- [31] W. Wu, S. Liu, M. Duan, X. Tan, C. Chen, Y. Xie, Y. Lan, X.-Q. Dong, X. Zhang, *Org. Lett.* **2016**, *18*, 2938.
- [32] Z. Császár, R. Kovács, M. Fonyó, J. Simon, A. Bényei, G. Lendvay, J. Bakos, G. Farkas, *Mol. Catal.* **2022**, *529*, 112531.
- [33] W. Gong, Y. Liu, J. Xue, Z. Xie, Y. Li, *Chem. Lett.* **2012**, *41*, 1597.
- [34] S. Mahato, P. Rawal, A. K. Devadkar, M. Joshi, A. Roy Choudhury, B. Biswas, P. Gupta, T. K. Panda, *Org. Biomol. Chem.* **2022**, *20*, 1103.
- [35] R. Yoneda, S. Harusawa, T. Kurihara, *Tetrahedron Lett.* **1989**, *30*, 3681.
- [36] H. Zhan, Z. Hu, W. Tao, M. Ling, W. Cao, J. Lin, Z. Liu, Y. Wang, Z. Fang, *SynOpen* **2019**, *03*, 16.
- [37] M. Mujahid Alam, S. R. Adapa, *Synth. Commun.* **2003**, *33*, 59.
- [38] Y.-B. Tang, J.-Z. Liu, S.-E. Zhang, X. Du, F. Nie, J.-Y. Tian, F. Ye, K. Huang, J.-P. Hu, Y. Li et al., *ChemMedChem* **2014**, *9*, 918.

- [39] P. Patel, *J. Org. Chem.* **2022**, *87*, 4852.
- [40] J. Z. Patel, T. Parkkari, T. Laitinen, A. A. Kaczor, S. M. Saario, J. R. Savinainen, D. Navia-Paldanius, M. Cipriano, J. Leppänen, I. O. Koshevoy et al., *J. Med. Chem.* **2013**, *56*, 8484.
- [41] S. Garakyaraghi, C. E. McCusker, S. Khan, P. Koutnik, A. T. Bui, F. N. Castellano, *Inorg. Chem.* **2018**, *57*, 2296.
- [42] R. Fayad, S. Engl, E. O. Danilov, C. E. Hauke, O. Reiser, F. N. Castellano, *J. Phys. Chem. Lett.* **2020**, *11*, 5345.
- [43] Q. Y. Li, S. N. Gockel, G. A. Lutovsky, K. S. DeGlopper, N. J. Baldwin, M. W. Bundesmann, J. W. Tucker, S. W. Bagley, T. P. Yoon, *Nat. Chem.* **2022**, *14*, 94.
- [44] M. Peng, H. Li, X. Kang, E. Du, D. Li, *Water Sci Technol.* **2017**, *75*, 2935.
- [45] R. E. Cowley, L. Tian, E. I. Solomon, *Proc. Natl. Acad. Sci. U.S.A.* **2016**, *113*, 12035.
- [46] A. Hossain, A. Vidyasagar, C. Eichinger, C. Lankes, J. Phan, J. Rehbein, O. Reiser, *Angew. Chem. Int. Ed.* **2018**, *57*, 8288.
- [47] S. Engl, O. Reiser, *Chem. Soc. Rev.* **2022**, *51*, 5287.
- [48] a) P. Xu, P. López-Rojas, T. Ritter, *J. Am. Chem. Soc.* **2021**, *143*, 5349; b) W. Su, P. Xu, T. Ritter, *Angew. Chem. Int. Ed.* **2021**, *60*, 24012; c) P. Xu, W. Su, T. Ritter, *Chem. Sci.* **2022**, *13*, 13611.

Chapter 3 Cu(I)-photocatalyzed Bromonitroalkylation of Olefins

Abstract

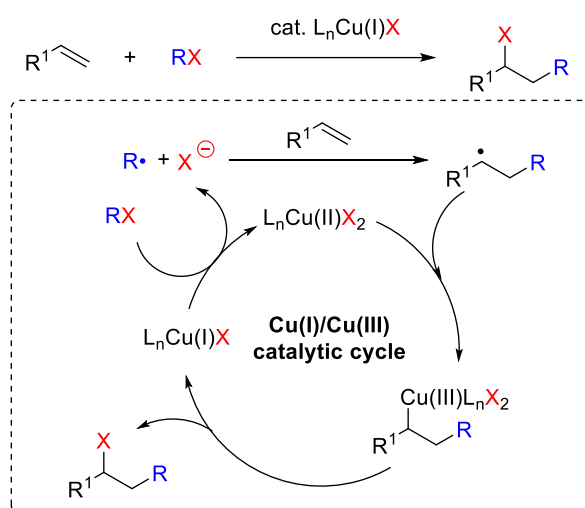
The vicinal difunctionalization of olefins utilizing bromonitroalkanes as atom transfer radical addition (ATRA) reagents has been developed in a visible light-mediated copper-catalyzed protocol. This procedure, which allows the rapid functionalization of activated and unactivated olefins, excels with high yields, fast reaction times, environmentally benign reaction conditions, and exceptional scope. Moreover, the methodology allows late-stage functionalization of biologically active molecules and upscaling to gram quantities. Manifold possibilities for further transformations exist, e.g. access to nitro- and aminocyclopropanes. In addition to the synthetic value of the title transformation, this study undergirds copper's unique character in photoredox catalysis by demonstrating its capability to stabilize and interact with radical intermediates in its inner coordination sphere. According to EPR investigations, these interactions can even outperform a favorable cyclization of transient radical intermediates to highly stable persistent radicals compared to iridium-based photocatalysts.



This chapter is based on: [A. Reichle](#)⁺⁺, M. Koch⁺⁺, H. Sterzel, L.-J. Großkopf, J. Floss, J. Rehbein, O. Reiser, *Angew. Chem. Int. Ed.*, **2023**, e202219086. ([⁺⁺] Co-first authors.)

3.1 Introduction and Outline of the Study

Atom transfer radical addition (ATRA) reactions are an effective method to functionalize olefins in a step-economic and atom-efficient manner. The earliest examples of the development of these reactions date back to Kharasch's pioneering work in the 1940s.^[1] Up to this date, especially in combination with visible-light photoredox catalysis,^[2] ATRA reactions could be developed in great variety.^[3] In general, suitable precursors RX are added across a double bond of an alkene (especially effective for this type of transformation are Cu(I)-phenanthroline complexes, in particular [Cu(dap)₂]Cl (dap = 2,9-bis(*para*-anisyl)-1,10-phenanthroline) as a stand-alone photocatalyst or iridium-based photocatalysts in combination with Cu(II)-additives.^[4] This is based on the characteristics of Cu(II) being a persistent radical. Therefore, it can interact with a transient radical to ultimately deliver X⁻ via a Cu(III)-intermediate, as depicted in Scheme 1.



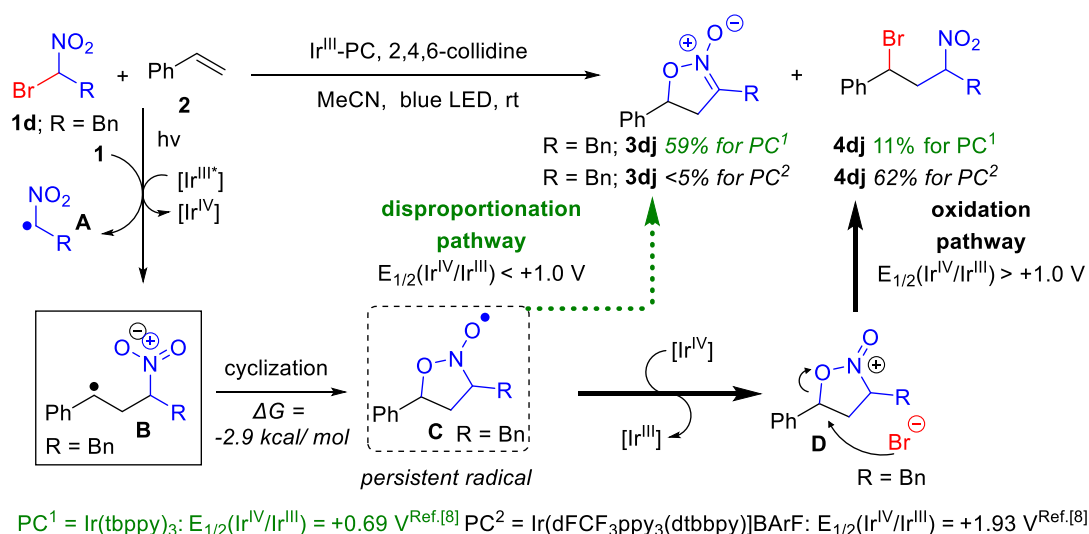
Scheme 1. General concept of Cu(I)-photocatalyzed ATRA reactions.

Many ATRA processes that are not feasible with other photoredox catalysts, such as ruthenium, iridium or organic dyes, have been shown to proceed in the presence of copper because of the unique character of copper-based (photo)catalysts to act in such an inner-sphere mode.^[5] Only a few reports of ATRA and associated reactions between organobromo nitroalkanes and alkenes have been published so far.^[6,7,8] We were intrigued by the report of Ooi co-workers^[8] who demonstrated the iridium(III)-catalyzed, photodivergent addition of bromonitroalkane **1d** to styrenes **2** (*vide infra*, Scheme 2A).

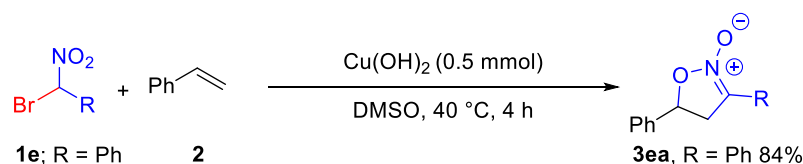
In respect to density-functional theory (DFT) calculations, the persistent radical **C** was proposed as the key intermediate, rapidly forming via **B**'s cyclization. It was demonstrated that the major product produced *via* a disproportionation pathway is the isoxazoline-*N*-oxide **3** if the oxidized photocatalyst cannot further oxidize **C** (*i.e.* $E_{1/2}(\text{Ir}^{\text{IV}}/\text{Ir}^{\text{III}}) < 1.0 \text{ V}$). On the other hand, for iridium photocatalysts with $E_{1/2}(\text{Ir}^{\text{IV}}/\text{Ir}^{\text{III}}) > 1.0 \text{ V}$, the ATRA product **4** is obtained as the major product *via* oxidation of **C** to **D**. Based on this research, it was expected that copper(II), for

example in $[\text{Cu}(\text{dap})_2]\text{Cl}$ ^[5] $E_{1/2}(\text{Cu}^{\text{II}}/\text{Cu}^{\text{I}}) = 0.62 \text{ V}$ vs. saturated calomel electrode (SCE)) having lower oxidizing power such as comparable photocatalysts $[\text{Ir}(\text{tbbpy})_3]^+$ $E_{1/2}(\text{Ir}^{\text{IV}}/\text{Ir}^{\text{III}}) = 0.69 \text{ V}$ vs. SCE^[8] or $[\text{Ir}(\text{ppy})_3]$ $E_{1/2}(\text{Ir}^{\text{IV}}/\text{Ir}^{\text{III}}) = 0.77 \text{ V}$ vs. SCE^[9] should also afford **3** except if Cu(II) could successfully compete with the cyclization to **C**. The related thermal reaction between **1e** and **2a** initiated by $\text{Cu}(\text{OH})_2$ (50 mol%) solely produces isoxazoline-*N*-oxide **3ea** in 84% yield and does not result in any ATRA-type products (Scheme 2B), as demonstrated by Iwasaki and co-workers.^[7]

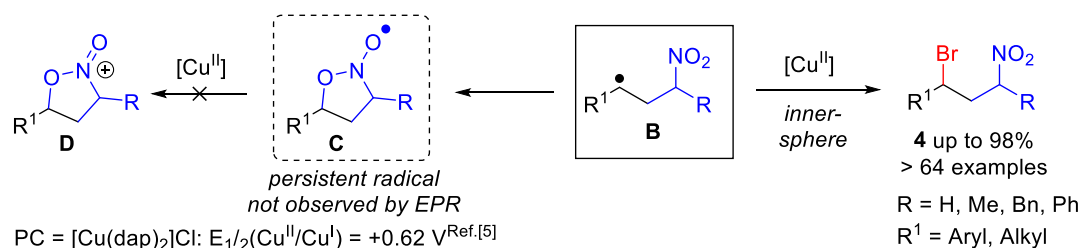
(A) Previous work: Ooi *et al.* (2020) Redox-regulated product formation



(B) Previous work: Iwasaki *et al.* (2020) Synthesis of 2-Isoxazoline-*N*-oxides



(C) This work: Inner-sphere controlled ATRA product formation



Scheme 2. Divergent pathways in ATRA reactions between bromonitroalkanes and alkenes in previous work.

3.2 Reaction Optimization

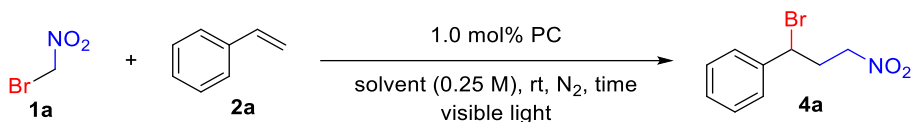
With an emphasis on the synthetic utility of the 1,3-functionalized compounds, we started our investigations with bromonitromethane^[10] (**1a**) and styrene (**2a**) in the presence of [Cu^I(dap)₂]Cl as the photocatalyst under visible light irradiation with a green LED ($\lambda_{\text{max}} = 530 \text{ nm}$) (Table 1). Typical solvents for ATRA processes, such as DCM or CDCl₃, gave moderate yields of the desired product (Table 1, entries 1–2), whereas only traces of the product were formed in THF, and no reaction was observed in the green solvent dimethyl carbonate (DMC) (entries 3–4). Using MeOH as a solvent, 44 % of the product was observed (entry 5).

Switching to MeCN as solvent afforded the corresponding ATRA product **4a** in high yield after 1 h of irradiation (entry 6). Next, we checked if a different starting material ratio would change the reaction yield. However, a distinct decrease in yield was observable if bromonitromethane (**1a**) was used in excess (entries 7–8). If the amount of styrene was increased, the yield stagnated (entries 9–10). Thus, the optimal ratio of ATRA reagent and olefin was found to be 1:1, which is optimal from an economic point of view.

It was also tried to decrease the catalyst loading. To our delight, the reaction still worked well with lower catalyst loading showing the high efficiency of the Cu(I)-photocatalyst. However, no increase in yield with higher catalyst loading was detected (entries 11–12). Considering the dilution as a reaction parameter, a change in product formation in higher or lower concentrations was not observable (entries 13–14).

Applying blue light for irradiation increased the yield to 90% (entry 15). Using 10 mol% of Cu^ICl or Cu^{II}Cl₂ as a potential standalone catalyst revealed the requirement of the photocatalyst in the reaction (entries 16–19). If solely 10 mol% of the ligand dap was used as the photocatalyst, no product was observable under green light irradiation (entry 20), but 35% of the product could be obtained under blue light irradiation (entry 21). Use of the ligand 2,9-dimethyl-1,10-phenanthroline (dmp) in 10 mol% under 455 nm irradiation gave 8% of **4a** (entry 23).

In the absence of any photocatalyst but with irradiation at 530 nm or 455 nm, no reaction was detected, indicating the requirement of the copper photocatalyst (entries 23–24). In the absence of light, but in the presence of the photocatalyst, neither with the Cu(I)- nor with the Cu(II)-complex product formation was observable, revealing the necessity of light (entries 25–26). Initiating a radical chain process with AIBN under thermal conditions was unsuccessful, confirming the importance of copper for the catalytic process (entry 27).

Table 1. Reaction optimization of bromonitromethylation.^a

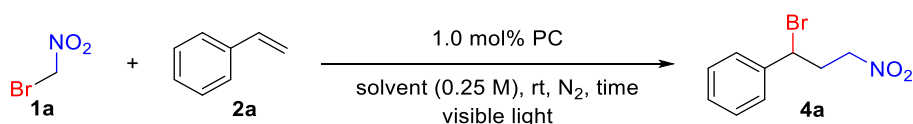
Entry	Photocatalyst	λ_{\max} [nm]	Solvent	Variations	Yield ^b (%)
1	[Cu ^I (dap) ₂]Cl	530	DCM	-	55
2	[Cu ^I (dap) ₂]Cl	530	CHCl ₃	-	67
3	[Cu ^I (dap) ₂]Cl	530	THF	-	traces
4	[Cu ^I (dap) ₂]Cl	530	DMC	-	0
5	[Cu ^I (dap) ₂]Cl	530	MeOH	-	44
6	[Cu ^I (dap) ₂]Cl	530	MeCN	-	87
7	[Cu ^I (dap) ₂]Cl	530	MeCN	equivalents (1a: 2a) = 2:1	57
8	[Cu ^I (dap) ₂]Cl	530	MeCN	equivalents (1a: 2a) = 1.5:1	51
9	[Cu ^I (dap) ₂]Cl	530	MeCN	equivalents (1a: 2a) = 1:1.5	81
10	[Cu ^I (dap) ₂]Cl	530	MeCN	equivalents (1a: 2a) = 1:2	86
11	[Cu ^I (dap) ₂]Cl	530	MeCN	catalyst loading 0.25 mol%	78
12	[Cu ^I (dap) ₂]Cl	530	MeCN	catalyst loading 1.5 mol%	85
13	[Cu ^I (dap) ₂]Cl	530	MeCN	0.5 M	87
14	[Cu ^I (dap) ₂]Cl	530	MeCN	0.125 M	86
15	[Cu ^I (dap) ₂]Cl	444	MeCN	wavelength	90
16	CuCl	530	MeCN	catalyst loading 10 mol%, 3h	nr
17	CuCl	455	MeCN	catalyst loading 10 mol%, 2h	nr
18	CuCl ₂	no	MeCN	catalyst loading 10 mol%, 3h	nr ^c
19	CuCl ₂	455	MeCN	catalyst loading 10 mol%, 3h	nr ^c
20	dap	530	MeCN	catalyst loading 10 mol%, 3h	nr
21	dap	455	MeCN	catalyst loading 10 mol%, 2h	35
22	dmp	455	MeCN	catalyst loading 10 mol%, 2h	8
23	no	530	MeCN	-	nr
24	no	455	MeCN	-	nr ^c
25	[Cu ^I (dap) ₂]Cl	no	MeCN	-	nr ^c
26	[Cu ^{II} (dap)Cl ₂]	no	MeCN	-	nr ^c
27	no	no	MeCN	AIBN (10 mol%), T=80°C, 24h	nr ^{bc}

^aStandard conditions: bromonitromethane (1a) (0.25 mmol, 1.0 equiv), styrene (2a) (0.25 mmol, 1.0 equiv), photocatalyst (2.50 μ mol, 1.0 mol%), in the solvent (anh., degassed, 1.0 mL, 0.25 M); Irradiation at indicated wavelength λ under N₂ atmosphere for 1 h at room temperature (25°C). ^bNMR yield using 1,1,2,2-tetrachloroethane as internal standard. nr = no reaction. crm = complex reaction mixture. ^canalyzed *via* TLC.

3.3 Comparison with other Photocatalysts

Following these initial findings, we were interested in the catalytic activity of different copper-based photocatalysts (Table 2). To our delight, with $[\text{Cu}^{\text{II}}(\text{dap})\text{Cl}_2]$, which is readily reduced under photochemical conditions to $[\text{Cu}^{\text{I}}(\text{dap})_2]\text{Cl}$ by homolysis of the Cu–Cl bond^[11], the ATRA product **4a** was exclusively obtained in high yield (entry 3).

Table 2. Comparison with other photocatalysts.^a



Entry	Photocatalyst	λ_{max} [nm]	$E_{1/2}(\text{PC}^{\text{n}+1} / \text{PC}^{\text{n}})$ [V] vs. SCE ^c	Reaction time [h]	Yield ^b (%)
1	$[\text{Cu}^{\text{I}}(\text{dap})_2]\text{Cl}$	530	+ 0.62 ^f	1	87
2	$[\text{Cu}^{\text{I}}(\text{dap})_2]\text{Cl}$	455	+ 0.62 ^g	1	90(90) ^d
3	$[\text{Cu}^{\text{II}}(\text{dap})\text{Cl}_2]$	530	-	2	87
4	$[\text{Cu}^{\text{I}}(\text{dmp})_2]\text{Cl}$	455	+ 0.63 ^h	2	80
5	$[\text{Cu}^{\text{I}}(\text{dmp})_2]\text{Cl}$	530	+ 0.63 ^f	2	75
6	$[\text{Cu}^{\text{II}}(\text{dmp})\text{Cl}]\text{Cl}$	455	-	2	80
7	$[\text{Cu}^{\text{I}}(\text{Xanthphos})(\text{dmp})]\text{BF}_4$	455	-	3	83
8	$[\text{Ru}(\text{bpy})_3](\text{BF}_4)_2$	455	+ 1.29 ^g	18	9
9	$[\text{Ir}(\text{dtbbpy})(\text{ppy})_2]\text{PF}_6$	455	+ 1.21 ^h	3	68
10	$(\text{Ir}[\text{dF}(\text{CF}_3)\text{ppy}]_2(\text{dtbpy}))\text{PF}_6$	455	+ 1.69 ^h	18	52
11	4-CzIPN	455	+ 1.52 ⁱ	3	59
12	Na ₂ -Eosin Y	530	+ 0.78 ^j	18	nr
13	Na ₂ -Rose Bengal	530	+ 1.00 ^k	18	nr
14	Rhodamine 6G	530	- 1.00 ^l	18	nr
15	$[\text{Fe}(\text{phen})_3](\text{NTf}_2)_2$	530	-	18	nr ^e

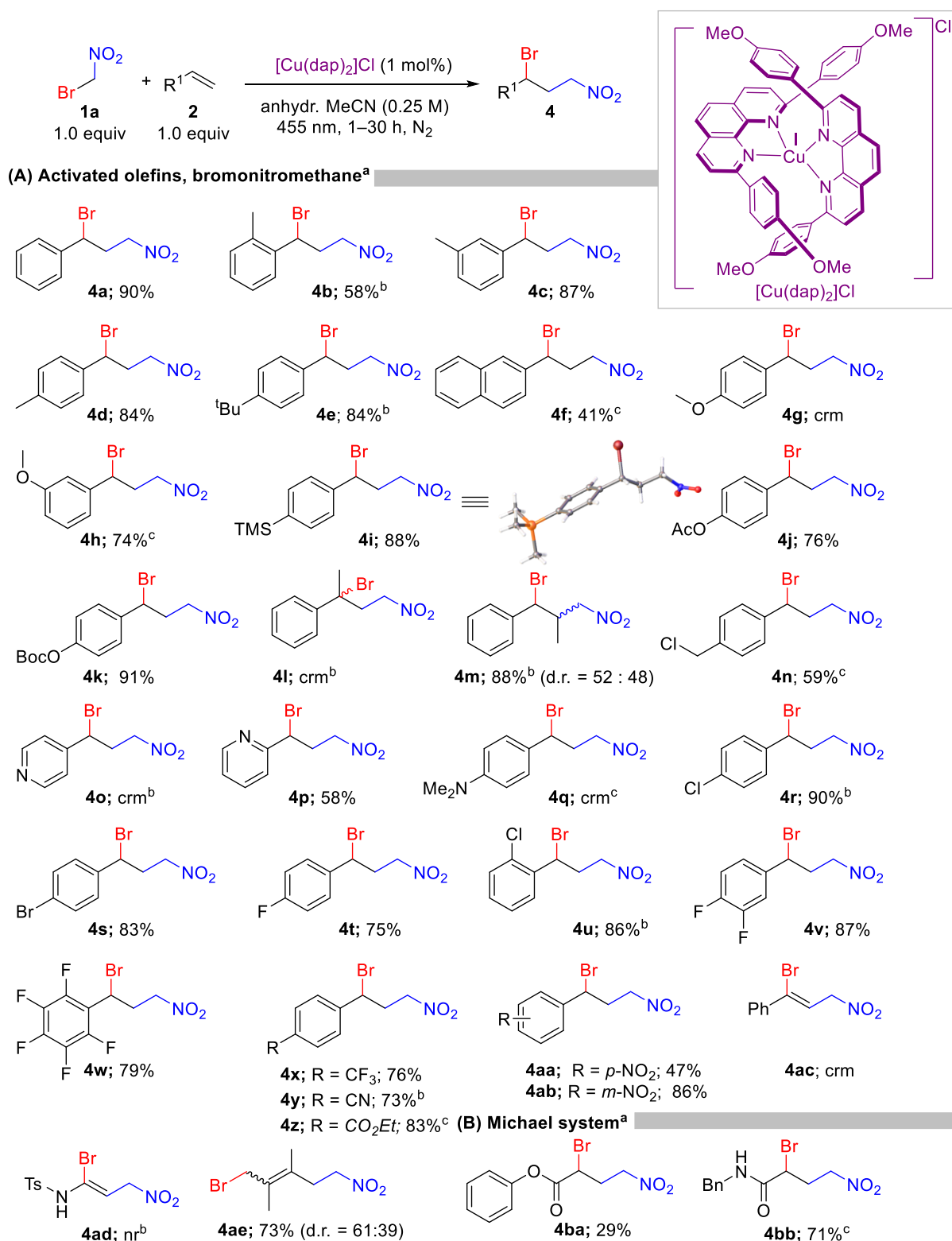
^aStandard conditions: bromonitromethane (**1a**) (0.25 mmol, 1.0 equiv), styrene (**2a**) (0.25 mmol, 1.0 equiv), photocatalyst (2.50 μmol , 1 mol%), in MeCN (anh., degassed, 1.0 mL, 0.25 M); Irradiation at indicated wavelength λ under N₂ atmosphere for given time at room temperature (25 °C). ^bNMR yield using 1,1,2,2-tetrachloroethane as internal standard. ^cReactions were stopped, after styrene was consumed completely. ^disolated yield. nr = no reaction. ^eanalyzed via TLC. ^fRef.^[5] ^gRef.^[12] ^hRef.^[13] ⁱRef.^[14] ^jRef.^[15] ^kRef.^[16] ^lRef.^[17]

Further, environmentally friendly and cheap complexes $[\text{Cu}^{\text{I}}(\text{dmp})_2]\text{Cl}$ and $[\text{Cu}^{\text{II}}(\text{dmp})_2]\text{Cl}$ ^[5] as well as heteroleptic complex $[\text{Cu}^{\text{I}}(\text{Xanthphos})(\text{dmp})]\text{BF}_4$ gave access to the desired product **4a** in high yield (entries 4–7). Finally, commonly employed photocatalysts, such as ruthenium(II), iridium(III) or organic dye-based were tested on their activity. With $[\text{Ru}(\text{bpy})_3](\text{BF}_4)_2$ only 9% of the product was observed, even after a long reaction time (entry 8). With higher oxidizing Ir(III)-based photocatalysts, such as $[\text{Ir}(\text{dtbbpy})(\text{ppy})_2]\text{PF}_6$ or $(\text{Ir}[\text{dF}(\text{CF}_3)\text{ppy}]_2(\text{dtbpy}))\text{PF}_6$ the product was delivered in moderate yields again with prolonged reaction time (entries 9–10).

Considering organic-dye based photocatalysts as low-cost alternatives,^[18] several established representatives were utilized under optimized reaction conditions. Whereas 4-CzIPN under blue irradiation delivered the product in 59% after 3h (entry 11), no reaction was observable for various organic dyes (with lower oxidation power), such as Eosin Y or Rhodamine 6G. (entries 12–14). When considering an iron-based photocatalyst for the title transformation, no catalytic activity was observed (entry 15). Thus, the importance and strength of copper as a photocatalyst promoting the title transformation were successfully demonstrated.

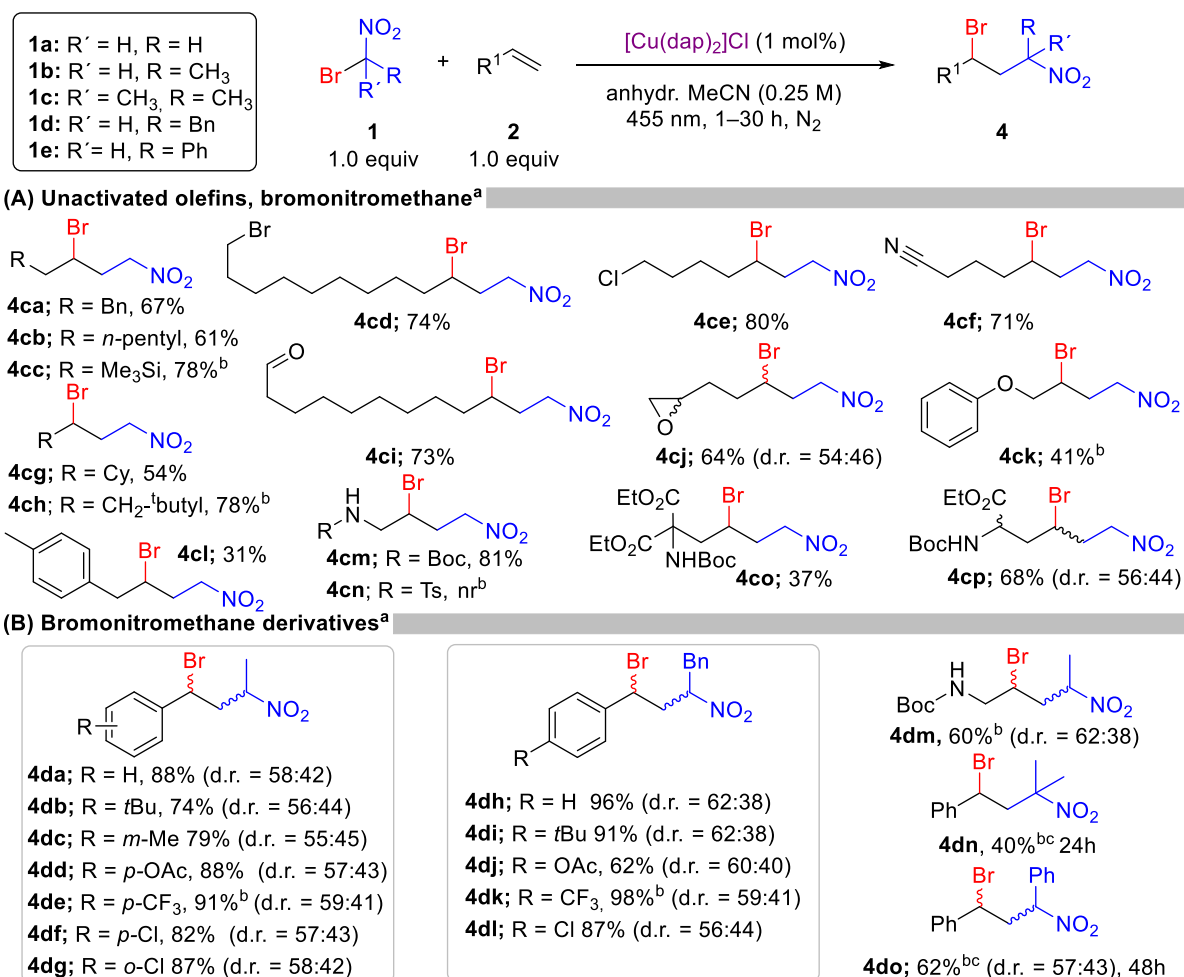
3.4 Substrate Scope

Next to having identified the superiority of Cu(I)-based photocatalysts in this transformation, we next explored the scope of olefins (Scheme 3). To our delight, electron-donating alkyl substitutions at the ortho, meta, or para positions of styrenes accessed the desired products **4b-4e** in high yield. However, further increasing the electron-donating character, such as *p*-OMe, resulted in a complex reaction mixture that agrees with previous studies on Cu(I)-catalyzed ATRA reactions.^[19] When the methoxy group is placed in meta position, fulfilling more the character of an acceptor, the product **4h** was obtained in 74% yield. TMS-substituted product **4i** was obtained in 88% and successfully crystallized. While α -substitution on the styrene-moiety led to a complex reaction mixture, we were pleased to see that β -substitution was tolerated and accessed product **4m** in good yield. A benzyl-chloride-containing styrene, which could have undergone a photoreduction to form a benzyl radical,^[20] successfully underwent the ATRA process, providing product **4n** in 59%. Employing heterocycles, we were pleased to see that 2-vinyl pyridine delivered the corresponding product **4p** with a yield of 58%. However, a complex reaction mixture was observed when the vinyl-moiety was placed in *p*-position. Styrene derivatives bearing electron-withdrawing halogen substitutions in different positions were tolerated well and yielded products **4r-4w** in high yields. Further increasing the electron-withdrawing character of the substrates, such as *p*-CF₃, *p*-CN, or *p*-NO₂ was possible, and corresponding bromonitromethylated products **4x-4ab** were obtained. A limitation regarding the protocol was observed for alkynes. A complex reaction mixture for **4ac** or no conversion was observed in the case of **4ad**. Moreover, this method could also be applied to the substrate class of conjugated dienes, accessing a 1,4-radical addition pattern in product **4ae** in 73% yield with an *E/Z* ratio of 61:39. The protocol was also suitable to convert α,β -unsaturated Michael systems, usually challenging for the addition of electrophilic radicals^[19,21] in moderate to good yields (Scheme 3B).



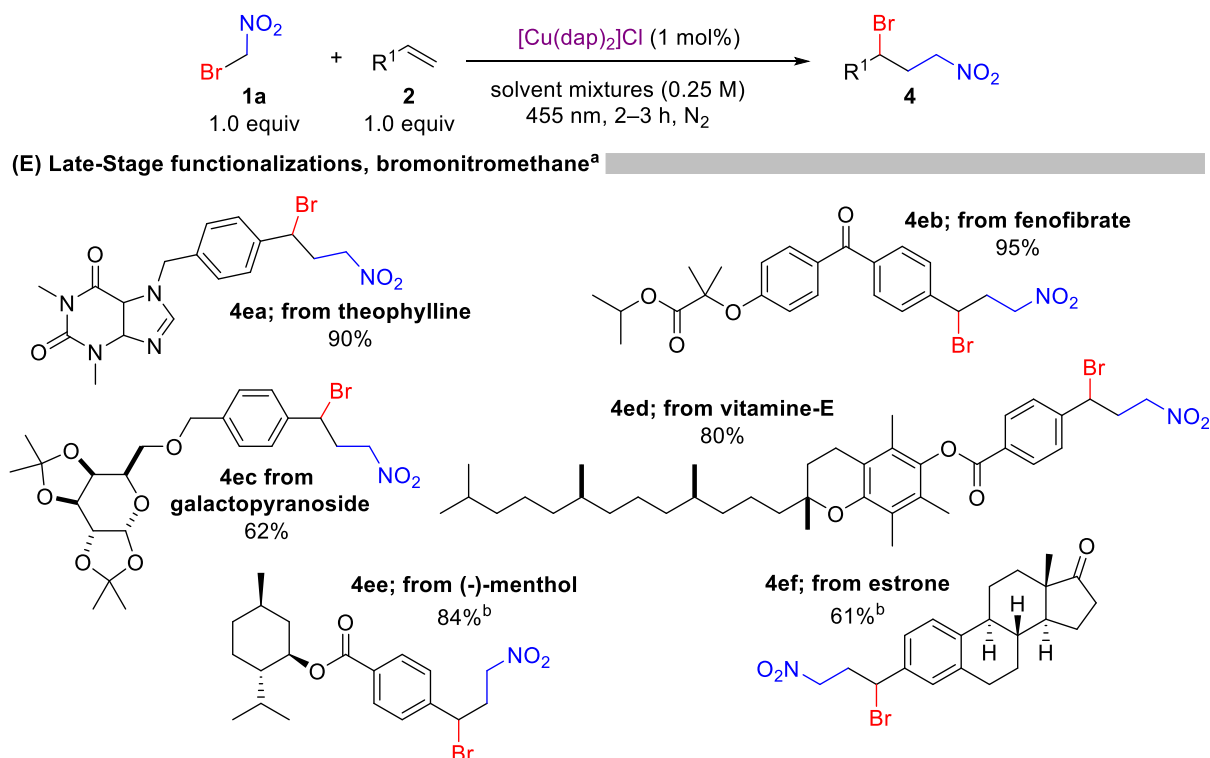
Scheme 3. Substrate Scope of activated olefins. ^aReaction conditions: 0.5 mmol scale in MeCN (degassed), irradiation at 455 nm under an atmosphere of N₂ for a given time at 25 °C. ^bPrepared by Magdalena Koch. ^cPrepared by Lea-Joy Großkopf. (Bachelor Thesis under supervision by Alexander Reichle). abbreviations as follows: crm = complex reaction mixture, nr = no reaction. Isolated yields are given unless otherwise stated.

Besides activated olefins, we were also interested in applying unactivated ones as suitable substrates (Scheme 4A). Indeed, various olefins with diverse functionalities, such as cyano-, epoxide-or aldehyde substituents, were well-tolerated, affording the desired products **4cf**, **4ci** and **4cj** in good to high yields. Boc-protected allylamine **4cm** was obtained in 81%, whereas Tosyl-protected derivative **4cn** was not accessible, stressing the importance of protecting groups for these substrates. We also explored other alkyl-substituted geminal bromonitroalkanes **1b–1e** (Scheme 4B). It was found that with increased alkyl-substitution, activated olefins can still be applied in this protocol, yielding the product in good to high yields, compared to iridium catalysis.^[8] However, the necessity of prolonged reaction times arises (for details, see chapter 5 experimental part). Notably, ATRA product **4do** derived from phenylbromonitromethane **1e** can be accessed via a photocatalytic process, in contrast to the thermal process mediated by Cu(OH)₂, which leads to the formation of the corresponding isoxazoline-*N*-oxide **3**.^[7]



Scheme 4. Substrate Scope of unactivated olefins and bromonitromethane derivatives. ^aReaction conditions: 0.5 mmol scale in MeCN (degassed), irradiation at 455 nm under an atmosphere of N₂ for a given time at 25 °C. ^bPrepared by Magdalena Koch. Abbreviations are as follows: crm = complex reaction mixture, nr = no reaction. ^cNMR yield using 1,3,5-trimethoxybenzene as the internal standard. Isolated yields are given unless otherwise stated.

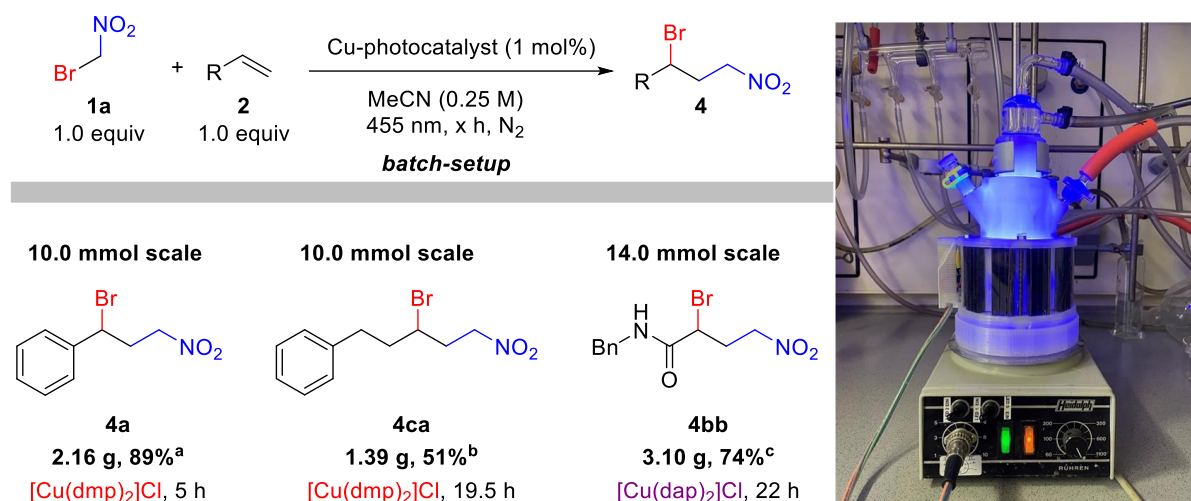
Moreover, we investigated the late-stage functionalization of more complex, biologically active molecules (Scheme 5). Due to solubility issues, solvent mixtures of MeCN/DCM and CDCl_3 were applied. Gratifyingly, theophylline- and fenofibrate derivatives delivered the corresponding 1,3-functionalized products in excellent yields, highlighting the benefit of the developed protocol in a multistep synthesis of complex molecules. Galactopyranoside derivative **2ec**, vitamin E derivative **2ed** and estrone-derived substrate **2ef** were diastereoselectively transformed to the desired products **4ec–4ef** in good to high yield.



Scheme 5. Substrate Scope for Late-Stage functionalization. ^aReaction conditions: 0.5 mmol scale in the solvent mixtures (MeCN/DCM/ CHCl_3 ; see experimental part for synthetic details) (degassed); irradiation at 455 nm under an atmosphere of N_2 for a given time at 25 °C. ^bPrepared by Lea-Joy Großkopf (Bachelor Thesis under supervision by Alexander Reichle). Isolated yields are given.

3.5 Upscaling and Synthetic Utility

After successful optimization and substrate scope investigation, we tested the protocol for synthetic utility. Increasing the scale by a factor of 20 and using environmentally benign and cheap complex $[\text{Cu}(\text{dmp})_2]\text{Cl}$, the bromonitromethylation product **4a** was obtained in multigram amounts with a yield of 89% in a simple batch setup with a slightly prolonged reaction time (Scheme 6). Along with product **4a**, we performed upscaling with olefin **2ca** and **2bb** and obtained the corresponding products **4ca** and **4bb** in good to high yield.

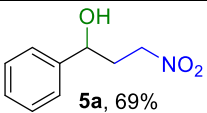
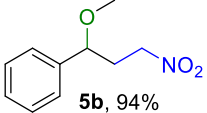
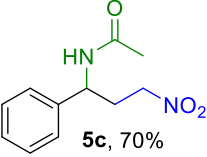
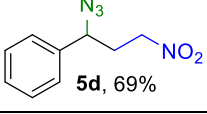
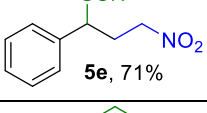
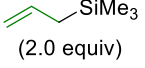
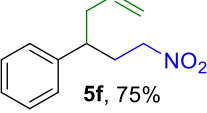
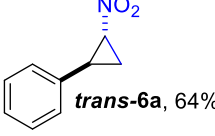
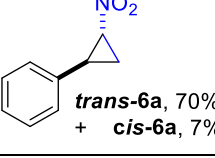
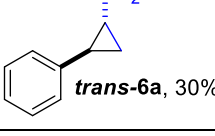


Scheme 6. Gram-scale functionalization of olefins. Standard conditions: olefin (**2**) (1.0 equiv), bromonitromethane (**1a**) (1.0 equiv) photocatalyst (1.0 mol%), in MeCN (anh., degassed, 0.25 M); Irradiation at indicated wavelength $\lambda = 455$ nm (blue LEDs) under N_2 atmosphere for given time at room temperature (25°C). ^aPrepared by Magdalena Koch. ^bPrepared by Lea-Joy Großkopf (Bachelor Thesis under supervision by Alexander Reichle) ^cPrepared by Johannes Floß.

3.5.1 Nucleophilic Substitutions and Eliminations

Benzylic halides are valuable intermediates in organic synthesis. Therefore, we were interested in finding out how the synthesized benzylic bromide could be applied in various transformations. Different nucleophiles could be successfully introduced, giving access to new 1,3-difunctionalized nitro compounds (*vide infra*, Table 3). Substitution with oxygen-based nucleophiles accesses 1,3-nitroalcohol **5a** (entry 1), which can be further converted to the corresponding 1,3-aminoalcohol, according to another literature report.^[22] Nitroether **5b** can be accessed with high yield utilizing MeOH as nucleophile (entry 2). No reaction was observable under the same conditions with phenol as a nucleophile (entry 3). With nitrogen-based nucleophiles, we could observe the formation of 1,3-aminonitro compounds **5c** and **5d** (entries 4–5) in good yield. A sulfur-based nucleophile 1,3-nitrothio-product **5e** was readily obtained (entry 6). As for a carbon-based nucleophile, we appreciated that adding an allyl silane in the presence of iron chloride gave us substituted nitroolefin **5f** in good yield (entry 7). Applying NaCN as a nucleophile, nitrocyclopropane *trans*-**6a** was isolated, which is also formed in the presence of 1,8-diazabicyclo[5.4.0]undec-7-ene (DBU) as base (entries 8–9). This could be explained by the fact that NaCN and DBU act both as a base rather than a nucleophile by deprotonating the methyl group and thus allowing intramolecular reaction prior to intermolecular reaction. Aiming towards a synthesis of a β -nitro ketone, according to a literature report,^[23] nitrocyclopropane *trans*-**6a** was again observed, although in low yield (entry 10). Considering the benzylic bromide pattern for Grignard-type reactivity to access deuteration or arylation^[24] showed no reactivity or resulted in a complex reaction mixture (entries 11–12).

Table 3. Nucleophilic substitutions and eliminations for compound **4a**.

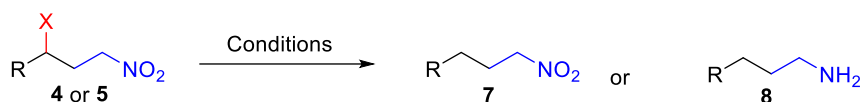
Entry	Reagent X	Conditions	Yield ^g
1 ^a	H ₂ O (solvent)	acetone/ H ₂ O (1:1) reflux, 2 h	 5a , 69%
2 ^a	MeOH (solvent)	MeOH, 65 °C, 2 h	 5b , 94%
3	PhOH (1.2 equiv)	MeCN, reflux, 24h	nr
4 ^b	MeCN (solvent)	FeCl ₃ • 6 H ₂ O, (4.0 equiv), MeCN, 80 °C, 2 h	 5c , 70%
5 ^a	NaN ₃ (5.0 equiv)	DMF, 2 h, rt	 5d , 69%
6 ^a	NaSCN (5.0 equiv)	DMF, rt, 2 h	 5e , 71%
7 ^b	 (2.0 equiv)	FeCl ₃ (5.0 mol%), DCM, rt, 2 h	 5f , 75%
8	NaCN (5.0 equiv)	DMF, rt, 2 h	 trans-6a , 64%
9 ^c	DBU (2.0 equiv)	THF, rt, 30 min	 trans-6a , 70% + cis-6a , 7%
10 ^d	pyridine- <i>N</i> -oxide (1.0 equiv)	AgO (0.5 equiv), MeCN, rt, 17 h	 trans-6a , 30%
11 ^f	D ₂ O (workup solvent)	1,2-dibromoethane (0.01 equiv), Mg (1.05 equiv), THF, rt, 19 h	nr
12 ^{ef}	<i>p</i> -MeOPhMgBr (1.0 equiv)	THF, rt, 19 h	crm

Reaction conditions: reactions were conducted with 0.5 mmol of **4a** in the solvent under stated conditions. rt = room temperature = 25 °C, ^abased on Ref.^[25], ^bbased on Ref.^[26], ^cinspired by Ref.^[27] ^dbased on Ref.^[23], ^ebased on Ref.^[24], ^fconducted by Lea-Joy Großkopf (Bachelor Thesis under supervision by Alexander Reichle). nr = no reaction. ^gisolated yields are given. crm = complex reaction mixture.

3.5.2 Hydrogenation and Reduction

Subsequently, after investigating nucleophilic substitutions, we aimed to synthesize aliphatic nitro- or amino compounds using standard techniques, such as hydrogenation with Pd/C or the reduction with Zn in aqueous acetic acid (Table 4):

Table 4. Hydrogenation and Reduction reactions of selected bromonitroalkylated compounds.



Entry	Compound	Reaction conditions	Product
1 ^d		10 mol% Pd/ C, MeOH, rt, H ₂ (1013 mbar) 22 h	 7a, 99%
2 ^b		Zn (24.0 equiv), aq. AcOH, rt, 4 h	 8a, 72%
3 ^{bc}		10 mol% Pd/ C, EtOH, rt, 4 h	 8a, 86%
4 ^d		10 mol% Pd/ C, MeOH, rt, H ₂ (1013 mbar) 22 h	nr
5 ^e		10 mol% Pd/ C, MeOH, rt, H ₂ (1013 mbar) 22 h	crm
6		10 mol% Pd/ C, MeOH, rt, H ₂ (1013 mbar) 22 h	crm

Reaction conditions: reactions were performed on a 0.5 mmol scale for compound **4** or **5** (1.0 equiv) under given conditions at room temperature (25 °C). ^bprepared by Magdalena Koch on a 2.0 mmol scale. ^con a 1.0 mmol scale. Isolated yields are reported unless otherwise stated. ^dconducted by Lea-Joy Großkopf (Bachelor Thesis under supervision by Alexander Reichle). nr = no reaction. crm = complex reaction mixture. ^ecompound **5ca** prepared by Lea-Joy Großkopf (Bachelor thesis under supervision by Alexander Reichle).

We started our investigations with the hydrogenation of ATRA product **4a** in the presence of 10 mol% of Pd/C in MeOH at 1013 bar. After 22 h, aliphatic nitro compound **7a** was isolated in quantitative amounts (entry 1), which is otherwise not straightforwardly accessible.^[28] Next, the reduction of **4a** with Zn in acetic acid was investigated. To our delight, 72% of aliphatic amine **8a** was obtained (entry 2). Further, we noticed that hydrogenation of nitro cyclopropane **trans-6a** with palladium could also access the ring-opened amine **8a** in high yield (entry 3).

Reduction of the aliphatic ATRA product **4ca** with Pd/H₂ was not successful, and starting material was reisolated (entry 4). Aliphatic diamines are useful compounds,^[29] e.g., ligands for metal complexes. Unfortunately, our attempts to reduce azide derivatives **5ca** or **5d** with Pd/H₂ to access aliphatic diamines failed (entry 5–6), and a complex reaction mixture was observed. Further attempts aiming at this type of compounds are ongoing in our laboratory.

3.5.3 Nitro- and Aminocyclopropane Synthesis

Given the importance of amino cyclopropanes as a structural motif in several bioactive compounds,^[30] we investigated the formation of these synthetically valuable compounds (Table 5). Treatment of bromonitromethylated product **4a** with DBU as base leads to the formation of nitrocyclopropane **trans-6a**, which can be easily converted according to a literature report^[31] to well-known monoamine oxidase inhibitor tranylcypromine (**trans-9a**) (entry 1).^[32]

According to another literature report,^[33] histone demethylase LSD1 inhibitor **9k** can be accessed from nitrocyclopropane **6k** (entry 2). In the same way, ATRA product **4v** can be converted into an amino-cyclopropane building block,^[34] which is required to construct ticagrelor^[27] (**9v**), an important platelet aggregation inhibitor (entry 3).

To highlight the synthetic methodology for synthesizing nitrocyclopropanes, aliphatic ATRA product **4ca** and acrylamide derivative **4bb** were used to access nitrocyclopropanes **6bb** and **6ca** (entries 4–5). An attempt to reduce **6bb** to the corresponding aminocyclopropane building block using Zn in aqueous acetic acid failed, but ring opening was observed (entry 4). Estrone derivative **4ef** was utilized to synthesize the highly substituted nitrocyclopropane **6ef** in diastereoselective fashion (entry 6).

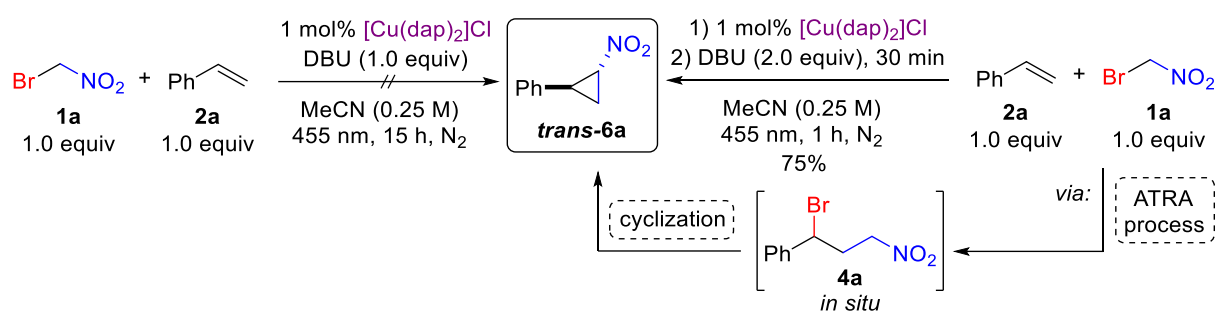
Contrary to our expectations, treatment of ATRA product **4da** with base under standard cyclization procedures resulted in isoxazoline-*N*-oxide **3da** as the major product, next to nitrocyclopropane **6da** as the minor in *trans* diastereoselective fashion (entry 7). This might be caused by the fact that after initial deprotonation, the negative charge was stabilized by the electron-withdrawing effect of the nitro-group towards the oxygen of the NO₂-group, which subsequently attacks the benzyl bromide to afford the isoxazoline-*N*-oxide product. In fact, this represents the more stable product, due to less ring strain effect, compared to the cyclopropane product.

Table 5. Cyclization of ATRA products and reported follow-up transformations.^a

Entry	ATRA product	Yield	Further (reported) transformations of 6	Ref.
1		 <i>trans-6a</i> , 70%	 <i>trans-9a</i>	[31]
2		 <i>trans-6k</i> , 62%	 <i>trans-9k</i>	[33]
3		 <i>trans-6v</i> accessible acc. to Ref.		[34]
4 ^b		 <i>trans-6bb</i> , 62%	 9bb , not isolated	-
5 ^c		 6ca , 72% <i>trans/cis</i> = 60/40	-	-
6		 <i>trans-6ef</i> , 67%	-	-
7		 <i>trans-6da</i> , 22%	 3da , 65%	-

^aReaction conditions: ATRA product **4** (0.5 mmol, 1.0 equiv), DBU (1.0 mmol, 2.0 equiv) in THF (0.25 M) stirred for 30 min at 25 °C. (reaction condition inspired from Ref.^[27]) ^bReaction condition for reduction of **6bb**: cyclopropane **6bb** (0.5 mmol, 1.0 equiv), Zn (2.5 mmol, 5.0 equiv.) in 50% aq. AcOH (3.0 mL); compound **9bb** was observed by Magdalena Koch but not isolated. ^ccyclopropane **6ca** prepared by Magdalena Koch on a 2.0 mmol scale.

After demonstrating the nitro cyclopropane syntheses starting from the isolated ATRA products, we investigated the issue of whether if having the base directly present in the photochemical process would lead to the cyclopropane product (Scheme 7). However, a complex reaction mixture was formed when DBU participated in the elaborated standard reaction conditions (the reaction mixture was followed *via* TLC and the time was increased because a significant product formation was not observable). As the presence of base is not possible in the photoreaction, we investigated if the base can be added in a one-pot fashion into the reaction mixture. Notably, a one-pot reaction sequence generated the corresponding nitro-cyclopropane **trans-6a** yielding 75% by applying DBU immediately after the photoreaction, followed by stirring for 30 minutes at room temperature.



Scheme 7. One-pot route to obtain nitro cyclopropane **trans-6a**.

3.6 Mechanistic Investigations

3.6.1 UV-vis Studies

An UV-vis investigation was conducted to obtain more insight into the photoreaction mechanism (Figure 1). Consequently, the absorption spectrum of the copper(I)-photocatalyst was measured. Every single component of the reaction mixture (bromonitromethane (**1a**) and styrene (**2a**)) was subsequently added, and the corresponding absorbance spectra were recorded. Given the copper(I)-photocatalyst's absorbance in the absence of a substrate, the blue part of the spectrum shows considerably higher absorbance. As can be seen from the recorded spectrum, if $[\text{Cu}^{\text{I}}(\text{dap})_2]\text{Cl}$ and bromonitromethane (**1a**) are mixed (blue line), the absorbance increases slightly in the absence of light, indicating an interaction between the ATRA reagent and the photocatalyst. This can be perceived as a precoordination of both components prior to single electron transfer (SET). If styrene (**2a**) is subsequently added to the reaction mixture, an increase in the absorbance along with a red shift (yellow line) is observed. After 1 h, the absorbance is even more red-shifted compared to the reaction mixture before irradiation (green line). The absorption spectrum of product **4a** (dark blue line) was measured to exclude any photoactive process of the product with light. It revealed no significant absorbance at the irradiated wavelength.

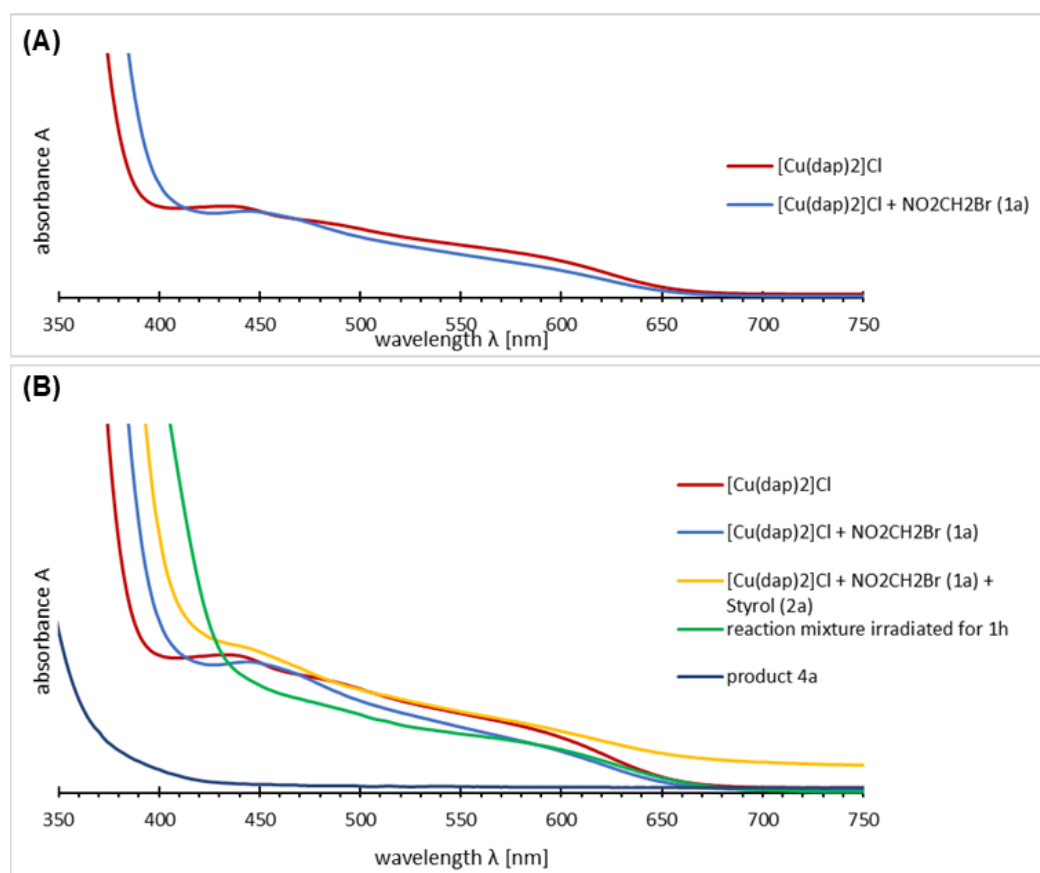


Figure 1. UV-Vis Investigations: (A) Comparison of absorbance of photocatalyst (red line) with a mixture of photocatalyst and bromonitromethane. (Blue line). (B) Addition of styrene (**2a**) (yellow line) and absorbance after irradiation (green line). ATRA product (**4a**) (dark blue line).

3.6.2 Stern-Volmer Interaction Analysis

We investigated whether the photocatalyst $[\text{Cu}^{\text{I}}(\text{dap})_2]\text{Cl}$ is interacting with the ATRA reagent bromonitromethane (**1a**) or styrene (**2a**). For this purpose, Stern-Volmer Analysis was employed. The technology allows the analysis of the kinetics of the photophysical intermolecular deactivation (fluorescence quenching) process. The presence of another chemical species can speed up the decay rate of the photocatalysts in their excited state if an interaction occurs. The fluorescence emission of the photocatalyst $[\text{Cu}^{\text{I}}(\text{dap})_2]\text{Cl}$ was measured in dry MeCN with varying concentrations of bromonitromethane as a quencher. As shown in Figure 2, increasing the concentration of bromonitromethane decreases the photocatalyst's fluorescence emission.

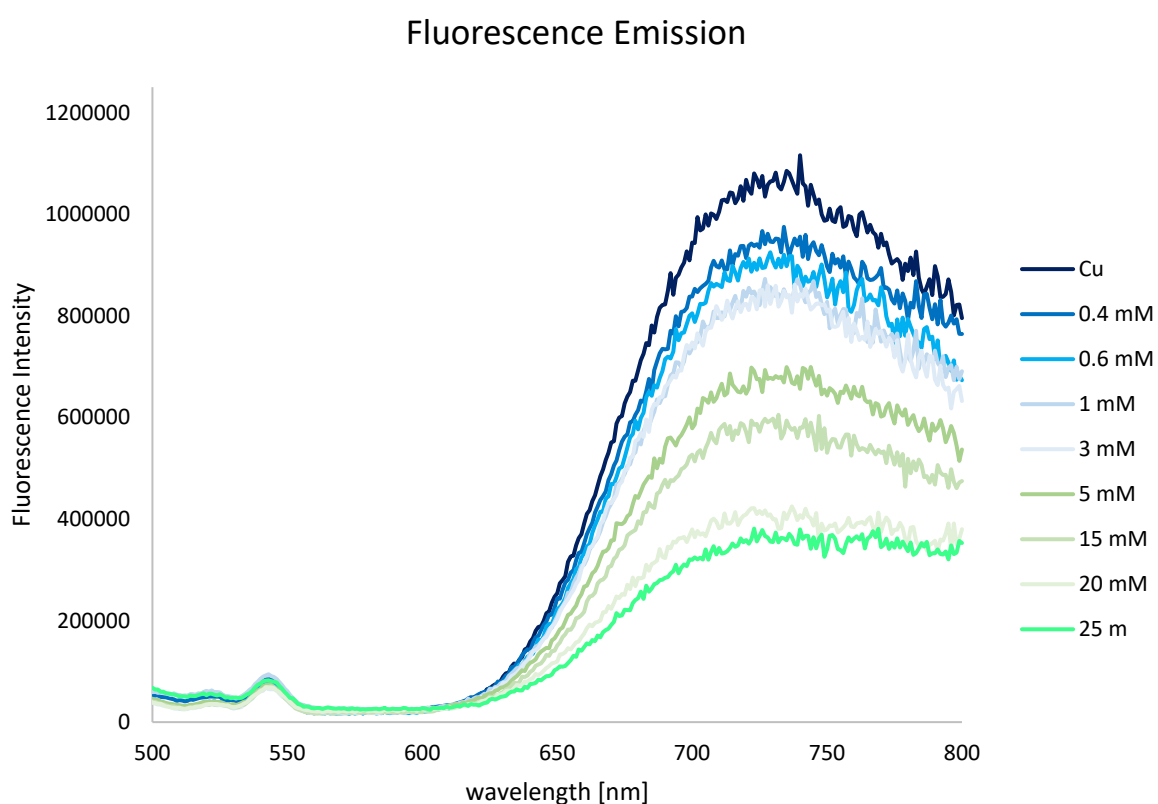


Figure 2. Fluorescence emission spectra of a 0.2 mM solution of $[\text{Cu}(\text{dap})_2]\text{Cl}$ in MeCN with varying concentrations of the quencher bromonitromethane (**1a**).

Besides bromonitromethane, styrene could also interact with the excited photocatalyst, thereby quenching it. To examine this type of interaction, fluorescence emission spectra of $[\text{Cu}^{\text{I}}(\text{dap})_2]\text{Cl}$ were recorded with varying concentrations of styrene in dry MeCN. Only in the presence of ATRA reagent bromonitromethane (**1a**) an interaction was observable by the decrease of the fluorescence signal, whereas in the presence of styrene, no decline was observable (Figure 3A).

In 2020, Daniel and co-workers reported Cu(I)-complexes of the type $[\text{Cu}^{\text{I}}(\text{L})_2]\text{X}$ (L = alkyl-substituted phenanthroline-derived ligand), which rapidly undergo ligand exchange in the presence of MeCN as solvent.^[35]

We performed additional quenching experiments to exclude this interaction for $[\text{Cu}^{\text{I}}(\text{dap})_2]\text{Cl}$ as a photocatalyst. The fluorescence emission of $[\text{Cu}^{\text{I}}(\text{dap})_2]\text{Cl}$ in dry DCM was recorded, and varying amounts of MeCN as possible quenching reagent were added. Figure 3B shows no quenching occurred with MeCN as a possible quenching partner.

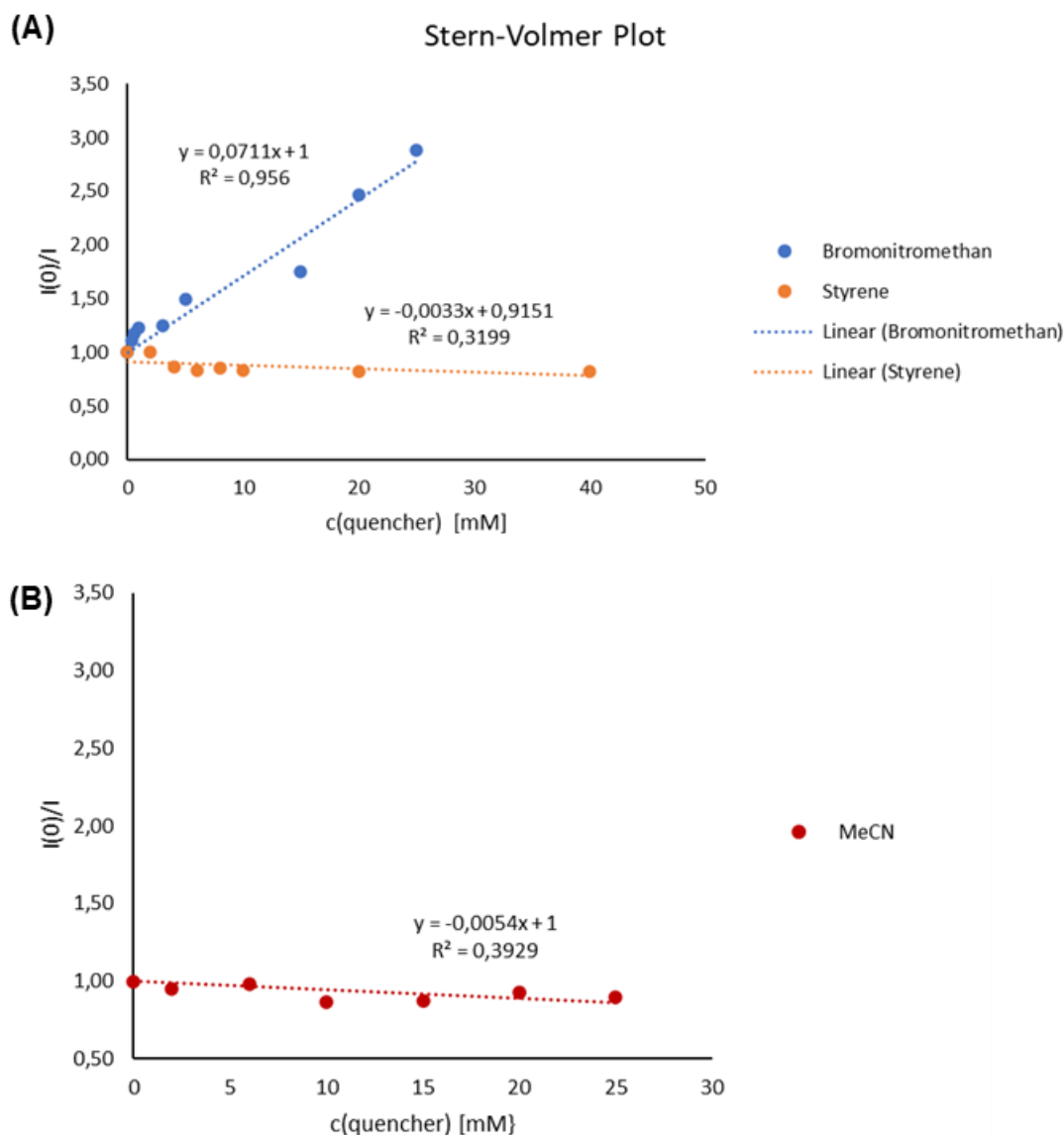
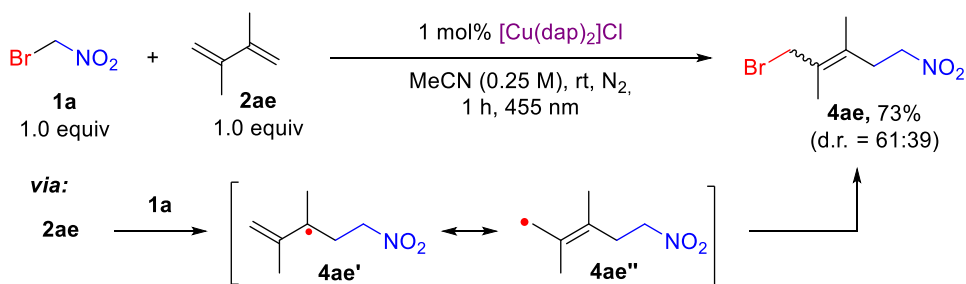


Figure 3. (A) Stern-Volmer plot for $[\text{Cu}^{\text{I}}(\text{dap})_2]\text{Cl}$ and the ATRA reagent bromonitromethane (**1a**) (blue line) and for $[\text{Cu}^{\text{I}}(\text{dap})_2]\text{Cl}$ and styrene (**2a**) in dry MeCN. Quenching experiments of $[\text{Cu}^{\text{I}}(\text{dap})_2]\text{Cl}$ and styrene were performed by Magdalena Koch. (B) Stern-Volmer plot for $[\text{Cu}^{\text{I}}(\text{dap})_2]\text{Cl}$ and MeCN (red line) recorded in dry DCM.

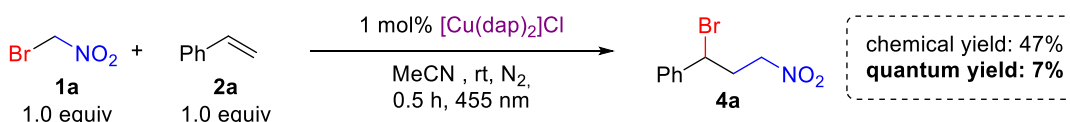
3.6.3 Investigation on Radical Character/ Determination of the Quantum Yield

The following experiments were conducted to get further mechanistic insight into the radical character of the photoreaction. Performing the title reaction on diene **2ae** led to the formation of product **4ae** with exclusive 1,4-selectivity occasioned by the resonance of radical intermediate **4ae'**, resulting in the higher substituted double bond (Scheme 8) This result further confirms the radical nature of the title reaction.

(A) 1,4-Selectivity on dienes



(B) Determination of the Quantum Yield



Scheme 8. Additional mechanistic Investigations on the Cu(I)-photocatalyzed bromonitromethylation of olefins. For detailed reaction conditions, see experimental part.

Additionally, the efficiency of the photoabsorption can give important indications regarding the nature of a radical process of a photoreaction, e.g. a radical chain process. Hence, we measured the quantum yield of the Cu(I)-photocatalyzed bromonitromethylation. The quantum yield was found to be 7%, whereas the chemical yield was determined to be 47%. This suggests that a photoinitiated radical chain process can be excluded, typically displaying values greater than 100%. Nevertheless, such interpretations should be considered with great caution, as they do not consider the participation of other photoinitiated shorter chain events or processes that do not result in the formation of the ATRA product.

3.6.4 Investigations on the Homolysis of $[\text{Cu}^{\text{I}}(\text{dap})_2]\text{Cl}$

An irradiation experiment was carried out to get a deeper insight into the activation of the ATRA reagent bromonitromethane by the photocatalyst $[\text{Cu}^{\text{I}}(\text{dap})_2]\text{Cl}$. Therefore, a solution of bromonitromethane (**1a**) in excess (1.25 mmol, 250.0 equiv) in MeCN and $[\text{Cu}^{\text{I}}(\text{dap})_2]\text{Cl}$ (5.0 μmol , 1.0 equiv) was irradiated under a nitrogen atmosphere for 1 h with blue LED (455 nm). The prior red solution changed upon irradiation to bright green. After 5 days, single crystals suitable for X-ray analysis were obtained, showing the molecular structure of $[\text{Cu}^{\text{II}}(\text{dap})\text{BrCl}]$ (**10**) (Figure 5).

The experiment shows that upon irradiation, dissociating one dap ligand from the copper center leads to a vacant coordination side on the catalyst. The coordination side is occupied by bromine anions, as seen in the X-ray structure. Hence, it was shown that upon irradiation, a SET step in the presence of the ATRA reagent bromonitromethane and ligand homolysis of $[\text{Cu}^{\text{I}}(\text{dap})_2]\text{Cl}$ occur.

Crystallization of $[\text{Cu}^{\text{II}}(\text{dap})\text{BrCl}]$

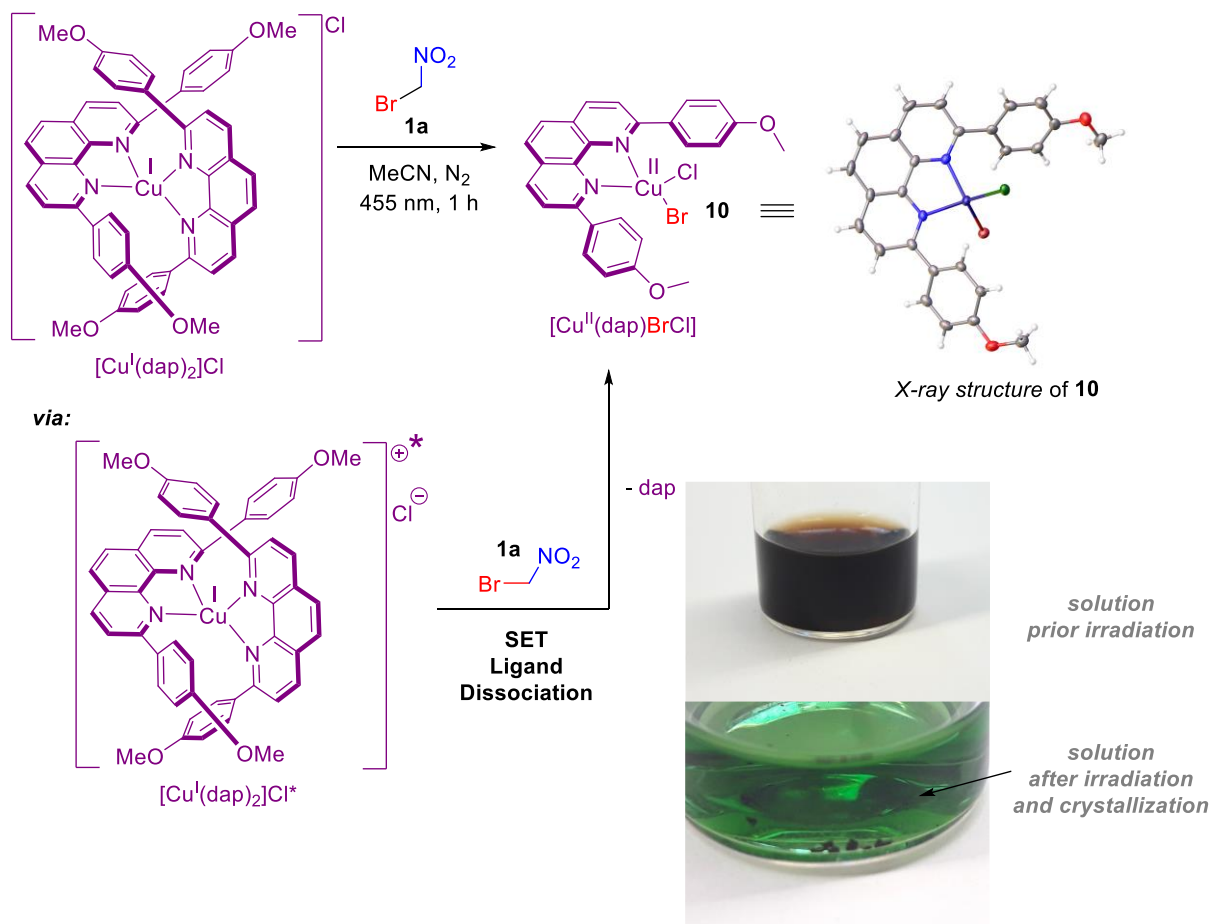


Figure 4. Irradiation Experiment of the photocatalyst $[\text{Cu}^{\text{I}}(\text{dap})_2]\text{Cl}$ in presence of bromonitromethane (1a).

A corresponding control experiment (*vide infra*, Figure 5) by irradiating the Cu(I)-complex in the absence of any substrate showed no ligand dissociation, proving the photostability of the photocatalyst *via* $^1\text{H-NMR}$ analysis.

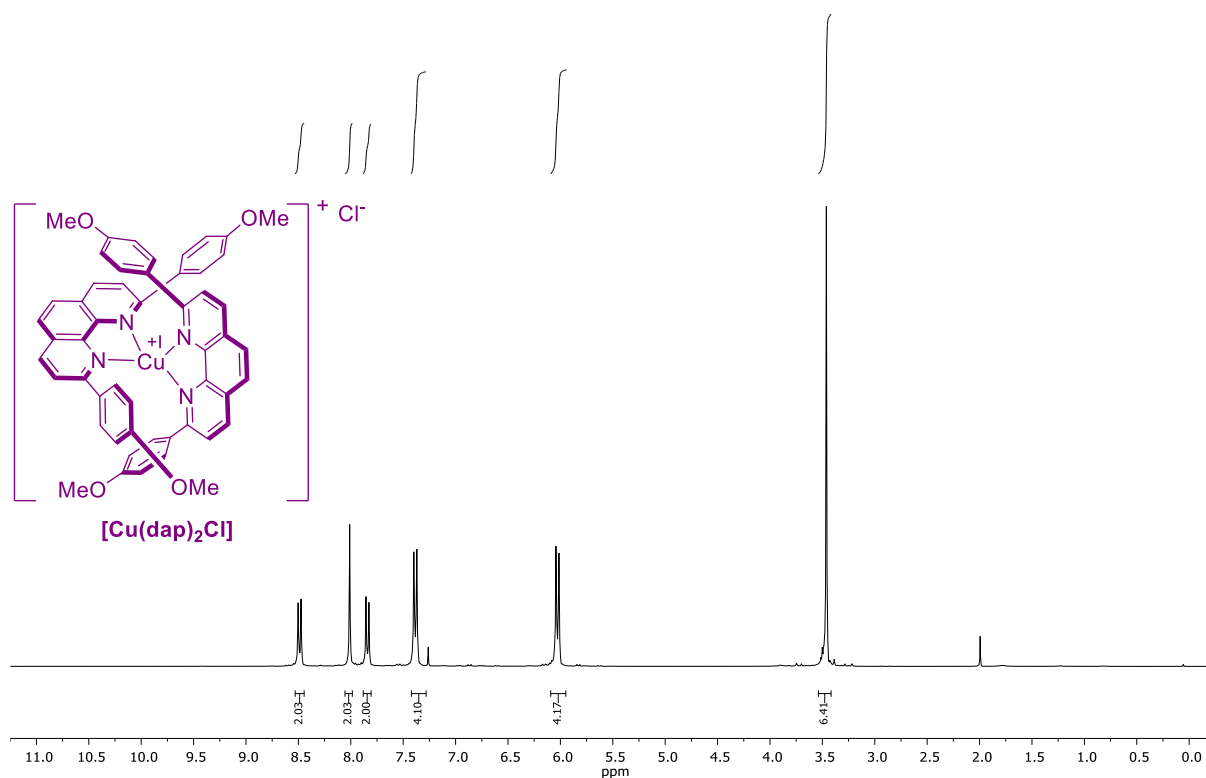


Figure 5. Crude $^1\text{H-NMR}$ of the photocatalyst $[\text{Cu}^{\text{I}}(\text{dap})_2]\text{Cl}$ (0.375 mmol) in dry MeCN (3.0 mL, 0.125 M) after an irradiation period of 3 h showed no dap ligand homolysis (no free dap ligand was detected).

3.6.5 Experiments on Product Formation with different Bromonitroalkanes

Ooi and coworkers reported a correlation between the formation of ATRA product compared to the formation of the isoxazoline-*N*-oxide depending on the oxidation potential of the oxidized photocatalyst species, as already stated in Chapter 3.1 Introduction and Outline of the Study.^[8] According to their observations, ATRA product from benzylbromonitromethane (**1d**) with styrene would only be obtained if the oxidized photocatalyst species after single electron transfer (SET) would show an oxidation potential equal or higher 1.0 V. Addition of a photocatalyst which shows a lower oxidation potential of its oxidized species would result in the formation of the isoxazoline-*N*-oxide. $[\text{Cu}^{\text{I}}(\text{dap})_2]\text{Cl}$ shows an oxidation potential of + 0.62 V of its oxidized ground state species,^[5] applying Ooi's correlation, it should thereby not form the ATRA product but instead, lead to the formation of isoxazoline-*N*-oxide. Nevertheless, we obtained only ATRA product using bromonitroalkane (**1a**) with styrene. Thus, we questioned how these seemingly contradicting results could be explained. Consequently, the type of product under photocatalytic conditions (isoxazoline-*N*-oxide **3** vs. ATRA product **4**) for three different bromonitroalkanes in combination with styrene (**2a**) as olefin was investigated concerning the photocatalysts (Table 6):

Table 6. Investigations on the product in comparison with the conditions reported by Ooi.^a

Entry	Catalyst	$E_{1/2}(\text{PC}^{n+1} / \text{PC}^n)$ [V] vs. SCE	Additive (1.0 equiv)	ATRA Reagent	Yield ^b 3 (%)	Yield ^b 4 (%)
1	[Cu ^I (dap) ₂]Cl	+0.62	-		0	99
2	<i>fac</i> -Ir(ppy) ₃	+0.78	-		0	44
3	[Cu ^I (dap) ₂]Cl	+0.62	Collidine		traces	82
4	<i>fac</i> Ir(ppy) ₃	+0.78	Collidine	1d	62 (40 ^e)	13 (18 ^e)
5	[Cu ^I (dap) ₂]Cl	+0.62	-		0	88 ^{df}
6	<i>fac</i> Ir(ppy) ₃	+0.78	-		7	31
7	[Cu ^I (dap) ₂]Cl	+0.62	Collidine		0	90 ^f
8	<i>fac</i> Ir(ppy) ₃	+0.78	Collidine	1b	57	traces
9	[Cu ^I (dap) ₂]Cl	+0.62	-		0	90 ^{df}
10	<i>fac</i> Ir(ppy) ₃	+0.78	-		0	40
11	[Cu ^I (dap) ₂]Cl	+0.62	Collidine		0	66 ^{cf}
12	<i>fac</i> Ir(ppy) ₃	+0.78	Collidine	1a	0	nd

^aStandard conditions: bromonitromethane (**1a**) (0.25 mmol, 1.0 equiv), styrene (**2a**) (0.25 mmol, 1.0 equiv), photocatalyst (2.5 μmol, 1 mol%), in MeCN (anh., degassed, 1.0 mL, 0.25 M); Irradiation at indicated wavelength λ under N₂ atmosphere for given time at room temperature (25 °C). ^bNMR yield using 1,1,2,2-tetrachloroethane as internal standard. ^cReaction stopped after 2h. ^disolated yield. ^eYield reported by Ooi and co-workers.^[8] ^fexperiment carried out by Magdalena Koch. nd = not detected.

It was found that for all bromonitroalkanes in combination with styrene, only the ATRA product was observable in high yield if [Cu^I(dap)₂]Cl was employed as a photocatalyst (entries 1, 5 and 9). Utilizing collidine (1.0 equiv) as an additive, as reported by Ooi and coworkers,^[8] again gave only traces of cyclization products **3** and high amounts of ATRA products **4** (entries 3, 7, 11). On the other hand, if low-oxidizing *fac*-Ir(ppy)₃ was utilized as photocatalyst according to the reported reaction conditions of Ooi and co-workers^[8] (1.0 equiv of collidine as additive), the ATRA products **4** were not observable, but the isoxazoline-*N*-oxide products **3** (entries 4 and 8).

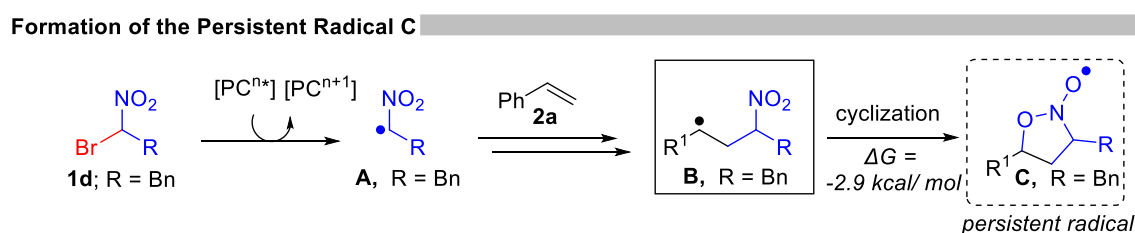
For bromonitromethane (**1a**) in combination with styrene, no product **3a** was observed under the catalysis of Ir(ppy)₃ and the presence of collidine (entry 12). A reasonable explanation might be given through investigations of Tartakovsky and co-workers, who reported the instability of the corresponding unsubstituted isoxazoline-*N*-oxide **3a**.^[36] On the other hand, if the photoreactions were performed in the absence of collidine as an additive with low-oxidizing *fac*-Ir(ppy)₃, the ATRA products **4** were observed, but with low yield (entries 2, 6 and 10).

In summary, the divergence in the type of product formation, as reported for the Ir-catalyzed photoreaction, cannot be transferred to the Cu-photocatalyst. These observations indicate that the Cu-photocatalyst must, in fact, catalyze the photoreaction from a mechanistic point of view differently than the photocatalyst based on iridium,^[8] e.g. through an inner-sphere type mechanism^[5] (*vide* chapter 3.1).

3.6.6 EPR Studies

With our collaboration partner, the Rehbein group, EPR (electron paramagnetic resonance) experiments were conducted to acquire insight into the mechanistic divergences between Cu(II)- and Ir(IV)-catalysis. Please take note that while we prepared the relevant reaction solutions for EPR measurements (in collaboration with Magdalena Koch), the Rehbein group conducted, analyzed, and interpreted the EPR measurements. Therefore, a plausible mechanistic picture was obtained for the Cu(I)-photocatalyzed bromonitroalkylation, contrasting Ir(IV)-catalysis. This chapter on EPR Studies is shown here for the sake of completeness.

By using CW-EPR spectroscopy (X-band), additional mechanistic details on the postulated key steps and intermediates under the Cu(I) catalysis were investigated in direct comparison to Ooi's Ir(III)-catalysis. Particular attention was paid to the experimental identification of the postulated persistent radical **C** (R = Bn), which Ooi *et al.* predicted based on DFT calculations (Scheme 9).^[8]



Scheme 9. Persistent Radical **C**, as predicted by Ooi and co-workers.^[8]

The opposing product selectivity of the Cu- vs. Ir(ppy)₃-catalysis was found to be closely linked to the presence (Ir) or absence (Cu) of the radical **C** based on the redox potentials of the different catalysts and the unique ability of copper for ligand exchange. In fact, the formation of an organic radical ($g_{\text{iso}} = 2.006$) was observed if Ir(ppy)₃ was utilized as a photocatalyst (Figure 6). The detected typical triplet signature of a nitrogen-centered radical with a g -value of 2.006 and a_N of 1.4 mT exhibited comparable parameters to TEMPO ($a_N = 1.6 \text{ mT}$) and related nitronic ester radicals.^[37]

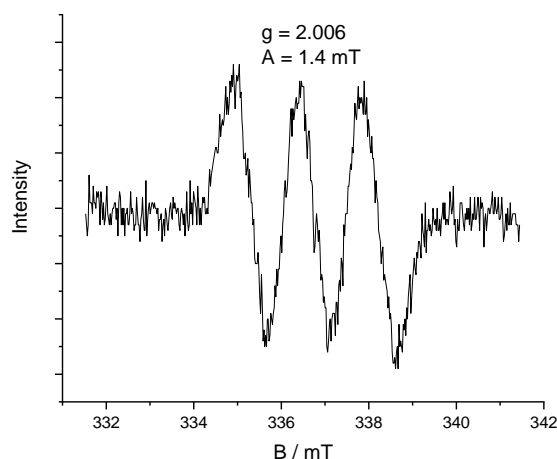


Figure 6. EPR Spectra of Ir(ppy)₃ (5 μmol, 1 mol%), bromonitromethane (**1a**) (0.5 mmol, 1 equiv) and styrene (**2a**) (0.5 mmol, 1 equiv) in MeCN (2 mL); Frequency: 0.4570 GHz; Modulation amplitude: 0.7 mT; MW attenuation: 10 dB; Gain: 10; Time constant: 0 s; B₀-field: 337 mT; B₀-sweep: 10 mT; Average of 5 runs. (Measurements were carried out by the Rehbein group and the shown graphics were kindly provided by them).

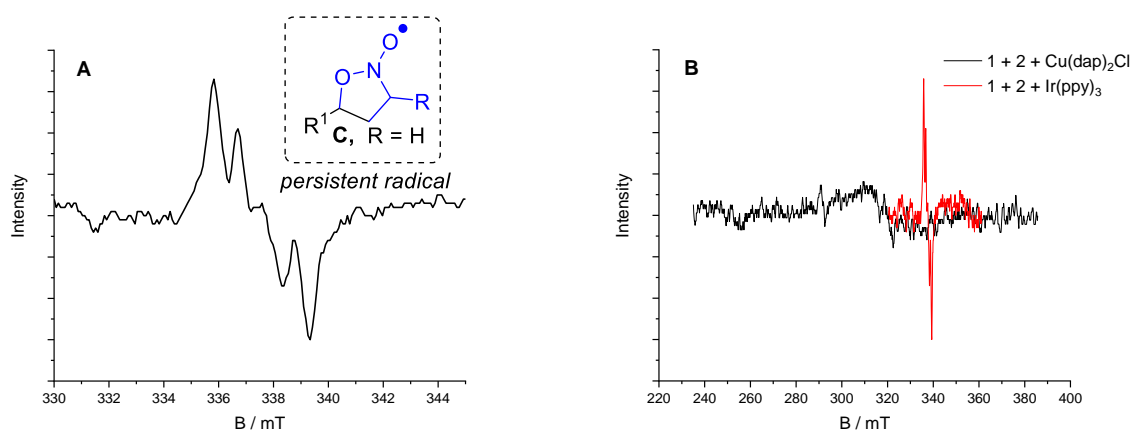


Figure 7. EPR spectra of photocatalyst (5 μmol, 1 mol%), bromonitromethane (**1a**) (0.5 mmol, 1 equiv) and styrene (**2a**) (0.5 mmol, 1 equiv) in MeCN (2 mL); Frequency: 0.4577 GHz; Modulation amplitude: 0.7 mT; MW attenuation: 10 dB; Gain: 10; Time constant: 1 s; Average of 3 runs; A) Photocatalyst: Ir(ppy)₃; 60 min irradiation at 455 nm; B₀-field: 340 mT; B₀-sweep: 40 mT; B) Comparison between photocatalyst [Cu^I(dap)₂]Cl (B₀-field: 310 mT; B₀-sweep: 150 mT) and Ir(ppy)₃ after irradiation at 455 nm. (Measurements were carried out by the Rehbein group and the shown graphics were kindly provided by them).

The acyclic carbon-centered radical **B** was ruled out to cause this signal based on the EPR signal's triplet signature. Additionally, the radical **A** generated by mesolytic cleavage of the carbon-bromine bond of the radical anion of **1** was also excluded for the following three reasons: the different splitting pattern, its expected short lifetime, as well as the fact that the recorded EPR signals showed in Figure 6–9 only arose in the presence of styrene (**2a**). The anisotropy in the hyperfine splitting and *g*-values and the coupling to the H-atoms of the nitronic-ester radicals could be partially resolved by increasing the time constant (*vide* Figure 7–9A).

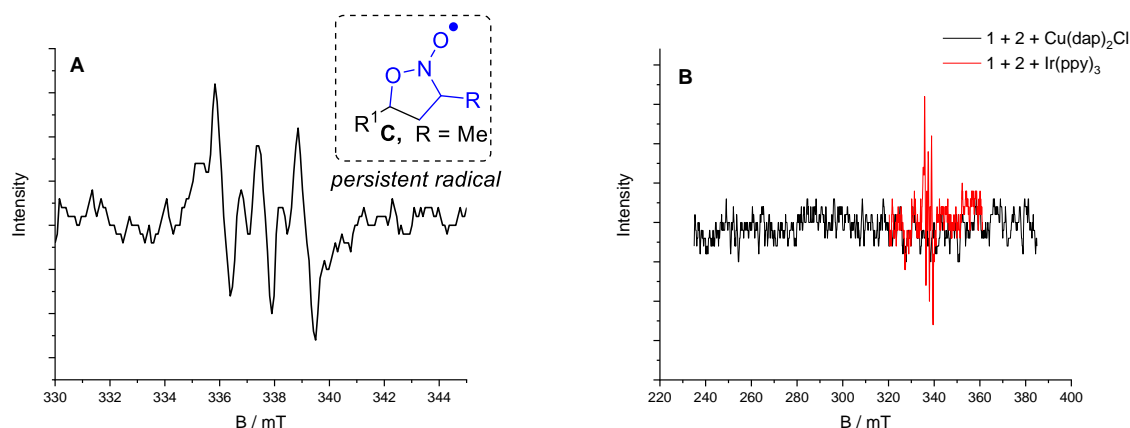


Figure 8. EPR spectra of photocatalyst (5 μmol , 1 mol%), bromonitroethane (**1b**) (0.5 mmol, 1 equiv) and styrene (**2a**) (0.5 mmol, 1 equiv) in MeCN (2 mL); Frequency: 0.4568 GHz; Modulation amplitude: 0.7 mT; MW attenuation: 10 dB; Gain: 10; Time constant: 1 s; Average of 3 runs; A) Photocatalyst: Ir(ppy)₃: 30 min irradiation at 455 nm; B₀-field: 340 mT; B₀-sweep: 40 mT; B) Comparison between Photocatalyst [Cu^I(dap)₂]Cl (B₀-field: 310 mT; B₀-sweep: 150 mT) and Ir(ppy)₃ after irradiation at 455 nm. (Measurements were carried out by the Rehbein group and the shown graphics were kindly provided by them).

The observed radical signature in the Ir-catalyzed reaction could not be detected when [Cu(dap)₂]Cl was used as the photocatalyst (Figure 7B, 8B and 9B). It was demonstrated that an emerging Cu(II)-signal does not overlap with the organic radical signal (Figure 9B).

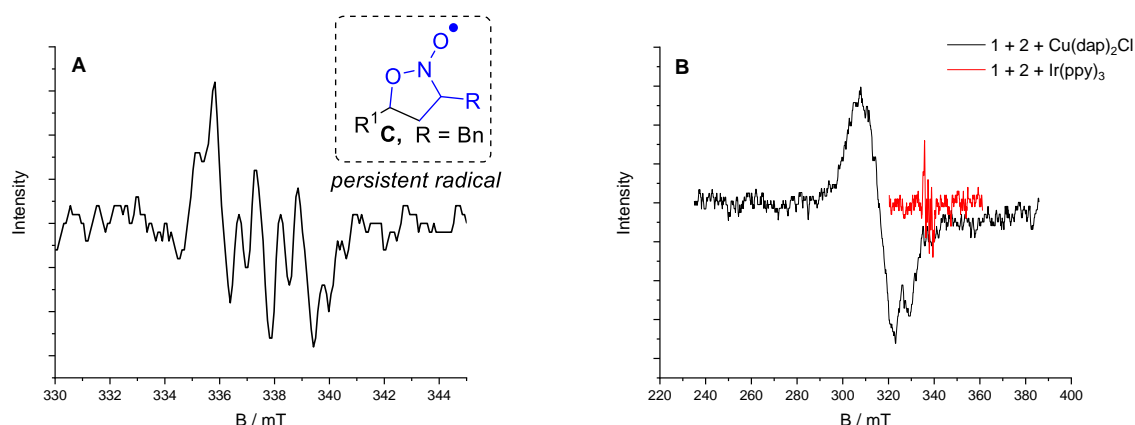


Figure 9. EPR spectra of photocatalyst (5 μmol , 1 mol%), bromonitrobenzylmethane (**1d**) (0.5 mmol, 1 equiv) and styrene (**2a**) (0.5 mmol, 1 equiv) in MeCN (2 mL); Frequency: 0.4569 GHz; Modulation amplitude: 0.7 mT; MW attenuation: 10 dB; Gain: 10; Time constant: 1 s, average of 3 runs; A) Photocatalyst: Ir(ppy)₃: 60 min irradiation at 455 nm; B₀-field: 340 mT; B₀-sweep: 40 mT; B) Comparison between photocatalyst [Cu^I(dap)₂]Cl (B₀-field: 310 mT; B₀-sweep: 150 mT) and Ir(ppy)₃ after irradiation at 455 nm. (Measurements were carried out by the Rehbein group and the shown graphics were kindly provided by them).

Moreover, the radical signature ($g = 2.006$) only appears in the presence of both ATRA reagent and styrene in the Ir-catalyzed reaction and grows over a period of at least 15 min (Figure 10).

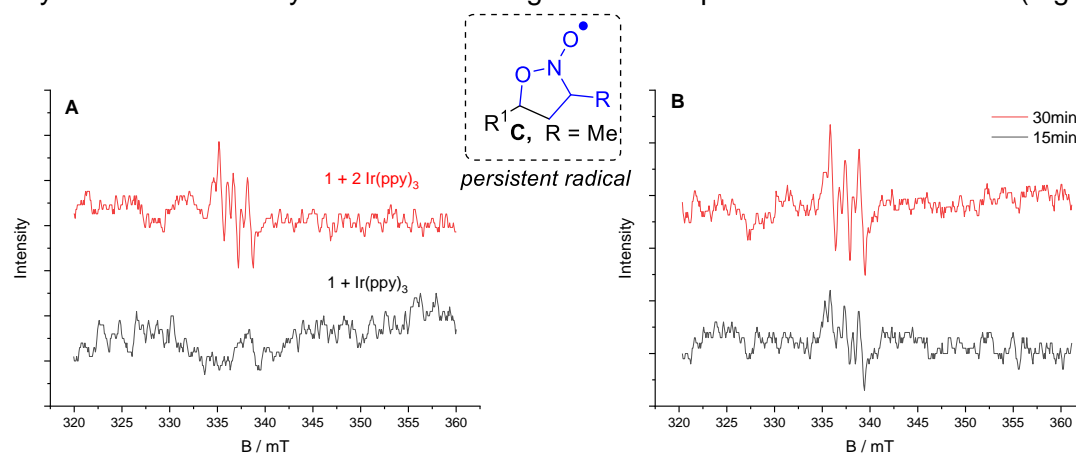


Figure 10. EPR spectra of $\text{Ir}(\text{ppy})_3$ ($5 \mu\text{mol}$, 1 mol%), bromonitroethane (**1b**) (0.5 mmol , 1 equiv) and styrene (**2a**) (0.5 mmol , 1 equiv) in MeCN (2 mL); Frequency: 0.4568 GHz ; Modulation amplitude: 0.7 mT ; MW attenuation: 10 dB ; Gain: 10; Time constant: 1 s; B0-field: 340 mT ; B0-sweep; Average of 3 runs; A) Comparison of the spectra with (red line) and without styrene (**2a**) (black line) after 45 min irradiation at 455 nm . B) Signal growth from 15 to 30 min irradiation at 455 nm . (Measurements were carried out by the Rehbein group and the shown graphics were kindly provided by them).

Next, the binary mixture of $[\text{Cu}^{\text{I}}(\text{dap})_2]\text{Cl}$ and bromonitroethane (**1b**) was measured in stoichiometric amounts to further clarify the formation of a Cu(II) species in the $[\text{Cu}^{\text{I}}(\text{dap})_2]\text{Cl}$ catalyzed process. The equimolar mixture displayed a well-resolved Cu(II) signal (Figure 11), indicating the ligands' octahedral coordination and axial elongation. Even low catalyst loadings, using only 10 mol% of the Cu-catalyst, still generate a signal, indicating the formation of Cu(II). Styrene (**2a**) addition immediately reduces signal intensity while leaving the signal pattern unchanged.

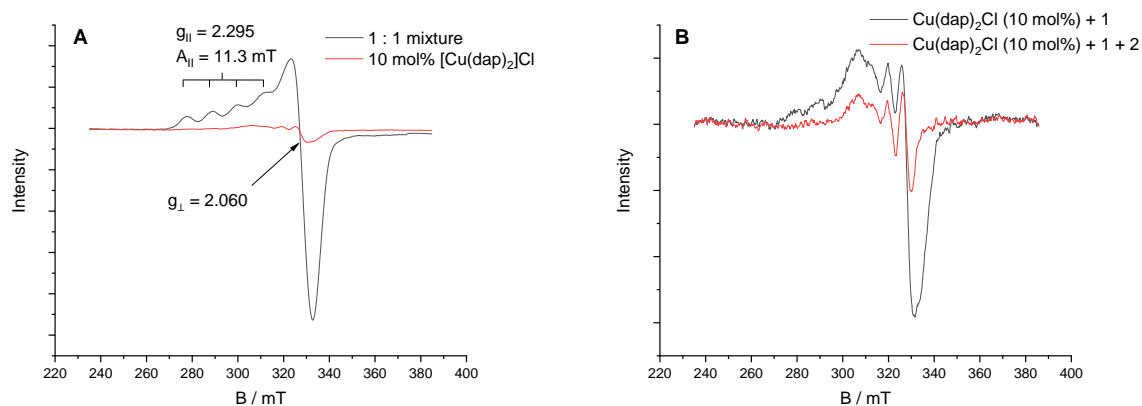


Figure 11. EPR spectra of A) $[\text{Cu}(\text{dap})_2]\text{Cl}$ ($50 \mu\text{mol}$, 1 equiv), bromonitroethane (**1b**) ($50 \mu\text{mol}$, 1 equiv) (black line) and $[\text{Cu}(\text{dap})_2]\text{Cl}$ ($50 \mu\text{mol}$, 10 mol%), bromonitroethane (**1b**) (0.5 mmol , 1 equiv) (red line) in MeCN (2 mL); B) Addition of styrene (**2a**) (0.5 mmol , 1 equiv) to a mixture of $[\text{Cu}(\text{dap})_2]\text{Cl}$ ($50 \mu\text{mol}$, 10 mol%), bromonitroethane (**1b**) (0.5 mmol , 1 equiv) in MeCN (2 mL); Frequency: 0.4575 GHz ; Modulation amplitude: 0.7 mT ; MW attenuation: 10 dB ; Gain: 10; Time constant: 1 s; B0-field: 340 mT ; B0-sweep; Average of 3 runs. (Measurements were carried out by the Rehbein group and the shown graphics were kindly provided by them).

A quick turnover of radical **C** in the presence of Cu(II) may be another explanation for the absence of the radical signature of **C** in the EPR under Cu(I) catalysis. To verify this, $[\text{Cu}^{\text{II}}(\text{dap})\text{Cl}_2]$ (1 mol%) was added to the reaction solution after a nitronic ester radical had been generated *in situ* via Ir-catalysis (*vide* Figure 12).

The reaction solution was monitored for 50 minutes. In the presence of Cu(II), a weaker signal intensity or even a total bleach of the nitronic ester radical signal would have suggested that the radical had been consumed, either by oxidation to **D** (*vide* chapter 3.7 chapter proposed reaction mechanism) or at the very least by binding of the radical. However, after the addition of $[\text{Cu}^{\text{II}}(\text{dap})\text{Cl}_2]$ neither did it immediately, nor over 50 minutes quench the signal of the nitronic ester radical. This suggests that Cu(II) is either not trapping the nitronic ester radical at all or not to a significant extent.

As a consequence, if **C** would be a key intermediate also under Cu-catalysis conditions (neglecting here the fact that the redox potential of Cu(II) is not sufficient to oxidize **C** to furnish **4** as the final product), a fast and effective binding would be required to explain the observed quick conversion of the starting materials to **4** under Cu-catalysis conditions (1h reaction time for 88% conversion).

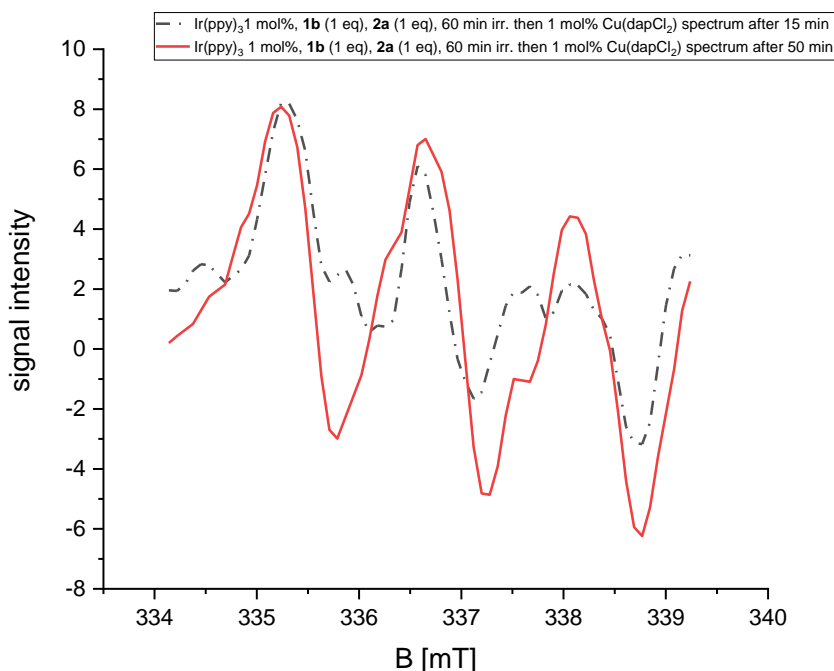


Figure 12. EPR spectra of $\text{Ir}(\text{ppy})_3$ (5 μmol , 1 mol%), bromonitroethane (**1b**) (0.5 mmol, 1 equiv) and styrene (**2a**) (0.5 mmol, 1 equiv) in MeCN (2 mL); solutions as indicated with addition of $[\text{Cu}(\text{dap})\text{Cl}_2]$ (1.0 mol%) after conformation of the occurrence of the nitronic ester radical. Frequency: 9.4595 GHz; B_0 -Field = 340 mT; B_0 -Sweep = 40 mT; Sweep-Time = 30 s; Number of runs = 3; Samples = 512; mod. Ampl. = 0.7 mT; MW Att. = 10 dB; Gain = 10; Time Const. = 0.1 s. (Measurements were carried out by the Rehbein group and the shown graphics were kindly provided by them).

Next, TEMPO was employed as a related radical to precisely examine the ability of nitroxyl-type radicals to attach to $[\text{Cu}^{\text{II}}(\text{dap})\text{Cl}_2]$ in a defined manner. Radical stabilization energies can be used to infer the thermodynamic stability similarities between TEMPO and the nitronic ester radical. Their spin delocalization (more significant for the nitronic ester radicals) and shielding of the spin center at the NO-unit affect their kinetic inertness (slightly higher for TEMPO). For the EPR studies, a stock solution of $[\text{Cu}(\text{dap})\text{Cl}_2]$ (10 mM) in MeCN and two TEMPO solutions (B1 1 mM and B2 0.1 mM) in MeCN was produced. As reference values, 0.2 mL aliquots of these solutions were measured in the EPR (two-fold determination).

Cu(II) solution and TEMPO solution (B1, B2) were mixed for the binding studies, and the results were measured after 15 minutes (twofold-determination, *vide* Figure 13 for the averaged spectra). Even in excess of 10- to 100-fold, the spectra reveal that only a small portion of free TEMPO is bound by the photocatalyst $[\text{Cu}^{\text{II}}(\text{dap})\text{Cl}_2]$.

The TEMPO concentration was reduced by around 60% (or 40% of the initial signal strength) in response to a 10-fold increase of Cu(II). According to the hypothesized mechanism (see Chapter 3.7 Proposed Reaction Mechanism), Cu(II) would be present in the catalysis in a 1:1 stoichiometry with the organic radical preceding **C**, indicating that if **C** were to be generated at all, Cu(II) would bind to an even less fraction of it.

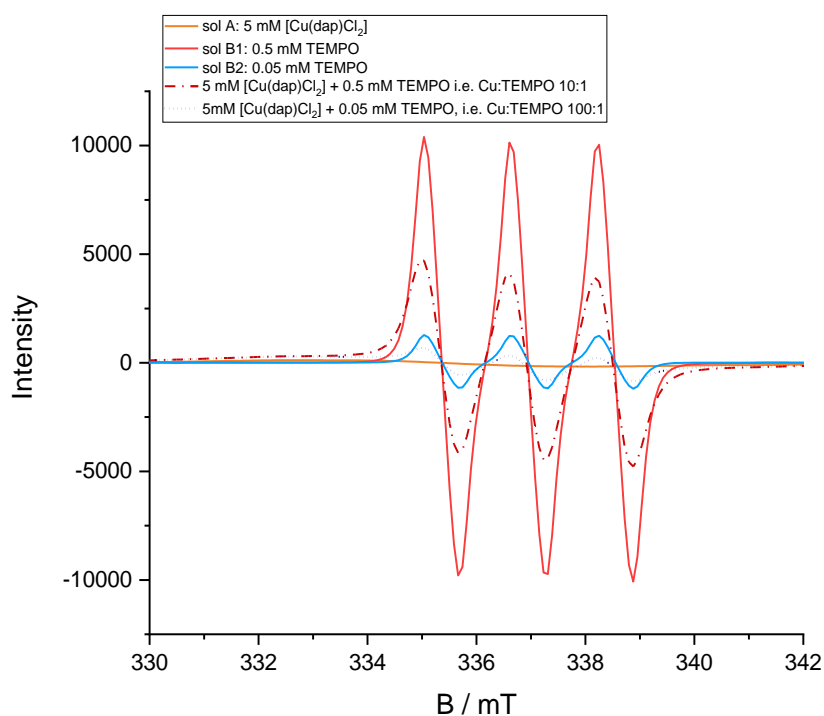


Figure 13. EPR spectra (averaged of two runs) of TEMPO and $[\text{Cu}(\text{dap})\text{Cl}_2]$ in MeCN and mixtures of TEMPO and Cu(II) stock-solutions. Frequency: 9.459 GHz; B_0 -Field = 320 mT; B_0 -Sweep = 80 mT; Sweep-Time = 60 s; Number of runs = 3; Samples = 1024; mod. Ampl. = 0.7 mT; MW Att. = 12 dB; Gain = 10; Time Const. = 0.1 s (Measurements were carried out by the Rehbein group and the shown graphics were kindly provided by them).

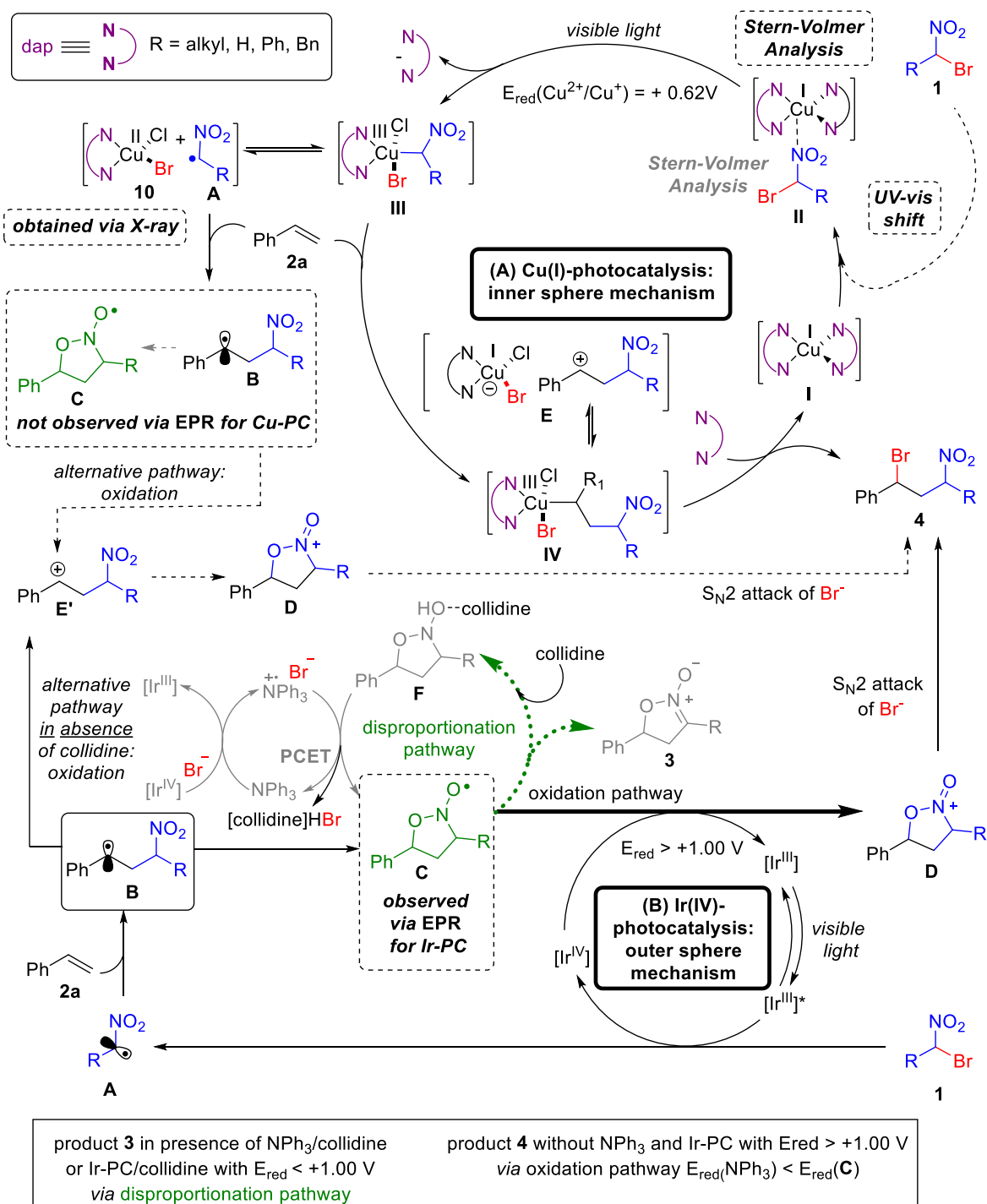
3.7 Proposed Reaction Mechanism

With all findings at hand, a plausible mechanistic picture can be proposed (Scheme 10A, Cu(I)-photocatalyzed process): It starts with the coordination of ATRA reagent **1** to the photocatalyst **I** as indicated by UV/Vis absorption shifts of the binary mixture of photocatalyst $[\text{Cu}^{\text{I}}(\text{dap})_2]\text{Cl}$ and bromonitroalkane **1** prior to irradiation. Single electron transfer from **II** to ATRA reagent **1** and subsequent C-Br bond cleavage results in intermediate **III** and radical **A**. Stern-Volmer studies demonstrate that only bromonitromethane (**1a**) can quench the photocatalyst $[\text{Cu}^{\text{I}}(\text{dap})_2]\text{Cl}$ in its excited state; but not styrene (**2a**). X-ray analysis of single crystals obtained from a solution of $[\text{Cu}^{\text{I}}(\text{dap})_2]\text{Cl}$ in the presence of **1a**, having the molecular structure $[\text{Cu}^{\text{II}}(\text{dap})\text{ClBr}]$ (**10**), provided additional evidence for this oxidation step. EPR measurements of an equimolar solution of $[\text{Cu}^{\text{I}}(\text{dap})_2]\text{Cl}$ and bromonitroethane (**1b**) in MeCN provided a characteristic Cu(II) spectrum showing octahedral coordination with an axial elongation of the ligands, revealing "in situ" evidence of this redox change. This Cu(II) species was even detectable in the presence of 10 mol% $[\text{Cu}^{\text{I}}(\text{dap})_2]\text{Cl}$, indicating that this step is likely to occur under catalytic conditions as well. Since an organic radical was not detected in the EPR studies of the Cu-catalyzed photoreaction, it is assumed that Cu alters the radical reactivity by coordination or by the formation of a (formal) Cu(III)-intermediate^{[38][39][40]} **IV** (or ion pair **E** representing the direct oxidation of radical **B**). Consequently, the cyclization pathway to radical **C** is no longer competitive with the formation of the ATRA product. (*Vide* Chapter 3.6.6 EPR Studies). By Insertion of olefin **2** into the Cu-carbon bond of **III** and subsequent reductive elimination, the formation of **4** can be explained. A polar pathway that provided **4** along with the high oxidation power Ir-catalysts would rely on the oxidation of **B** to the carbocation **E'**. Due to its lower oxidation power, this polar pathway was shown to be inefficient for Cu(II), suggesting that the radical pathway similar to those in ATRA reactions is the most plausible.

In contrast to Cu-catalysis, the Ir-catalyzed process is believed to proceed by the following mechanism, according to Ooi and colleagues (Scheme 10B, Ir(IV)-photocatalyzed process): After SET to bromonitroalkane **1** with simultaneous photocatalyst oxidation followed by addition of the generated radical **A** to styrene (**2a**), intermediate **B** rapidly cyclizes to the persistent nitrosyl radical **C** in a highly favorable 5-exo-trig cyclization (in the presence of collidine). The ATRA product **4** will only be produced if the oxidation potential of the oxidized photocatalyst, iridium(IV), is sufficiently high, as in $[\text{Ir}(\text{dtbbpy})(\text{ppy})_2]\text{PF}_6$ ($E_{\text{red}}(\text{Ir}^{4+} / \text{Ir}^{3+}) = +1.21 \text{ V}$),^[13] to oxidize **C** further to **D**. (*Nota bene*: In the absence of collidine, we observed the production of ATRA product **4** but in lower yield, indicating that concurrent oxidation of benzylic radical **B** to **E'** can take place as side reaction – an observation, which was not described by Ooi *et al.*).

Nevertheless, only a minor amount of the ATRA product **4** is observed if the oxidation potential of the oxidized photocatalyst ($E_{\text{red}} < +1.0$ V) is insufficient to oxidize radical **C**; instead, isoxazoline-*N*-oxide **3** is the major product. Additionally, in combination with 2,4,6-collidine, triphenylamine as a sacrificed electron donor reduces the oxidized iridium(IV) catalyst, resulting once again solely in the formation of isoxazoline-*N*-oxide **3** instead of the ATRA product **4**.

Detailed mechanistic comparison of Cu(I)- and Ir(IV)-photocatalysis



Scheme 10. Detailed mechanistic comparison/ proposed reaction mechanism of the bromonitroalkylation.

3.8 Studies with Chiral Ligands

Encouraged by the high efficiency of copper-catalyzed inner-sphere ATRA processes^[41] compared to outer-sphere ionic mechanism, we aimed the development of an asymmetric bromonitromethylation protocol by using a chiral ligand on the metal center. As starting point, we used three chiral ligands belonging to the family of (aza)-bisoxazoline ligands and (*R*)-BINAP (Table 7). Therefore, replacing the photocatalyst [Cu^I(dap)₂]Cl with a combination of 10 mol% Cu^ICl and the chiral ligand should enable the ATRA process in an enantioselective fashion. We started our investigations under 455 nm irradiation. Since a reaction was not observed, it might be the case that the *in situ* formed photocatalyst did not show sufficient absorption at this wavelength. Therefore, we switched after 2h of irradiation to 400 nm and again after 2h to 367 nm irradiation. Unfortunately, product formation was not detected in any of these reactions. One plausible explanation could be that the chiral copper complexes do not have the redox power required to activate bromonitromethane (**1a**). A suitable strategy might be, e.g. to apply the well-established strategy of dual catalysis.^[4,42] The radical could be successfully generated e.g. with an Ir(IV)-based photocatalyst and trapped by a chiral copper(II)-complex. Further studies about this type of activation are currently ongoing in our laboratory.

Table 7. Studies with chiral ligands towards enantioselective ATRA process ^a

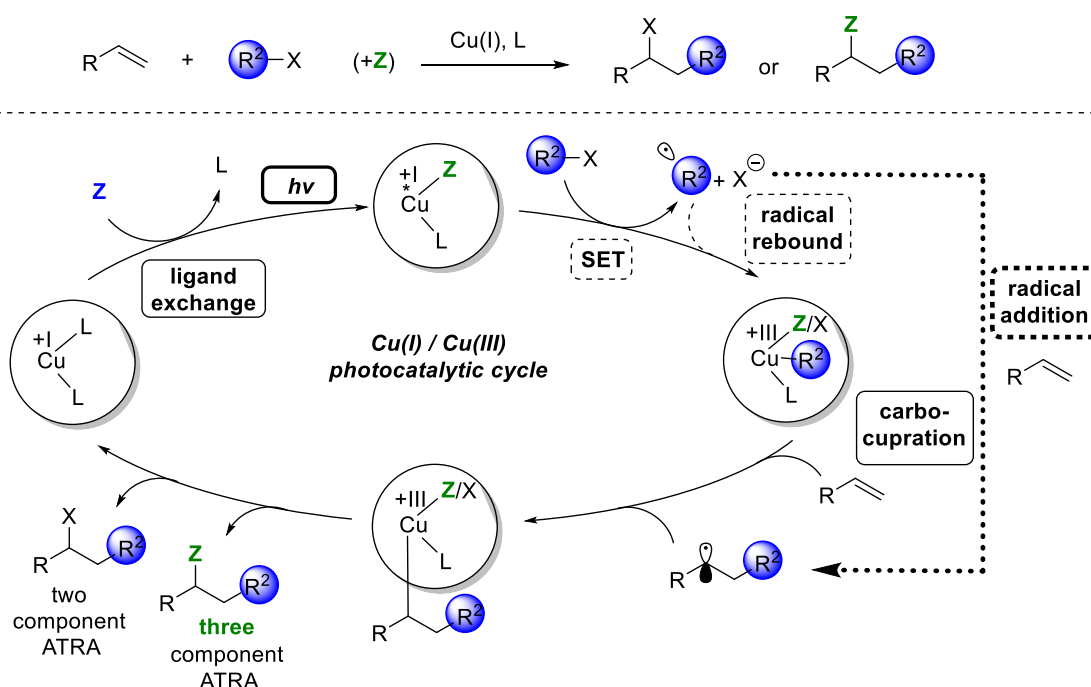
Reaction scheme: **1a** (1.0 equiv) + **2a** (1.0 equiv) $\xrightarrow[\text{MeCN (0.25 M), rt, N}_2, 2 \text{ h}, 0 \text{ }^\circ\text{C, 455 nm}]{10 \text{ mol\% chiral L}^*, 10 \text{ mol\% CuCl}}$ **4a**

Entry	Ligand	wavelengths [nm]	Irradiation time [h]	Yield ^b
1		455 403 367	2 2 2	nd
2		455 403 367	2 2 2	nd
3		455 403 367	2 2 2	nd
4		455 403 367	2 2 2	nd

^aReaction conditions: reactions were performed on a 0.25 mmol scale for ATRA reagent **1a** (1.0 equiv) under given conditions in an ice bath (0 °C) and N₂ atmosphere. ^b¹H-NMR yield using 1,1,2,2-tetrachloroethane as the internal standard. nd = not detected.

3.9 Studies on Three-Component Type ATRA Reactions

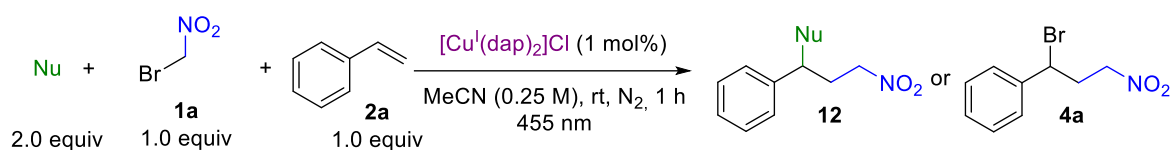
During the last years, besides Iridium- or Ruthenium polypyridinyl complexes, especially copper(I)-complexes are widely used photocatalysts in the reductive quenching cycles.^[41] Due to the benefits of these photocatalysts, acting as low-cost, more robust, easily accessible alternatives, the focus has shifted from rare earth metal complexes towards 3d metals, e.g. copper. Because of the unique character of copper, the possibility of ligand exchange and the ability to stabilize and interact with radical species through the inner-sphere type mechanism, a unique opportunity to achieve new bond formation has been developed. Moreover, three-component type ATRA reactions offer the possibility of achieving enantioselective product formation using chiral Cu(I)-complexes, which is not possible using other photocatalysts, such as iridium- and ruthenium-based, or organic dye photocatalysts.^[4] Scheme 11 gives an overview of the mechanistic details for a Cu(I)/ Cu(III) photocatalyzed ATRA reaction with respect to two- or three-component ATRA-type reactions. In principle, a Cu(I)-complex can undergo ligand exchange with a suitable third component **Z**. After excitation by light, SET to an ATRA reagent can occur. Thereby a radical **R²** is formed. Now either radical addition to an olefin or radical rebound can take place. In the first pathway, the radical addition product binds back to the Cu(II)-intermediate, affording a Cu(III)-species. In the second pathway, the carbocupration of an olefin leads to Cu(III)-species. Reductive elimination upon extrusion of the two- or three-component ATRA product regenerates the photocatalyst.



Scheme 11. Mechanistic picture for Cu(I)-photocatalyzed two- and three-component ATRA reactions.

Motivated by the impressive literature, we aimed at achieving a photocatalytic ATRA reaction with bromonitromethane (**1a**), styrene (**2a**) and [Cu^I(dap)₂]Cl as photocatalyst in a three-component type fashion to obtain other 1,3-difunctionalized organonitro products of type **12** (Table 8). Therefore, we started our investigations with TMSCN as the third component in the photochemical process (Table 8, entry 1). Contrary to our expectations, the desired product was not observed, but ATRA product **4a** was obtained with good yield. Moving to other third components, we also observed the formation of the two-component product **4a** in good to high yield (Table 8, entries 2–4).

Table 8. Attempts towards three-component ATRA reactions with nucleophiles.^a

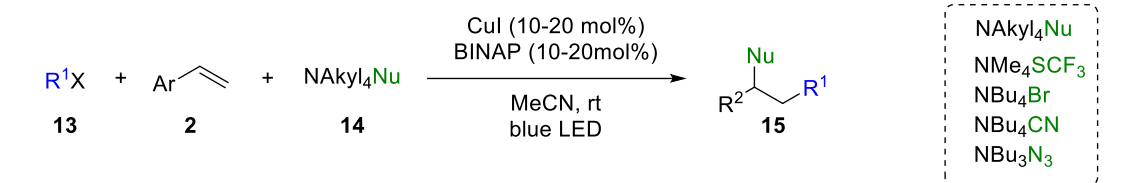


Entry	Nucleophile	Yield Product 12 ^b	Yield Product 4a ^b
1	TMSCN	0	77
2	TMSN ₃	0	84
3	H ₂ O	0	83
4	TMSCF ₃	0	87

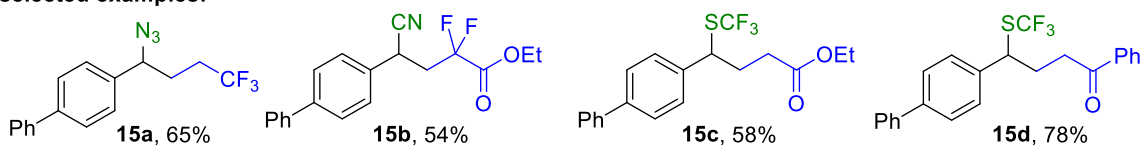
^aReaction conditions: reactions were performed on a 0.25 mmol scale for ATRA Reagent **1a** (1.0 equiv) under given conditions at room temperature (25 °C) and N₂ atmosphere. ^bNMR yield using 1,1,2,2-tetrachloroethane as the internal standard.

In 2018, Fu, Peters and coworkers elaborated a visible-light mediated Cu(I)-photocatalyzed three-component ATRA process using a combination of Cu(I) iodide and racemic BINOL as the photocatalyst under blue LED irradiation in MeCN.^[43] They were able to activate donor-acceptor substituted ATRA reagents (**13**) and quaternary (alkyl)-ammonium salts (**14**) as the third component to obtain products of type **15** in good yield (Scheme 12).

Fu, Peters *et al.* (2018)



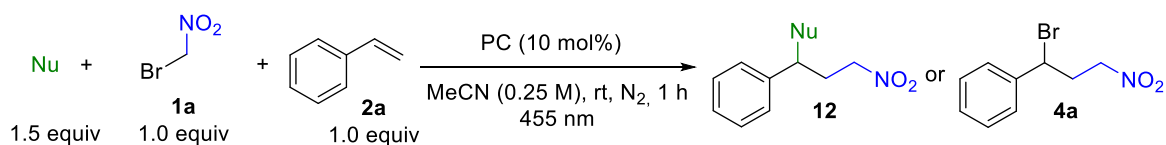
selected examples:



Scheme 12. Reported three-component ATRA process by Fu and Peters *et al.*^[43].

Intrigued by this literature, we questioned if the reaction conditions were transferrable to our system using bromonitromethane (**1a**) to obtain products **12**. Unfortunately, having neither BINAP nor BINOL as a ligand in the reaction mixture gave the expected products, only bromonitromethane as ATRA reagent was decomposed under these reaction conditions (Table 9, entries 1–3).

Table 9. Attempts towards three-component ATRA processes based on Fu and Peters.^a

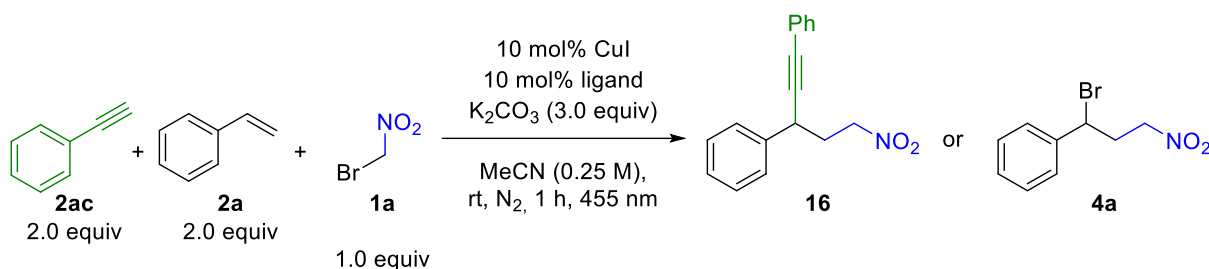


Entry	Photocatalyst (PC)	Nucleophile	Product 12 ^b	Product 4a ^b
1	CuI + rac. BINOL	NBu ₄ N ₃	0	0
2	CuI + rac. BINAP	NBu ₄ N ₃	0	0
3	CuI + rac. BINAP	NBu ₄ CN	0	0

^aReaction conditions: reactions were performed on a 0.50 mmol scale for bromonitromethane (**1a**) (1.0 equiv), styrene (**2a**) (1.0 equiv), nucleophile (1.5 equiv) under given conditions at room temperature (25 °C). ^b¹H-NMR yield using 1,1,2,2-tetrachloroethane as internal standard.

Furthermore, we aimed toward a three-component-type process, using phenylacetylene as the third component, which is amply documented in the literature.^[41] Therefore, different types of ligands, such as dmp, terpyridine or 4,4'-di-*tert*-butyl-2,2'-dipyridyl (dtbbpy), were screened since, usually the type of ligand plays a crucial role^[4,44] for the success of this type of reactions (Table 10, entries 1–4).

Table 10. Three-component ATRA reaction with phenylacetylene.^a



Entry	Ligand	Product 16 ^b	Product 4a ^b
1	dmp	0	0
2	terpyridine	0	0
3	bathocuproine	0	0
4	dtbbpy	0	0

^aReaction conditions: reactions were performed on a 0.5 mmol scale for bromonitromethane (**1a**) (1.0 equiv) phenylacetylene (2.0 equiv), styrene (**2a**) (1.0 equiv) and K₂CO₃ (3.0 equiv) under given conditions at room temperature (25 °C). ^b¹H-NMR yield using 1,1,2,2-tetrachloroethane as internal standard.

However, in the presence of a base (which is necessary to obtain a copper(I)-acetylide species^[41] initially) neither the desired product (**16**), nor the ATRA product (**4a**) was observable. Instead the ATRA reagent was destroyed due to deprotonation by K_2CO_3 as a base.^[10] Therefore, no further investigations were carried out on three-component processes involving phenylacetylene.

3.10 Conclusion and Outlook

In conclusion, a highly efficient visible light-mediated ATRA reaction of bromonitromethane derivatives and olefins catalyzed by a copper(I)-photocatalyst was developed. Moreover, evidence is provided for the highly effective rebound of Cu(II) to radical intermediates that can even outcompete a highly advantageous intramolecular radical cyclization to a persistent radical, in addition to the synthetic value of the title reaction concerning the scope and further transformations of the products. It is well known that the isolation of a Cu(III)-intermediate along the reaction pathway would serve as the mechanistic proposal's ultimate proof. However, this poses a significant challenge^{[38][39][40]} due to the rapid reductive elimination that can occur to produce the ATRA product while concurrently regenerating the Cu(I)-photocatalyst. Further investigations regarding three-component ATRA-type reactions with bromonitromethane and other derivatizations of the bromonitroalkylated products are currently carried out in our laboratory.

3.11 References

- [1] a) M. S. Kharasch, W. H. Urry, E. V. Jensen, *J. Am. Chem. Soc.* **1945**, *67*, 1626; b) M. S. Kharasch, E. V. Jensen, W. H. Urry, *Science* **1945**, *102*, 128; c) M. S. Kharasch, P. S. Skell, P. Fisher, *J. Am. Chem. Soc.* **1948**, *70*, 1055.
- [2] M. H. Shaw, J. Twilton, D. W. C. MacMillan, *J. Org. Chem.* **2016**, *81*, 6898.
- [3] T. Courant, G. Masson, *J. Org. Chem.* **2016**, *81*, 6945.
- [4] A. Hossain, A. Bhattacharyya, O. Reiser, *Science* **2019**, 364.
- [5] S. Engl, O. Reiser, *Eur. J. Org. Chem.* **2020**, 2020, 1523.
- [6] a) H. Cao, S. Ma, Y. Feng, Y. Guo, P. Jiao, *Chem. Commun.* **2022**, 58, 1780; b) G. Hirata, T. Shimada, T. Nishikata, *Org. Lett.* **2020**, *22*, 8952.
- [7] M. Iwasaki, Y. Ikemoto, Y. Nishihara, *Org. Lett.* **2020**, *22*, 7577.
- [8] Y. Tsuchiya, R. Onai, D. Uruguchi, T. Ooi, *Chem. Commun.* **2020**, 56, 11014.
- [9] C. K. Prier, D. A. Rankic, D. W. C. MacMillan, *Chem. Rev.* **2013**, *113*, 5322.
- [10] M. P. Thorpe, A. N. Smith, M. S. Crocker, J. N. Johnston, *J. Org. Chem.* **2022**, *87*, 5451.
- [11] A. Hossain, S. Engl, E. Lutsker, O. Reiser, *ACS Catal.* **2019**, *9*, 1103.
- [12] N. Corrigan, S. Shanmugam, J. Xu, C. Boyer, *Chem. Soc. Rev.* **2016**, *45*, 6165.
- [13] M. S. Lowry, J. I. Goldsmith, J. D. Slinker, R. Rohl, S. Bernhard, G. G. Malliaras, *Chem. Mater.* **2005**, 5712–5719.
- [14] H. Uoyama, K. Goushi, K. Shizu, H. Nomura, C. Adachi, *Nature* **2012**, *492*, 234.
- [15] X.-F. Zhang, I. Zhang, L. Liu, *Photochem. Photobiol.* **2010**, *86*, 492.
- [16] C. R. Lambert, I. E. Kochevar, *Photochem. Photobiol.* **1997**, *66*, 15.
- [17] I. Ghosh, B. König, *Angew. Chem. Int. Ed.* **2016**, *55*, 7676.
- [18] D. A. Nicewicz, T. M. Nguyen, *ACS Catal.* **2014**, *4*, 355.
- [19] S. Engl, O. Reiser, *ACS Catal.* **2020**, *10*, 9899.
- [20] S. Paria, M. Pirtsch, V. Kais, O. Reiser, *Synth.* **2013**, *45*, 2689.
- [21] X.-J. Tang, W. R. Dolbier, *Angew. Chem. Int. Ed.* **2015**, *54*, 4246.
- [22] S. Tanaka, S. Kohmoto, M. Yamamoto, K. Yamada, *Shokuhin Kagaku Kogaku Kaishi* **1989**, 1742.
- [23] D. X. Chen, C. M. Ho, Q. Y. R. Wu, P. R. Wu, F. M. Wong, W. Wu, *Tetrahedron Lett.* **2008**, *49*, 4147.

- [24] S.-Y. Li, Z.-Y. Guan, J. Xue, G.-Y. Zhang, X.-Y. Guan, Q.-H. Deng, *Org. Chem. Front.* **2020**, *7*, 2449.
- [25] S. Engl, O. Reiser, *Org. Lett.* **2021**, *23*, 5581.
- [26] J. Han, Z. Cui, J. Wang, Z. Liu, *Synth. Commun.* **2010**, *40*, 2042.
- [27] M. Rasparini, M. Taddei, E. Cini, C. Minelli, N. Turner, K. G. Hugentobler, *EP2589587A1* **2013**.
- [28] M. Orlandi, D. Brenna, R. Harms, S. Jost, M. Benaglia, *Org. Process Res. Dev.* **2018**, *22*, 430.
- [29] X. Ji, H. Huang, *Org. Biomol. Chem.* **2016**, *14*, 10557.
- [30] a) T. Akasaka, S. Kurosaka, Y. Uchida, M. Tanaka, K. Sato, I. Hayakawa, *Antimicrob. Agents Chemother.* **1998**, *42*, 1284; b) S. Kawamura, Y. Unno, A. List, A. Mizuno, M. Tanaka, T. Sasaki, M. Arisawa, A. Asai, M. Groll, S. Shuto, *J. Med. Chem.* **2013**, *56*, 3689; c) H.-L. Teng, Y. Luo, B. Wang, L. Zhang, M. Nishiura, Z. Hou, *Angew. Chem. Int. Ed.* **2016**, *55*, 15406.
- [31] B. Moreau, D. Alberico, V. N. Lindsay, A. B. Charette, *Tetrahedron* **2012**, *68*, 3487.
- [32] S. Ulrich, R. Ricken, M. Adli, *Eur. Neuropsychopharmacol.* **2017**, *27*, 697.
- [33] N. Hoang, X. Zhang, C. Zhang, van Vo, F. Leng, L. Saxena, F. Yin, F. Lu, G. Zheng, P. Bhowmik et al., *Bioorg. Med. Chem.* **2018**, *26*, 1523.
- [34] K. G. Hugentobler, H. Sharif, M. Rasparini, R. S. Heath, N. J. Turner, *Org. Biomol. Chem.* **2016**, *14*, 8064.
- [35] L. Gimeno, E. Blart, J.-N. Rebilly, M. Coupeau, M. Allain, T. Roisnel, A. Quarré de Verneuil, C. Gourlaouen, C. Daniel, Y. Pellegrin, *Chem. Eur. J.* **2020**, *26*, 11887.
- [36] R. A. Kunetsky, A. D. Dilman, S. L. Ioffe, M. I. Struchkova, Y. A. Strelenko, V. A. Tartakovsky, *Org. Lett.* **2003**, *5*, 4907.
- [37] J. E. T. Corrie, B. C. Gilbert, V. R. N. Munasinghe, A. C. Whitwood, *J. Chem. Soc., Perkin Trans. 2* **2000**, 2483.
- [38] L. M. Huffman, S. S. Stahl, *J. Am. Chem. Soc.* **2008**, *130*, 9196.
- [39] A. E. King, L. M. Huffman, A. Casitas, M. Costas, X. Ribas, S. S. Stahl, *J. Am. Chem. Soc.* **2010**, *132*, 12068.
- [40] L. M. Huffman, A. Casitas, M. Font, M. Canta, M. Costas, X. Ribas, S. S. Stahl, *Chem. Eur. J* **2011**, *17*, 10643.
- [41] S. Engl, O. Reiser, *Chem. Soc. Rev.* **2022**, *51*, 5287.

- [42] K. L. Skubi, T. R. Blum, T. P. Yoon, *Chem. Rev.* **2016**, *116*, 10035.
- [43] J. He, C. Chen, G. C. Fu, J. C. Peters, *ACS Catal.* **2018**, *8*, 11741.
- [44] R. Trammell, K. Rajabimoghadam, I. Garcia-Bosch, *Chem. Rev.* **2019**, *119*, 2954.

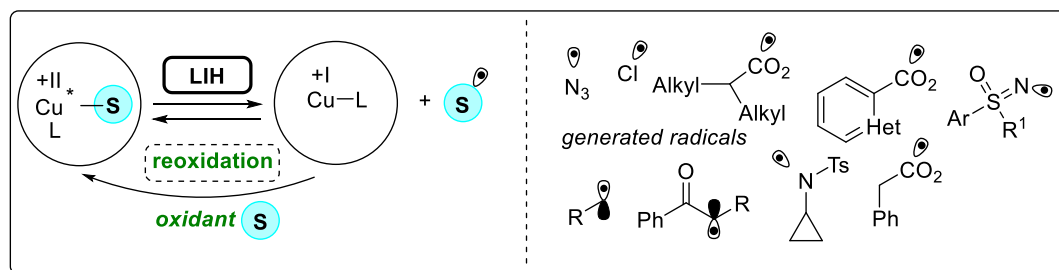
Chapter 4 Summary/ Zusammenfassung

4.1 Summary

Light-Induced Homolysis (LIH) of Copper(II)-complexes

This chapter is based on: [A. Reichle](#)[†] and O. Reiser[†], *Chem. Sci.*, **2023**, *14*, 4449. ([†]A.R. and O.R. jointly wrote the manuscript.).

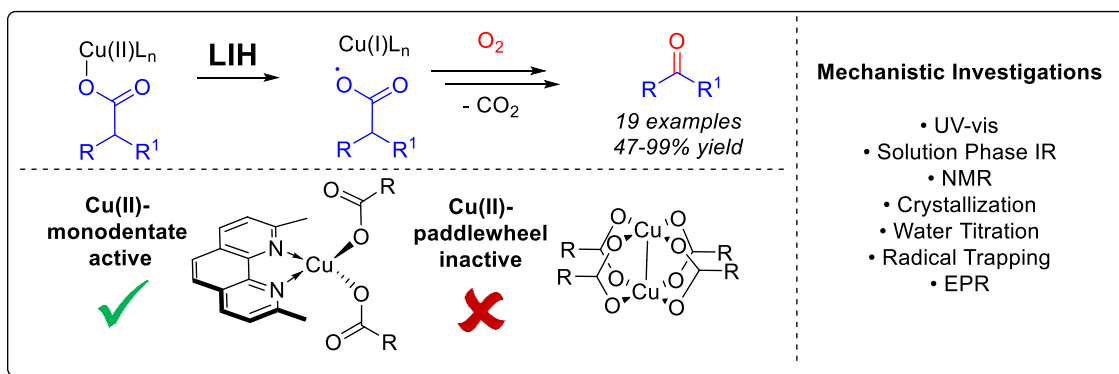
In the past ten years powerful strategies have been developed in the field of photocatalysis regarding the functionalization of compounds via radical intermediaries in a selective manner. The shift towards earth-abundant metal-based photocatalysts is currently less explored, in comparison to the well-established iridium- or ruthenium-based photocatalysts, which fulfil the requirements of a photocatalyst, such as long excited-state lifetimes and photostability. Although only having excited-state lifetimes in the low millisecond range or below, the idea of light-induced homolysis (LIH) for producing radicals has recently attracted significant interest as a potential strategy for initiating photoreactions using earth-abundant 3d metal complexes, such as Iron, Cobalt, Nickel or Copper. Exploiting this idea involves the use of Cu(II)-complexes, which will be presented by demonstrating current advancements in organic synthesis with an eye toward the field's prospects.



Photocatalytic Decarboxylation of Copper(II)-carboxylates

This chapter is based on: [A. Reichle](#), H. Sterzel, P. Kreitmeier, R. Fayad, F. N. Castellano, J. Rehbein, O. Reiser, *Chem. Commun.* **2022**, *58*, 4456.

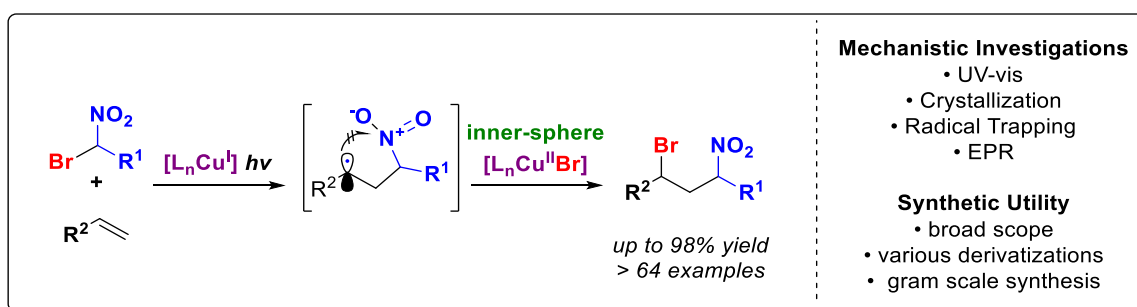
In this chapter, we applied the concept of light-induced homolysis (LIH) of Cu(II)-carboxylates to generate radicals. A protocol for the decarboxylative oxygenation of carboxylic acids with molecular oxygen as the terminal oxidant is described. Therefore, two Cu(II)-carboxylate complexes with different coordination geometries were synthesized and characterized by X-ray analysis. Diverse mechanistic investigations (in collaboration with our partners, the Castellano and Rehbein group) were carried out, e.g., UV-vis absorption spectra, solution-phase IR spectra as well as EPR studies supporting the light-induced homolysis of monodentate Cu(II)-carboxylate, rather than paddle-wheel type chelation. The protocol can be successfully applied to nonsteroidal anti-inflammatory drugs (NSAIDs) such as felbinac, ibuprofen, or naproxen delivering the corresponding decarboxylated products in high yields.



Copper(I)-photocatalyzed Bromonitroalkylation of Olefins – Evidence for Highly Efficient Inner-Sphere Pathways

This chapter is based on: [A. Reichle⁺⁺, M. Koch⁺⁺, H. Sterzel, L.-J. Großkopf, J. Floss, J. Rehbein, O. Reiser, *Angew. Chem. Int. Ed.*, **2023**, e202219086.](#) ([⁺⁺] Co-first authors.)

A visible light-mediated copper-catalyzed protocol has been developed to enable the highly economic, vicinal difunctionalization of olefins utilizing bromonitroalkanes as ATRA reagents. This procedure, which allows the rapid functionalization of activated and unactivated olefins, excels by high yields and fast reaction times under environmentally benign reaction conditions with exceptional scope. Moreover, the methodology allows late-stage functionalization of biologically active molecules and upscaling to gram quantities. Manifold possibilities for subsequent transformations, *e.g.*, access to nitro- and aminocyclopropanes are feasible. In addition to the synthetic value of the title transformation, this study undergirds copper's unique character in photoredox catalysis by demonstrating its capacity to stabilize and interact with radical intermediates in its inner coordination sphere. According to EPR investigations, these interactions can even outperform a favorable cyclization of transient radical intermediates to highly stable persistent radicals compared to iridium-based photocatalysts.



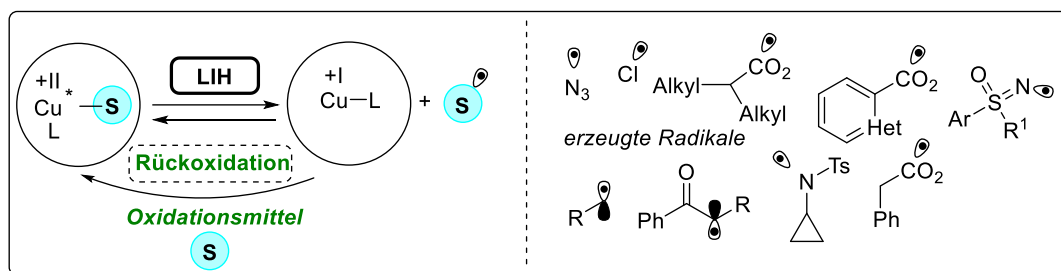
4.2 Zusammenfassung

Licht induzierte Homolyse (LIH) von Kupfer(II)-Komplexen

Dieses Kapitel basiert auf: A. Reichle[†] und O. Reiser[†], *Chem. Sci.*, **2023**, *14*, 4449.

([†]A.R. and O.R. haben das Manuscript gemeinsam erstellt.).

Dieses Kapitel fasst die Entwicklungen auf dem Gebiet der lichtinduzierten Homolyse von Cu(II)-Komplexen zusammen. In der letzten Dekade hat sich die Photokatalyse zu einer leistungsfähigen Strategie für die selektive Funktionalisierung von Molekülen durch radikalische Intermediate entwickelt. Der Wandel hin zu Photokatalysatoren auf der Basis von auf der Erde häufig vorkommenden Metallen ist derzeit weniger erforscht als die gut etablierten Photokatalysatoren auf Iridium- oder Ruthenium-Basis. Diese erfüllen die Anforderungen eines Photokatalysators, wie z.B. eine lange Lebensdauer des angeregten Zustands und Photostabilität. Das Konzept der durch (sichtbares) Licht induzierten Homolyse (LIH) zur Erzeugung von Radikalen hat kürzlich großes Interesse als neue Strategie zur Initiierung von Photoreaktionen basierend auf Metallkomplexen mit nachhaltigen 3d-Metallen geweckt, obwohl diese nur eine Lebensdauer des angeregten Zustands haben, welcher sich im niedrigen Nanosekundenbereich oder sogar darunter befindet. Obwohl die Idee der lichtinduzierten Homolyse (LIH) zur Erzeugung von Radikalen nur Lebensdauern angeregter Zustände im niedrigen Millisekundenbereich oder darunter aufweist, hat sie in jüngster Zeit großes Interesse als potenzielle Strategie zur Initiierung von Photoreaktionen unter Verwendung auf der Erde häufig vorkommender 3D-Metallkomplexe geweckt, z.B. Eisen, Kobalt, Nickel oder Kupfer. Die Nutzung dieser Idee beinhaltet die Verwendung von Cu(II)-Komplexen, die anhand aktueller Fortschritte in der organischen Synthese mit Blick auf die Zukunftsaussichten des Fachgebiets vorgestellt werden.

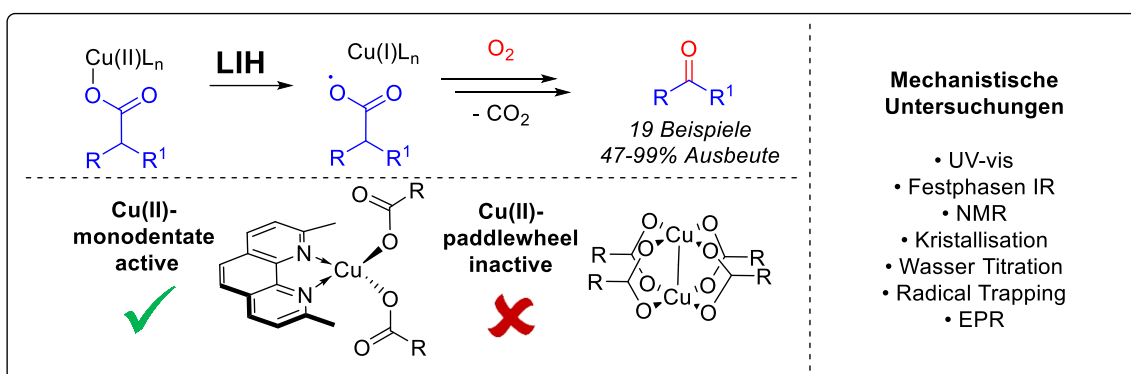


Photokatalytische Decarboxylierung von Kupfer(II)-carboxylaten

Dieses Kapitel basiert auf: A. Reichle, H. Sterzel, P. Kreitmeier, R. Fayad, F. N. Castellano, J. Rehbein, O. Reiser, *Chem. Commun.* **2022**, 58, 4456.

In diesem Kapitel wendeten wir das Konzept der lichtinduzierten Homolyse (LIH) von Cu(II)-Carboxylaten zur Erzeugung von Radikalen an. Eine Vorschrift für die decarboxylative Oxygenierung von Carbonsäuren mit molekularem Sauerstoff als terminalem Oxidationsmittel wird beschrieben. Daher wurden zwei Cu(II)-carboxylat Komplexe mit unterschiedlichen Koordinationsgeometrien synthetisiert und durch Röntgenstrukturanalyse charakterisiert.

Es wurden diverse mechanistische Untersuchungen (in Zusammenarbeit mit unseren Partnern, der Castellano und Rehbein Gruppe) durchgeführt, z.B. UV-Vis-Absorptionsspektren, solution-phase-IR-Spektren sowie EPR-Studien, die die lichtinduzierte Homolyse von einzähnigen Cu(II)-carboxylat unterstützen, eher als die paddle-wheel Koordination von Cu(II)-carboxylat. Die Synthesevorschrift kann erfolgreich auf nichtsteroidale entzündungshemmende Medikamente (NSAIDs) wie Felbinac, Ibuprofen oder Naproxen angewendet werden, welche die entsprechenden decarboxylierten Produkte in hohen Ausbeuten liefern.

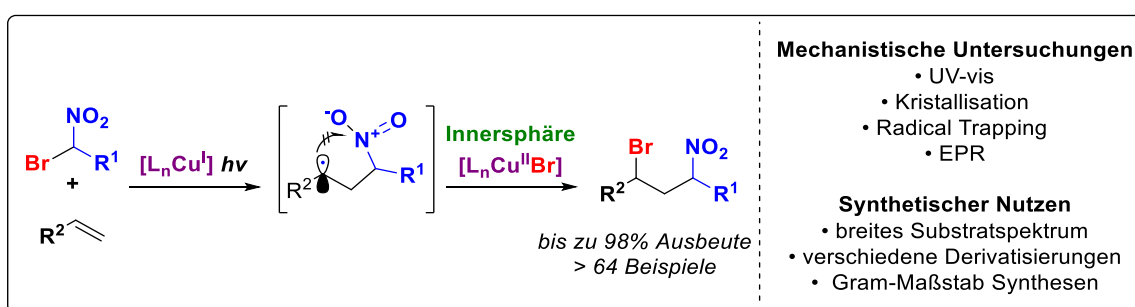


Kupfer(I)-photokatalysierte Bromnitroalkylierung von Olefinen – Hinweise für hocheffizienten Innersphären-Mechanismus

Dieses Kapitel basiert auf: A. Reichle⁺⁺, M. Koch⁺⁺, H. Sterzel, L.-J. Großkopf, J. Floss, J. Rehbein, O. Reiser, *Angew. Chem. Int. Ed.*, **2023**, e202219086. ([⁺⁺] Co-Erstautoren.)

Es wurde ein durch sichtbares Licht vermitteltes kupferkatalysiertes Protokoll entwickelt, das die äußerst wirtschaftliche, vicinale Difunktionalisierung von Olefinen unter Verwendung von Bromnitroalkanen als ATRA-Reagenzien ermöglicht. Dieses Verfahren, das die schnelle Funktionalisierung sowohl aktivierter als auch inaktivierter Olefine ermöglicht, zeichnet sich durch hohe Ausbeuten, schnelle Reaktionszeiten unter umweltfreundlichen Reaktionsbedingungen und außergewöhnliche Anwendungsbreite aus.

Darüber hinaus ermöglicht die Methodik die Funktionalisierung biologisch aktiver Moleküle im späten Stadium sowie die Hochskalierbarkeit der Reaktion in den Gramm-Maßstab. Vielfältige Möglichkeiten für weitere synthetische Transformationen, z.B. Zugang zu Nitro- und Aminocyclopropanen sind möglich. Neben dem synthetischen Wert der Titelreaktion untermauert diese Studie den einzigartigen Charakter von Kupfer in der Photoredoxkatalyse, indem seine Fähigkeit zur Stabilisierung und Wechselwirkung mit radikalischen Zwischenstufen in seiner inneren Koordinationssphäre demonstriert wird. Gemäß EPR-Untersuchungen können diese Interaktionen im Vergleich zu Iridium-basierten Photokatalysatoren sogar eine begünstigte Zyklisierung von transienten radikalischen Intermediaten zu hochstabilen persistenten Radikalen überwinden.



Chapter 5 Experimental Part

5.1 General Information

Commercially available chemicals were used without further purifications, unless otherwise stated. Synthesized compounds were purified according to common standard procedures.^[1] All photochemical reactions were carried out in oven-dried glassware. Reactions were carried out under atmospheric conditions unless otherwise stated. Reaction mixtures were degassed using three freeze-pump-thaw cycles. Petroleum ether (hexanes) and ethyl acetate (EtOAc) were distilled prior to use. The reported yields are referred to isolated compounds unless otherwise stated.

Chromatography

For thin layer chromatography (TLC), precoated aluminum sheets (Merck silica gel 60 F₂₅₄) were used. UV light ($\lambda = 254$ nm) was applied for visualization. Staining was done with vanillin (6.0 g vanillin, 100.0 mL ethanol (95%) and 1.0 mL conc. sulfuric acid), ninhydrin (300.0 mg ninhydrin, 3.0 mL conc. acetic acid, 100.0 mL ethanol) or potassium permanganate (1.0 g KMnO₄, 2.0 g Na₂CO₃ and 100.0 mL distilled water) followed by heating. Column chromatography was performed with silica gel (Merck, Geduran 80, 0.063 – 0.200 mm particle size) and flash silica gel (Merck, 0.040 – 0.200 mm particle size).

NMR-Spectroscopy

¹H-NMR- and ¹³C-NMR Spectra were recorded on *Avance III* Systems of the Company Bruker, Rheinstetten:

Bruker Avance 300 FT-NMR (for 300 MHz ¹H -NMR- and 75 MHz ¹³C-NMR)

Bruker Avance 400 FT-NMR (for 400 MHz ¹H -NMR- and 101 MHz ¹³C-NMR and 377 MHz ¹⁹F-NMR)

Field strengths are expressed in MHz and chemical shifts are reported relative to the solvent residual peak of commercially available NMR-solvents CDCl₃: δ ppm = 7.26. The designation of the peak multiplicities is implemented as follow: s–singlet, d–doublet, dd–doublet of doublet, ddd–doublet of doublet of doublet, dt–doublet of triplet, dtd–doublet of triplet of doublet, t–triplet, td–triplet of doublet, q–quartet, p–pentet, m–multiplet.

IR-Spectroscopy

FTIR spectroscopy was performed on a Cary 630 FTIR spectrometer. Solid and liquid compounds were measured neatly, and the wave numbers are reported as cm⁻¹.

Mass Spectroscopy

Mass spectra were recorded by the Central Analytical Laboratory at the Department of Chemistry of the University of Regensburg on a Varian MAT311A, Finnigan MAT 95, Thermoquest Finnigan TSQ 7000 or Agilent Technologies 6540 UHD Accurate-Mass Q-TOF LC/MS. High-resolution mass spectra were performed using electrospray ionization (ESI) or electron ionization (EI) with a quadrupole time-of-flight (Q-TOF) detector.

Melting Point

For melting point measurements an SRS MPA 100 OptiMelt was used with a heating rate of 1 °C/min.

X-ray

X-ray crystallographic analysis was performed by the Central Analytic Department of the University of Regensburg using an Agilent Technologies SuperNova, Agilent Technologies Gemini R Ultra, Agilent GV 50 or Rigaku GV 50. Suitable crystals were mounted on a Lindemann tube oil and kept at a steady temperature of $T = 293$ K during data collection. The structures were solved with the ShelXT (Scheldrick 2015) structure solution program using the Intrinsic Phasing solution method and by using Olex2 as the graphical interface. The model was refined with ShelXL using Least Squares minimization.

Light Source

All photochemical reactions were performed using a LED-stick as irradiation source. (for more details, see chapter 5.2 Photochemical Setup).

5.2 Photochemical Setup

5.2.1 Schlenk Tube Setup

The internal irradiation setup was developed by O. Reiser *et. al.* (Figure 1).^[2] All photochemical reactions were performed using a LED-stick as irradiation source. The LED is placed on a glass rod (8 mm diameter; borosilicate glass; Schott Borofloat® 33) as fiber optics, which directly immerses in the reaction mixture.

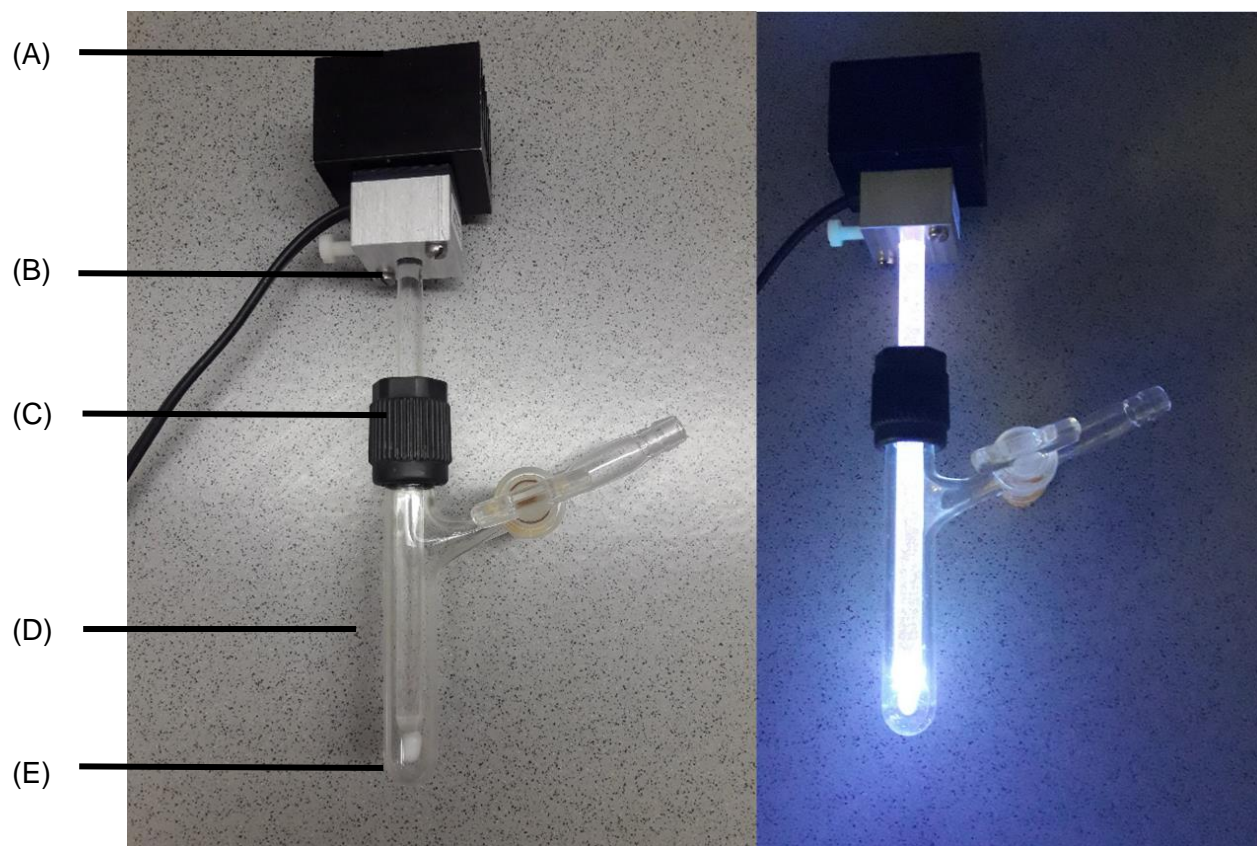


Figure 1. Irradiation setup for photochemical reactions: (A) LED; (B) glass rod; (C) Teflon adapter; (D) Schlenk tube (10.0 mL size); (E) Teflon-coated stirring bar.

Light Source

For all photochemical reactions monochromatic light emitting diodes (LED) were used as irradiation source. All relevant data are taken from the official data sheets provided by Osram, which are available free of charge via the internet at the Osram web page.

UV light irradiation was performed using a Seoul Viosys CUN66A1B (3 W, 500 mA, $\lambda_{\text{max}} = 367 \text{ nm}$), NVSU233A (3 W, 700 mA, $\lambda_{\text{max}} = 367 \text{ nm}$) and a Luminus SST-10 (3 W, 720 mA, $\lambda_{\text{max}} = 365 \text{ nm}$ or 405 nm).

Determination of the radiant flux for the “Immersed light guide”

The radiant flux and emission spectra of the LED light sources were measured, mounted on a glass or quartz rod ($8 \times 150 \text{ mm}$), were determined using an integrating sphere (2π geometry) with an Avantes AvaSpec 3648 spectrometer, coupled with a fiber optic. The spectrometer response of this setup was referenced against LEDs with known radiant flux, determined independently with a calibrated FieldMate Power Meter, Edmund Optics.

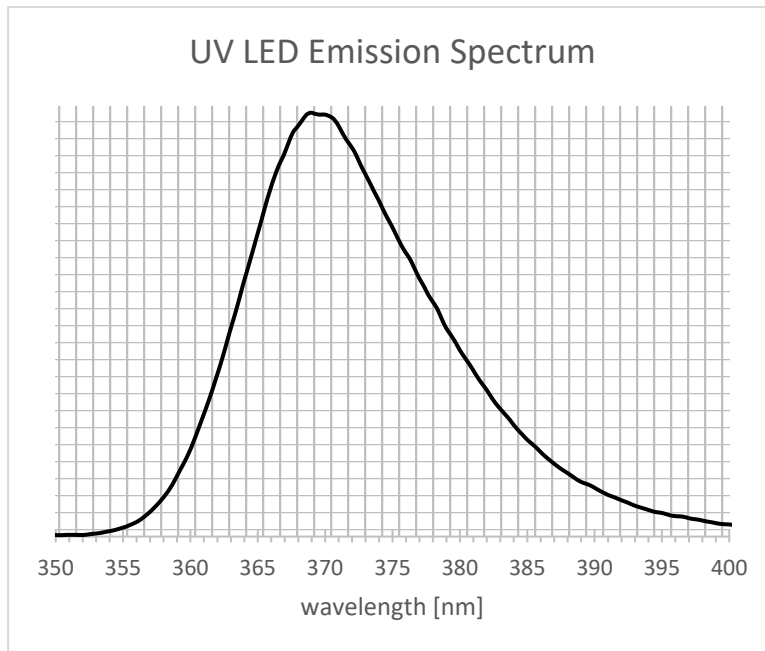


Figure 2. Emission Spectrum of Luminus SST-10.

Blue light irradiation was performed using an OSLO® 80 rb (3 W, 700 mA, $\lambda_{\text{max}} = 455 \text{ nm}$), Osram OSOLON® SSL deep blue (3 W, 700 mA, dominant wavelength $\lambda_{\text{dom}} = 455 \text{ nm}$, spectral bandwidth at 50% $I_{\text{max}} = 20 \text{ nm}$, radiant power at 25 °C and 700 mA ~ 900 mW), CREE XP rb LED (3 W, 700 mA, $\lambda_{\text{max}} = 455 \text{ nm}$).

Green light irradiation was performed using an Osram OSOLON® SSL 80 green (3 W, 700 mA, dominant wavelength $\lambda_{\text{dom}} = 530 \text{ nm}$, spectral bandwidth at 50% $I_{\text{max}} = 30 \text{ nm}$, luminous flux at 25 °C and 700 mA ~ 250 lum).

5.2.2 Upscaling Reactors

Photochemical upscaling reactions were performed in a Schlenk reaction vessel (40 mL), custom designed at the university of Regensburg by O. Reiser *et. al.* (Figure 3). The setup consists of an inner cooling mantle (A), cooling the reaction mixture during the reaction, giving an internal reactor volume of 40 mL with a short irradiation path after solvent displacement by the cooling mantle. The glass reaction vessel itself (C) sitting directly on top of the magnet stirrer was irradiated from the outside by twenty Osram OSOLON® SSL 80 deep blue ca. 3W/LED at 700 mA, $\lambda_{\max} = 455$ nm LEDs, arranged around the outside wall of the reaction vessel in an LED array (D). The LEDs were air-cooled by a fan driven by the magnetic stir plate. This LED array (D) contained the glass reaction vessel itself (C) sitting directly on top of the magnet stirrer.

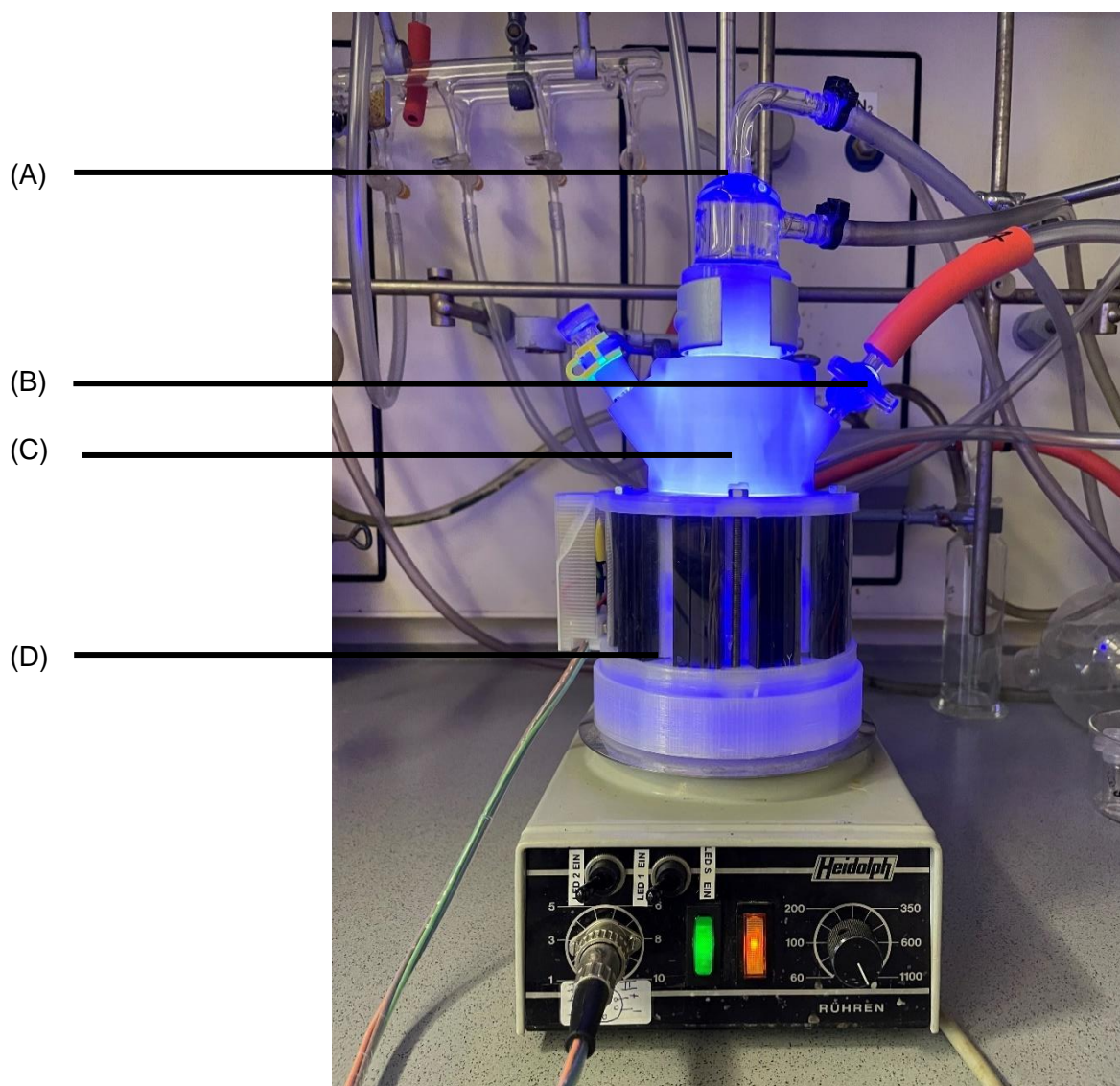


Figure 3. Irradiation setup for upscaling of photochemical reactions: (A) Inner cooling mantle; (B) glass stock (attached to schlenk line); (C) glass reaction vessel; (D) LED array around the reactor.

Next to the upscaling reactor for 455 nm also a setup for UV-irradiation (368 nm) was designed by Dr. Peter Kreitmeier (Figure 4). Therefore, the photochemical upscaling reaction was performed in a Schlenk reaction vessel (with adjustable filling volume). The setup consists of an inner cooling mantle (A), cooling the reaction mixture during the reaction, giving an adjustable internal reactor volume with a short irradiation path after solvent displacement by the cooling mantle. The glass reaction vessel itself (C) sitting directly on top of the magnet stirrer was irradiated from the outside by 4 x 12 Luminus SST-10 UV LEDs (SST-10-UV-B130-G385-00) ca. 3W/LED at 700 mA, $\lambda_{\text{max}} = 455 \text{ nm}$ LEDs, arranged around the outside wall of the reaction vessel in LED Zones (D). The LEDs were water-cooled by a cooling block circulating inbetween the Zones. The LED Zones (D) contained the glass reaction vessel itself (C) sitting directly on top of the magnet stirrer. Depending on the filling volume of the reactor, the corresponding LED Zones 1–4 were employed. To shield dangerous scatter light, an aluminum mantle was used.

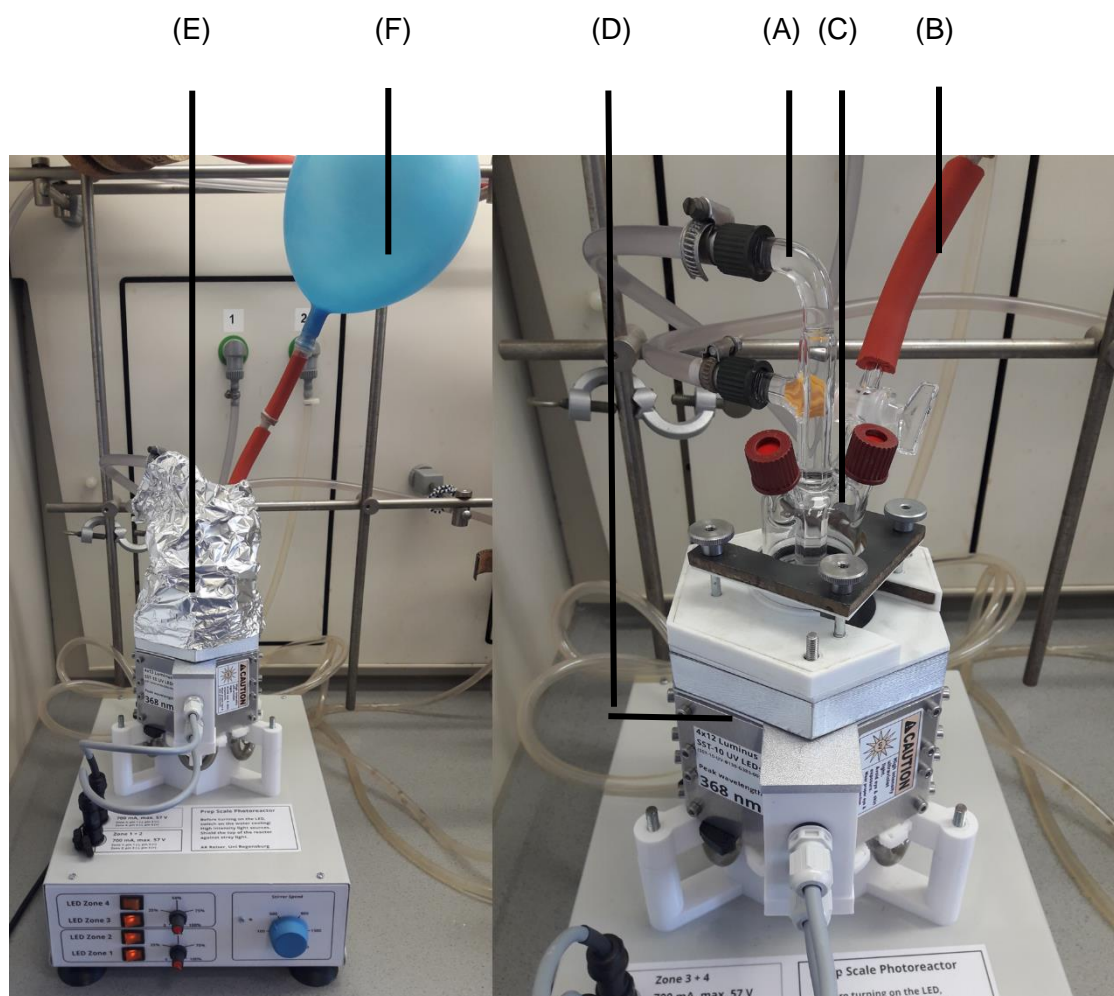


Figure 4. Irradiation setup for upscaling of photochemical reactions at 368 nm: (A) Inner cooling finger; (B) glass stock (attached to oxygen balloon); (C) glass reaction vessel; (D) LED Zones around the reactor with cooling block. (E) Aluminium mantle, to shield dangerous scatter light (F) oxygen balloon.

5.3 Experimental Part for Chapter 2

5.3.1 UV-vis Absorption Measurements

All UV-vis measurements were recorded on a SPECTRORECORD 200 PLUS of the company analytikjena using a Macro cell type 110-QS quartz cuvette with PTFE stopper (Hellma Analytics quartz cuvette, 10 × 10 mm, 3.5 mL). For UV-vis spectra of the Cu-complexes **2** and **3**, stock solutions with a concentration of $2.5 \cdot 10^{-3}$ mol/L. (referred to Cu(II)) were prepared. A volume of 200 μ L was transferred to a cuvette, containing acetonitrile (2 mL) and water (45 μ L). Then the spectra were recorded.

For UV-Vis monitoring (Figure 5), 4-methoxyphenylacetic acid (**1a**) (41.5 mg, 0.25 mmol, 1.0 equiv) and [Cu(dmp)(**1a**)₂] (**3**) (15.1 mg, 25.0 μ mol, 10 mol%) were dissolved in dry MeCN (2.0 mL, 0.125 M) and water (45 μ L, 2.2 Vol%). The mixture was irradiated at 367 nm under O₂ atmosphere for 24 h at room temperature (30 °C). After 24h, 10 μ L of the reaction mixture was dissolved into 2 mL of acetonitrile, showing the typical absorption at 450 nm for [Cu(I)(dmp)]⁺. UV-vis spectra of **1a** and the product **4a** showed no increased absorbance at 367 and 450 nm.

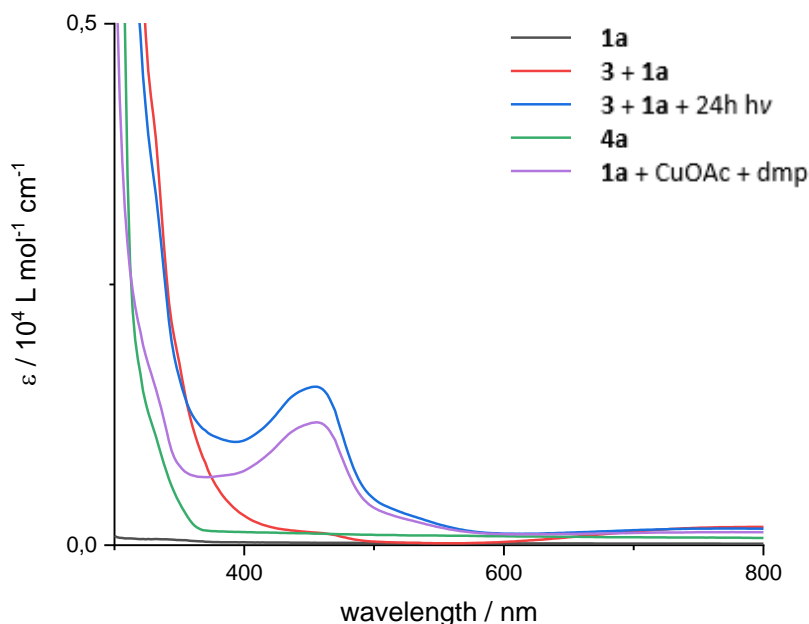


Figure 5. UV-vis monitoring of the reaction solution and absorbance spectra of **1a** and **4a**.

5.3.2 Radical Trap Experiment and Reaction under N₂-Atmosphere

5.3.2.1 TEMPO Trapping

For TEMPO trapping experiments, 4-methoxyphenylacetic acid (**1a**) (41.5 mg, 0.25 mmol, 1.0 equiv) and [Cu(dmp)(**1a**)₂] (**3**) (15.1 mg, 25.0 μmol, 10 mol%) and (2,2,6,6-tetramethylpiperidin-1-yl)oxyl (TEMPO) (46.9 mg, 0.30 mmol, 1.2 equiv) were dissolved in dry MeCN (2.0 mL, 0.125 M) and water (45 μL, 2.2 Vol%). The mixture was irradiated at 367 nm under O₂ atmosphere for 24 h at room temperature (30°C).

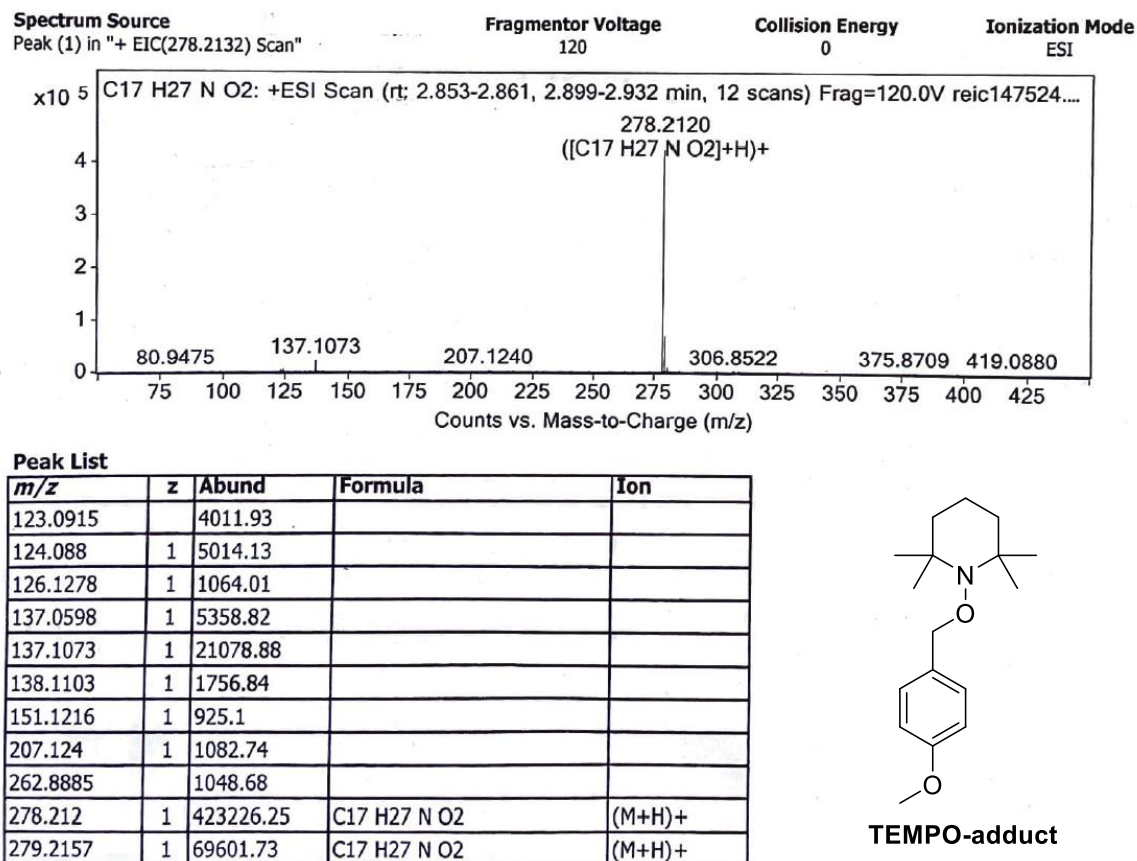
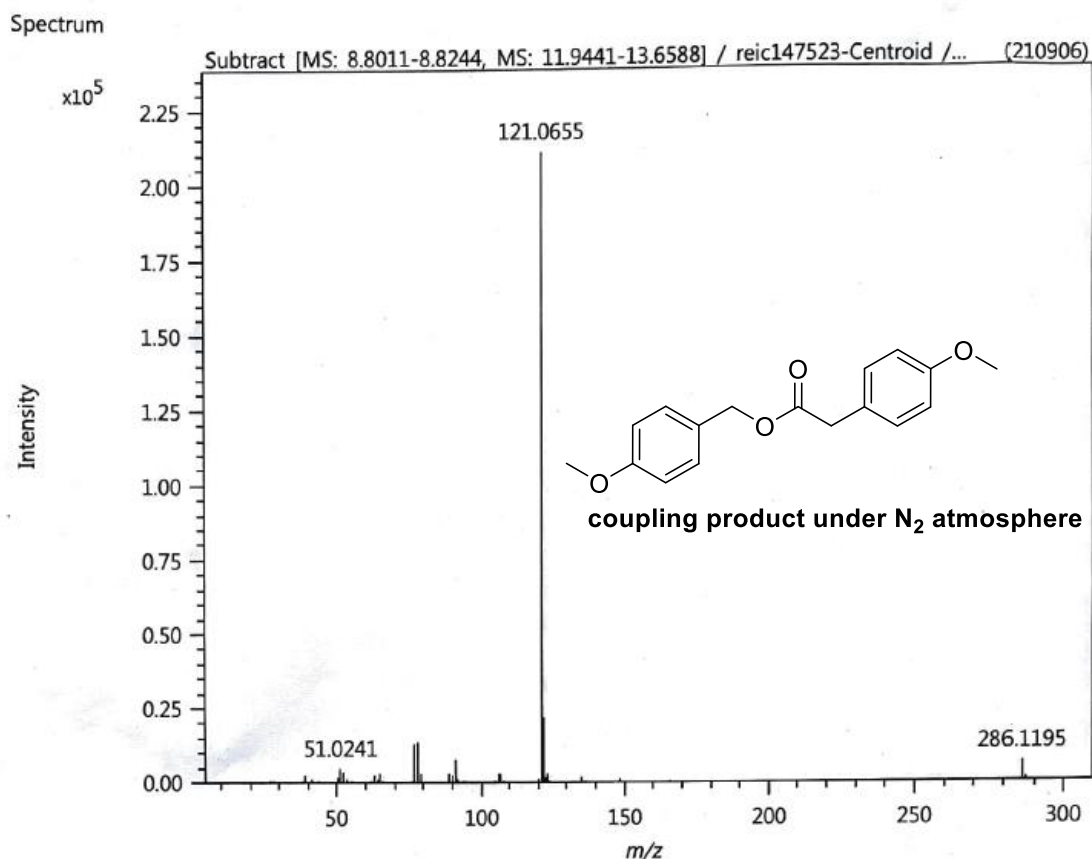


Figure 6. HRMS of TEMPO trap experiment (crude reaction mixture was submitted for analysis).

The decarboxylation reaction is completely suppressed and the TEMPO-adduct was observed by ESI-HRMS (calc. for C₁₇H₂₇NO₂ [M+H]⁺: 278.2115, found 278.2120). The result indicates the formation of free radicals in the mechanistic pathway (*vide supra*, Figure 6).

5.3.2.2 Reaction under N₂-Atmosphere

For the reaction under N₂-atmosphere, 4-methoxyphenylacetic acid (**1a**) (0.25 mmol, 1.0 equiv), Cu(OAc)₂ (25 μmol, 10 mol%) and dmp (2,9-dimethyl-1,10-phenanthroline) (25 μmol, 10 mol%) were dissolved in dry MeCN (2.0 mL, 0.125 M), water (45 μL, 2.2 Vol%). The reaction mixture was degassed three times applying freeze-pump-thaw-cycles. Irradiation at 367nm under N₂ atmosphere for 24 h at room temperature (30°C).



Elemental Composition

Parameters

Tolerance: 10.00 ppm
 Electron: Odd/Even
 Charge: +1
 DBE: -1.5 - 50.0

Elements:

Symbol	C	H	N	O	Cl	S	Se	Sen
Min	0	0	0	0	0	0	0	0
Max	100	100	0	5	0	0	0	0

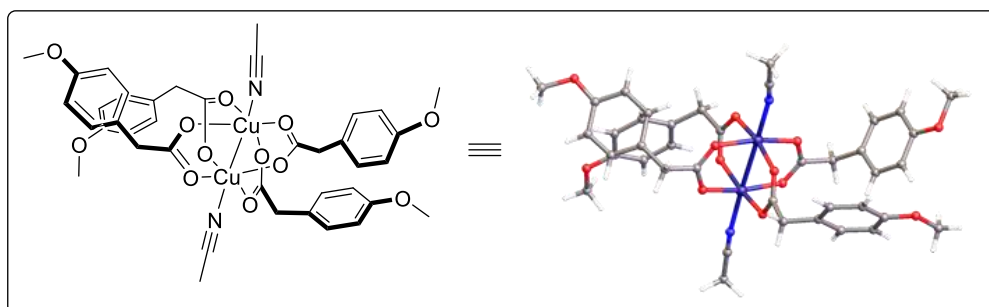
Results

Mass	Intensity	Formula	Calculated Mass	Mass Difference [mDa]	Mass Difference [ppm]	DBE
286.11953	6713.13	C ₁₇ H ₁₈ O ₄	286.11996	-0.43	-1.52	9.0

Figure 7. HRMS of Reaction under N₂-Atmosphere (crude reaction mixture was submitted for analysis).

5.3.3 Synthesis of Copper(II)-carboxylates

$\text{Cu}_2(4\text{-MeOpa})_4(\text{MeCN})_2$ (**2**)



The procedure for the synthesis of copper-carboxylate was slightly modified from the literature.^[3] 4-methoxy phenylacetic acid (**1a**) (2.0 g, 12.0 mmol, 1.0 equiv) and 1M aq. NaOH (12.0 mL, 12.0 mmol, 1.0 equiv) were combined and sonicated for 5 minutes. Then copper(II)-sulfate pentahydrate (1.50 g, 6.02 mmol, 0.5 equiv) was added to the reaction mixture. The product precipitated immediately. After stirring for 30 min, the precipitate was collected by filtration and washed with water and diethyl ether. The precipitate was dried *in vacuo* for 3 h at 100 °C (heatgun), to afford copper(II) arylacetate (2.05 g, 86%) as parise-greenish powder.

Characterization of the copper(II) arylacetate precipitate:

mp: 215 °C (decomposition).

Elemental microanalysis (%): calculated for $(\text{Cu}(\mathbf{1a})_2)_n \cong (\text{C}_{18}\text{H}_{18}\text{CuO}_6)_n$: C 54.89, H 4.61
found: C 51.83, H 4.95.

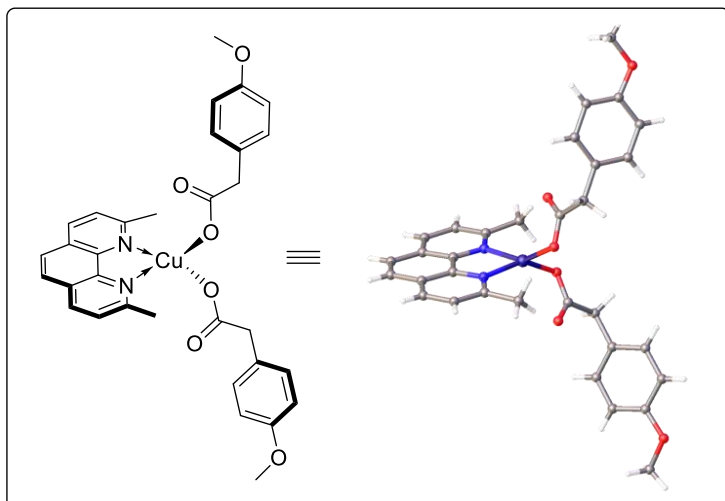
IR (neat, cm^{-1}): 3541, 3429, 3008, 2914, 2840, 1580, 1513, 1464, 1431, 1401, 1304, 1248, 1177, 1032, 924, 861, 823, 738, 700.

Single crystals suitable for X-ray analysis of the paddle-wheel complex (**2**) were obtained by crystallization of the precipitate *via* vapor diffusion of Et_2O into MeCN solution (1.0 mL).

mp: 205 °C (decomposition).

Elemental microanalysis (%): calculated for $[\text{Cu}_2(\mathbf{1a})_4(\text{MeCN})_2] \cong \text{C}_{40}\text{H}_{42}\text{Cu}_2\text{N}_2\text{O}_{12}$: C 55.23, H 4.87
found: C 52.54, H 4.72.

IR (neat, cm^{-1}): 3046, 3000, 2937, 2911, 2836, 1584, 1513, 1464, 1394, 1300, 1244, 1177, 1107, 1032, 939, 857, 820, 730, 700.

Bis(2-(4-methoxyphenyl)acetoxy) neocuproino cuprate (3)

A round-bottomed flask was charged with copper(II) carboxylate (**2**) (200 mg, 508 μmol , 1.0 equiv) followed by addition of CHCl_3 (3 mL). The suspension was placed in an ultrasonic bath for 5 min. Afterward, neocuproine (dmp) (106 mg, 508 μmol , 1.0 equiv) was added to the reaction mixture. A color change from dark greenish to bright greenish was observable. The reaction mixture was stirred for 1 h at 25 $^\circ\text{C}$. Cold diethyl ether was added to precipitate the product. Filtration and subsequent drying *in vacuo* afforded the desired complex $[\text{Cu}(\text{dmp})(\mathbf{1a})_2]$ (**3**) as a bright greenish solid (291 mg, 483 μmol , 95%).

mp: 254 $^\circ\text{C}$ (decomposition).

IR (neat, cm^{-1}): 3026, 2989, 2840, 1595, 1509, 1446, 1358, 1300, 1274, 1241, 1177, 1148, 1107, 1025, 924, 861, 823, 685.

Elemental microanalysis (%): calculated for $\text{C}_{32}\text{H}_{30}\text{CuN}_2\text{O}_6$: C 63.83, H 5.02, N 4.65 found: C 62.97, H 5.04, N 4.55.

HRMS (ESI-MS) exact mass calc. for $[\text{Cu}(\text{neocup})_2]^+$: m/z 479.1297, found: m/z 479.1311.

Single crystals suitable for X-ray analysis of copper complex (**3**) were obtained by vapor diffusion of pentane into CHCl_3 solution (1.0 mL).

5.3.4 Synthesis of Compounds via Photocatalytic Decarboxylation

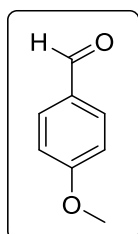
General Procedure for Cu(II)-photocatalyzed Decarboxylative Oxygenation of Carboxylic Acids (GP-A)

A flame-dried Schlenk tube (10.0 mL size) equipped with a magnetic stirring bar was charged with anhydrous $\text{Cu}(\text{OAc})_2$ (4.5 mg, 25 μmol , 10 mol%), dmp (5.2 mg, 25 μmol , 10 mol%) and the carboxylic acid (0.25 mmol, 1.0 equiv). Subsequently, the solvent mixture MeCN (2.0 mL) and water (45 μL , 2.2 Vol%) was added. The reaction tube was flushed with oxygen and a balloon containing oxygen was added. A Teflon sealed inlet for a glass rod was placed on the reaction tube, through which irradiation with LED took place from above. The mixture was stirred in an aluminum block at room temperature (30 °C) for 24 h; for a detailed setup see Figure 1, Chapter 5.2 Photochemical Setup. The reaction was monitored by TLC. Afterwards, two equal reaction mixtures were united and the solvent was removed under reduced pressure (200 mbar) to afford the crude.

Two different work-up procedures were used. Work-up Procedure A: The residue was dissolved in DCM/ EtOAc and the solution was filtered through a pad of basic aluminum oxide (washed three times) and the filtrate was concentrated *in vacuo* (200 mbar).

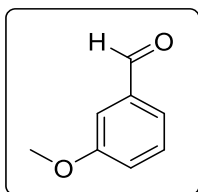
Work-up-Procedure B: The residue was purified by flash column chromatography on silica gel (eluent hexanes/ EtOAc).

4-methoxybenzaldehyde (4a)



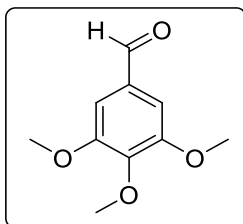
Following general procedure (GP-A) using 4-methoxyphenylacetic acid (**1a**) (83.1 mg, 0.5 mmol, 1.0 equiv), dmp (10.4 mg, 50 μmol , 10 mol%), dry $\text{Cu}(\text{OAc})_2$ (9.1 mg, 50 μmol , 10 mol%) in the solvent mixture at room temperature (30 °C) and irradiation with UV-LED ($\lambda_{\text{max}} = 367 \text{ nm}$; radiant power of 400 mW) for 24 h yielded 63.5 mg (446 μmol , 93%) of 4-methoxybenzaldehyde (**4a**) as a colorless oil, using work-up procedure A. Spectral data are in accordance to literature.^[4] **Rf** (5:1 hexanes / EtOAc) = 0.51.

¹H NMR (300 MHz, CDCl_3) δ [ppm] = 9.85 (s, 1H), 7.81 (d, $J = 8.8 \text{ Hz}$, 2H), 6.97 (d, $J = 8.7 \text{ Hz}$, 2H), 3.85 (s, 3H). **¹³C NMR** (75 MHz, CDCl_3) δ [ppm] = 190.9, 164.7, 132.0, 130.0, 114.4, 55.6.

3-methoxybenzaldehyde (4b)

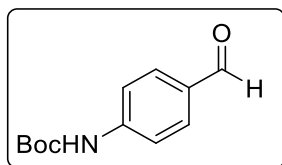
Following general procedure (GP-A) using 3-methoxyphenylacetic acid (**1b**) (83.1 mg, 0.5 mmol, 1.0 equiv), dmp (10.4 mg, 50 μ mol, 10 mol%), dry $\text{Cu}(\text{OAc})_2$ (9.1 mg, 50 μ mol, 10 mol%) and the solvent mixture at room temperature (30 $^\circ\text{C}$) and irradiation with UV-LED ($\lambda_{\text{max}} = 367$ nm, radiant power of 400 mW) for 24 h yielded 60.0 mg (441 μ mol, 88%) of 3-methoxybenzaldehyde (**4b**) as a colorless oil, using work-up procedure A. Spectral data are in accordance to literature.^[5] R_f (5:1 hexanes / EtOAc) = 0.51.

$^1\text{H NMR}$ (300 MHz, CDCl_3) δ [ppm] = 9.98 (s, 1H), 7.49 – 7.44 (m, 2H), 7.41 – 7.37 (m, 1H), 7.22 – 7.14 (m, 1H), 3.87 (s, 3H). $^{13}\text{C NMR}$ (75 MHz, CDCl_3) δ [ppm] = 192.3, 160.3, 137.9, 130.2, 123.7, 121.7, 112.1, 55.6.

3,4,5-trimethoxybenzaldehyde (4c)

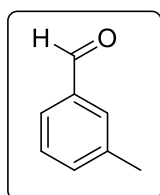
Following general procedure (GP-A) using 3,4,5-trimethoxyphenylacetic acid (**1c**) (113.1 mg, 0.5 mmol, 1.0 equiv), dmp (10.4 mg, 50 μ mol, 10 mol%), dry $\text{Cu}(\text{OAc})_2$ (9.1 mg, 50 μ mol, 10 mol%) and the solvent mixture at room temperature (30 $^\circ\text{C}$) and irradiation with UV-LED ($\lambda_{\text{max}} = 367$ nm, radiant power of 400 mW) for 24 h yielded 83.8 mg (427 μ mol, 85%) of 3,4,5-trimethoxybenzaldehyde (**4c**) as a white solid, using work-up procedure B (hexanes / EtOAc 5:1). Spectral data are in accordance to literature.^[6] R_f (5:1 hexanes / EtOAc) = 0.24.

$^1\text{H NMR}$ (400 MHz, CDCl_3) δ [ppm] = 9.83 (s, 1H), 7.09 (s, 2H), 3.89 (s, 9H). $^{13}\text{C NMR}$ (101 MHz, CDCl_3) δ [ppm] = 191.1, 153.7, 143.6, 131.8, 106.8, 61.0, 56.3.

tert-butyl (4-formylphenyl)carbamate (4d)

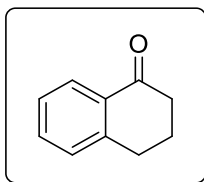
Following general procedure (GP-A) using 2-(4-((tert-butoxycarbonyl)amino)phenyl)acetic acid (**1d**) (125.6 mg, 0.5 mmol, 1.0 equiv), dmp (10.4 mg, 50 μ mol, 10 mol%), dry $\text{Cu}(\text{OAc})_2$ (9.1 mg, 50 μ mol, 10 mol%) and the solvent mixture at room temperature (30 $^\circ\text{C}$) and irradiation with UV-LED ($\lambda_{\text{max}} = 367$ nm, radiant power of 400 mW) for 24 h yielded 107.3 mg (485 μ mol, 97%) of tert-butyl (4-formylphenyl)carbamate (**4d**) as a white solid, using work-up procedure B (hexanes / EtOAc 5:1). Spectral data are in accordance to literature.^[7] R_f (5:1 hexanes / EtOAc) = 0.39.

$^1\text{H NMR}$ (400 MHz, CDCl_3) δ [ppm] = 9.88 (s, 1H), 7.81 (d, $J = 8.2$ Hz, 2H), 7.54 (d, $J = 8.2$ Hz, 2H), 6.94 (s, 1H), 1.52 (s, 9H). $^{13}\text{C NMR}$ (101 MHz, CDCl_3) δ [ppm] = 191.1, 152.2, 144.4, 131.4, 131.4, 117.9, 81.6, 28.4.

3-methylbenzaldehyde (4e)

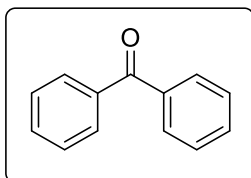
Following general procedure (GP-A) using 3-methylphenylacetic acid (**1e**) (83.1 mg, 0.5 mmol, 1.0 equiv), dmp (10.4 mg, 50 μ mol, 10 mol%), dry $\text{Cu}(\text{OAc})_2$ (9.1 mg, 50 μ mol, 10 mol%) and the solvent mixture at room temperature (30 $^\circ\text{C}$) and irradiation with UV-LED ($\lambda_{\text{max}} = 367$ nm, radiant power of 400 mW) for 24 h yielded 53.3 mg (444 μ mol, 89%) of 3-methylbenzaldehyde (**4e**) as a pale yellow oil, using work-up procedure B (hexanes / EtOAc 1:2). Spectral data are in accordance to literature.^[4] R_f (5:1 hexanes / EtOAc) = 0.82.

$^1\text{H NMR}$ (300 MHz, CDCl_3) δ [ppm] = 9.96 (s, 1H), 7.49 – 7.36 (m, 3H), 7.17 (dt, $J = 5.9, 2.8$ Hz, 1H), 3.85 (s, 3H). $^{13}\text{C NMR}$ (101 MHz, CDCl_3) δ [ppm] = 192.3, 160.3, 138.0, 130.2, 123.7, 121.7, 112.2, 55.6.

3,4-dihydronaphthalen-1(2H)-one (4h)

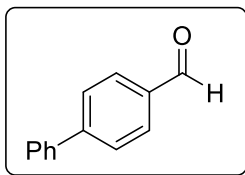
Following general procedure (GP-A) using 1,2,3,4-tetrahydronaphthalene-1-carboxylic acid (**1h**) (88.1 mg, 0.5 mmol, 1.0 equiv), dmp (10.4 mg, 50 μ mol, 10 mol%), dry $\text{Cu}(\text{OAc})_2$ (9.1 mg, 50 μ mol, 10 mol%) and the solvent mixture at room temperature (30 °C) and irradiation with UV-LED ($\lambda_{\text{max}} = 367$ nm, radiant power of 400 mW) for 24 h yielded 60.3 mg (412 μ mol, 82%) of 3,4-dihydronaphthalen-1(2H)-one (**4h**) as a yellowish oil, using work-up procedure B (hexanes / EtOAc 5:1). Spectral data are in accordance to literature.^[8] **Rf** (5:1 hexanes / EtOAc) = 0.67.

¹H NMR (400 MHz, CDCl_3) δ [ppm] = 8.03 (dd, $J = 7.9, 1.4$ Hz, 1H), 7.47 (td, $J = 7.5, 1.5$ Hz, 1H), 7.33 – 7.28 (m, 1H), 7.25 (d, $J = 7.2$ Hz, 1H), 2.97 (t, $J = 6.1$ Hz, 2H), 2.66 (dd, $J = 7.3, 5.8$ Hz, 2H), 2.14 (p, $J = 6.5$ Hz, 2H). **¹³C NMR** (101 MHz, CDCl_3) δ [ppm] = 198.5, 144.6, 133.5, 132.8, 128.9, 127.3, 126.8, 39.3, 29.9, 23.4.

benzophenone (4i)

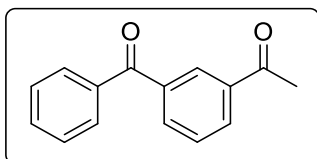
Following general procedure (GP-A) using 2,2-diphenylacetic acid (**1i**) (106.1 mg, 0.5 mmol, 1.0 equiv), dmp (10.4 mg, 50 μ mol, 10 mol%), dry $\text{Cu}(\text{OAc})_2$ (9.1 mg, 50 μ mol, 10 mol%) and the solvent mixture at room temperature (30 °C) and irradiation with UV-LED ($\lambda_{\text{max}} = 367$ nm, radiant power of 400 mW) for 24 h yielded 90.2 mg (495 μ mol, 99%) of benzophenone (**4i**) as a colorless oil, using work-up procedure B (hexanes / EtOAc 5:1). Spectral data are in accordance to literature.^[8] **Rf** (5:1 hexanes / EtOAc) = 0.60.

¹H NMR (400 MHz, CDCl_3) δ [ppm] = 7.84 – 7.77 (m, 4H), 7.62 – 7.56 (m, 2H), 7.55 – 7.44 (m, 4H). **¹³C NMR** (101 MHz, CDCl_3) δ [ppm] = 196.8, 137.6, 132.4, 130.1, 128.3.

[1,1'-biphenyl]-4-carbaldehyde (4j)

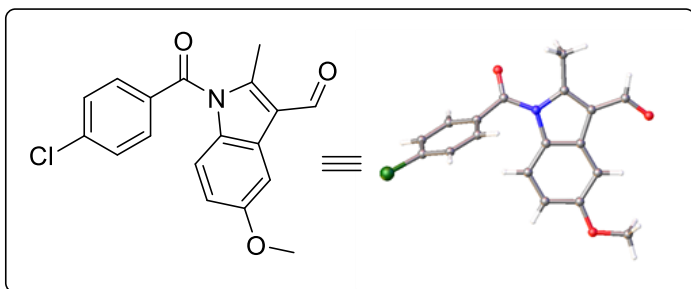
Following general procedure (GP-A) using 2-([1,1'-biphenyl]-4-yl)acetic acid (**1j**) (106.1 mg, 0.5 mmol, 1.0 equiv), dmp (10.4 mg, 50 μ mol, 10 mol%), dry $\text{Cu}(\text{OAc})_2$ (9.1 mg, 50 μ mol, 10 mol%) and the solvent mixture at room temperature (30 $^\circ\text{C}$) and irradiation with UV-LED ($\lambda_{\text{max}} = 367$ nm, radiant power of 160 mW) for 24 h yielded 68.8 mg (378 μ mol, 76%) of [1,1'-biphenyl]-4-carbaldehyde (**4j**) as a white solid, using work-up procedure B (hexanes / EtOAc 10:1). Ca. 15% of side product 4-methyl-1,1'-biphenyl were detected. Spectral data of **4j** are in accordance to literature.^[6] **Rf** (10:1 hexanes / EtOAc) = 0.38.

$^1\text{H NMR}$ (400 MHz, CDCl_3) δ [ppm] = 10.06 (s, 1H), 8.00 – 7.91 (m, 2H), 7.79 – 7.72 (m, 2H), 7.68 – 7.60 (m, 2H), 7.53 – 7.44 (m, 2H), 7.47 – 7.37 (m, 1H). **$^{13}\text{C NMR}$** (101 MHz, CDCl_3) δ [ppm] = 192.1, 147.3, 139.8, 135.3, 130.4, 129.1, 128.6, 127.8, 127.5.

1-(3-benzoylphenyl)ethan-1-one (4k)

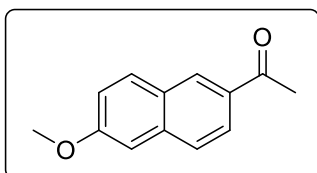
Following general procedure (GP-A) using 2-(4-benzoylphenyl)propanoic acid (ketoprofen) (**1k**) (134.1 mg, 0.5 mmol, 1.0 equiv), dmp (10.4 mg, 50 μ mol, 10 mol%), dry $\text{Cu}(\text{OAc})_2$ (9.1 mg, 50 μ mol, 10 mol%) and the solvent mixture at room temperature (30 $^\circ\text{C}$) and irradiation with UV-LED ($\lambda_{\text{max}} = 367$ nm, radiant power of 400 mW) for 24 h yielded 74.5 mg (332 μ mol, 66%) of 1-(3-benzoylphenyl)ethan-1-one (**4k**) as a white solid, using work-up procedure B (hexanes / EtOAc 5:1). Spectral data are in accordance to literature.^[6] **Rf** (5:1 hexanes / EtOAc) = 0.38.

$^1\text{H NMR}$ (400 MHz, CDCl_3) δ [ppm] = 8.36 (td, $J = 1.8, 0.6$ Hz, 1H), 8.18 (ddd, $J = 7.8, 1.8, 1.2$ Hz, 1H), 8.01 – 7.97 (m, 1H), 7.82 – 7.76 (m, 2H), 7.65 – 7.57 (m, 2H), 7.54 – 7.45 (m, 2H), 2.65 (s, 3H). **$^{13}\text{C NMR}$** (101 MHz, CDCl_3) δ [ppm] = 197.4, 196.0, 138.2, 137.3, 137.1, 134.4, 133.0, 131.9, 130.2, 129.8, 128.9, 128.6, 26.9.

1-(4-chlorobenzoyl)-5-methoxy-2-methyl-1H-indole-3-carbaldehyde (4l)

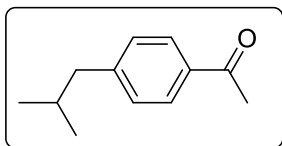
Following general procedure (GP-A) using indometacine (**1l**) (178.9 mg, 0.5 mmol, 1.0 equiv), dmp (10.4 mg, 50 μ mol, 10 mol%), dry $\text{Cu}(\text{OAc})_2$ (9.1 mg, 50 μ mol, 10 mol%) and the solvent mixture at room temperature (30 °C) and irradiation with UV-LED ($\lambda_{\text{max}} = 367$ nm, radiant power of 160 mW) for 24 h yielded 76.5 mg (223 μ mol, 47%) of 1-(4-chlorobenzoyl)-5-methoxy-2-methyl-1H-indole-3-carbaldehyde (**4l**) as a white crystalline solid, using work-up procedure B (hexanes / EtOAc 5:1). Spectral data are in accordance to literature.^[6] *Rf* (5:1 hexanes / EtOAc) = 0.33.

¹H NMR (400 MHz, CDCl_3) δ [ppm] = 10.32 (s, 1H), 7.81 (t, $J = 1.6$ Hz, 1H), 7.72 – 7.68 (m, 2H), 7.53 – 7.47 (m, 2H), 6.73 (d, $J = 1.6$ Hz, 2H), 3.87 (s, 3H), 2.76 (s, 3H). **¹³C NMR** (101 MHz, CDCl_3) δ [ppm] = 185.9, 168.4, 157.3, 148.6, 141.1, 132.2, 131.8, 130.8, 129.6, 127.1, 118.5, 114.4, 114.0, 103.5, 55.9, 12.8. Single crystals suitable for X-ray analysis compound **2l** were obtained by crystallization from CHCl_3 (1.0 mL).

1-(6-methoxynaphthalen-2-yl)ethan-1-one (4m)

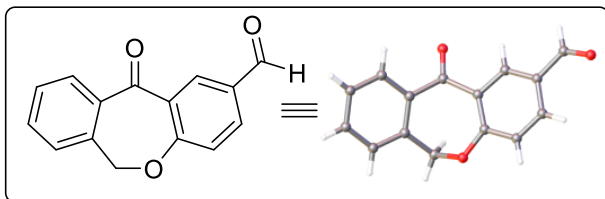
Following general procedure (GP-A) using 2-(6-methoxynaphthalen-2-yl)propanoic acid/naproxene (**1m**) (115.1 mg, 0.5 mmol, 1.0 equiv), dmp (10.4 mg, 50 μ mol, 10 mol%), dry $\text{Cu}(\text{OAc})_2$ (9.1 mg, 50 μ mol, 10 mol%) and the solvent mixture at room temperature (30 °C) and irradiation with UV-LED ($\lambda_{\text{max}} = 367$ nm, radiant power of 400 mW) for 24 h yielded 99.7 mg (498 μ mol, 99%) of 1-(6-methoxynaphthalen-2-yl)ethan-1-one (**4m**) as a white crystalline solid, using work-up procedure B (hexanes / EtOAc 5:1). Spectral data are in accordance to literature.^[9] *Rf* (5:1 hexanes / EtOAc) = 0.36.

¹H NMR (300 MHz, CDCl_3) δ [ppm] = 8.38 (d, $J = 1.8$ Hz, 1H), 8.00 (dd, $J = 8.6, 1.8$ Hz, 1H), 7.84 (dt, $J = 8.9, 0.7$ Hz, 1H), 7.79 – 7.70 (m, 1H), 7.20 (dd, $J = 8.9, 2.5$ Hz, 1H), 7.14 (d, $J = 2.5$ Hz, 1H), 3.94 (s, 3H), 2.69 (s, 3H). **¹³C NMR** (75 MHz, CDCl_3) δ [ppm] = 198.0, 159.8, 137.4, 132.7, 131.2, 130.2, 127.9, 127.2, 124.8, 119.8, 105.8, 55.5, 26.7.

1-(4-isobutylphenyl)ethan-1-one (4n)

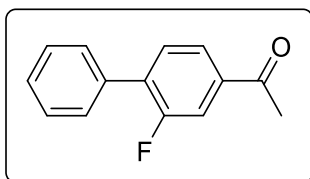
Following general procedure (GP-A) using 2-(4-isobutylphenyl)propanoic acid / ibuprofen (**1n**) (115.1 mg, 0.5 mmol, 1.0 equiv), dmp (10.4 mg, 50 μ mol, 10 mol%), dry $\text{Cu}(\text{OAc})_2$ (9.1 mg, 50 μ mol, 10 mol%) and the solvent mixture at room temperature (30 $^\circ\text{C}$) and irradiation with UV-LED ($\lambda_{\text{max}} = 367$ nm, radiant power of 400 mW) for 24 h yielded 86.0 mg (488 μ mol, 98%) of 1-(4-isobutylphenyl)ethan-1-one (**4n**) as a colorless oil, using work-up procedure B (hexanes / EtOAc 5:1). Spectral data are in accordance to literature.^[4] **Rf** (5:1 hexanes / EtOAc) = 0.83.

^1H NMR (300 MHz, CDCl_3) δ [ppm] = 7.91 – 7.80 (m, 2H), 7.25 – 7.20 (m, 2H), 2.58 (s, 3H), 2.52 (d, $J = 7.2$ Hz, 2H), 1.89 (dt, $J = 13.9, 7.0$ Hz, 1H), 0.90 (d, $J = 6.6$ Hz, 6H). **^{13}C NMR** (75 MHz, CDCl_3) δ [ppm] = 198.0, 147.7, 135.1, 129.4, 128.4, 45.5, 30.2, 26.7, 22.4.

11-oxo-6,11-dihydrodibenzo[b,e]oxepine-2-carbaldehyde (4o)

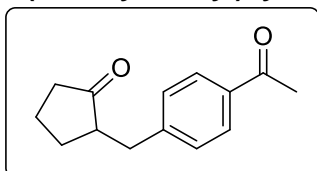
Following general procedure (GP-A) using 2-(11-oxo-6,11-dihydrodibenzo[b,e]oxepin-2-yl)acetic acid (**1o**) (134.1 mg, 0.5 mmol, 1.0 equiv), dmp (10.4 mg, 50 μ mol, 10 mol%), dry $\text{Cu}(\text{OAc})_2$ (9.1 mg, 50 μ mol, 10 mol%) and the solvent mixture at room temperature (30 $^\circ\text{C}$) and irradiation with UV-LED ($\lambda_{\text{max}} = 367$ nm, radiant power of 160 mW) for 24 h yielded 67.0 mg (281 μ mol, 56%) of 11-oxo-6,11-dihydrodibenzo[b,e]oxepine-2-carbaldehyde (**4o**) as a yellowish solid, using work-up procedure B (hexanes / EtOAc 5:1). Spectral data are in accordance to literature.^[6] **Rf** (5:1 hexanes / EtOAc) = 0.33.

^1H NMR (300 MHz, CDCl_3) δ [ppm] = 9.97 (s, 1H), 8.71 (d, $J = 2.2$ Hz, 1H), 8.00 (dd, $J = 8.6, 2.2$ Hz, 1H), 7.87 (dd, $J = 7.6, 1.5$ Hz, 1H), 7.59 (td, $J = 7.4, 1.5$ Hz, 1H), 7.49 (td, $J = 7.6, 1.4$ Hz, 1H), 7.40 (d, $J = 7.4$ Hz, 1H), 7.15 (d, $J = 8.0$ Hz, 1H), 5.27 (s, 2H). **^{13}C NMR** (75 MHz, CDCl_3) δ [ppm] = 190.5, 190.3, 165.6, 140.4, 137.5, 134.6, 133.5, 133.3, 131.0, 129.8, 129.5, 128.3, 125.1, 122.3, 73.7. Single crystals suitable for X-ray analysis compound **2n** were obtained by crystallization from CHCl_3 (1.0 mL).

1-(2-fluoro-[1,1'-biphenyl]-4-yl)ethan-1-one (4p)

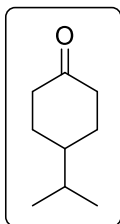
Following general procedure (GP-A) using 2-(2-fluoro-[1,1'-biphenyl]-4-yl)propanoic acid / fluorobiprofen (**1p**) (122.1 mg, 0.5 mmol, 1.0 equiv), dmp (10.4 mg, 50 μ mol, 10 mol%), dry $\text{Cu}(\text{OAc})_2$ (9.1 mg, 50 μ mol, 10 mol%) and the solvent mixture at room temperature (30 $^\circ\text{C}$) and irradiation with UV-LED ($\lambda_{\text{max}} = 367$ nm, radiant power of 400 mW) for 24 h yielded 100.7 mg (470 μ mol, 94%) of 1-(2-fluoro-[1,1'-biphenyl]-4-yl)ethan-1-one (**4p**) as a white crystalline solid, using work-up procedure B (hexanes / EtOAc 10:1). Spectral data are in accordance to literature.^[6] **Rf** (10:1 hexanes / EtOAc) = 0.33.

^1H NMR (400 MHz, CDCl_3) δ 7.80 (dd, $J = 8.0, 1.7$ Hz, 1H), 7.74 (dd, $J = 11.1, 1.7$ Hz, 1H), 7.58 (d, $J = 8.5$ Hz, 2H), 7.54 (t, $J = 7.9$ Hz, 1H), 7.47 (t, $J = 7.3$ Hz, 2H), 7.42 (t, $J = 7.2$ Hz, 1H), 2.62 (s, 3H). **^{13}C NMR** (101 MHz, CDCl_3) δ [ppm] = 196.5 (d, $J = 1.9$ Hz), 159.8 (d, $J = 249.9$ Hz), 137.9 (d, $J = 6.5$ Hz), 134.8 (d, $J = 1.6$ Hz), 133.9 (d, $J = 13.7$ Hz), 131.0 (d, $J = 3.4$ Hz), 129.1 (d, $J = 3.1$ Hz), 128.7, 128.6, 124.4 (d, $J = 3.5$ Hz), 116.0 (d, $J = 24.0$ Hz), 26.7. **^{19}F NMR** (376 MHz, CDCl_3) δ [ppm] = -117.19 (ddt, $J = 9.2, 7.5, 1.9$ Hz).

2-(4-acetylbenzyl)cyclopentan-1-one (4q)

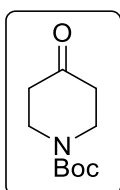
Following general procedure (GP-A) using 2-(4-((2-oxocyclopentyl)methyl)phenyl)propanoic acid (**1q**) (123.2 mg, 0.5 mmol, 1.0 equiv), dmp (10.4 mg, 50 μ mol, 10 mol%), dry $\text{Cu}(\text{OAc})_2$ (9.1 mg, 50 μ mol, 10 mol%) and the solvent mixture at room temperature (30 $^\circ\text{C}$) and irradiation with UV-LED ($\lambda_{\text{max}} = 367$ nm, radiant power of 400 mW) for 24 h yielded 106.5 mg (492 μ mol, 98%) of 2-(4-acetylbenzyl)cyclopentan-1-one (**4q**) as a colorless oil, using work-up procedure B (hexanes / EtOAc 3:1). **Rf** (3:1 hexanes / EtOAc) = 0.35.

^1H NMR (400 MHz, CDCl_3) δ [ppm] = 7.85 (d, $J = 8.3$ Hz, 2H), 7.23 (d, $J = 8.2$ Hz, 2H), 3.15 (dd, $J = 13.9, 4.3$ Hz, 1H), 2.63 – 2.56 (m, 1H), 2.55 (s, 3H), 2.38 – 2.21 (m, 2H), 2.14 – 2.01 (m, 2H), 1.99 – 1.87 (m, 1H), 1.78 – 1.64 (m, 1H), 1.50 (dtd, $J = 12.5, 11.0, 6.5$ Hz, 1H). **^{13}C NMR** (101 MHz, CDCl_3) δ [ppm] = 219.5, 197.8, 145.9, 135.4, 129.2, 128.6, 50.7, 38.1, 35.6, 29.2, 26.6, 20.6. **IR** (neat, cm^{-1}): 2963, 2877, 2363, 1736, 1681, 1606, 1572, 1412, 1360, 1267, 1185, 1121, 1017, 957, 861, 820, 693. **HRMS** (EI-MS) exact mass calc. for $\text{C}_{14}\text{H}_{16}\text{O}_2$ $[\text{M}]^+$ m/z 216.11448, found: m/z 216.11411.

4-isopropylcyclohexan-1-one (4r)

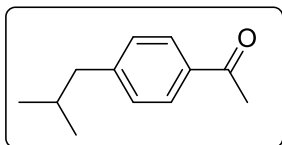
Following general procedure (GP-A) using 4-isopropylcyclohexane-1-carboxylic acid (**1r**) (85.2 mg, 0.5 mmol, 1.0 equiv), dmp (10.4 mg, 50 μ mol, 10 mol%), dry $\text{Cu}(\text{OAc})_2$ (9.1 mg, 50 μ mol, 10 mol%) and the solvent mixture at room temperature (30 °C) and irradiation with UV-LED ($\lambda_{\text{max}} = 367$ nm, radiant power of 400 mW) for 24 h yielded 39.9 mg (285 μ mol, 57%) of 4-isopropylcyclohexan-1-one (**4r**) as a colorless smelly oil, using work-up procedure B (hexanes / EtOAc 10:1). Spectral data are in accordance to literature.^[10] **Rf** (5:1 hexanes / EtOAc) = 0.54. Vanillin-Stain.

¹H NMR (400 MHz, CDCl_3) δ [ppm] = 2.48 – 2.21 (m, 4H), 2.05 – 1.91 (m, 2H), 1.61 – 1.38 (m, 4H), 0.92 (d, $J = 6.7$ Hz, 6H). **¹³C NMR** (101 MHz, CDCl_3) δ [ppm] = 212.8, 42.7, 41.2, 31.9, 29.8, 20.1.

tert-butyl 4-oxopiperidine-1-carboxylate (4s)

Following general procedure (GP-A) using 1-(tert-butoxycarbonyl)piperidine-4-carboxylic acid (**1s**) (114.6 mg, 0.5 mmol, 1.0 equiv), dmp (10.4 mg, 50 μ mol, 10 mol%), dry $\text{Cu}(\text{OAc})_2$ (9.1 mg, 50 μ mol, 10 mol%) and the solvent mixture at room temperature (30 °C) and irradiation with UV-LED ($\lambda_{\text{max}} = 367$ nm, radiant power of 400 mW) for 24 h yielded 72.0 mg (361 μ mol, 72%) of tert-butyl 4-oxopiperidine-1-carboxylate (**4s**) as a colorless solid, using work-up procedure B (hexanes / EtOAc 5:1). Spectral data are in accordance to literature.^[11] **Rf** (5:1 hexanes / EtOAc) = 0.34. Vanillin-Stain.

¹H NMR (400 MHz, CDCl_3) δ [ppm] = 3.70 (t, $J = 6.2$ Hz, 4H), 2.42 (t, $J = 6.2$ Hz, 4H), 1.47 (s, 9H). **¹³C NMR** (101 MHz, CDCl_3) δ [ppm] = 208.0, 154.7, 80.6, 43.1, 41.3, 28.5.

Gram-Scale Experiment**1-(4-isobutylphenyl)ethan-1-one (4n)**

The oven-dried schlenk tube of the photochemical UV-upscaling reactor (Inlet A + Vessel A, Irradiation Zones 1-3) (see chapter 5.2.2 Upscaling Reactors) equipped with a stirring bar was charged with anhydrous $\text{Cu}(\text{OAc})_2$ (136.2 mg, 750.0 μmol , 10 mol%), dmp (156.2 mg, 750.0 μmol , 10 mol%) and 2-(4-isobutylphenyl)propanoic acid / ibuprofen (**1n**) (1.55 g, 7.5 mmol, 1.0 equiv). Subsequently, the solvent mixture MeCN (60.0 mL) and water (1.36 mL, 2.2 Vol%) was added. The reaction tube was flushed with oxygen, the corresponding cooling finger was connected and a balloon containing oxygen was added. The stirring speed was 400 rpm and zones 1-3 were irradiated for 18 h with UV-light ($\lambda_{\text{max}} = 368 \text{ nm}$). Completeness of the reaction was monitored via TLC. Subsequently, the reaction mixture was concentrated in vacuo. Silica column chromatography (hexanes / EtOAc 10:1) yielded 1.20 g (8.82 mmol, 91%) of 1-(4-isobutylphenyl)ethan-1-one (**4n**) as a colorless oil. Spectral data are in accordance to literature.^[4] R_f (5:1 hexanes / EtOAc) = 0.83.

$^1\text{H NMR}$ (300 MHz, CDCl_3) δ [ppm] = 7.91 – 7.80 (m, 2H), 7.25 – 7.20 (m, 2H), 2.58 (s, 3H), 2.52 (d, $J = 7.2 \text{ Hz}$, 2H), 1.89 (dt, $J = 13.9, 7.0 \text{ Hz}$, 1H), 0.90 (d, $J = 6.6 \text{ Hz}$, 6H).

5.4 Experimental Part for Chapter 3

5.4.1 Selected Olefins Photocatalyst Comparison

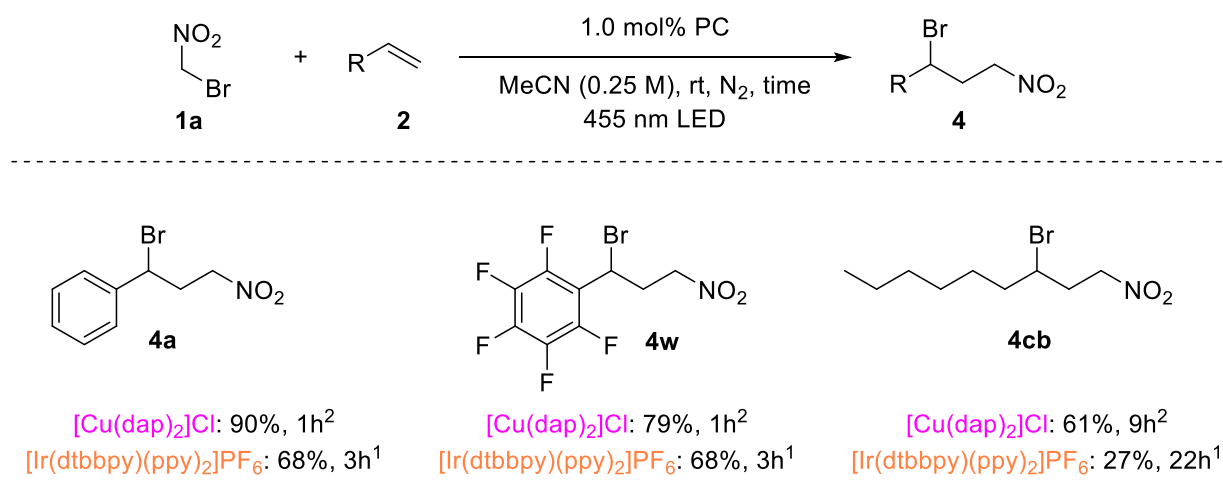


Figure 8. Selected Photocatalyst Comparison Copper(I) vs. Iridium(IV).

Reaction was stopped when olefin consumed.¹ on 0.25 mmol scale. NMR yield with 1,1,2,2-tetrachloroethane as the internal standard. ²isolated yield 0.5 mmol scale.

5.4.2 UV-vis Absorption Measurements

For UV-vis absorption measurements, bromonitromethane (**1a**) (0.25 mmol, 1.0 equiv), styrene (**2a**) (0.25 mmol, 1.0 equiv), and [Cu(dap)₂]Cl (1 mol%) were dissolved in dry degassed MeCN (1.0 mL, 0.25 M). After given time, 20 μ L of the reaction mixture was dissolved into 2 mL of acetonitrile. All UV-vis measurements were recorded on a SPECTRORECORD 200 PLUS of the company analytikjena. using a Macro cell type 110-QS quartz cuvette with PTFE stopper (Hellma Analytics quartz cuvette, 10 x 10 mm, 3.5 mL).

5.4.3 Quantum Yield Measurement

The quantum yield Φ of the visible light-mediated Cu(I)-catalyzed bromonitromethylation of bromonitromethane (**1a**) with styrene (**2a**) was determined using a method developed by Riedle and co-workers.^[12] For irradiation, a blue LED (1000 mA operating current, $\lambda_{\text{max}} = 451$ nm, Osram OSLON SSL80 LD-CQ7P-2U3U) was used. The radiant power was detected with a commercial power meter (PowerMax USB – PS19Q Power Sensor from Coherent) using computer-aided read out with PowerMax software. The measurement was carried out in diluted solution, since the undiluted reaction solution showed to high absorbance.

An oven dried schlenk flask equipped with a stirring bar was charged with $[\text{Cu}(\text{dap})_2]\text{Cl}$ (4.4 mg, 1 mol%, 0.01 equiv) Then dry MeCN (10 mL) was added under positive nitrogen atmosphere. The solution was degassed by three freeze-pump-thaw cycles.

Afterwards bromonitromethane (**1a**) (70.0 mg, 36.0 μL , 0.5 mmol, 1.0 equiv) and styrene (**2a**) (52.1 mg, 58.0 μL , 0.5 mmol, 1.0 equiv) were added under a slight nitrogen overpressure. An oven-dried fluorescence cuvette equipped with a magnetic stirring bar and a septum was flushed with nitrogen. Immediately prior to the quantum yield measurement, 2.0 mL of the reaction solution was transferred to the fluorescence cuvette under nitrogen atmosphere. The whole measurement was carried out in a dark room to minimize ambient light. First, the radiant power of light transmitted by a fluorescence cuvette with blank solution P_{ref} was measured. After that, the fluorescence cuvette with the blank solution was exchanged by the fluorescence cuvette containing the diluted reaction mixture and the transmitted radiant power P_{sample} was determined for an irradiation time of $\Delta t = 30$ min. Finally, the reaction yield or rather the molar amount of product molecules generated n_{product} was determined by $^1\text{H-NMR}$ analysis with 1,1,2,2-tetrachloroethane as an internal standard.

The quantum yield Φ was calculated as the following:

$$\Phi = \frac{N_{\text{product}}}{N_{\text{ph,abs}}} = \frac{n_{\text{product}} \cdot N_{\text{A}} \cdot h \cdot c}{P_{\text{abs}} \cdot \Delta t \cdot \lambda} = \frac{n_{\text{product}} \cdot N_{\text{A}} \cdot h \cdot c}{(P_{\text{ref}} - P_{\text{sample}}) \cdot \Delta t \cdot \lambda \cdot f}$$

Here, Φ is the quantum yield, N_{product} is the number of created product molecules, $N_{\text{ph,abs}}$ is the number of absorbed photons, n_{product} is the molar amount of product molecules generated in [mol], N_{A} is Avogadro's constant in [mol^{-1}], h is Plank's constant in [Js], c is the speed of light in [m/s], P_{abs} is the radiant power absorbed in [W], Δt is the irradiation time in [s], λ is the wavelength of the irradiation source in [m], P_{ref} is the radiant power transmitted by a fluorescence cuvette with blank solution in [W], P_{sample} is the radiant power transmitted by the fluorescence cuvette containing the reaction sample in [W] and f is a correction factor depending on the reflection coefficient R of the air-glass-interface.

Neglecting second order effects, the correction factor f can be calculated from:

$$f = \frac{1 + R \cdot \frac{P_{\text{sample}}}{P_{\text{ref}}}}{1 - R}$$

The reflection coefficient R for a fused silica cuvette and an irradiation wavelength of

$\lambda = 451$ nm is equal to $R = 0.0357$.

With this formula, the preceding data obtained from the measurement could be used to calculate the final value for the quantum yield Φ as the following:

n_{product}	$0.235 \cdot 10^{-3} \text{ mol}$	N_A	$6.022 \cdot 10^{23} \text{ mol}^{-1}$
P_{sample}	$5.8 \cdot 10^{-3} \text{ W}$	h	$6.626 \cdot 10^{-34} \text{ Js}$
P_{ref}	$104.0 \cdot 10^{-3} \text{ W}$	c	$2.998 \cdot 10^8 \text{ ms}$

$$f = \frac{1 + R \cdot \frac{P_{\text{sample}}}{P_{\text{ref}}}}{1 - R} = \frac{1 + R \cdot \frac{5.8 \cdot 10^{-3} \text{ W}}{104.0 \cdot 10^{-3} \text{ W}}}{1 - 0.0357} = 1.039$$

$$\Phi = \frac{N_{\text{product}}}{N_{\text{ph,abs}}} = \frac{n_{\text{product}} \cdot N_A \cdot h \cdot c}{P_{\text{abs}} \cdot \Delta t \cdot \lambda} =$$

$$= \frac{0.235 \cdot 10^{-3} \text{ mol} \cdot 6.022 \cdot 10^{23} \text{ mol}^{-1} \cdot 6.626 \cdot 10^{-34} \text{ Js} \cdot 2.998 \cdot 10^8 \text{ ms}}{(104.0 \cdot 10^{-3} \text{ W} - 5.8 \cdot 10^{-3} \text{ W}) \cdot 1800 \text{ s} \cdot 451 \cdot 10^{-9} \text{ m} \cdot 1.039}$$

$$= \mathbf{0.06788} \cong 7\%$$

5.4.4 Fluorescence Quenching Interactions (Stern-Volmer)

The interaction of the photocatalyst $\text{Cu}(\text{dap})_2\text{Cl}$ with ATRA-reagent bromonitromethane (**1a**) was measured recording fluorescence emission spectra. All measurements were recorded with a HORIBA Fluoromax-4 of the company Horbia Scientific, using a High Precision Cell 117100F-10-40 quartz cuvette with scew cap (Hellma Analytics quartz cuvette, 10 × 10 mm, 3.5 mL).

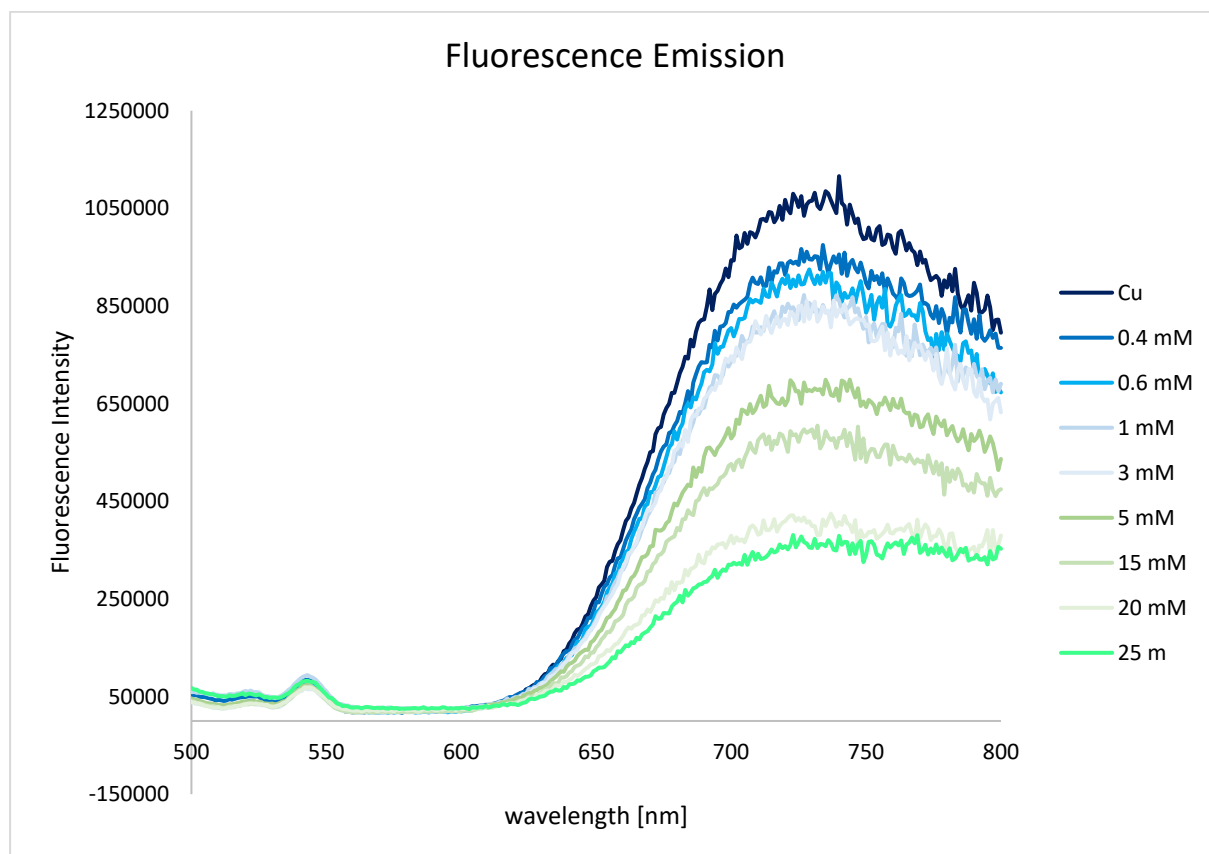


Figure 9. Fluorescence Emission Spectra of a 0.2 mM solution of $[\text{Cu}(\text{dap})_2]\text{Cl}$ in MeCN with varying concentrations of the quencher bromonitromethane (**1a**).

Stern-Volmer plots and quenching constants for the emission of $[\text{Cu}(\text{dap})_2]\text{Cl}$ quenched by bromonitromethane (**1a**) showed an interaction between the photocatalyst and the ATRA reagent prior to reaction. Solutions were prepared under nitrogen atmosphere immediately prior measurement.

For excitation, mixtures were irradiated with 467 nm and the data at maximum of the fluorescence emission (722 nm) was taken for preparing the Stern-Volmer plot. Interaction was only detected between $[\text{Cu}(\text{dap})_2]\text{Cl}$ and bromonitromethane (**1a**) not with styrene (**2a**).

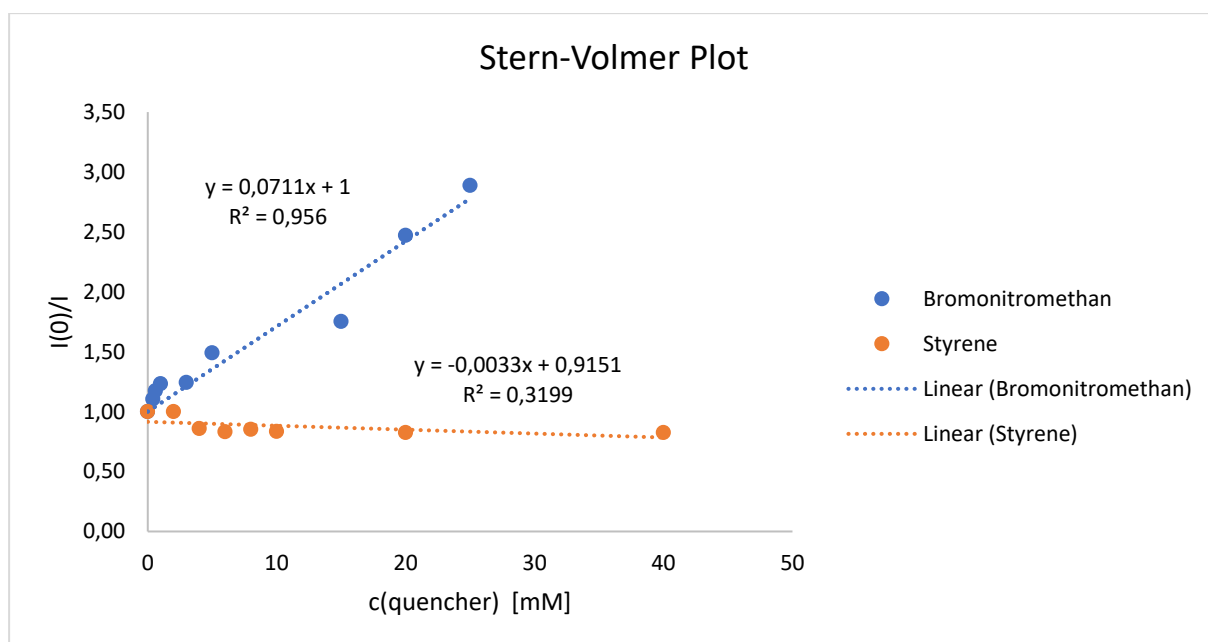


Figure 10. Stern-Volmer plot for $[\text{Cu}(\text{dap})_2]\text{Cl}$ and the ATRA reagent bromonitromethane (**1a**) (blue line) and for $[\text{Cu}(\text{dap})_2]\text{Cl}$ and styrene (**2a**), showing interaction of photocatalyst and quencher in case of bromonitromethane (**1a**).

Stern-Volmer Plot for $[\text{Cu}(\text{dap})_2]\text{Cl}$ vs. MeCN recorded in DCM (degassed) showed no quenching (Figure 11).

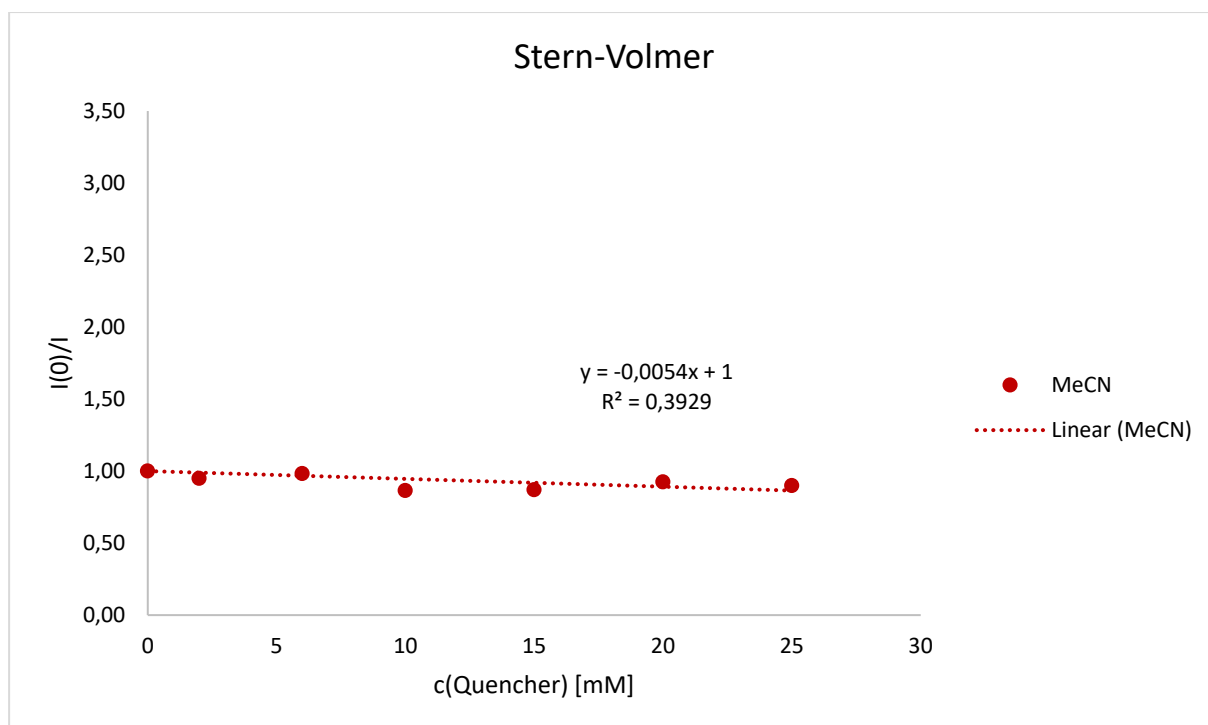


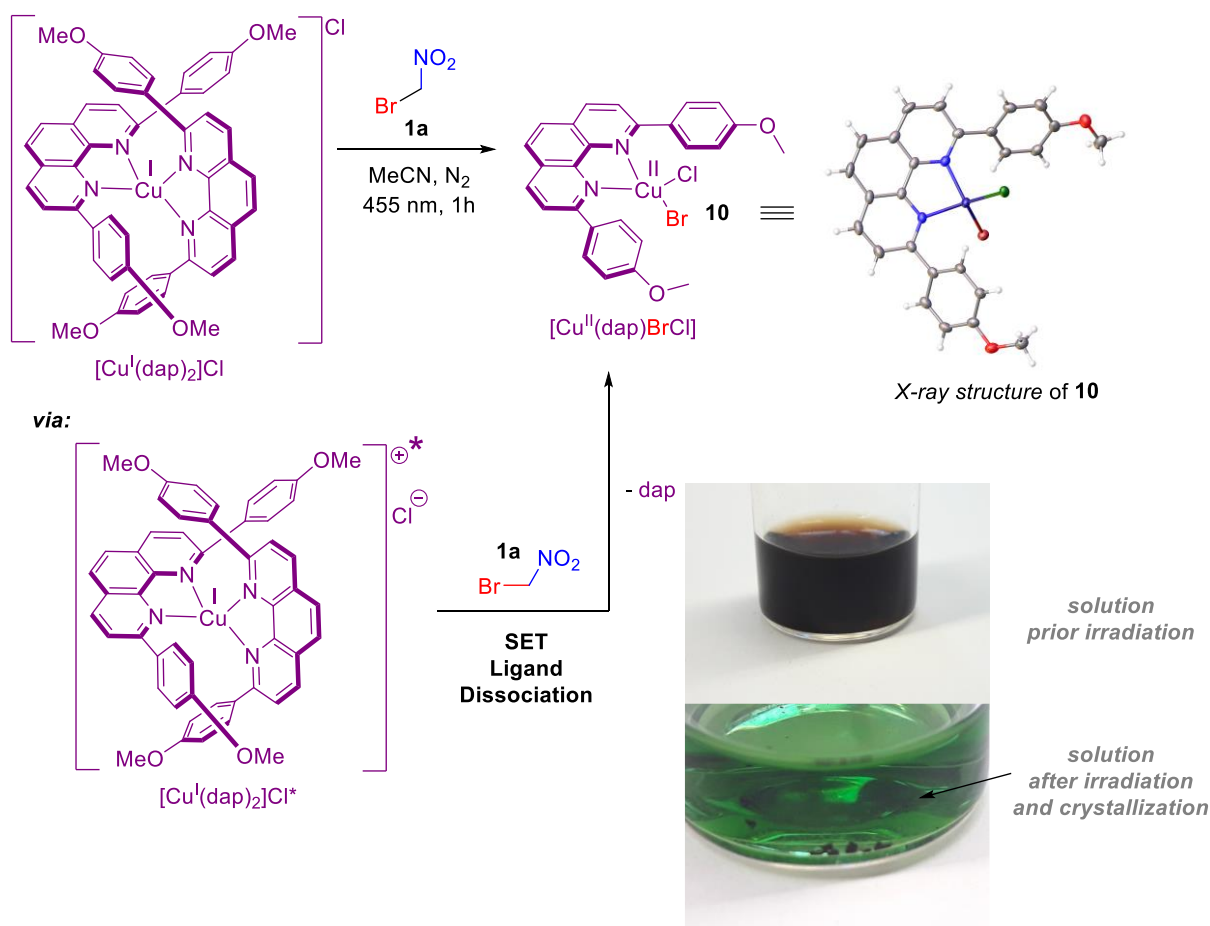
Figure 11. Stern-Volmer plot for $[\text{Cu}(\text{dap})_2]\text{Cl}$ and MeCN (red line), recorded in degassed DCM to exclude ligand exchange prior excitation.

5.4.5 Investigations on Homolysis of [Cu^I(dap)₂]Cl

5.4.5.1 [Cu^I(dap)₂]Cl in Presence of Bromonitromethane (1a)

An oven dried schlenk tube (10 mL size) equipped with a stirring bar was charged with [Cu(dap)₂]Cl (4.4 mg, 5.0 μmol, 1.0 equiv) Then dry MeCN (2.0 mL, 0.625 M) was added under positive nitrogen atmosphere. The solution was degassed by three freeze-pump-thaw cycles. Then bromonitromethane (**1a**) (175.0 mg, 1.25 mmol, 250.0 equiv) was added under nitrogen atmosphere. A Teflon sealed inlet for a glass rod was placed on the reaction tube, through which irradiation with LED_{455nm} took place from above for a period of 1 h (for a detailed setup see chapter 5.2.1 Schlenk Tube Setup). The mixture was stirred in an aluminum block at room temperature (25 °C). After 5 days, greenish-blue crystals of complex **10** were growing. X-ray analysis showed the incorporation of bromine (Scheme 1). Detailed X-ray parameter can be found in chapter 6.4 Crystallographic Data for Chapter 3.

Crystallization of [Cu^{II}(dap)BrCl]



Scheme 1. Irradiation Experiment of the photocatalyst [Cu^I(dap)₂]Cl in presence of bromonitromethane (**1a**).

3.4.5.2 [Cu^I(dap)₂]Cl in Absence of Bromonitromethane (1a)

An oven dried schlenk tube (10 mL size) equipped with a stirring bar was charged with [Cu(dap)₂]Cl (66.0 mg, 0.375 mmol) Then dry MeCN (3mL, 0.125 M) was added under positive nitrogen atmosphere. The solution was degassed by three freeze-pump-thaw cycles. A Teflon sealed inlet for a glass rod was placed on the reaction tube, through which irradiation with LED_{455nm} took place from above for a period of 3 h (for a detailed setup see chapter 5.2.1 Schlenk Tube Setup). Afterwards the solution was concentrated in *vacuo*. ¹H-NMR analysis showed no homolysis of the complex, since no free dap ligand was detected (Figure 12).

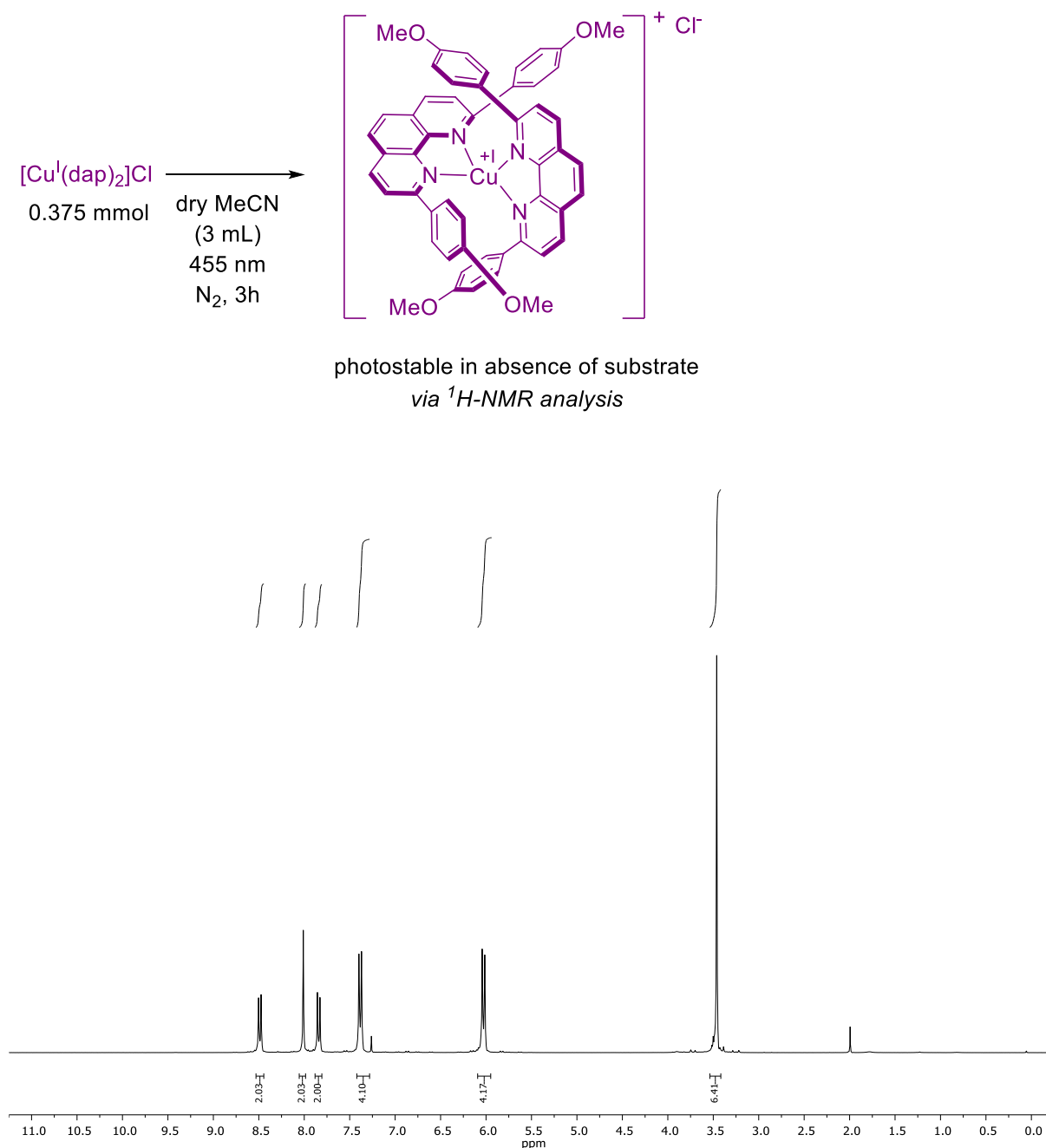
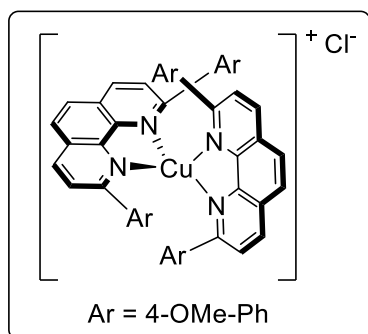


Figure 12. Crude ¹H-NMR of the photocatalyst [Cu(dap)₂]Cl after an irradiation period of 3h in MeCN showed no dap ligand homolysis.

5.4.6 Synthesis of Compounds

5.4.6.1 Synthesis of literature-known Compounds

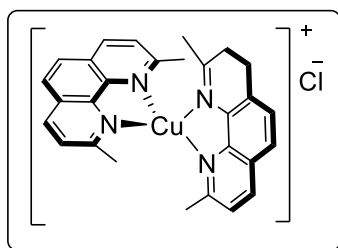
[Cu(dap)₂]Cl



A 50 mL round-bottom flask equipped with a magnetic stirring bar was charged with CuCl (98.4 mg, 993.7 μmol , 1.3 equiv) and dissolved in CHCl_3 (15 mL, 0.10 M) and 9-bis(4-methoxyphenyl)-1,10-phenanthroline (dap) was added (600.0 mg, 1.53 mmol, 2.0 equiv). The solution was stirred at 60 $^\circ\text{C}$ for 1h. Then the reaction mixture was stirred for 24 h at room temperature (25 $^\circ\text{C}$). Afterward, the solution was filtered over cotton. Addition of cold diethyl ether resulted in precipitation of the product. Filtration and subsequent drying *in vacuo* afforded the desired complex [Cu(dap)₂]Cl as a violet-black solid in 650.0 mg (735.4 μmol , 96%). Spectral data are in accordance with literature.^[13]

¹H NMR (400 MHz, CDCl_3) δ [ppm] = 8.50 (d, J = 8.3 Hz, 1H), 8.02 (s, 1H), 7.86 (d, J = 8.3 Hz, 1H), 7.40 (d, J = 8.3 Hz, 2H), 6.05 (d, J = 8.3 Hz, 2H), 3.48 (s, 3H). ¹³C NMR (101 MHz, CDCl_3) δ [ppm] = 160.3, 156.5, 143.6, 137.2, 131.2, 129.3, 127.9, 126.2, 124.6, 112.7, 55.4.

[Cu(dmp)₂]Cl

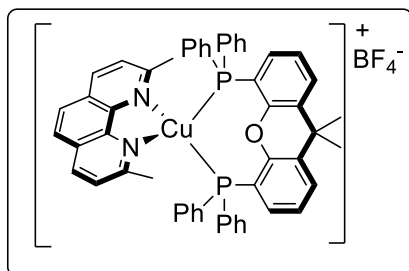


Based on a slightly modified literature procedure,^[14] a round-bottom flask equipped with a magnetic stirring bar was charged with 2,9-dimethyl-1,10-phenanthroline (624.8 mg, 3.0 mmol, 2.0 equiv), dissolved in chloroform (40 mL) and stirred at room temperature (25 $^\circ\text{C}$) for 30 min. CuCl (148.5 mg, 1.5 mmol, 1.0 equiv) was added and the resulting mixture was stirred for 18 h at room temperature (25 $^\circ\text{C}$). Afterwards it was concentrated *in vacuo* (to a volume of 25 mL) and the complex was precipitated using diethylether. The red precipitate was collected by vacuum filtration using a fritted funnel. The solid was washed with cold diethyl ether and dried

in vacuo to yield 728.0 mg (1.4 mmol, 94%) of $[\text{Cu}(\text{dmp})_2]\text{Cl}$ as a bright red solid. Spectral data are in accordance with literature.^[14]

$^1\text{H NMR}$ (400 MHz, CDCl_3) δ [ppm] = 8.54 (d, J = 8.3 Hz, 2H), 8.05 (s, 2H), 7.79 (d, J = 8.2 Hz, 2H), 2.41 (s, 6H). $^{13}\text{C NMR}$ (101 MHz, CDCl_3) δ [ppm] = 157.7, 143.1, 137.5, 127.7, 126.3, 125.7, 26.0.

$[\text{Cu}(\text{Xanthphos})(\text{dmp})]\text{BF}_4$

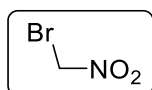


Slightly modified from literature.^[15] $[\text{Cu}(\text{MeCN})_4\text{BF}_4]$ (220.2 mg, 0.7 mmol, 1 equiv) and Xanthphos (405.1 mg, 0.7 mmol, 1 equiv) were dissolved in anhydrous DCM (50 mL) for 1 h. After 1 h, dmp (2,9-dimethylphenanthroline) (145.8 mg, 0.7 mmol, 1 equiv) was added. The yellowish solution was stirred for 1 h at room temperature (25 °C), concentrated *in vacuo* to a volume of 25 mL and the complex was precipitated by adding diethylether. The product was collected by filtration to yield 561.7 mg (500.3 μmol , 86%) as a yellow solid.

Spectral data are in accordance to literature.^[15]

$^1\text{H NMR}$ (400 MHz, CDCl_3) δ [ppm] = 8.60 (d, J = 8.2 Hz, 2H), 8.09 (s, 2H), 7.89 (dd, J = 7.8, 1.4 Hz, 2H), 7.79 (d, J = 8.3 Hz, 2H), 7.53 – 7.39 (m, 6H), 7.26 (q, J = 3.3 Hz, 16H), 7.12 (dt, J = 7.8, 3.8 Hz, 2H), 2.49 (s, 6H), 1.99 (s, 6H). $^{13}\text{C NMR}$ (101 MHz, CDCl_3) δ [ppm] = 158.5, 155.2, 142.9, 138.2, 133.0 (t, J = 7.7 Hz), 132.9, 131.5 (t, J = 16.3 Hz), 130.5, 130.1, 128.73 (t, J = 4.6 Hz), 127.9, 127.5, 126.2, 125.5, 125.4, 121.9, 121.8, 36.2, 28.6, 27.2.

bromonitromethane (1a)

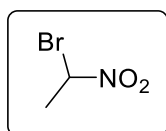


Commercially available, technical grade bromonitromethane was further purified *via* Kugelrohr distillation at 40 °C and a pressure of 10 mbar.

$^1\text{H NMR}$ (400 MHz, CDCl_3) δ [ppm] = 5.71 (s, 2H). $^{13}\text{C NMR}$ (101 MHz, CDCl_3) δ [ppm] = 60.9.

Please note for the Bromonitroalkanes 1b-1d: all following bromonitroalkanes were provided by Dr. Peter Kreitmeier and Johannes Floss according to optimized literature procedures. The procedures and spectra are shown in the experimental part for the sake of completeness.

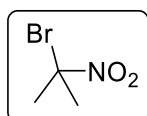
1-bromo-1-nitroethane (1b)



Following literature procedure^[16], sodium hydroxide (2.34g, 58.6 mmol, 1.0 equiv) was dissolved in water (79 mL). Nitroethane (4.40 g, 4.19 mL, 58.6 mmol, 1.0 equiv) was added and the mixture was cooled to -10°C by a salt-ice mixture. Bromine (9.37 g, 3.00 mL, 58.6 mmol, 1.0 equiv) was added, the mixture warmed to room temperature (25 °C) and stirred for 20 min. Afterwards the pH was adjusted to acidic pH by addition of HCl solution (2M). The mixture was extracted with saturated thiosulfate solution (3 x) and solvent removed under reduced pressure. The crude was distilled at 42°C and 13 mbar yielding 4.74 g (30.8 mmol, 53%) of colorless liquid. Spectral data are in accordance with literature.^[17]

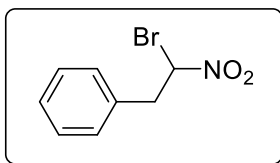
¹H NMR (300 MHz, CDCl₃) δ [ppm] = 6.05 (q, *J* = 6.5 Hz, 1H), 2.18 (d, *J* = 6.5 Hz, 3H). ¹³C NMR (101 MHz, CDCl₃) δ [ppm] = 74.6, 24.6.

2-bromo-2-nitropropane (1c)



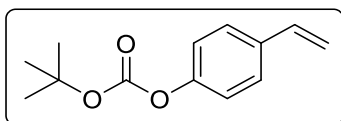
Following literature procedure,^[16] sodium hydroxide (784 mg, 19.6 mmol, 1.0 equiv) was dissolved in water (27 mL). 2-Nitropropane (1.75 g, 1.84 mL, 19.6 mmol, 1.0 equiv) was added and the mixture was cooled to -10°C by a salt-ice mixture. Bromine (3.13 g, 1.00 mL, 19.6 mmol, 1.0 equiv) was added, the mixture warmed to room temperature (25 °C) and stirred for 20 min. Afterwards the pH was adjusted to acidic pH by addition of HCl solution (2M). The mixture was extracted with saturated thiosulfate solution (3 x) and solvent removed under reduced pressure. The crude was distilled at 42°C and 13 mbar yielding 3.29 g (19.6 mmol, 99%) of **2c** as colorless liquid. Spectral data are in accordance with literature.^[17]

¹H NMR (400 MHz, CDCl₃) δ [ppm] = 2.27 (s, 6H). ¹³C NMR (101 MHz, CDCl₃) δ [ppm] = 89.0, 32.5.

(2-bromo-2-nitroethyl)benzene (1d)

Following modified literature procedure^[16], (2-nitroethyl)benzene (1.98 g, 13.1 mmol, 1.0 equiv) was added to a mixture of solid KOH (735 mg, 13.1 mmol, 1.0 equiv), CH₃OH (11 mL) and H₂O (22 mL) at room temperature. The mixture was vigorously stirred until complete dissolution of the starting nitro compound (30 min), and then cooled to 0 °C. Bromine (670 μL, 13.1 mmol, 1.0 equiv) in CH₂Cl₂ (22 mL, precooled to – 78 °C) was added in one pot. The cooling bath was removed, and the mixture was vigorously stirred for 5 min. The mixture was poured in a separation funnel and shaken, subsequently adding small portions of Na₂S₂O₃ until all remaining bromine was quenched. The phases were separated and the organic phase was washed with water (30 mL) and brine (30 mL), dried over anhydrous Na₂SO₄, and concentrated via rotary evaporation. The crude mixture was purified by filtration over a small plug of silica eluting with hexanes. After removing the solvent via rotary evaporation the yellowish turbid oil was distilled via Kugelrohr at 110°C and 4.4 mbar yielding 2.1 g (9.09 mmol, 69%) of **1d** as a colorless liquid. Spectral data are in accordance with literature.^[18]

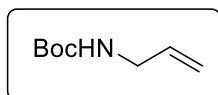
¹H NMR (400 MHz, CDCl₃) δ [ppm] = 7.39 – 7.30 (m, 3H), 7.24 – 7.18 (m, 2H), 6.05 (dd, *J* = 8.2, 6.1 Hz, 1H), 3.76 (dd, *J* = 14.6, 8.2 Hz, 1H), 3.51 (dd, *J* = 14.6, 6.1 Hz, 1H). ¹³C NMR (101 MHz, CDCl₃) δ [ppm] = 133.4, 129.3, 129.2, 128.5, 79.3, 43.6.

***tert*-butyl (4-vinylphenyl) carbonate (2k)**

Following literature procedure,^[19] 4-vinylphenyl acetate (900 mg, 5.55 mmol, 1.0 equiv) was dissolved in 25wt% tetramethylammonium hydroxide solution (5.06 g, 13.87 mmol, 2.5 equiv) at 0 °C. The solution was allowed to stir for 2h at room temperature (25 °C). Then it was cooled to 0 °C and di-*tert*-butyl-dicarbonate (1.21 g, 5.5 mmol, 1.0 equiv) was added to the reaction mixture. It was stirred for 24 h. Afterwards the product was extracted with diethylether (3 x 10 mL). The combined organic phases were washed with brine and dried over MgSO₄ and the solvent was removed under reduced pressure. Column chromatography (hexanes / EtOAc 9:1) followed by Kugelrohr distillation (5 mbar and 80 °C) yielded 660 mg (3.00 mmol, 54%) of *tert*-butyl (4-vinylphenyl) carbonate as colorless oil. Spectral data are in accordance with literature.^[20] **Rf** (hexanes / EtOAc 5:1 on silica) = 0.97, Staining: UV, KMnO₄.

¹H NMR (300 MHz, CDCl₃) δ [ppm] = 7.48 – 7.33 (m, 2H), 7.18 – 7.09 (m, 2H), 6.70 (dd, *J* = 17.6, 10.9 Hz, 1H), 5.70 (dd, *J* = 17.6, 0.9 Hz, 1H), 5.24 (dd, *J* = 10.8, 0.9 Hz, 1H), 1.56 (s, 9H). **¹³C NMR** (75 MHz, CDCl₃) δ [ppm] = 151.9, 150.7, 136.0, 135.4, 127.3, 121.4, 114.2, 83.7, 27.8.

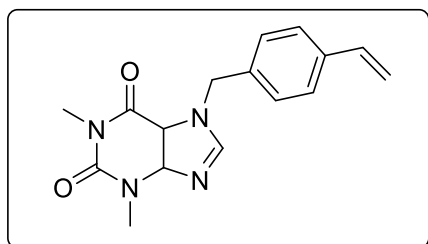
***tert*-butyl allylcarbamate (2cm)**



Following literature procedure,^[21] a round-bottom flask equipped with a magnetic stirring bar was charged with allylamine (1.87 mL, 1.43 g, 25.0 mmol, 1.0 equiv) and dissolved in DCM (60 mL). Then a solution of Boc₂O (6.0 g, 27.50 mmol, 1.1 equiv) in DCM (50 mL) was added dropwise at 0 °C. The resulting reaction mixture was allowed to warm up to room temperature (25 °C) and stirred for 18 h. Afterwards the solvent was removed under reduced pressure and the product was dried *in vacuo* to yield 2.94 g (18.7 mmol, 75%) of *tert*-butyl allylcarbamate as a white solid. Spectral data are in accordance to literature.^[21] **R_f** (hexanes / EtOAc 5:1 on silica) = 0.53, Staining: Ninhydrin.

¹H NMR (300 MHz, CDCl₃) δ [ppm] = 5.83 (ddt, *J* = 17.2, 10.3, 5.5 Hz, 1H), 5.23 – 5.03 (m, 2H), 4.60 (s, NH), 3.73 (d, *J* = 5.4 Hz, 2H), 1.44 (s, 9H). **¹³C NMR** (101 MHz, CDCl₃) δ [ppm] = 155.9, 135.1, 115.7, 79.4, 43.2, 28.5.

1,3-dimethyl-7-(4-vinylbenzyl)-3,4,5,7-tetrahydro-1H-purine-2,6-dione (2ea)

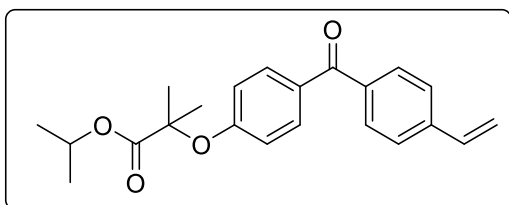


According to a slightly modified literature procedure,^[22] a round-bottom flask equipped with a magnetic stirring bar was charged with theophylline (1.82 g, 10.0 mmol, 1.0 equiv) and K₂CO₃ (2.76 g, 20.0 mmol, 2.0 equiv) and dissolved in DMF (24 mL). Afterwards, freshly distilled 1-(chloromethyl)-4-vinylbenzene (3.05 g, 2.82 mL, 2.0 equiv) was added. The yellowish suspension was stirred for 24 h at room temperature (25 °C). Followed by this, water (50 mL) was added, and the reaction mixture was cooled to 0°C for 2 h. The formed, white precipitate was collected by filtration, washed with water, and redissolved in DCM (40 mL). Then it was reprecipitated using diethylether (20 mL). The product was collected by filtration and washed with diethylether (10 mL). After drying under vacuum, 2.24 g (7.51 mmol, 75%) of 1,3-dimethyl-

7-(vinylbenzyl)-3,4,5,7-tetrahydro-1H-purine-2,6-dione (**2ea**) was obtained as white solid. R_f (hexanes / EtOAc 1:2 on silica) = 0.51, Staining: UV; KMnO_4 -solution.

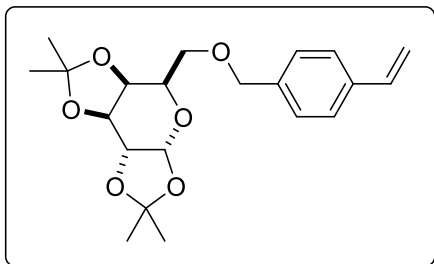
$^1\text{H NMR}$ (400 MHz, CDCl_3) δ [ppm] = 7.56 (s, 1H), 7.39 (d, $J = 8.2$ Hz, 2H), 7.28 (d, $J = 8.2$ Hz, 2H), 6.68 (dd, $J = 17.6, 10.9$ Hz, 1H), 5.74 (dd, $J = 17.6, 0.9$ Hz, 1H), 5.47 (s, 2H), 5.26 (dd, $J = 10.9, 0.8$ Hz, 1H), 3.57 (s, 3H), 3.39 (s, 3H). $^{13}\text{C NMR}$ (101 MHz, CDCl_3) δ [ppm] = 155.4, 151.8, 149.0, 140.9, 138.1, 136.1, 134.8, 128.3, 127.0, 115.0, 107.1, 50.2, 29.9, 28.1. **IR** (neat, cm^{-1}): 3101, 3004, 2948, 1699, 1654, 1543, 1472, 1423, 1371, 1289, 1230, 1192, 1125, 1028, 976, 905, 875, 827, 749, 670. **HRMS** (ESI-MS) exact mass calc. for $\text{C}_{16}\text{H}_{16}\text{N}_4\text{O}_2$ $[\text{M}+\text{Na}]^+$ 319.1165 m/z , found: 319.1167 m/z .

isopropyl 2-methyl-2-(4-(4-vinylbenzoyl)phenoxy)propanoate (**2eb**)



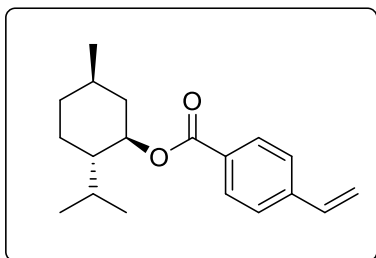
Based on literature procedure,^[23] a dry round-bottom flask was charged with isopropyl 2-(4-(4-chlorobenzoyl)phenoxy)-2-methylpropanoate (Fenofibrate) (721.7 g, 2.0 mmol, 1.0 equiv), potassium vinyltrifluoroborate (468.8 g, 3.5 mmol, 1.8 equiv), Cs_2CO_3 (1.95 g, 6.0 mmol, 3.0 equiv), PdCl_2 (17.7 mg, 0.1 mmol, 5.0 mol%), RuPhos (93.3 mg, 0.20 mmol, 10.0 mol%) and THF / water (7:1, 5.33 mL) and stirred at 85 °C for 48 h. The reaction was monitored by TLC. Afterwards, the reaction mixture was diluted with H_2O (50 mL) and extracted three times with diethylether (3 x 25 mL). The combined organic layers were dried over anhydrous MgSO_4 , filtered, and concentrated *in vacuo*. The residue was purified by flash column chromatography (hexanes / EtOAc 20:1) to yield 478.0 mg (1.36 mmol, 68%) of isopropyl 2-methyl-2-(4-(4-vinylbenzoyl)phenoxy)propanoate (**2eb**) as a white solid. Spectral data are in accordance with literature.^[23] R_f (hexanes / EtOAc 5:1 on silica) = 0.52, Staining: UV, Vanillin.

$^1\text{H NMR}$ (400 MHz, CDCl_3) δ [ppm] = 7.78 – 7.70 (m, 4H), 7.52 – 7.46 (m, 2H), 6.89 – 6.84 (m, 2H), 6.78 (dd, $J = 17.6, 10.9$ Hz, 1H), 5.88 (dd, $J = 17.6, 0.8$ Hz, 1H), 5.39 (dd, $J = 10.9, 0.8$ Hz, 1H), 5.09 (hept, $J = 6.3$ Hz, 1H), 1.66 (s, 6H), 1.20 (d, $J = 6.3$ Hz, 6H). $^{13}\text{C NMR}$ (101 MHz, CDCl_3) δ 195.1, 173.3, 159.6, 141.3, 137.4, 136.2, 132.1, 130.9, 130.4, 126.1, 117.3, 116.5, 79.5, 69.5, 25.5, 21.7.

(3a*R*,5*R*,5a*S*,8a*S*,8b*R*)-2,2,7,7-tetramethyl-5-(((4-vinylbenzyl)oxy)methyl)tetrahydro-5*H*-bis([1,3]dioxolo)[4,5-*b*:4',5'-*d*]pyran (2ec)

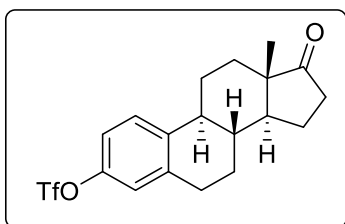
According to a slightly modified procedure,^[24] a dry round-bottom flask equipped with a magnetic stirring bar was charged with 1,2,3,4-di-O-isopropylidene- α -D-galactopyranoside (1.30 g, 5.0 mmol, 1.0 equiv) dissolved in dry DMF (7 mL). Followed by this, sodium hydride (145 mg, 6.1 mmol, 1.2 equiv) was added and the yellowish solution was stirred for 2 h. Afterwards, freshly distilled 1-(chloromethyl)-4-vinylbenzene (801 mg, 740 μ L, 1.1 equiv) was added. The reaction mixture was heated in an oil bath at 50 °C for 6 h. Followed by this, the solution was quenched with water (25 mL) and extracted with toluene (3 x 10 mL). The combined organic layers were dried over anhydrous MgSO₄, filtered, and concentrated *in vacuo*. The residue was purified by flash column chromatography (hexanes / EtOAc 20:1) to yield 410.0 mg (1.09 mmol, 1.09 mmol, 22%) of (3a*R*,5*R*,5a*S*,8a*S*,8b*R*)-2,2,7,7-tetramethyl-5-(((4-vinylbenzyl)oxy)methyl)tetrahydro-5*H*-bis([1,3]dioxolo)[4,5-*b*:4',5'-*d*]pyran (**2ec**) as a colorless sticky oil. **Rf** (hexanes / EtOAc 5:1 on silica) = 0.52, Staining: UV, Vanillin.

¹H NMR (400 MHz, CDCl₃) δ [ppm] = 7.40 – 7.34 (m, 2H), 7.31 (d, *J* = 8.2 Hz, 2H), 6.71 (dd, *J* = 17.6, 10.9 Hz, 1H), 5.73 (dd, *J* = 17.6, 0.9 Hz, 1H), 5.55 (d, *J* = 5.0 Hz, 1H), 5.23 (dd, *J* = 10.9, 0.9 Hz, 1H), 4.64 – 4.51 (m, 3H), 4.31 (dd, *J* = 5.0, 2.4 Hz, 1H), 4.27 (dd, *J* = 7.9, 1.9 Hz, 1H), 4.00 (td, *J* = 6.3, 1.9 Hz, 1H), 3.69 (dd, *J* = 10.1, 5.9 Hz, 1H), 3.62 (dd, *J* = 10.1, 6.7 Hz, 1H), 1.54 (s, 3H), 1.44 (s, 3H), 1.33 (d, *J* = 2.0 Hz, 6H). **¹³C NMR** (101 MHz, CDCl₃) δ [ppm] = 138.1, 137.1, 136.7, 128.1, 126.3, 113.8, 109.4, 108.7, 96.5, 73.2, 71.3, 70.8, 70.8, 69.0, 67.1, 26.3, 26.1, 25.1, 24.6. **IR** (neat, cm⁻¹): 3086, 2985, 2933, 1628, 1457, 1371, 1252, 1207, 1170, 1103, 1066, 998, 827, 764, 719, 678. **HRMS** (ESI-MS) exact mass calc. for C₂₁H₂₈O₆ [M+H]⁺ 377.1959 m/z, found: 377.1963 m/z and exact mass calc. for C₂₁H₂₈O₆ [M+Na]⁺ 399.1778 m/z, found: 399.1783 m/z and exact mass calc. for C₂₁H₂₈O₆ [M+NH₄]⁺ 394.2224 m/z, found: 394.2230 m/z.

(1*R*,2*S*,5*R*)-2-isopropyl-5-methylcyclohexyl 4-vinylbenzoate (2ed)

Based on a literature procedure,^[25] a round-bottom flask was charged with (-)-menthol (562.6 mg, 3.6 mmol, 1.2 equiv), 4-vinylbenzoic acid (444.5 mg, 3.0 mmol, 1.0 equiv), DCC (*N,N*-Dicyclohexylcarbodiimide) (742.8 mg, 3.6 mmol, 1.2 equiv) and DMAP (73.3 mg, 0.6 mmol, 20 mol%) and DCM (6 mL) was added. The resulting solution was stirred at room temperature (25 °C) for 48 h. Afterwards, the reaction mixture was quenched with H₂O (40 mL) and extracted with DCM (3 x 25 mL). The combined organic layers were washed with brine, dried over anhydrous MgSO₄, filtered and concentrated *in vacuo*. The residue was purified by flash column chromatography (hexanes / EtOAc 10:1) to yield 528.5 mg (1.85 mmol, 62%) of (1*R*,2*S*,5*R*)-2-isopropyl-5-methylcyclohexyl 4-vinylbenzoate (**2ed**) as colorless oil. Spectral data are in accordance to literature.^[25] *R_f* (hexanes/ EtOAc 5:1) on silica = 0.90, Staining: KMnO₄-solution.

¹H NMR (400 MHz, CDCl₃) δ [ppm] = 8.00 (d, *J* = 8.3 Hz, 2H), 7.46 (d, *J* = 8.3 Hz, 2H), 6.76 (dd, *J* = 17.6, 10.9 Hz, 1H), 5.86 (dd, *J* = 17.6, 0.8 Hz, 1H), 5.37 (dd, *J* = 10.8, 0.8 Hz, 1H), 4.93 (td, *J* = 10.9, 4.4 Hz, 1H), 2.18 – 2.08 (m, 1H), 2.00 – 1.86 (m, 1H), 1.78 – 1.68 (m, 2H), 1.62 – 1.49 (m, 2H), 1.18 – 1.03 (m, 2H), 0.95 (m, 1H), 0.92 (dd, *J* = 6.8, 5.3 Hz, 6H), 0.79 (d, *J* = 7.0 Hz, 3H). ¹³C NMR (101 MHz, CDCl₃) δ [ppm] = 166.01, 141.89, 136.23, 130.15, 130.01, 126.19, 116.46, 74.96, 47.45, 41.14, 34.49, 31.61, 26.69, 23.84, 22.21, 20.92, 16.72.

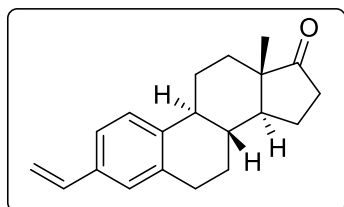
(8*R*,9*S*,13*S*,14*S*)-13-methyl-17-oxo-7,8,9,11,12,13,14,15,16,17-decahydro-6*H*-cyclopenta[*a*]phenanthren-3-yl trifluoromethanesulfonate (2ef')

Based on literature procedure,^[26] a flame-dried round-bottom schlenk flask was charged with estrone (1.35 g, 5.0 mmol, 1.0 equiv), pyridine (806 μL, 791 mg, 10.0 mmol, 2.0 equiv) and anhydrous DCM (15 mL, 0.3 M). The resulting reaction mixture was cooled to 0 °C and triflic

anhydride (1.01 mL, 1.69 g, 6.0 mmol, 1.2 equiv) was added dropwise. The reaction was allowed to warm to room temperature (25 °C) and stirred for 1 h. Afterwards, the reaction mixture was diluted with H₂O (10 mL) and extracted three times with DCM (3 x 20 mL). The combined organic layers were dried over anhydrous MgSO₄, filtered, and concentrated *in vacuo*. The residue was purified by flash column chromatography (hexanes / EtOAc 10:1 to 5:1) to yield 1.74 g (4.32 mmol, 87%) of (8*R*,9*S*,13*S*,14*S*)-13-methyl-17-oxo-7,8,9,11,12,13,14,15,16,17-decahydro-6*H*-cyclopenta[*a*]phenanthren-3-yl trifluoromethane sulfonate (**2ef**) as a white solid. Spectral data are in accordance with literature.^[26] *R*_f (hexanes / EtOAc 5:1 on silica) = 0.56, Staining: KMnO₄-solution.

¹H NMR (400 MHz, CDCl₃) δ [ppm] = 7.33 (d, *J* = 8.7 Hz, 1H), 7.02 (d, *J* = 8.6 Hz, 1H), 6.99 (s, 1H), 2.93 (dd, *J* = 9.1, 4.3 Hz, 2H), 2.50 (dd, *J* = 18.7, 8.7 Hz, 1H), 2.39 (dt, *J* = 12.8, 3.6 Hz, 1H), 2.29 (td, *J* = 10.8, 4.2 Hz, 1H), 2.21 – 1.91 (m, 4H), 1.68 – 1.38 (m, 6H), 0.91 (s, 3H). **¹³C NMR** (101 MHz, CDCl₃) δ [ppm] = 220.5, 147.7, 140.4, 139.4, 127.3, 121.3, 118.8 (d, *J* = 320.8 Hz), 118.4, 50.4, 47.9, 44.2, 37.8, 35.9, 31.6, 29.5, 26.2, 25.8, 21.6. **¹⁹F NMR** (376 MHz, CDCl₃) δ [ppm] = -73.52 (s, 3F).

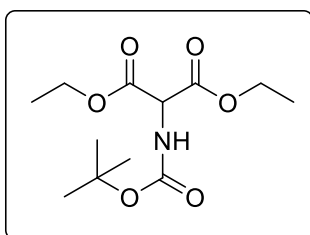
(8*R*,9*S*,13*S*,14*S*)-13-methyl-3-vinyl-6,7,8,9,11,12,13,14,15,16-decahydro-17*H*-cyclopenta[*a*]phenanthren-17-one (2ef)



Based on literature procedure,^[26] a round-bottom schlenk flask was charged with (8*R*,9*S*,13*S*,14*S*)-13-methyl-17-oxo-7,8,9,11,12,13,14,15,16,17-decahydro-6*H*-cyclopenta[*a*]phenanthren-3-yl trifluoromethanesulfonate (1.61 g, 4.0 mmol, 1.0 equiv), potassium vinyltrifluoroborate (535.8 mg, 4.0 mmol, 1.0 equiv), Cs₂CO₃ (3.91 g, 12.0 mmol, 3.0 equiv), PdCl₂ (14.2 mg, 0.08 mmol, 2 mol%), PPh₃ (67.2 mg, 0.26 mmol, 6 mol%) and THF/water (9:1, 8 mL) and stirred under reflux conditions for 21 h. The reaction was monitored by TLC. Afterwards, the reaction mixture was diluted with H₂O (40 mL) and extracted three times with DCM (3 x 25 mL). The combined organic layers were dried over anhydrous MgSO₄, filtered, and concentrated *in vacuo*. The residue was purified by flash column chromatography (hexanes / EtOAc 5:1) to yield 590.2 mg (2.10 mmol, 53%) of (8*R*,9*S*,13*S*,14*S*)-13-methyl-3-vinyl-6,7,8,9,11,12,13,14,15,16-decahydro-17*H*-cyclopenta[*a*]phenanthren-17-one (**2ef**) as a white solid. Spectral data are in accordance with literature.^[26] *R*_f (hexanes / EtOAc 5:1 on silica) = 0.50, Staining: KMnO₄-solution.

¹H NMR (300 MHz, CDCl₃) δ [ppm] = 7.29 – 7.19 (m, 2H), 7.15 (d, *J* = 1.7 Hz, 1H), 6.67 (dd, *J* = 17.6, 10.9 Hz, 1H), 5.71 (dd, *J* = 17.6, 1.0 Hz, 1H), 5.20 (dd, *J* = 10.8, 1.0 Hz, 1H), 2.92 (dd, *J* = 8.9, 4.2 Hz, 2H), 2.58 – 2.39 (m, 2H), 2.38 – 2.25 (m, 1H), 2.22 – 1.92 (m, 4H), 1.72 – 1.35 (m, 6H), 0.91 (s, 3H). **¹³C NMR** (101 MHz, CDCl₃) δ [ppm] = 221.0, 139.7, 136.7, 135.3, 127.0, 125.7, 123.7, 113.3, 50.6, 48.1, 44.6, 38.3, 36.0, 31.7, 29.5, 26.6, 25.9, 21.7, 14.0.

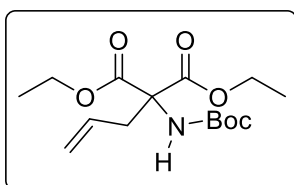
diethyl 2-((*tert*-butoxycarbonyl)amino)malonate (2co⁴)



Based on literature procedure,^[27] a round-bottom schlenk flask was charged with diethylaminomalonate hydrochloride (25.0 g, 118.2 mmol, 1.0 equiv), NaHCO₃ (10.4 g, 130.0 mmol, 1.1 equiv) and dissolved in water (150 mL) and dioxane (220 mL). DMAP (144 mg, 1.2 mmol, 1 mol%) was added and a solution of Boc₂O (27.07 g, 124.1 mmol, 1.1 equiv) in dioxane (80 mL) was added dropwise and stirred at room temperature (25 °C) for 18 h. Afterwards, the solvent was evaporated *in vacuo* and the reaction mixture was diluted with EtOAc (100 mL) and washed with a solution of 5% KHSO₄ (50 mL), sat. NaHCO₃ (50 mL) and brine. The organic layer was dried over anhydrous MgSO₄, filtered, and concentrated *in vacuo* to obtain 27.4 g (118.12 mmol, 100%) of diethyl 2-((*tert*-butoxycarbonyl)amino)malonate (2co⁴) as a yellow oil. Spectral data are in accordance with literature.^[27]

¹H NMR (400 MHz, CDCl₃) δ [ppm] = 5.55 (d, *J* = 7.8 Hz, 1H), 4.94 (d, *J* = 7.7 Hz, 1H), 4.34 – 4.16 (m, 6H), 1.45 (s, 9H), 1.29 (t, *J* = 7.1 Hz, 4H). **¹³C NMR** (101 MHz, CDCl₃) δ [ppm] = 166.8, 154.9, 80.8, 62.6, 57.7, 28.4, 14.1.

diethyl 2-allyl-2-((*tert*-butoxycarbonyl)amino)malonate (2co)

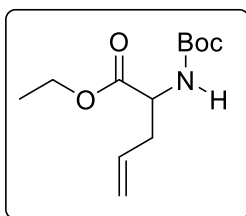


Based on literature procedure,^[28] a round-bottom schlenk flask was charged with diethyl 2-((*tert*-butoxycarbonyl)amino)malonate (5.5 g, 20.0 mmol, 1.0 equiv), and dissolved in THF (50 mL). NaH (60% w/w in mineral oil, 840 mg, 21.0 mmol, 1.1 equiv) and allylbromide (1.51 g, 1.08 mL, 21.0 mmol, 1.1 equiv) was added. The reaction mixture was stirred under reflux

conditions for 1 h. Afterwards, the reaction mixture was diluted with H₂O (40 mL) and extracted with CHCl₃ (3 x 50 mL). The combined organic layers were dried over anhydrous MgSO₄, filtered, and concentrated *in vacuo*. The residue was purified by flash column chromatography (hexanes / EtOAc 10:1) to yield 6.0 g (19.0 mmol, 95%) diethyl 2-allyl-2-((*tert*-butoxycarbonyl)amino)malonate (**2co**) as a colorless oil. Spectral data are in accordance with literature.^[28] **R_f** (hexanes / EtOAc 5:1 on silica) = 0.58, Staining: UV; KMnO₄-solution.

¹H NMR (400 MHz, CDCl₃) δ [ppm] = 5.89 (s, 1H), 5.72 – 5.56 (m, 1H), 5.15 – 5.05 (m, 2H), 4.30 – 4.16 (m, 4H), 3.03 (d, *J* = 7.4 Hz, 2H), 1.42 (s, 9H), 1.25 (t, *J* = 7.1 Hz, 6H). **¹³C NMR** (101 MHz, CDCl₃) δ [ppm] = 168.0, 131.6, 119.8, 80.3, 66.3, 62.6, 37.6, 28.3, 14.2.

racemic ethyl 2-((*tert*-butoxycarbonyl)amino)pent-4-enoate (**2cp**)

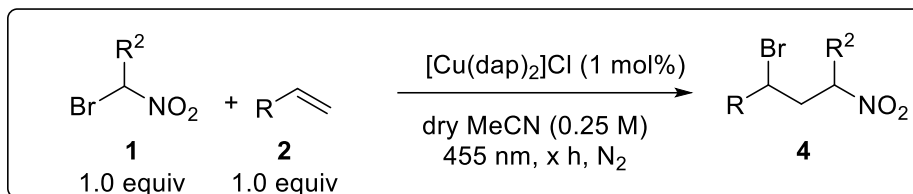


Based on literature procedure,^[29] a round-bottom schlenk flask was charged with diethyl 2-allyl-2-((*tert*-butoxycarbonyl)amino)malonate (**2co**) (3.01 g, 9.54 mmol, 1.0 equiv) and dissolved in EtOH (6.2 mL) and 1M NaOH (1.0 equiv) was added. The reaction mixture was stirred at room temperature (25 °C) for 16 h under nitrogen atmosphere. Afterwards, the reaction mixture was diluted with H₂O (20 mL) and extracted with EtOAc (3 x 25 mL). The combined organic layers were dried over anhydrous MgSO₄, filtered, and concentrated *in vacuo*. The residue was refluxed for 2h in xylene (20 mL). Then the solvent was removed *in vacuo*. The crude product was purified by flash column chromatography (hexanes / EtOAc 6:1) to yield 1.67 g (6.86 mmol, 71 %) of ethyl 2-((*tert*-butoxycarbonyl)amino)pent-4-enoate (**2cp**) as a colorless oil. Spectral data are in accordance with literature.^[29] **R_f** (hexanes / EtOAc 5:1 on silica) = 0.61, Staining: UV; KMnO₄-solution.

¹H NMR (300 MHz, CDCl₃) δ [ppm] = 5.69 (ddt, *J* = 16.9, 9.6, 7.2 Hz, 1H), 5.19 – 5.07 (m, 2H), 5.07 – 4.95 (m, 1H), 4.35 (q, *J* = 6.8, 6.2 Hz, 1H), 4.27 – 4.10 (m, 2H), 2.63 – 2.37 (m, 2H), 1.43 (s, 9H), 1.27 (t, *J* = 7.1 Hz, 3H). **¹³C NMR** (101 MHz, CDCl₃) δ [ppm] = 172.2, 155.3, 132.5, 119.2, 80.0, 61.4, 53.1, 37.0, 28.4, 14.4.

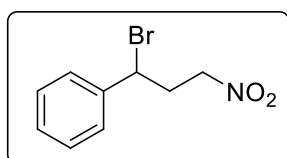
5.4.6.2 Compound Characterization of Bromonitromethylation Products

General Procedure for Bromonitromethylation of Olefins (GP-A)



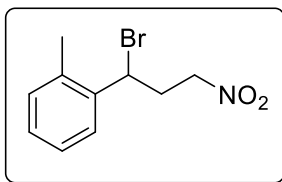
An oven dried schlenk tube (10 mL size) equipped with a stirring bar was charged with $[\text{Cu}(\text{dap})_2]\text{Cl}$ (4.4 mg, 1 mol%, 0.01 equiv) Then dry MeCN (2 mL, 0.25 M) was added under positive nitrogen atmosphere. The solution was degassed by three freeze-pump-thaw cycles. Then bromonitromethane-reagent **1** (0.5 mmol, 1.0 equiv) and desired olefin **2** was added (0.5 mmol, 1.0 equiv) under nitrogen atmosphere. A Teflon sealed inlet for a glass rod was placed on the reaction tube, through which irradiation with LED_{455nm} took place from above (for a detailed setup see, Figure 1, 5.1 General Information). The mixture was stirred in an aluminum block at room temperature (25 °C). After completion of the reaction (monitored via TLC), the reaction mixture was transferred to a round-bottom flask, concentrated *in vacuo*, and the crude residue was purified by flash column chromatography on silica gel (eluent hexanes/EtOAc) to afford the product **4**.

Scope of Activated Olefins

(1-bromo-3-nitropropyl)benzene (**4a**)

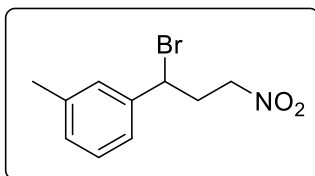
Following general procedure (GP-A) using styrene (**2a**) (52.1 mg, 58.0 μL , 0.5 mmol, 1.0 equiv), bromonitromethane (**1a**) (70.0 mg, 36.0 μL , 0.5 mmol, 1.0 equiv), $[\text{Cu}(\text{dap})_2]\text{Cl}$ (4.4 mg, 5.0 μmol , 1 mol%) and dry MeCN (2.0 mL, 0.25 M) at room temperature (25 °C) and irradiation with blue LED ($\lambda_{\text{max}} = 455 \text{ nm}$) for 1 h yielded 110.0 mg (450.6 μmol , 90%) of (1-bromo-3-nitropropyl)benzene (**4a**) as colorless oil after flash column purification (hexanes / EtOAc 10:1). R_f (hexanes / EtOAc 5:1 on silica) = 0.63, Staining: UV; KMnO_4 -solution.

$^1\text{H NMR}$ (300 MHz, CDCl_3) δ [ppm] = 7.48 – 7.30 (m, 5H), 5.05 (dd, $J = 9.1, 5.9 \text{ Hz}$, 1H), 4.72 – 4.38 (m, 2H), 3.10 – 2.64 (m, 2H). $^{13}\text{C NMR}$ (75 MHz, CDCl_3) δ [ppm] = 140.2, 129.2, 129.2, 127.3, 73.6, 50.3, 37.1. **IR** (neat, cm^{-1}): 3063, 3034, 2922, 1546, 1494, 1453, 1427, 1379, 1289, 1159, 1088, 1058, 998, 961, 864, 831, 760, 693. **HRMS** (EI-MS) exact mass calc. for $\text{C}_9\text{H}_{10}\text{NO}_2$ $[\text{M}]^+$ 164.07060 m/z , found: 164.07018 m/z and exact mass calc. for $\text{C}_7\text{H}_6\text{Br}$ $[\text{M}]^+$ 168.96474 m/z , found: 168.96489 m/z .

1-(1-bromo-3-nitropropyl)-2-methylbenzene (4b)

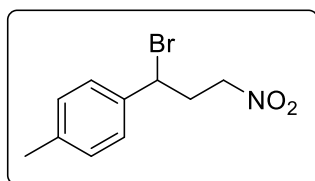
Following general procedure (GP-A) using 2-methylstyrene (**2b**) (59.1 mg, 65.0 μL , 0.5 mmol, 1.0 equiv), bromonitromethane (**1a**) (70.0 mg, 36.0 μL , 0.5 mmol, 1.0 equiv), $[\text{Cu}(\text{dap})_2]\text{Cl}$ (4.4 mg, 5.0 μmol , 1 mol%) and dry MeCN (2.0 mL, 0.25 M) at room temperature (25 $^\circ\text{C}$) and irradiation with blue LED ($\lambda_{\text{max}} = 455 \text{ nm}$) for 1 h yielded 75.0 mg (290.5 μmol , 58%) of 1-(1-bromo-3-nitropropyl)-2-methylbenzene (**4b**) as pale yellowish oil after flash column purification (hexanes / EtOAc 20:1). R_f (hexanes / EtOAc 20:1 on silica) = 0.38, Staining: UV; KMnO_4 -solution.

$^1\text{H NMR}$ (300 MHz, CDCl_3) δ [ppm] = 7.48 (dd, $J = 7.1, 2.1 \text{ Hz}$, 1H), 7.23 (ddtd, $J = 12.0, 9.3, 7.0, 2.2 \text{ Hz}$, 3H), 5.31 (dd, $J = 9.5, 5.3 \text{ Hz}$, 1H), 4.76 – 4.48 (m, 2H), 3.07 – 2.71 (m, 2H), 2.39 (s, 3H). **$^{13}\text{C NMR}$** (101 MHz, CDCl_3) δ [ppm] = 138.2, 135.7, 131.2, 129.0, 127.1, 126.6, 73.6, 46.8, 36.0, 19.1. **IR** (neat, cm^{-1}): 3026, 2922, 1550, 1490, 1461, 1427, 1379, 1155, 864, 760, 723. **HRMS** (APCI-MS) exact mass calc. for $\text{C}_{10}\text{H}_{10}\text{BrNO}_2$ $[\text{M}+\text{NH}_4]^+$ 275.0390 m/z, found: 275.0392 m/z.

1-(1-bromo-3-nitropropyl)-3-methylbenzene (4c)

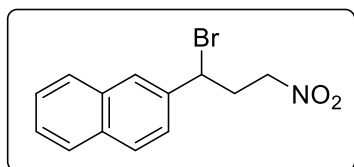
Following general procedure (GP-A) using 3-methylstyrene (**2c**) (59.1 mg, 66.4 μL , 0.5 mmol, 1.0 equiv), bromonitromethane (**1a**) (70.0 mg, 36.0 μL , 0.5 mmol, 1.0 equiv), $[\text{Cu}(\text{dap})_2]\text{Cl}$ (4.4 mg, 5.0 μmol , 1 mol%) and dry MeCN (2.0 mL, 0.25 M) at room temperature (25 $^\circ\text{C}$) and irradiation with blue LED ($\lambda_{\text{max}} = 455 \text{ nm}$) for 2 h yielded 112.2 mg (434.7 μmol , 87%) of 1-(1-bromo-3-nitropropyl)-3-methylbenzene (**3c**) as pale yellowish oil after flash column purification (hexanes / EtOAc 20:1). R_f (hexanes / EtOAc 5:1 on silica) = 0.63, Staining: UV; KMnO_4 -solution.

$^1\text{H NMR}$ (300 MHz, CDCl_3) δ [ppm] = 7.31 – 7.23 (m, 1H), 7.23 – 7.11 (m, 3H), 5.02 (dd, $J = 9.0, 5.9 \text{ Hz}$, 1H), 4.68 – 4.36 (m, 2H), 2.96 – 2.68 (m, 2H), 2.37 (s, 3H). **$^{13}\text{C NMR}$** (75 MHz, CDCl_3) δ [ppm] = 140.1, 139.0, 130.0, 129.1, 127.9, 124.3, 73.6, 50.4, 37.1, 21.5. **IR** (neat, cm^{-1}): 2922, 1550, 1427, 1379, 1159, 786, 700. **HRMS** (APCI-MS) exact mass calc. for $\text{C}_{10}\text{H}_{12}\text{BrNO}_2$ $[\text{M}+\text{NH}_4]^+$ 275.0390 m/z, found: 275.0389 m/z.

1-(1-bromo-3-nitropropyl)-4-methylbenzene (3d)

Following general procedure (GP-A) using 4-methylstyrene (**2d**) (59.1 mg, 66.0 μL , 0.5 mmol, 1.0 equiv), bromonitromethane (**1a**) (70.0 mg, 36.0 μL , 0.5 mmol, 1.0 equiv), $[\text{Cu}(\text{dap})_2]\text{Cl}$ (4.4 mg, 5.0 μmol , 1 mol%) and dry MeCN (2.0 mL, 0.25 M) at room temperature (25 $^\circ\text{C}$) and irradiation with blue LED ($\lambda_{\text{max}} = 455 \text{ nm}$) for 1 h yielded 107.8 mg (417.6 μmol , 84%) of 1-(1-bromo-3-nitropropyl)-4-methylbenzene (**4d**) as pale yellowish oil after flash column purification (hexanes / EtOAc 10:1). R_f (hexanes / EtOAc 5:1 on silica) = 0.44, Staining: UV; KMnO_4 -solution.

$^1\text{H NMR}$ (300 MHz, CDCl_3) δ [ppm] = 7.30 (d, $J = 8.2 \text{ Hz}$, 2H), 7.19 (d, $J = 7.9 \text{ Hz}$, 2H), 5.04 (dd, $J = 9.1, 5.9 \text{ Hz}$, 1H), 4.64 – 4.42 (m, 2H), 2.97 – 2.71 (m, 2H), 2.36 (s, 3H). $^{13}\text{C NMR}$ (75 MHz, CDCl_3) δ [ppm] = 139.2, 137.3, 129.8, 127.1, 73.6, 50.4, 37.0, 21.3. **IR** (neat, cm^{-1}): 3026, 2922, 1610, 1550, 1427, 1516, 1427, 1379, 1338, 1285, 1185, 1162, 1118, 1039, 969, 909, 868, 816, 734. **HRMS** (EI-MS) exact mass calc. for $\text{C}_{10}\text{H}_{12}\text{NO}_2\text{Br}$ $[\text{M}]^+$ 257.00459 m/z, found: 257.00409 m/z.

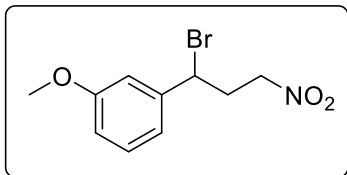
2-(1-bromo-3-nitropropyl)naphthalene (4f)

Following general procedure (GP-A) using 2-vinylnaphthalene (**2f**) (77.1 mg, 0.5 mmol, 1.0 equiv), bromonitromethane (**1a**) (70.0 mg, 36.0 μL , 0.5 mmol, 1.0 equiv), $[\text{Cu}(\text{dap})_2]\text{Cl}$ (4.4 mg, 5.0 μmol , 1 mol%) and dry MeCN (2.0 mL, 0.25 M) at room temperature (25 $^\circ\text{C}$) and irradiation with blue LED ($\lambda_{\text{max}} = 455 \text{ nm}$) for 2 h yielded 59.5 mg (202.3 μmol , 41%) of 2-(1-bromo-3-nitropropyl)naphthalene (**4f**) as pale yellowish oil after flash column purification (hexanes / EtOAc 20:1). **mp**: 74 $^\circ\text{C}$ R_f (hexanes / EtOAc 5:1 on silica) = 0.56, Staining: UV; KMnO_4 -solution.

$^1\text{H NMR}$ (400 MHz, CDCl_3) δ [ppm] = 7.93 – 7.77 (m, 4H), 7.58 – 7.47 (m, 3H), 5.24 (dd, $J = 9.1, 5.9 \text{ Hz}$, 1H), 4.61 (ddd, $J = 13.8, 7.3, 6.3 \text{ Hz}$, 1H), 4.51 (dt, $J = 14.0, 6.4 \text{ Hz}$, 1H), 2.99 (ddt, $J = 15.4, 9.1, 6.3 \text{ Hz}$, 1H), 2.88 (ddt, $J = 15.1, 7.3, 6.2 \text{ Hz}$, 1H). $^{13}\text{C NMR}$ (101 MHz, CDCl_3) δ [ppm] = 137.3, 133.5, 133.1, 129.4, 128.2, 127.9, 127.1, 127.0, 126.3, 124.6, 73.5, 50.7, 36.9. **IR** (neat, cm^{-1}): 3049, 2952, 2922, 2113, 1599, 1543, 1408, 1364, 1166, 1125, 1095,

1021, 954, 864, 820, 752, 670. **HRMS** (APCI-MS) exact mass calc. for $C_{13}H_{12}BrNO_2$ $[M+NH_4]^+$ 311.0390 m/z, found: 311.0391 m/z.

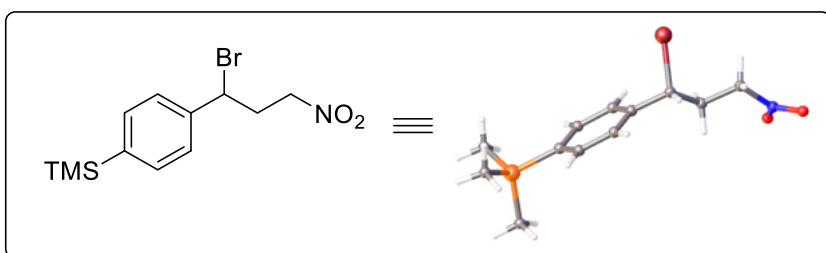
1-(1-bromo-3-nitropropyl)-3-methoxybenzene (**4h**)



Following general procedure (GP-A) using 1-methoxy-3-vinylbenzene (**2h**) (67.1 mg, 69.4 μ L, 0.5 mmol, 1.0 equiv), bromonitromethane (**1a**) (70.0 mg, 36.0 μ L, 0.5 mmol, 1.0 equiv), $[Cu(dap)_2]Cl$ (4.4 mg, 5.0 μ mol, 1 mol%) and dry MeCN (2.0 mL, 0.25 M) at room temperature (25 °C) and irradiation with blue LED (λ_{max} = 455 nm) for 2 h yielded 102.2 mg (372.8 μ mol, 74%) of 1-(1-bromo-3-nitropropyl)-3-methoxybenzene (**4h**) as colorless oil after flash column purification (hexanes / EtOAc 20:1). R_f (hexanes / EtOAc 5:1 on silica) = 0.46, Staining: UV; $KMnO_4$ -solution.

1H NMR (300 MHz, $CDCl_3$) δ [ppm] = 7.29 (t, J = 7.9 Hz, 1H), 7.00 – 6.96 (m, 1H), 6.93 (t, J = 2.1 Hz, 1H), 6.87 (ddd, J = 8.3, 2.5, 0.9 Hz, 1H), 5.01 (dd, J = 9.0, 6.0 Hz, 1H), 4.52 (ddt, J = 20.4, 14.0, 6.5 Hz, 2H), 3.82 (s, 3H), 2.96 – 2.70 (m, 2H). ^{13}C NMR (75 MHz, $CDCl_3$) δ [ppm] = 160.0, 141.6, 130.2, 119.4, 114.5, 113.1, 73.5, 55.4, 50.1, 37.0. IR (neat, cm^{-1}): 3086, 3026, 2926, 2862, 1602, 1535, 1494, 1485, 1364, 1319, 1181, 1095, 1051, 909, 857, 749, 700. **HRMS** (APCI-MS) exact mass calc. for $C_{10}H_{12}BrNO_3$ $[M+NH_4]^+$ 291.0339 m/z, found: 291.0341 m/z.

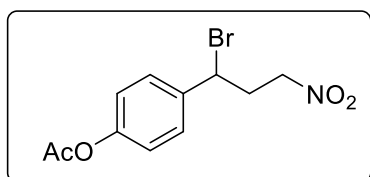
(4-(1-bromo-3-nitropropyl)phenyl)trimethylsilane (**4i**)



Following general procedure (GP-A) using trimethyl(4-vinylphenyl)silane (**2i**) (88.2 mg, 102.5 μ L, 0.5 mmol, 1.0 equiv), bromonitromethane (**1a**) (70.0 mg, 36.0 μ L, 0.5 mmol, 1.0 equiv), $[Cu(dap)_2]Cl$ (4.4 mg, 5.0 μ mol, 1 mol%) and dry MeCN (2.0 mL, 0.25 M) at room temperature (25 °C) and irradiation with blue LED (λ_{max} = 455 nm) for 2 h yielded 138.9 mg (439.2 μ mol, 88%) of (4-(1-bromo-3-nitropropyl)phenyl)trimethylsilane (**4i**) as a white solid after flash column purification (hexanes / EtOAc 20:1). **mp**: 59 °C R_f (hexanes / EtOAc 5:1 on silica) = 0.66, Staining: UV; $KMnO_4$ -solution. Single crystals suitable for X-ray analysis of compound **4i** were obtained by vapor diffusion of pentane into DCM solution (1.0 mL).

¹H NMR (400 MHz, CDCl₃) δ [ppm] = 7.54 (d, *J* = 8.1 Hz, 2H), 7.38 (d, *J* = 8.1 Hz, 2H), 5.05 (dd, *J* = 9.1, 5.8 Hz, 1H), 4.60 (dt, *J* = 13.8, 6.8 Hz, 1H), 4.51 (dt, *J* = 13.9, 6.3 Hz, 1H), 2.95 – 2.74 (m, 2H), 0.28 (s, 9H). **¹³C NMR** (101 MHz, CDCl₃) δ [ppm] = 142.2, 140.6, 134.2, 126.5, 73.6, 50.3, 37.0, -1.1. **IR** (neat, cm⁻¹): 3019, 2952, 2896, 1599, 1546, 1423, 1382, 1289, 1244, 1166, 1110, 1062, 920, 823, 756, 723, 689. **HRMS** (APCI-MS) exact mass calc. for C₁₀H₁₈BrNO₂Si [M+H]⁺ 316.0363 m/z, found: 316.0359 m/z and [M+NH₄]⁺ 333.0628 m/z, found: 333.0629 m/z.

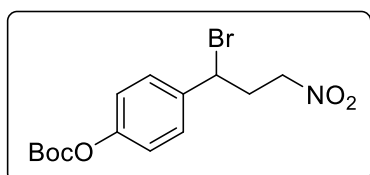
4-(1-bromo-3-nitropropyl)phenyl acetate (**4j**)



Following general procedure (GP-A) using 4-vinylphenyl acetate (**2j**) (81.1 mg, 76.5 μL, 0.5 mmol, 1.0 equiv), bromonitromethane (**1a**) (70.0 mg, 36.0 μL, 0.5 mmol, 1.0 equiv), [Cu(dap)₂]Cl (4.4 mg, 5.0 μmol, 1 mol%) and dry MeCN (2.0 mL, 0.25 M) at room temperature (25 °C) and irradiation with blue LED (λ_{max} = 455 nm) for 3 h yielded 115.1 mg (381.0 μmol, 76%) of 4-(1-bromo-3-nitropropyl)phenyl acetate (**4j**) as pale yellowish oil after flash column purification (hexanes / EtOAc 5:1). *R_f* (hexanes / EtOAc 20:1 on silica) = 0.29, Staining: UV; KMnO₄-solution.

¹H NMR (300 MHz, CDCl₃) δ [ppm] = 7.41 (d, *J* = 8.6 Hz, 2H), 7.10 (d, *J* = 8.6 Hz, 2H), 5.04 (dd, *J* = 9.1, 5.8 Hz, 1H), 4.71 – 4.37 (m, 2H), 2.94 – 2.67 (m, 2H), 2.30 (s, 3H). **¹³C NMR** (101 MHz, CDCl₃) δ [ppm] = 169.3, 151.0, 137.8, 128.5, 122.3, 73.5, 49.5, 37.1, 21.2. **IR** (neat, cm⁻¹): 2922, 1759, 1550, 1505, 1423, 1367, 1189, 1013, 909, 849. **HRMS** (APCI-MS) exact mass calc. for C₁₁H₁₂BrNO₄ [M+NH₄]⁺ 319.0288 m/z, found: 319.0289 m/z.

4-(1-bromo-3-nitropropyl)phenyl *tert*-butyl carbonate (**4k**)



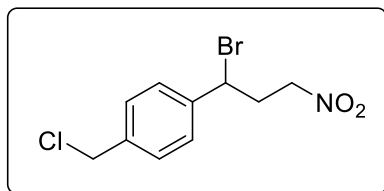
Following general procedure (GP-A) using *tert*-butyl (4-vinylphenyl) carbonate (**2k**) (110.1 mg, 0.5 mmol, 1.0 equiv), bromonitromethane (**1a**) (70.0 mg, 36.0 μL, 0.5 mmol, 1.0 equiv), [Cu(dap)₂]Cl (4.4 mg, 5.0 μmol, 1 mol%) and dry MeCN (2.0 mL, 0.25 M) at room temperature (25 °C) and irradiation with blue LED (λ_{max} = 455 nm) for 3 h yielded 163.8 mg (454.7 μmol,

91%) of 4-(1-bromo-3-nitropropyl)phenyl *tert*-butyl carbonate (**4k**) as pale yellowish oil after flash column purification (hexanes / EtOAc 5:1). R_f (hexanes / EtOAc 20:1 on silica) = 0.45, Staining: UV; KMnO_4 -solution.

$^1\text{H NMR}$ (300 MHz, CDCl_3) δ [ppm] = 7.42 (d, J = 8.6 Hz, 2H), 7.19 (d, J = 8.7 Hz, 2H), 5.04 (dd, J = 9.2, 5.8 Hz, 1H), 4.67 – 4.44 (m, 2H), 2.93 – 2.67 (m, 2H), 1.56 (s, 9H). $^{13}\text{C NMR}$ (101 MHz, CDCl_3) δ [ppm] = 151.7, 151.4, 137.8, 128.5, 122.1, 84.1, 73.5, 49.4, 37.2, 27.8.

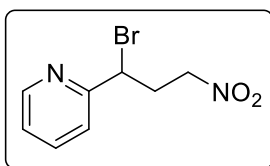
IR (neat, cm^{-1}): 2981, 2933, 1751, 1606, 1554, 1509, 1423, 1371, 1256, 1222, 1140, 1047, 1017, 961, 894, 838, 782, 663. HRMS (ESI-MS) exact mass calc. for $\text{C}_{14}\text{H}_{18}\text{BrNO}_5$ $[\text{M}+\text{H}]^+$ 398.0000 m/z, found: 397.999 m/z and exact mass calc. for $\text{C}_{14}\text{H}_{18}\text{BrNO}_5$ $[\text{M}+\text{Na}]^+$ 382.0261 m/z, found: 382.0264 m/z and exact mass calc. for $\text{C}_{14}\text{H}_{18}\text{BrNO}_5$ $[\text{M}+\text{NH}_4]^+$ 377.0707 m/z, found: 377.0709 m/z.

1-(1-bromo-3-nitropropyl)-4-(chloromethyl)benzene (**4n**)



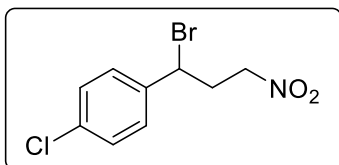
Following general procedure (GP-A) using ethyl 1-(chloromethyl)-4-vinylbenzene (**2n**) (76.3 mg, 66.1 μL , 0.5 mmol, 1.0 equiv), bromonitromethane (**1a**) (70.0 mg, 36.0 μL , 0.5 mmol, 1.0 equiv), $[\text{Cu}(\text{dap})_2]\text{Cl}$ (4.4 mg, 5.0 μmol , 1 mol%) and dry MeCN (2.0 mL, 0.25 M) at room temperature (25 $^\circ\text{C}$) and irradiation with blue LED ($\lambda_{\text{max}} = 455$ nm) for 1 h yielded 86.8 mg (296.7 μmol , 59%) of 1-(1-bromo-3-nitropropyl)-4-(chloromethyl)benzene (**4n**) as pale yellowish oil after flash column purification (hexanes / EtOAc 20:1). R_f (hexanes / EtOAc 5:1) on silica) = 0.59, Staining: UV; KMnO_4 -solution.

$^1\text{H NMR}$ (300 MHz, CDCl_3) δ [ppm] = 7.41 (s, 5H), 5.04 (dd, J = 9.1, 5.8 Hz, 1H), 4.69 – 4.43 (m, 4H), 2.95 – 2.65 (m, 2H). $^{13}\text{C NMR}$ (101 MHz, CDCl_3) δ [ppm] = 140.5, 138.5, 129.4, 127.7, 73.5, 49.6, 45.6, 37.0. IR (neat, cm^{-1}): 3034, 2959, 2922, 1550, 1423, 1379, 1267, 1233, 1162, 1114, 1021, 981, 916, 834, 779, 745, 678. HRMS (APCI-MS) exact mass calc. for $\text{C}_{10}\text{H}_{11}\text{BrClNO}_2$ $[\text{M}+\text{NH}_4]^+$ 310.0030 m/z, found: 310.0033 m/z.

2-(1-bromo-3-nitropropyl)pyridine (4p)

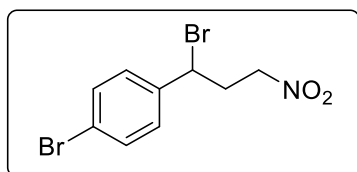
Following general procedure (GP-A) using freshly distilled 2-vinylpyridine (**2p**) (52.6 mg, 54.2 μL , 0.5 mmol, 1.0 equiv), bromonitromethane (**1a**) (70.0 mg, 36.0 μL , 0.5 mmol, 1.0 equiv), $[\text{Cu}(\text{dap})_2]\text{Cl}$ (4.4 mg, 5.0 μmol , 1 mol%) and dry MeCN (2.0 mL, 0.25 M) at room temperature (25 $^\circ\text{C}$) and irradiation with blue LED ($\lambda_{\text{max}} = 455 \text{ nm}$) for 4 h yielded 71.3 mg (290.9 μmol , 58%) of 2-(1-bromo-3-nitropropyl)pyridine (**4p**) as brownish oil after flash column purification (hexanes / EtOAc 5:1). R_f (hexanes / EtOAc 5:1 on silica) = 0.27, Staining: UV; KMnO_4 -solution.

$^1\text{H NMR}$ (400 MHz, CDCl_3) δ [ppm] = 8.58 (ddd, $J = 4.8, 1.9, 0.9 \text{ Hz}$, 1H), 7.70 (td, $J = 7.7, 1.8 \text{ Hz}$, 1H), 7.39 (dt, $J = 7.8, 1.1 \text{ Hz}$, 1H), 7.23 (ddd, $J = 7.6, 4.8, 1.1 \text{ Hz}$, 1H), 5.15 (dd, $J = 8.2, 6.2 \text{ Hz}$, 1H), 4.72 – 4.53 (m, 2H), 3.07 – 2.87 (m, 2H). **$^{13}\text{C NMR}$** (101 MHz, CDCl_3) δ [ppm] = 158.1, 149.8, 137.4, 123.7, 122.9, 73.5, 49.8, 34.4. **IR** (neat, cm^{-1}): 3052, 2926, 1587, 1546, 1472, 1435, 1379, 1289, 1151, 1103, 1051, 995, 961, 913, 868, 782, 745, 670. **HRMS** (APCI-MS) exact mass calc. for $\text{C}_8\text{H}_9\text{BrN}_2\text{O}_2$ $[\text{M}+\text{NH}_4]^+$ 244.9920 m/z, found: 244.9921 m/z.

1-(1-bromo-3-nitropropyl)-4-chlorobenzene (4r)

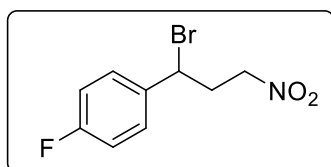
Following general procedure (GP-A) using 4-chlorostyrene (**2r**) (69.3 mg, 63.6 μL , 0.5 mmol, 1.0 equiv), bromonitromethane (**1a**) (70.0 mg, 36.0 μL , 0.5 mmol, 1.0 equiv), $[\text{Cu}(\text{dap})_2]\text{Cl}$ (4.4 mg, 5.0 μmol , 1 mol%) and dry MeCN (2.0 mL, 0.25 M) at room temperature (25 $^\circ\text{C}$) and irradiation with blue LED ($\lambda_{\text{max}} = 455 \text{ nm}$) for 1 h yielded 125.4 mg (450.2 μmol , 90%) of 1-(1-bromo-3-nitropropyl)-4-chlorobenzene (**4r**) as pale yellowish oil after flash column purification (hexanes / EtOAc 20:1). R_f (hexanes / EtOAc 9:1 on silica) = 0.25, Staining: UV, KMnO_4 -solution

$^1\text{H NMR}$ (300 MHz, CDCl_3) δ [ppm] = 7.35 (s, 4H), 5.01 (dd, $J = 9.2, 5.8 \text{ Hz}$, 1H), 4.68 – 4.41 (m, 2H), 2.93 – 2.64 (m, 2H). **$^{13}\text{C NMR}$** (75 MHz, CDCl_3) δ [ppm] = 138.8, 134.9, 129.4, 128.6, 73.4, 49.2, 36.9. **IR** (neat, cm^{-1}): 2922, 1550, 1490, 1427, 1379, 1162, 1092, 831. **HRMS** (APCI-MS) exact mass calc. for $\text{C}_9\text{H}_9\text{BrClNO}_2$ $[\text{M}+\text{NH}_4]^+$ 294.9843 m/z, found: 294.9843 m/z.

1-bromo-4-(1-bromo-3-nitropropyl)benzene (4s)

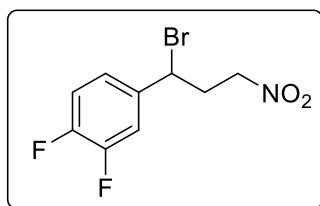
Following general procedure (GP-A) using 4-bromostyrene (**2s**) (91.5 mg, 65.3 μ L, 0.5 mmol, 1.0 equiv), bromonitromethane (**1a**) (70.0 mg, 36.0 μ L, 0.5 mmol, 1.0 equiv), [Cu(dap)₂]Cl (4.4 mg, 5.0 μ mol, 1 mol%) and dry MeCN (2.0 mL, 0.25 M) at room temperature (25 °C) and irradiation with blue LED ($\lambda_{\text{max}} = 455$ nm) for 3 h yielded 133.9 mg (414.6 μ mol, 83%) of 1-bromo-4-(1-bromo-3-nitropropyl)benzene (**4s**) as pale yellowish oil after flash column purification (hexanes / EtOAc 20:1). R_f (hexanes / EtOAc 20:1 on silica) = 0.24, Staining: UV; KMnO₄-solution.

¹H NMR (300 MHz, CDCl₃) δ [ppm] = 7.51 (dd, 2H), 7.28 (dd, $J = 8.8, 2.4$ Hz, 2H), 5.00 (dd, $J = 9.2, 5.8$ Hz, 1H), 4.76 – 4.35 (m, 2H), 2.97 – 2.66 (m, 2H). ¹³C NMR (75 MHz, CDCl₃) δ [ppm] = 139.3, 132.4, 128.9, 123.2, 73.4, 49.2, 36.9. IR (neat, cm⁻¹): 2926, 1587, 1550, 1490, 1338, 1170, 1073, 1010, 827. HRMS (APCI-MS) exact mass calc. for C₉H₉Br₂NO₂ [M+NH₄]⁺ 338.9338 m/z, found: 338.9343 m/z.

1-fluoro-4-(1-bromo-3-nitropropyl)benzene (4t)

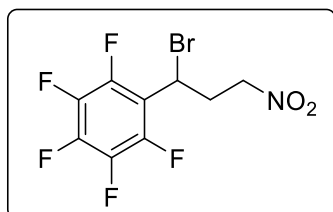
Following general procedure (GP-A) using 4-fluorostyrene (**2t**) (61.1 mg, 59.6 μ L, 0.5 mmol, 1.0 equiv), bromonitromethane (**1a**) (70.0 mg, 36.0 μ L, 0.5 mmol, 1.0 equiv), [Cu(dap)₂]Cl (4.4 mg, 5.0 μ mol, 1 mol%) and dry MeCN (2.0 mL, 0.25 M) at room temperature (25 °C) and irradiation with blue LED ($\lambda_{\text{max}} = 455$ nm) for 1 h yielded 97.9 mg (373.6 μ mol, 75%) of 1-fluoro-4-(1-bromo-3-nitropropyl)benzene (**4t**) as pale yellowish oil after flash column purification (hexanes / EtOAc 20:1). R_f (hexanes / EtOAc 5:1 on silica) = 0.66, Staining: UV; KMnO₄-solution.

¹H NMR (300 MHz, CDCl₃) δ [ppm] = 7.46 – 7.34 (m, 2H), 7.14 – 7.01 (m, 2H), 5.04 (dd, $J = 9.2, 5.8$ Hz, 1H), 4.73 – 4.42 (m, 2H), 2.98 – 2.68 (m, 2H). ¹³C NMR (75 MHz, CDCl₃) δ [ppm] = 136.3 (d, $J = 3.5$ Hz), 129.2 (d, $J = 8.5$ Hz), 116.2 (d, $J = 21.9$ Hz), 73.5, 49.3, 37.2. ¹⁹F NMR (377 MHz, CDCl₃) δ [ppm] = -112.35. IR (neat, cm⁻¹): 3049, 2922, 1602, 1550, 1509, 1423, 1379, 1297, 1226, 1159, 1103, 1062, 961, 916, 834, 767. HRMS (APCI-MS) exact mass calc. for C₉H₉BrFNO₂ [M+NH₄]⁺ 279.0139 m/z, found: 279.0140 m/z.

4-(1-bromo-3-nitropropyl)-1,2-difluorobenzene (4v)

Following general procedure (GP-A) using 3,4-difluorostyrene (**2v**) (70.1 mg, 62.0 μL , 0.5 mmol, 1.0 equiv), bromonitromethane (**1a**) (70.0 mg, 36.0 μL , 0.5 mmol, 1.0 equiv), $[\text{Cu}(\text{dap})_2]\text{Cl}$ (4.4 mg, 5.0 μmol , 1 mol%) and dry MeCN (2.0 mL, 0.25 M) at room temperature (25 °C) and irradiation with blue LED ($\lambda_{\text{max}} = 455 \text{ nm}$) for 1 h yielded 121.9 mg (435.3 μmol , 87%) of 4-(1-bromo-3-nitropropyl)-1,2-difluorobenzene (**4v**) as pale yellowish oil after flash column purification (hexanes / EtOAc 20:1). R_f (hexanes / EtOAc 20:1 on silica) = 0.29, Staining: UV; KMnO_4 -solution.

$^1\text{H NMR}$ (400 MHz, CDCl_3) δ [ppm] = 7.29 – 7.23 (m, 1H), 7.21 – 7.11 (m, 2H), 5.00 (dd, $J = 9.1, 5.8 \text{ Hz}$, 1H), 4.61 (ddd, $J = 13.8, 7.5, 6.1 \text{ Hz}$, 1H), 4.52 (dt, $J = 14.1, 6.2 \text{ Hz}$, 1H), 2.86 – 2.68 (m, 2H). $^{13}\text{C NMR}$ (101 MHz, CDCl_3) δ [ppm] = 151.7 (dd, $J = 11.9, 6.6 \text{ Hz}$), 149.2 (dd, $J = 11.9, 5.2 \text{ Hz}$), 137.4 (dd, $J = 5.5, 3.9 \text{ Hz}$), 123.5 (dd, $J = 6.6, 3.7 \text{ Hz}$), 118.0 (d, $J = 17.4 \text{ Hz}$), 116.6 (d, $J = 18.2 \text{ Hz}$), 73.3, 48.4 (d, $J = 1.7 \text{ Hz}$), 37.0. $^{19}\text{F NMR}$ (376 MHz, CDCl_3) δ [ppm] = -136.09 (ddd, $J = 21.6, 10.7, 6.4 \text{ Hz}$), -136.64 – -136.78 (m). **IR** (neat, cm^{-1}): 3063, 2922, 1610, 1550, 1517, 1435, 1379, 1282, 1207, 1162, 1118, 1073, 1039, 998, 956, 909, 857, 820, 782. **HRMS** (APCI-MS) exact mass calc. for $\text{C}_9\text{H}_8\text{BrF}_2\text{NO}_2$ $[\text{M}+\text{NH}_4]^+$ 297.0045 m/z, found: 297.0043 m/z.

1-(1-bromo-3-nitropropyl)-2,3,4,5,6-pentafluorobenzene (4w)

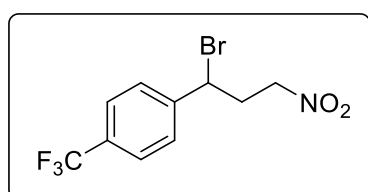
Following general procedure (GP-A) using 2,3,4,5,6-pentafluorostyrene (**2w**) (97.1 mg, 69.0 μL , 0.5 mmol, 1.0 equiv), bromonitromethane (**1a**) (70.0 mg, 36.0 μL , 0.5 mmol, 1.0 equiv), $[\text{Cu}(\text{dap})_2]\text{Cl}$ (4.4 mg, 5.0 μmol , 1 mol%) and dry MeCN (2.0 mL, 0.25 M) at room temperature (25 °C) and irradiation with blue LED ($\lambda_{\text{max}} = 455 \text{ nm}$) for 3 h yielded 132.5 mg (396.7 μmol , 79%) of 1-(1-bromo-3-nitropropyl)-2,3,4,5,6-pentafluorobenzene (**4w**) as colorless oil after flash column purification (hexanes / EtOAc 20:1). R_f (hexanes / EtOAc 20:1 on silica) = 0.24, Staining: UV; KMnO_4 -solution.

¹H NMR (300 MHz, CDCl₃) δ [ppm] = 5.33 (dd, *J* = 10.3, 5.0 Hz, 1H), 4.77 – 4.40 (m, 2H), 3.15 – 2.95 (m, 1H), 2.84 (ddt, *J* = 15.5, 8.3, 5.2 Hz, 1H). **¹³C NMR** (101 MHz, CDCl₃) δ [ppm] = 146.6 – 143.5 (m), 143.4 – 140.3 (m), 139.6 – 136.5 (m), 114.7 – 114.0(m), 34.2 (t, *J* = 3.4 Hz).

¹⁹F NMR (377 MHz, CDCl₃) δ [ppm] = -140.58 (s, 2F), -152.32 (tt, *J* = 20.9, 3.0 Hz, 1F), -160.85 (td, *J* = 21.6, 8.0 Hz, 2F). **IR** (neat, cm⁻¹): 1664, 1558, 1505, 1427, 1371, 1133, 991, 957.

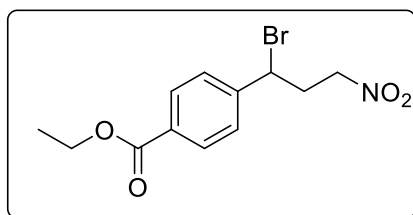
HRMS (EI-MS) exact mass calc. for C₉H₅NO₂F₅ [M]⁺ 254.02350 m/z, found: 254.02356 m/z and exact mass calc. for C₇HF₅Br [M]⁺ 258.91763 m/z, found: 258.91791 m/z and exact mass calc. for C₉H₅F₅Br [M]⁺ 286.94893 m/z, found: m/z 286.94747.

1-(1-bromo-3-nitropropyl)-4-(trifluoromethyl)benzene (**4x**)



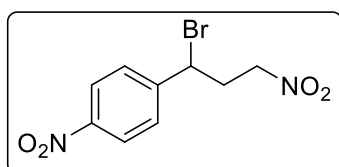
Following general procedure (GP-A) using 4-trifluoromethylstyrene (**2x**) (86.1 mg, 73.9 μL, 0.5 mmol, 1.0 equiv), bromonitromethane (**1a**) (70.0 mg, 36.0 μL, 0.5 mmol, 1.0 equiv), [Cu(dap)₂]Cl (4.4 mg, 5.0 μmol, 1 mol%) and dry MeCN (2.0 mL, 0.25 M) at room temperature (25 °C) and irradiation with blue LED (λ_{max} = 455 nm) for 1 h yielded 119.2 mg (382.0 μmol, 76%) of 1-(1-bromo-3-nitropropyl)-4-(trifluoromethyl)benzene (**4x**) as pale yellowish oil after flash column purification (hexanes / EtOAc 20:1). *R_f* (hexanes / EtOAc 20:1 on silica) = 0.20, Staining: UV; KMnO₄-solution.

¹H NMR (400 MHz, CDCl₃) δ [ppm] = 7.65 (d, *J* = 8.2 Hz, 2H), 7.54 (d, *J* = 8.1 Hz, 2H), 5.07 (dd, *J* = 9.3, 5.6 Hz, 1H), 4.64 (ddd, *J* = 13.8, 7.6, 6.1 Hz, 1H), 4.53 (dt, *J* = 14.1, 6.1 Hz, 1H), 2.96 – 2.67 (m, 2H). **¹³C NMR** (101 MHz, CDCl₃) δ [ppm] = 144.2, 131.3 (q, *J* = 32.8 Hz), 127.8, 126.2 (q, *J* = 3.8 Hz), 123.8 (d, *J* = 272.3 Hz), 73.3, 48.7, 36.8. **¹⁹F NMR** (376 MHz, CDCl₃) δ [ppm] = -63.30 (3F). **IR** (neat, cm⁻¹): 2922, 1617, 1554, 1423, 1379, 1319, 1244, 1162, 1110, 1066, 1017, 957, 913, 842, 760. **HRMS** (APCI-MS) exact mass calc. for C₁₀H₉BrF₃NO₂ [M+NH₄]⁺ 329.0107 m/z, found: 329.0107 m/z.

ethyl 4-(1-bromo-3-nitropropyl)benzoate (4z)

Following general procedure (GP-A) using ethyl 4-vinylbenzoate (**2z**) (88.1 mg, 84.7 μL , 0.5 mmol, 1.0 equiv), bromonitromethane (**1a**) (70.0 mg, 36.0 μL , 0.5 mmol, 1.0 equiv), $[\text{Cu}(\text{dap})_2]\text{Cl}$ (4.4 mg, 5.0 μmol , 1 mol%) and dry MeCN (2.0 mL, 0.25 M) at room temperature (25 $^\circ\text{C}$) and irradiation with blue LED ($\lambda_{\text{max}} = 455 \text{ nm}$) for 1 h yielded 131.6 mg (416.3 μmol , 83%) of ethyl 4-(1-bromo-3-nitropropyl)benzoate (**4z**) as yellowish oil after flash column purification (hexanes / EtOAc 20:1). R_f (hexanes / EtOAc 5:1 on silica) = 0.67, Staining: UV; KMnO_4 -solution.

$^1\text{H NMR}$ (400 MHz, CDCl_3) δ [ppm] = 8.04 (d, $J = 8.4 \text{ Hz}$, 2H), 7.46 (d, $J = 8.4 \text{ Hz}$, 2H), 5.06 (dd, $J = 9.3, 5.6 \text{ Hz}$, 1H), 4.61 (ddd, $J = 13.8, 7.5, 6.1 \text{ Hz}$, 1H), 4.51 (dt, $J = 14.1, 6.2 \text{ Hz}$, 1H), 4.37 (q, $J = 7.1 \text{ Hz}$, 2H), 2.93 – 2.70 (m, 2H), 1.38 (t, $J = 7.1 \text{ Hz}$, 3H). $^{13}\text{C NMR}$ (101 MHz, CDCl_3) δ [ppm] = 165.8, 144.8, 131.2, 130.4, 127.3, 73.3, 61.3, 49.1, 36.7, 14.4. IR (neat, cm^{-1}): 2981, 1710, 1610, 1550, 1420, 1387, 1274, 1177, 1103, 1021, 916, 857, 823, 771, 700. HRMS (APCI-MS) exact mass calc. for $\text{C}_{12}\text{H}_{14}\text{BrNO}_4$ $[\text{M}+\text{H}]^+$ 316.0179 m/z, found: 316.0182 m/z.

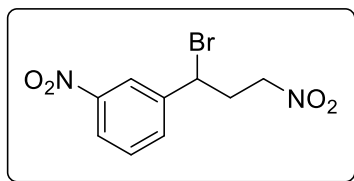
1-(1-bromo-3-nitropropyl)-4-nitrobenzene (4aa)

Following general procedure (GP-A) using 4-nitrostyrene (**2aa**) (74.5 mg, 65.0 μL , 0.5 mmol, 1.0 equiv), bromonitromethane (**1a**) (70.0 mg, 36.0 μL , 0.5 mmol, 1.0 equiv), $[\text{Cu}(\text{dap})_2]\text{Cl}$ (4.4 mg, 5.0 μmol , 1 mol%) and dry MeCN (2.0 mL, 0.25 M) at room temperature (25 $^\circ\text{C}$) and irradiation with blue LED ($\lambda_{\text{max}} = 455 \text{ nm}$) for 1 h yielded 67.7 mg (234.2 μmol , 47%) of 1-(1-bromo-3-nitropropyl)-4-nitrobenzene (**4aa**) as pale yellowish oil after flash column purification (hexanes / EtOAc 10:1). R_f (hexanes / EtOAc 5:1 on silica) = 0.29, Staining: UV; KMnO_4 -solution.

$^1\text{H NMR}$ (400 MHz, CDCl_3) = δ 8.24 (d, $J = 8.8 \text{ Hz}$, 2H), 7.60 (d, $J = 8.8 \text{ Hz}$, 2H), 5.36 – 5.09 (m, 1H), 4.72 – 4.62 (m, 1H), 4.62 – 4.51 (m, 1H), 2.82 (dtd, $J = 7.5, 6.0, 4.2 \text{ Hz}$, 2H). $^{13}\text{C NMR}$ (101 MHz, CDCl_3) δ [ppm] = 148.1, 147.1, 128.4, 124.5, 73.1, 47.9, 36.6. IR (neat, cm^{-1}): 3112, 3082, 2959, 2858, 1606, 1550, 1520, 1427, 1379, 1349, 1293, 1230, 1166, 1100, 1066, 961,

916, 853, 820, 752, 697. **HRMS** (APCI-MS) exact mass calc. for $C_9H_9N_2O_4Br$ $[M+NH_4]^+$ 306.0084 m/z, found: 306.0083 m/z.

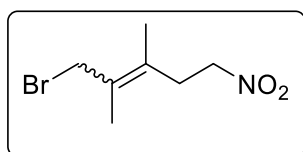
1-(1-bromo-3-nitropropyl)-3-nitrobenzene (**4ab**)



Following general procedure (GP-A) using 3-nitrostyrene (**2ab**) (74.5 mg, 69.7 μ L, 0.5 mmol, 1.0 equiv), bromonitromethane (**1a**) (70.0 mg, 36.0 μ L, 0.5 mmol, 1.0 equiv), $[Cu(dap)_2]Cl$ (4.4 mg, 5.0 μ mol, 1 mol%) and dry MeCN (2.0 mL, 0.25 M) at room temperature (25 $^{\circ}C$) and irradiation with blue LED (λ_{max} = 455 nm) for 4 h yielded 124.3 mg (429.6 μ mol, 86%) of 1-(1-bromo-3-nitropropyl)-3-nitrobenzene (**4ab**) as pale yellowish oil after flash column purification (hexanes / EtOAc 5:1). R_f (hexanes / EtOAc 5:1 on silica) = 0.35, Staining: UV; $KMnO_4$ -solution.

1H NMR (400 MHz, $CDCl_3$) δ [ppm] = 8.29 (t, J = 2.0 Hz, 1H), 8.19 (ddd, J = 8.2, 2.2, 1.0 Hz, 1H), 7.79 – 7.73 (m, 1H), 7.59 (t, J = 8.0 Hz, 1H), 5.13 (dd, J = 9.1, 5.8 Hz, 1H), 4.68 (ddd, J = 13.9, 7.6, 6.1 Hz, 1H), 4.58 (dt, J = 14.2, 6.0 Hz, 1H), 2.94 – 2.73 (m, 2H). **^{13}C NMR** (101 MHz, $CDCl_3$) δ [ppm] = 148.7, 142.5, 133.4, 130.4, 124.1, 122.4, 73.2, 48.1, 36.7. **IR** (neat, cm^{-1}): 3086, 3015, 2922, 2873, 1550, 1524, 1427, 1349, 1230, 1203, 1162, 1099, 998, 965, 857, 805, 738, 685. **HRMS** (APCI-MS) exact mass calc. for $C_9H_9N_2O_4Br$ $[M+NH_4]^+$ 306.0084 m/z, found: 306.0086 m/z.

1-bromo-2,3-dimethyl-5-nitropent-2-ene (*E/Z* = 61:39) (**4ae**)



Following general procedure (GP-A) using 2,3-dimethylbuta-1,3-diene (**2ae**) (41.1 mg, 56.6 μ L, 0.5 mmol, 1.0 equiv), bromonitromethane (**1a**) (70.0 mg, 36.0 μ L, 0.5 mmol, 1.0 equiv), $[Cu(dap)_2]Cl$ (4.4 mg, 5.0 μ mol, 1 mol%) and dry MeCN (2.0 mL, 0.25 M) at room temperature (25 $^{\circ}C$) and irradiation with blue LED (λ_{max} = 455 nm) for 1 h yielded 81.2 mg (365.6 μ mol, 73%) of 1-bromo-2,3-dimethyl-5-nitropent-2-ene as an inseparable mixture of diastereomers (*E/Z* = 61:39) (**4ae**) as colorless oil after flash column purification (hexanes / EtOAc 20:1). R_f (hexanes / EtOAc 5:1 on silica) = 0.63 UV, $KMnO_4$ -solution.

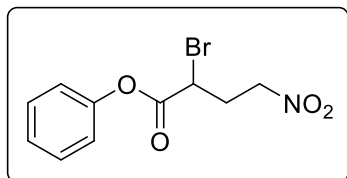
1H NMR (300 MHz, $CDCl_3$) δ [ppm] = 4.48 (d, J = 7.4 Hz, 2H, minor diastereomer), 4.41 (t, J = 7.6 Hz, 2H, major diastereomer), 4.01 (s, 2H, minor diastereomer), 3.97 (s, 2H, major

diastereomer), 2.87 (t, $J = 7.5$ Hz, 2H, minor diastereomer), 2.79 (t, $J = 7.6$ Hz, 2H, major diastereomer), 1.84 – 1.76 (m, 9H, both diastereomers), 1.75 – 1.72 (m, 3H, minor diastereomer). $^{13}\text{C NMR}$ (75 MHz, CDCl_3) δ [ppm] = 130.6 (minor diastereomer), 130.4 (major diastereomer), 129.6 (both diastereomers), 73.1 (major diastereomer), 73.1 (minor diastereomer), 35.2 (major diastereomer), 34.6 (minor diastereomer), 33.0 (major diastereomer), 32.3 (minor diastereomer), 18.9 (minor diastereomer), 18.0 (minor diastereomer), 18.0 (major diastereomer), 17.2 (major diastereomer).

IR (neat, cm^{-1}): 2922, 1654, 1550, 1431, 1379, 1278, 1203, 1080, 1013, 957, 920, 861, 756, 689. **HRMS** (APCI-MS) (minor diastereomer) exact mass calc. for $\text{C}_7\text{H}_{12}\text{Br}_2\text{O}_2$ $[\text{M}+\text{NH}_4]^+$ 239.0390 m/z, found: 239.0390 m/z and **HRMS** (APCI-MS) (major diastereomer) exact mass calc. for $\text{C}_7\text{H}_{12}\text{Br}_2\text{O}_2$ $[\text{M}+\text{NH}_4]^+$ 239.0390 m/z, found: 239.0392 m/z.

Scope of Michael Systems

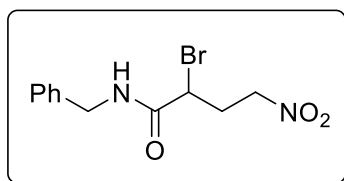
phenyl 2-bromo-4-nitrobutanoate (**4ba**)



Following general procedure (GP-A) using phenyl acrylate (**2ba**) (74.1 mg, 59.3 μL , 0.5 mmol, 1.0 equiv), bromonitromethane (**1a**) (70.0 mg, 36.0 μL , 0.5 mmol, 1.0 equiv), $[\text{Cu}(\text{dap})_2]\text{Cl}$ (4.4 mg, 5.0 μmol , 1 mol%) and dry MeCN (2.0 mL, 0.25 M) at room temperature (25 $^\circ\text{C}$) and irradiation with blue LED ($\lambda_{\text{max}} = 455$ nm) for 30 h yielded 41.8 mg (145.1 μmol , 29%) of phenyl 2-bromo-4-nitrobutanoate (**4ba**) as pale yellowish oil after flash column purification (hexanes / EtOAc 10:1). R_f (hexanes / EtOAc 5:1 on silica) = 0.41, Staining: KMnO_4 -solution.

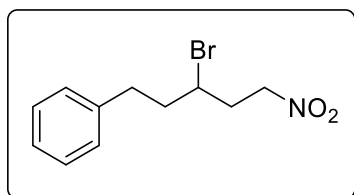
$^1\text{H NMR}$ (300 MHz, CDCl_3) δ [ppm] = 7.51 – 7.36 (m, 2H), 7.35 – 7.22 (m, 1H), 7.19 – 7.09 (m, 2H), 4.74 – 4.62 (m, 3H), 2.89 (dtd, $J = 15.5, 6.8, 5.5$ Hz, 1H), 2.72 (ddt, $J = 15.6, 8.6, 6.0$ Hz, 1H). $^{13}\text{C NMR}$ (101 MHz, CDCl_3) δ [ppm] = 167.4, 150.3, 129.8, 126.7, 121.0, 72.3, 41.1, 31.5.

IR (neat, cm^{-1}): 3019, 2922, 1751, 1591, 1550, 1490, 1427, 1367, 1315, 1259, 1230, 1189, 1133, 1069, 965, 913, 857, 812, 752, 685. **HRMS** (APCI-MS) exact mass calc. for $\text{C}_{10}\text{H}_{10}\text{BrNO}_4$ $[\text{M}+\text{NH}_4]^+$ 305.0131 m/z, found: 305.0133 m/z.

***N*-benzyl-2-bromo-4-nitrobutanamide (4bb)**

Following general procedure (GP-A) using *N*-benzylacrylamide (**2bb**) (74.1 mg, 59.3 μ L, 0.5 mmol, 1.0 equiv), bromonitromethane (**1a**) (70.0 mg, 36.0 μ L, 0.5 mmol, 1.0 equiv), [Cu(dap)₂]Cl (4.4 mg, 5.0 μ mol, 1 mol%) and dry MeCN (2.0 mL, 0.25 M) at room temperature (25 °C) and irradiation with blue LED ($\lambda_{\text{max}} = 455$ nm) for 22 h yielded 107.1 mg (355.7 μ mol, 71%) of *N*-benzyl-2-bromo-4-nitrobutanamide (**4bb**) as colorless oil after flash column purification (hexanes / EtOAc 5:1). R_f (hexanes / EtOAc 5:1 on silica) = 0.08, Staining: KMnO₄-solution.

¹H NMR (300 MHz, CDCl₃) δ [ppm] = 7.50 – 7.30 (m, 5H), 7.04 (s, NH), 4.65 (td, $J = 6.4, 1.4$ Hz, 2H), 4.62 – 4.36 (m, 3H), 2.97 – 2.79 (m, 1H), 2.78 – 2.59 (m, 1H). **¹³C NMR** (101 MHz, CDCl₃) δ [ppm] = 167.5, 137.2, 128.9, 127.9, 127.7, 72.8, 45.1, 44.2, 32.3. **IR** (neat, cm⁻¹): 3399, 3287, 3067, 3034, 2926, 1654, 1546, 1453, 1423, 1371, 1271, 1241, 1207, 1162, 1107, 1028, 985, 909, 857, 805, 730, 697. **HRMS** (ESI-MS) exact mass calc. for C₁₁H₁₃N₂O₃ [M+Na]⁺ 323.0002 m/z, found: 323.0003 m/z.

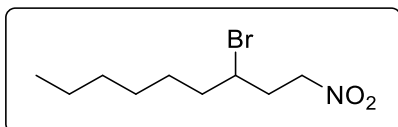
Unactivated Olefins**(3-bromo-5-nitropentyl)benzene (4ca)**

Following general procedure (GP-A) using but-3-en-1-ylbenzene (**2ca**) (66.1 mg, 75.1 μ L, 0.5 mmol, 1.0 equiv), bromonitromethane (**1a**) (70.0 mg, 36.0 μ L, 0.5 mmol, 1.0 equiv), [Cu(dap)₂]Cl (4.4 mg, 5.0 μ mol, 1 mol%) and dry MeCN (2.0 mL, 0.25 M) at room temperature (25 °C) and irradiation with blue LED ($\lambda_{\text{max}} = 455$ nm) for 9 h yielded 91.0 mg (334.4 μ mol, 67%) of 1 *tert*-butyl (2-bromo-4-nitrobutyl)carbamate (**4ca**) as pale yellowish oil after flash column purification (hexanes / EtOAc 5:1). R_f (hexanes / EtOAc 5:1 on silica) = 0.37, Staining: UV; KMnO₄-solution.

¹H NMR (300 MHz, CDCl₃) δ [ppm] = 7.37 – 7.28 (m, 2H), 7.26 – 7.14 (m, 3H), 4.62 (dd, $J = 7.5, 6.2$ Hz, 2H), 3.99 (dddd, $J = 10.2, 8.2, 5.0, 3.1$ Hz, 1H), 2.93 (ddd, $J = 14.0, 8.4, 5.7$ Hz, 1H), 2.78 (dt, $J = 13.8, 8.0$ Hz, 1H), 2.62 (dtd, $J = 15.1, 7.5, 3.1$ Hz, 1H), 2.39 (ddt, $J = 15.1,$

10.2, 6.2 Hz, 1H), 2.23 – 2.12 (m, 2H). ^{13}C NMR (75 MHz, CDCl_3) δ [ppm] = 140.2, 128.8, 128.6, 126.5, 73.6, 51.9, 40.8, 36.2, 33.6. IR (neat, cm^{-1}): 3063, 3026, 2926, 2862, 1602, 1550, 1498, 1431, 1386, 1297, 1237, 1177, 1084, 1028, 909, 849, 797, 752, 700. HRMS (EI-MS) exact mass calc. for $\text{C}_{11}\text{H}_{14}\text{NO}_2\text{Br}$ $[\text{M}]^+$ 271.0202 m/z, found: 271.0209 m/z.

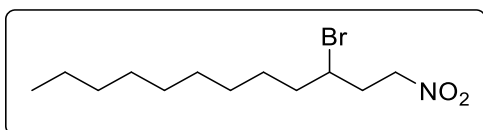
3-bromo-1-nitrononane (4cb)



Following general procedure (GP-A) using 1-pente (**2cb**) (56.1 mg, 78.5 μL , 0.5 mmol, 1.0 equiv), bromonitromethane (**1a**) (70.0 mg, 36.0 μL , 0.5 mmol, 1.0 equiv), $[\text{Cu}(\text{dap})_2]\text{Cl}$ (4.4 mg, 5.0 μmol , 1 mol%) and dry MeCN (2.0 mL, 0.25 M) at room temperature (25 $^\circ\text{C}$) and irradiation with blue LED ($\lambda_{\text{max}} = 455$ nm) for 9 h yielded 76.8 mg (304.6 μmol , 61%) of 3-bromo-1-nitrononane (**4cb**) as colorless oil after flash column purification (hexanes / EtOAc 50:1). R_f (hexanes / EtOAc 10:1 on silica) = 0.47, Staining: KMnO_4 -solution.

^1H NMR (400 MHz, CDCl_3) δ [ppm] = 4.69 – 4.55 (m, 2H), 4.04 (dddd, $J = 10.6, 8.2, 5.3, 3.0$ Hz, 1H), 2.61 (dtd, $J = 15.1, 7.5, 3.0$ Hz, 1H), 2.34 (dddd, $J = 15.4, 10.2, 6.6, 5.5$ Hz, 1H), 1.95 – 1.77 (m, 2H), 1.67 – 1.18 (m, 8H), 0.94 – 0.84 (m, 3H). ^{13}C NMR (101 MHz, CDCl_3) δ [ppm] = 73.7, 52.8, 39.3, 36.2, 31.7, 28.6, 27.5, 22.7, 14.2. IR (neat, cm^{-1}): 2929, 2858, 1550, 1461, 1431, 1379, 1289, 1218, 1170, 1125, 1058, 1006, 879, 842, 797, 723. HRMS (APCI-MS) exact mass calc. for $\text{C}_9\text{H}_{18}\text{BrNO}_2$ $[\text{M}+\text{NH}_4]^+$ 269.0859 m/z, found: 269.0858 m/z.

3,12-dibromo-1-nitrododecane (4cd)

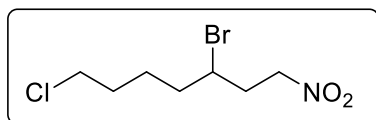


Following general procedure (GP-A) using 11-bromoundec-1-ene (**2cd**) (116.6 mg, 109.7 μL , 0.5 mmol, 1.0 equiv), bromonitromethane (**1a**) (70.0 mg, 36.0 μL , 0.5 mmol, 1.0 equiv), $[\text{Cu}(\text{dap})_2]\text{Cl}$ (4.4 mg, 5.0 μmol , 1 mol%) and dry MeCN (2.0 mL, 0.25 M) at room temperature (25 $^\circ\text{C}$) and irradiation with blue LED ($\lambda_{\text{max}} = 455$ nm) for 6 h yielded 137.2 mg (367.7 μmol , 74%) of 3,12-dibromo-1-nitrododecane (**4cd**) as colorless oil after flash column purification (hexanes / EtOAc 50:1). R_f (hexanes / EtOAc 5:1 on silica) = 0.68, Staining: KMnO_4 -solution.

^1H NMR (400 MHz, CDCl_3) δ [ppm] = 4.69 – 4.53 (m, 2H), 4.03 (dddd, $J = 10.6, 8.2, 5.3, 3.1$ Hz, 1H), 3.39 (t, $J = 6.9$ Hz, 2H), 2.60 (dtd, $J = 15.1, 7.6, 3.1$ Hz, 1H), 2.33 (dddd, $J = 15.4, 10.2, 6.5, 5.5$ Hz, 1H), 1.95 – 1.75 (m, 3H), 1.62 – 1.49 (m, 1H), 1.51 – 1.33 (m, 3H), 1.29 (s, 9H).

^{13}C NMR (101 MHz, CDCl_3) δ [ppm] = 73.7, 52.8, 39.2, 36.1, 34.1, 32.9, 29.4, 29.3, 28.9, 28.8, 28.2, 27.4. **IR** (neat, cm^{-1}): 2926, 2855, 1550, 1461, 1431, 1382, 1289, 1256, 1170, 1133, 1051, 998, 909, 853, 797, 723. **HRMS** (APCI-MS) exact mass calc. for $\text{C}_{12}\text{H}_{23}\text{Br}_2\text{NO}_2$ $[\text{M}+\text{NH}_4]^+$ 389.0434 m/z, found: 389.0423 m/z.

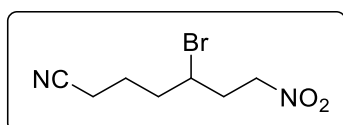
3-bromo-7-chloro-1-nitroheptane (**4ce**)



Following general procedure (GP-A) using 6-chlorohex-1-ene (**2ce**) (59.3 mg, 66.2 μL , 0.5 mmol, 1.0 equiv), bromonitromethane (**1a**) (70.0 mg, 36.0 μL , 0.5 mmol, 1.0 equiv), $[\text{Cu}(\text{dap})_2]\text{Cl}$ (4.4 mg, 5.0 μmol , 1 mol%) and dry MeCN (2.0 mL, 0.25 M) at room temperature (25 $^\circ\text{C}$) and irradiation with blue LED ($\lambda_{\text{max}} = 455$ nm) for 6 h yielded 103.2 mg (399.2 μmol , 80%) of 3-bromo-7-chloro-1-nitroheptane (**4ce**) as colorless oil after flash column purification (hexanes / EtOAc 20:1). R_f (hexanes / EtOAc 5:1 on silica) = 0.51, Staining: KMnO_4 -solution.

^1H NMR (300 MHz, CDCl_3) δ [ppm] = 4.71 – 4.52 (m, 2H), 4.03 (ddt, $J = 13.2, 6.4, 3.0$ Hz, 1H), 3.54 (t, $J = 6.3$ Hz, 2H), 2.67 – 2.52 (m, 1H), 2.42 – 2.25 (m, 1H), 1.95 – 1.53 (m, 6H). **^{13}C NMR** (75 MHz, CDCl_3) δ [ppm] = 73.6, 52.2, 44.7, 38.4, 36.0, 31.8, 24.9. **IR** (neat, cm^{-1}): 2944, 2870, 1550, 1431, 1382, 1308, 1230, 1174, 1088, 995, 846, 790, 723. **HRMS** (APCI-MS) exact mass calc. for $\text{C}_7\text{H}_{13}\text{BrClNO}_2$ $[\text{M}+\text{NH}_4]^+$ 277.0134 m/z, found: 277.0137 m/z.

5-bromo-7-nitroheptanenitrile (**4cf**)

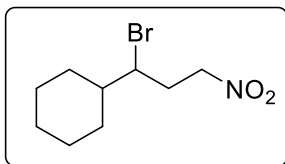


Following general procedure (GP-A) using hex-5-enenitrile (**2cf**) (47.6 mg, 56.6 μL , 0.5 mmol, 1.0 equiv), bromonitromethane (**1a**) (70.0 mg, 36.0 μL , 0.5 mmol, 1.0 equiv), $[\text{Cu}(\text{dap})_2]\text{Cl}$ (4.4 mg, 5.0 μmol , 1 mol%) and dry MeCN (2.0 mL, 0.25 M) at room temperature (25 $^\circ\text{C}$) and irradiation with blue LED ($\lambda_{\text{max}} = 455$ nm) for 24 h yielded 83.9 mg (356.9 μmol , 71%) of 5-bromo-7-nitroheptanenitrile (**4cf**) as pale yellowish oil after flash column purification (hexanes / EtOAc 5:1). R_f (hexanes / EtOAc 5:1 on silica) = 0.13, Staining: KMnO_4 -solution.

^1H NMR (400 MHz, CDCl_3) δ [ppm] = 4.61 (qd, $J = 7.7, 7.3, 5.7$ Hz, 2H), 4.07 – 3.96 (m, 1H), 2.61 (dddd, $J = 15.1, 8.1, 6.8, 3.1$ Hz, 1H), 2.46 – 2.27 (m, 3H), 2.08 – 1.92 (m, 3H), 1.88 – 1.71 (m, 1H). **^{13}C NMR** (101 MHz, CDCl_3) δ [ppm] = 119.1, 73.3, 51.0, 37.7, 36.0, 23.5, 16.6.

IR (neat, cm^{-1}): 2933, 2247, 1550, 1427, 1382, 1304, 1233, 1177, 1092, 1036, 957, 909, 861, 793, 738. **HRMS** (APCI-MS) exact mass calc. for $\text{C}_7\text{H}_{11}\text{BrN}_2\text{O}_2$ $[\text{M}+\text{NH}_4]^+$ 252.0342 m/z, found: 252.0344 m/z.

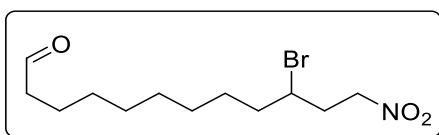
(1-bromo-3-nitropropyl)cyclohexane (4cg)



Following general procedure (GP-A) using vinylcyclohexane (**2cg**) (55.1 mg, 68.5 μL , 0.5 mmol, 1.0 equiv), bromonitromethane (**1a**) (70.0 mg, 36.0 μL , 0.5 mmol, 1.0 equiv), $[\text{Cu}(\text{dap})_2]\text{Cl}$ (4.4 mg, 5.0 μmol , 1 mol%) and dry MeCN (2.0 mL, 0.25 M) at room temperature (25 $^\circ\text{C}$) and irradiation with blue LED ($\lambda_{\text{max}} = 455$ nm) for 2 h yielded 68.1 mg (272.3 μmol , 54 %) of (1-bromo-3-nitropropyl)cyclohexane (**4cg**) as colorless oil after flash column purification (hexanes / EtOAc 5:1). R_f (hexanes / EtOAc 5:1 on silica) = 0.24, Staining: KMnO_4 -solution.

^1H NMR (300 MHz, CDCl_3) δ [ppm] = 4.62 (dd, $J = 7.6, 5.9$ Hz, 2H), 3.96 (ddd, $J = 11.0, 4.5, 2.6$ Hz, 1H), 2.59 (dtd, $J = 15.2, 7.7, 2.6$ Hz, 1H), 2.44 – 2.28 (m, 1H), 1.97 – 1.71 (m, 4H), 1.72 – 1.44 (m, 2H), 1.38 – 0.95 (m, 5H). **^{13}C NMR** (75 MHz, CDCl_3) δ [ppm] = 74.1, 59.6, 44.7, 33.5, 30.7, 29.5, 26.2, 26., 26.0. **IR** (neat, cm^{-1}): 2929, 2855, 1550, 1446, 1382, 1304, 1241, 1170, 1095, 1066, 1028, 961, 857, 797, 715. **HRMS** (APCI-MS) exact mass calc. for $\text{C}_9\text{H}_{16}\text{BrNO}_2$ $[\text{M}+\text{NH}_4]^+$ 267.0703 m/z, found: 267.0706 m/z.

10-bromo-12-nitrododecanal (4ci)

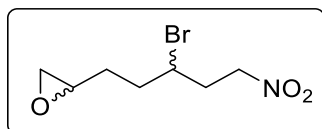


Following general procedure (GP-A) using undec-10-enal (**2ci**) (84.1 mg, 102.0 μL , 0.5 mmol, 1.0 equiv), bromonitromethane (**1a**) (70.0 mg, 36.0 μL , 0.5 mmol, 1.0 equiv), $[\text{Cu}(\text{dap})_2]\text{Cl}$ (4.4 mg, 5.0 μmol , 1 mol%) and dry MeCN (2.0 mL, 0.25 M) at room temperature (25 $^\circ\text{C}$) and irradiation with blue LED ($\lambda_{\text{max}} = 455$ nm) for 3 h yielded 111.8 mg (362.7 μmol , 73%) of 10-bromo-12-nitrododecanal (**4ci**) as colorless oil after flash column purification (hexanes / EtOAc 20:1). R_f (hexanes / EtOAc 5:1 on silica) = 0.33, Staining: KMnO_4 -solution.

^1H NMR (400 MHz, CDCl_3) δ [ppm] = 9.75 (t, $J = 1.8$ Hz, 1H), 4.68 – 4.55 (m, 2H), 4.02 (dddd, $J = 10.6, 8.2, 5.3, 3.0$ Hz, 1H), 2.59 (dtd, $J = 15.1, 7.5, 3.1$ Hz, 1H), 2.41 (td, $J = 7.3, 1.9$ Hz, 2H), 2.38 – 2.27 (m, 1H), 1.94 – 1.76 (m, 2H), 1.67 – 1.58 (m, 2H), 1.58 – 1.48 (m, 1H), 1.48

– 1.37 (m, 1H), 1.37 – 1.25 (m, 8H). $^{13}\text{C NMR}$ (101 MHz, CDCl_3) δ [ppm] = 203.0, 73.7, 52.8, 44.0, 39.2, 36.1, 29.3, 29.2, 29.2, 28.8, 27.4, 22.1. **IR** (neat, cm^{-1}): 2929, 2855, 2721, 1722, 1550, 1431, 1382, 1293, 1230, 1174, 1110, 853, 797, 723. **HRMS** (APCI-MS) exact mass calc. for $\text{C}_{12}\text{H}_{22}\text{BrNO}_3$ $[\text{M}+\text{NH}_4]^+$ 325.1121 m/z, found: 325.1121 m/z.

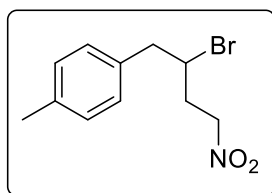
2-(3-bromo-5-nitropentyl)oxirane (**4c**)



Following general procedure (GP-A) using 2-(but-3-en-1-yl)oxirane (**2c**) (49.1 mg, 54.5 μL , 0.5 mmol, 1.0 equiv), bromonitromethane (**1a**) (70.0 mg, 36.0 μL , 0.5 mmol, 1.0 equiv), $[\text{Cu}(\text{dap})_2]\text{Cl}$ (4.4 mg, 5.0 μmol , 1 mol%) and dry MeCN (2.0 mL, 0.25 M) at room temperature (25 $^\circ\text{C}$) and irradiation with blue LED ($\lambda_{\text{max}} = 455$ nm) for 4 h yielded 75.7 mg (318.0 μmol , 64%) of 2-(3-bromo-5-nitropentyl)oxirane (**4c**) as an inseparable mixture of two diastereomers (d.r. = 54:46; diastereomeric ratio was determined using GC-MS) as pale yellowish oil after flash column purification (hexanes / EtOAc 5:1). R_f (hexanes / EtOAc 5:1 on silica) = 0.15, Staining: KMnO_4 -solution.

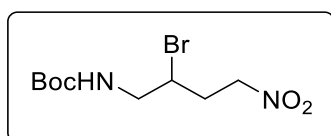
$^1\text{H NMR}$ (300 MHz, CDCl_3) δ [ppm] = 4.71 – 4.53 (m, 4H, both diastereomers), 4.15 – 3.99 (m, 2H, both diastereomers), 2.98 – 2.87 (m, 2H, both diastereomers), 2.80 – 2.72 (m, 2H, both diastereomers), 2.70 – 2.54 (m, 2H, both diastereomers), 2.54 – 2.45 (m, 2H, both diastereomers), 2.43 – 2.26 (m, 2H, both diastereomers), 2.15 – 1.62 (m, 7H, both diastereomers), 1.61 – 1.45 (m, 1H, diastereomer). $^{13}\text{C NMR}$ (75 MHz, CDCl_3) δ [ppm] = 73.5, 73.5, 52.1, 51.8, 51.6, 51.1, 47.1, 47.0, 36.2, 36.0, 35.9, 35.3, 30.7, 30.2. **IR** (neat, cm^{-1}): 2993, 2926, 1550, 1483, 1431, 1431, 1382, 1285, 1222, 1170, 1099, 1002, 972, 913, 838, 752, 667.

HRMS (APCI-MS) (minor diastereomer) exact mass calc. for $\text{C}_7\text{H}_{12}\text{BrNO}_3$ $[\text{M}+\text{NH}_4]^+$ 238.0073 m/z, found: 238.0069 m/z exact mass calc. for $\text{C}_7\text{H}_{12}\text{BrNO}_3$ $[\text{M}+\text{NH}_4]^+$ 255.0339 m/z, found: 255.0348 m/z and **HRMS** (APCI-MS) (major diastereomer) exact mass calc. for $\text{C}_7\text{H}_{12}\text{BrNO}_3$ $[\text{M}+\text{NH}_4]^+$ 238.0073 m/z, found: 238.0079 m/z and exact mass calc. for $\text{C}_7\text{H}_{12}\text{BrNO}_3$ $[\text{M}+\text{NH}_4]^+$ 255.0339 m/z, found: 255.0344 m/z.

1-(2-bromo-4-nitrobutyl)-4-methylbenzene (4cl)

Following general procedure (GP-A) using 1-allyl-4-methylbenzene (**2cl**) (66.1 mg, 43.8 μL , 0.5 mmol, 1.0 equiv), bromonitromethane (**1a**) (70.0 mg, 36.0 μL , 0.5 mmol, 1.0 equiv), $[\text{Cu}(\text{dap})_2]\text{Cl}$ (4.4 mg, 5.0 μmol , 1 mol%) and dry MeCN (2.0 mL, 0.25 M) at room temperature (25 $^\circ\text{C}$) and irradiation with blue LED ($\lambda_{\text{max}} = 455 \text{ nm}$) for 3 h yielded 42.7 mg (156.9 μmol , 31%) of 1-(2-bromo-4-nitrobutyl)-4-methylbenzene (**4cl**) as yellowish oil after flash column purification (hexanes / EtOAc 20:1). R_f (hexanes / EtOAc 5:1 on silica) = 0.66, Staining: KMnO_4 -solution.

$^1\text{H NMR}$ (400 MHz, CDCl_3) δ [ppm] = 7.15 (d, $J = 7.7 \text{ Hz}$, 2H), 7.10 (d, $J = 8.1 \text{ Hz}$, 2H), 4.60 (dd, $J = 7.7, 6.1 \text{ Hz}$, 2H), 4.23 (dtd, $J = 10.2, 7.1, 2.9 \text{ Hz}$, 1H), 3.26 (dd, $J = 14.2, 7.1 \text{ Hz}$, 1H), 3.14 (dd, $J = 14.2, 7.2 \text{ Hz}$, 1H), 2.62 (dtd, $J = 15.2, 7.7, 2.9 \text{ Hz}$, 1H), 2.34 (s, 3H), 2.34 – 2.22 (m, 1H). **$^{13}\text{C NMR}$** (101 MHz, CDCl_3) δ [ppm] = 137.1, 134.2, 129.5, 129.2, 73.7, 52.0, 45.3, 35.1, 21.2. **IR** (neat, cm^{-1}): 3022, 2922, 1550, 1500, 1431, 1382, 1300, 1162, 1110, 1043, 905, 805, 756. **HRMS** (APCI-MS) exact mass calc. for $\text{C}_{11}\text{H}_{14}\text{BrNO}_2$ $[\text{M}+\text{NH}_4]^+$ 289.0546 m/z, found: 289.0545 m/z.

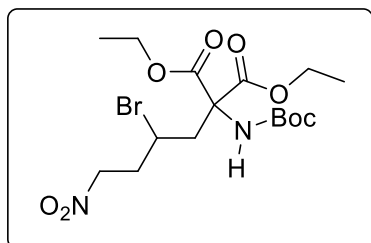
tert-butyl (2-bromo-4-nitrobutyl)carbamate (4cm)

Following general procedure (GP-A) using *tert*-butyl allylcarbamate (**2cm**) (78.6 mg, 0.5 mmol, 1.0 equiv), bromonitromethane (**1a**) (70.0 mg, 36.0 μL , 0.5 mmol, 1.0 equiv), $[\text{Cu}(\text{dap})_2]\text{Cl}$ (4.4 mg, 5.0 μmol , 1 mol%) and dry MeCN (2.0 mL, 0.25 M) at room temperature (25 $^\circ\text{C}$) and irradiation with blue LED ($\lambda_{\text{max}} = 455 \text{ nm}$) for 9 h yielded 120.4 mg (405.2 μmol , 81%) of 1 *tert*-butyl (2-bromo-4-nitrobutyl)carbamate (**4cm**) as pale yellowish oil after flash column purification (hexanes / EtOAc 5:1). **mp**: 74 $^\circ\text{C}$ R_f (hexanes / EtOAc 5:1 on silica) = 0.20, Staining: Ninhydrin-solution.

$^1\text{H NMR}$ (400 MHz, CDCl_3) δ [ppm] = 5.00 (s, 1H), 4.61 (dh, $J = 14.1, 6.7 \text{ Hz}$, 2H), 4.14 (tt, $J = 9.5, 4.4 \text{ Hz}$, 1H), 3.55 (dt, $J = 9.7, 5.9 \text{ Hz}$, 2H), 2.63 (dtd, $J = 15.0, 7.4, 3.7 \text{ Hz}$, 1H), 2.33 (ddt, $J = 15.8, 10.0, 6.2 \text{ Hz}$, 1H), 1.44 (s, 9H). **$^{13}\text{C NMR}$** (101 MHz, CDCl_3) δ [ppm] = 155.8, 80.2, 73.2, 51.2, 47.0, 32.9, 28.3. **IR** (neat, cm^{-1}): 3350, 2978, 2937, 1699, 1558, 1513, 1431, 1367,

1252, 1166, 1043, 913, 861. **HRMS** (ESI-MS) exact mass calc. for $C_9H_{17}BrN_2O_4Na$ $[M+Na]^+$ 319.0264 m/z, found: 319.0271 m/z.

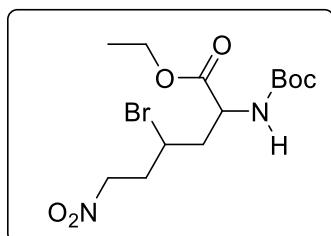
diethyl 2-(2-bromo-4-nitrobutyl)-2-((*tert*-butoxycarbonyl)amino)malonate (4co**)**



Following general procedure (GP-A) using diethyl 2-allyl-2-((*tert*-butoxycarbonyl)-amino)malonate (**2co**) (157.7 mg, 0.5 mmol, 1.0 equiv), bromonitromethane (**1a**) (70.0 mg, 36.0 μ L, 0.5 mmol, 1.0 equiv), $[Cu(dap)_2]Cl$ (4.4 mg, 5.0 μ mol, 1 mol%) and dry MeCN (2.0 mL, 0.25 M) at room temperature (25 °C) and irradiation with blue LED ($\lambda_{max}=455$ nm) for 6 h yielded 84.0 mg (184.5 μ mol, 37%) of diethyl 2-(2-bromo-4-nitrobutyl)-2-((*tert*-butoxycarbonyl)-amino)malonate (**4co**) as colorless oil after flash column purification (hexanes / EtOAc 5:1). R_f (hexanes / EtOAc 5:1 on silica) = 0.43, Staining: $KMnO_4$ -solution.

1H NMR (400 MHz, $CDCl_3$) δ [ppm] = 6.10 (s, NH), 4.65 – 4.48 (m, 2H), 4.34 – 4.13 (m, 2H), 4.09 – 4.00 (m, 1H), 3.10 (d, $J = 15.6$ Hz, 1H), 2.90 (dd, $J = 15.8, 9.6$ Hz, 1H), 2.64 – 2.50 (m, 1H), 2.47 – 2.34 (m, 1H), 1.42 (s, 9H), 1.25 (dt, $J = 14.5, 7.2$ Hz, 7H). ^{13}C NMR (101 MHz, $CDCl_3$) δ [ppm] = 167.7, 167.6, 154.3, 81.0, 73.0, 65.2, 63.3, 62.8, 45.7, 41.5, 36.8, 28.2, 14.1, 13.9. IR (neat, cm^{-1}): 3414, 2981, 2937, 2359, 1736, 1714, 1554, 1483, 1367. 1312, 1252, 1203, 1159, 1095, 1025, 894, 857, 816, 782. **HRMS** (ESI-MS) exact mass calc. for $C_{16}H_{27}BrN_2O_8$ $[M+H]^+$ 455.1024 m/z, found: 455.1018 m/z and exact mass calc. for $C_{16}H_{27}BrN_2O_8$ $[M+Na]^+$ 477.0843 m/z, found: 477.0841 m/z and exact mass calc. for $C_{16}H_{27}BrN_2O_8$ $[M+NH_4]^+$ 472.1289 m/z, found: 472.1285 m/z.

ethyl 4-bromo-2-((*tert*-butoxycarbonyl)amino)-6-nitrohexanoate (4cp**)**



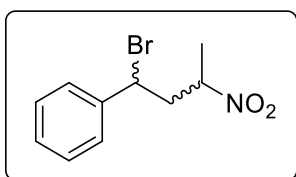
Following general procedure (GP-A) using two schlenk setups loaded each with racemic ethyl 2-((*tert*-butoxycarbonyl)amino)pent-4-enoate (**2cp**) (121.7 mg, 0.5 mmol, 1.0 equiv), bromonitromethane (**1a**) (70.0 mg, 36.0 μ L, 0.5 mmol, 1.0 equiv), $[Cu(dap)_2]Cl$ (4.4 mg, 5.0 μ mol, 1 mol%) and dry MeCN (2.0 mL, 0.25 M) at room temperature (25 °C) and irradiation

with blue LED (λ_{\max} = 455 nm) for 22 h yielded 129.5 mg (337.9 μ mol, 68%) of ethyl 4-bromo-2-((*tert*-butoxycarbonyl)amino)-6-nitrohexanoate (**4cp**) an inseparable mixture of two diastereomers as colorless oil after flash column purification (hexanes / EtOAc 5:1). Diastereomeric ratio was determined by crude $^1\text{H-NMR}$ analysis: d.r. = 56:44. R_f (hexanes / EtOAc 5:1 on silica) = 0.17, Staining: KMnO_4 -solution.

$^1\text{H NMR}$ (400 MHz, CDCl_3) δ [ppm] = 5.22 (s, NH, major diastereomer), 5.04 (s, NH, minor diastereomer), 4.72 – 4.56 (m, 4H, both diastereomers), 4.53 – 4.40 (m, 2H, minor diastereomer), 4.27 – 4.09 (m, 6H, both diastereomers), 2.79 – 2.68 (m, 1H, minor diastereomer), 2.69 – 2.57 (m, 1H, major diastereomer), 2.49 – 2.27 (m, 4H both diastereomers), 2.17 (s, 1H, minor diastereomer), 1.45 (s, 18H, both diastereomers), 1.30 (td, J = 7.1, 3.6 Hz, 6H, both diastereomers). $^{13}\text{C NMR}$ (101 MHz, CDCl_3) δ [ppm] = both diastereomers: 171.7, 171.4, 155.3, 80.5, 73.3, 62.0, 61.9, 52.3, 51.8, 47.9, 46.9, 42.1, 41.9, 36.0, 35.3, 28.3, 28.3, 14.2, 14.1. **IR** (neat, cm^{-1}): 3373, 2981, 2933, 2359, 2258, 2132, 1707, 1554, 1509, 1431, 1367, 1252, 1215, 1162, 1095, 1025, 913, 857, 782, 734. **HRMS** (ESI-MS) (minor diastereomer) exact mass calc. for $\text{C}_{13}\text{H}_{23}\text{BrN}_2\text{O}_6$ $[\text{M}+\text{H}]^+$ 383.0632 m/z, found: 383.0801 m/z and exact mass calc. for $\text{C}_{13}\text{H}_{23}\text{BrN}_2\text{O}_6$ $[\text{M}+\text{Na}]^+$ 405.0632 m/z, found: 405.0631 m/z and exact mass calc. for $\text{C}_{13}\text{H}_{23}\text{BrN}_2\text{O}_6$ $[\text{M}+\text{NH}_4]^+$ 400.1078 m/z, found: 400.1075 m/z and **HRMS** (ESI-MS) (major diastereomer) exact mass calc. for $\text{C}_{13}\text{H}_{23}\text{BrN}_2\text{O}_6$ $[\text{M}+\text{H}]^+$ 383.0812 m/z, found: 383.0808 m/z and exact mass calc. for $\text{C}_{13}\text{H}_{23}\text{BrN}_2\text{O}_6$ $[\text{M}+\text{Na}]^+$ 405.0632 m/z, found: 405.0635 m/z and exact mass calc. for $\text{C}_{13}\text{H}_{23}\text{BrN}_2\text{O}_6$ $[\text{M}+\text{NH}_4]^+$ 400.1078 m/z, found: 400.1077 m/z.

Scope of NO_2 -Reagent Derivatives

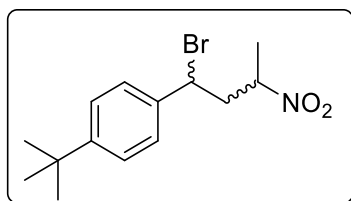
(1-bromo-3-nitrobutyl)benzene (**4da**)



Following general procedure (GP-A) using styrene (**2a**) (52.1 mg, 58.0 μ L, 0.5 mmol, 1.0 equiv), 1-bromo-1-nitroethane (**1b**) (77.0 mg, 0.5 mmol, 1.0 equiv), $[\text{Cu}(\text{dap})_2]\text{Cl}$ (4.4 mg, 5.0 μ mol, 1 mol%) and dry MeCN (2.0 mL, 0.25 M) at room temperature (25 $^\circ\text{C}$) and irradiation with blue LED (λ_{\max} = 455 nm) for 3.5 h yielded 113.1 mg (438.0 μ mol, 88%) of (1-bromo-3-nitrobutyl)benzene (**4da**) as an inseparable mixture of two diastereomers (d.r. = 58:42) as a colorless oil after flash column purification (hexanes / EtOAc 20:1). Spectra data are in accordance with literature.^[18] R_f (hexanes / EtOAc 20:1 on silica) = 0.42, Staining: KMnO_4 -solution.

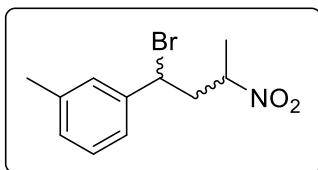
¹H NMR (400 MHz, CDCl₃) δ [ppm] = 7.41 – 7.29 (m, 10H, both diastereomers), 5.00 – 4.87 (m, 3H, both diastereomers), 4.47 (dq, *J* = 8.2, 6.7, 5.5 Hz, 1H, minor diastereomer), 3.06 (ddd, *J* = 14.7, 8.1, 7.4 Hz, 1H, minor diastereomer), 2.79 (dd, *J* = 9.5, 4.0 Hz, 1H, major diastereomer), 2.75 (dd, *J* = 9.5, 4.0 Hz, 1H, minor diastereomer), 2.59 – 2.45 (m, 4H, both diastereomers), 1.63 (d, *J* = 6.8 Hz, 3H, major diastereomer), 1.56 (d, *J* = 6.8 Hz, 3H, minor diastereomer). **¹³C NMR** (101 MHz, CDCl₃) δ [ppm] = 140.6, 140.0, 129.2, 129.2, 129.1, 129.1, 127.4, 127.2, 81.8, 81.6, 50.7, 49.0, 44.7, 44.7, 19.8, 19.1. **HRMS** (APCI-MS) exact mass calc. for C₁₀H₁₂BrNO₂ [M+NH₄]⁺ 275.0390 m/z, found: 275.0392 m/z.

1-(1-bromo-3-nitrobutyl)-4-(tert-butyl)benzene (**4db**)



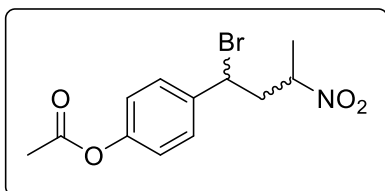
Following general procedure (GP-A) using 4-tertbutylstyrene (**2e**) (80.1 mg, 91.0 μL, 0.5 mmol, 1.0 equiv), 1-bromo-1-nitroethane (**1b**) (77.0 mg, 0.5 mmol, 1.0 equiv), [Cu(dap)₂]Cl (4.4 mg, 5.0 μmol, 1 mol%) and dry MeCN (2.0 mL, 0.25 M) at room temperature (25 °C) and irradiation with blue LED (λ_{max} = 455 nm) for 3.5 h yielded 115.6 mg (367.9 μmol, 74%) of 1-(1-bromo-3-nitrobutyl)-4-(tert-butyl)benzene (**4db**) as an inseparable mixture of two diastereomers (d.r. = 56:44) as a colorless oil after flash column purification (hexanes / EtOAc 20:1). **R_f** (hexanes / EtOAc 5:1 on silica) = 0.68, Staining: KMnO₄-solution.

¹H NMR (300 MHz, CDCl₃) δ [ppm] 7.43 – 7.27 (m, 8H), 5.02 – 4.84 (m, 3H, both diastereomers), 4.56 – 4.42 (m, 1H, minor diastereomer), 3.06 (ddd, *J* = 14.6, 8.1, 7.5 Hz, 1H, major diastereomer), 2.77 (ddd, *J* = 15.4, 9.5, 4.1 Hz, 3H, minor diastereomer), 2.62 – 2.44 (m, 3H, both diastereomer), 1.63 (d, *J* = 6.8 Hz, 1H, major diastereomer), 1.56 (d, *J* = 6.7 Hz, 3H, minor diastereomer), 1.32 (s, 9H, major diastereomer), 1.32 (s, 1H, minor diastereomer). **¹³C NMR** (101 MHz, CDCl₃) δ [ppm] = 152.4, 152.3, 137.6, 137.0, 127.1, 126.9, 126.2, 126.1, 81.8, 81.6, 50.8, 49.2, 44.7, 34.8, 34.8, 31.4, 19.8, 19.1. **IR** (neat, cm⁻¹): 2963, 2870, 1550, 1461, 1390, 1360, 1267, 1207, 1170, 1110, 1021, 894, 834, 752, 685. **HRMS** (APCI-MS) (major diastereomer) exact mass calc. for C₁₄H₂₀BrNO₂ [M+NH₄]⁺ 3331.1016 m/z, found: 331.1015 m/z and **HRMS** (APCI-MS) (minor diastereomer) exact mass calc. for C₁₂H₁₄BrNO₄ [M+NH₄]⁺ 331.1016 m/z, found: 3331.1015 m/z.

1-(1-bromo-3-nitrobutyl)-3-methylbenzene (4dc)

Following general procedure (GP-A) using 3-methylstyrene (**2c**) (69.3 mg, 60.0 μL , 0.5 mmol, 1.0 equiv), 1-bromo-1-nitroethane (**1b**) (77.0 mg, 0.5 mmol, 1.0 equiv), $[\text{Cu}(\text{dap})_2]\text{Cl}$ (4.4 mg, 5.0 μmol , 1 mol%) and dry MeCN (2.0 mL, 0.25 M) at room temperature (25 $^\circ\text{C}$) and irradiation with blue LED ($\lambda_{\text{max}} = 455 \text{ nm}$) for 3 h yielded 106.8 mg (392.4 μmol , 79%) of 1-(1-bromo-3-nitrobutyl)-3-methylbenzene (**4dc**) as an inseparable mixture of two diastereomers (d.r. = 55:45) as a colorless oil after flash column purification (hexanes / EtOAc 20:1). R_f (hexanes / EtOAc 5:1 on silica) = 0.71, Staining: KMnO_4 -solution.

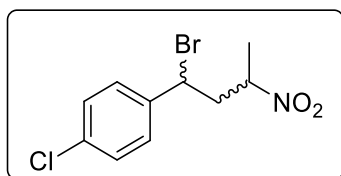
$^1\text{H NMR}$ (400 MHz, CDCl_3) δ [ppm] = 7.29 – 7.11 (m, 8H, both diastereomers), 5.01 – 4.82 (m, 3H, both diastereomers), 4.48 (dq, $J = 8.2, 6.7, 5.5 \text{ Hz}$, 1H, minor diastereomer), 3.05 (dt, $J = 14.6, 7.8 \text{ Hz}$, 1H, major diastereomer), 2.76 (ddd, $J = 15.4, 9.5, 4.1 \text{ Hz}$, 1H, minor diastereomer), 2.60 – 2.45 (m, 1H, major diastereomer), 2.40 – 2.33 (m, 3H, both diastereomers), 1.63 (d, $J = 6.8 \text{ Hz}$, 3H, major diastereomer), 1.56 (d, $J = 6.7 \text{ Hz}$, 3H, minor diastereomer). $^{13}\text{C NMR}$ (101 MHz, CDCl_3) δ [ppm] = 140.5, 139.9, 139.0, 138.9, 130.0, 129.9, 129.1, 129.0, 128.1, 127.8, 124.4, 124.2, 81.8, 81.6, 50.9, 49.2, 44.7, 44.6, 21.5, 21.5, 19.8, 19.1. IR (neat, cm^{-1}): 2989, 2922, 2363, 1550, 1453, 1394, 1356, 1259, 1174, 1129, 1095, 1051, 879, 790, 700, 670. HRMS (APCI-MS) (minor diastereomer) exact mass calc. for $\text{C}_{11}\text{H}_{14}\text{BrNO}_2$ $[\text{M}+\text{NH}_4]^+$ 289.0546 m/z, found: 289.0547 m/z and HRMS (APCI-MS) (major diastereomer) exact mass calc. for $\text{C}_{11}\text{H}_{14}\text{BrNO}_2$ $[\text{M}+\text{NH}_4]^+$ 289.0546 m/z, found: 289.0549 m/z.

4-(1-bromo-3-nitrobutyl)phenyl acetate (4dd)

Following general procedure (GP-A) using 4-vinylphenyl acetate (**2j**) (81.1 mg, 76.5 μL , 0.5 mmol, 1.0 equiv), 1-bromo-1-nitroethane (**1b**) (77.0 mg, 0.5 mmol, 1.0 equiv), $[\text{Cu}(\text{dap})_2]\text{Cl}$ (4.4 mg, 5.0 μmol , 1 mol%) and dry MeCN (2.0 mL, 0.25 M) at room temperature (25 $^\circ\text{C}$) and irradiation with blue LED ($\lambda_{\text{max}} = 455 \text{ nm}$) for 4.0 h yielded 139.0 mg (439.7 μmol , 88%) of 4-(1-bromo-3-nitrobutyl)phenyl acetate (**4dd**) as an inseparable mixture of two diastereomers (d.r. = 57:43) as a colorless oil after flash column purification (hexanes / EtOAc 20:1). R_f (hexanes / EtOAc 5:1 on silica) = 0.28, Staining: KMnO_4 -solution.

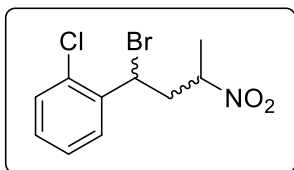
¹H NMR (400 MHz, CDCl₃) δ [ppm] = 7.42 – 7.36 (m, 4H, both diastereomers), 7.09 (dd, *J* = 8.5, 5.9 Hz, 4H, both diastereomers), 5.00 – 4.85 (m, 3H, both diastereomers), 4.53 – 4.41 (m, 1H, minor diastereomer), 3.03 (ddd, *J* = 14.7, 8.2, 7.4 Hz, 1H, major diastereomer), 2.73 (ddd, *J* = 15.4, 9.7, 3.8 Hz, 1H, minor diastereomer), 2.52 – 2.42 (m, 2H, both diastereomers), 2.30 (s, 3H, minor diastereomer), 2.30 (s, 3H, major diastereomer), 1.62 (d, *J* = 6.8 Hz, 3H, major diastereomer), 1.55 (d, *J* = 6.7 Hz, 3H, minor diastereomer). **¹³C NMR** (101 MHz, CDCl₃) δ [ppm] = 169.3, 169.3, 151.0, 150.9, 138.2, 137.5, 128.6, 128.37, 122.3, 122.3, 81.7, 81.5, 49.9, 48.1, 44.8, 44.7, 21.2, 19.9, 19.0. **IR** (neat, cm⁻¹): 2989, 2940, 1759, 1502, 1546, 1505, 1453, 1367, 1192, 1013, 946, 909, 853, 786, 734. **HRMS** (APCI-MS) (minor diastereomer) exact mass calc. for C₁₂H₁₄BrNO₄ [M+NH₄]⁺ 333.0444 m/z, found: 333.0443 m/z and **HRMS** (APCI-MS) (major diastereomer) exact mass calc. for C₁₂H₁₄BrNO₄ [M+NH₄]⁺ 333.0444 m/z, found: 333.0444 m/z.

(1-bromo-3-nitrobutyl)-4-chlorobenzene (**4df**)



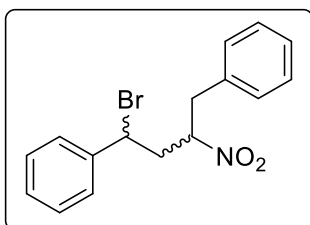
Following general procedure (GP-A) using 4-chlorostyrene (**2r**) (69.3 mg, 60.0 μL, 0.5 mmol, 1.0 equiv), 1-bromo-1-nitroethane (**1b**) (77.0 mg, 0.5 mmol, 1.0 equiv), [Cu(dap)₂]Cl (4.4 mg, 5.0 μmol, 1 mol%) and dry MeCN (2.0 mL, 0.25 M) at room temperature (25 °C) and irradiation with blue LED (λ_{max} = 455 nm) for 3.5 h yielded 120.3 mg (411.2 μmol, 82%) of (1-bromo-3-nitrobutyl)-4-chlorobenzene (**4df**) as an inseparable mixture of two diastereomers (d.r. = 57:43) as a colorless oil after flash column purification (hexanes / EtOAc 20:1). **R_f** (hexanes / EtOAc 5:1 on silica) = 0.71, Staining: KMnO₄-solution.

¹H NMR (400 MHz, CDCl₃) δ [ppm] = 7.38 – 7.29 (m, 8H, both diastereomers), 4.99 – 4.82 (m, 3H, both diastereomers), 4.44 (dq, *J* = 8.3, 6.7, 5.4 Hz, 1H, minor diastereomer), 3.02 (ddd, *J* = 14.7, 8.3, 7.3 Hz, 1H, major diastereomer), 2.72 (ddd, *J* = 15.5, 9.7, 3.9 Hz, 1H, minor diastereomer), 2.53 – 2.41 (m, 4H, both diastereomers), 1.63 (d, *J* = 6.8 Hz, 3H, major diastereomer), 1.55 (d, *J* = 6.7 Hz, 3H, minor diastereomer). **¹³C NMR** (101 MHz, CDCl₃) δ [ppm] = 139.2, 138.6, 135.0, 134.8, 129.4, 129.3, 128.8, 128.6, 81.7, 81.4, 49.6, 47.8, 44.6, 44.6, 19.9, 19.0. **IR** (neat, cm⁻¹): 2993, 2940, 2255, 1595, 1546, 1490, 1449, 1412, 1356, 1315, 1200, 1170, 1125, 1092, 1013, 909, 857, 827, 790, 730. **HRMS** (APCI-MS) (minor diastereomer) exact mass calc. for C₁₀H₁₁BrClNO₂ [M+NH₄]⁺ 310.9978 m/z, found: 310.9978 m/z and **HRMS** (APCI-MS) (major diastereomer) exact mass calc. for C₁₀H₁₁BrClNO₂ [M+NH₄]⁺ 310.9978 m/z, found: 310.9981 m/z.

1-(1-bromo-3-nitrobutyl)-2-chlorobenzene (4dg)

Following general procedure (GP-A) using 2-chlorostyrene (**2u**) (69.3 mg, 60.0 μL , 0.5 mmol, 1.0 equiv), 1-bromo-1-nitroethane (**1b**) (77.0 mg, 0.5 mmol, 1.0 equiv), $[\text{Cu}(\text{dap})_2]\text{Cl}$ (4.4 mg, 5.0 μmol , 1 mol%) and dry MeCN (2.0 mL, 0.25 M) at room temperature (25 $^\circ\text{C}$) and irradiation with blue LED ($\lambda_{\text{max}} = 455 \text{ nm}$) for 3.5 h yielded 127.8 mg (436.8 μmol , 87%) of (1-bromo-3-nitrobutyl)-2-chlorobenzene (**4dg**) as an inseparable mixture of two diastereomers (d.r. = 58:42) as a colorless oil after flash column purification (hexanes / EtOAc 20:1). R_f (hexanes / EtOAc 5:1 on silica) = 0.56, Staining: KMnO_4 -solution.

$^1\text{H NMR}$ (400 MHz, CDCl_3) δ [ppm] = 7.58 (dd, $J = 7.8, 1.7 \text{ Hz}$, 2H, both diastereomers), 7.37 (ddd, $J = 7.8, 4.6, 1.5 \text{ Hz}$, 2H, both diastereomers), 7.36 – 7.27 (m, 2H, both diastereomers), 7.31 – 7.21 (m, 2H, both diastereomers), 5.49 – 5.40 (m, 2H, both diastereomers), 4.90 (ddd, $J = 9.2, 6.7, 3.9 \text{ Hz}$, 1H, major diastereomer), 4.65 (q, $J = 6.8 \text{ Hz}$, 1H, minor diastereomer), 3.05 (ddd, $J = 14.7, 9.0, 6.6 \text{ Hz}$, 1H, minor diastereomer), 2.80 (ddd, $J = 15.3, 9.2, 4.5 \text{ Hz}$, 1H, major diastereomer), 2.61 – 2.46 (m, 4H, both diastereomers), 1.62 (t, $J = 6.7 \text{ Hz}$, 6H, both diastereomers). $^{13}\text{C NMR}$ (101 MHz, CDCl_3) δ [ppm] = 137.7, 137.4, 132.8, 132.7, 130.2, 130.2, 130.1, 130.1, 129.0, 128.8, 127.9, 127.8, 81.5, 81.4, 45.7, 44.6, 43.7, 43.3, 19.8, 18.7. **IR** (neat, cm^{-1}): 3067, 2989, 2259, 1550, 1476, 1446, 1390, 1356, 1289, 1200, 1170, 1133, 1036, 1004, 946, 898, 834, 760, 693. **HRMS** (APCI-MS) (minor diastereomer) exact mass calc. for $\text{C}_{10}\text{H}_{11}\text{BrClNO}_2$ $[\text{M}+\text{NH}_4]^+$ 310.9978 m/z, found: 310.9982 m/z and **HRMS** (APCI-MS) (major diastereomer) exact mass calc. for $\text{C}_{10}\text{H}_{11}\text{BrClNO}_2$ $[\text{M}+\text{NH}_4]^+$ 310.9978 m/z, found: 310.9980 m/z.

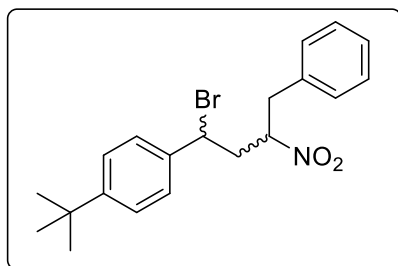
(1-bromo-3-nitrobutane-1,4-diyl)dibenzene (4dh)

Following general procedure (GP-A) using styrene (**2a**) (52.1 mg, 58.0 μL , 0.5 mmol, 1.0 equiv), (2-bromo-2-nitroethyl)benzene (**1d**) (115.0 mg, 0.5 mmol, 1.0 equiv), $[\text{Cu}(\text{dap})_2]\text{Cl}$ (4.4 mg, 5.0 μmol , 1 mol%) and dry MeCN (2.0 mL, 0.25 M) at room temperature (25 $^\circ\text{C}$) and irradiation with blue LED ($\lambda_{\text{max}} = 455 \text{ nm}$) for 3.5 h yielded 160.5 mg (480.3 μmol , 96%) of (1-

bromo-3-nitrobutane-1,4-diyl)dibenzene (**4dh**) as an inseparable mixture of two diastereomers (d.r. = 62:38) as a colorless oil after flash column purification (hexanes / EtOAc 20:1). Spectra data are in accordance with literature.^[18] R_f (hexanes / EtOAc 5:1 on silica) = 0.77, Staining: $KMnO_4$ -solution.

1H NMR (300 MHz, $CDCl_3$) δ [ppm] = 7.42 – 7.25 (m, 16H, both diastereomers), 7.23 – 7.18 (m, 2H, major diastereomer), 7.13 – 7.06 (m, 2H, minor diastereomer), 5.21 (dddd, J = 9.7, 8.0, 6.3, 3.3 Hz, 1H, major diastereomer), 4.95 – 4.85 (m, 2H, both diastereomers), 4.53 (dddd, J = 9.2, 7.8, 6.6, 4.1 Hz, 1H, minor diastereomer), 3.37 (dd, J = 14.2, 8.1 Hz, 1H, major diastereomer), 3.28 (dd, J = 14.1, 7.8 Hz, 1H, minor diastereomer), 3.17 (dd, J = 14.1, 6.3 Hz, 1H, major diastereomer), 3.12 – 3.00 (m, 2H, both diastereomers), 2.81 – 2.58 (m, 3H, both diastereomers). **^{13}C NMR** (75 MHz, $CDCl_3$) δ [ppm] = 140.6, 139.5, 134.7, 134.6, 129.2, 129.2, 129.1, 129.0, 129.0, 129.0, 127.8, 127.8, 127.4, 127.1, 87.8, 87.2, 50.6, 48.6, 42.7, 42.6, 40.2, 39.6. **HRMS** (APCI-MS) exact mass calc. for $C_{17}H_{15}BrF_3N_2O_2$ $[M+NH_4^+]^+$ 419.0577 m/z, found: 419.0580 m/z.

1-(1-bromo-3-nitro-4-phenylbutyl)-4-(tert-butyl)benzene (**4di**)

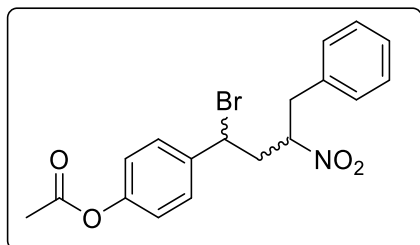


Following general procedure (GP-A) using 4-tertbutylstyrene (**2e**) (80.1 mg, 91.1 μ L, 0.5 mmol, 1.0 equiv), (2-bromo-2-nitroethyl)benzene (**1d**) (115.0 mg, 0.5 mmol, 1.0 equiv), $[Cu(dap)_2]Cl$ (4.4 mg, 5.0 μ mol, 1 mol%) and dry MeCN (2.0 mL, 0.25 M) at room temperature (25 $^{\circ}C$) and irradiation with blue LED (λ_{max} = 455 nm) for 3.5 h yielded 176.9 mg (453.1 μ mol, 91%) of 1-(1-bromo-3-nitro-4-phenylbutyl)-4-(tert-butyl)benzene (**4di**) as an inseparable mixture of two diastereomers (d.r. = 62:38) as a colorless oil after flash column purification (hexanes / EtOAc 20:1). Spectra data are in accordance with literature.^[18] R_f (hexanes / EtOAc 5:1 on silica) = 0.85, Staining: $KMnO_4$ -solution.

1H NMR (300 MHz, $CDCl_3$) δ [ppm] = 7.42 – 7.24 (m, 12H, both diastereomers), 7.24 – 7.15 (m, 4H, both diastereomers), 7.13 – 7.05 (m, 2H, both diastereomers), 5.20 (dddd, J = 9.7, 8.0, 6.3, 3.4 Hz, 1H, major diastereomer), 4.94 – 4.84 (m, 2H, both diastereomers), 4.55 (dddd, J = 9.1, 7.8, 6.5, 4.3 Hz, 1H, minor diastereomer), 3.36 (dd, J = 14.1, 8.0 Hz, 1H, major diastereomer), 3.28 (dd, J = 14.0, 7.9 Hz, 1H, major diastereomer), 3.16 (dd, J = 14.1, 6.3 Hz, 1H, major diastereomer), 3.12 – 2.96 (m, 2H, both diastereomers), 2.81 – 2.55 (m, 3H, both diastereomers), 1.34 (s, 9H, minor diastereomer), 1.33 (s, 9H, major diastereomer). **^{13}C NMR**

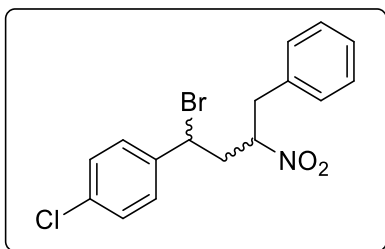
(75 MHz, CDCl₃) δ [ppm] = 152.4, 152.2, 137.6, 136.5, 134.8, 134.7, 129.1, 129.0, 127.8, 127.8, 127.1, 126.9, 126.1, 126.0, 87.9, 87.3, 50.7, 48.8, 42.8, 42.7, 40.2, 39.6, 34.8, 34.8, 31.3.

4-(1-bromo-3-nitro-4-phenylbutyl)phenyl acetate (**4dj**)



Following general procedure (GP-A) using 4-acetoxystyrene (**2i**) (81.1 mg, 76.5 μ L, 0.5 mmol, 1.0 equiv), (2-bromo-2-nitroethyl)benzene (**1d**) (115.0 mg, 0.5 mmol, 1.0 equiv), [Cu(dap)₂]Cl (4.4 mg, 5.0 μ mol, 1 mol%) and dry MeCN (2.0 mL, 0.25 M) at room temperature (25 °C) and irradiation with blue LED (λ_{max} = 455 nm) for 3.5 h yielded 122.6 mg (312.6 μ mol, 62%) of 4-(1-bromo-3-nitro-4-phenylbutyl)phenyl acetate (**4dj**) as an inseparable mixture of two diastereomers (d.r. = 60:40) as a colorless oil after flash column purification (hexanes / EtOAc 20:1). R_f (hexanes / EtOAc 5:1 on silica) = 0.39, Staining: KMnO₄-solution.

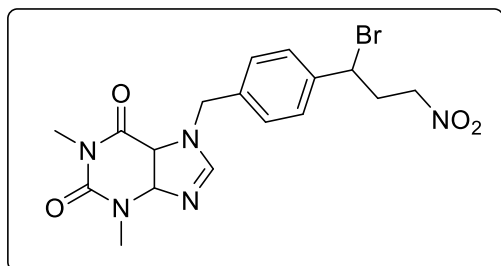
¹H NMR (300 MHz, CDCl₃) δ [ppm] = 7.40 – 7.21 (m, 10H, both diastereomers), 7.21 – 7.15 (m, 4H, both diastereomers), 7.13 – 7.02 (m, 4H, both diastereomers), 5.19 (dddd, J = 9.7, 7.8, 6.5, 3.0 Hz, 1H, major diastereomer), 4.91 – 4.80 (m, 2H, both diastereomers), 4.51 (dddd, J = 9.1, 7.7, 6.8, 4.1 Hz, 1H, minor diastereomer), 3.35 (dd, J = 14.1, 7.9 Hz, 1H, major diastereomer), 3.27 (dd, J = 14.1, 7.8 Hz, 1H, minor diastereomer), 3.14 (dd, J = 14.1, 6.5 Hz, 1H, major diastereomer), 3.12 – 2.93 (m, 2H, both diastereomers), 2.75 – 2.47 (m, 3H, both diastereomers), 2.31 (s, 3H, minor diastereomer), 2.30 (s, 3H, major diastereomer). **¹³C NMR** (75 MHz, CDCl₃) δ [ppm] = 169.3, 169.2, 151.0, 150.8, 138.2, 137.0, 134.6, 134.5, 129.1, 129.1, 129.0, 128.6, 128.3, 127.8, 127.8, 122.3, 122.2, 87.7, 87.1, 49.8, 47.7, 42.8, 42.6, 40.2, 39.5, 21.2, 21.2. **IR** (neat, cm⁻¹): 3063, 3034, 2926, 1759, 1602, 1550, 1505, 1423, 1367, 1192, 1080, 1043, 969, 909, 853, 730. **HRMS** (APCI-MS) exact mass calc. for C₁₈H₁₈BrNO₄ [M+NH₄]⁺ 409.0757 m/z, found: 409.0755 m/z.

1-(1-bromo-3-nitro-4-phenylbutyl)-4-chlorobenzene (4dl)

Following general procedure (GP-A) using 4-chlorostyrene (**2r**) (69.3 mg, 63.6 μL , 0.5 mmol, 1.0 equiv), (2-bromo-2-nitroethyl)benzene (**1d**) (115.0 mg, 0.5 mmol, 1.0 equiv), $[\text{Cu}(\text{dap})_2]\text{Cl}$ (4.4 mg, 5.0 μmol , 1 mol%) and dry MeCN (2.0 mL, 0.25 M) at room temperature (25 $^\circ\text{C}$) and irradiation with blue LED ($\lambda_{\text{max}} = 455 \text{ nm}$) for 3.5 h yielded 160.3 mg (480.3 μmol , 87%) of 1-(1-bromo-3-nitro-4-phenylbutyl)-4-chlorobenzene (**4dl**) as an inseparable mixture of two diastereomers (d.r. = 56:44) as a colorless oil after flash column purification (hexanes / EtOAc 20:1). Spectra data are in accordance with literature.^[18] R_f (hexanes / EtOAc 5:1 on silica) = 0.58, Staining: KMnO_4 -solution.

$^1\text{H NMR}$ (300 MHz, CDCl_3) δ [ppm] = 7.40 – 7.23 (m, 12H, both diastereomers), 7.21 – 7.13 (m, 4H, both diastereomers), 7.12 – 7.05 (m, 2H, both diastereomers), 5.17 (dddd, $J = 9.8, 8.0, 6.4, 3.0 \text{ Hz}$, 1H, major diastereomer), 4.87 – 4.78 (m, 2H, both diastereomers), 4.45 (dtd, $J = 9.5, 7.3, 3.9 \text{ Hz}$, 1H, minor diastereomer), 3.36 (dd, $J = 14.3, 8.0 \text{ Hz}$, 1H, major diastereomer), 3.28 (dd, $J = 14.0, 7.4 \text{ Hz}$, 1H, minor diastereomer), 3.15 (dd, $J = 14.0, 6.5 \text{ Hz}$, 1H, major diastereomer), 3.10 – 2.94 (m, 2H, both diastereomers), 2.76 – 2.48 (m, 3H, both diastereomers). $^{13}\text{C NMR}$ (75 MHz, CDCl_3) δ [ppm] = 139.1, 138.0, 135.0, 134.8, 134.6, 134.4, 129.4, 129.3, 129.1, 129.0, 128.8, 128.6, 127.9, 87.7, 87.1, 49.4, 47.3, 42.6, 42.5, 40.2, 39.6.

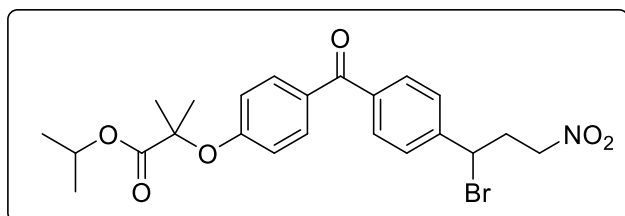
Late-Stage Functionalizations

7-(4-(1-bromo-3-nitropropyl)benzyl)-1,3-dimethyl-3,4,5,7-tetrahydro-1*H*-purine-2,6-dione (**4ea**)

Following general procedure (GP-A) using 1,3-dimethyl-7-(4-vinylbenzyl)-3,4,5,7-tetrahydro-1*H*-purine-2,6-dione (Theophylline) (**2ea**) (149.2 mg, 0.5 mmol, 1.0 equiv), bromonitromethane (**1a**) (70.0 mg, 36.0 μL , 0.5 mmol, 1.0 equiv), $[\text{Cu}(\text{dap})_2]\text{Cl}$ (4.4 mg, 5.0 μmol , 1. mol%) and solvent mixture (MeCN/DCM/ CHCl_3 2/1/1, 4.0 mL, dry) at room temperature (25 $^\circ\text{C}$) and irradiation with blue LED ($\lambda_{\text{max}} = 455 \text{ nm}$) for 2 h yielded 196.7 mg (448.8 μmol , 90%) of 7-(4-(1-bromo-3-nitropropyl)benzyl)-1,3-dimethyl-3,4,5,7-tetrahydro-1*H*-purine-2,6-dione (**4ea**) as sticky yellowish oil after flash column purification (EtOAc). R_f (EtOAc on silica) = 0.25, Staining: KMnO_4 -solution.

$^1\text{H NMR}$ (300 MHz, CDCl_3) δ [ppm] = 7.61 (s, 1H), 7.37 (d, $J = 8.4 \text{ Hz}$, 2H), 7.31 (d, $J = 8.3 \text{ Hz}$, 2H), 5.47 (s, 2H), 4.99 (dd, $J = 9.1, 5.7 \text{ Hz}$, 1H), 4.64 – 4.39 (m, 2H), 3.55 (s, 3H), 3.36 (s, 3H), 2.90 – 2.62 (m, 2H). $^{13}\text{C NMR}$ (101 MHz, CDCl_3) δ [ppm] = 155.3, 151.7, 149.0, 140.9, 140.6, 136.5, 128.6, 128.0, 106.9, 73.4, 49.7, 49.4, 36.8, 29.9, 28.1. **IR** (neat, cm^{-1}): 3112, 2952, 2251, 1699, 1651, 1546, 1472, 1423, 1375, 1289, 1230, 1189, 1118, 1066, 1025, 909, 864, 805, 726.

HRMS (ESI-MS) exact mass calc. for $\text{C}_{17}\text{H}_{18}\text{BrN}_5\text{O}_4$ $[\text{M}+\text{Na}]^+$ 460.0416 m/z, found: 460.0416 m/z.

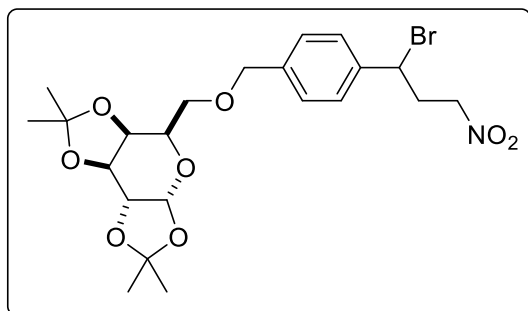
isopropyl 2-(4-(4-(1-bromo-3-nitropropyl)benzoyl)phenoxy)-2-methylpropanoate (**4eb**)

Following general procedure (GP-A) using isopropyl 2-methyl-2-(4-(4-vinylbenzoyl)phenoxy)propanoate (Fenofibrate Derivative) (**2eb**) (176.2 mg, 0.5 mmol, 1.0 equiv), bromonitromethane (**1a**) (70.0 mg, 36.0 μL , 0.5 mmol, 1.0 equiv), $[\text{Cu}(\text{dap})_2]\text{Cl}$ (4.4 mg, 5.0 μmol , 1. mol%) and the solvent mixture (MeCN/ CHCl_3 1/1, 2.0 mL, dry) at room temperature (25 $^\circ\text{C}$) and irradiation with blue LED ($\lambda_{\text{max}} = 455 \text{ nm}$) for 2 h yielded 234.2 mg

(475.4 μmol , 95%) of isopropyl 2-(4-(4-(1-bromo-3-nitropropyl)benzoyl)phenoxy)-2-methylpropanoate (**4eb**) as sticky yellowish oil after flash column purification (hexanes / EtOAc 10:1). R_f (hexanes / EtOAc 5:1 on silica) = 0.23, Staining: KMnO_4 -solution.

$^1\text{H NMR}$ (400 MHz, CDCl_3) δ [ppm] = 7.74 (dd, J = 8.6, 2.7 Hz, 4H), 7.52 – 7.45 (m, 2H), 6.90 – 6.83 (m, 2H), 5.15 – 4.99 (m, 2H), 4.63 (ddd, J = 13.8, 7.5, 6.2 Hz, 1H), 4.53 (dt, J = 14.0, 6.2 Hz, 1H), 2.93 – 2.73 (m, 2H), 1.65 (s, 6H), 1.19 (d, J = 6.3 Hz, 6H). $^{13}\text{C NMR}$ (101 MHz, CDCl_3) δ [ppm] = 194.5, 173.1, 159.9, 143.9, 138.8, 132.1, 130.5, 130.2, 127.2, 117.3, 79.5, 73.3, 69.4, 49.2, 36.8, 25.5, 21.6. **IR** (neat, cm^{-1}): 2989, 2933, 2251, 1554, 1427, 1379, 1308, 1252, 1166, 1066, 1002, 909, 820, 726. **HRMS** (ESI-MS) exact mass calc. for $\text{C}_{23}\text{H}_{26}\text{BrNO}_6$ $[\text{M}+\text{H}]^+$ 494.0999 m/z, found: 494.1007 m/z and $\text{C}_{23}\text{H}_{26}\text{BrNO}_6$ $[\text{M}+\text{Na}]^+$ 516.0819 m/z, found: 516.0827 m/z.

(3aR,5R,5aS,8aS,8bR)-5-(((4-(1-bromo-3-nitropropyl)benzyl)oxy)methyl)-2,2,7,7-tetramethyltetrahydro-5H-bis([1,3]dioxolo)[4,5-b:4',5'-d]pyran (4ec)



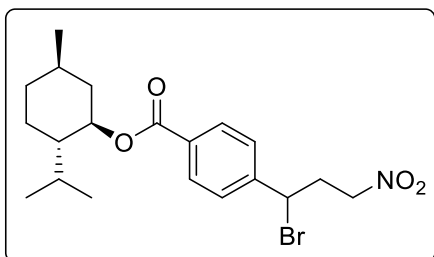
Following general procedure (GP-A) using (3aR,5R,5aS,8aS,8bR)-2,2,7,7-tetramethyl-5-(((4-vinylbenzyl)oxy)methyl)tetrahydro-5H-bis([1,3]dioxolo)[4,5-b:4',5'-d]pyran (Galactopyranosid-Derivative) (**2ec**) (188.2 mg, 0.5 mmol, 1.0 equiv), bromonitromethane (**1a**) (70.0 mg, 36.0 μL , 0.5 mmol, 1.0 equiv), $[\text{Cu}(\text{dap})_2]\text{Cl}$ (4.4 mg, 5.0 μmol , 1. mol%) and the solvent mixture (MeCN/ CHCl_3 1/1, 2.0 mL, dry) at room temperature (25 $^\circ\text{C}$) and irradiation with blue LED (λ_{max} = 455 nm) for 2 h yielded 158.8 mg (307.5 μmol , 62%) of (3aR,5R,5aS,8aS,8bR)-5-(((4-(1-bromo-3-nitropropyl)benzyl)oxy)methyl)-2,2,7,7-tetramethyltetrahydro-5H-bis([1,3]dioxolo)[4,5-b:4',5'-d]pyran (**4ec**) as sticky yellowish oil after flash column purification (hexanes / EtOAc 5:1 to 2:1). R_f (hexanes / EtOAc 5:1 on silica) = 0.13, Staining: KMnO_4 -solution.

$^1\text{H NMR}$ (400 MHz, CDCl_3) δ [ppm] = 7.36 (s, 4H), 5.54 (d, J = 5.0 Hz, 1H), 5.03 (dd, J = 9.1, 5.8 Hz, 1H), 4.64 – 4.43 (m, 5H), 4.31 (dd, J = 5.0, 2.4 Hz, 1H), 4.26 (dd, J = 7.9, 1.9 Hz, 1H), 4.01 (ddd, J = 7.3, 5.8, 1.8 Hz, 1H), 3.70 (ddd, J = 10.1, 5.7, 1.2 Hz, 1H), 3.63 (dd, J = 10.1, 6.8 Hz, 1H), 2.93 – 2.70 (m, 2H), 1.54 (s, 3H), 1.43 (s, 3H), 1.33 (d, J = 2.2 Hz, 6H). $^{13}\text{C NMR}$ (101 MHz, CDCl_3) δ [ppm] = 139.6, 139.4, 128.3, 127.3, 109.4, 108.7, 96.5, 73.5, 72.8, 71.3,

70.8, 70.6, 69.3, 67.0, 50.1, 37.0, 26.2, 26.1, 25.0, 24.6. **IR** (neat, cm^{-1}): 2985, 2937, 2255, 1729, 1651, 1599, 1554, 1505, 1468, 1420, 1382, 1282, 1252, 1177, 1103, 972, 905, 767, 726.

HRMS (ESI-MS) exact mass calc. for $\text{C}_{22}\text{H}_{30}\text{BrNO}_8$ $[\text{M}+\text{H}]^+$ 518.1211 m/z, found: 518.1220 m/z $[\text{M}+\text{Na}]^+$ 540.1030 m/z, found: 540.1038 m/z and $[\text{M}+\text{NH}_4]^+$ 535.1476 m/z, found: 535.1484 m/z.

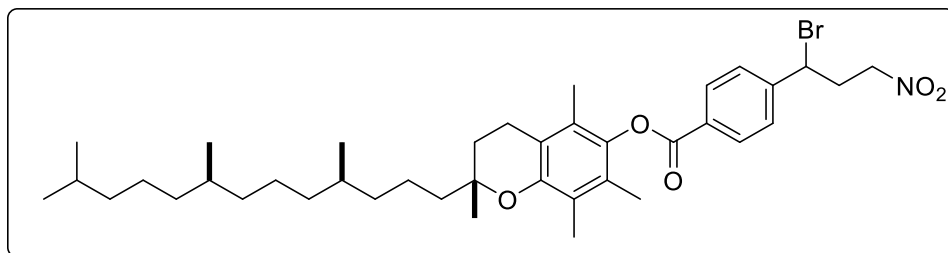
(1*R*,2*S*,5*R*)-2-isopropyl-5-methylcyclohexyl 4-(1-bromo-3-nitropropyl)benzoate (4ed)



Following general procedure (GP-A) using (1*R*,2*S*,5*R*)-2-isopropyl-5-methylcyclohexyl 4-vinylbenzoate (**2ed**) (143.2 mg, 0.5 mmol, 1.0 equiv), bromonitromethane (**1a**) (70.0 mg, 36.0 μL , 0.5 mmol, 1.0 equiv), $[\text{Cu}(\text{dap})_2]\text{Cl}$ (4.4 mg, 5.0 μmol , 1 mol%) dry MeCN (2.0 mL, 0.25 M) at room temperature (25 $^\circ\text{C}$) and irradiation with blue LED ($\lambda_{\text{max}}=455$ nm) for 3 h yielded 179.8 mg (400.1 μmol , 84%) of (1*R*,2*S*,5*R*)-2-isopropyl-5-methylcyclohexyl 4-(1-bromo-3-nitropropyl)benzoate (**4ed**) as colorless smelly oil after flash column purification (hexanes / EtOAc 20:1). R_f (hexanes / EtOAc 5:1 on silica) = 0.49, Staining: KMnO_4 -solution.

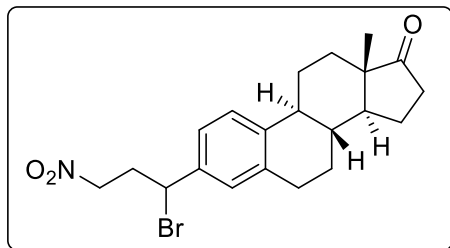
$^1\text{H NMR}$ (300 MHz, CDCl_3) δ [ppm] = 8.05 (d, $J = 8.4$ Hz, 2H), 7.48 (d, $J = 8.4$ Hz, 2H), 5.07 (dd, $J = 9.2, 5.8$ Hz, 1H), 4.93 (td, $J = 10.8, 4.4$ Hz, 1H), 4.72 – 4.39 (m, 2H), 2.98 – 2.62 (m, 2H), 2.22 – 2.04 (m, 1H), 1.93 (pt, $J = 9.2, 4.6$ Hz, 1H), 1.81 – 1.66 (m, 2H), 1.64 – 1.45 (m, 2H), 1.19 – 1.00 (m, 2H), 0.92 (dd, $J = 6.8, 3.9$ Hz, 7H), 0.78 (d, $J = 6.9$ Hz, 3H). **$^{13}\text{C NMR}$** (75 MHz, CDCl_3) δ [ppm] = 165.3, 144.7, 131.6, 130.4, 127.3, 75.3, 73.3, 49.1, 49.1, 47.3, 41.0, 36.8, 36.7, 34.4, 31.6, 26.6, 23.7, 22.2, 20.9, 16.6. **IR** (neat, cm^{-1}): 2955, 2926, 2870, 1707, 1610, 1554, 1453, 1420, 1371, 1274, 1177, 1110, 1039, 916, 857, 771, 734, 704, 663. **HRMS** (ESI-MS) exact mass calc. for $\text{C}_{20}\text{H}_{28}\text{BrNO}_4$ $[\text{M}+\text{Na}]^+$ 450.1076 m/z, found: 450.1082 m/z.

2,5,7,8-tetramethyl-2-((4*R*,8*R*)-4,8,12-trimethyltridecyl)chroman-6-yl 4-(1-bromo-3-nitropropyl)benzoate (4ee**)**



Following general procedure (GP-A) using 2,5,7,8-tetramethyl-2-(4,8,12-trimethyltridecyl)chroman-6-yl 4-vinylbenzoate (**2ee**) (280.0 mg, 0.5 mmol, 1.0 equiv), bromonitromethane (**1a**) (70.0 mg, 36.0 μ L, 0.5 mmol, 1.0 equiv), [Cu(dap)₂]Cl (4.4 mg, 5.0 μ mol, 1. mol%) and the solvent mixture (MeCN/CHCl₃ 2/1, 3.0 mL, dry) at room temperature (25 °C) and irradiation with blue LED (λ_{max} = 455 nm) for 2 h yielded 281.0 mg (401.0 μ mol, 80%) of 2,5,7,8-tetramethyl-2-(4,8,12-trimethyltridecyl)chroman-6-yl 4-(1-bromo-3-nitropropyl)- benzoate (**4ee**) as sticky yellowish oil after flash column purification (hexanes / EtOAc 10:1). R_f (hexanes / EtOAc 5:1 on silica) = 0.63, Staining: KMnO₄-solution.

¹H NMR (400 MHz, CDCl₃) δ [ppm] = 8.26 (d, J = 8.4 Hz, 2H), 7.57 (d, J = 8.4 Hz, 2H), 5.11 (dd, J = 9.2, 5.7 Hz, 1H), 4.65 (ddd, J = 13.7, 7.5, 6.1 Hz, 1H), 4.60 – 4.48 (m, 1H), 2.97 – 2.75 (m, 2H), 2.62 (t, J = 6.8 Hz, 2H), 2.13 (s, 3H), 2.05 (s, 3H), 2.01 (s, 3H), 1.92 – 1.72 (m, 2H), 1.68 – 1.02 (m, 16H), 0.89 – 0.80 (m, 12H). **¹³C NMR** (101 MHz, CDCl₃) δ [ppm] = 164.5, 149.7, 145.5, 140.7, 131.1, 130.4, 127.6, 126.9, 125.2, 123.4, 117.7, 75.3, 73.4, 49.0, 39.5, 37.7, 37.6, 37.6, 37.5, 36.8, 33.0, 32.9, 32.9, 28.1, 25.0, 24.9, 24.6, 24.4, 23.9, 22.9, 22.8, 21.2, 20.8, 19.9, 19.9, 19.8, 13.2, 12.4, 12.0. **IR** (neat, cm⁻¹): 2926, 2866, 1733, 1610, 1558, 1481, 1379, 1334, 1274, 1237, 1181, 1095, 1017, 916, 857, 767, 708. **HRMS** (APCI-MS) exact mass calc. for C₃₉H₅₈BrNO₅ [M+NH₄]⁺ 719.3824 m/z, found: 719.3821 m/z and exact mass calc. for C₃₉H₅₈BrNO₅ [M+H]⁺ 702.3559 m/z, found: 702.3556 m/z.

(8*R*,9*S*,13*S*,14*S*)-3-(1-bromo-3-nitropropyl)-13-methyl-6,7,8,9,11,12,13,14,15,16-decahydro-17*H*-cyclopenta[*a*]phenanthren-17-one (4ef)

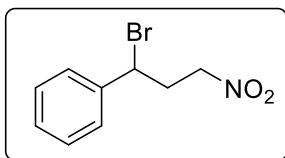
Following general procedure (GP-A) using (8*R*,9*S*,13*S*,14*S*)-13-methyl-3-vinyl-6,7,8,9,11,12,13,14,15,16-decahydro-17*H*-cyclopenta[*a*]phenanthren-17-one (**2ef**) (140.2 mg, 0.5 mmol, 1.0 equiv), bromonitromethane (**1a**) (70.0 mg, 36.0 μ L, 0.5 mmol, 1.0 equiv), [Cu(dap)₂]Cl (4.4 mg, 5.0 μ mol, 1 mol%) and the solvent mixture (dry MeCN (1.0 mL) and dry CHCl₃ (1.0 mL)) at room temperature (25 °C) and irradiation with blue LED (λ_{max} = 455 nm) for 3 h yielded 127.9 mg (304.3 μ mol, 61%) of (8*R*,9*S*,13*S*,14*S*)-3-(1-bromo-3-nitropropyl)-13-methyl-6,7,8,9,11,12,13,14,15,16-decahydro-17*H*-cyclopenta[*a*]phenanthren-17-one (**4ef**) as colorless oil after flash column purification (hexanes / EtOAc 10:1 to 5:1). *R_f* (hexanes / EtOAc 5:1) on silica = 0.31, Staining: KMnO₄-solution.

¹H NMR (300 MHz, CDCl₃) δ [ppm] = 7.30 (dd, *J* = 8.2, 1.0 Hz, 1H), 7.18 (dd, *J* = 8.1, 2.1 Hz, 1H), 7.12 (d, *J* = 1.9 Hz, 1H), 5.01 (dd, *J* = 9.1, 5.9 Hz, 1H), 4.67 – 4.41 (m, 2H), 2.96 – 2.70 (m, 4H), 2.51 (dd, *J* = 18.3, 8.4 Hz, 1H), 2.46 – 2.36 (m, 1H), 2.29 (td, *J* = 10.5, 4.3 Hz, 1H), 2.22 – 1.91 (m, 4H), 1.67 – 1.38 (m, 6H), 0.91 (s, 3H). **¹³C NMR** (75 MHz, CDCl₃) *rotamer 1 (rotamer 2)* δ [ppm] = 220.8, 141.1, 137.6, 137.5, (137.5), 127.8, 126.2, 124.5, 73.6, 50.5, 50.4, (50.3), 48.0, 44.5, 38.0, (38.0), 36.9, (36.9), 35.9, 31.6, 29.5, 26.4, 25.7, 21.7, 13.9. **IR** (neat, cm⁻¹): 2929, 2862, 1736, 1550, 1498, 1453, 1431, 1379, 1289, 1259, 1162, 1084, 1054, 1006, 961, 909, 823, 730. **HRMS** (ESI-MS) exact mass calc. for C₂₁H₂₆BrNO₃ [M+H]⁺ 422.1151 m/z, found: 422.1152 m/z and C₂₁H₂₆BrNO₃ [M+Na]⁺ 444.0970 m/z, found: 444.0976 m/z and C₂₁H₂₆BrNO₃[M+NH₄]⁺ 439.1417 m/z, found: 439.1416 m/z.

Gram-Scale Experiments

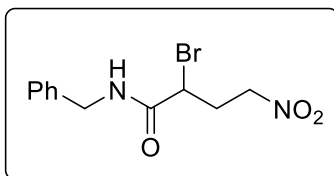
General procedure B (GP-B) for upscaling reactions: The oven-dried schlenk tube of the photochemical upscaling reactor (Figure 3, 5.2.2 Upscaling Reactors) equipped with a stirring bar was charged with the Cu-photocatalyst (1 mol%). Dry MeCN (40 mL) was degassed, using three freeze-pump-thaw cycles. Then dry MeCN (40.0 mL) was added under positive nitrogen atmosphere to the Schlenk tube. Then desired olefin (**2**) (10.0 mmol, 1.0 equiv) and bromonitromethane (**1a**) (1.4 g, 710 μ L, 10.0 mmol, 1.0 equiv) were added under nitrogen atmosphere. The cooling finger was added to the photoreactor and irradiation at 455 nm took place, while the mixture was magnetically stirred at room temperature (25 °C). The reaction was monitored by TLC. After completion of the reaction, the mixture was transferred to a round-bottom flask, concentrated *in vacuo* and the crude residue was purified by flash column chromatography on silica gel (hexanes / EtOAc).

(1-bromo-3-nitropropyl)benzene (**4a**)



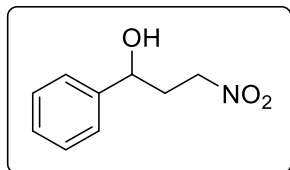
Reaction performed by Magdalena Koch: Following general procedure (GP-B) using styrene (**2a**) (1.40 g, 710.0 μ L, 10.0 mmol, 1.0 equiv), bromonitromethane (**1a**) (1.4 g, 710.0 μ L, 10.0 mmol, 1.0 equiv), [Cu(dmp)₂]Cl (52.0 mg, 1 mol%,) and dry MeCN (40.0 mL, 0.25 M) at room temperature (25 °C) and irradiation with blue LED ($\lambda_{\text{max}} = 455$ nm) for 5 h yielded yield 2.17 g (8.89 mmol, 89%) of **4a** as colorless oil after flash column purification (hexanes / EtOAc 20:1). R_f (hexanes / EtOAc 5:1 on silica) = 0.63, Staining: UV; KMnO₄-solution.

N-benzyl-2-bromo-4-nitrobutanamide (**4bb**)



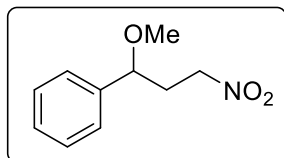
Reaction performed by Johannes Floss: Following general procedure (GP-B) using *N*-benzylacrylamide (**2bb**) (2.26 g, 14.0 mmol, 1.0 equiv), bromonitromethane (**1a**) (1.96 g, 14.0 mmol, 1.0 equiv), [Cu(dap)₂]Cl (124.0 mg, 140.0 μ mol, 1 mol%) and dry MeCN (56.0 mL, 0.25 M) at room temperature (25 °C) and irradiation with blue LED ($\lambda_{\text{max}} = 455$ nm) for 22 h yielded 3.10 g (10.3 mmol, 74%) of *N*-benzyl-2-bromo-4-nitrobutanamide (**4bb**) as colorless oil after flash column purification (hexanes / EtOAc 5:1). R_f (hexanes / EtOAc 5:1 on silica) = 0.08, Staining: KMnO₄-solution.

5.4.6.3 Compound Characterization of Further Transformations

3-nitro-1-phenylpropan-1-ol (**5a**)

A pressure tube equipped with a magnetic stirring bar was charged with (1-bromo-3-nitropropyl)benzene (**4a**) (122.0 mg, 0.5 mmol, 1.0 equiv) and a mixture of MeCN and water (1:1, 4.0 mL) was added. The reaction mixture was then refluxed for 2.5 h. After completion of the reaction, it was concentrated *in vacuo* and the residue was purified by flash column chromatography on silica gel (hexanes / EtOAc 5:1) to yield 62.9 mg (347.2 μmol , 69%) of 3-nitro-1-phenylpropan-1-ol (**5a**) as yellowish oil. R_f (hexanes / EtOAc 5:1 on silica) = 0.25, Staining: UV; KMnO_4 -solution.

$^1\text{H NMR}$ (400 MHz, CDCl_3) δ [ppm] = 7.44 – 7.27 (m, 5H), 4.81 (dd, J = 8.4, 4.7 Hz, 1H), 4.59 (dt, J = 13.7, 7.1 Hz, 1H), 4.44 (dt, J = 13.3, 6.5 Hz, 1H), 2.48 – 2.29 (m, 2H), 2.21 (s, OH). $^{13}\text{C NMR}$ (101 MHz, CDCl_3) δ [ppm] = 143.0, 128.9, 128.4, 125.7, 72.4, 71.2, 36.1. **IR** (neat, cm^{-1}): 3537, 3410, 1546, 1453, 1379, 1069, 913, 764, 700. **MS** (APCI-MS) exact mass calc. for $\text{C}_9\text{H}_{11}\text{NO}_3$ $[\text{M}+\text{NH}_4]^+$ 188.108 m/z, found: 199.108 m/z.

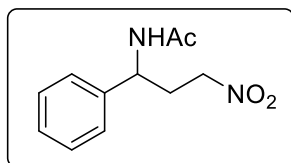
(1-methoxy-3-nitropropyl)benzene (**5b**)

Slightly modified from literature procedure,^[30] a pressure tube equipped with a magnetic stirring bar was charged with (1-bromo-3-nitropropyl)benzene (**4a**) (122.0 mg, 0.5 mmol, 1.0 equiv) and MeOH (4.0 mL) was added. The reaction mixture was then refluxed for 2.5 h. After completion of the reaction, it was concentrated *in vacuo* and the residue was purified by flash column chromatography on silica (hexanes / EtOAc 5:1) to yield 91.7 mg (496.7 μmol , 94%) of (1-methoxy-3-nitropropyl)benzene (**5b**) as pale yellowish oil. R_f (hexanes / EtOAc 5:1 on silica) = 0.86, Staining: UV; KMnO_4 -solution.

$^1\text{H NMR}$ (400 MHz, CDCl_3) δ [ppm] = 7.43 – 7.27 (m, 5H), 4.59 (dt, J = 13.3, 7.1 Hz, 1H), 4.43 (dt, J = 13.2, 6.4 Hz, 1H), 4.24 (t, J = 6.6 Hz, 1H), 3.22 (s, 3H), 2.46 – 2.24 (m, 2H). $^{13}\text{C NMR}$ (101 MHz, CDCl_3) δ [ppm] = 140.5, 128.9, 128.4, 126.5, 80.4, 72.5, 57.0, 35.7. **IR** (neat, cm^{-1}): 3063, 3030, 2985, 2937, 2829, 2363, 2340, 1738, 1554, 1494, 1453, 1382, 1285, 1177, 1110,

909, 868, 700. **MS** (APCI-MS) exact mass calc. for $C_{10}H_{13}NO_3NH_4$ $[M+NH_4]^+$ 213.124 m/z, found: 213.124 m/z.

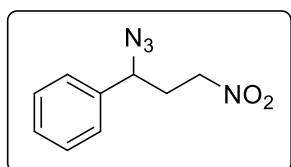
***N*-(3-nitro-1-phenylpropyl)acetamide (5c)**



Based on a literature procedure,^[31] a round-bottom flask equipped with a magnetic stirring bar was charged with irontrichlorid hexahydrate (540.6 mg, 1.2 mmol, 4.0 equiv) and dissolved in MeCN (2.0 mL). To the latter a solution of (1-bromo-3-nitropropyl)benzene (**4a**) (122.0 mg, 0.5 mmol, 1.0 equiv) in MeCN (1.0 mL) was added dropwise at room temperature (25 °C). The resulting reaction mixture was stirred for 2 h at 80 °C. The reaction was monitored by TLC. Afterwards, the reaction mixture was quenched with water and extracted three times with EtOAc. The combined organic layers were washed with water, brine, dried over anhydrous MgSO₄, filtered, concentrated in vacuo and the residue was purified by flash column chromatography on silica (hexanes / EtOAc 1:2) to yield 77.7 mg (349.6 μmol, 70%) of *N*-(3-nitro-1-phenylpropyl)acetamide (**5c**) as a white solid. **mp**: 114 °C **R_f** (hexanes / EtOAc 1:2 on silica) = 0.29, Staining: UV (very weak).

¹H NMR (300 MHz, CDCl₃) δ [ppm] = 7.40 – 7.24 (m, 5H), 6.54 (s, NH), 5.06 (dd, *J* = 14.9, 8.4 Hz, 1H), 4.38 (t, *J* = 7.2 Hz, 2H), 2.63 – 2.36 (m, 2H), 1.95 (s, 3H). **¹³C NMR** (75 MHz, CDCl₃) δ [ppm] = 170.2, 140.2, 129.2, 128.3, 126.5, 72.8, 51., 33.4, 23.3. **IR** (neat, cm⁻¹): 3309, 3063, 2970, 2937, 2383, 1647, 1528, 1427, 1371, 1289, 1218, 1189, 1118, 1028, 935, 823, 752, 697. **MS** (APCI-MS) exact mass calc. for $C_{11}H_{14}N_2O_3$ $[M+H]^+$ 223.1077 m/z, found: 223.1078 m/z.

(1-azido-3-nitropropyl)benzene (5d)

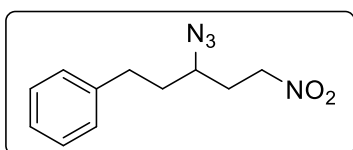


A pressure tube equipped with a magnetic stirring bar was charged with (1-bromo-3-nitropropyl)benzene (**4a**) (122.0 mg, 0.5 mmol, 1.0 equiv), sodium azide (162.5 mg, 2.5 mmol, 5.0 equiv) and DMF (4.0 mL) was added. The reaction mixture was then stirred at room temperature (25 °C) for 24 h. After completion the reaction was quenched with water and extracted with diethyl ether (3 x 25 mL). The combined organic phases were washed with water, then brine and dried over MgSO₄. Concentration *in vacuo* and purification by flash column chromatography (hexanes / EtOAc 20:1) yielded 71.6 mg (347.2 μmol, 69%) of 1-

azido-3-nitropropyl)benzene (**5d**) as colorless oil. R_f (hexanes / EtOAc 5:1 on silica) = 0.57, Staining: UV; KMnO₄-solution.

¹H NMR (300 MHz, CDCl₃) δ [ppm] = 7.47 – 7.29 (m, 6H), 4.65 (t, J = 7.2 Hz, 1H), 4.53 (dt, J = 13.9, 7.0 Hz, 1H), 4.40 (dt, J = 13.8, 6.4 Hz, 1H), 2.40 (q, J = 6.9 Hz, 2H). ¹³C NMR (75 MHz, CDCl₃) δ [ppm] = 137.8, 129.4, 129.2, 126.9, 72.1, 63.0, 33.8. IR (neat, cm⁻¹): 3063, 3034, 2933, 2359, 2102, 1554, 1494, 1453, 1382, 1312, 1244, 1062, 984, 887, 764, 700. HRMS (ESI-MS) exact mass calc. for C₉H₁₀N₄O₂Na [M+Na]⁺ 229.0696 m/z, found: 229.0693 m/z.

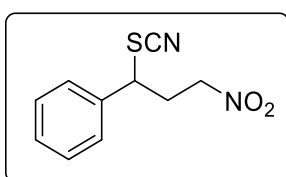
(3-azido-5-nitropentyl)benzene (**5ca**)



A round-bottomed flask equipped with a magnetic stirring bar was charged with ((3-bromo-5-nitropentyl)benzene (**4ca**) (408.2 mg, 1.5 mmol, 1.0 equiv), sodium azide (487.6 mg, 7.5 mmol, 5.0 equiv) and DMF (4.0 mL) was added. The reaction mixture was then stirred at room temperature for 5 d. After completion of the reaction, the reaction was quenched with water and extracted with diethyl ether (3x 25 mL). The combined organic phases were washed with water and brine and dried over MgSO₄. Then it was concentrated *in vacuo* and the residue was purified by flash column chromatography on silica gel (PE/ EE 20:1) to yield 193.0 mg (55%) (3-azido-5-nitropentyl)benzene (**5ca**) as colorless oil.

R_f (hexanes/ EtOAc 5:1) on silica) = 0.6, Staining: UV; KMnO₄-solution. ¹H NMR (300 MHz, CDCl₃) δ [ppm] = 7.36 – 7.28 (m, 2H), 7.26 – 7.17 (m, 3H), 4.60 – 4.43 (m, 2H), 3.44 (dddd, J = 9.4, 7.8, 5.4, 3.6 Hz, 1H), 2.90 – 2.66 (m, 2H), 2.32 (dddd, J = 14.9, 7.9, 7.2, 3.6 Hz, 1H), 2.14 – 2.00 (m, 1H), 2.00 – 1.82 (m, 2H). ¹³C NMR (75 MHz, CDCl₃) δ [ppm] = 140.4, 128.8, 128.5, 126.5, 72.3, 59.0, 36.3, 32.2, 32.0. IR (neat, cm⁻¹): 3036, 3026, 2929, 2862, 2098, 1602, 1550, 1494, 1453, 1382, 1259, 1092, 1051, 909, 872, 848, 805, 749, 700. HRMS (ESI-MS) exact mass calc. for C₁₁H₁₄N₄O₂ [M+Na]⁺ 257.1009 m/z, found: 257.1008 m/z.

(3-nitro-1-thiocyanatopropyl)benzene (**5e**)

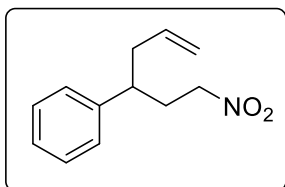


A pressure tube equipped with a magnetic stirring bar was charged with (1-bromo-3-nitropropyl)benzene (**4a**) (122.0 mg, 0.5 mmol, 1.0 equiv), sodium thiocyanate (202.7 mg,

2.5 mmol, 5.0 equiv) and DMF (4.0 mL) was added. The reaction mixture was then stirred at room temperature (25 °C) for 3 h. After completion of the reaction, it was quenched with water and extracted with diethyl ether (3 x 25 mL). The combined organic phase was washed with water and brine and dried over MgSO₄. Concentration *in vacuo* and purification by flash column chromatography (hexanes / EtOAc 5:1) yielded 78.4 mg (352.7 μmol, 71%) of (3-nitro-1-thiocyanatopropyl)benzene (**5e**) as pale yellowish oil. *R_f* (hexanes / EtOAc 5:1 on silica) = 0.27, Staining: UV; KMnO₄-solution.

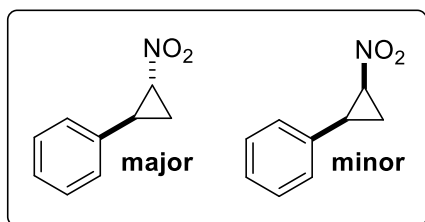
¹H NMR (400 MHz, CDCl₃) δ (ppm) = 7.47 – 7.31 (m, 5H), 4.55 – 4.41 (m, 2H), 4.35 (ddd, *J* = 13.9, 7.7, 5.8 Hz, 1H), 3.02 – 2.87 (m, 1H), 2.80 (ddt, *J* = 15.0, 9.1, 6.2 Hz, 1H). **¹³C NMR** (75 MHz, CDCl₃) δ [ppm] = 136.1, 129.9, 129.7, 127.4, 110.5, 72.2, 49.5, 32.8. **IR** (neat, cm⁻¹): 3034, 2929, 2154, 1722, 1550, 1453, 1431, 1379, 1181, 868, 764, 697. **MS** (APCI-MS) exact mass calc. for C₁₀H₁₀N₂O₂S [M+Na]⁺ 245.0355 m/z, found: 245.0357 m/z.

(1-nitrohex-5-en-3-yl)benzene (**5f**)



Based on a literature procedure,^[32] a round-bottom flask equipped with a magnetic stirring bar was charged with iron trichloride (4.1 mg, 25.0 μmol, 5 mol%) and (1-bromo-3-nitropropyl)benzene (**4a**) (122.0 mg, 0.5 mmol, 1.0 equiv) in DCM (2.0 mL). Then allyltrimethylsilane (114.2 mg, 158.9 μL, 2.0 equiv) was added. The resulting reaction mixture was stirred for 2 h at room temperature (25 °C). The reaction was monitored by TLC. Afterwards, the reaction mixture was concentrated *in vacuo* and the residue was purified by flash column chromatography on silica (hexanes / EtOAc 20:1) to yield 76.8 mg (374.2 μmol, 75%) of (1-nitrohex-5-en-3-yl)benzene (**5f**) as a colorless oil. *R_f* (hexanes / EtOAc 5:1 on silica) = 0.78, Staining: UV (very weak).

¹H NMR (300 MHz, CDCl₃) δ [ppm] = 7.39 – 7.31 (m, 2H), 7.30 – 7.22 (m, 1H), 7.20 – 7.14 (m, 2H), 5.75 – 5.58 (m, 1H), 5.09 – 5.02 (m, 1H), 5.02 – 4.98 (m, 1H), 4.20 (dd, *J* = 8.0, 6.5 Hz, 2H), 2.72 (ddt, *J* = 11.4, 7.3, 3.6 Hz, 1H), 2.60 – 2.35 (m, 3H), 2.17 (ddt, *J* = 14.1, 11.0, 6.6 Hz, 1H). **¹³C NMR** (75 MHz, CDCl₃) δ [ppm] = 142.4, 135.8, 129.0, 127.6, 127.2, 117.1, 73.9, 42.8, 41.2, 33.2. **IR** (neat, cm⁻¹): 3063, 3030, 2978, 2922, 1640, 1602, 1550, 1494, 1453, 1379, 1185, 1073, 995, 916, 764, 700. **HRMS** (ESI-MS) exact mass calc. for C₁₂H₁₅NO₂ [M+NH₄]⁺ 223.1441 m/z, found: 223.1442 m/z.

2-nitrocyclopropyl)benzene (6a)

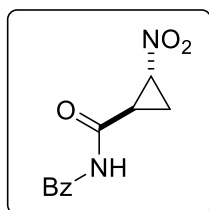
One-pot procedure from **1a** and **2a**: Following general procedure (GP-A) using styrene (**2a**) (52.1 mg, 58.0 μ L, 0.5 mmol, 1.0 equiv), bromonitromethane (**1a**) (70.0 mg, 36.0 μ L, 0.5 mmol, 1.0 equiv), [Cu(dap)₂]Cl (4.4 mg, 5.0 μ mol, 1 mol%) and dry MeCN (2.0 mL, 0.25 M) at room temperature (25 °C) and irradiation with blue LED ($\lambda_{\text{max}} = 455$ nm) for 1 h. After irradiation DBU (1,8-diazabicyclo[5.4.0]undec-7-ene) (152.4 mg, 148.4 μ L, 1.0 mmol, 2.0 equiv) was added to the reaction mixture, and stirred for 30 min at room temperature (25 °C). After completion, the reaction acidified using 1 M HCl. The aqueous phase was extracted with EtOAc (3 x 25 mL). The combined organic phase was washed with water, brine and dried over MgSO₄. It was concentrated *in vacuo* and the residue was purified by flash column chromatography on silica (hexanes / EtOAc 20:1 to 10:1) to yield 61.2 mg (375.1 μ mol, 75%) of *trans*-2-nitrocyclopropyl)benzene (**trans-6a**). Corresponding *cis*-diastereomer was not isolated. Diastereomeric ratio was determined by crude ¹H-NMR analysis: d.r. = 85:15. R_f (**trans-6a**) (hexanes / EtOAc 5:1 on silica) = 0.79, Staining: UV; KMnO₄-solution.

Procedure starting from compound **4a**: A pressure tube equipped with a magnetic stirring bar was charged with (1-bromo-3-nitropropyl)benzene (**4a**) (122.0 mg, 0.5 mmol, 1.0 equiv), and dissolved in THF (4.0 mL). DBU (152.4 mg, 148.4 μ L, 1.0 mmol, 2.0 equiv) was added. The reaction mixture was then stirred at room temperature (25 °C) for 30 min. After completion, the reaction acidified using 1 M HCl. The aqueous phase was extracted with EtOAc (3 x 25 mL). The combined organic phase was washed with water, brine and dried over MgSO₄. It was concentrated *in vacuo* and the residue was purified by flash column chromatography on silica (hexanes / EtOAc 20:1 to 10:1) to yield 57.0 mg (349.3 μ mol, 70%) of *trans*-2-nitrocyclopropyl)benzene (**trans-6a**) and 5.5 mg (33.7 μ mol, 7%) of *cis*-nitrocyclopropyl)benzene (**cis-6a**) colorless oil. Spectral data are in accordance with literature.^[33] Diastereomeric ratio was determined by crude ¹H-NMR analysis: d.r. = 85:15. R_f (**trans-6a**) (hexanes / EtOAc 5:1 on silica) = 0.79, Staining: UV; KMnO₄-solution. R_f (**cis-6a**) (hexanes / EtOAc 5:1 on silica) = 0.40, Staining: UV; KMnO₄-solution.

trans-6a: $^1\text{H NMR}$ (400 MHz, CDCl_3) δ [ppm] = 7.39 – 7.23 (m, 3H), 7.17 – 7.04 (m, 2H), 4.42 (ddd, J = 7.1, 3.9, 3.0 Hz, 1H), 3.14 (ddd, J = 10.8, 7.9, 3.0 Hz, 1H), 2.25 (ddd, J = 10.5, 6.2, 3.9 Hz, 1H), 1.68 (ddd, J = 7.9, 7.3, 6.2 Hz, 1H). $^{13}\text{C NMR}$ (101 MHz, CDCl_3) δ [ppm] = 136.5, 128.9, 127.8, 126.8, 61.8, 29.5, 18.9. **IR** (neat, cm^{-1}): 3093, 3034, 1535, 1431, 1360, 1077, 1017, 931, 752, 697. **HRMS** (APCI-MS) exact mass calc. for $\text{C}_9\text{H}_9\text{NO}_2$ $[\text{M}+\text{H}]^+$ 164.0706 m/z, found: 164.0705 m/z.

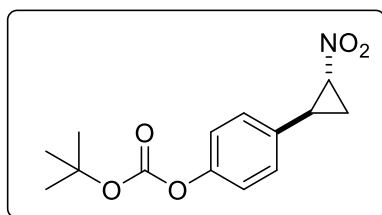
cis-6a: $^1\text{H NMR}$ (300 MHz, CDCl_3) δ [ppm] = 7.37 – 7.27 (m, 5H), 4.64 (ddd, J = 8.4, 6.6, 4.2 Hz, 1H), 2.86 (q, J = 9.0 Hz, 1H), 2.36 (ddd, J = 9.0, 6.8, 4.1 Hz, 1H), 1.65 (dt, J = 9.5, 6.6 Hz, 1H). $^{13}\text{C NMR}$ (75 MHz, CDCl_3) δ [ppm] = 132.6, 129.3, 128.6, 128.1, 60.6, 28.7, 13.6.

trans-N-2-nitrocyclopropane-1-carbonyl)benzamide (trans-6bb)



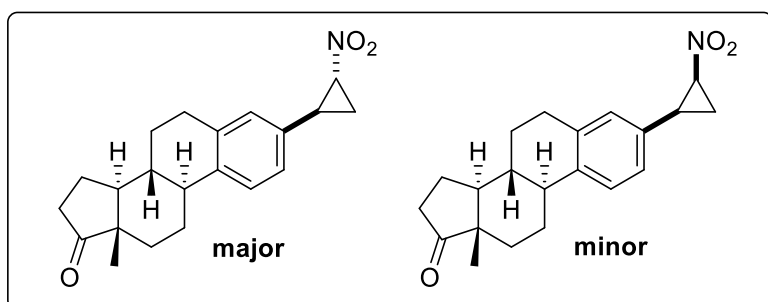
A round-bottom flask equipped with a magnetic stirring bar was charged with *N*-benzyl-2-bromo-4-nitrobutanamide (**4bb**) (150.6 mg, 0.5 mmol, 1.0 equiv), and dissolved in THF (4.0 mL). DBU (152.4 mg, 148.4 μL , 1.0 mmol, 2.0 equiv) was added. The reaction mixture was then stirred at room temperature (25 $^\circ\text{C}$) for 30 min. After completion, the reaction acidified using 1N HCl. The aqueous phase was extracted with EtOAc (3 x 25 mL). The combined organic phase was washed with water, brine and dried over MgSO_4 . It was concentrated *in vacuo* and the residue was purified by flash column chromatography on silica (hexanes / EtOAc 2:1) to yield 67.7 mg (307.4 μmol , 62%) of *trans*-*N*-2-nitrocyclopropane-1-carbonyl)-benzamide (**trans-6bb**) as a white solid. **mp**: 132 $^\circ\text{C}$ **R_f** (hexanes / EtOAc 5:1 on silica) = 0.16, Staining: UV; KMnO_4 -solution.

$^1\text{H NMR}$ (400 MHz, CDCl_3) δ [ppm] = 7.38 – 7.21 (m, 5H), 6.49 (s, 1H), 4.54 (ddd, J = 7.5, 4.2, 2.6 Hz, 1H), 4.39 (d, J = 5.7 Hz, 2H), 2.53 (ddd, J = 9.9, 7.1, 2.7 Hz, 1H), 1.94 (ddd, J = 9.9, 5.6, 4.3 Hz, 1H), 1.73 (td, J = 7.3, 5.6 Hz, 1H). $^{13}\text{C NMR}$ (101 MHz, CDCl_3) δ [ppm] = 167.3, 137.4, 129.0, 128.0, 128.0, 59.3, 44.3, 26.8, 16.8. **IR** (neat, cm^{-1}): 3298, 3123, 3060, 2922, 1636, 1535, 1467, 1423, 1364, 1222, 998, 939, 890, 805, 752, 693. **HRMS** (ESI-MS) exact mass calc. for $\text{C}_{11}\text{H}_{12}\text{N}_2\text{O}_3$ $[\text{M}+\text{H}]^+$ 221.0921 m/z, found: 221.0919 m/z and exact mass calc. for $\text{C}_{11}\text{H}_{12}\text{N}_2\text{O}_3$ $[\text{M}+\text{Na}]^+$ 243.0740 m/z, found: 243.0737 m/z.

trans-tert-butyl (4-(2-nitrocyclopropyl)phenyl) carbonate (trans-6k)

A round-bottom flask equipped with a magnetic stirring bar was charged with 4-(1-bromo-3-nitropropyl)phenyl *tert*-butyl carbonate (**4k**) (180.1 mg, 0.5 mmol, 1.0 equiv), and dissolved in THF (4.0 mL). DBU (152.4 mg, 148.4 μ L, 1.0 mmol, 2.0 equiv) was added. The reaction mixture was then stirred at room temperature (25 °C) for 30 min. After completion, the reaction acidified using 1M HCl. The aqueous phase was extracted with EtOAc (3 x 25 mL). The combined organic phase was washed with water, brine and dried over MgSO₄. It was concentrated *in vacuo* and the residue was purified by flash column chromatography on silica (hexanes / EtOAc 10:1) to yield 86.1mg (308.3 μ mol, 62%) of *trans-tert*-butyl (4-(2-nitrocyclopropyl)phenyl) carbonate (**trans-6k**) as colorless oil. The corresponding *cis*-diastereomer was not isolated. *trans*-diastereomer was designated based coupling constants of literature^[33] for cyclopropanes. *R_f* (hexanes / EtOAc 5:1 on silica) = 0.78, Staining: UV; KMnO₄-solution.

¹H NMR (400 MHz, CDCl₃) δ [ppm] = 7.13 (s, 4H), 4.37 (ddd, *J* = 7.2, 3.9, 3.0 Hz, 1H), 3.12 (ddd, *J* = 10.8, 7.9, 3.0 Hz, 1H), 2.21 (ddd, *J* = 10.5, 6.3, 3.9 Hz, 1H), 1.68 – 1.60 (m, 1H), 1.55 (s, 9H). **¹³C NMR** (101 MHz, CDCl₃) δ [ppm] = 151.8, 150.6, 133.8, 127.9, 121.8, 83.9, 61.6, 28.8, 27.8, 18.7. **IR** (neat, cm⁻¹): 3101, 2981, 2933, 1751, 1543, 1476, 1364, 1256, 1222, 1140, 1051, 1013, 931, 894, 827, 782, 678. **HRMS** (ESI-MS) exact mass calc. for C₁₄H₁₇NO₅ [M+H]⁺ 280.1179 m/z, found: 280.1179 m/z and exact mass calc. for C₁₄H₁₇NO₅ [M+Na]⁺ 302.0999 m/z, found: 302.1002 m/z and exact mass calc. for C₁₄H₁₇NO₅ [M+NH₄]⁺ 297.1445 m/z, found: 297.1444 m/z.

trans-(8R,9S,13S,14S)-13-methyl-3-((1S,2R)-2-nitrocyclopropyl)-***6,7,8,9,11,12,13,14,15,16-decahydro-17H-cyclopenta[a]phenanthren-17-one (trans-6ef)***

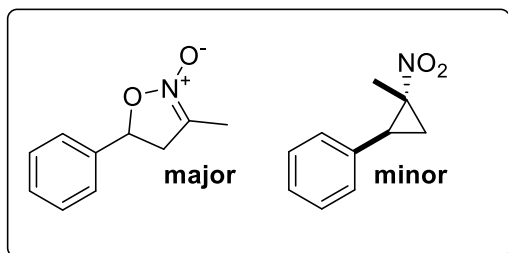
A round-bottom flask equipped with a magnetic stirring bar was charged with (8*R*,9*S*,13*S*,14*S*)-3-(1-bromo-3-nitropropyl)-13-methyl-6,7,8,9,11,12,13,14,15,16-decahydro-17*H*-

cyclopenta[a]phenanthren-17-one (**4ef**) (229.6 mg, 0.5 mmol, 1.0 equiv), and dissolved in THF (4.0 mL). DBU (152.4 mg, 148.4 μ L, 1.0 mmol, 2.0 equiv) was added. The reaction mixture was then stirred at room temperature (25 °C) for 30 min. After completion, the reaction acidified using 1M HCl. The aqueous phase was extracted with EtOAc (3 x 25 mL). The combined organic phase was washed with water, brine and dried over MgSO₄. It was concentrated *in vacuo* and the residue was purified by flash column chromatography on silica (hexanes / EtOAc 5:1 to 2:1) to yield 114.4 mg (337.0 μ mol 67%) of *trans*-(8*R*,9*S*,13*S*,14*S*)-13-methyl-3-((1*S*,2*R*)-2-nitrocyclopropyl)-6,7,8,9,11,12,13,14,15,16-decahydro-17*H*-cyclopenta[a]phenanthren-17-one (**trans-6ef**) and 16.4 mg (48.3 μ mol, 9%) of *cis*-(8*R*,9*S*,13*S*,14*S*)-13-methyl-3-((1*S*,2*R*)-2-nitrocyclopropyl)-6,7,8,9,11,12,13,14,15,16-decahydro-17*H*-cyclopenta[a]phenanthren-17-one (**cis-6ef**) each as colorless sticky oil. Diastereomeric ratio was determined by crude ¹H-NMR analysis: d.r. = 91:9. Diastereomers were designated based coupling constants of literature^[33] for cyclopropanes. **R_f** (**trans-7ef**) (hexanes / EtOAc 2:1 on silica) = 0.75, Staining: UV; KMnO₄-solution. **R_f** (**cis-7ef**) (hexanes / EtOAc 2:1 on silica) = 0.58, Staining: UV; KMnO₄-solution.

trans-6ef: ¹H NMR (300 MHz, CDCl₃) δ [ppm] = 7.26 (d, *J* = 8.0 Hz, 1H), 6.95 – 6.83 (m, 2H), 4.38 (dt, *J* = 6.8, 3.4 Hz, 1H), 3.08 (ddd, *J* = 10.7, 7.9, 3.0 Hz, 1H), 2.90 (dd, *J* = 8.8, 4.2 Hz, 2H), 2.51 (dd, *J* = 18.3, 8.5 Hz, 1H), 2.45 – 2.35 (m, 1H), 2.35 – 1.90 (m, 5H), 1.73 – 1.36 (m, 7H), 0.91 (s, 3H). **¹³C NMR** *rotamer 1+2* (101 MHz, CDCl₃) δ [ppm] = 220.8, 139.6, 137.3, 133.9, 127.6, 127.5, 126.0, 124.1, 124.0, 61.8, 50.6, 48.1, 44.4, 38.2, 36.0, 31.7, 29.5, 29.3, 26.5, 25.9, 21.7, 18.8, 18.8, 14.0. **IR** (neat, cm⁻¹): 3093, 2929, 2862, 2251, 1736, 1539, 1505, 1453, 1408, 1360, 1289, 1269, 1215, 1166, 1118, 1080, 1054, 1006, 950, 909, 846, 782, 730, 662. **HRMS** (EI-MS) exact mass calc. for C₂₁H₂₅NO₃ [M]⁺ 339.18290 m/z, found: 339.18342 m/z.

cis-6ef: ¹H NMR (400 MHz, CDCl₃) δ [ppm] = 7.23 (d, *J* = 8.1 Hz, 1H), 7.06 (dt, *J* = 8.1, 2.6 Hz, 1H), 7.01 (d, *J* = 2.6 Hz, 1H), 4.61 (ddd, *J* = 8.4, 6.5, 4.1 Hz, 1H), 2.89 (q, *J* = 4.5 Hz, 3H), 2.79 (q, *J* = 9.0 Hz, 1H), 2.50 (dd, *J* = 18.7, 8.6 Hz, 1H), 2.45 – 2.22 (m, 3H), 2.22 – 1.91 (m, 3H), 1.68 – 1.38 (m, 6H), 0.91 (s, 3H). **¹³C NMR** *rotamer 1+2* (101 MHz, CDCl₃) δ [ppm] = 221.0, 139.7, 136.7, 129.9, 129.8, 126.6, 126.6, 125.6, 60.7, 50.7, 48.1, 44.4, 38.1, 36.0, 31.7, 29.4, 28.4, 26.6, 25.7, 21.7, 14.0, 13.6. **IR** (neat, cm⁻¹): 2929, 2862, 1736, 1539, 1453, 1408, 1367, 1259, 1215, 1118, 1084, 1054, 1006, 909, 823, 730. **HRMS** (EI-MS) exact mass calc. for C₂₁H₂₅NO₃ [M]⁺ 339.18290 m/z, found: 339.18196 m/z.

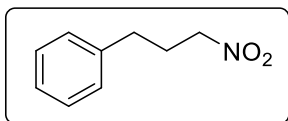
3-methyl-5-phenyl-4,5-dihydroisoxazole 2-oxide (3da) and *trans*-2-methyl-2-nitrocyclopropyl)benzene (*trans*-6da)



A pressure tube equipped with a magnetic stirring bar was charged with (1-bromo-3-nitrobutyl)benzene (**4da**) (129.1 mg, 0.5 mmol, 1.0 equiv), and dissolved in THF (4.0 mL). DBU (152.4 mg, 148.4 μ L, 1.0 mmol, 2.0 equiv) was added. The reaction mixture was then stirred at room temperature (25 °C) for 30 min. After completion, the reaction acidified using 1 M HCl. The aqueous phase was extracted with EtOAc (3 x 25 mL). The combined organic phase was washed with water, brine and dried over MgSO_4 . It was concentrated *in vacuo* and the residue was purified by flash column chromatography on silica (hexanes / EtOAc 20:1 to pure EE) to yield 19.3 mg (108.9 μ mol, 22%) of *trans*-2-methyl-2-nitrocyclopropyl)benzene (**3da**) as colorless oil and 57.4 mg (323.9 μ mol, 65%) of 3-methyl-5-phenyl-4,5-dihydroisoxazole 2-oxide (***trans*-6da**) as a white solid. Spectral data of isoxazoline-*N*-oxide are in accordance with literature.^[18] R_f (***trans*-6da**, cyclopropane) (hexanes / EtOAc 5:1 on silica) = 0.83, Staining: UV; KMnO_4 -solution. R_f (**3da**, isoxazoline-*N*-oxide) (hexanes / EtOAc 5:1 on silica) = 0.08, Staining: UV; KMnO_4 -solution.

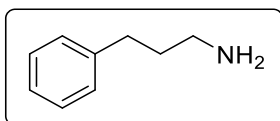
***trans*-2-methyl-2-nitrocyclopropyl)benzene (*trans*-6da):** $^1\text{H NMR}$ (400 MHz, CDCl_3) δ [ppm] = 7.40 – 7.27 (m, 3H), 7.22 – 7.14 (m, 2H), 3.38 (dd, J = 10.5, 8.2 Hz, 1H), 2.36 (dd, J = 10.5, 5.9 Hz, 1H), 1.55 (dd, J = 8.2, 5.9 Hz, 1H), 1.44 (s, 3H). $^{13}\text{C NMR}$ (101 MHz, CDCl_3) δ [ppm] = 134.7, 128.9, 128.8, 127.9, 65.7, 35.0, 22.2, 15.4. **IR** (neat, cm^{-1}): 3034, 2985, 2940, 2870, 2363, 1736, 1531, 1449, 1394, 1353, 1319, 1207, 1092, 1054, 954, 894, 853, 756, 700.

3-methyl-5-phenyl-4,5-dihydroisoxazole 2-oxide (3da): $^1\text{H NMR}$ (300 MHz, CDCl_3) δ [ppm] = 7.43 – 7.28 (m, 5H), 5.57 (dd, J = 9.6, 7.5 Hz, 1H), 3.47 (ddq, J = 17.1, 9.6, 1.7 Hz, 1H), 3.06 (ddd, J = 17.1, 7.6, 1.8 Hz, 1H), 2.00 (t, J = 1.8 Hz, 3H). $^{13}\text{C NMR}$ (75 MHz, CDCl_3) δ [ppm] = 139.0, 129.0, 128.8, 125.7, 125.6, 112.4, 75.4, 42.3, 11.9.

(3-nitropropyl)benzene (7a)

A pressure tube equipped with a magnetic stirring bar was charged with (1-bromo-3-nitropropyl)benzene (**4a**) (122.0 mg, 0.5 mmol, 1.0 equiv), Pd on charcoal (5.3 mg, 50.0 μ mol, 10 mol%) dissolved in MeOH (1.0 mL). The reaction mixture was then equipped with a balloon containing H₂. The reaction was stirred for 22 h at room temperature (25 °C). The solution was filtered over a pad of celite to obtain 82.2 mg (497.6 μ mol, 99%) of (3-nitropropyl)benzene (**7a**) as orange oil. Spectral data are in accordance with literature.^[34] R_f (hexanes / EtOAc 5:1 on silica) = 0.81, Staining: UV; KMnO₄-solution.

¹H NMR (400 MHz, CDCl₃) δ [ppm] = 7.31 (t, J = 7.3 Hz, 2H), 7.26 – 7.14 (m, 3H), 4.36 (t, J = 6.9 Hz, 2H), 2.71 (t, J = 7.5 Hz, 2H), 2.32 (p, J = 7.1 Hz, 2H). **¹³C NMR** (101 MHz, CDCl₃) δ [ppm] = 139.6, 128.9, 128.6, 126.7, 74.8, 32.4, 29.0.

3-phenylpropan-1-amine (8a)

A round-bottom flask equipped with a magnetic stirring bar was charged with (1-bromo-3-nitropropyl)benzene (**4a**) (195.3 mg, 0.8 mmol, 1.0 equiv), Zn dust (1.26 g, 19.20 mmol, 24.0 equiv) and aqueous acetic acid (50% V/V, 4 mL, 0.15 M) was added. The resulting reaction mixture was stirred at room temperature (25 °C) for 18 h. The reaction solution was then filtered over cotton to remove excess of Zn. Afterwards, the reaction mixture was quenched with conc. NaOH solution till pH = 12. Celite was added and the solution was filtered off. The filter was washed with EtOAc (3 x 20 mL). Followed by this, the mixture was extracted three times with EtOAc. The combined organic layers were washed with conc. NaOH solution, dried over anhydrous MgSO₄, filtered, concentrated *in vacuo* to yield 78.3 mg (579.1 μ mol, 72%) of 3-phenylpropan-1-amine (**8a**) as a yellowish oil. Spectral data are in accordance with literature.^[35]

¹H NMR (300 MHz, CDCl₃) δ [ppm] = 7.34 – 7.14 (m, 5H), 2.72 (t, J = 7.1 Hz, 2H), 2.65 (t, J = 7.6 Hz, 2H), 2.01 (s, 2H), 1.85 – 1.69 (m, 2H). **¹³C NMR** (75 MHz, CDCl₃) δ [ppm] = 142.1, 128.4, 128.4, 125.8, 41.7, 35.2, 33.3.

5.5 References for Experimental Part

- [1] W. L. F. Armarego, *Purification of laboratory chemicals*, Butterworth-Heinemann, Kidlington, Oxford, United Kingdom, Cambridge, MA, **2017**.
- [2] D. Rackl, V. Kais, P. Kreitmeier, O. Reiser, *Beilstein J. Org. Chem.* **2014**, *10*, 2157.
- [3] P. J. Moon, A. Fahandej-Sadi, W. Qian, R. J. Lundgren, *Angew. Chem. Int. Ed.* **2018**, *57*, 4612.
- [4] Q. Feng, Q. Song, *J. Org. Chem.* **2014**, *79*, 1867.
- [5] L. Han, P. Xing, B. Jiang, *Org. Lett.* **2014**, *16*, 3428.
- [6] Y. Sakakibara, P. Cooper, K. Murakami, K. Itami, *Chem. Asian. J.* **2018**, *13*, 2410.
- [7] E. V. Vinogradova, N. H. Park, B. P. Fors, S. L. Buchwald, *Org. Lett.* **2013**, *15*, 1394.
- [8] D. Shen, C. Miao, D. Xu, C. Xia, W. Sun, *Org. Lett.* **2015**, *17*, 54.
- [9] Z. Chen, C. Liu, J. Liu, J. Li, S. Xi, X. Chi, H. Xu, I.-H. Park, X. Peng, X. Li et al., *Adv. Mater.* **2020**, *32*, e1906437.
- [10] S. Harusawa, S. Nakamura, S. Yagi, T. Kurihara, Y. Hamada, T. Shioiri, *Synth. Commun.* **1984**, *14*, 1365.
- [11] W. Wang, S. Wang, Y. Liu, G. Dong, Y. Cao, Z. Miao, J. Yao, W. Zhang, C. Sheng, *Eur. J. Med. Chem.* **2010**, *45*, 6020.
- [12] U. Megerle, R. Lechner, B. König, E. Riedle, *Photochem. Photobiol. Sci.* **2010**, *9*, 1400.
- [13] S. Engl, O. Reiser, *ACS Catal.* **2020**, *10*, 9899.
- [14] S. Engl, O. Reiser, *Eur. J. Org. Chem.* **2020**, *2020*, 1523.
- [15] C. Minozzi, A. Caron, J.-C. Grenier-Petel, J. Santandrea, S. K. Collins, *Angew. Chem. Int. Ed.* **2018**, *57*, 5477.
- [16] B. R. Fishwick, D. K. Rowles, C. J. M. Stirling, *J. Chem. Soc., Perkin Trans. 1* **1986**, 1171.
- [17] A. I. Ilovaisky, V. M. Merkulova, Y. N. Ogibin, G. I. Nikishin, *Russ. Chem. Bull.* **2005**, *54*, 1585.
- [18] Y. Tsuchiya, R. Onai, D. Uruguchi, T. Ooi, *Chem. Commun.* **2020**, *56*, 11014.
- [19] F. Lo Galbo, E. G. Occhiato, A. Guarna, C. Faggi, *J. Org. Chem.* **2003**, *68*, 6360.
- [20] M. Iseki, Y. Hiraoka, C. Jing, H. Okamura, E. Sato, A. Matsumoto, *J. Appl. Polym. Sci.* **2018**, *135*, 46252.
- [21] F. Ratsch, H.-G. Schmalz, *Synlett* **2018**, *29*, 785.

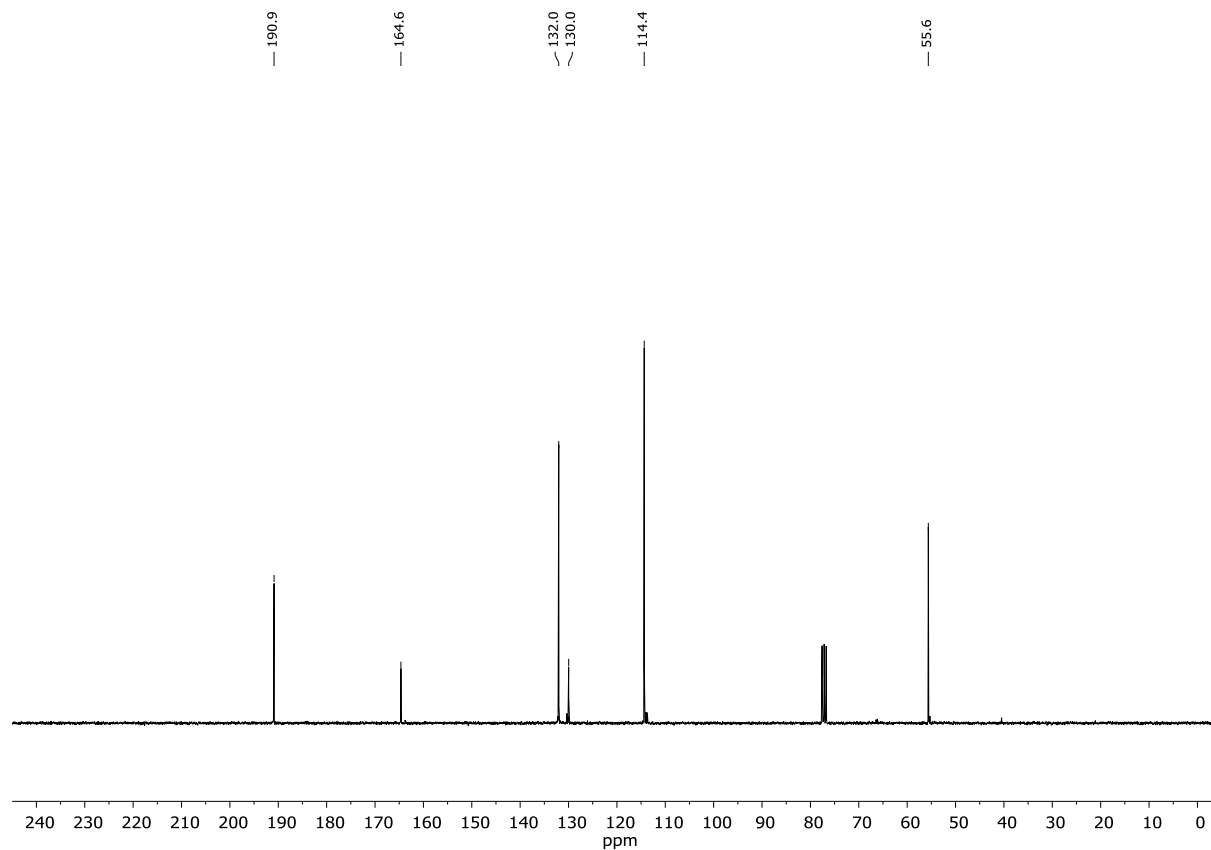
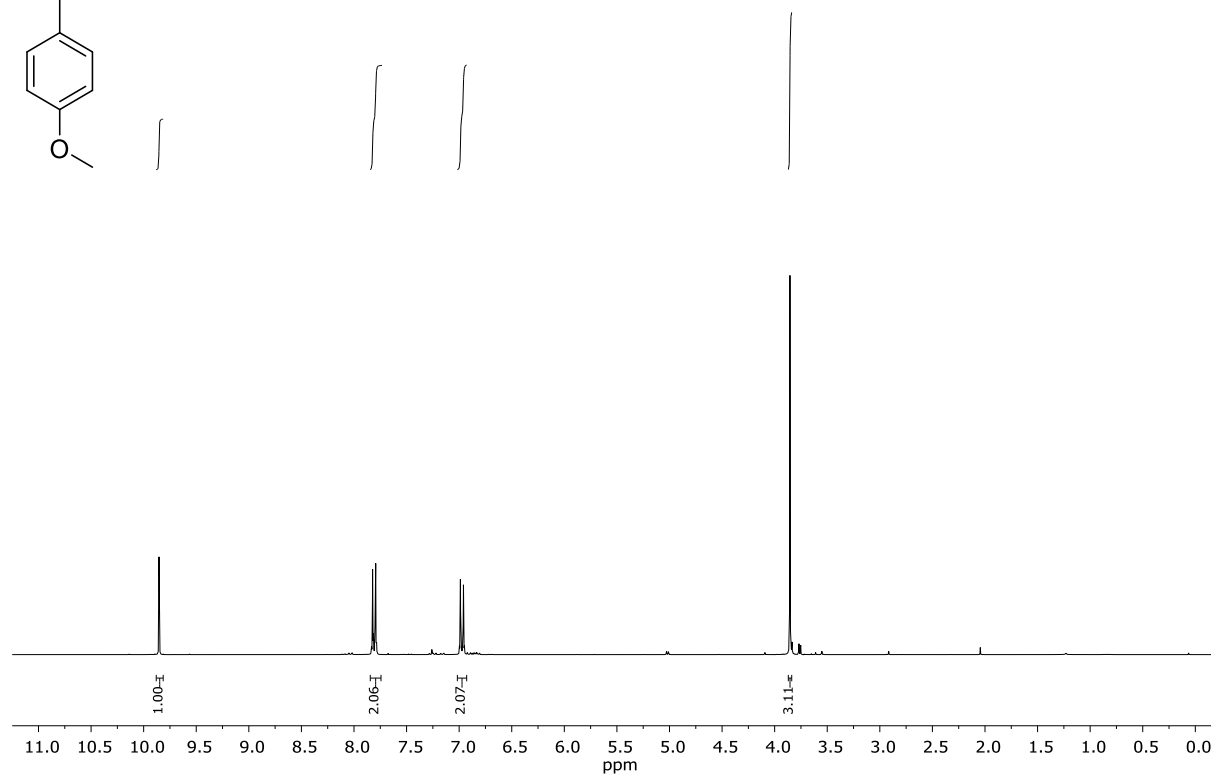
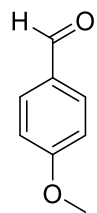
- [22] B. Bertrand, L. Stefan, M. Pirrotta, D. Monchaud, E. Bodio, P. Richard, P. Le Gendre, E. Warmerdam, M. H. de Jager, G. M. M. Groothuis et al., *Inorg. Chem.* **2014**, *53*, 2296.
- [23] M. Mato, B. Herlé, A. M. Echavarren, *Org. Lett.* **2018**, *20*, 4341.
- [24] S. Loykulnant, M. Hayashi, A. Hirao, *Macromolecules* **1998**, *31*, 9121.
- [25] M. Zhang, M. Chen, X. Ding, J. Kang, Y. Gao, X. He, Z. Wang, A. Lu, Q. Wang, *Chem. Commun.* **2021**, *57*, 9140.
- [26] M. Ratushnyy, M. Kamenova, V. Gevorgyan, *Chem. Sci.* **2018**, *9*, 7193.
- [27] A. H. Mai, S. Pawar, W. M. de Borggraeve, *Tetrahedron Lett.* **2014**, *55*, 4664.
- [28] T. Honjo, M. Nakao, S. Sano, M. Shiro, K. Yamaguchi, Y. Sei, Y. Nagao, *Org. Lett.* **2007**, *9*, 509.
- [29] H. Schneider, G. Sigmund, B. Schrickler, K. Thirring, H. Berner, *J. Org. Chem.* **1993**, *58*, 683.
- [30] S. Engl, O. Reiser, *Org. Lett.* **2021**, *23*, 5581.
- [31] H. R. F. Karabulut, M. Kacan, *Synth. Commun.* **2002**, *32*, 2345.
- [32] J. Han, Z. Cui, J. Wang, Z. Liu, *Synth. Commun.* **2010**, *40*, 2042.
- [33] J. A. Ciaccio, C. E. Aman, *Synth. Commun.* **2006**, *36*, 1333.
- [34] A. Palmieri, S. Gabrielli, R. Ballini, *Beilstein J. Org. Chem.* **2013**, *9*, 533.
- [35] N. Ríos-Lombardía, C. Vidal, M. Cocina, F. Morís, J. García-Álvarez, J. González-Sabín, *Chem. Commun.* **2015**, *51*, 10937.

Chapter 6 Scientific Appendix

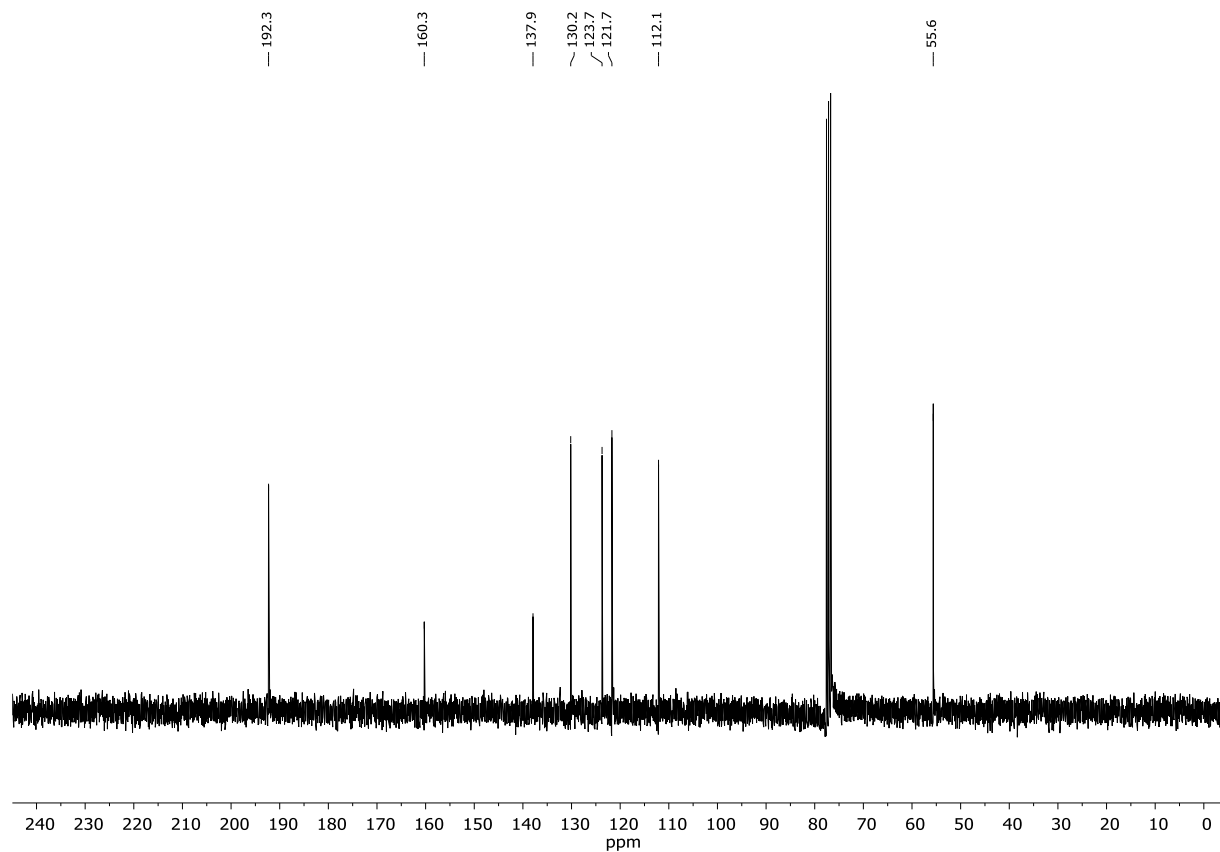
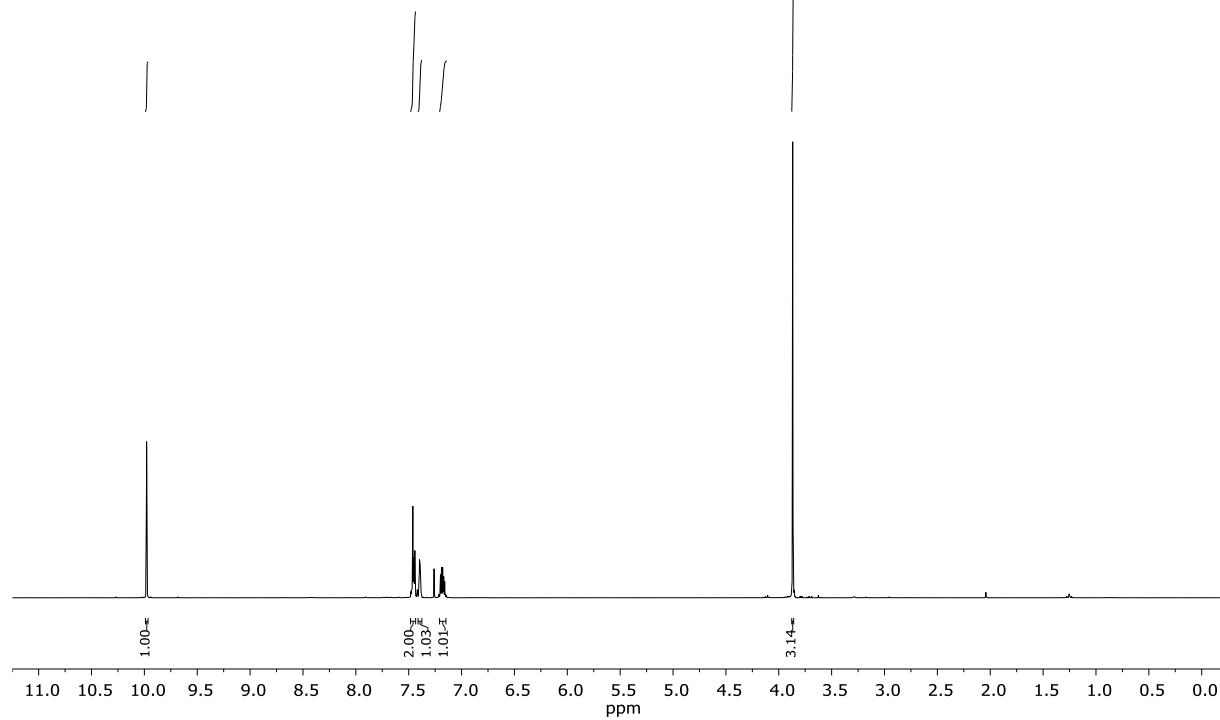
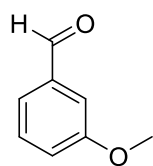
This chapter contains copies of all NMR spectra, as well as detailed data for X-ray analysis.

6.1 NMR Spectra for Chapter 2

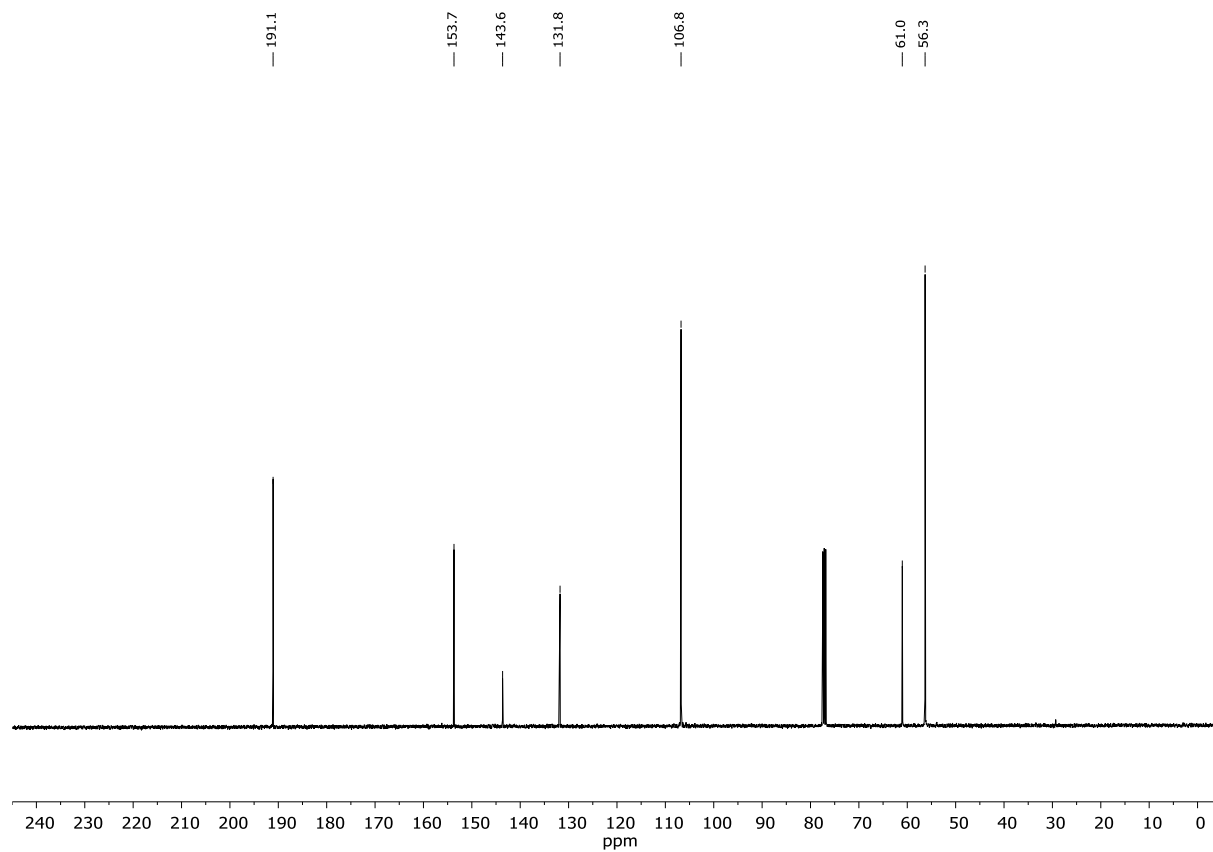
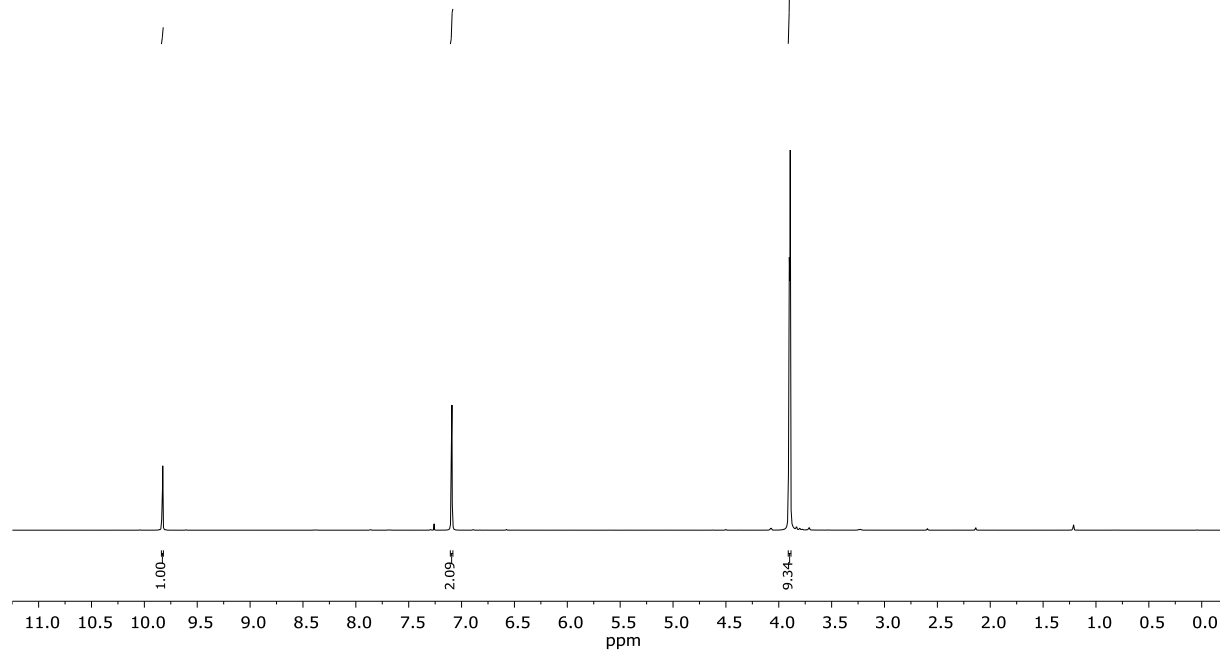
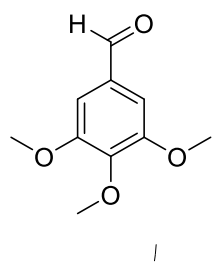
4-methoxybenzaldehyde (4a)



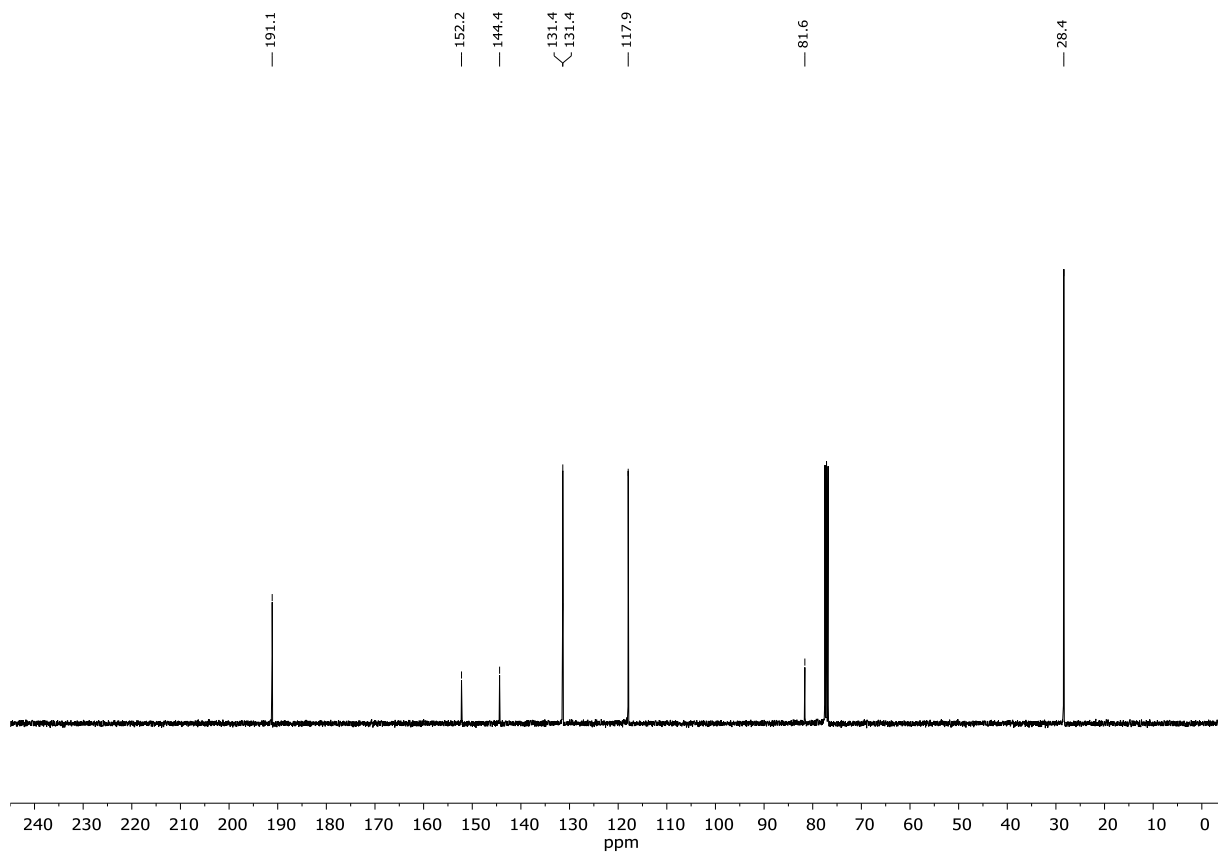
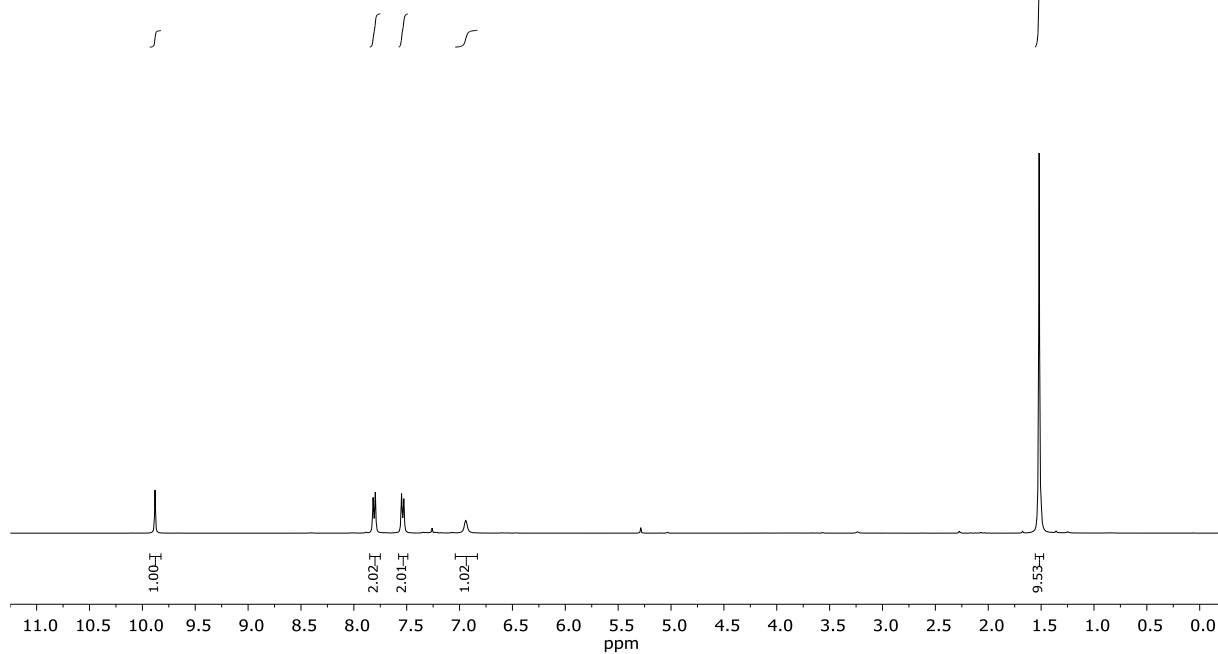
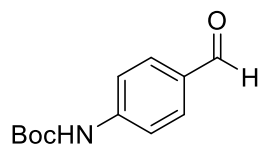
First image: $^1\text{H-NMR}$; Second image: $^{13}\text{C-NMR}$; NMR solvent: CDCl_3

3-methoxybenzaldehyde (4b)

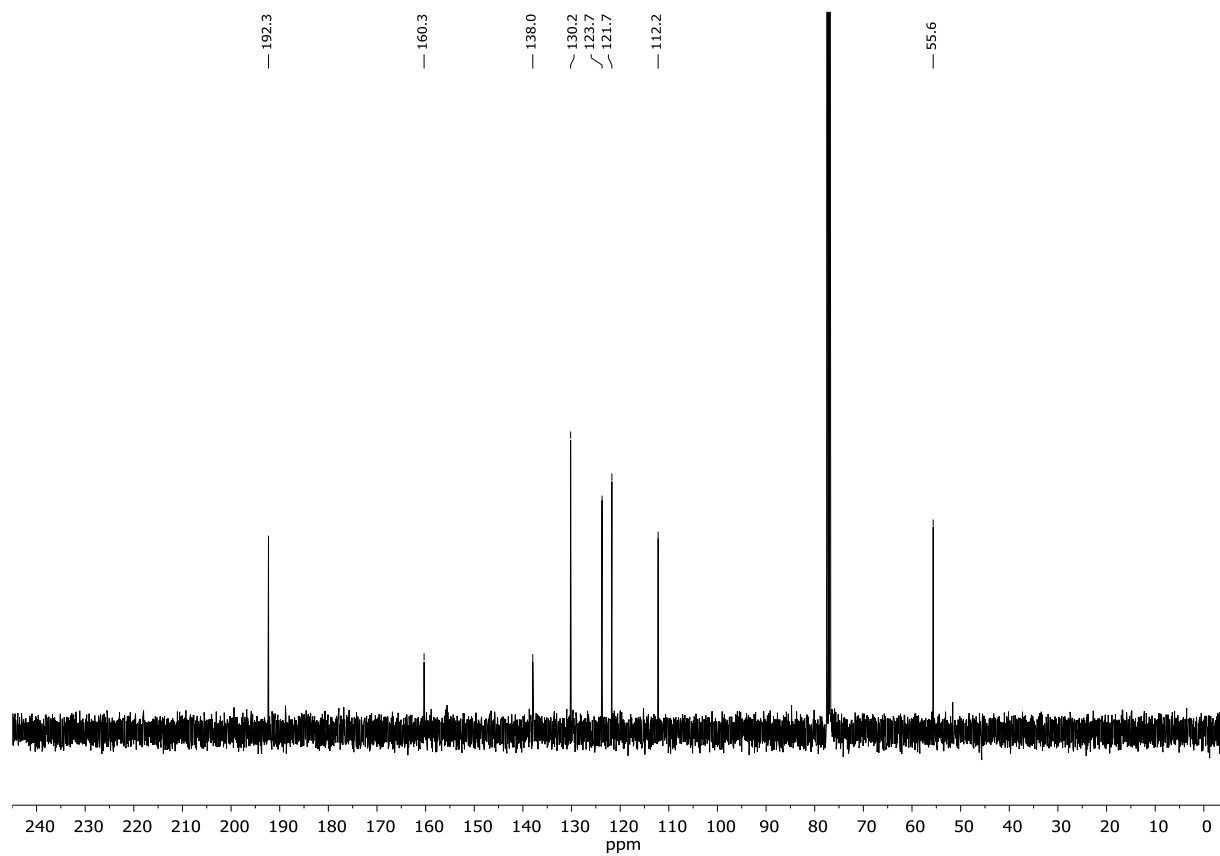
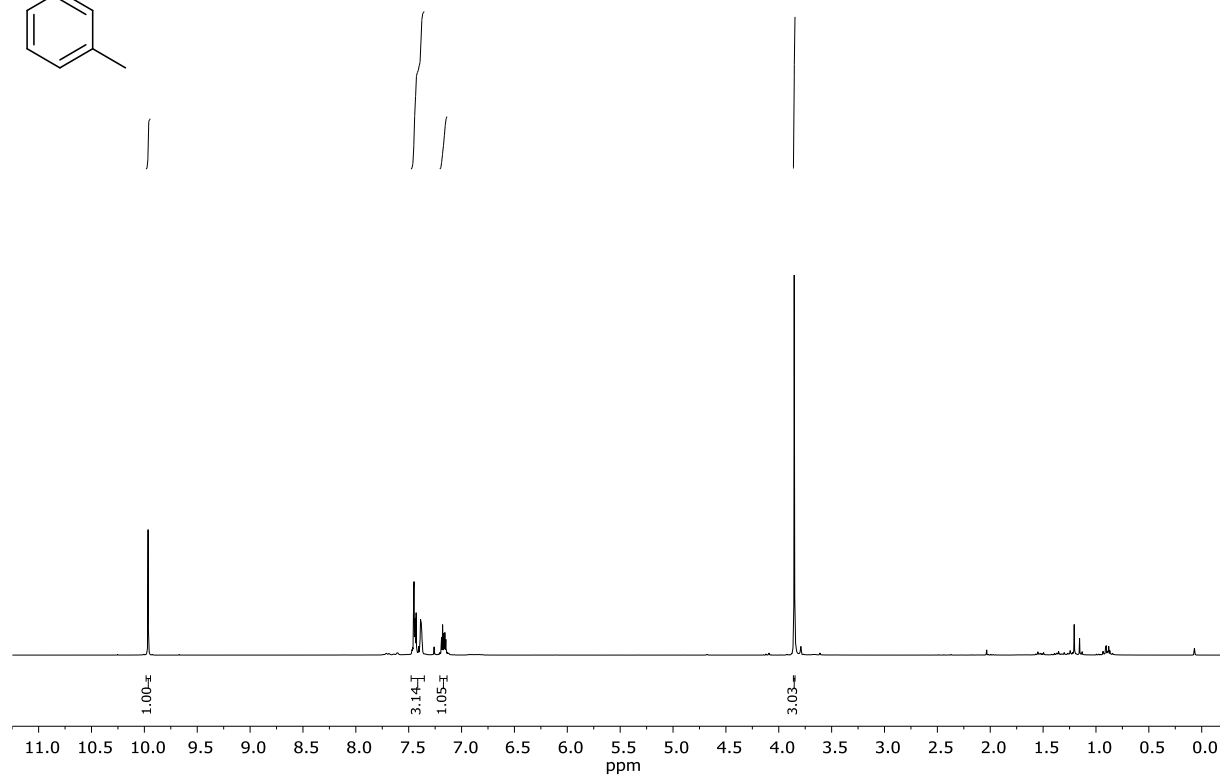
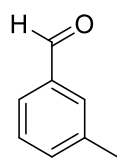
First image: $^1\text{H-NMR}$; Second image: $^{13}\text{C-NMR}$; NMR solvent: CDCl_3

3,4,5-trimethoxybenzaldehyde (4c)

First image: $^1\text{H-NMR}$; Second image: $^{13}\text{C-NMR}$; NMR solvent: CDCl_3

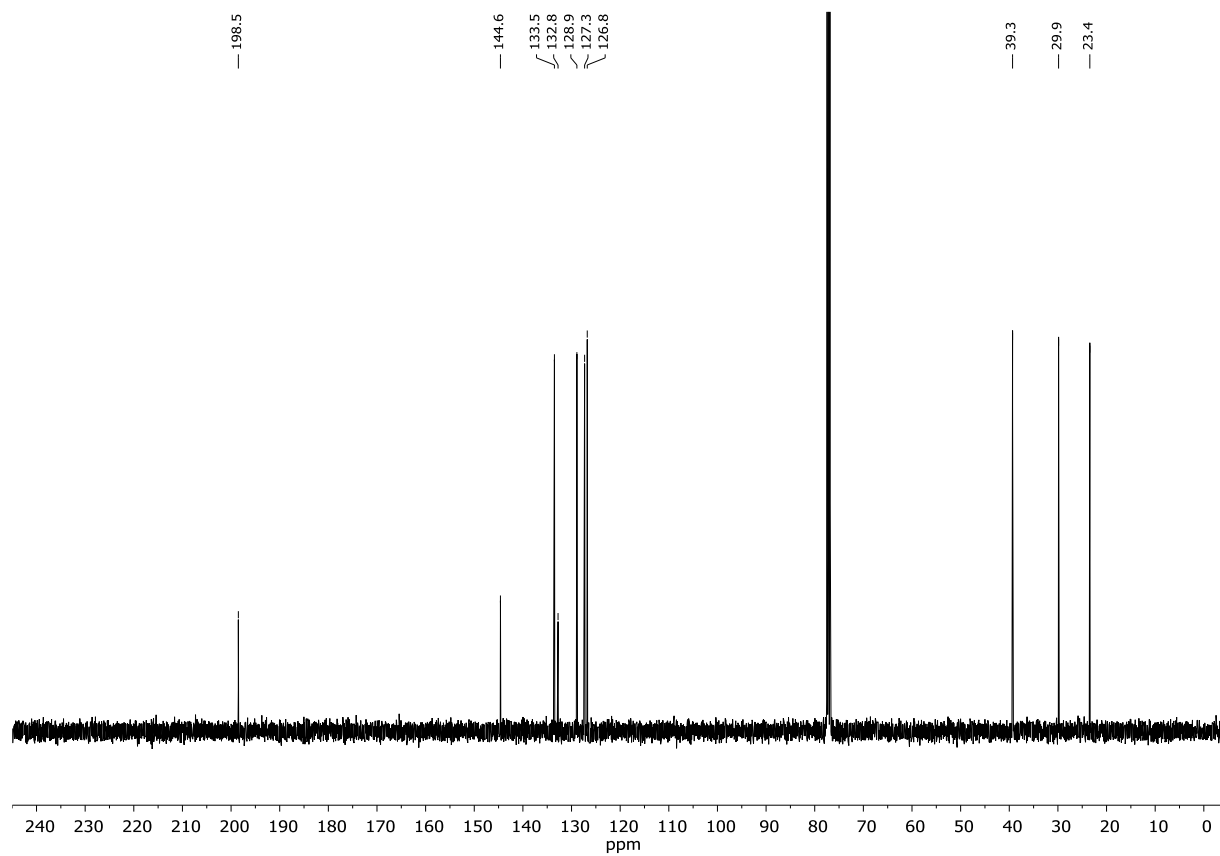
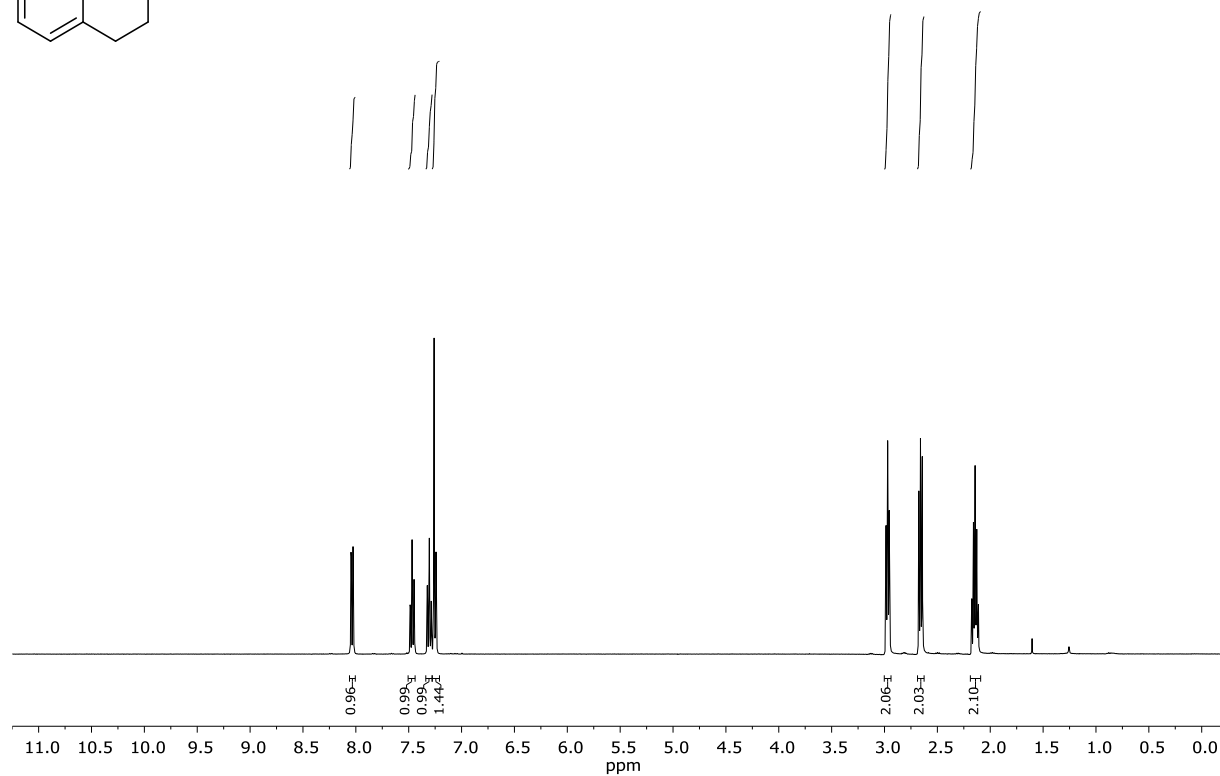
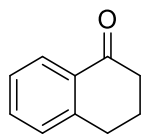
tert-butyl (4-formylphenyl)carbamate (4d)

First image: $^1\text{H-NMR}$; Second image: $^{13}\text{C-NMR}$; NMR solvent: CDCl_3

3-methylbenzaldehyde (4e)

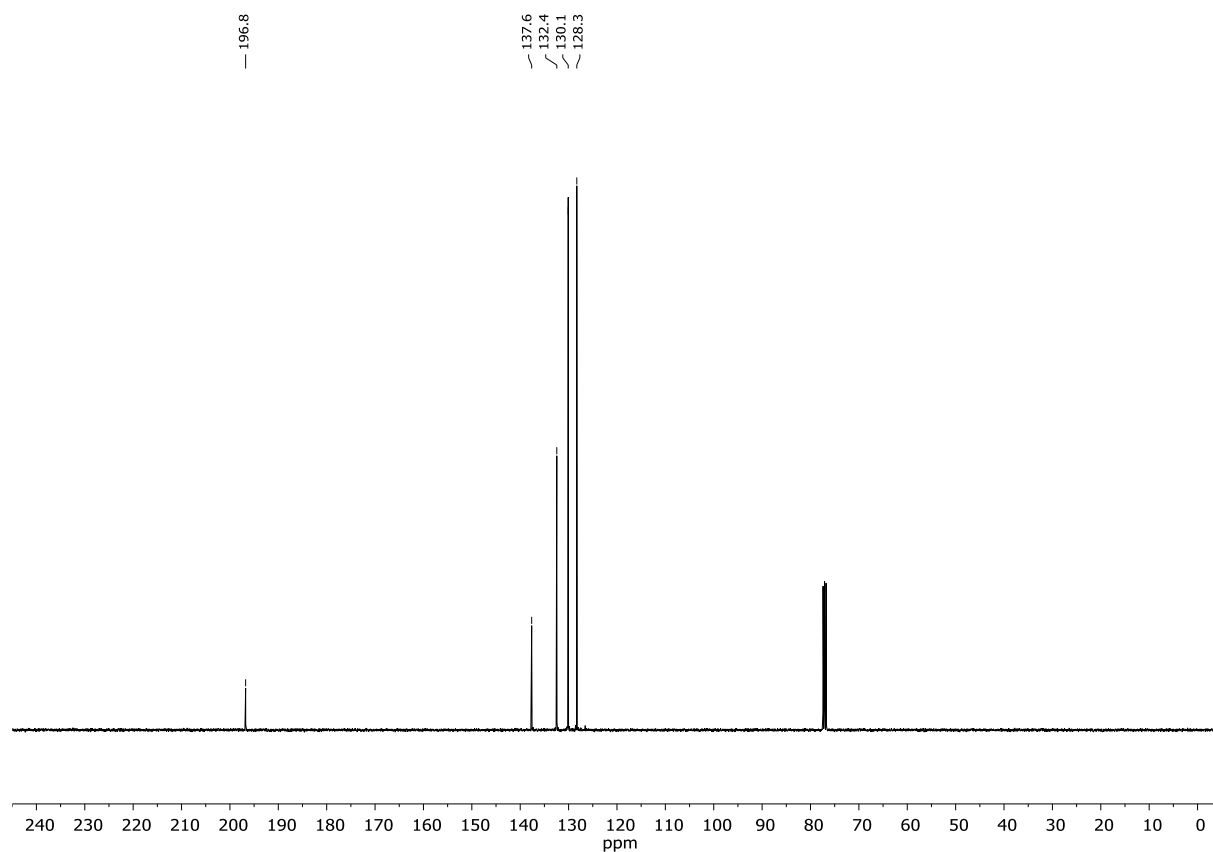
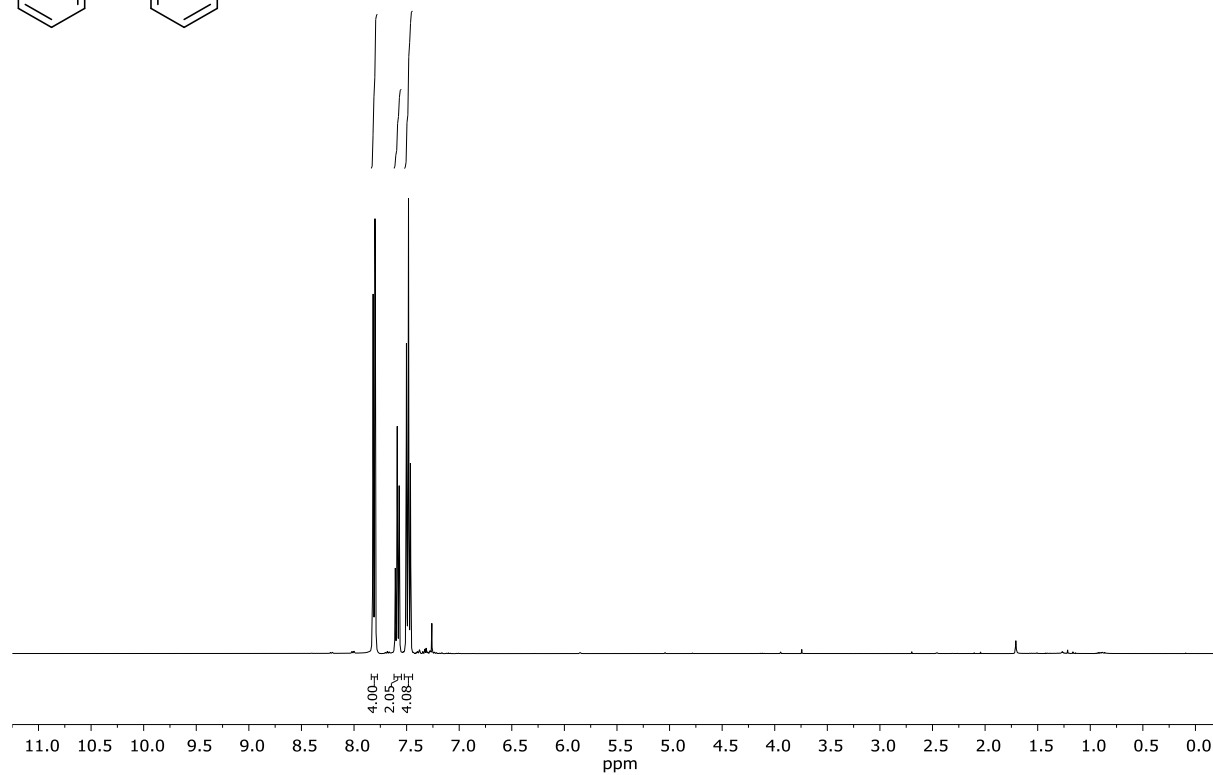
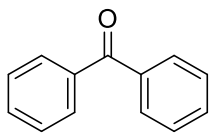
First image: ¹H-NMR; Second image: ¹³C-NMR; NMR solvent: CDCl₃

3,4-dihydronaphthalen-1(2H)-one (4h)

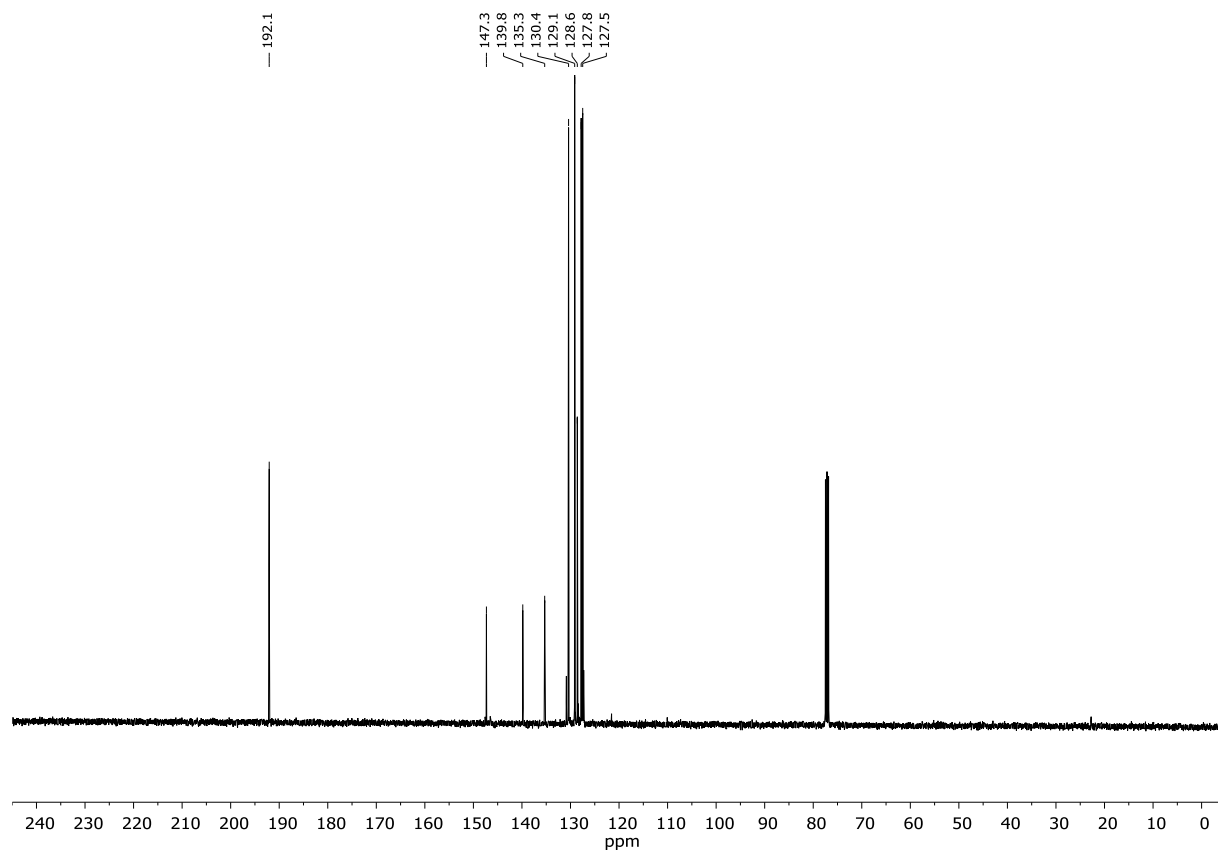
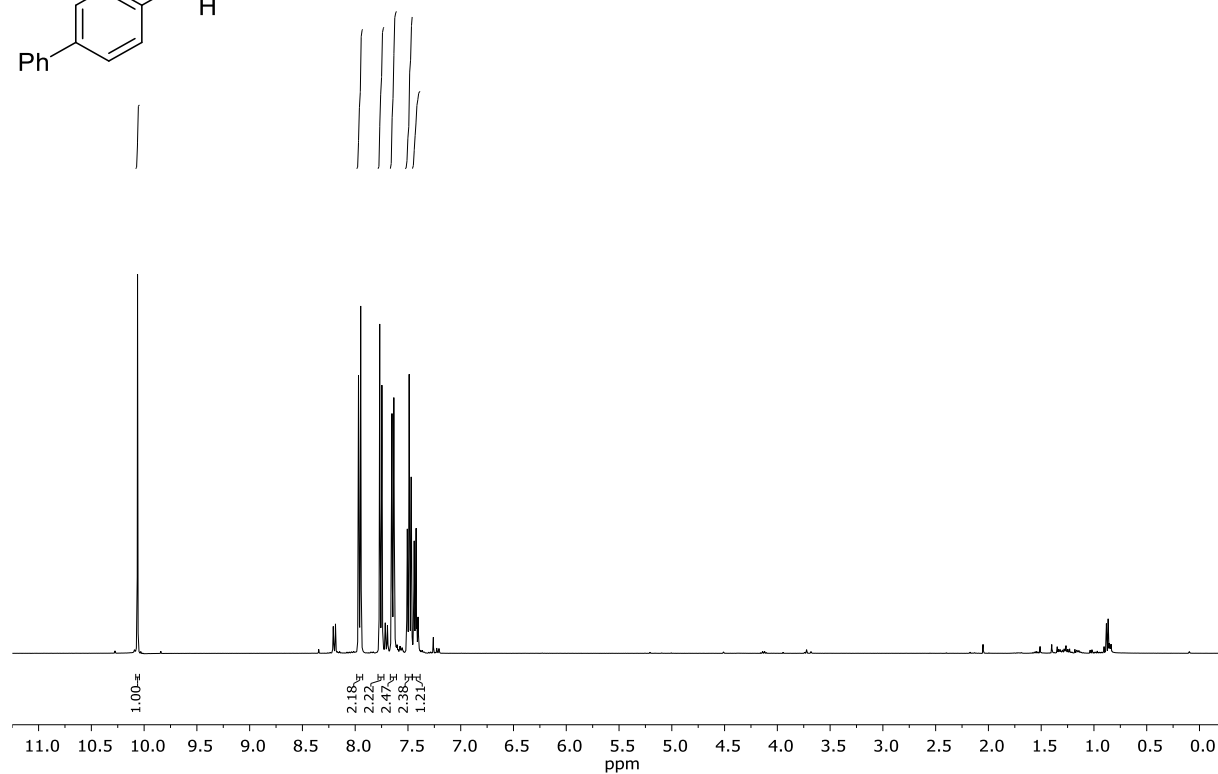
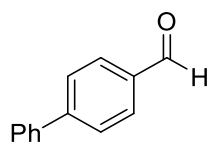


First image: ¹H-NMR; Second image: ¹³C-NMR; NMR solvent: CDCl₃

benzophenone (4i)

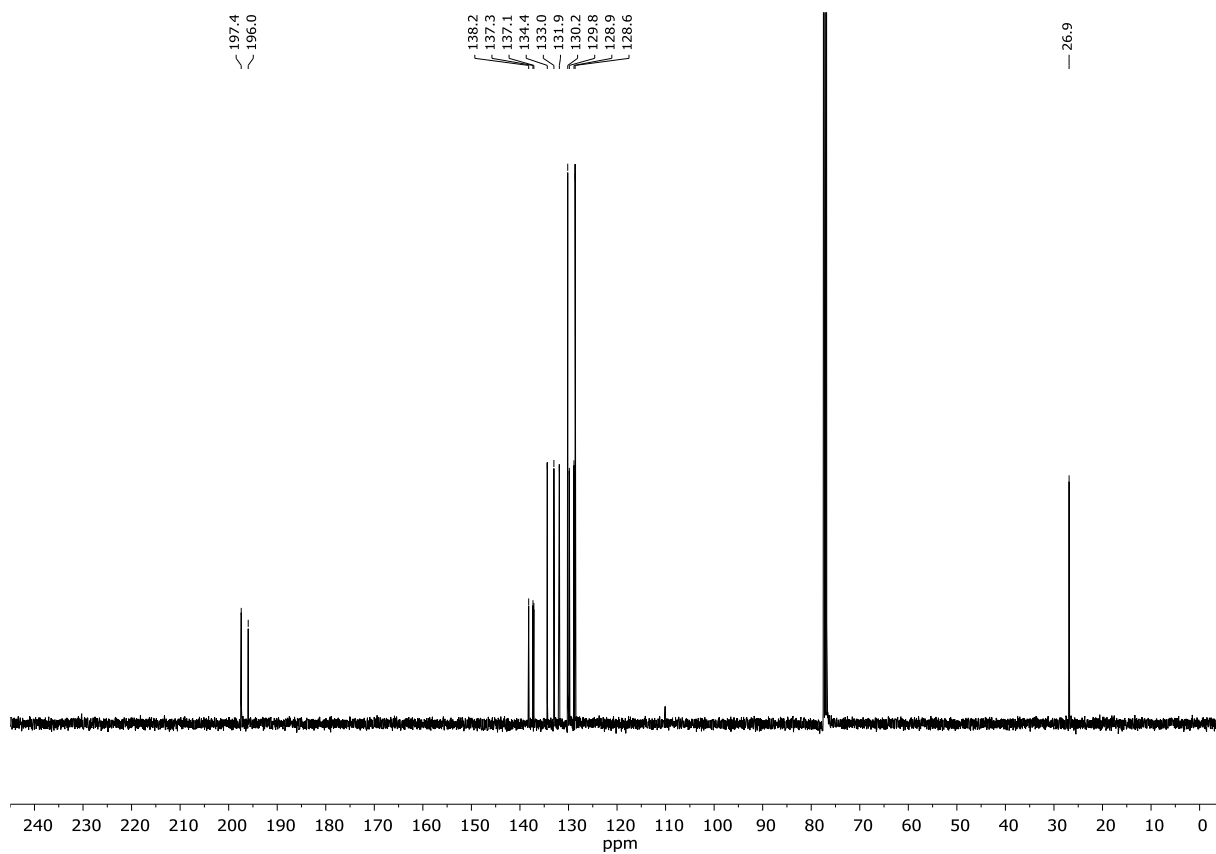
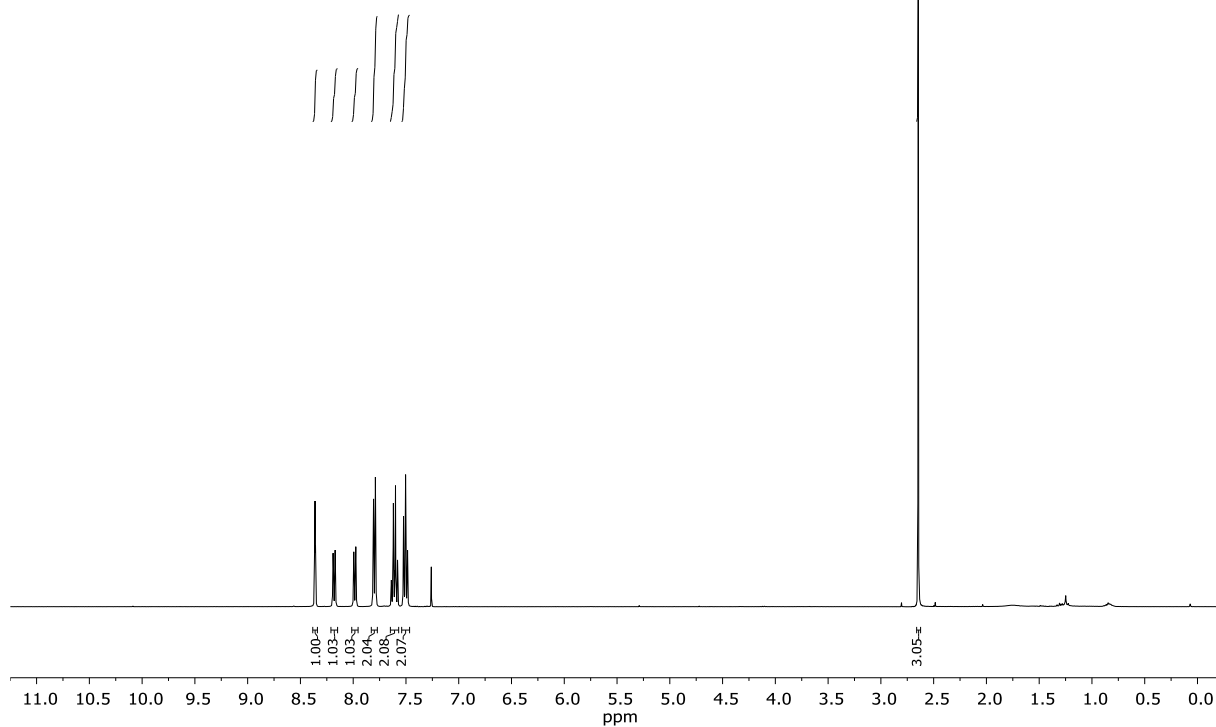
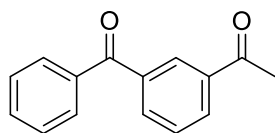


First image: $^1\text{H-NMR}$; Second image: $^{13}\text{C-NMR}$; NMR solvent: CDCl_3

[1,1'-biphenyl]-4-carbaldehyde (4j)

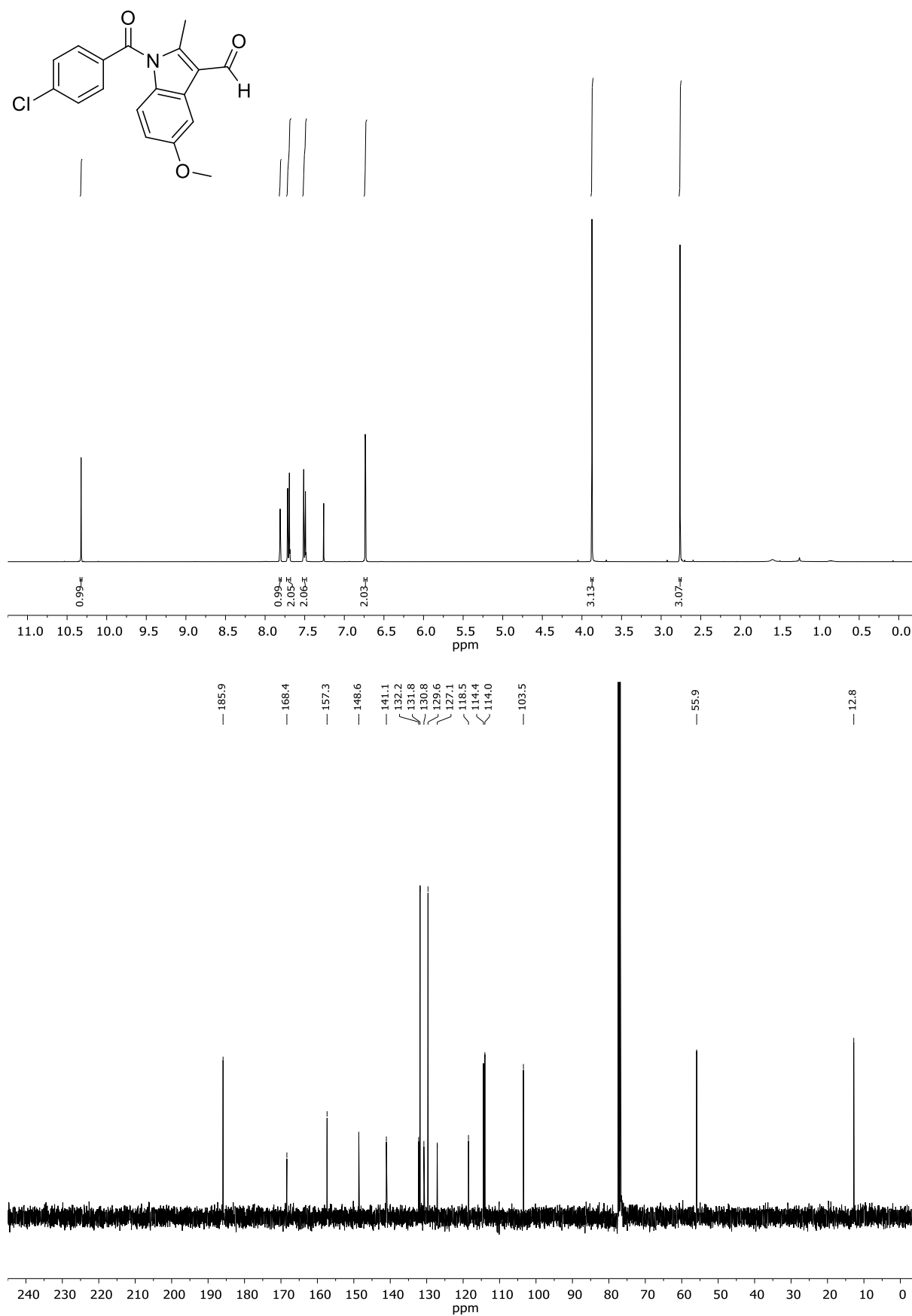
First image: $^1\text{H-NMR}$; Second image: $^{13}\text{C-NMR}$; NMR solvent: CDCl_3

1-(3-benzoylphenyl)ethan-1-one (4k)



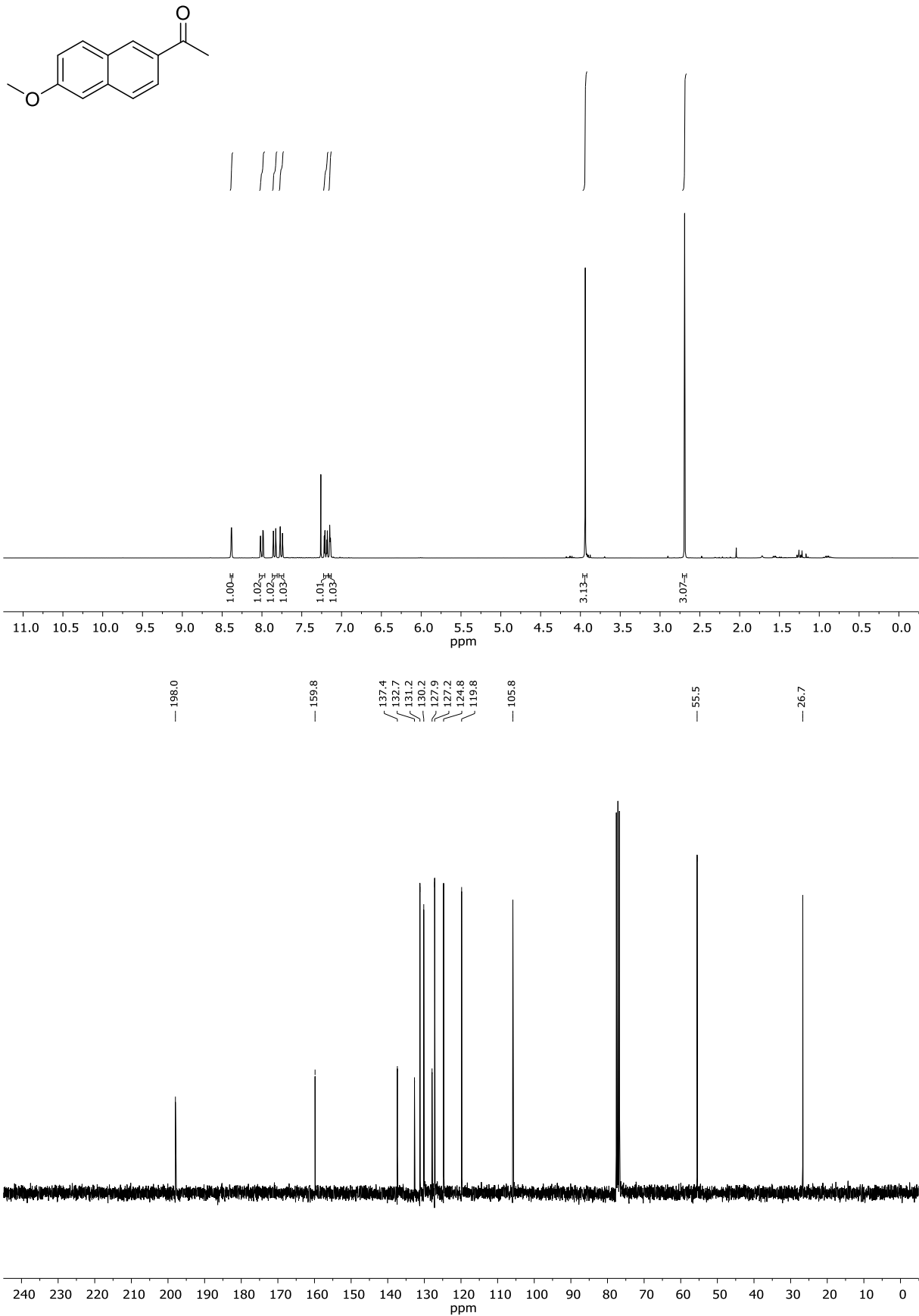
First image: ¹H-NMR; Second image: ¹³C-NMR; NMR solvent: CDCl₃

1-(4-chlorobenzoyl)-5-methoxy-2-methyl-1H-indole-3-carbaldehyde (4I)



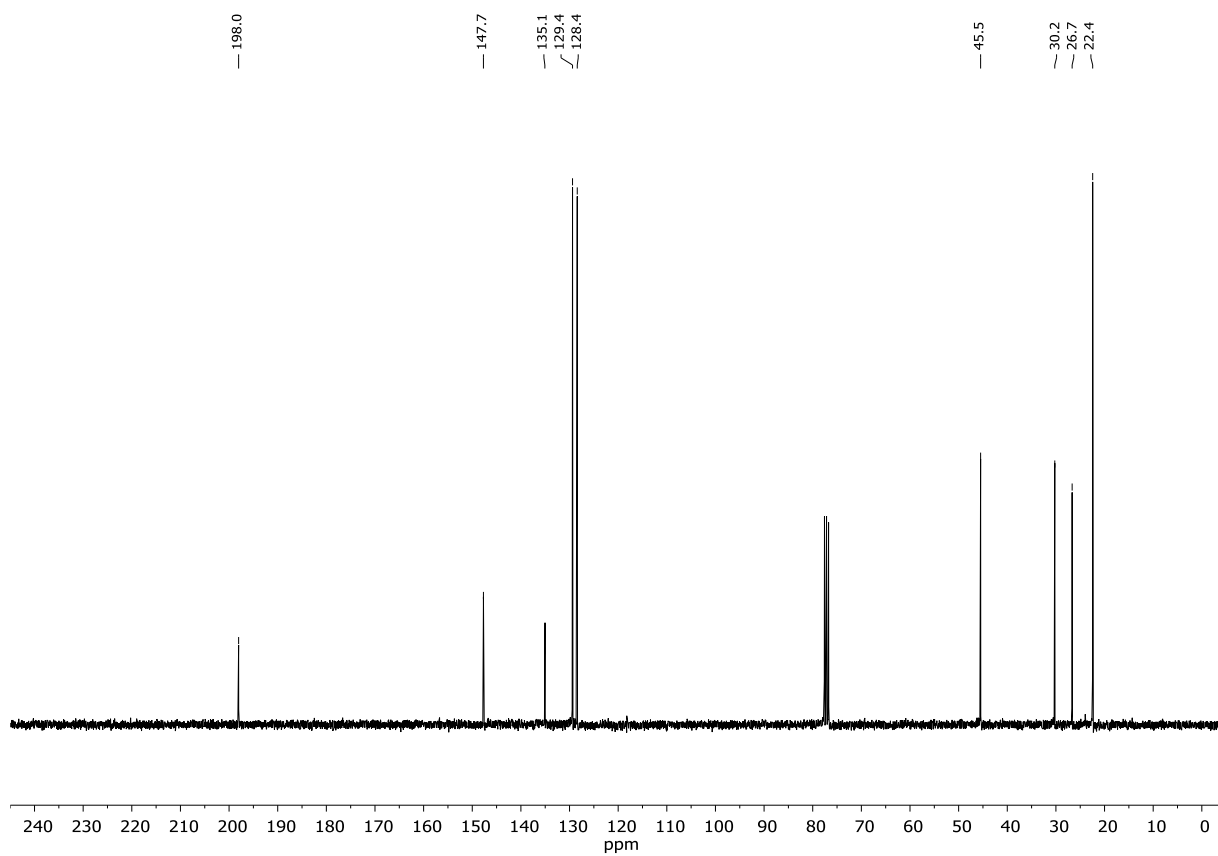
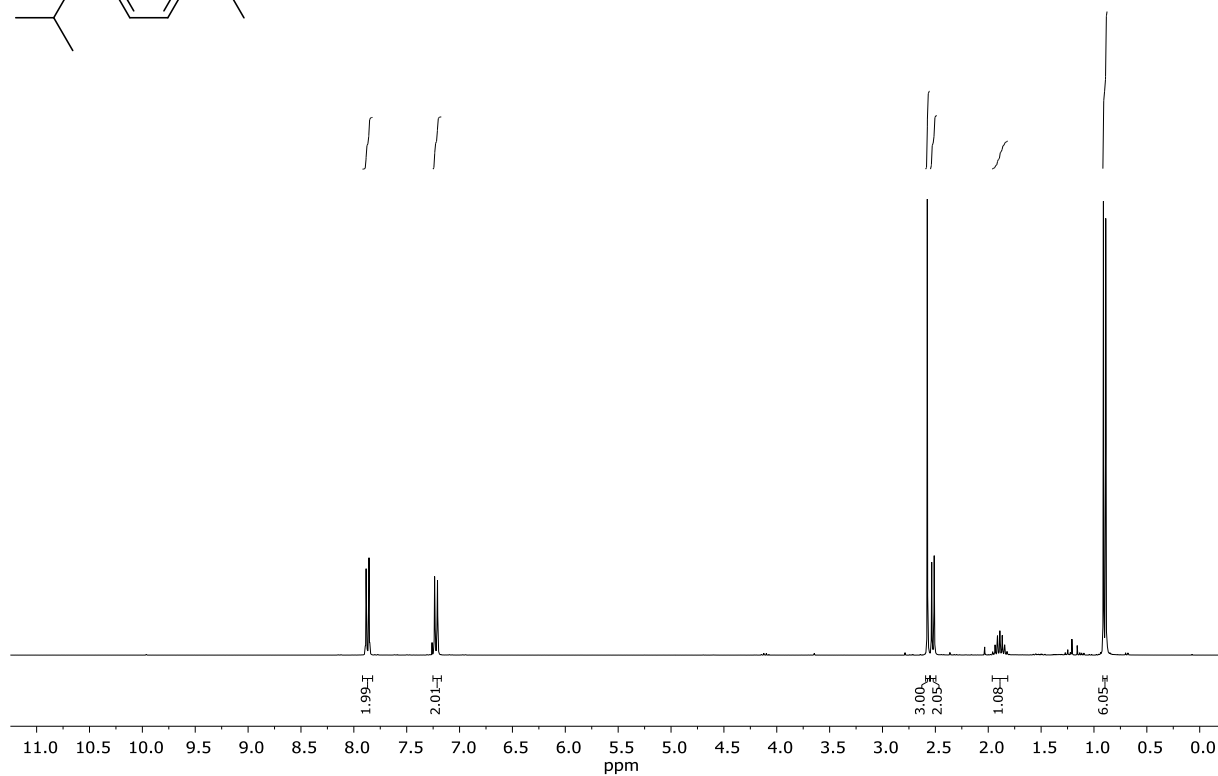
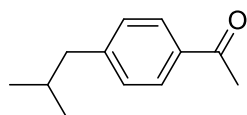
First image: ¹H-NMR; Second image: ¹³C-NMR; NMR solvent: CDCl₃

1-(6-methoxynaphthalen-2-yl)ethan-1-one/ naproxene (4m)

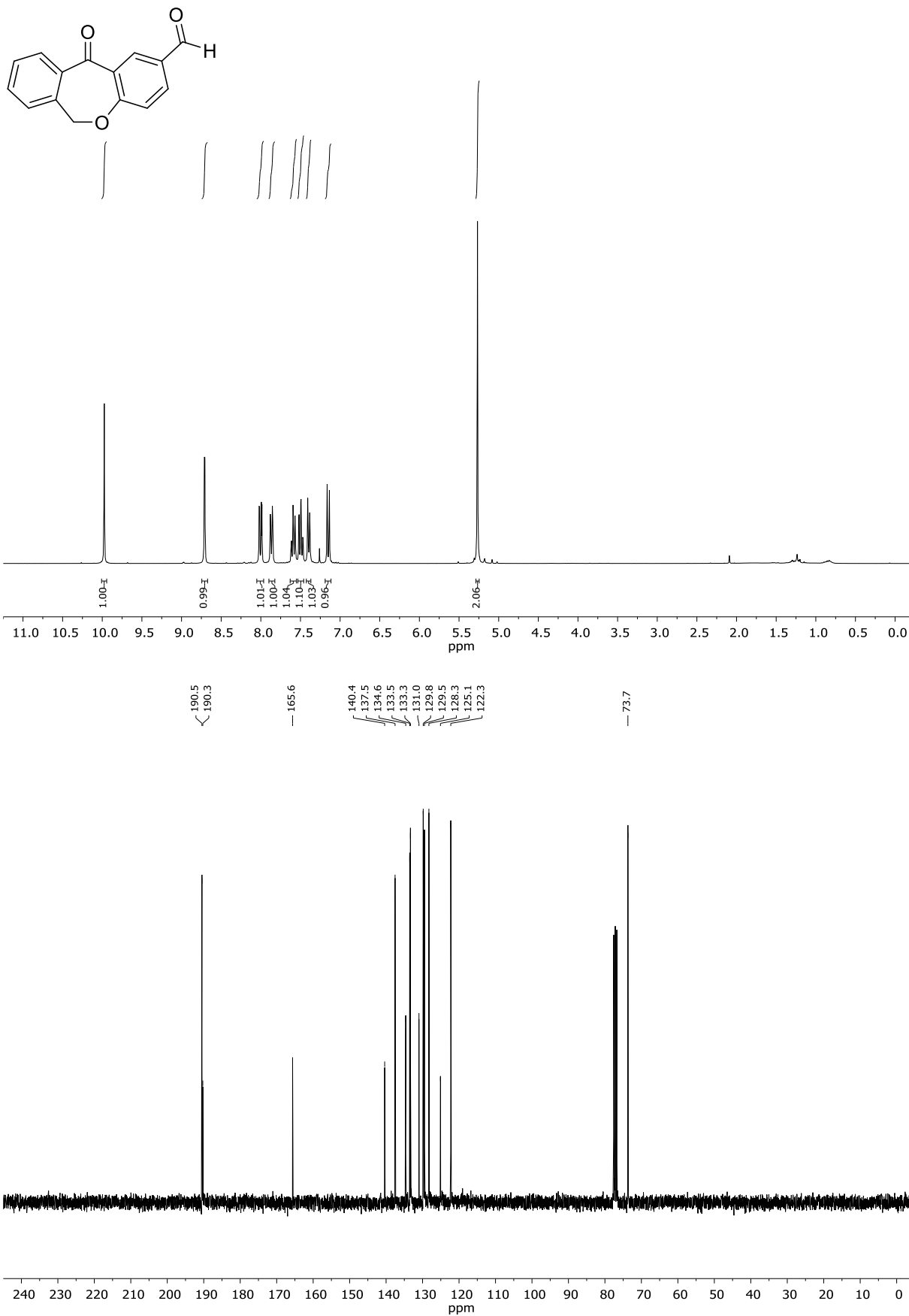


First image: ¹H-NMR; Second image: ¹³C-NMR; NMR solvent: CDCl₃

1-(4-isobutylphenyl)ethan-1-one (4n)

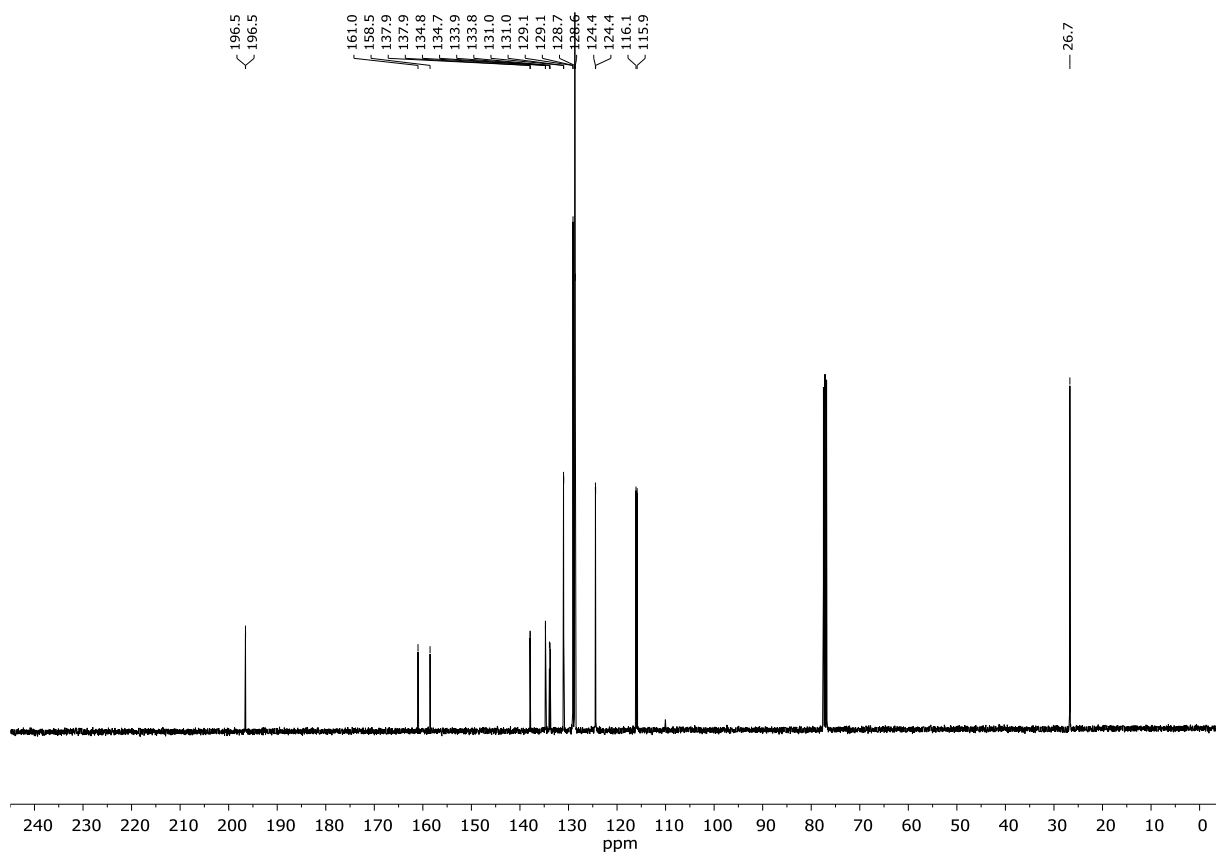
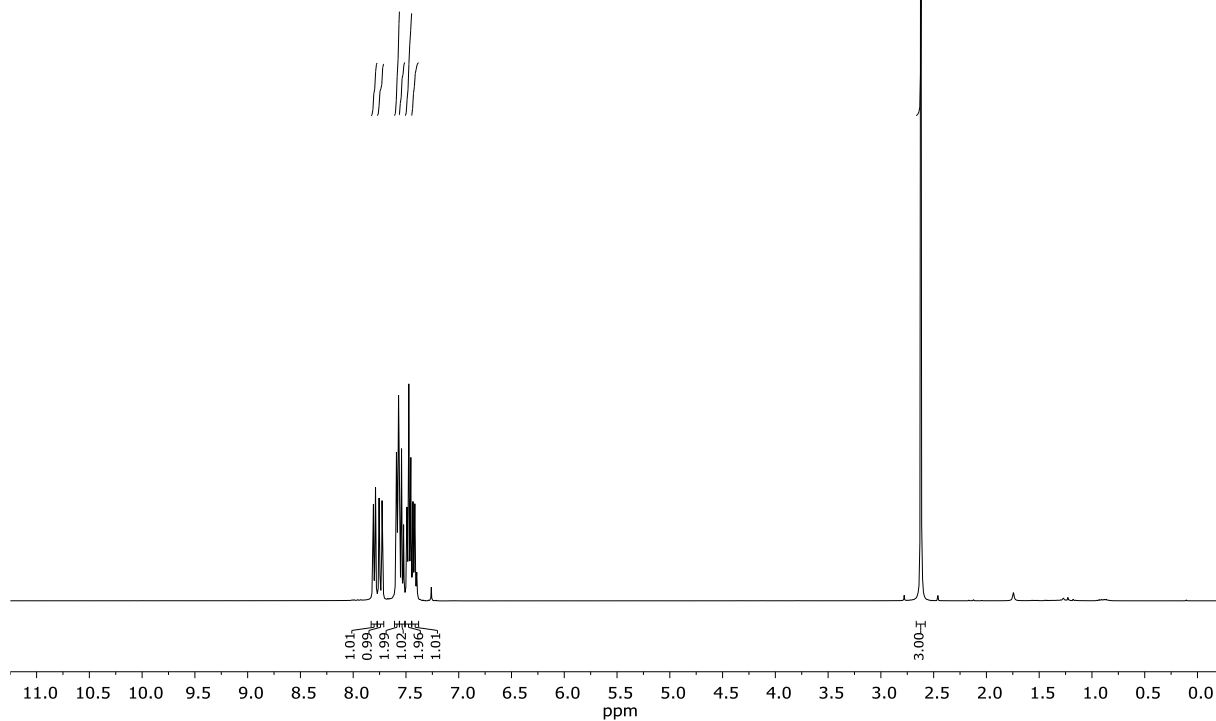
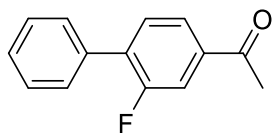


First image: $^1\text{H-NMR}$; Second image: $^{13}\text{C-NMR}$; NMR solvent: CDCl_3

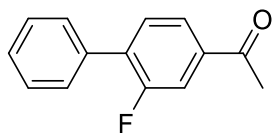
11-oxo-6,11-dihydrodibenzo[b,e]oxepine-2-carbaldehyde (4o)

First image: ¹H-NMR; Second image: ¹³C-NMR; NMR solvent: CDCl₃

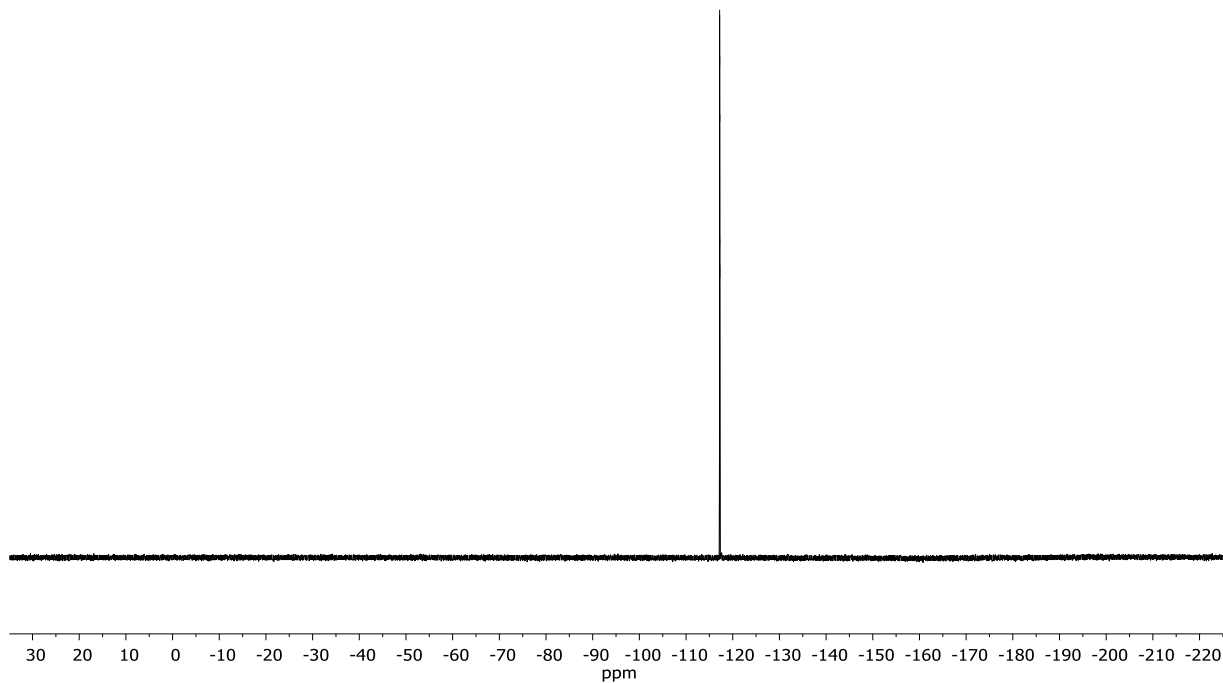
1-(2-fluoro-[1,1'-biphenyl]-4-yl)ethan-1-one (4p)



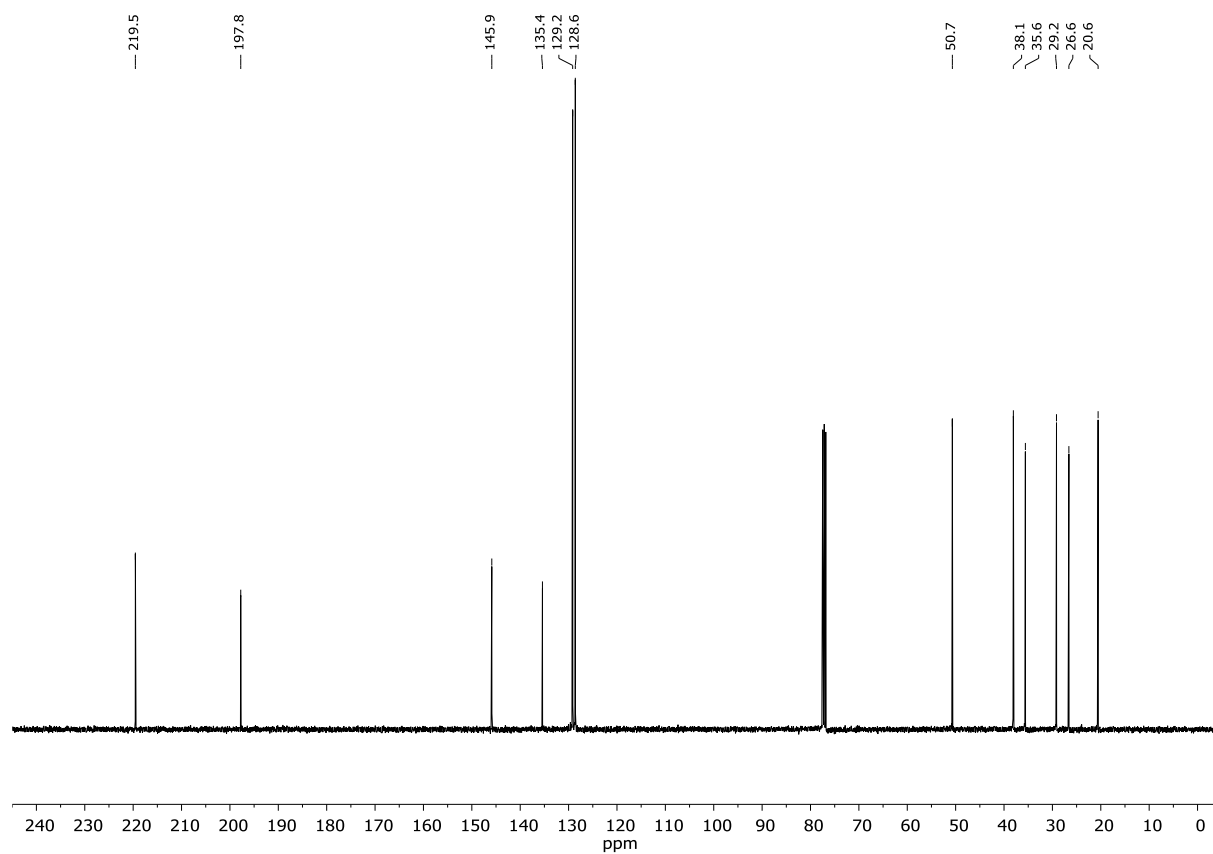
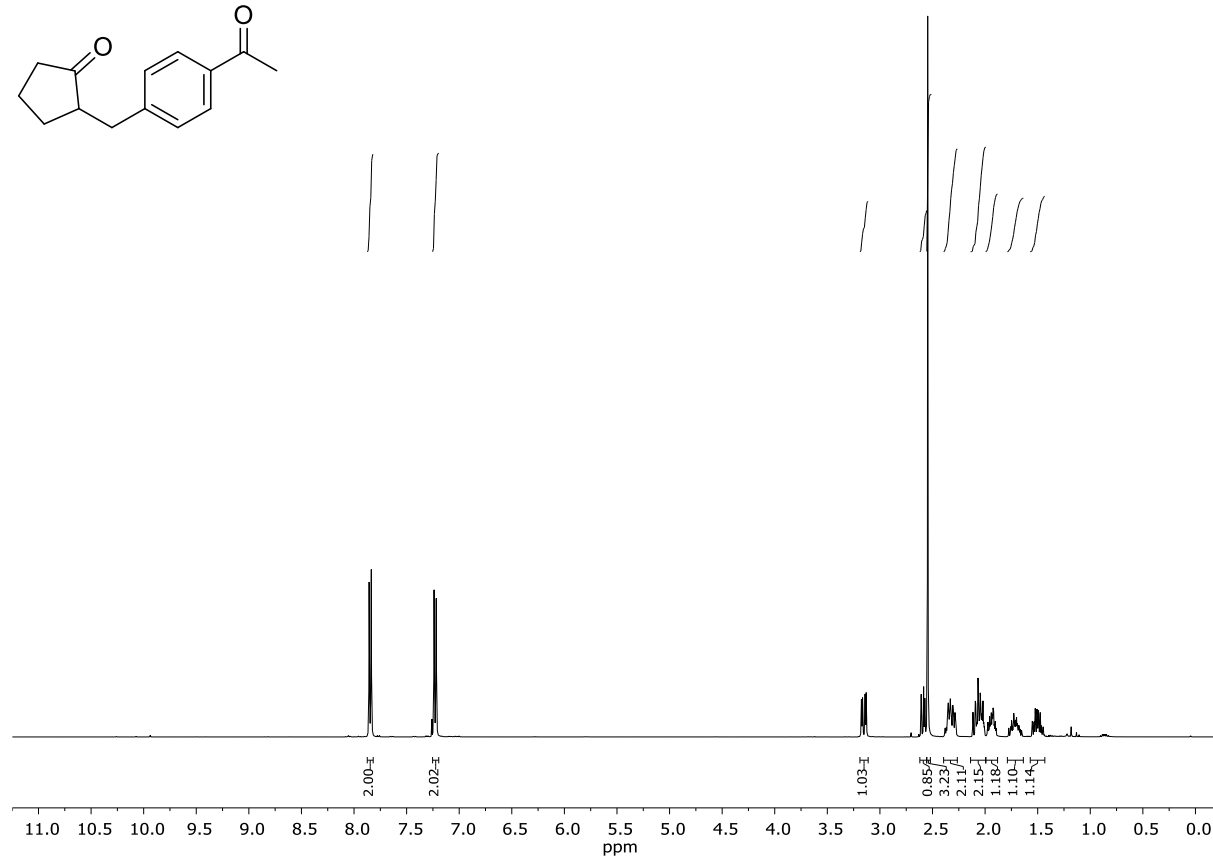
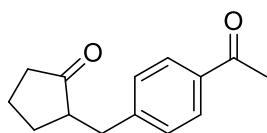
First image: $^1\text{H-NMR}$; Second image: $^{13}\text{C-NMR}$; NMR solvent: CDCl_3

1-(2-fluoro-[1,1'-biphenyl]-4-yl)ethan-1-one (4p)

-117.16
-117.17
-117.17
-117.19
-117.19
-117.20
-117.20
-117.21
-117.22

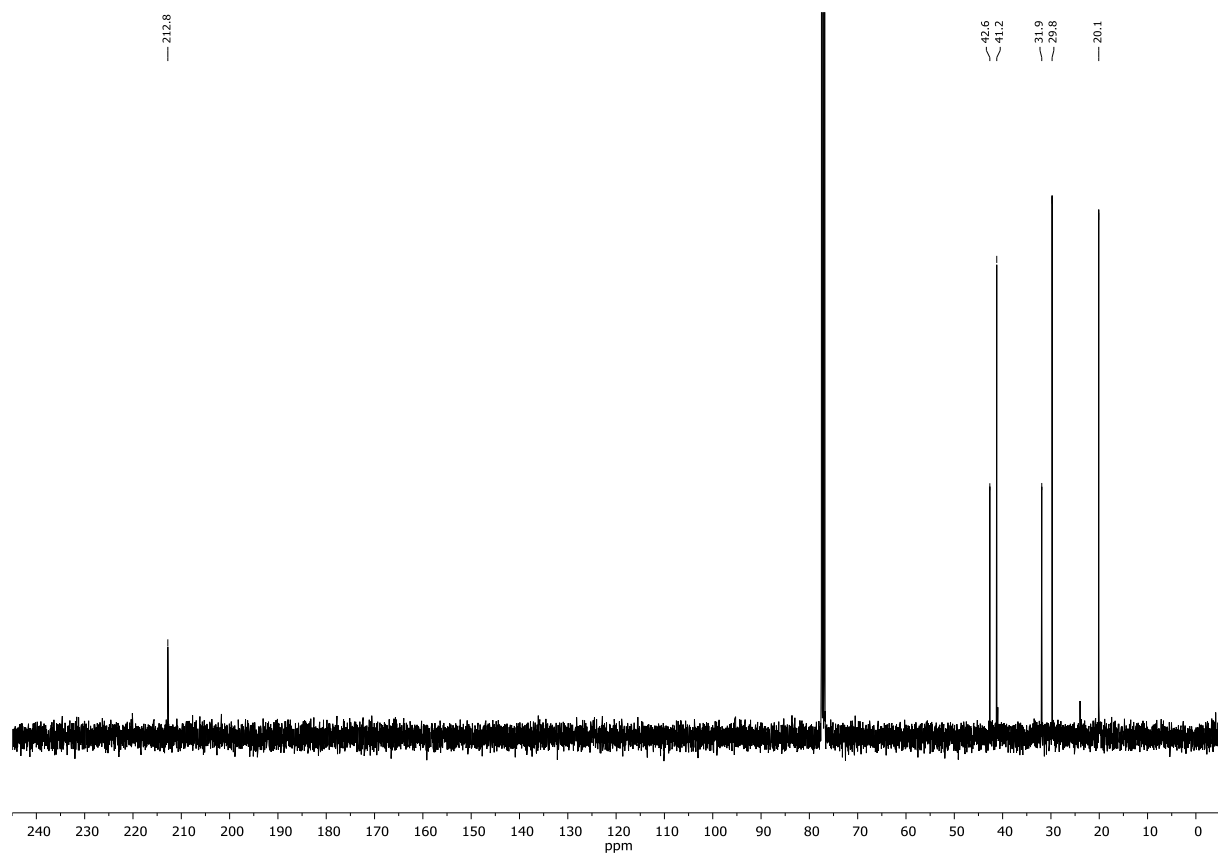
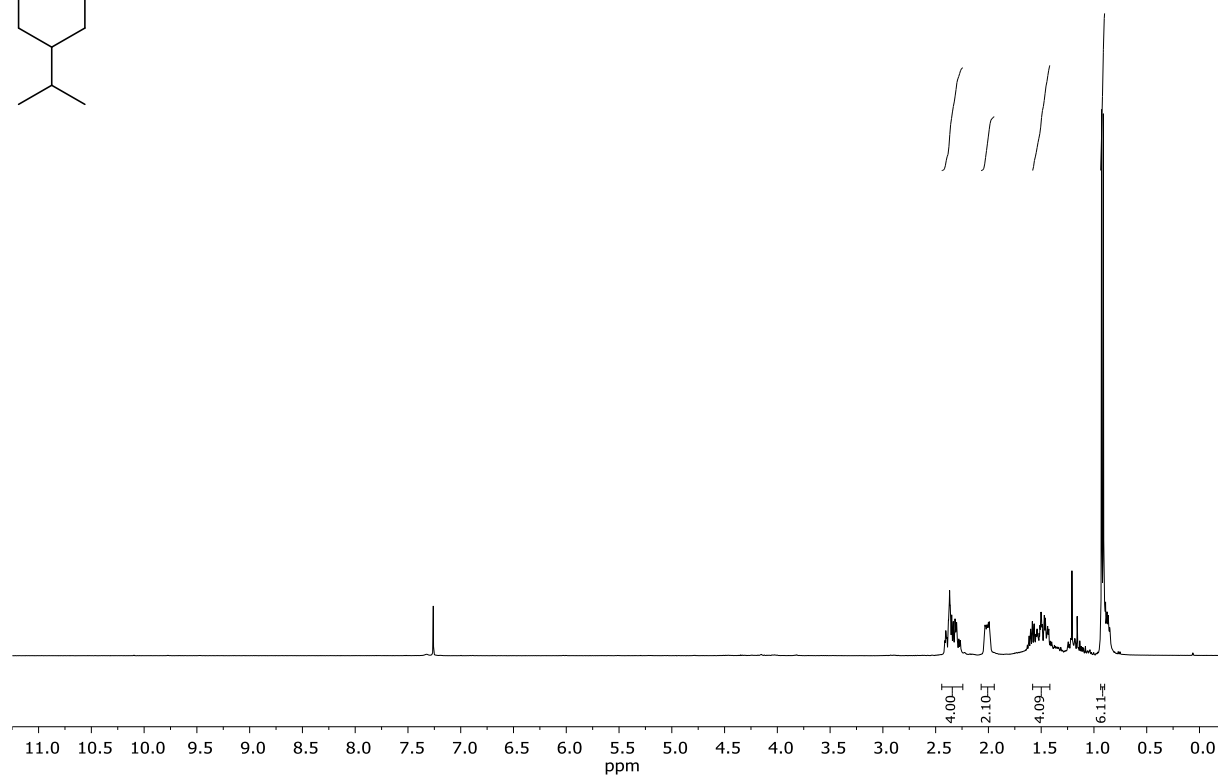
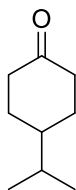


Third image: ^{19}F -NMR NMR; NMR solvent: CDCl_3

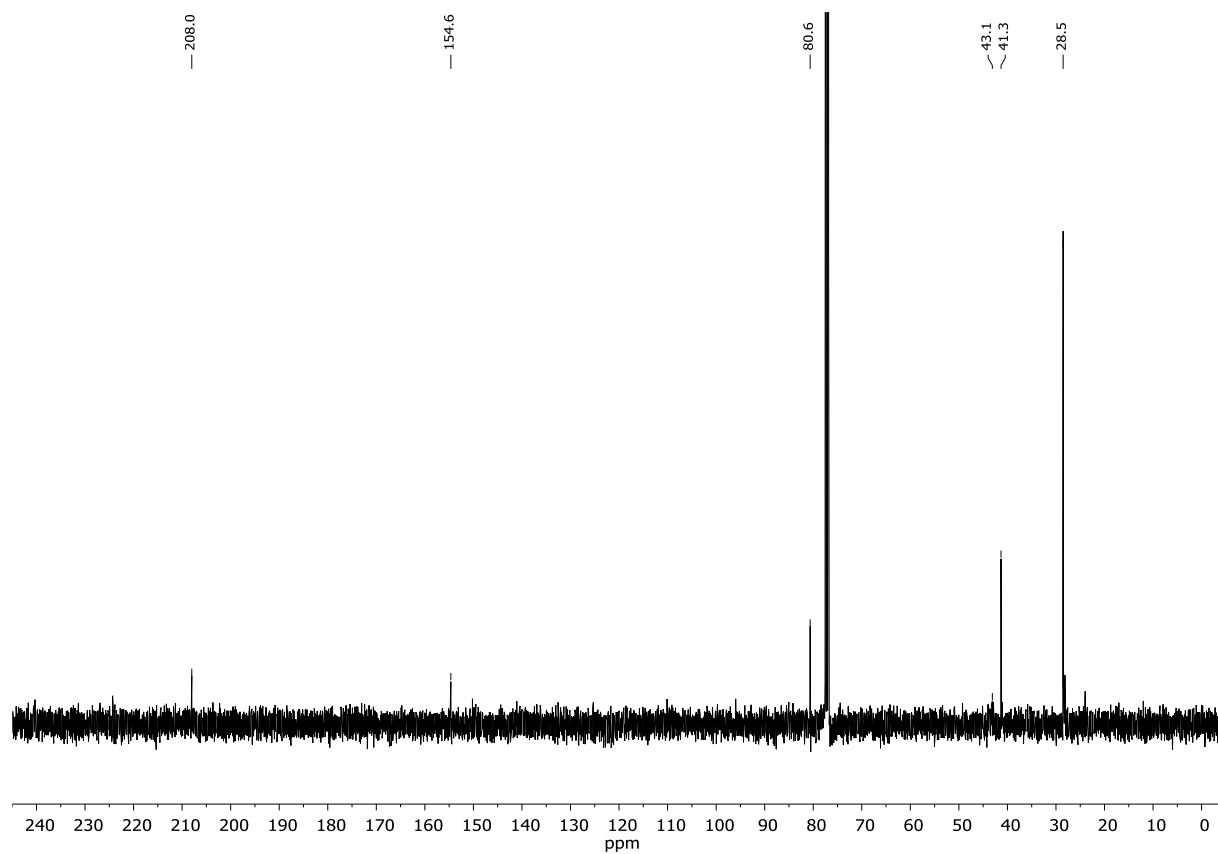
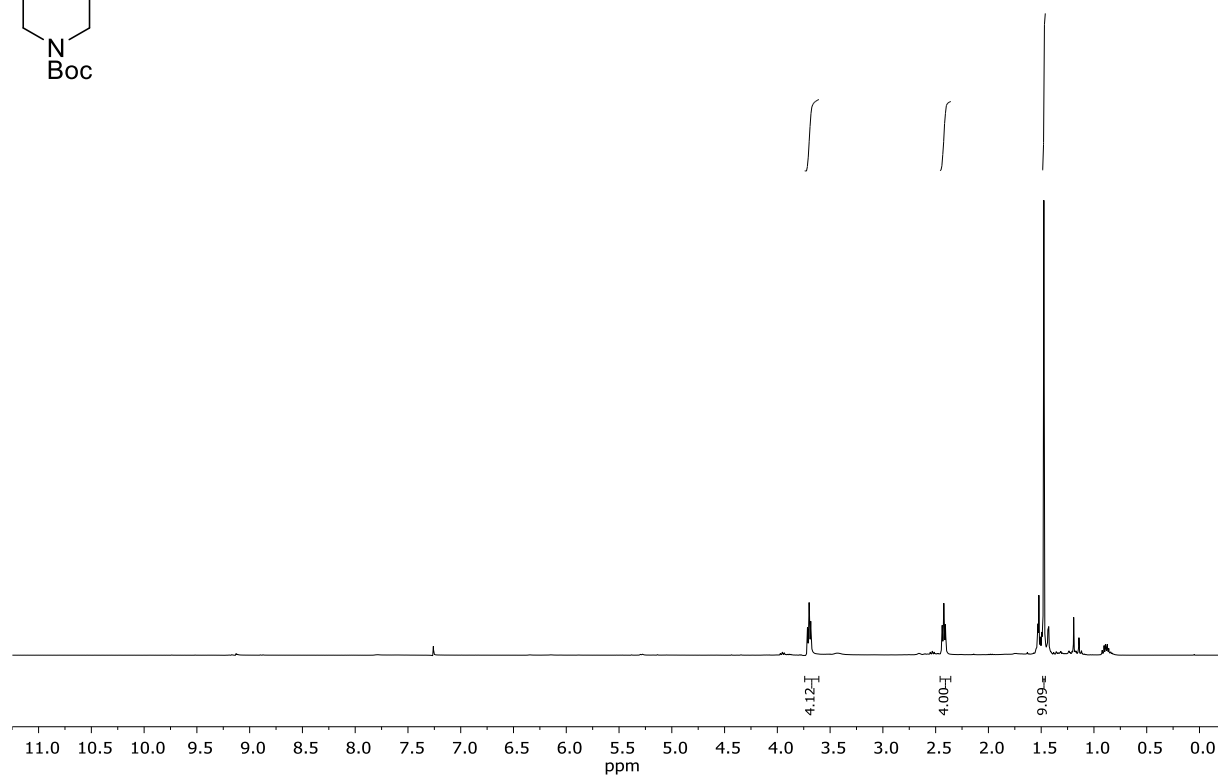
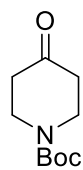
2-(4-acetylbenzyl)cyclopentan-1-one (4q)

First image: $^1\text{H-NMR}$; Second image: $^{13}\text{C-NMR}$; NMR solvent: CDCl_3

4-isopropylcyclohexan-1-one (4r)



First image: $^1\text{H-NMR}$; Second image: $^{13}\text{C-NMR}$; NMR solvent: CDCl_3

tert-butyl 4-oxopiperidine-1-carboxylate (4s)

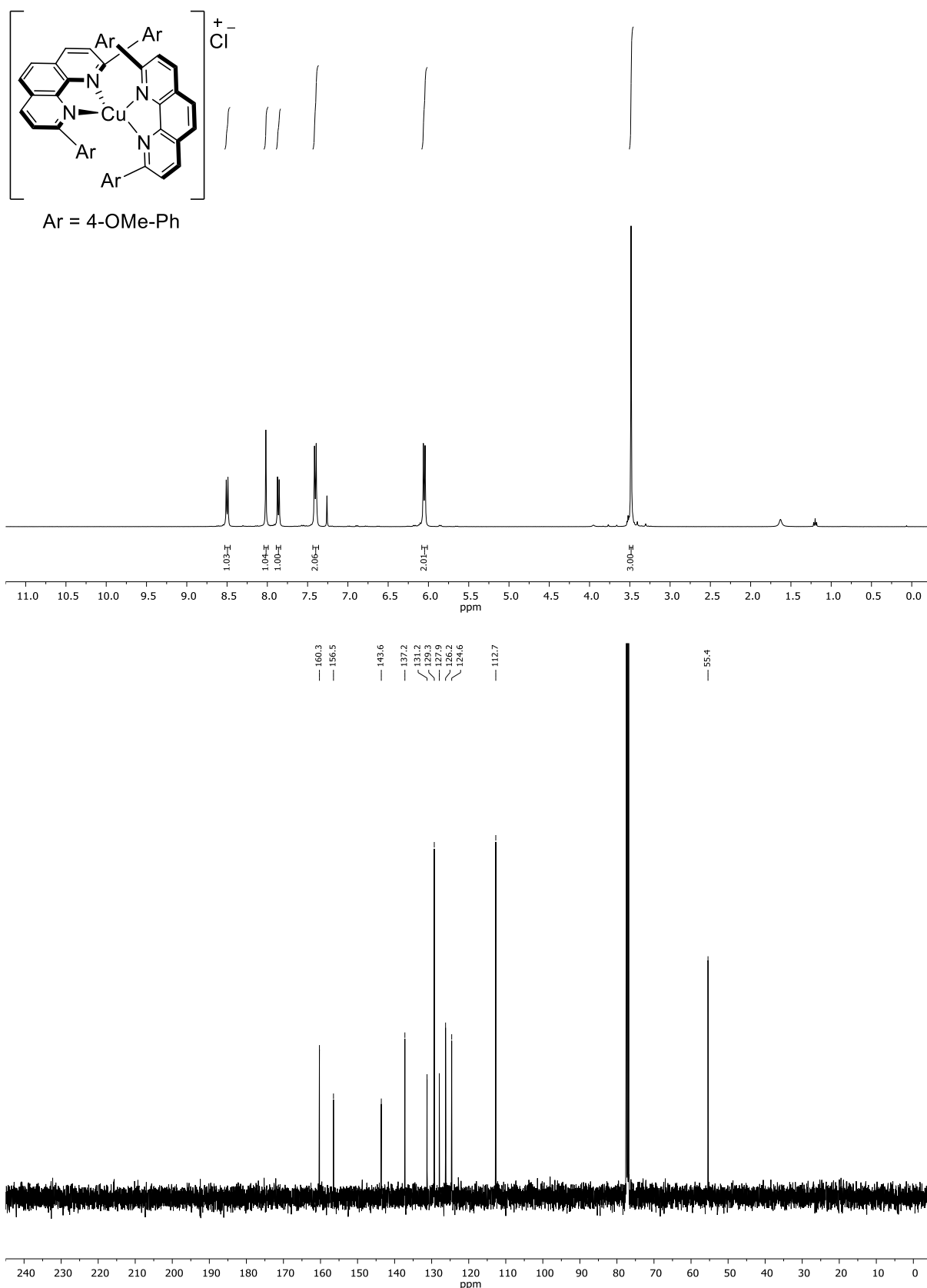
First image: $^1\text{H-NMR}$; Second image: $^{13}\text{C-NMR}$; NMR solvent: CDCl_3

6.2 Crystallographic Data for Chapter 2

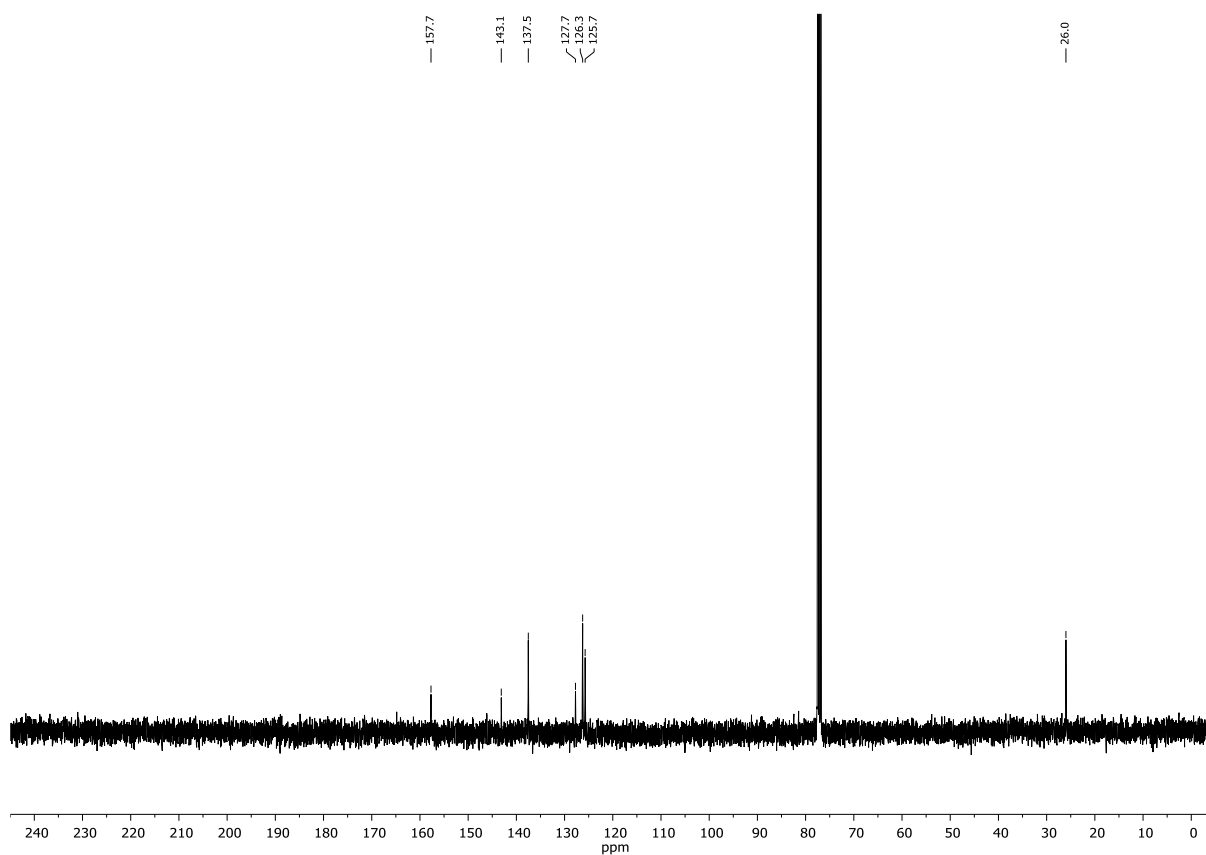
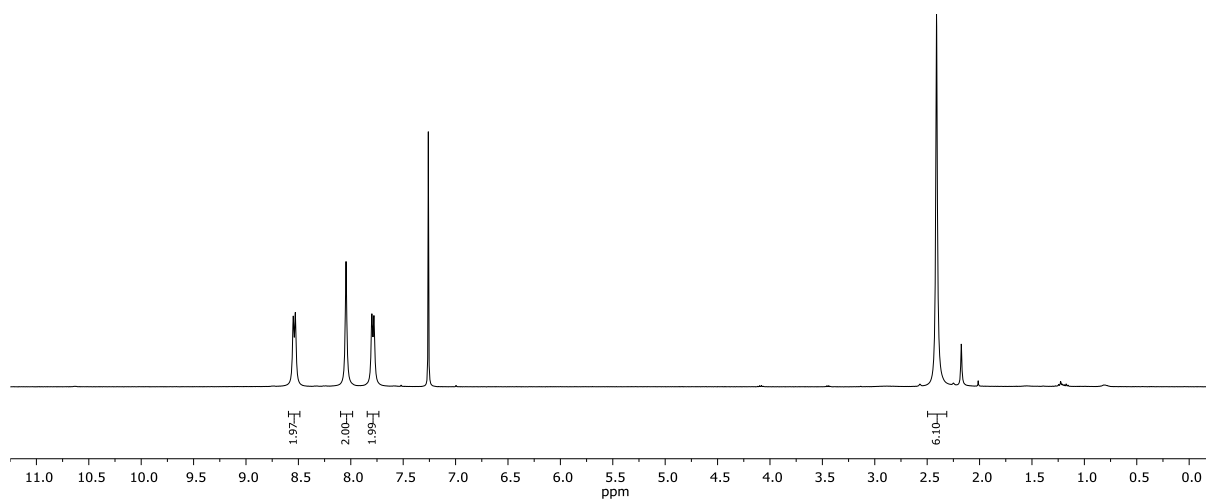
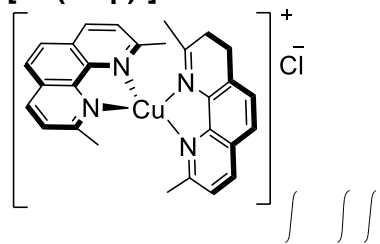
Table 1. Crystallographic Data for Chapter 2.

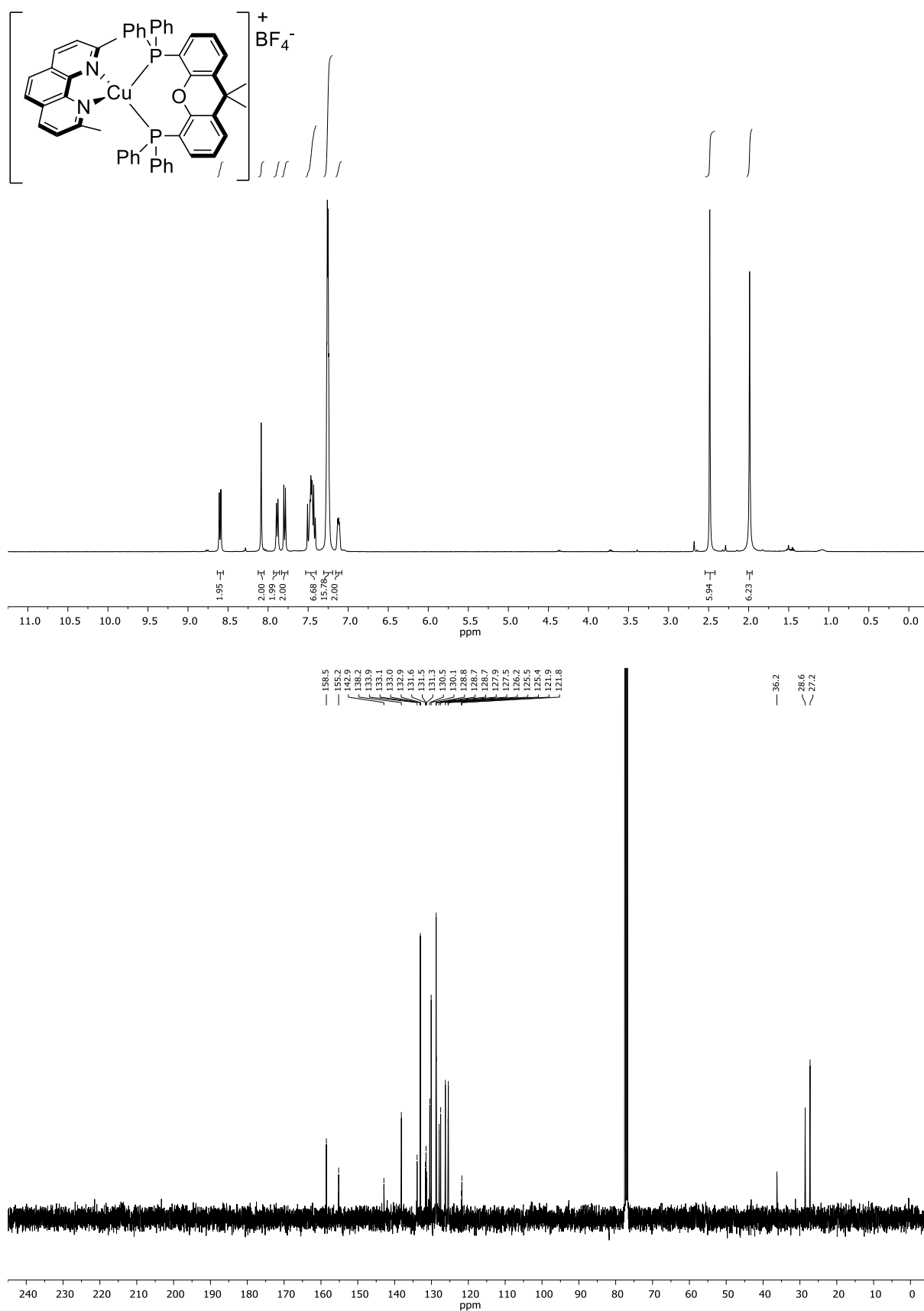
Compound	[Cu ₂ (1a) ₄ (MeCN) ₂] (2)	[Cu(dmp)(1a) ₂] (3)	Isoxepac Derivative (4o)	Indometacin Derivative (4I)
CCDC	2144482	2144474	2144480	2144485
Formula	C ₂₀ H ₂₁ CuNO ₆	C ₃₂ H ₃₀ CuN ₂ O ₆	C ₁₅ H ₁₀ O ₃	C ₁₈ H ₁₄ ClNO ₃
D _{calc.} / g cm ⁻³	1.502	1.451	1.448	1.445
μ /mm ⁻¹	1.930	1.529	0.830	2.377
Formula Weight	434.92	602.12	238.23	327.75
Colour	clear blue	clear green	clear colorless	clear colorless
Shape	plate-shaped	plate	plate-shaped	prism-shaped
Size/mm ³	0.23x0.15x0.06	0.15x0.10x0.05	0.17x0.11x0.06	0.09x0.08x0.08
T/K	123.01(10)	123.01(10)	122.97(10)	123.00(10)
Crystal System	triclinic	monoclinic	monoclinic	monoclinic
Space Group	P-1	C2/c	C2/c	P2 ₁ /c
a/Å	9.8246(2)	25.6472(6)	13.7617(9)	16.06989(7)
b/Å	13.6030(3)	16.1411(4)	8.1050(4)	7.09422(3)
c/Å	14.54570(10)	13.7447(3)	19.5997(12)	26.42930(11)
α /°	83.192(2)	90	90	90
β /°	85.2690(10)	104.289(3)	91.551(6)	90.3024(4)
γ /°	88.081(2)	90	90	90
V/Å ³	1923.11(6)	5513.9(2)	2185.3(2)	3012.99(2)
Z	4	8	8	8
Z'	2	1	1	2
Wavelength/Å	1.54184	1.54184	1.54184	1.54184
Radiation type	Cu K α	CuK α	Cu K α	Cu K α
θ_{min} /°	3.069	3.265	4.514	2.750
θ_{max} /°	73.028	74.143	73.956	74.433
Measured Refl.	52324	14926	11611	66058
Independent Refl.	7274	5395	2140	6106
Refl's I > σ 2(I)	5785	4303	1916	5835
R _{int}	0.0848	0.0270	0.0445	0.0186
Parameters	511	374	163	419
Restraints	0	0	0	0
Largest Peak	0.607	0.941	0.310	0.263
Deepest Hole	-1.121	-0.435	-0.260	-0.395
GooF	1.126	1.018	1.046	1.048
wR ₂ (all data)	0.1544	0.1061	0.1339	0.0790
wR ₂	0.1461	0.0974	0.1311	0.0782
R ₁ (all data)	0.0676	0.0506	0.0568	0.0297
R ₁	0.0536	0.0380	0.0525	0.0286
Solution		Olex2 1.2-alpha		

6.3 NMR Spectra for Chapter 3

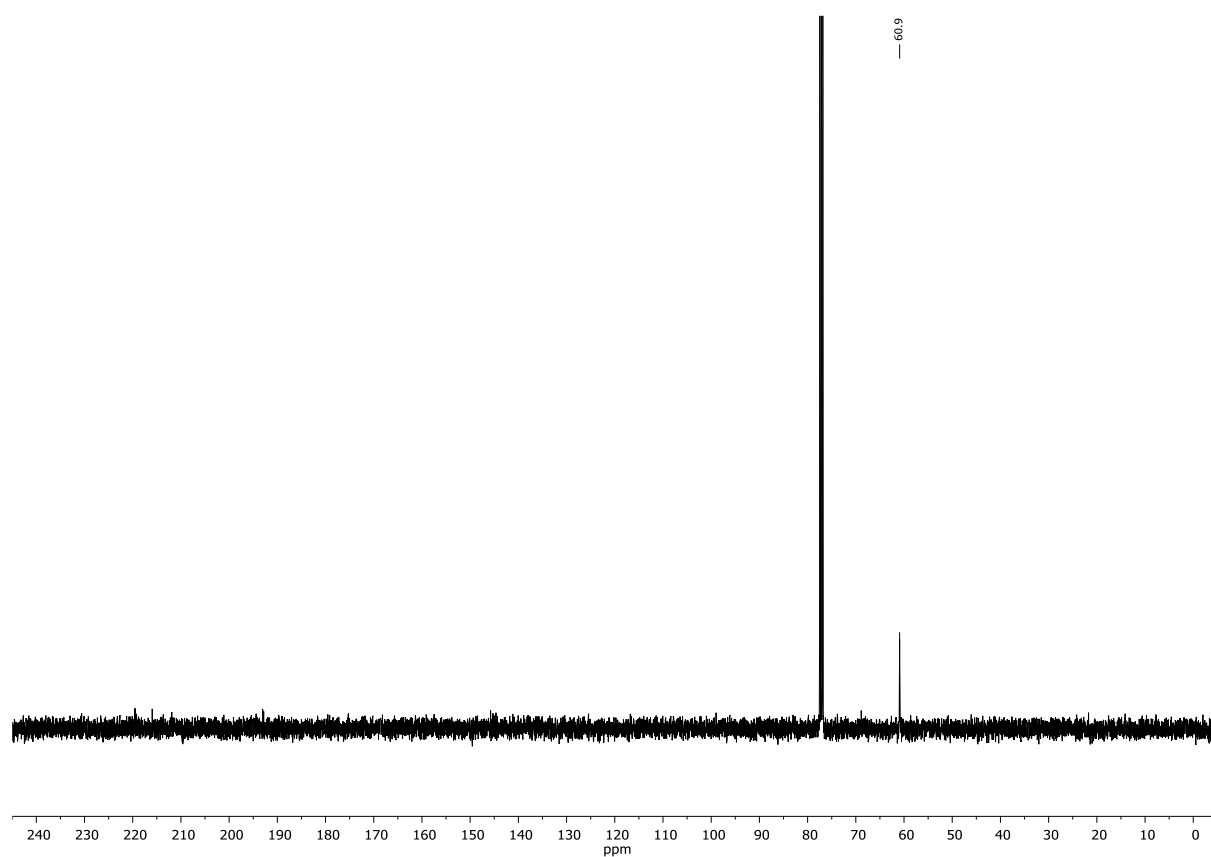
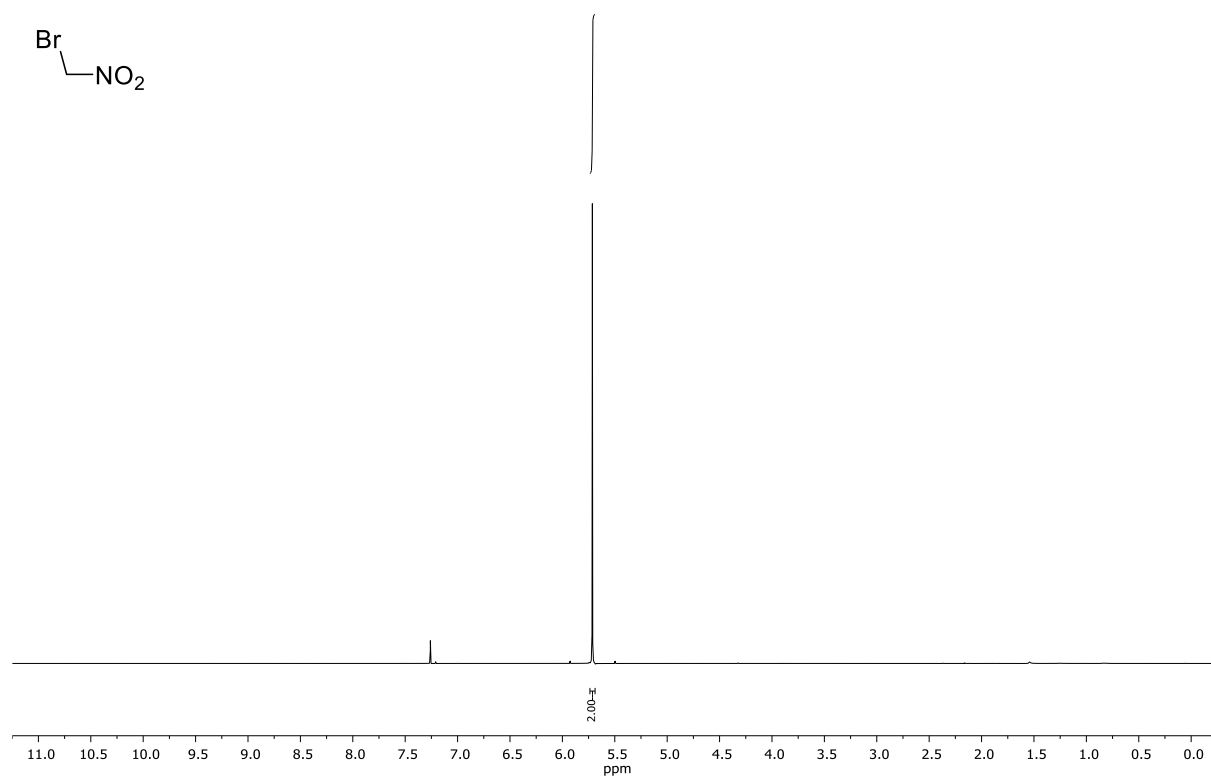
 $[\text{Cu}(\text{dap})_2]\text{Cl}$ 

First image: $^1\text{H-NMR}$; Second image: $^{13}\text{C-NMR}$; NMR solvent: CDCl_3

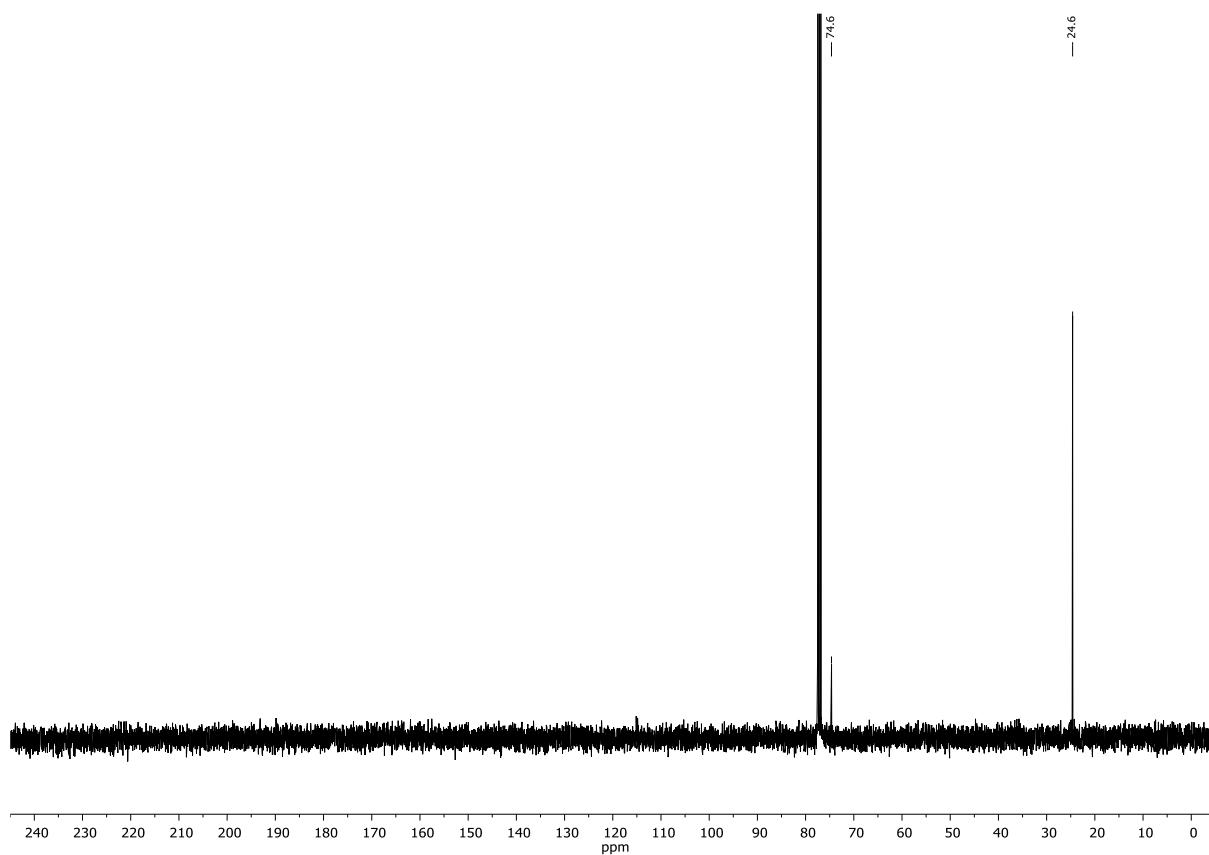
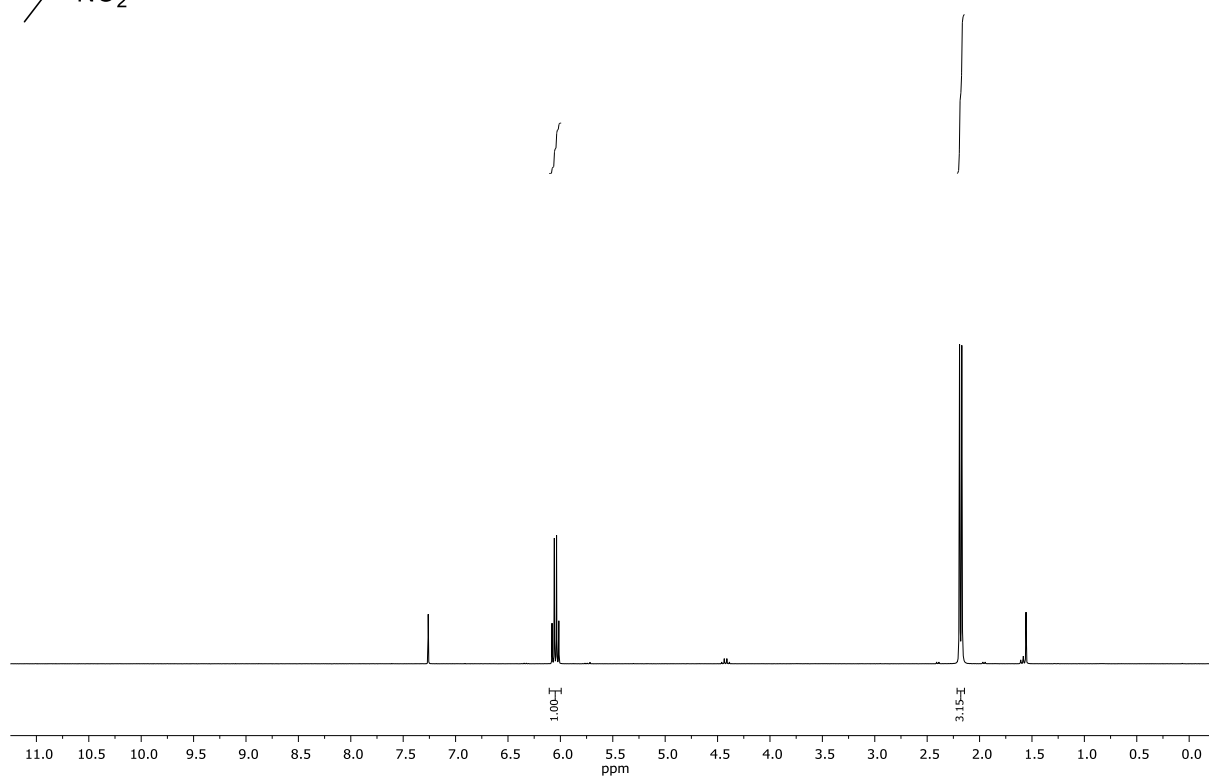
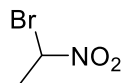
[Cu(dmp)₂]⁺Cl⁻First image: ¹H-NMR; Second image: ¹³C-NMR; NMR solvent: CDCl₃

[Cu(Xanthphos)(dmp)]BF₄

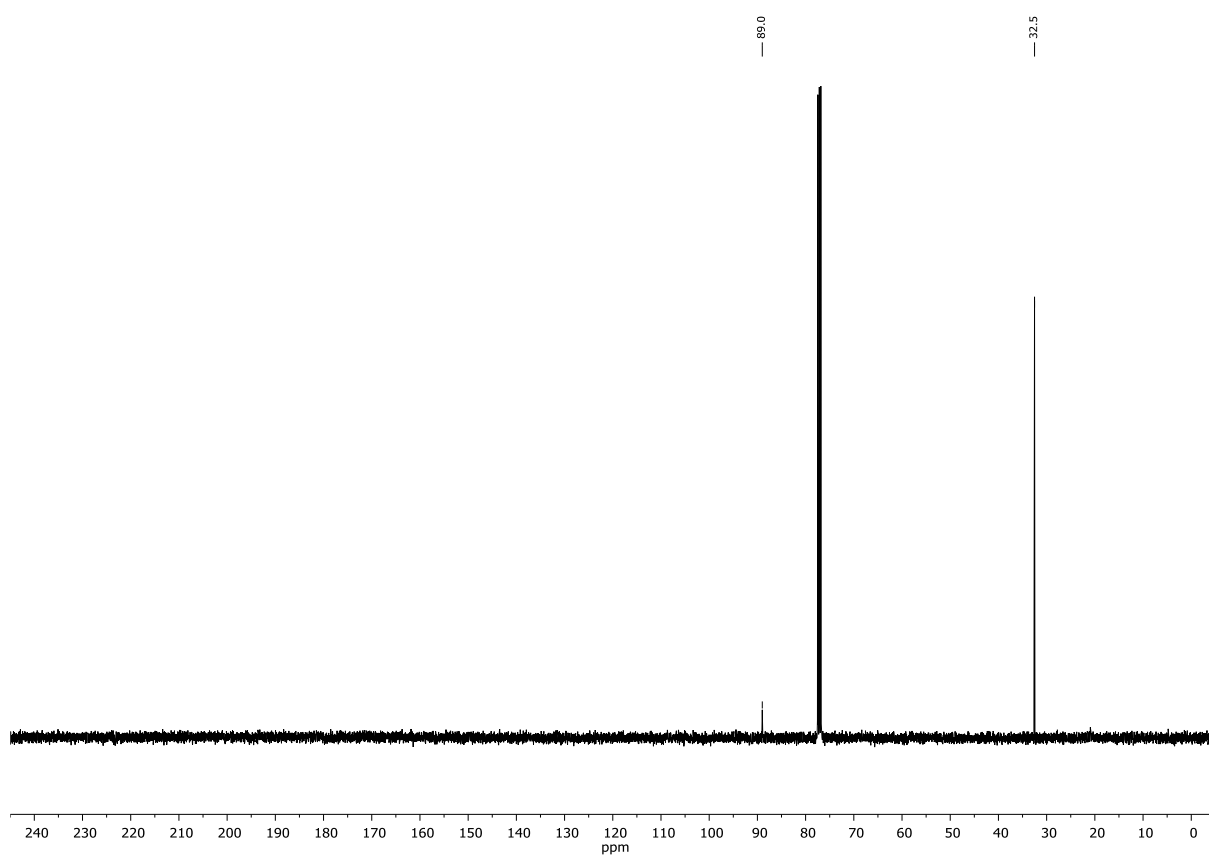
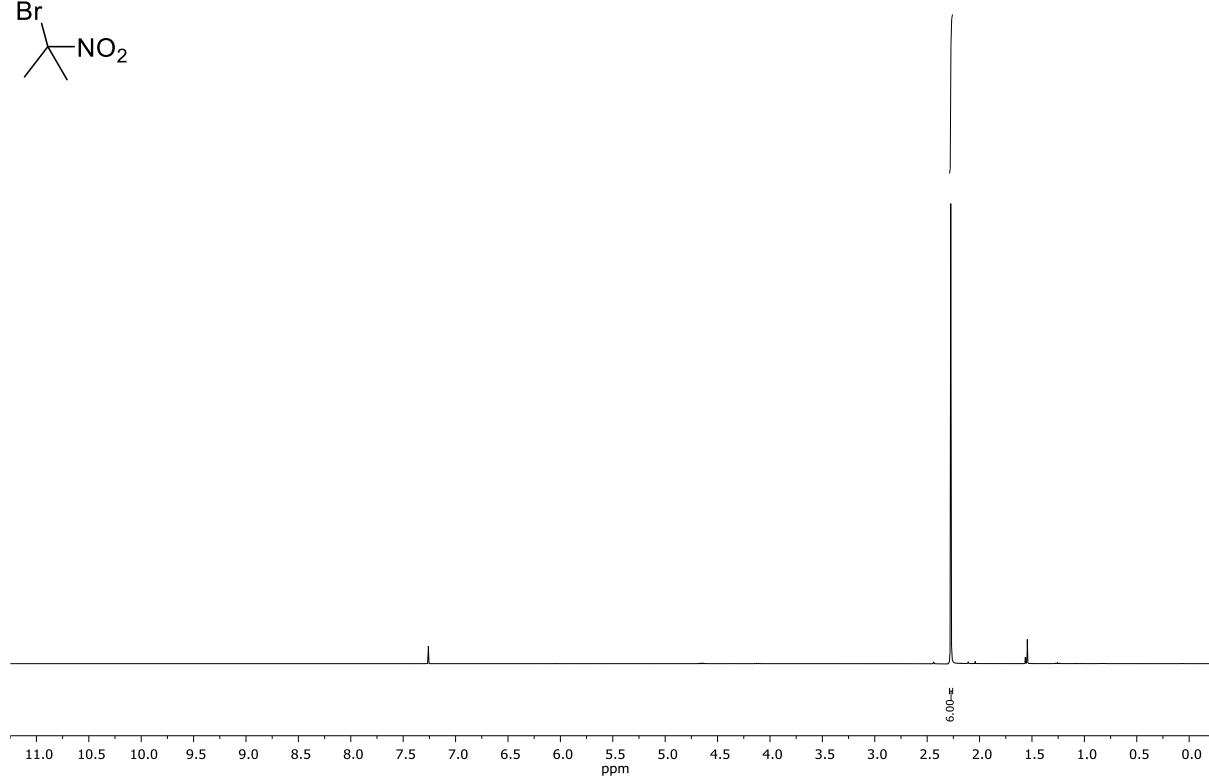
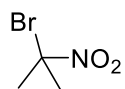
First image: ¹H-NMR; Second image: ¹³C-NMR; NMR solvent: CDCl₃

bromonitromethane (1a)

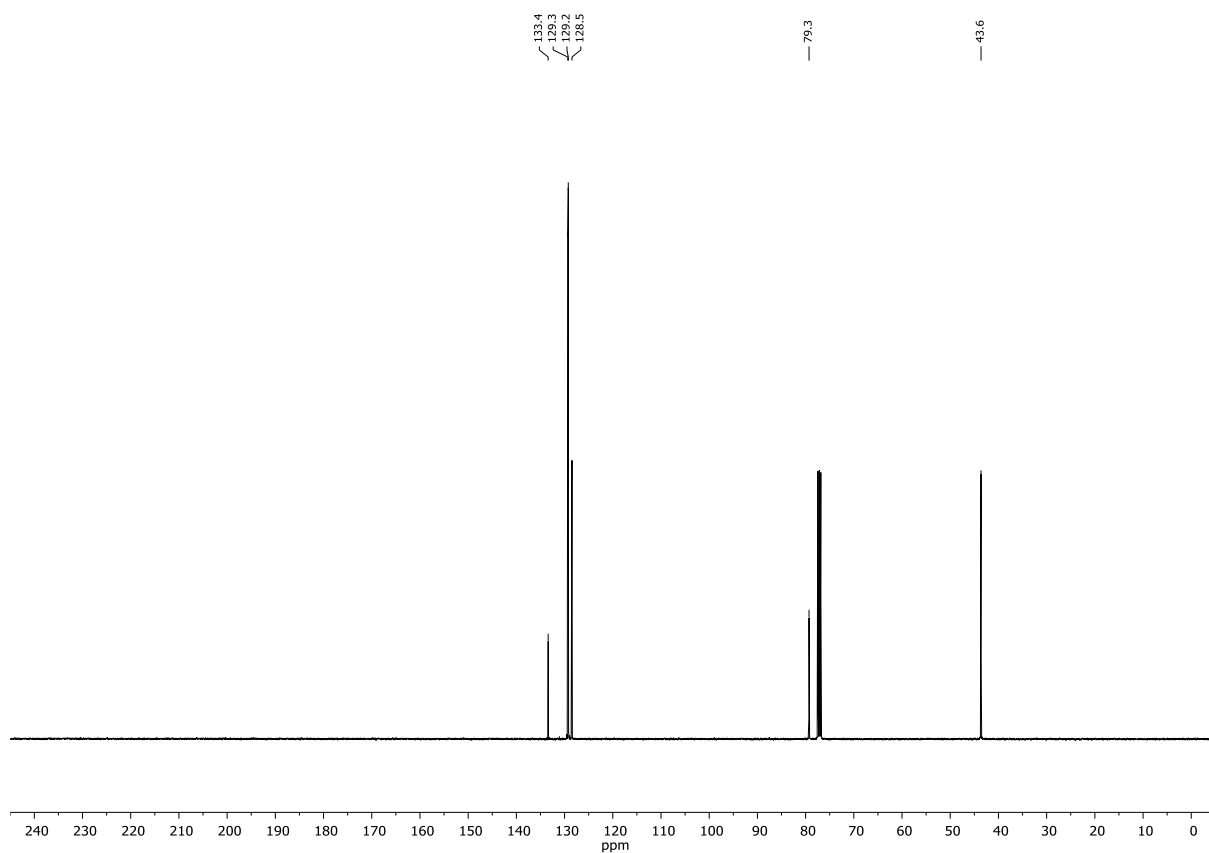
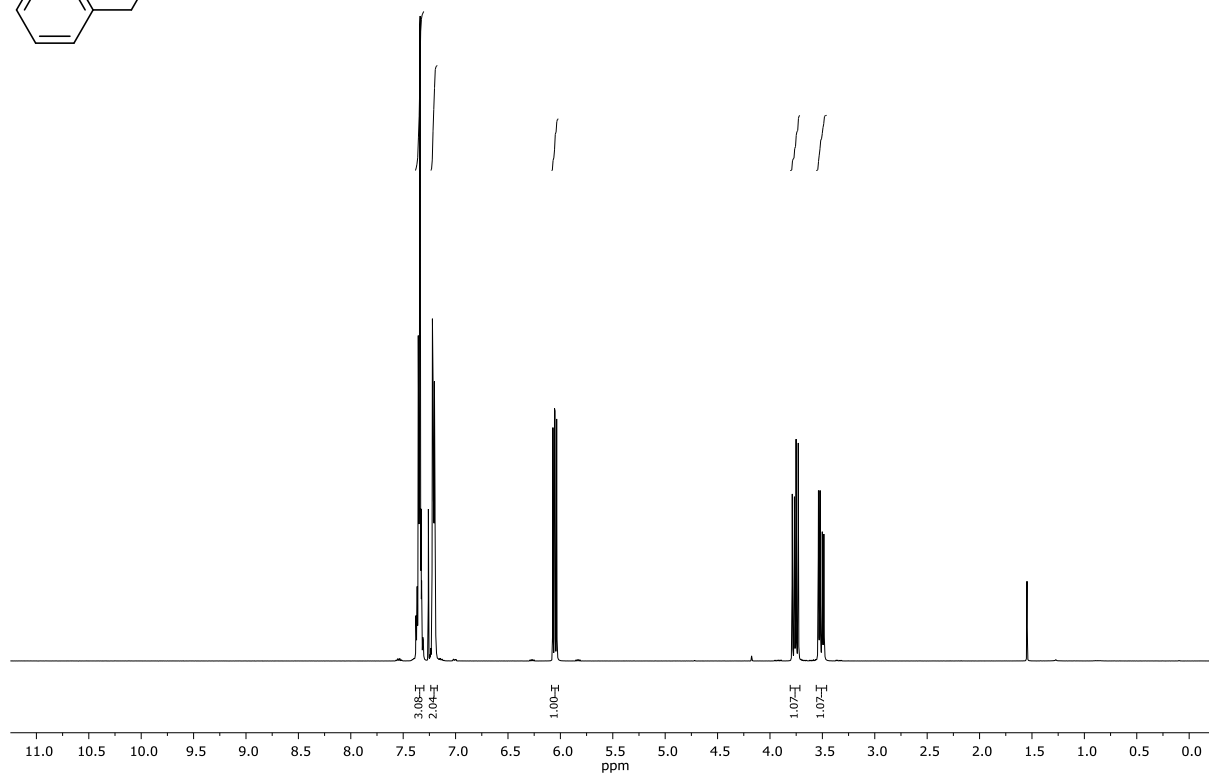
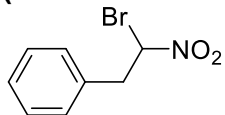
First image: ^1H -NMR; Second image: ^{13}C -NMR; NMR solvent: CDCl_3

1-bromo-1-nitroethane (1b)

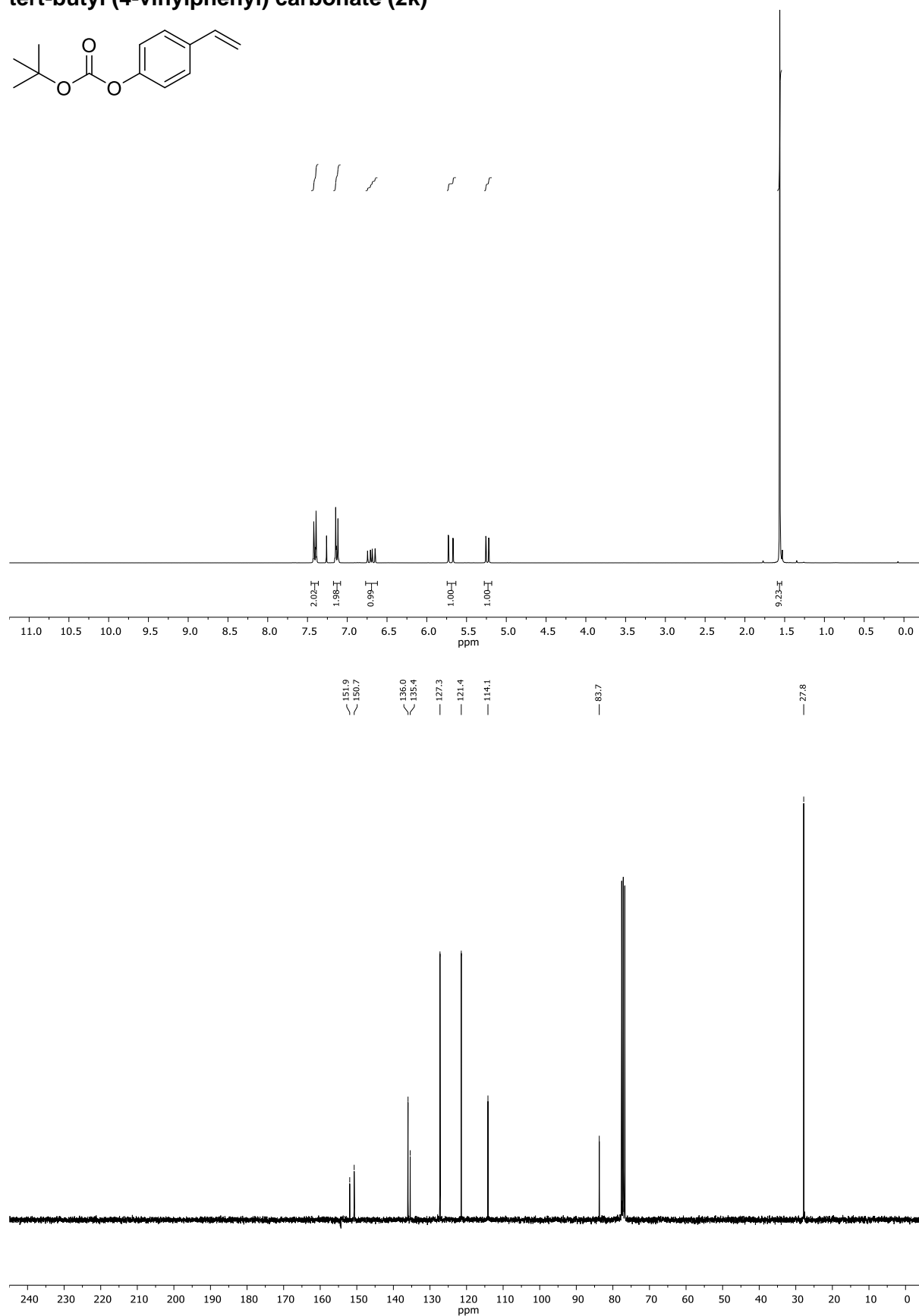
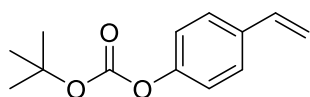
First image: ¹H-NMR; Second image: ¹³C-NMR; NMR solvent: CDCl₃

2-bromo-2-nitropropane (1c)

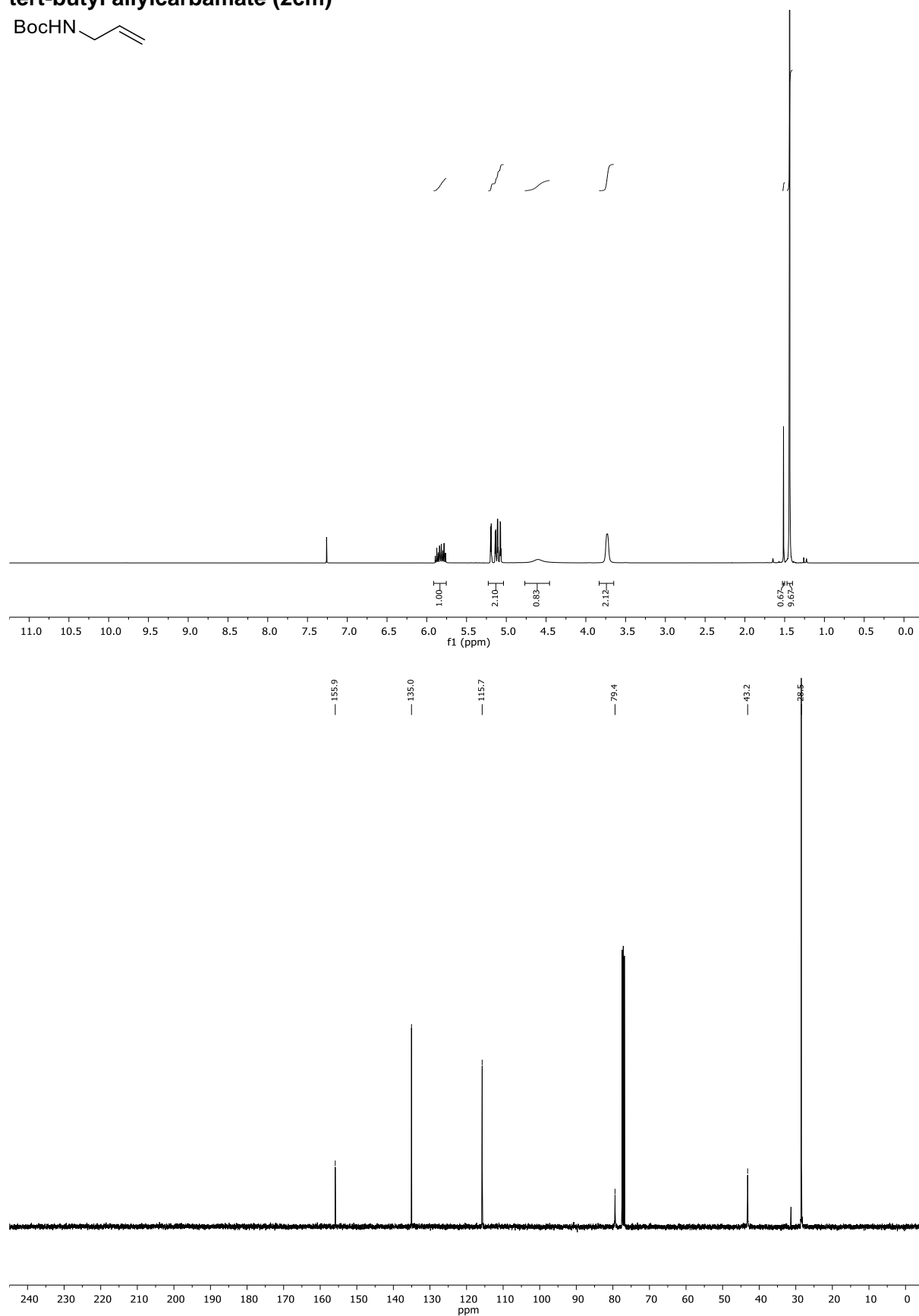
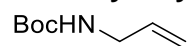
First image: ^1H -NMR; Second image: ^{13}C -NMR; NMR solvent: CDCl_3

(2-bromo-2-nitroethyl)benzene (1d)

First image: $^1\text{H-NMR}$; Second image: $^{13}\text{C-NMR}$; NMR solvent: CDCl_3

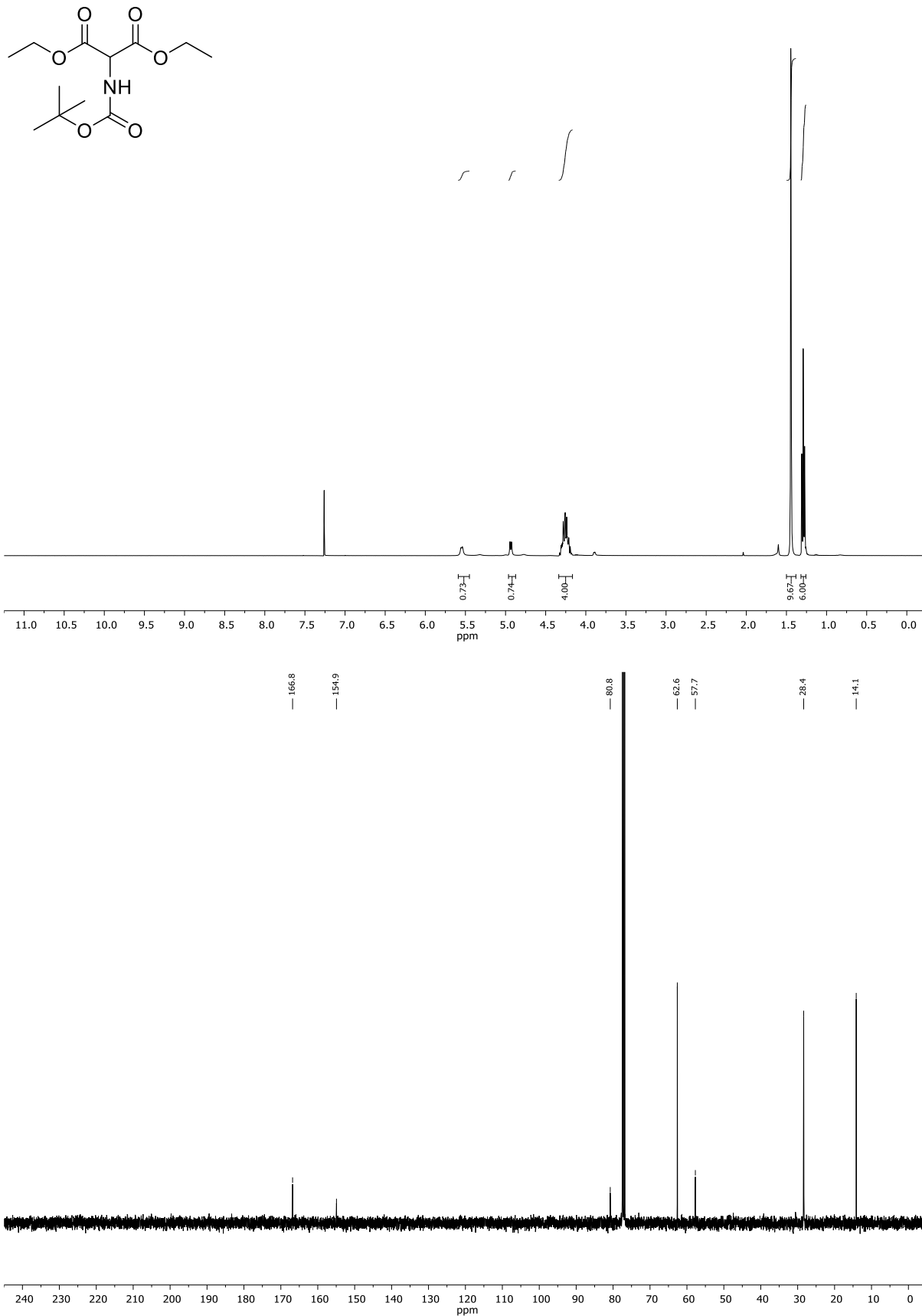
tert-butyl (4-vinylphenyl) carbonate (2k)

First image: $^1\text{H-NMR}$; Second image: $^{13}\text{C-NMR}$; NMR solvent: CDCl_3

tert-butyl allylcarbamate (2cm)

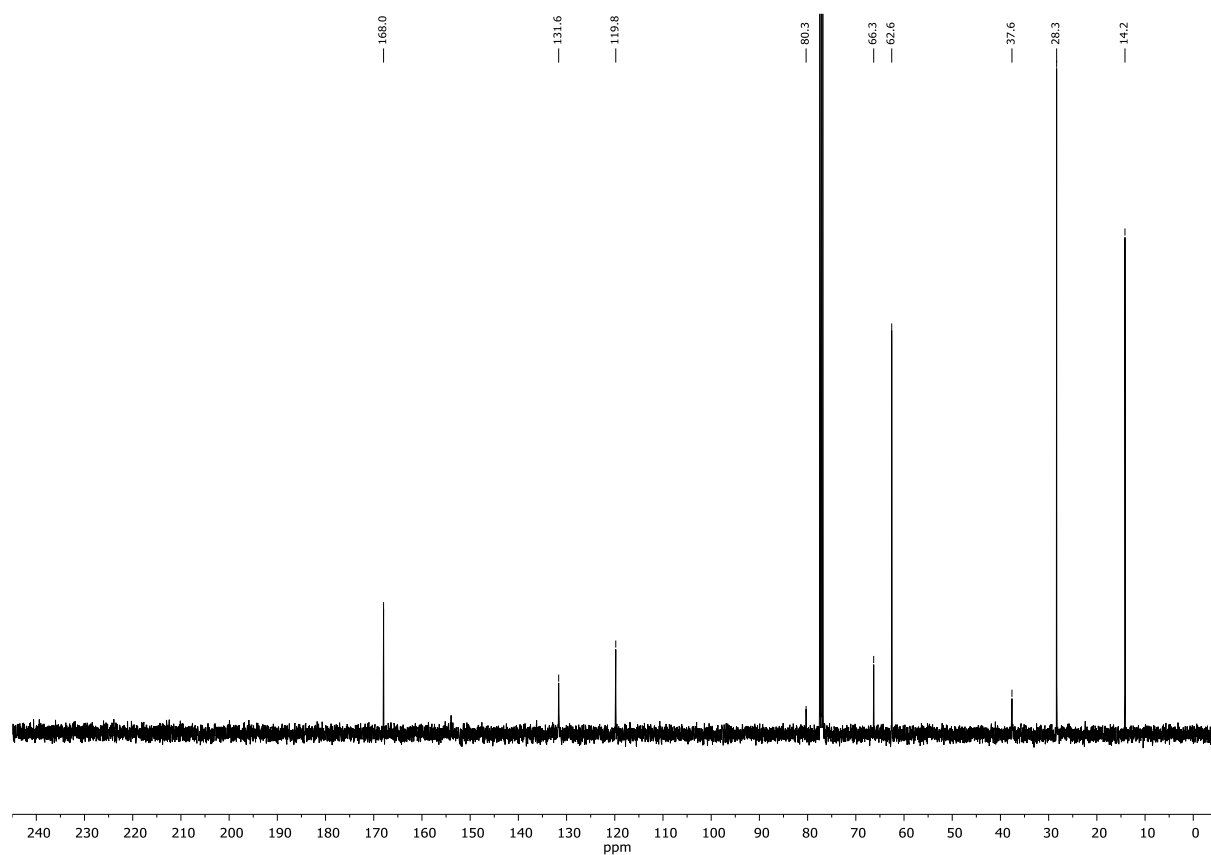
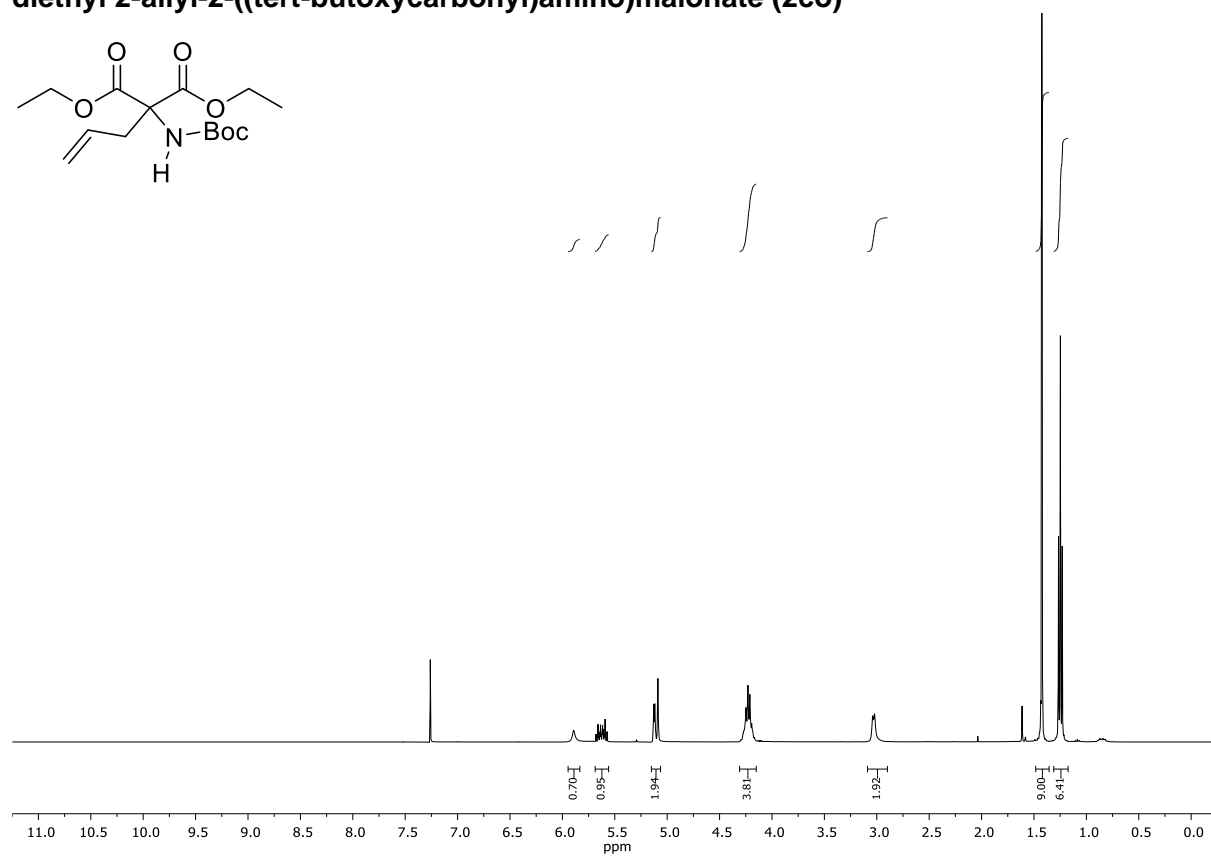
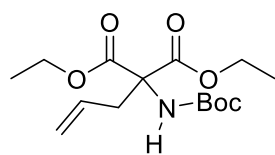
First image: $^1\text{H-NMR}$; Second image: $^{13}\text{C-NMR}$; NMR solvent: CDCl_3

diethyl 2-((tert-butoxycarbonyl)amino)malonate (2co')



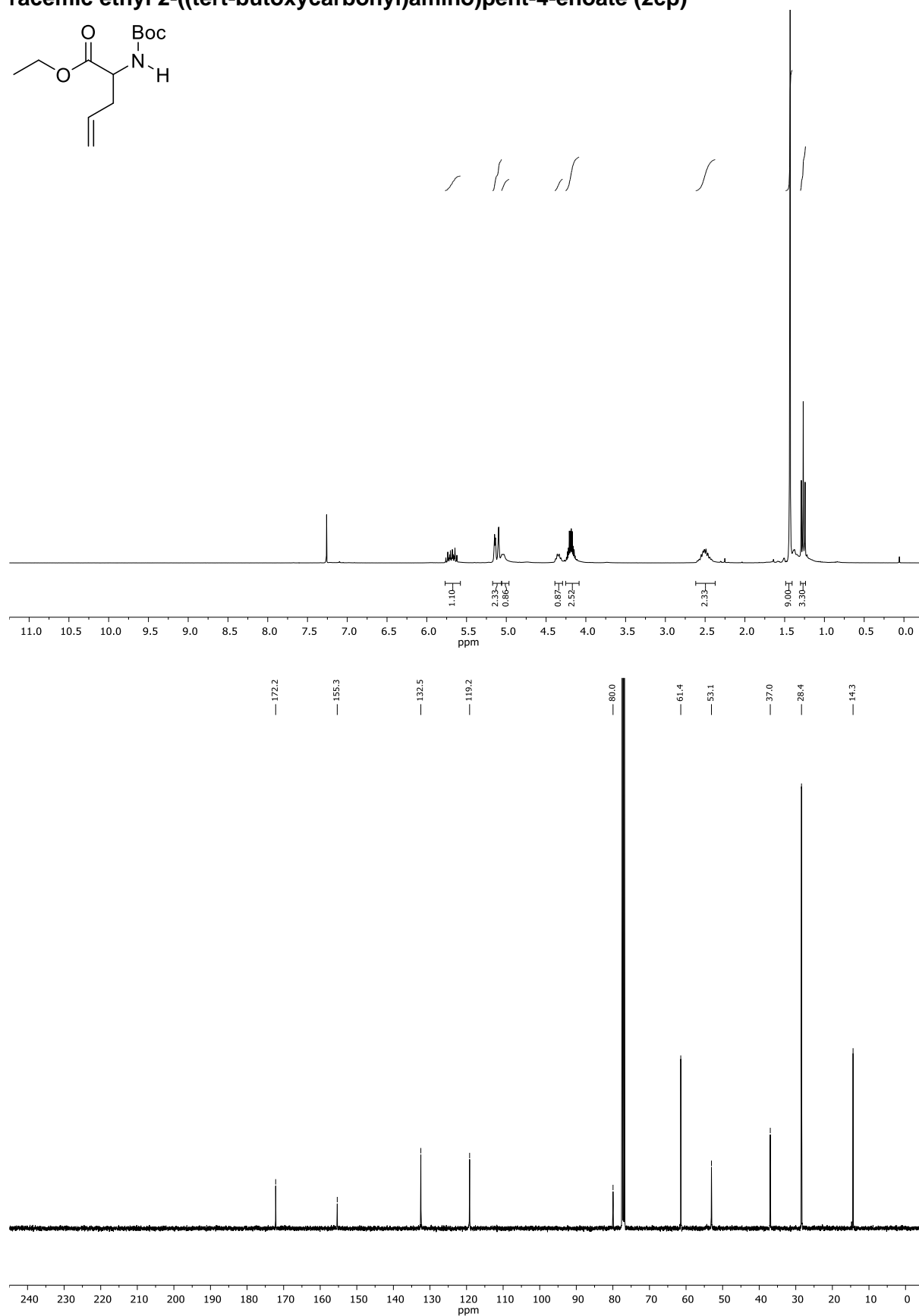
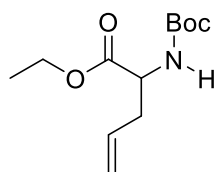
First image: ¹H-NMR; Second image: ¹³C-NMR; NMR solvent: CDCl₃

diethyl 2-allyl-2-((tert-butoxycarbonyl)amino)malonate (2co)



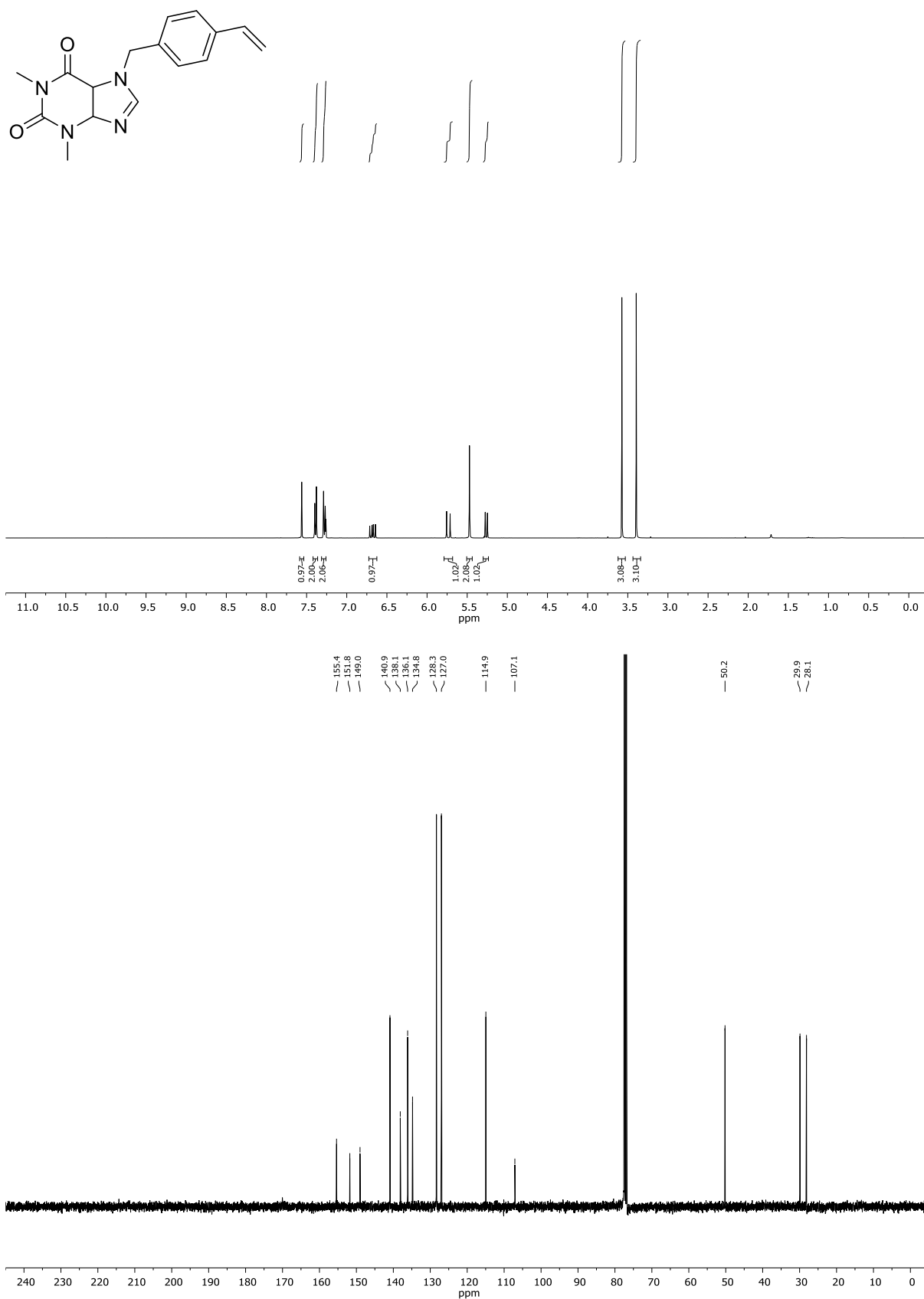
First image: $^1\text{H-NMR}$; Second image: $^{13}\text{C-NMR}$; NMR solvent: CDCl_3

racemic ethyl 2-((tert-butoxycarbonyl)amino)pent-4-enoate (2cp)



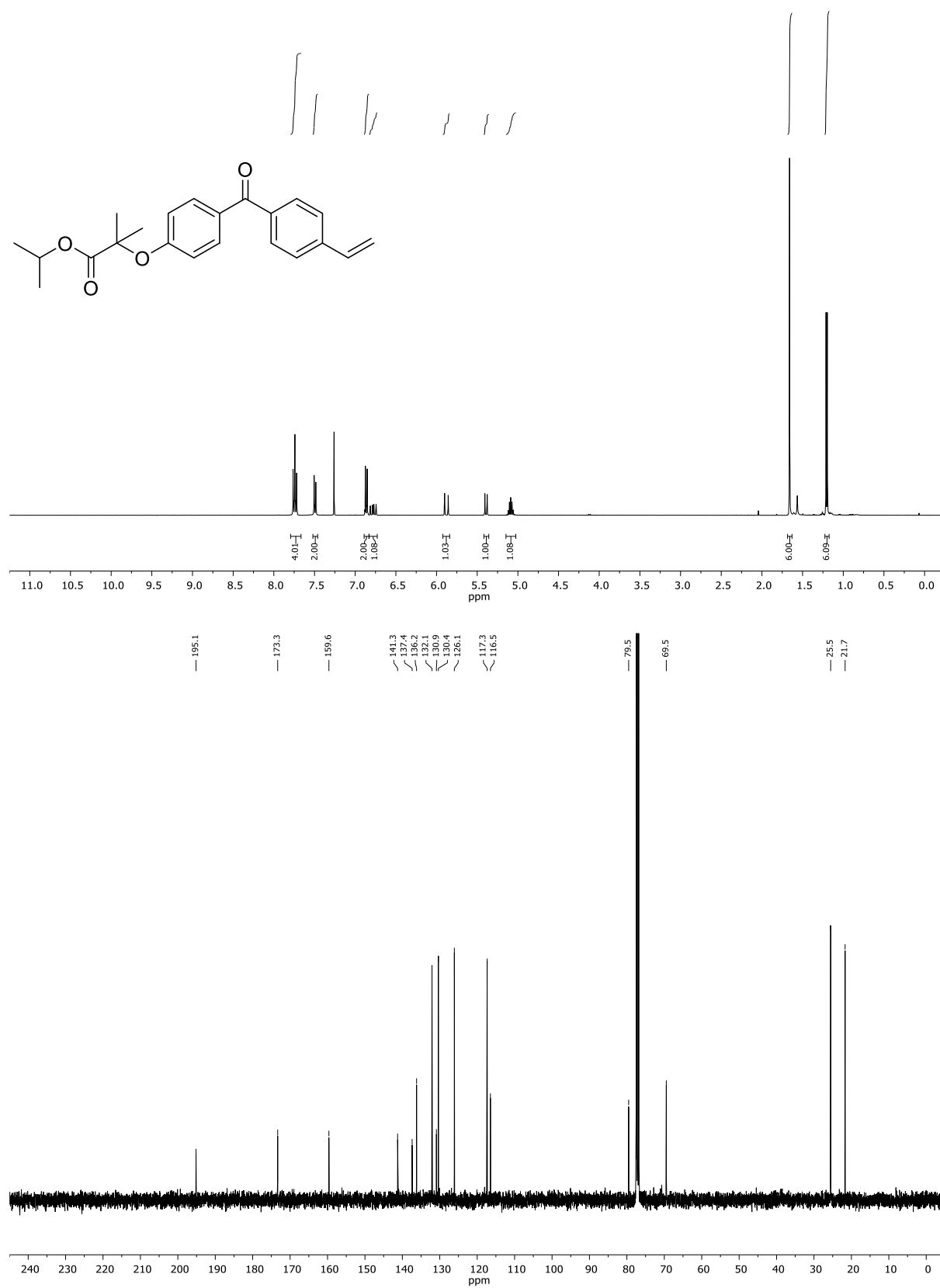
First image: $^1\text{H-NMR}$; Second image: $^{13}\text{C-NMR}$; NMR solvent: CDCl_3

1,3-dimethyl-7-(4-vinylbenzyl)-3,4,5,7-tetrahydro-1H-purine-2,6-dione (2ea)

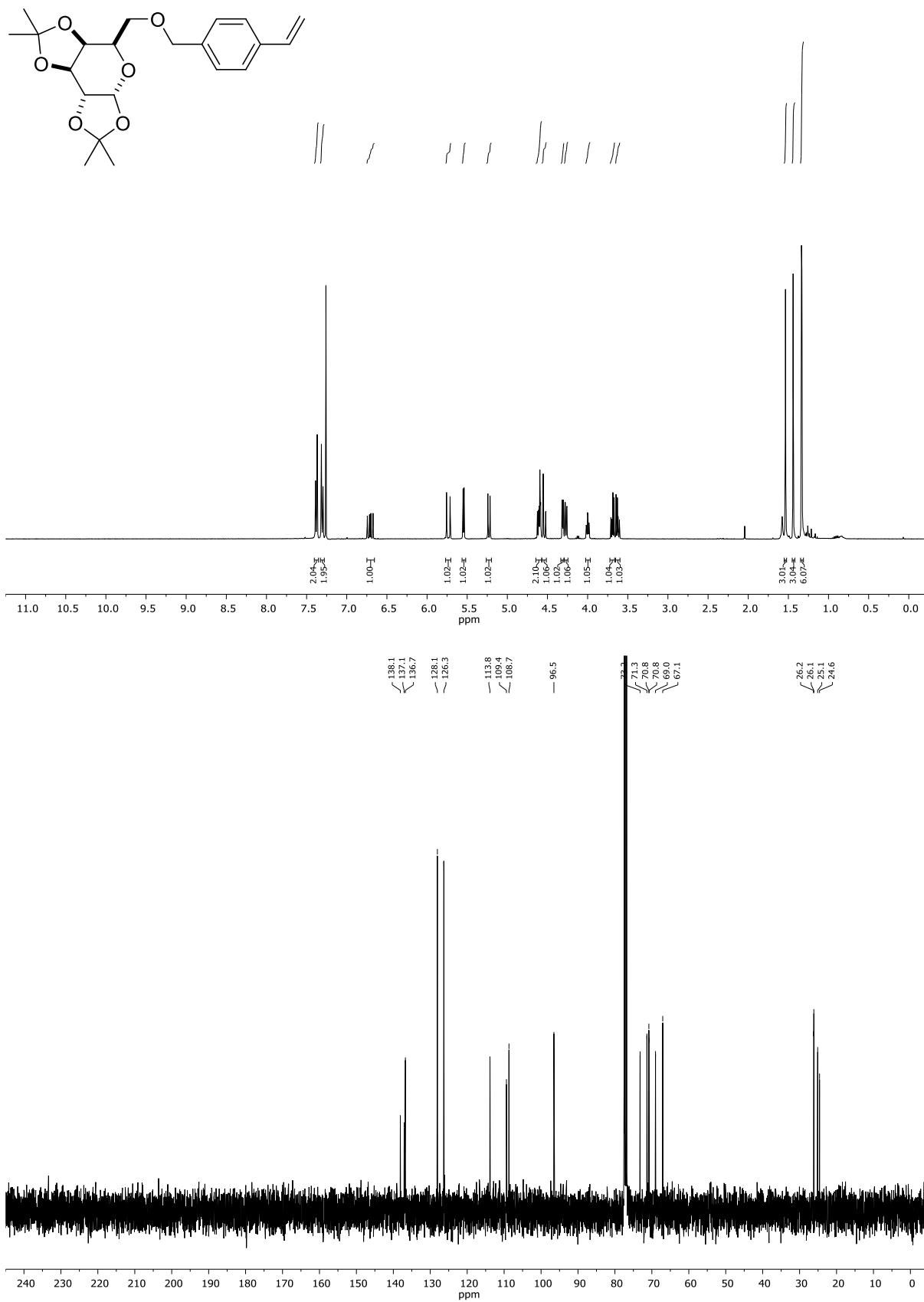


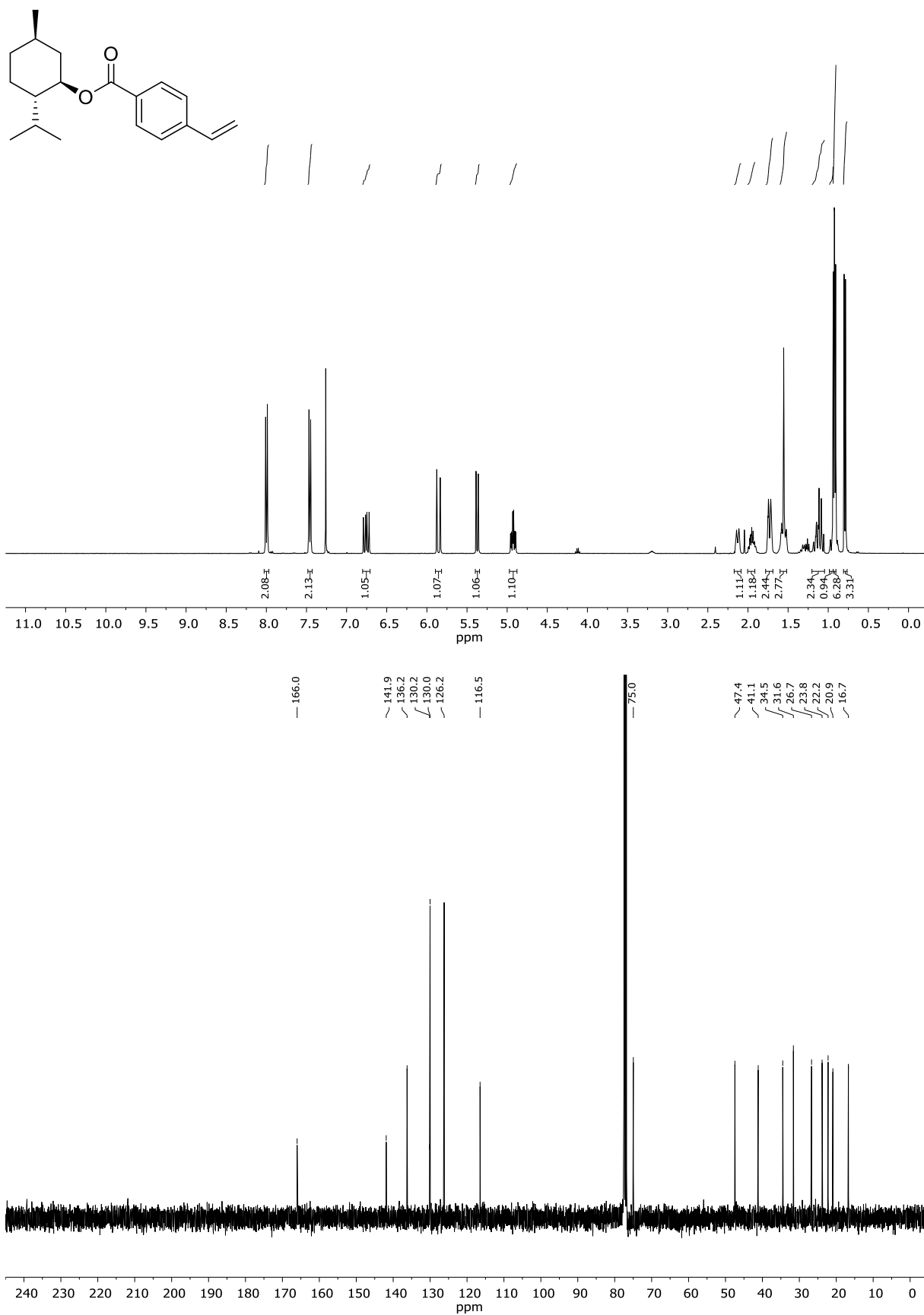
First image: ^1H -NMR; Second image: ^{13}C -NMR; NMR solvent: CDCl_3

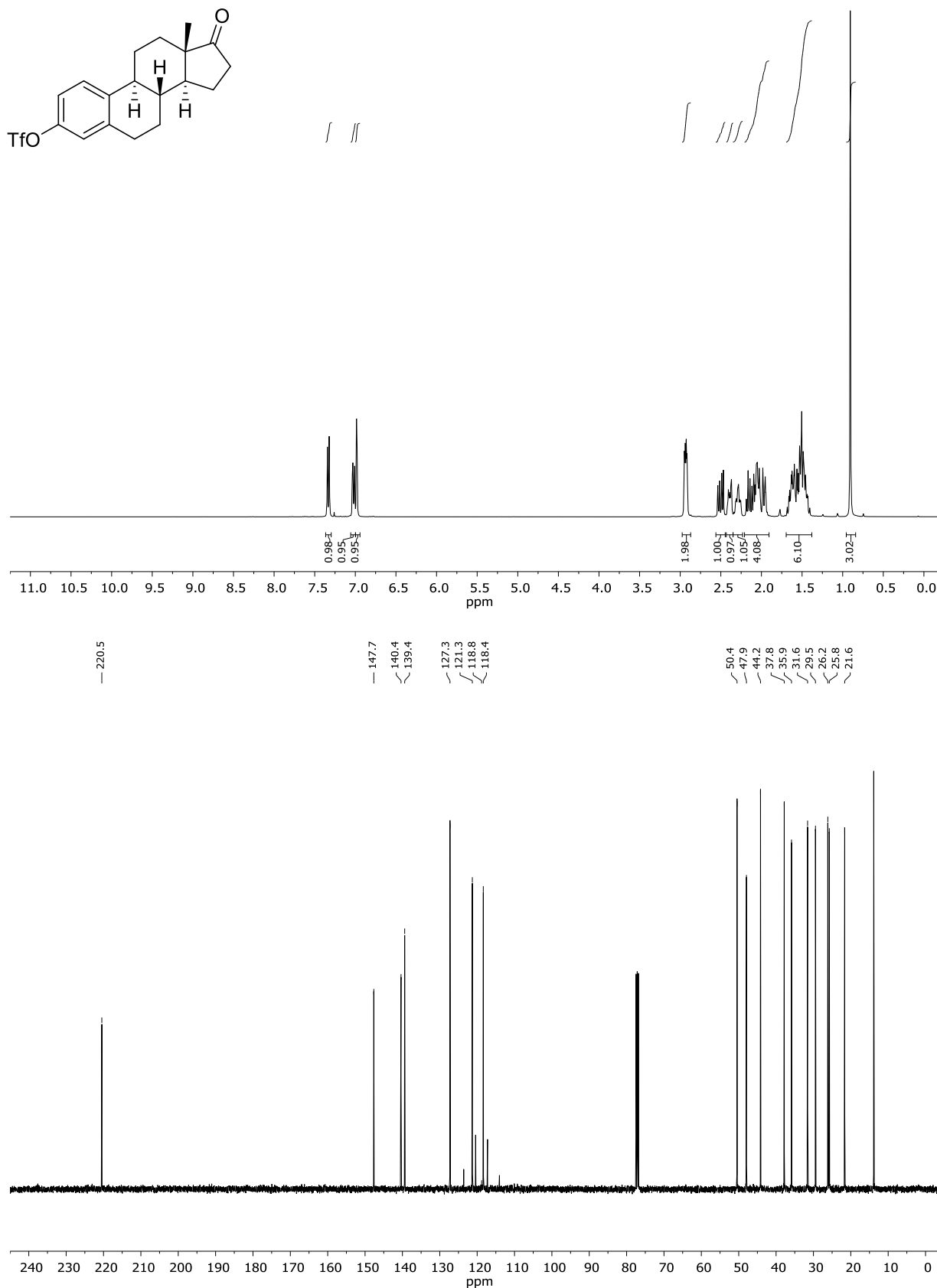
isopropyl 2-methyl-2-(4-(4-vinylbenzoyl)phenoxy)propanoate (2eb)

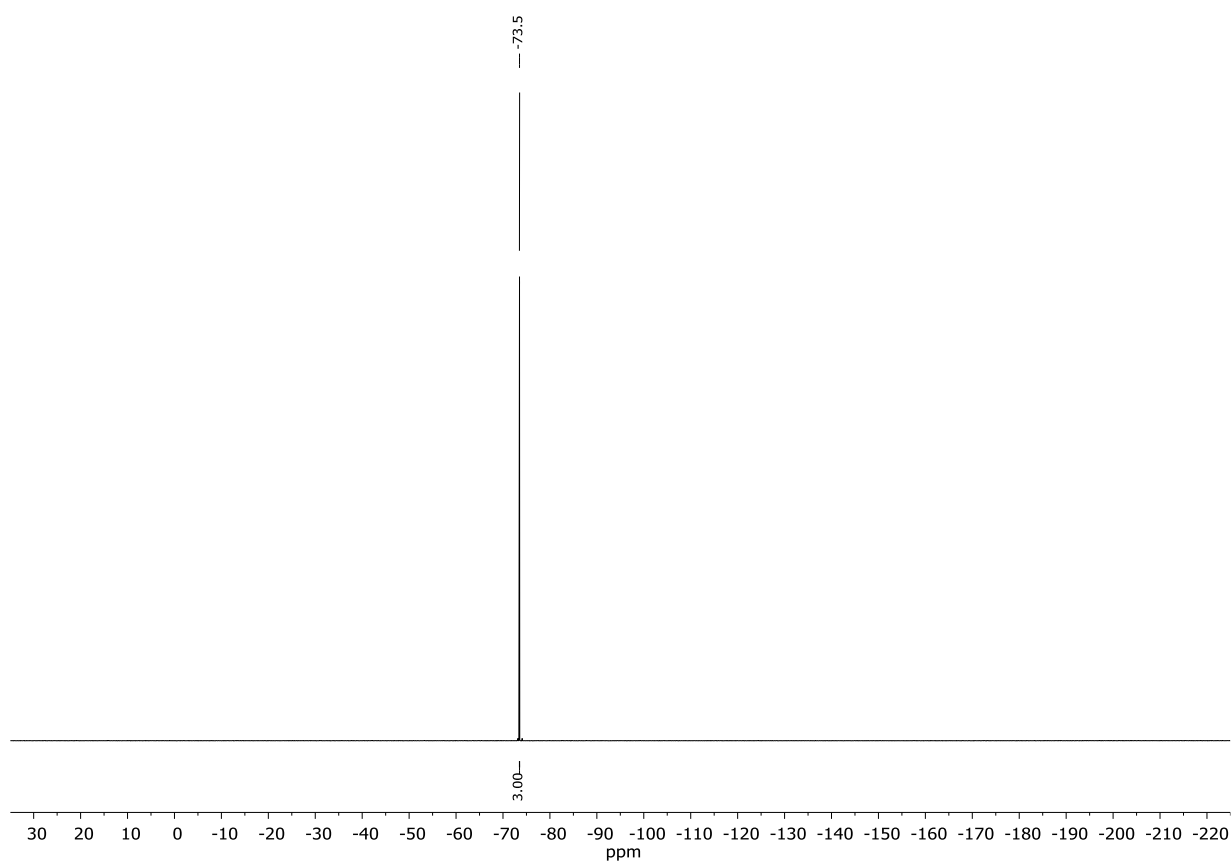


First image: ¹H-NMR; Second image: ¹³C-NMR; NMR solvent: CDCl₃

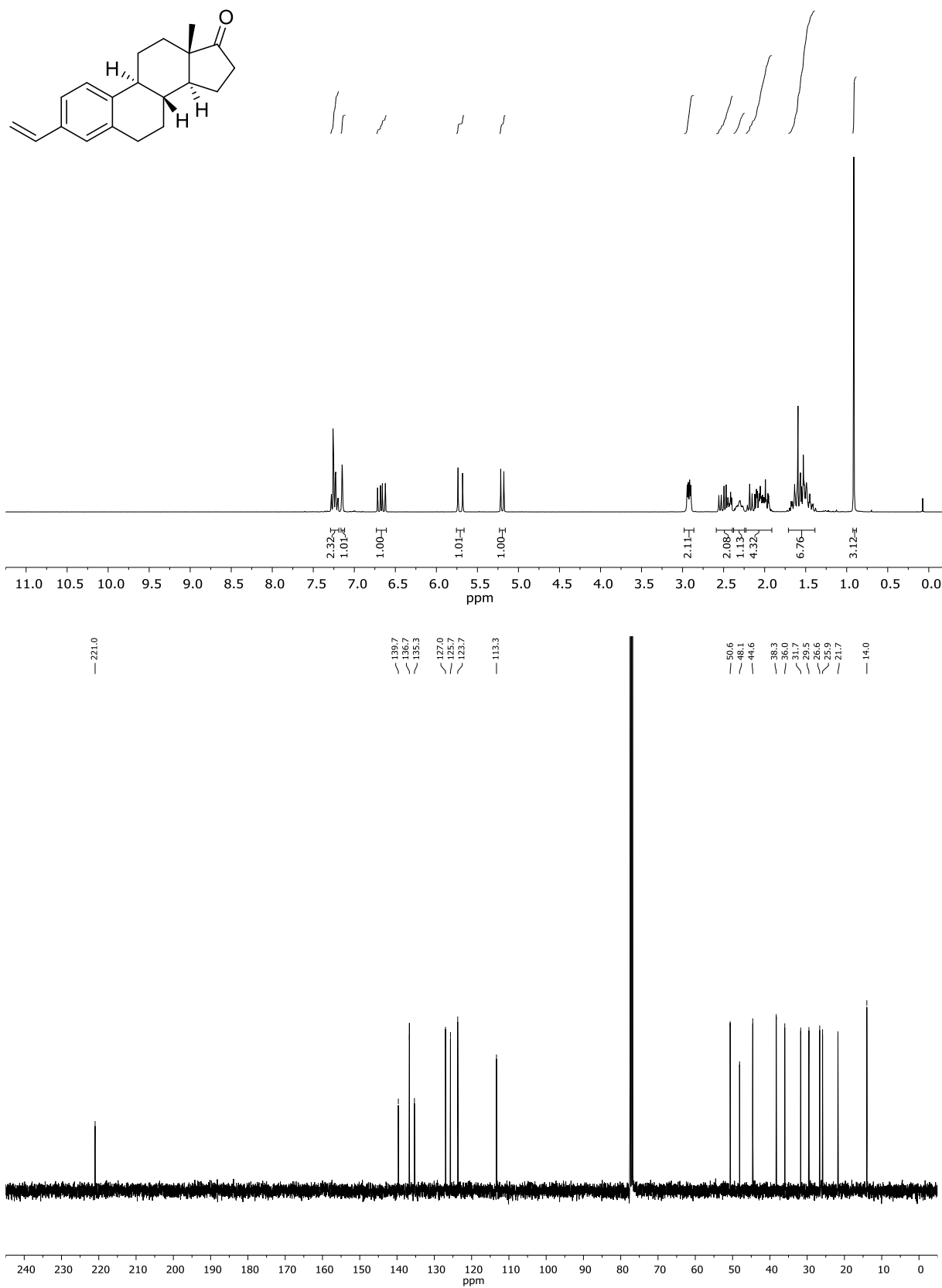
(3aR,5R,5aS,8aS,8bR)-2,2,7,7-tetramethyl-5-(((4-vinylbenzyl)oxy)methyl)tetrahydro-5H-bis[[1,3]dioxolo)[4,5-b:4',5'-d]pyran (2ec)First image: ¹H-NMR; Second image: ¹³C-NMR; NMR solvent: CDCl₃

(1R,2S,5R)-2-isopropyl-5-methylcyclohexyl 4-vinylbenzoate (2ed)First image: ¹H-NMR; Second image: ¹³C-NMR; NMR solvent: CDCl₃

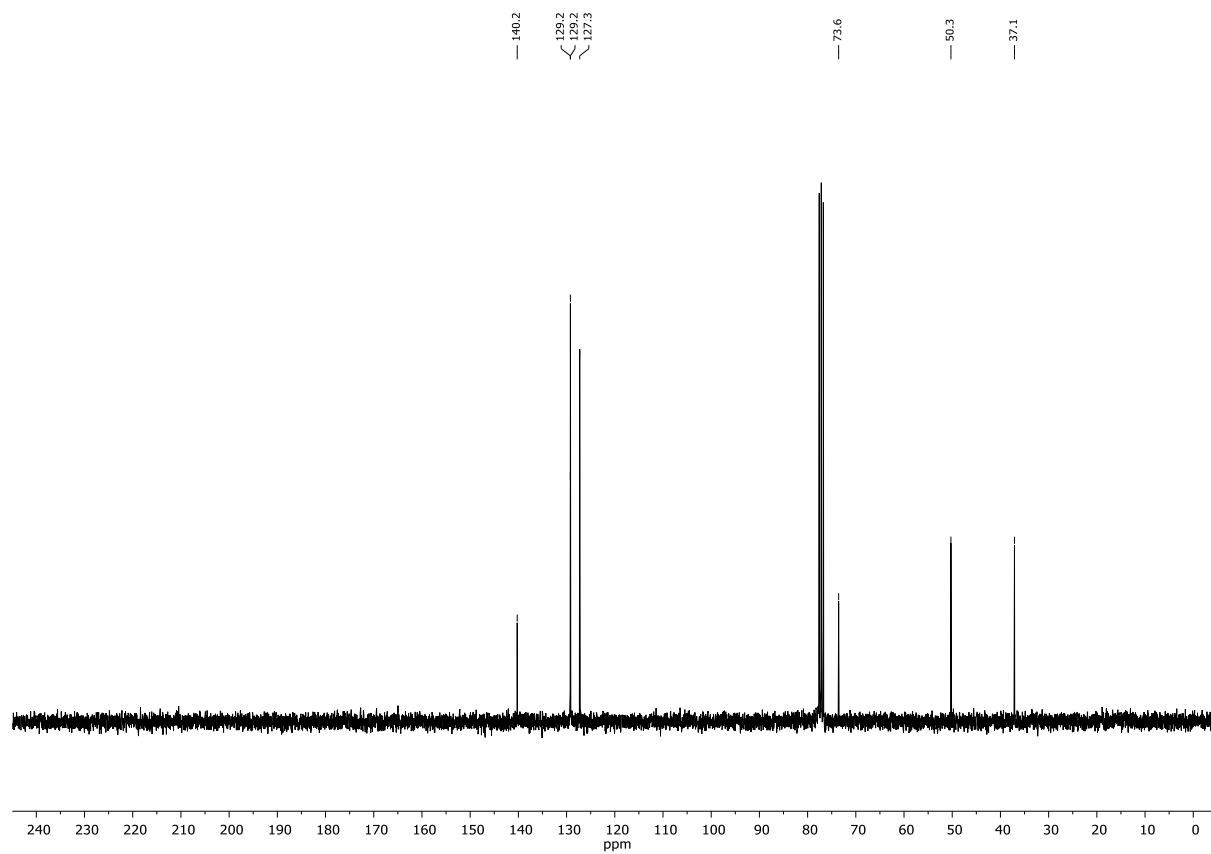
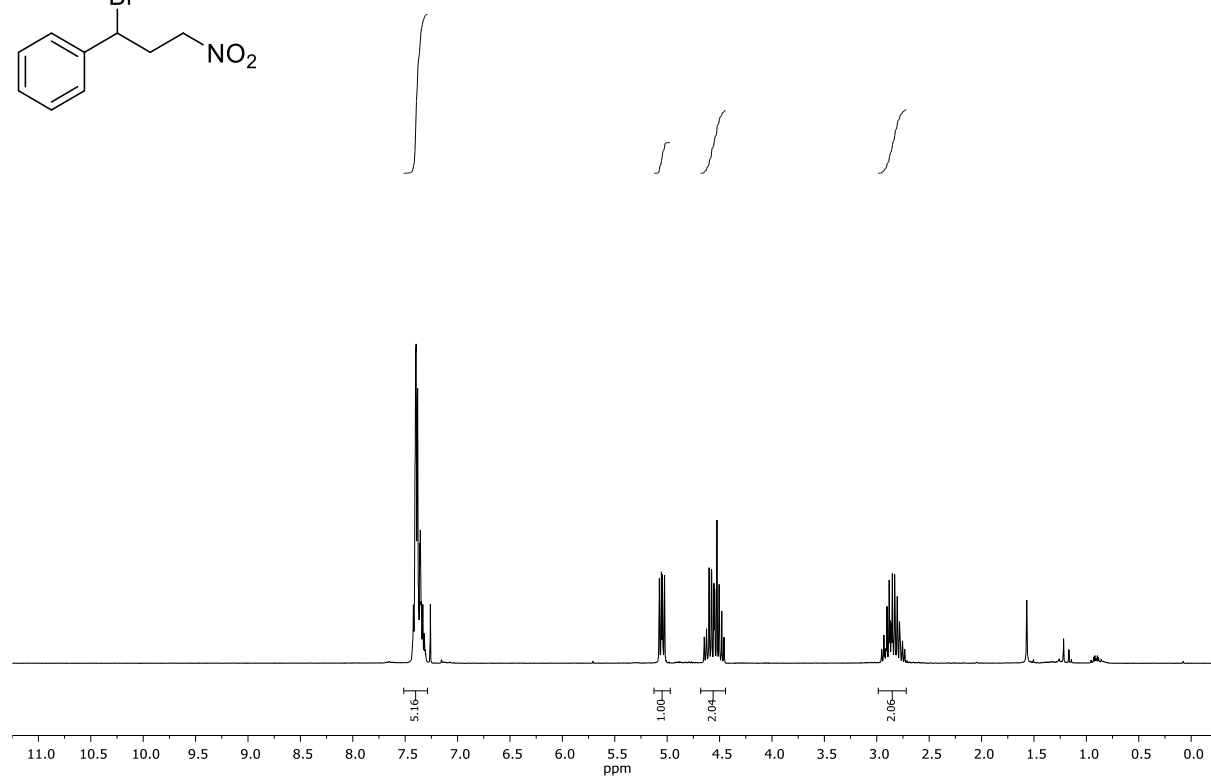
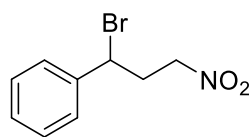
(8R,9S,13S,14S)-13-methyl-17-oxo-7,8,9,11,12,13,14,15,16,17-decahydro-6H-cyclopenta[a]phenanthren-3-yl trifluoromethanesulfonate (2ef')



First image: ^1H -NMR; Second image: ^{13}C -NMR; Thrid image: ^{19}F -NMR: NMR solvent: CDCl_3

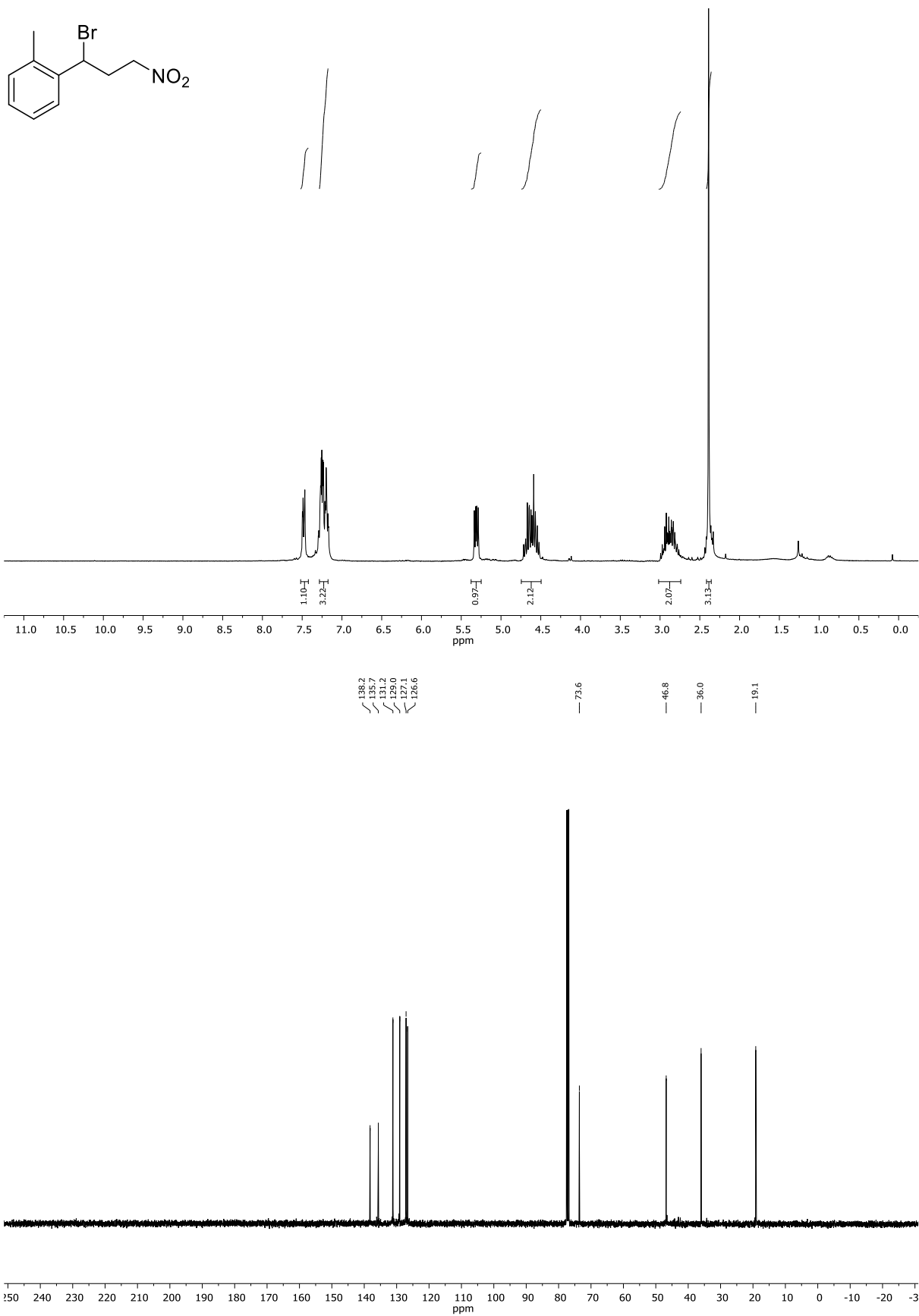
(8R,9S,13S,14S)-13-methyl-3-vinyl-6,7,8,9,11,12,13,14,15,16-decahydro-17H-cyclopenta[a]phenanthren-17-one (2ef)

First image: ¹H-NMR; Second image: ¹³C-NMR; NMR solvent: CDCl₃

(1-bromo-3-nitropropyl)benzene(4a)

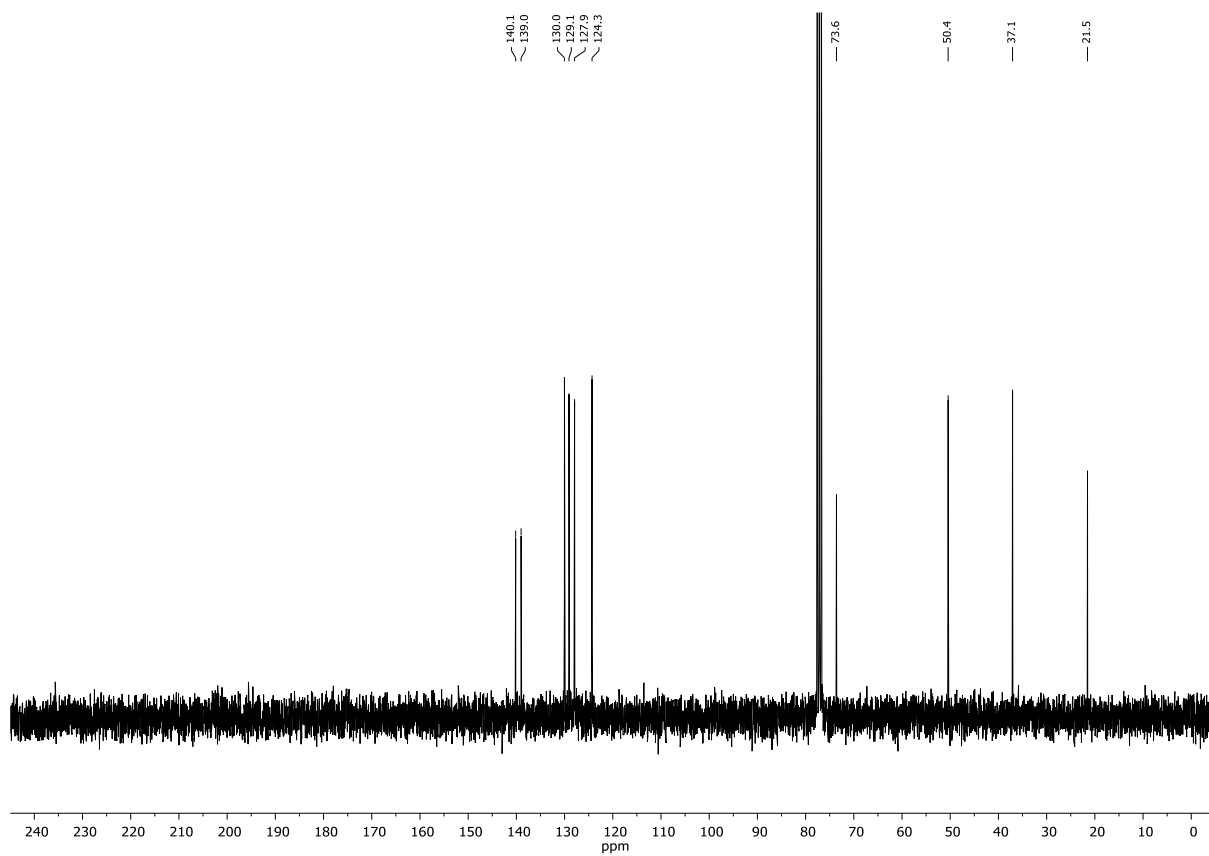
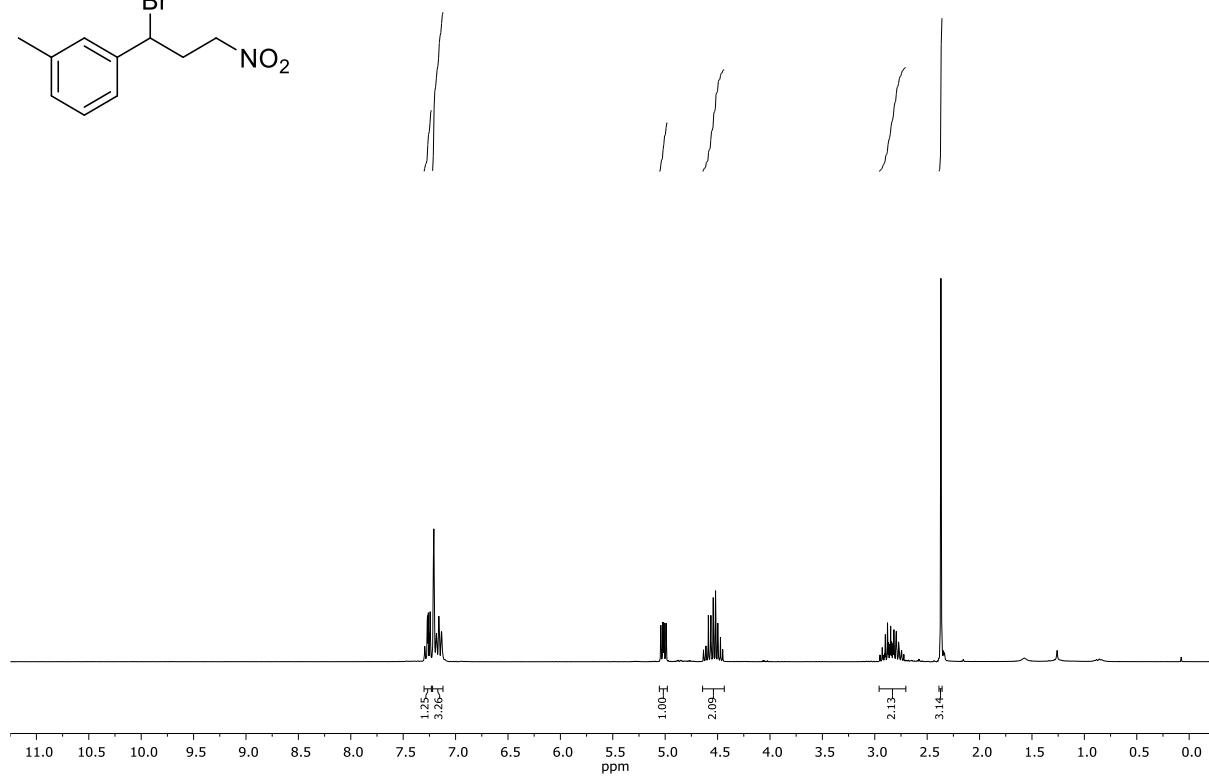
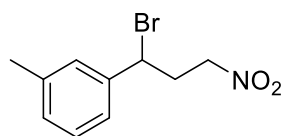
First image: $^1\text{H-NMR}$; Second image: $^{13}\text{C-NMR}$; NMR solvent: CDCl_3

1-(1-bromo-3-nitropropyl)-2-methylbenzene (4b)



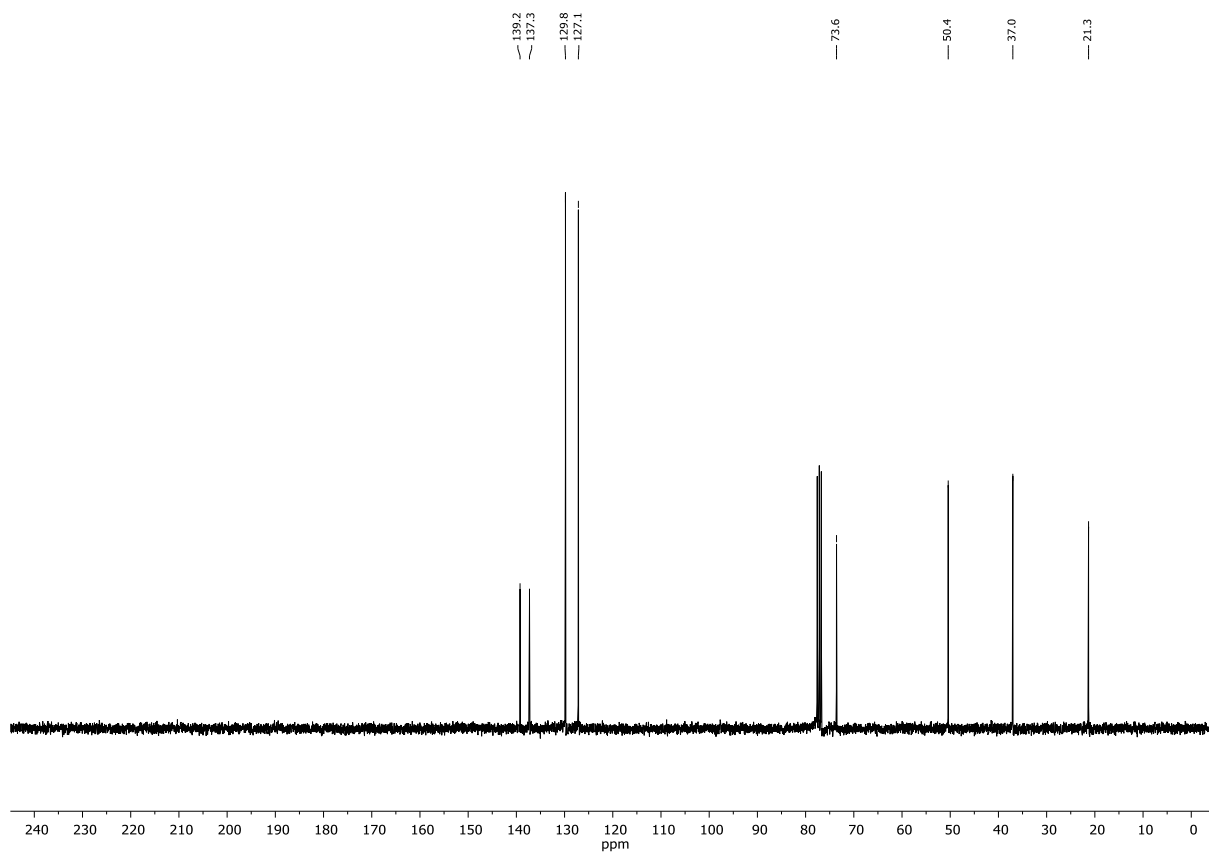
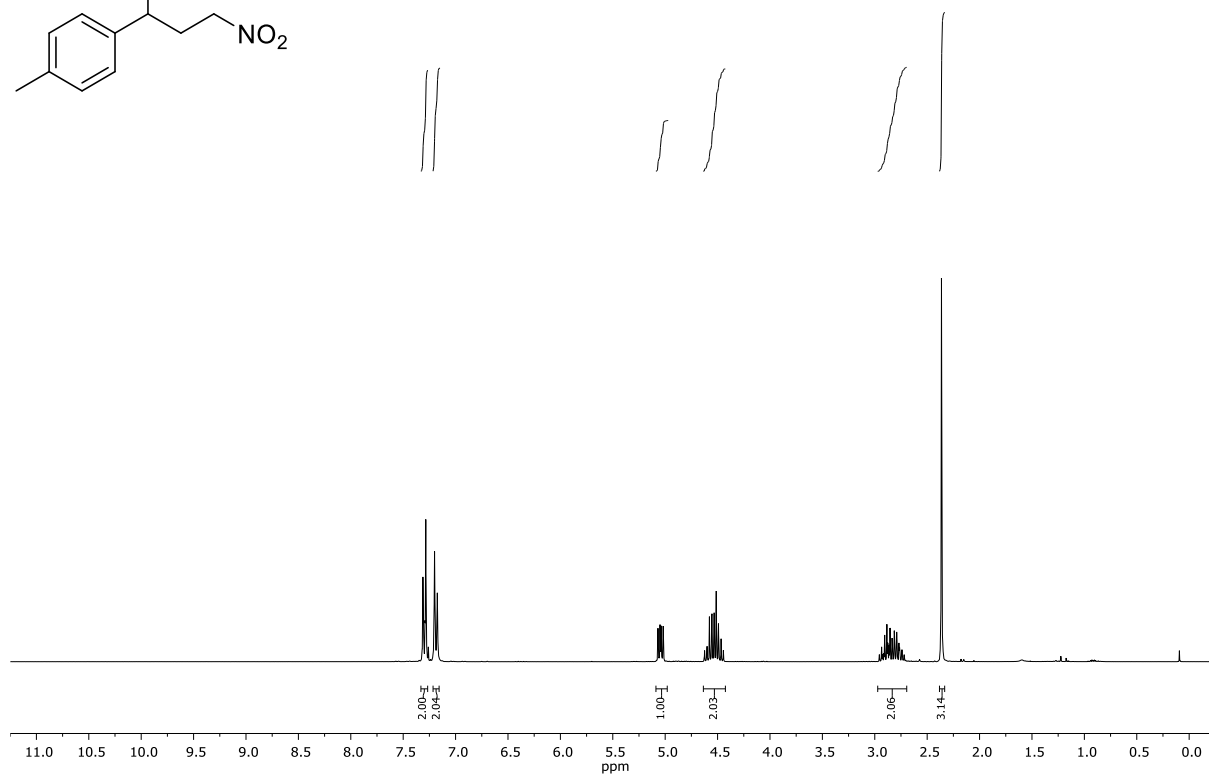
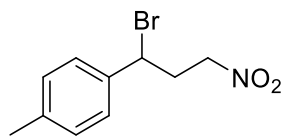
First image: ¹H-NMR; Second image: ¹³C-NMR; NMR solvent: CDCl₃

1-(1-bromo-3-nitropropyl)-3-methylbenzene (4c)



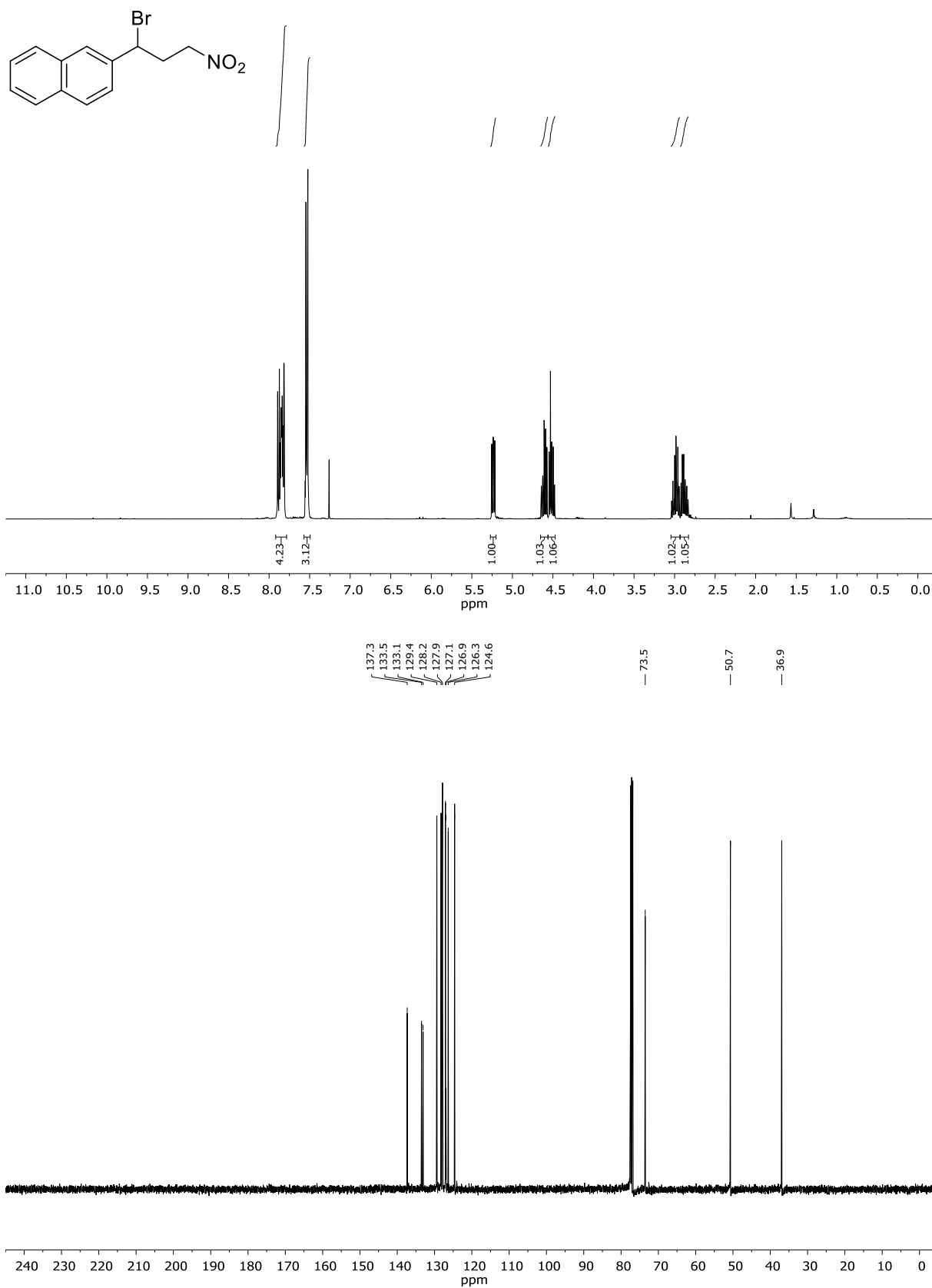
First image: $^1\text{H-NMR}$; Second image: $^{13}\text{C-NMR}$; NMR solvent: CDCl_3

1-(1-bromo-3-nitropropyl)-4-methylbenzene (4d)



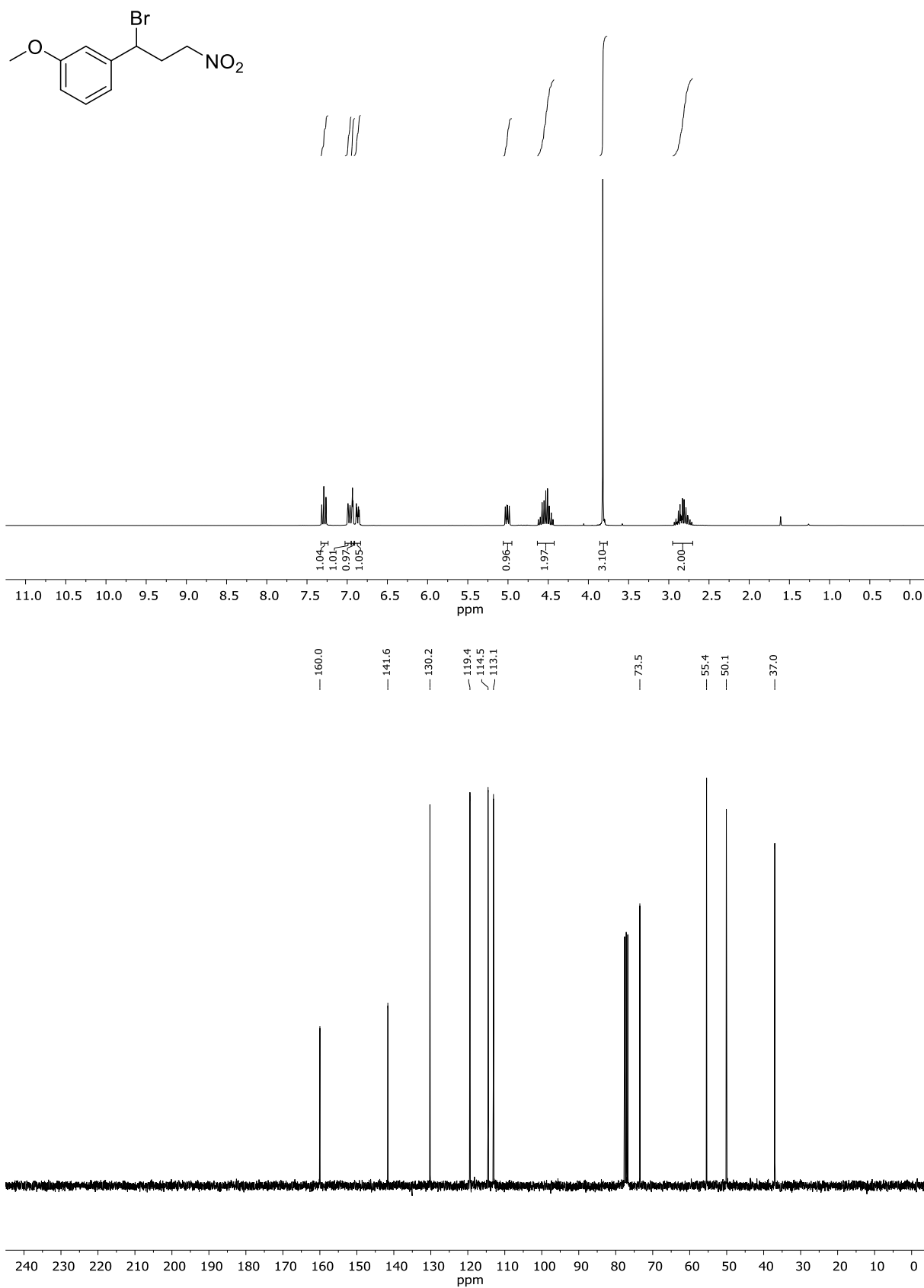
First image: $^1\text{H-NMR}$; Second image: $^{13}\text{C-NMR}$; NMR solvent: CDCl_3

2-(1-bromo-3-nitropropyl)naphthalene (4f)

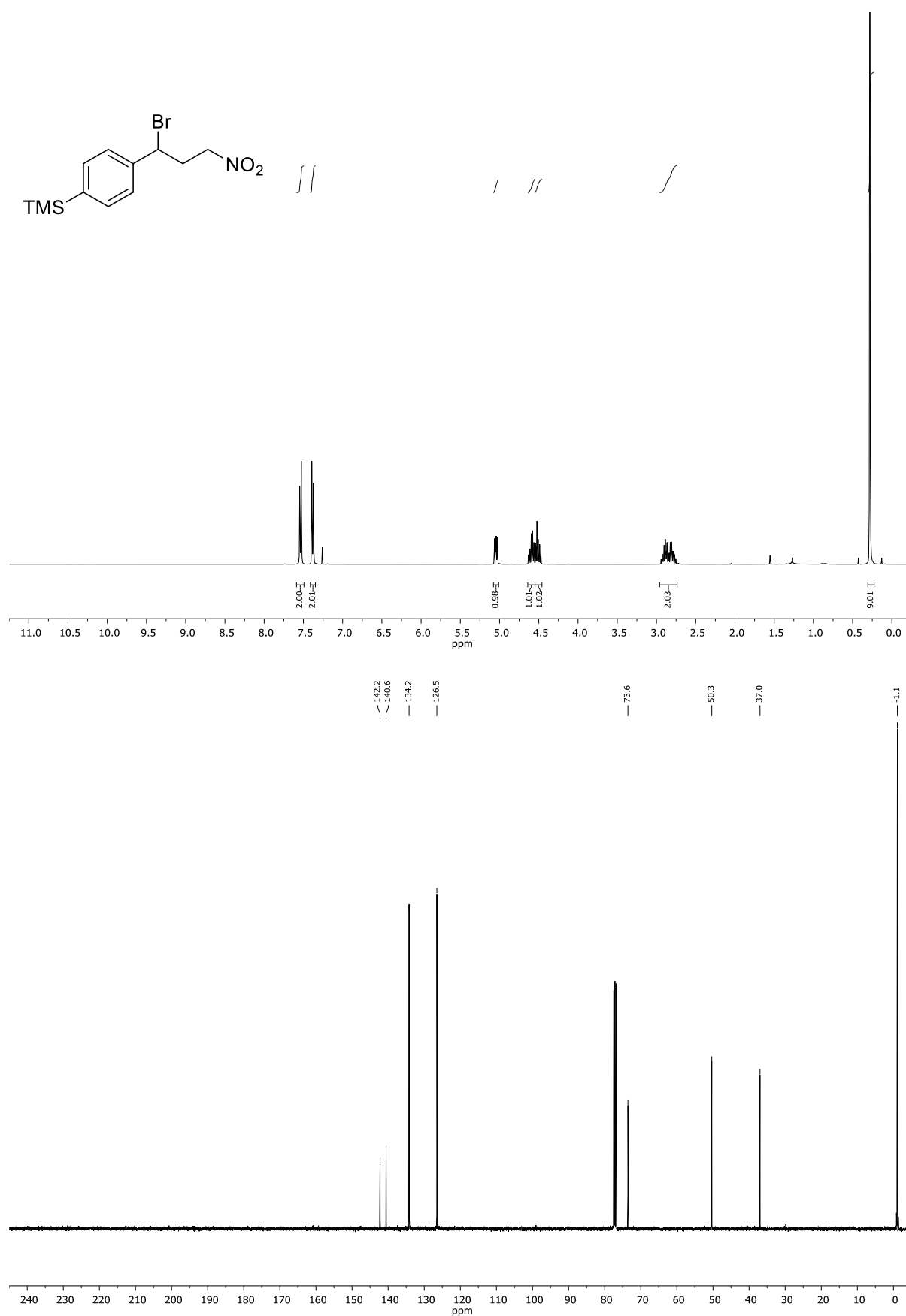


First image: ¹H-NMR; Second image: ¹³C-NMR; NMR solvent: CDCl₃

1-(1-bromo-3-nitropropyl)-3-methoxybenzene (4h)

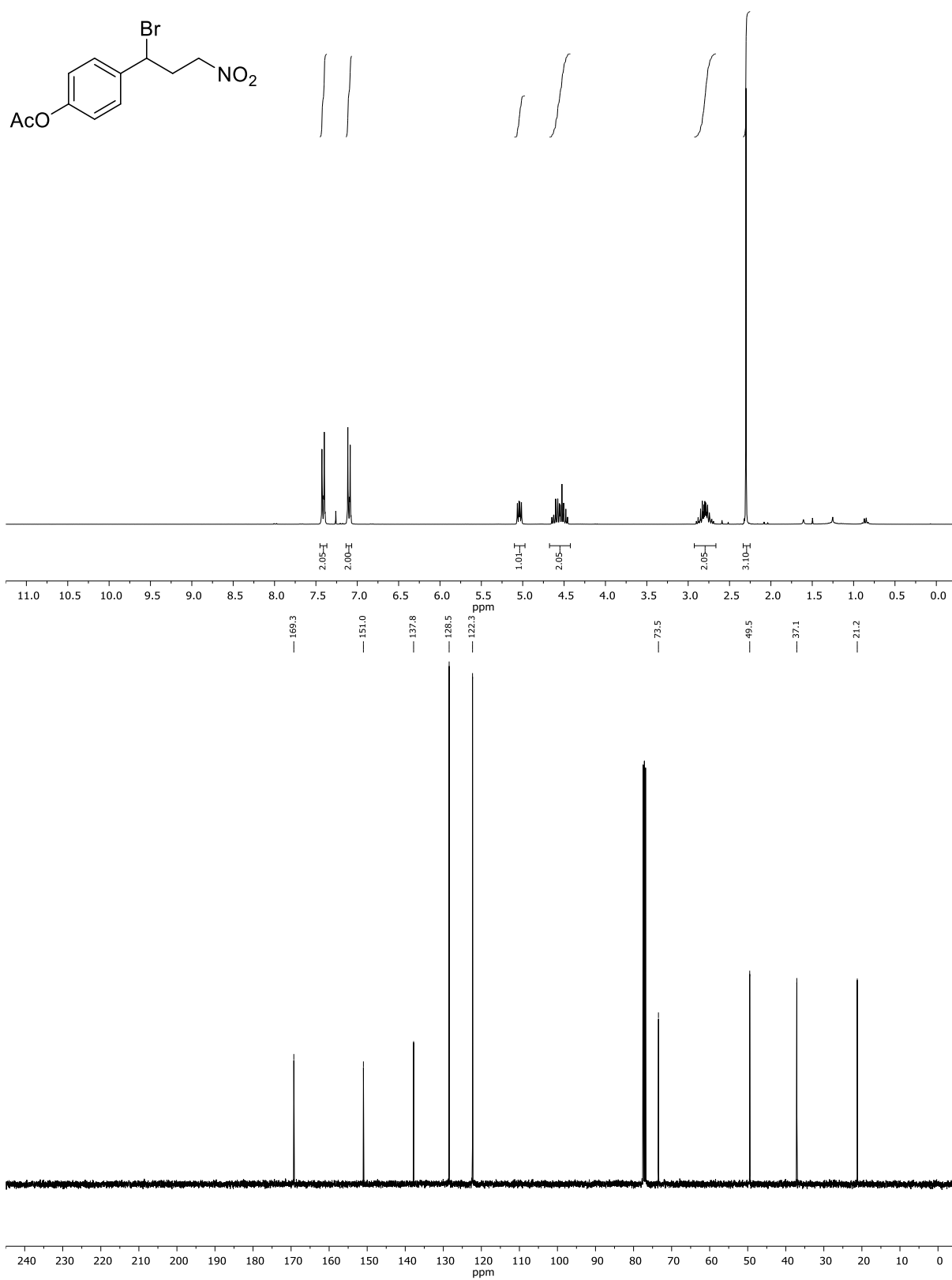


First image: ¹H-NMR; Second image: ¹³C-NMR; NMR solvent: CDCl₃

(4-(1-bromo-3-nitropropyl)phenyl)trimethylsilane (4i)

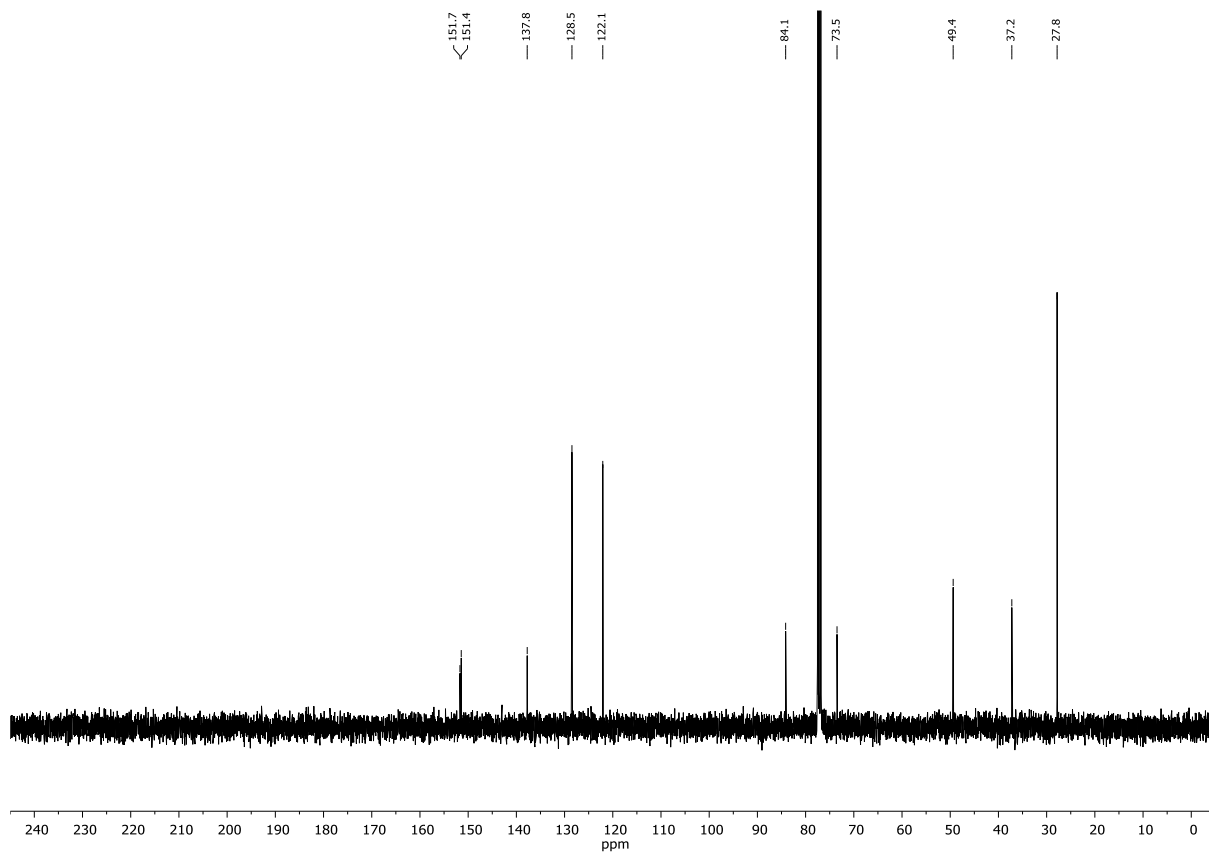
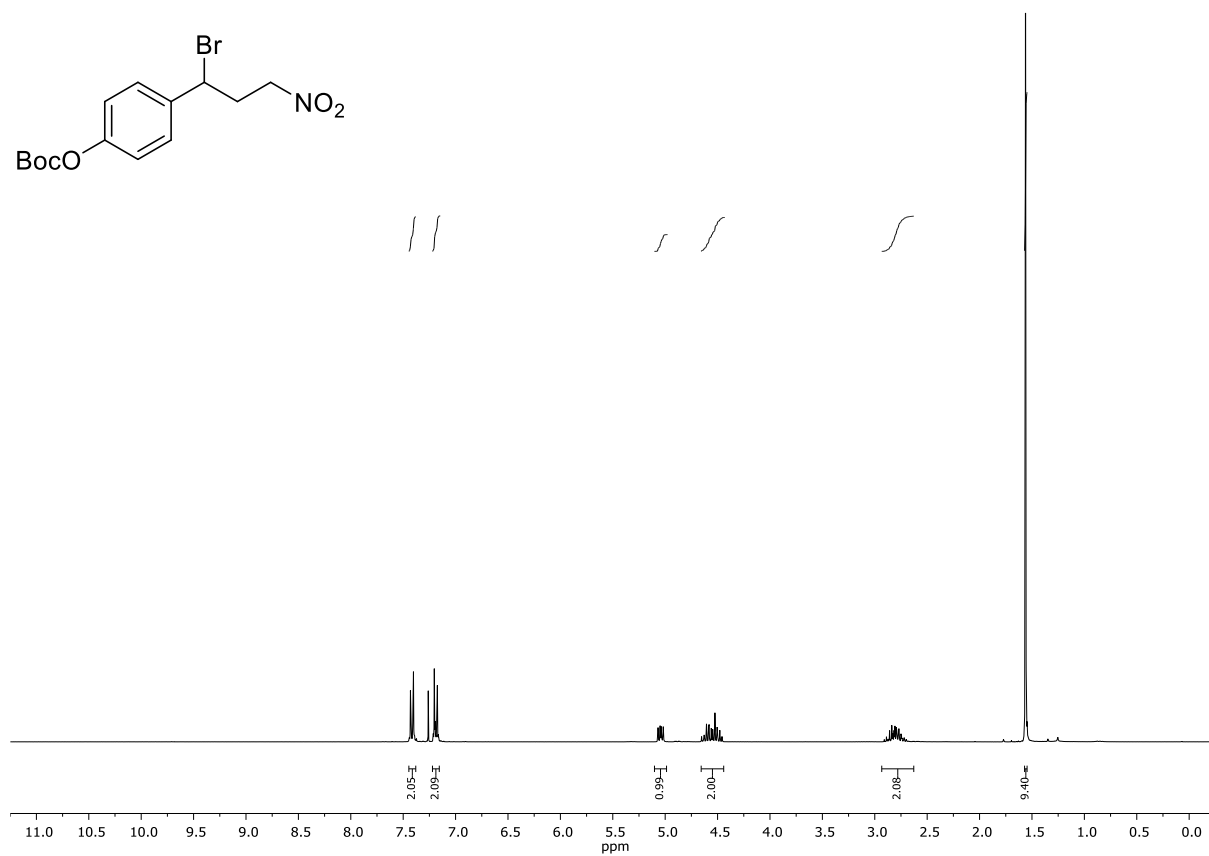
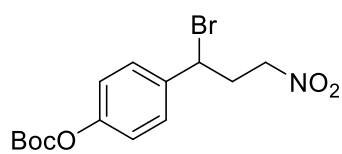
First image: ¹H-NMR; Second image: ¹³C-NMR; NMR solvent: CDCl₃

4-(1-bromo-3-nitropropyl)phenyl acetate(4j)



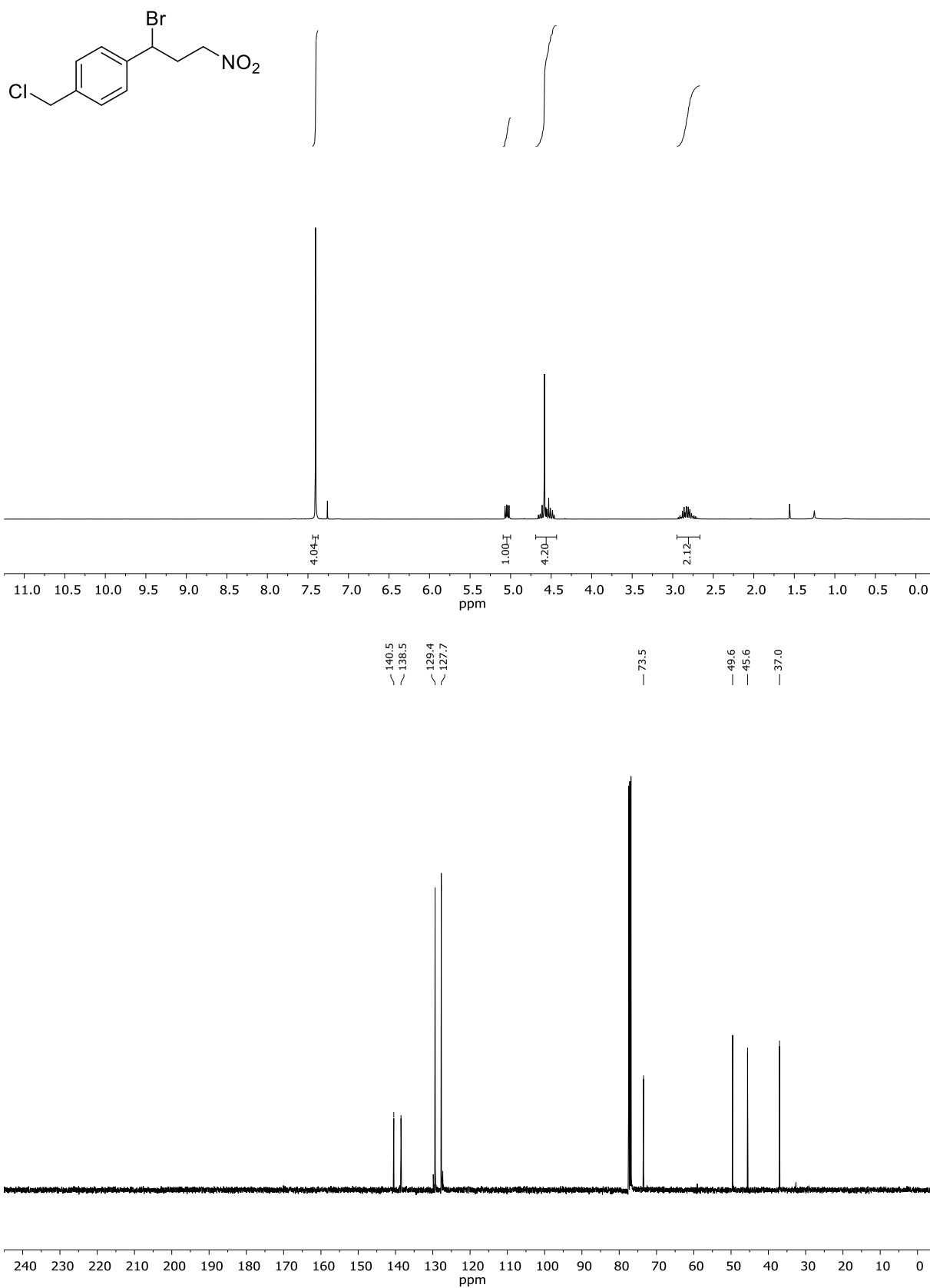
First image: ¹H-NMR; Second image: ¹³C-NMR; NMR solvent: CDCl₃

4-(1-bromo-3-nitropropyl)phenyl tert-butyl carbonate (4k)



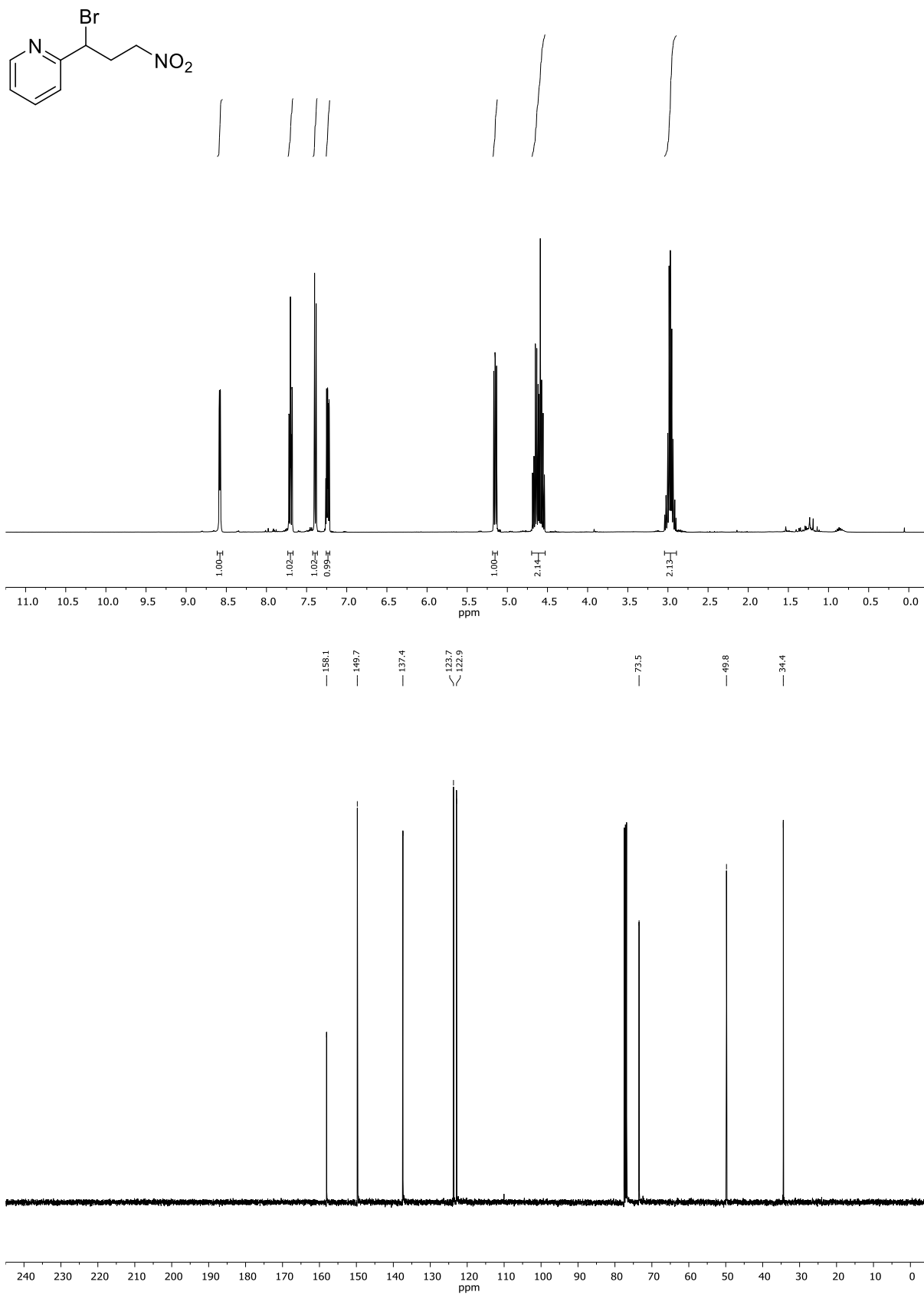
First image: $^1\text{H-NMR}$; Second image: $^{13}\text{C-NMR}$; NMR solvent: CDCl_3

1-(1-bromo-3-nitropropyl)-4-(chloromethyl)benzene (4n)



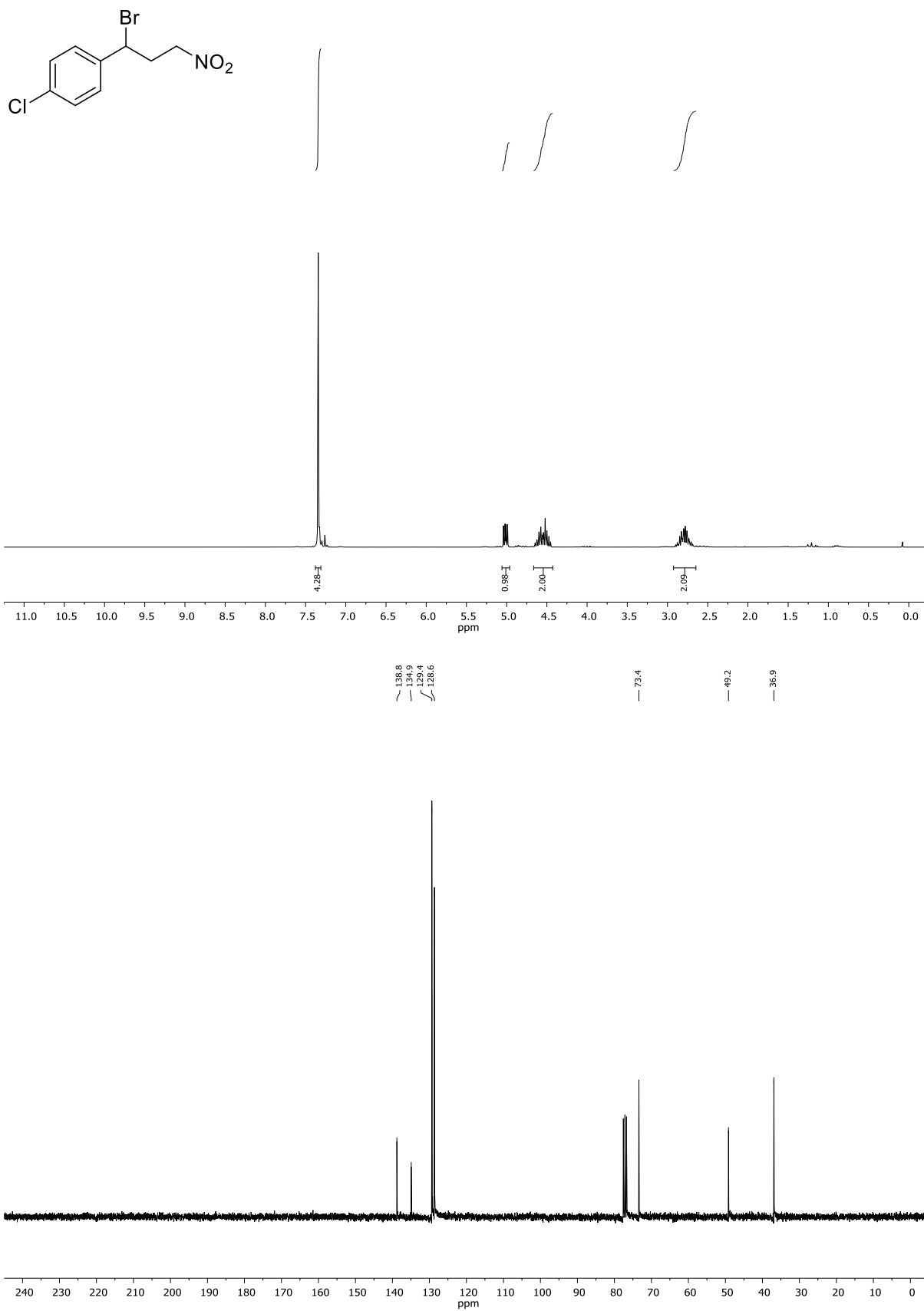
First image: ¹H-NMR; Second image: ¹³C-NMR; NMR solvent: CDCl₃

2-(1-bromo-3-nitropropyl)pyridine (4p)

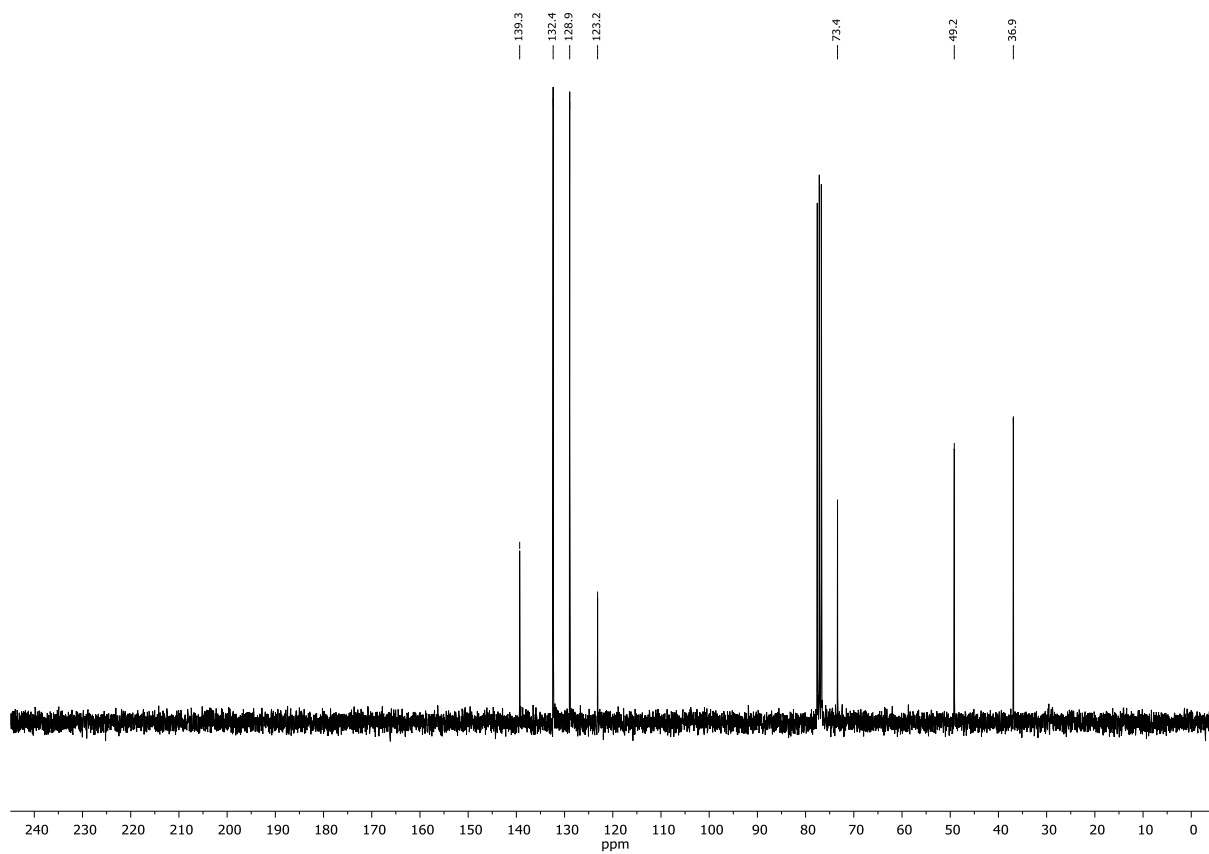
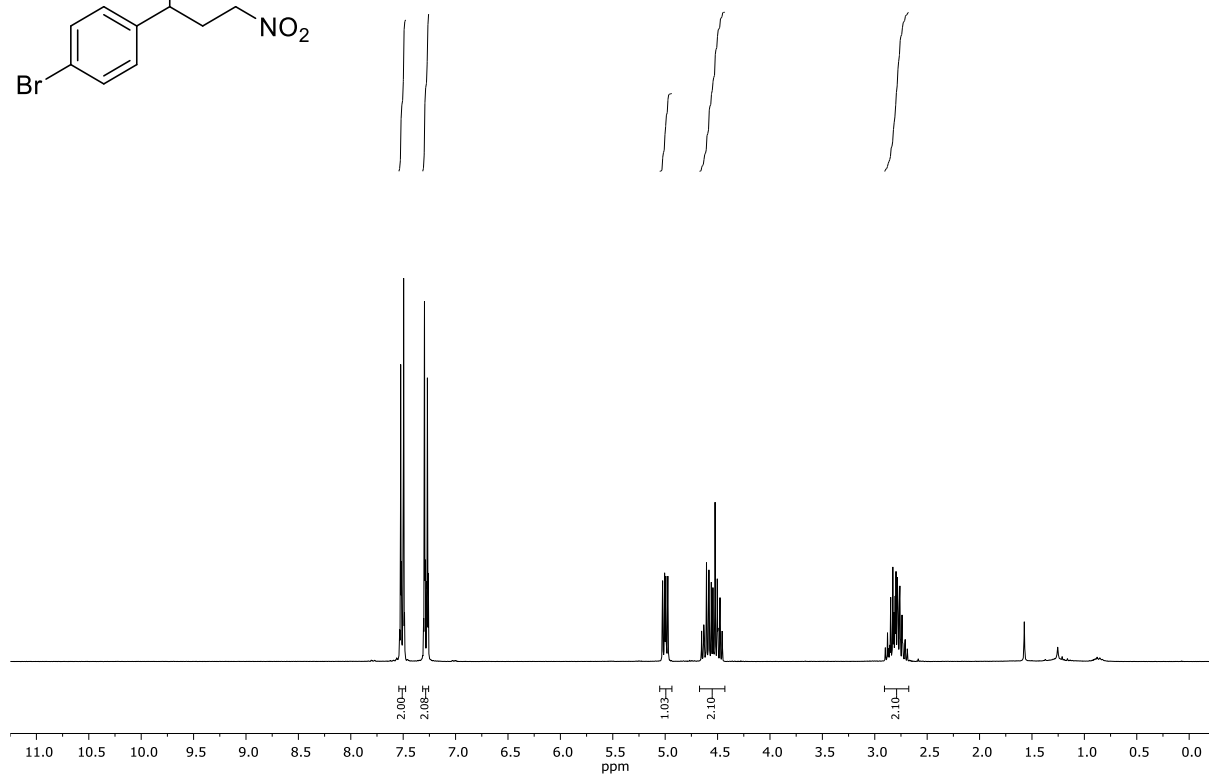
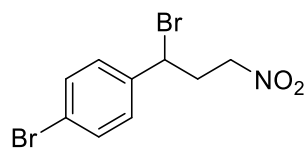


First image: ¹H-NMR; Second image: ¹³C-NMR; NMR solvent: CDCl₃

1-(1-bromo-3-nitropropyl)-4-chlorobenzene (4r)

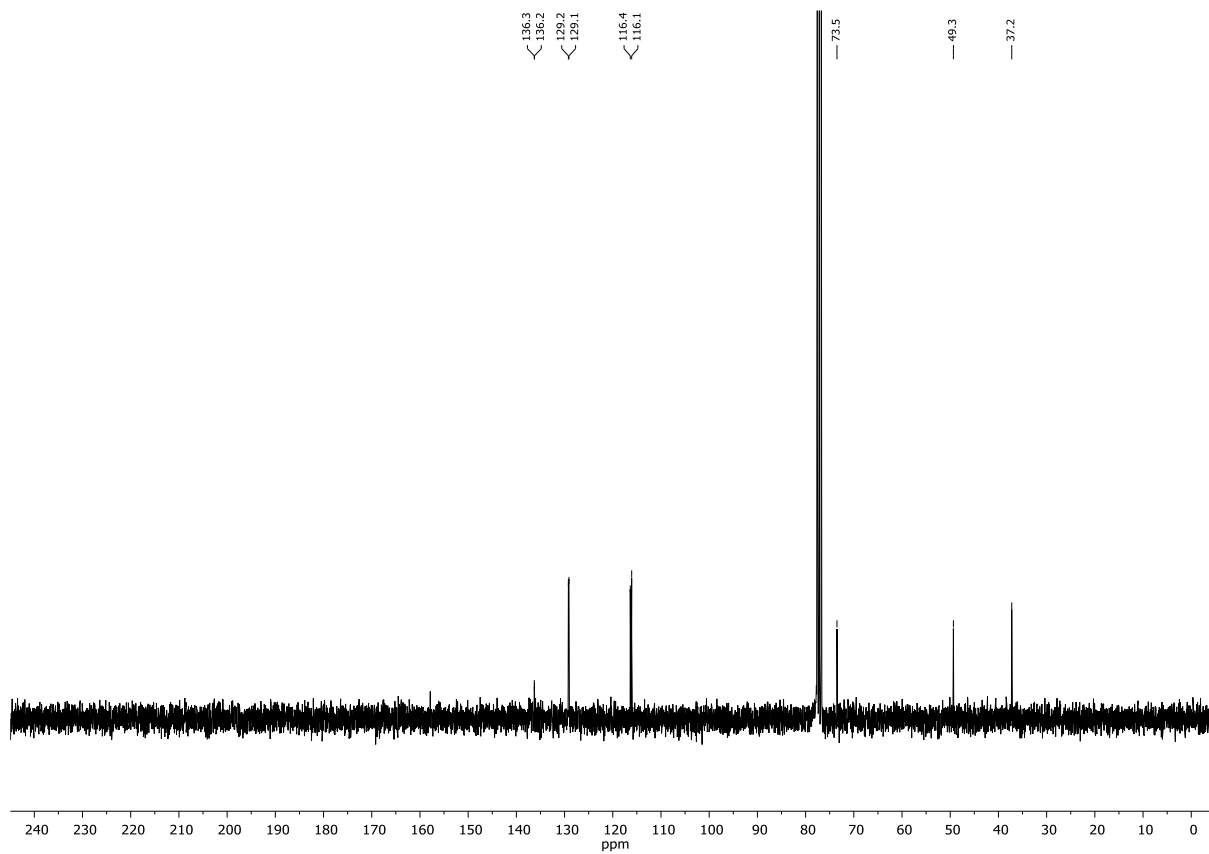
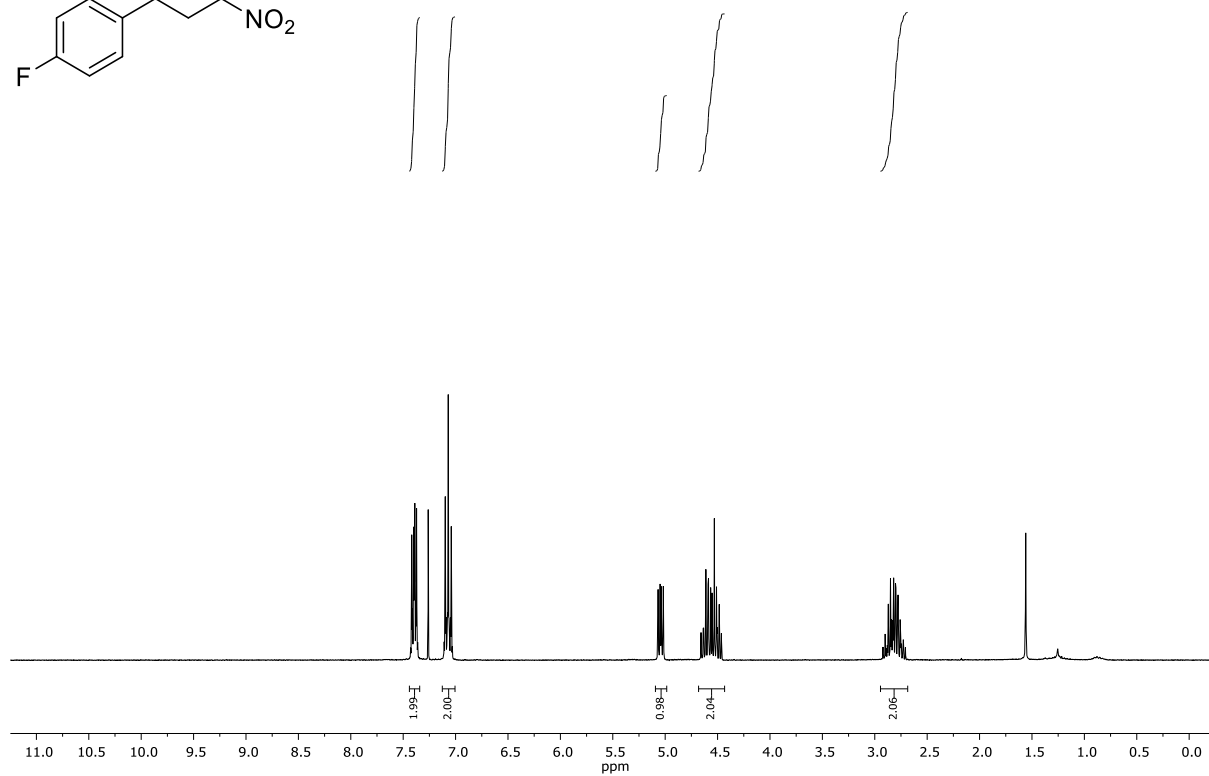
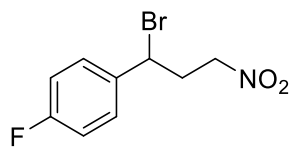


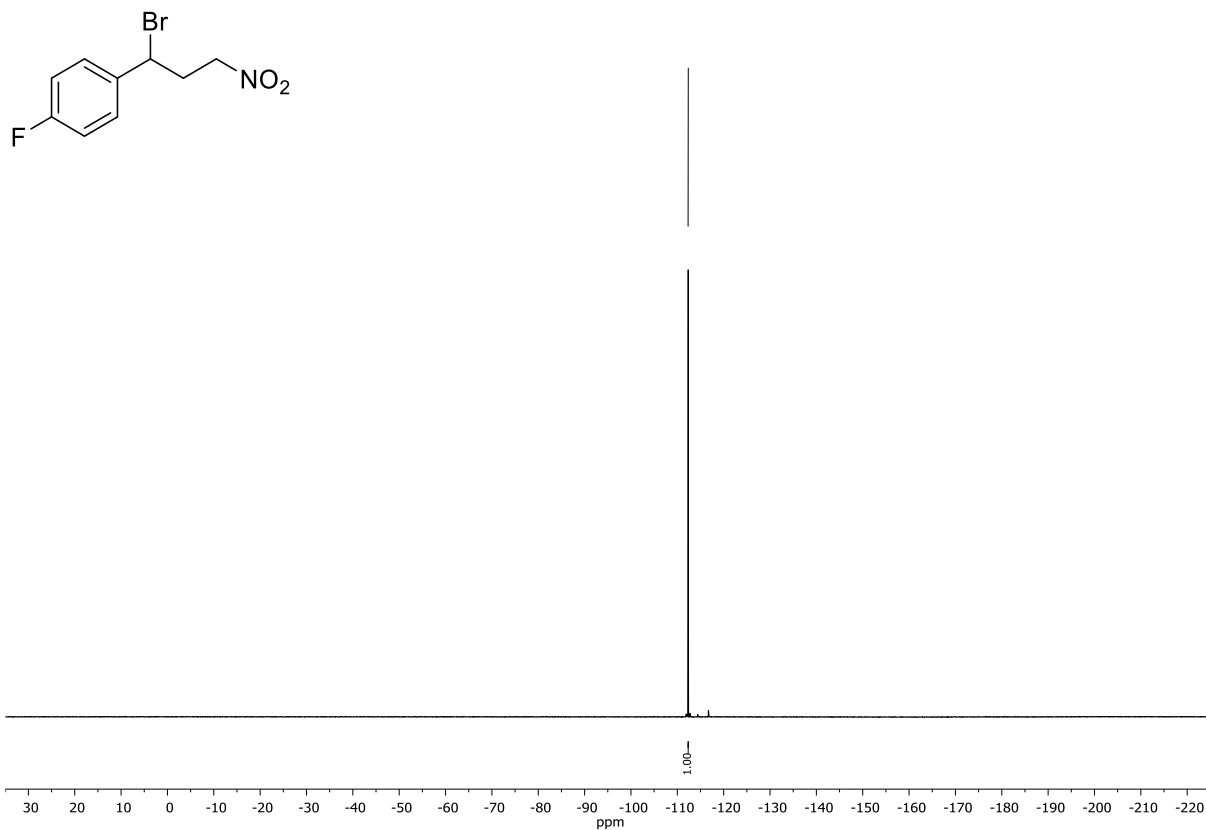
First image: ¹H-NMR; Second image: ¹³C-NMR; NMR solvent: CDCl₃

1-bromo-4-(1-bromo-3-nitropropyl)benzene (4s)

First image: $^1\text{H-NMR}$; Second image: $^{13}\text{C-NMR}$; NMR solvent: CDCl_3

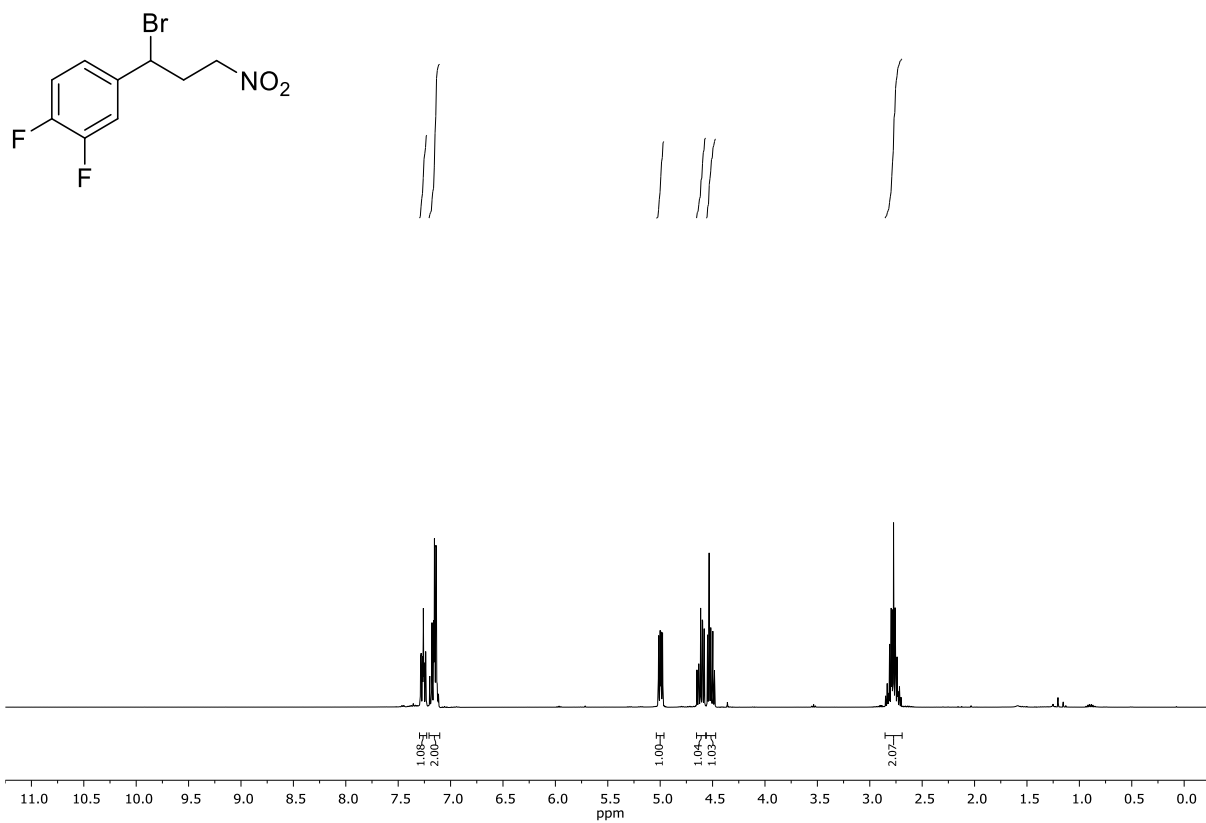
1-fluoro-4-(1-bromo-3-nitropropyl)benzene (4t)



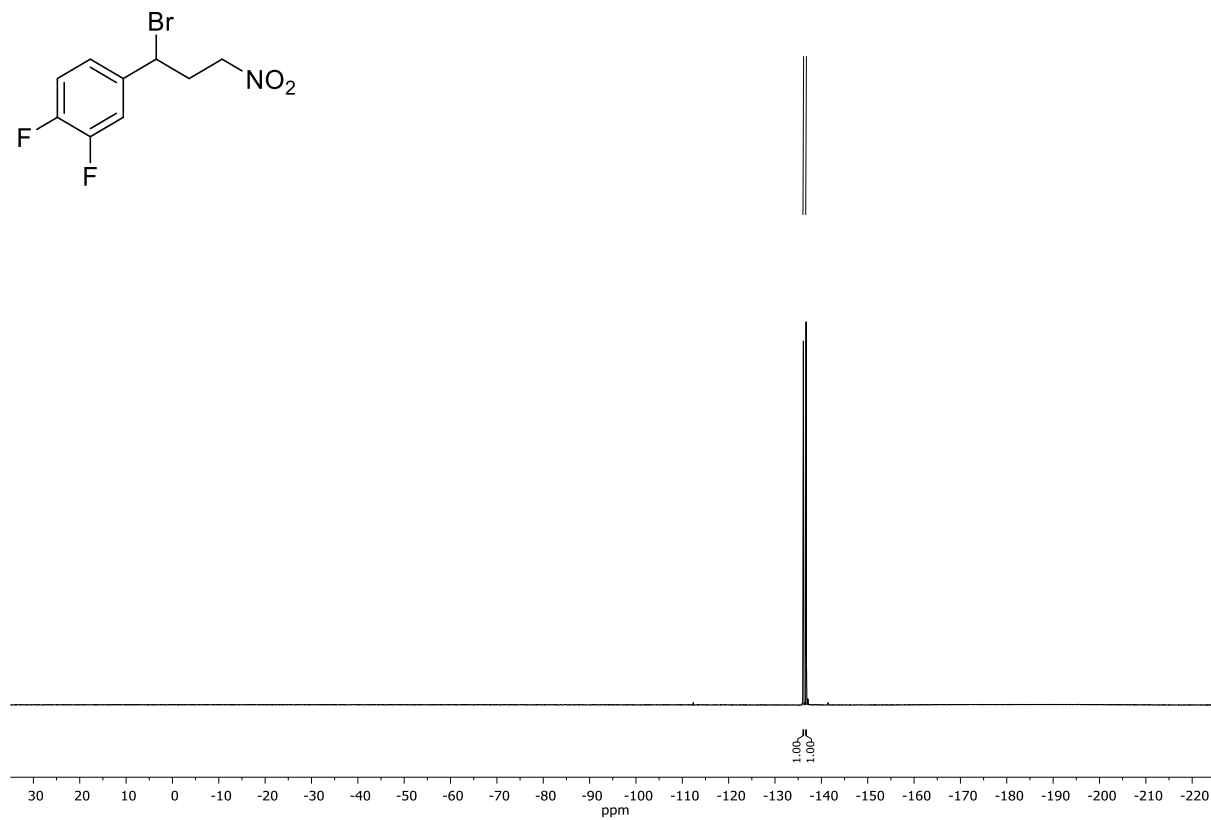
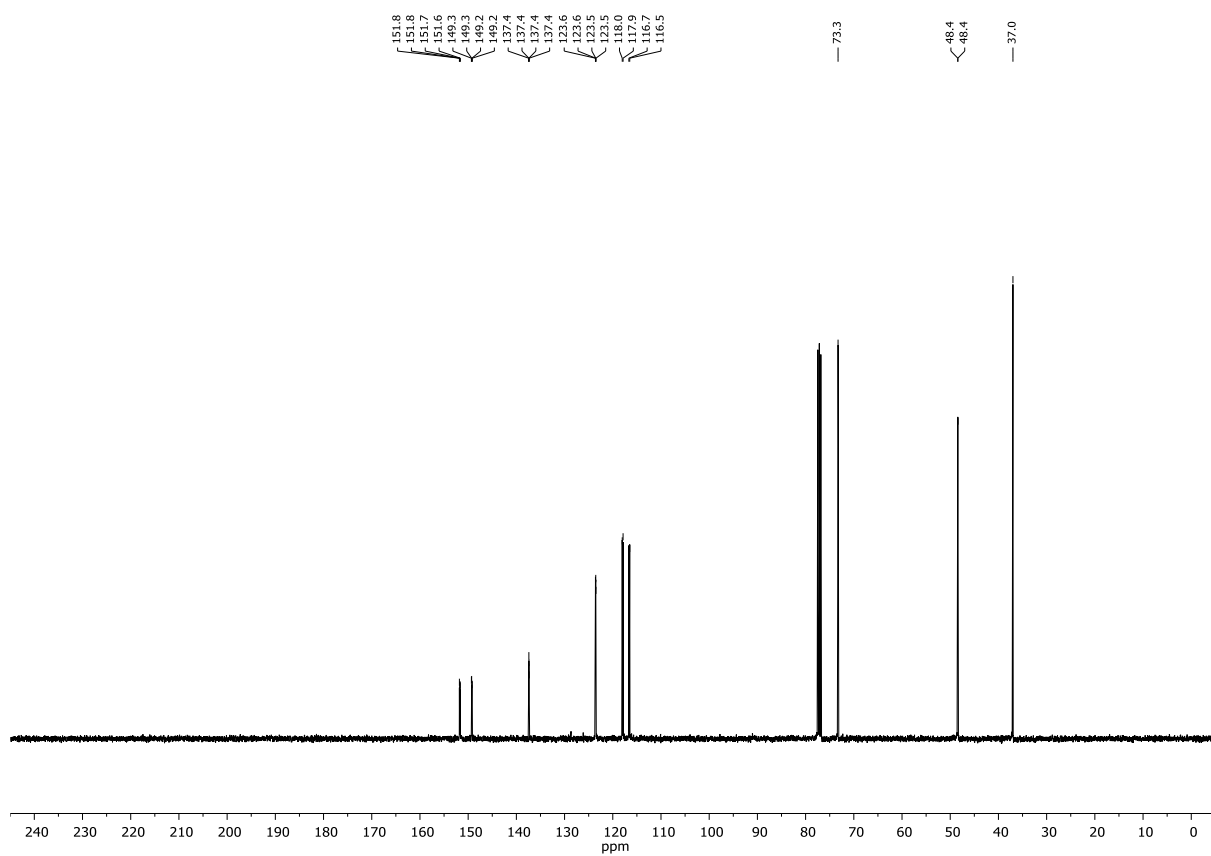


First image: $^1\text{H-NMR}$; Second image: $^{13}\text{C-NMR}$; Third image: $^{19}\text{F-NMR}$; NMR solvent: CDCl_3

4-(1-bromo-3-nitropropyl)-1,2-difluorobenzene (4v)

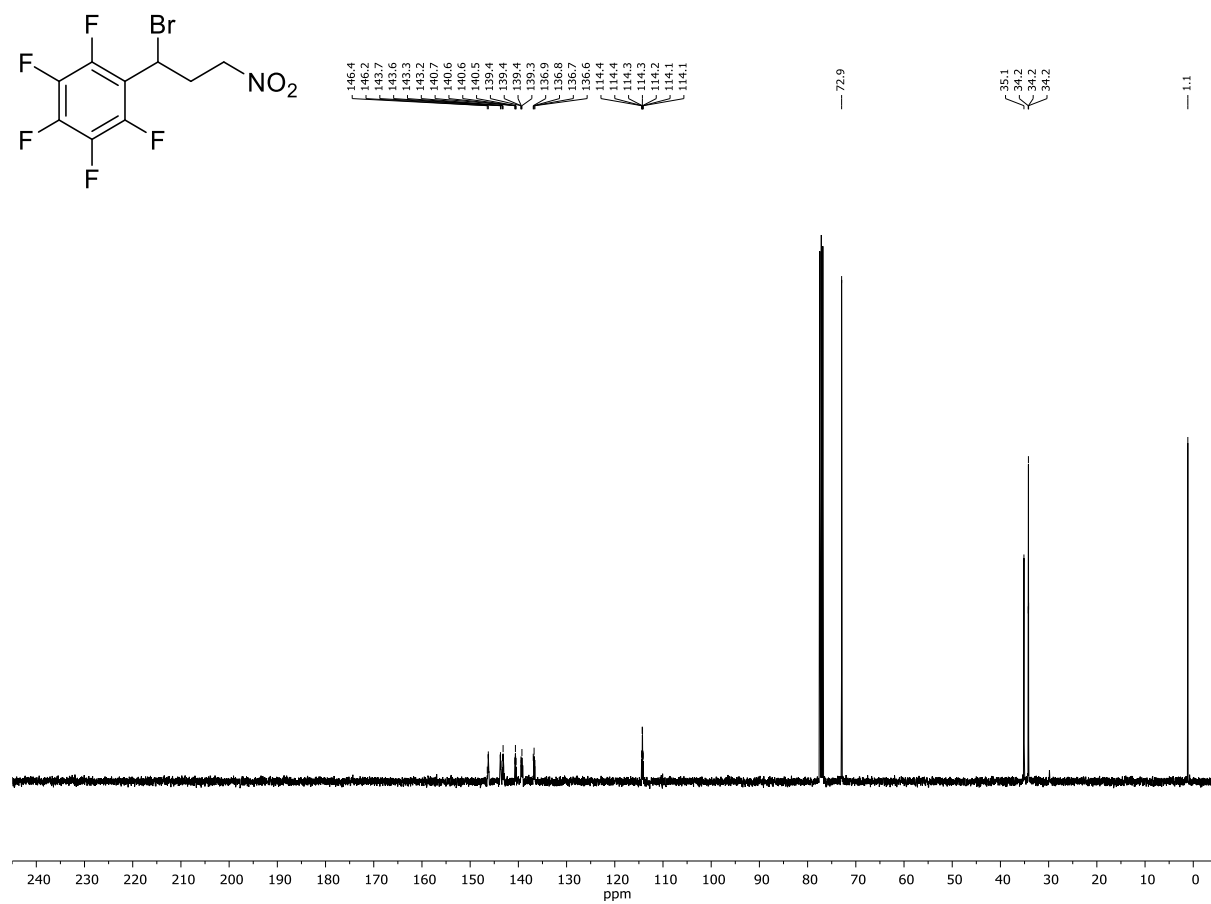
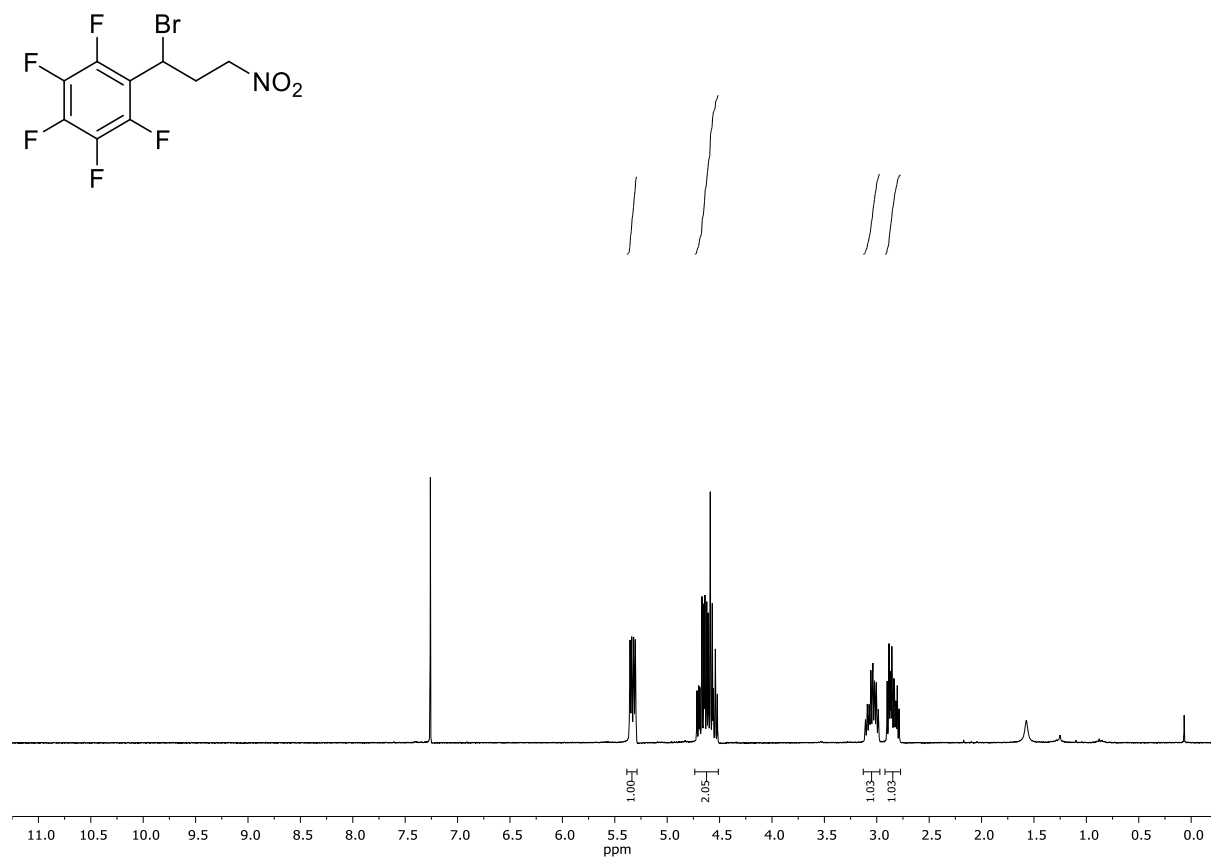


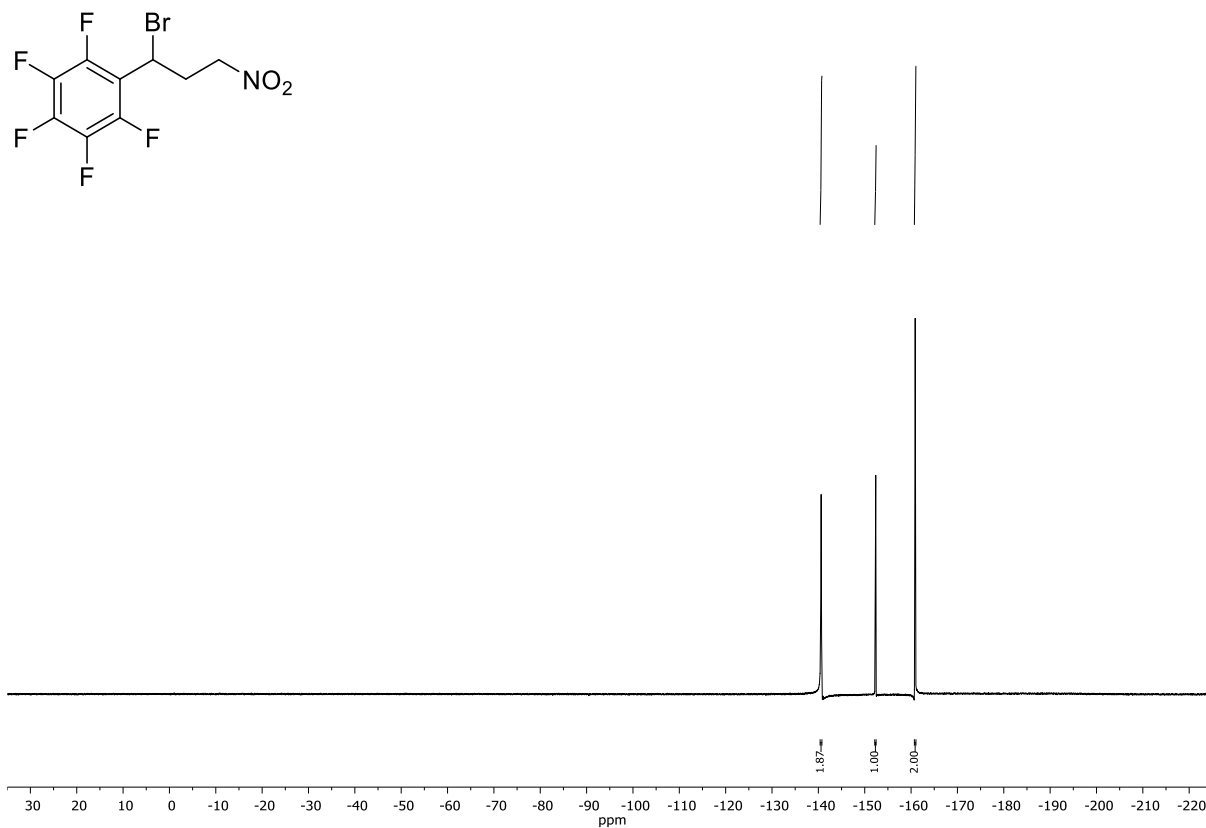
Chapter 6 Scientific Appendix



First image: ¹H-NMR; Second image: ¹³C-NMR; Third image: ¹⁹F-NMR; NMR solvent: CDCl₃

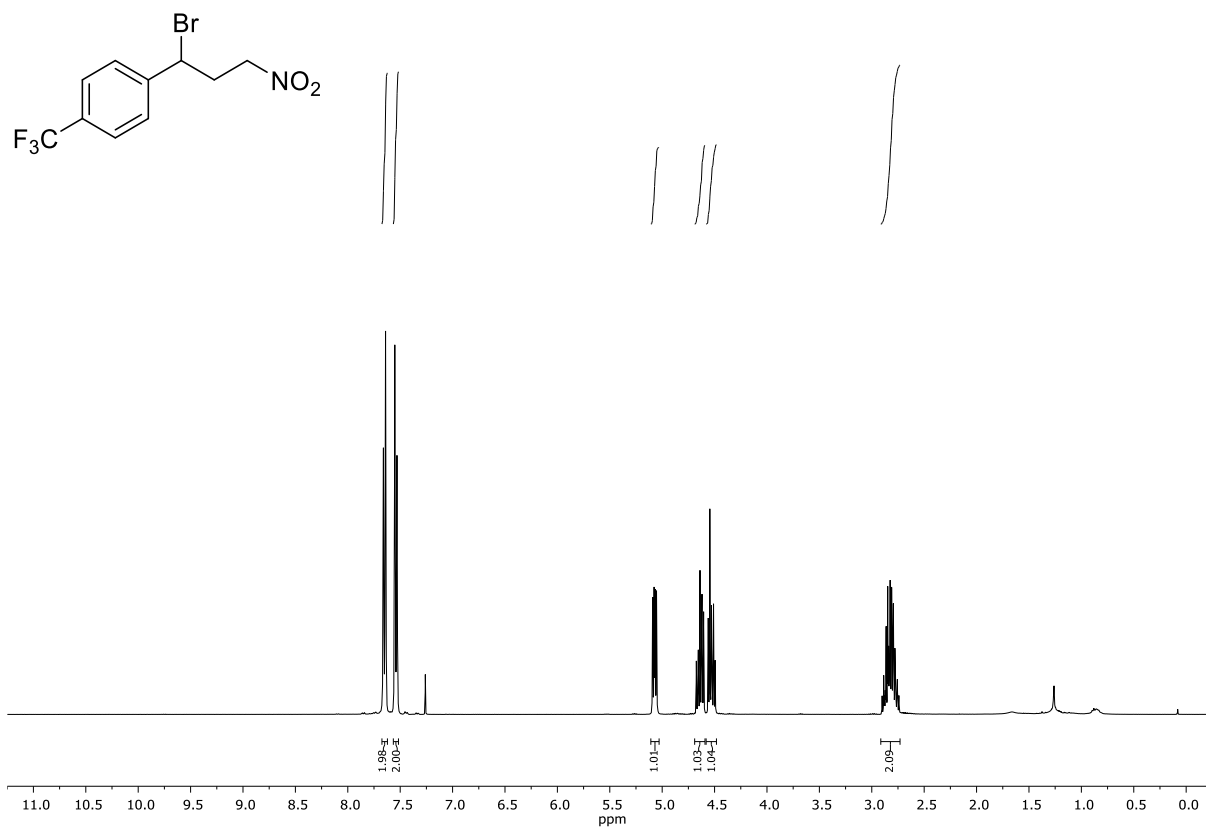
4-(1-bromo-3-nitropropyl)-1,2-difluorobenzene (4w)

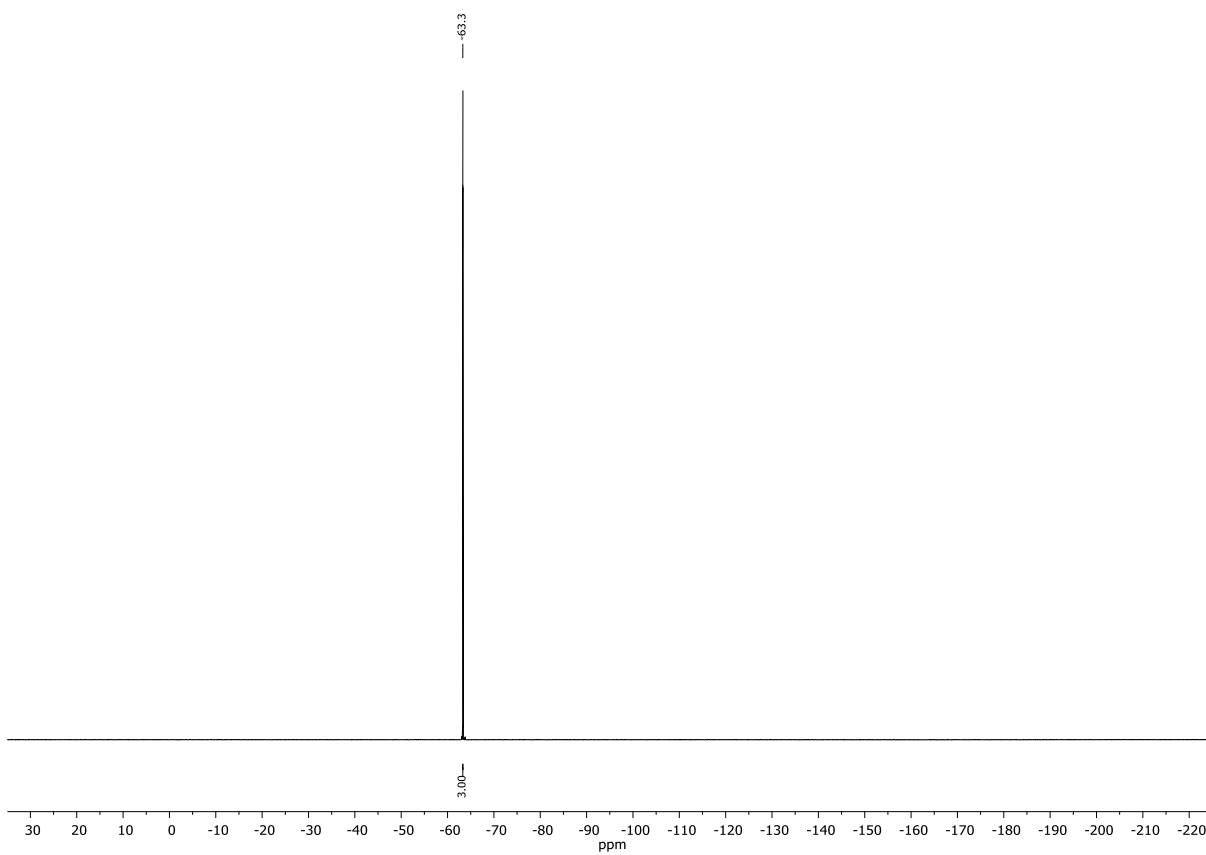
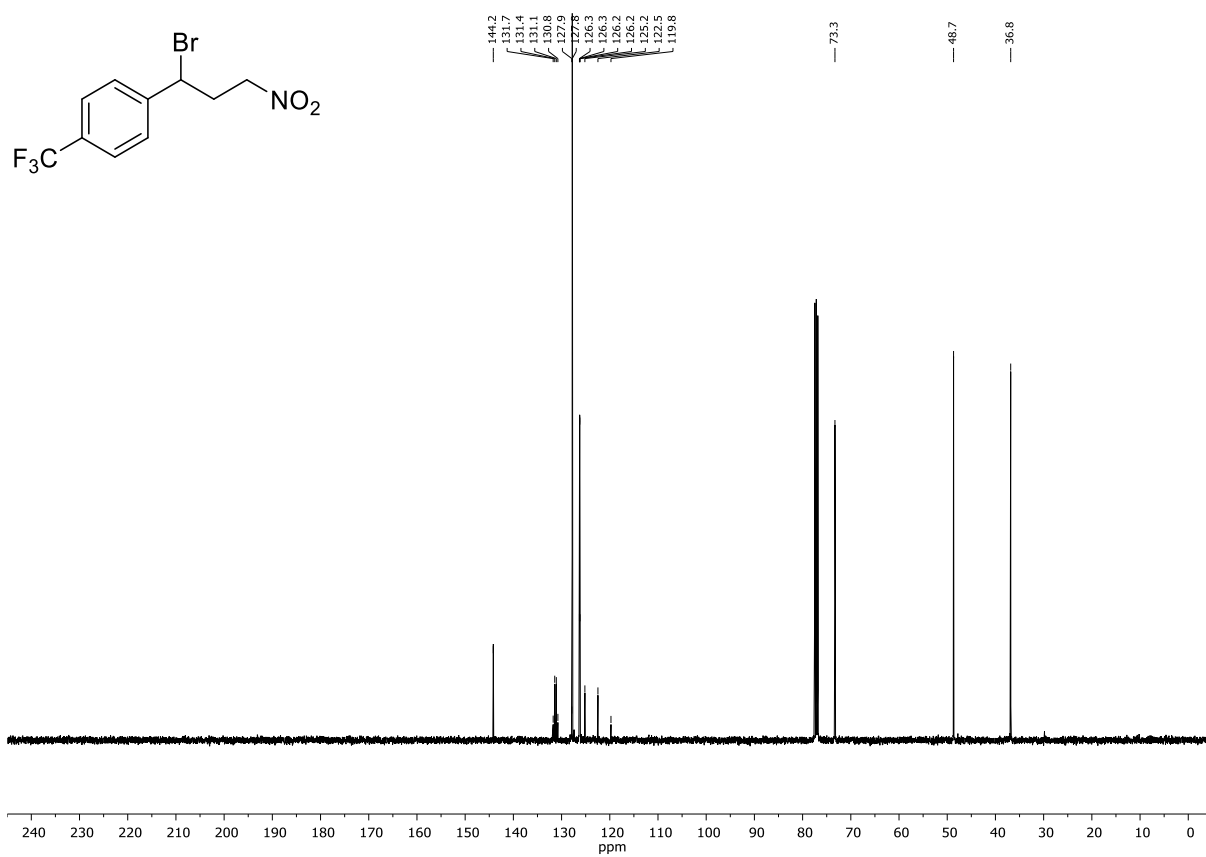




First image: $^1\text{H-NMR}$; Second image: $^{13}\text{C-NMR}$; Third image: $^{19}\text{F-NMR}$; NMR solvent: CDCl_3

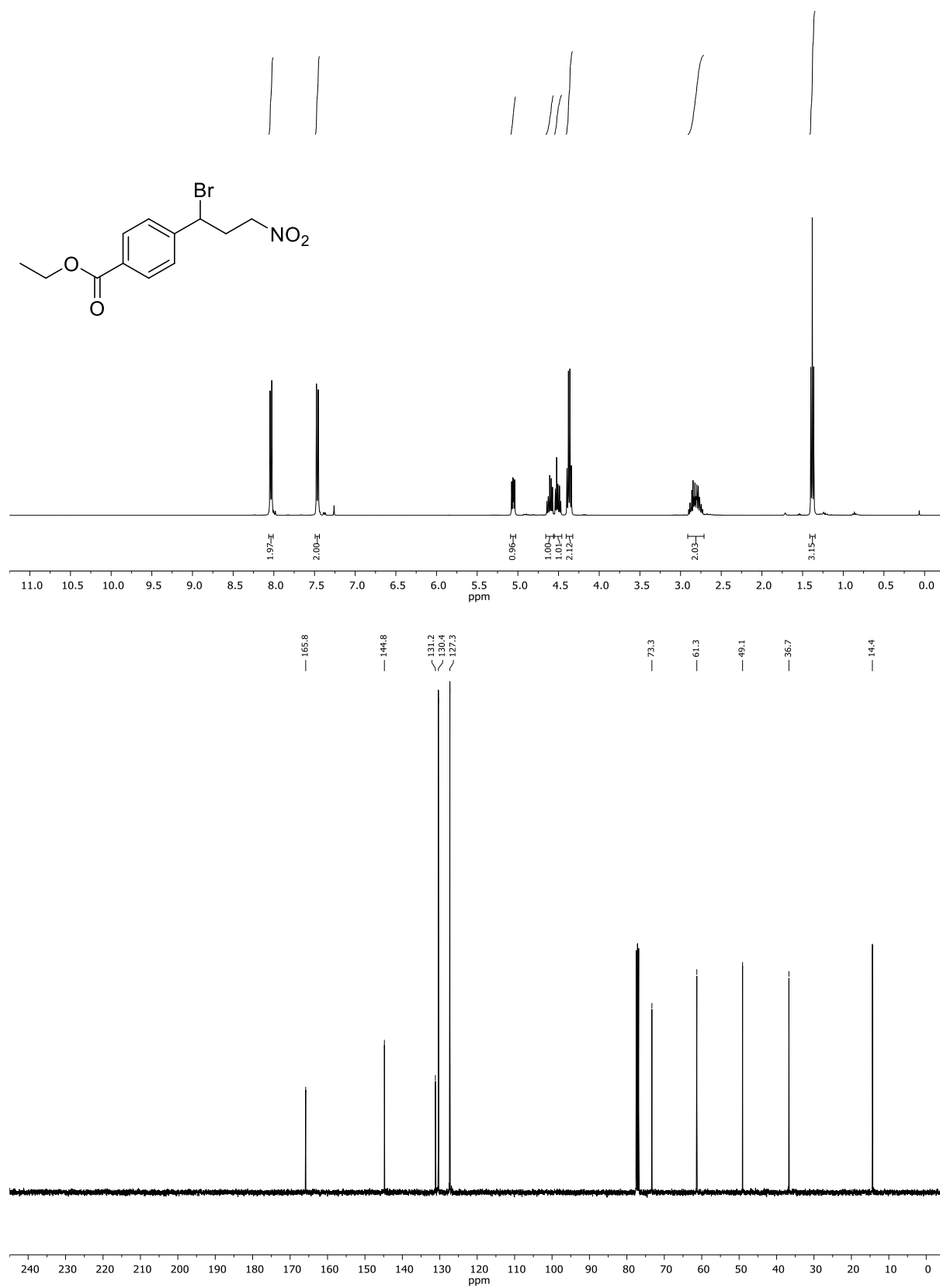
1-(1-bromo-3-nitropropyl)-4-(trifluoromethyl)benzene (4x)





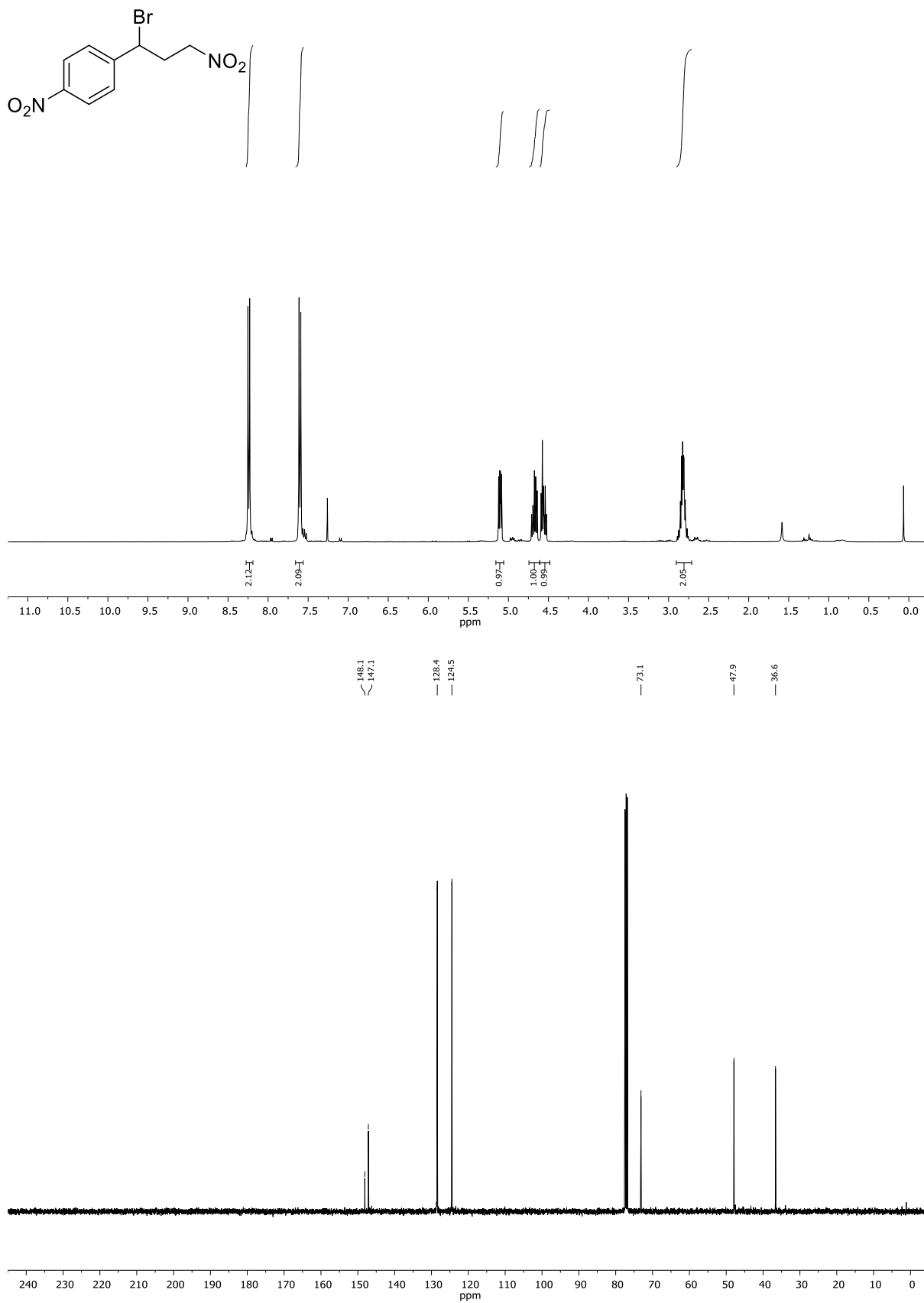
First image: ¹H-NMR; Second image: ¹³C-NMR; Third image: ¹⁹F-NMR; NMR solvent: CDCl₃

ethyl 4-(1-bromo-3-nitropropyl)benzoate (4z)



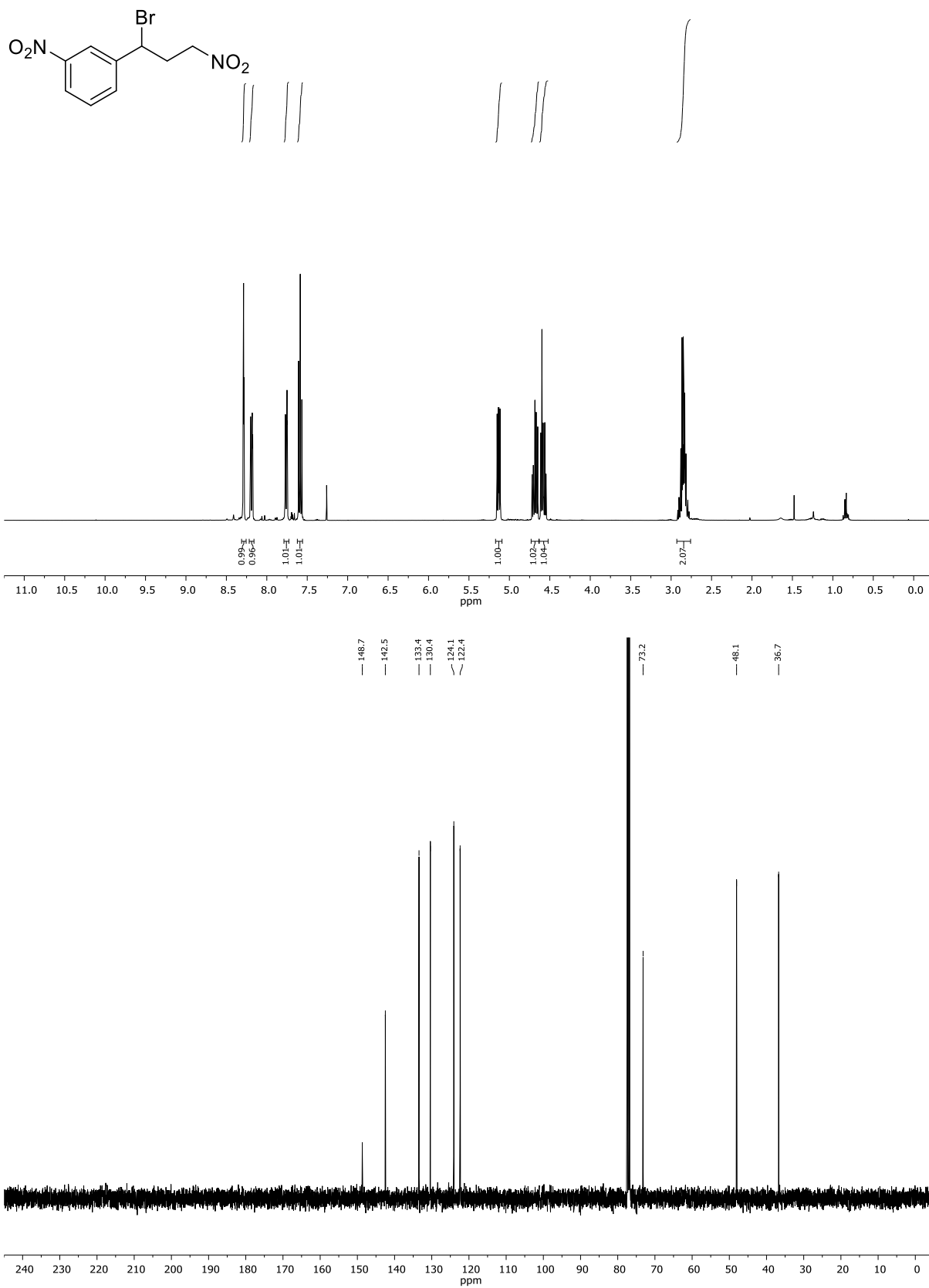
First image: ¹H-NMR; Second image: ¹³C-NMR; NMR solvent: CDCl₃

1-(1-bromo-3-nitropropyl)-4-nitrobenzene (4aa)



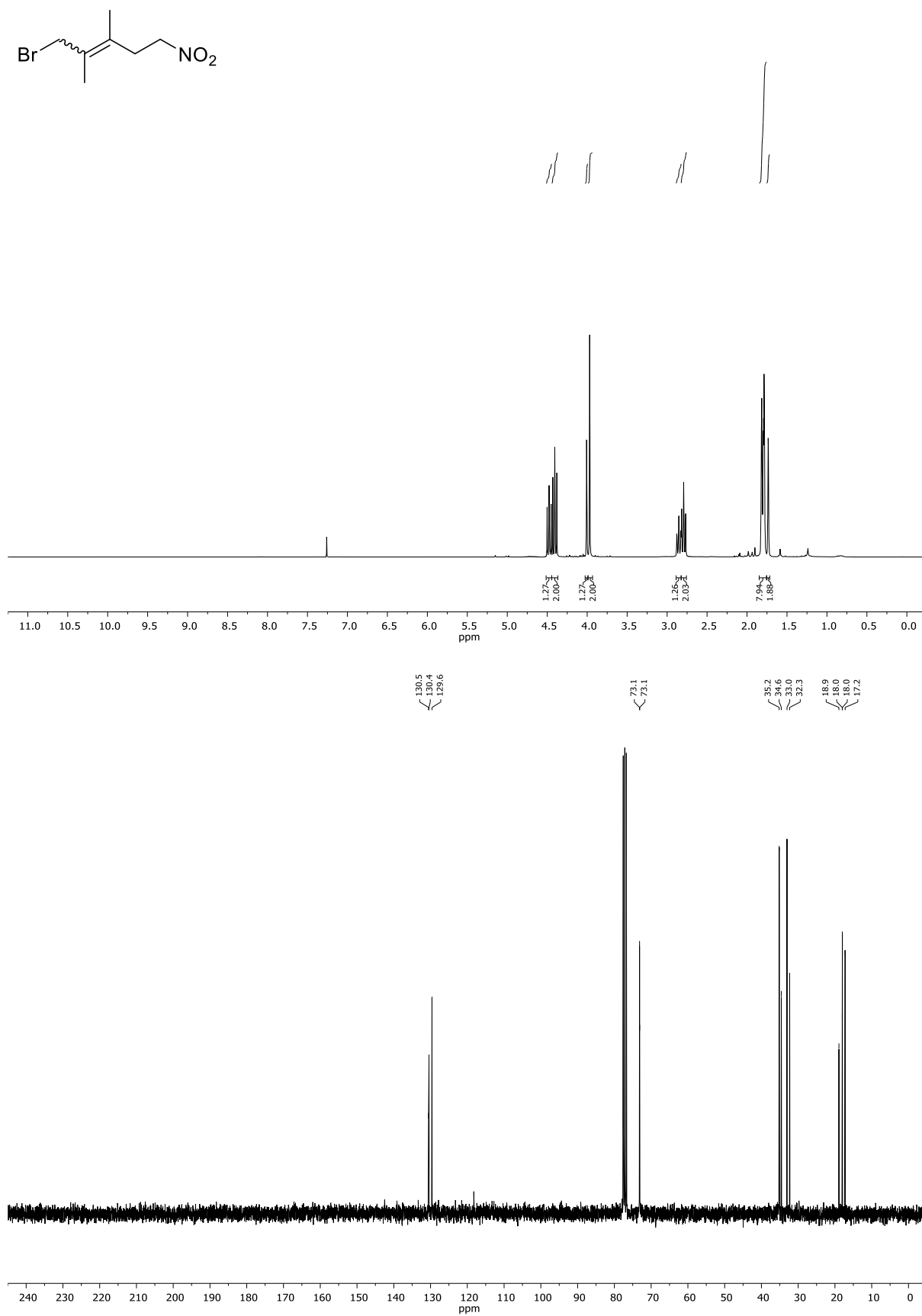
First image: ¹H-NMR; Second image: ¹³C-NMR; NMR solvent: CDCl₃

1-(1-bromo-3-nitropropyl)-3-nitrobenzene (4ab)



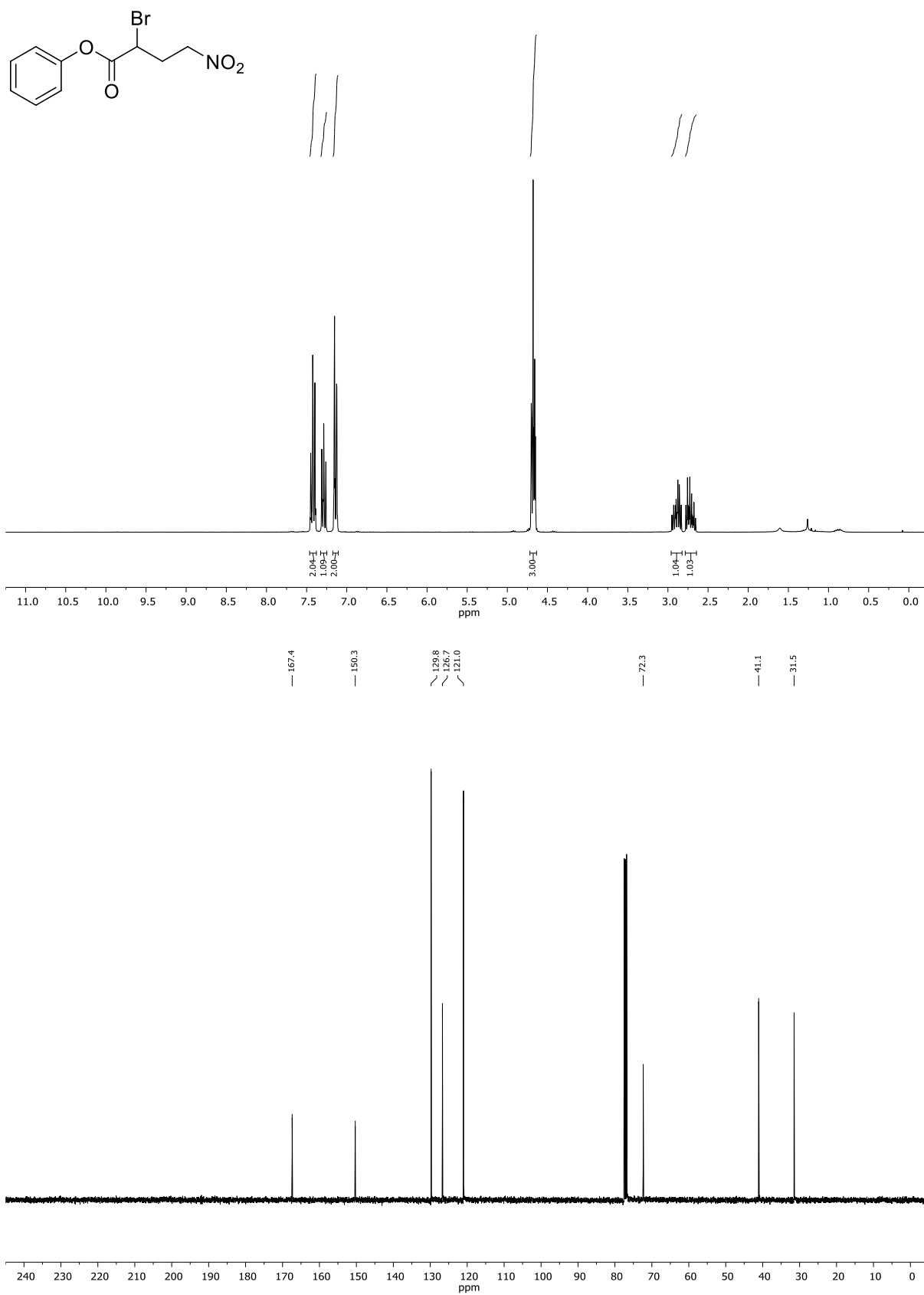
First image: $^1\text{H-NMR}$; Second image: $^{13}\text{C-NMR}$; NMR solvent: CDCl_3

1-bromo-2,3-dimethyl-5-nitropent-2-ene (E/Z = 61:39) (4ae)

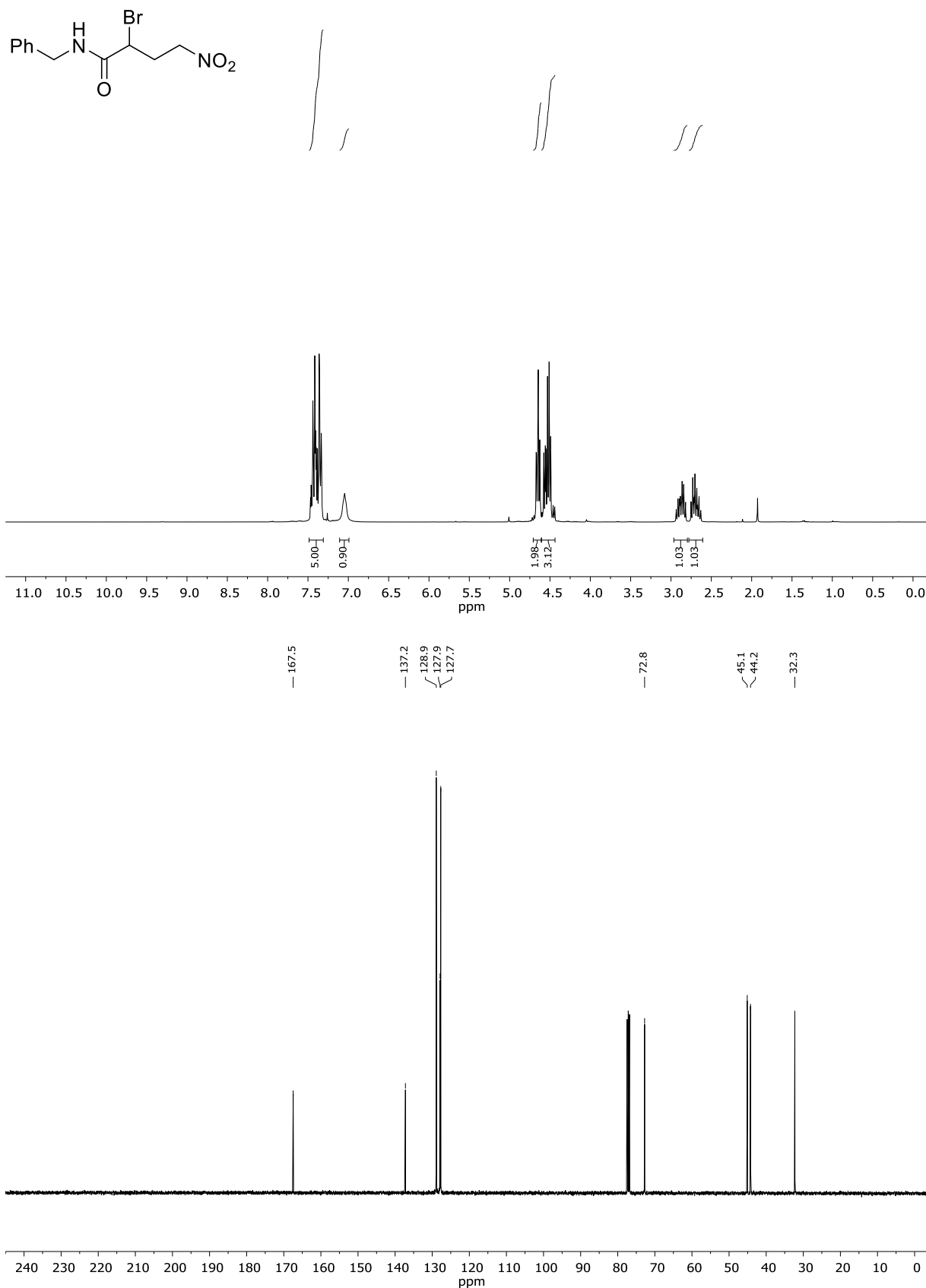


First image: ¹H-NMR; Second image: ¹³C-NMR; NMR solvent: CDCl₃

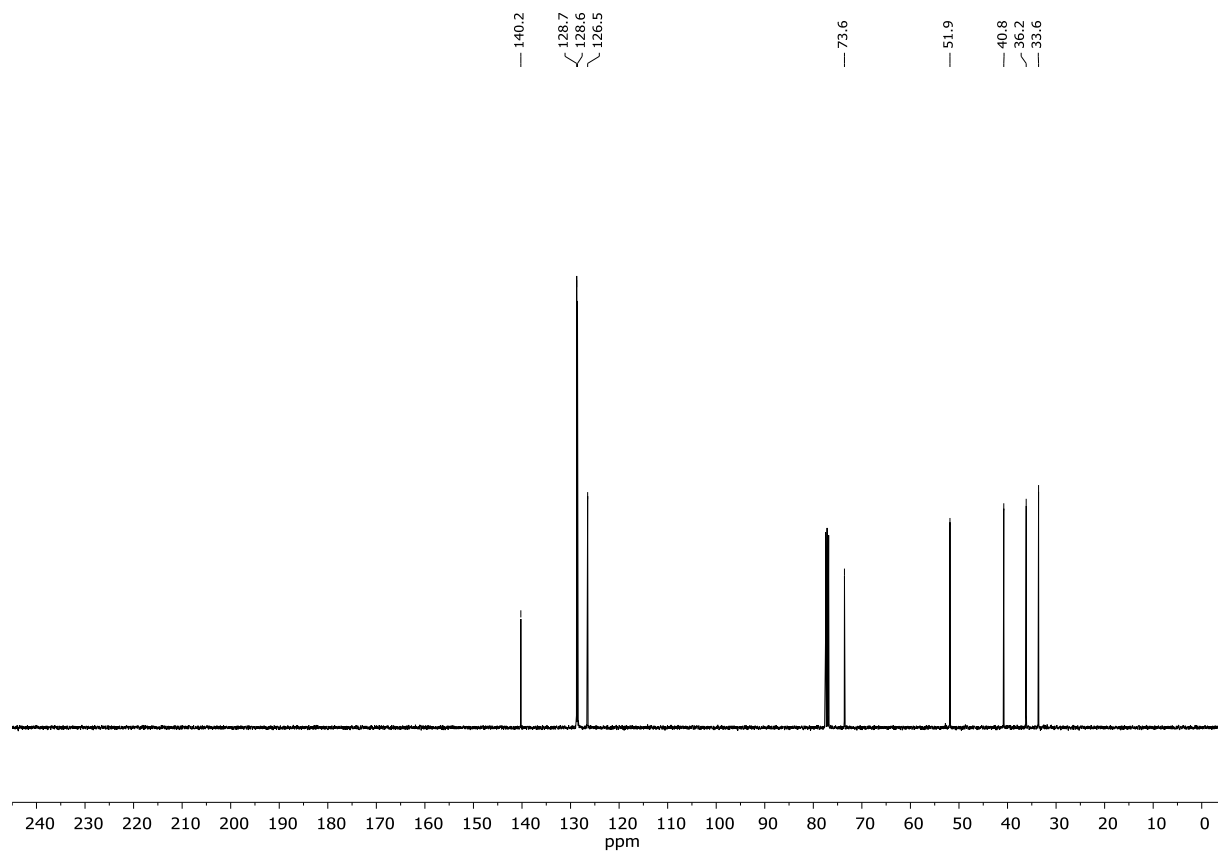
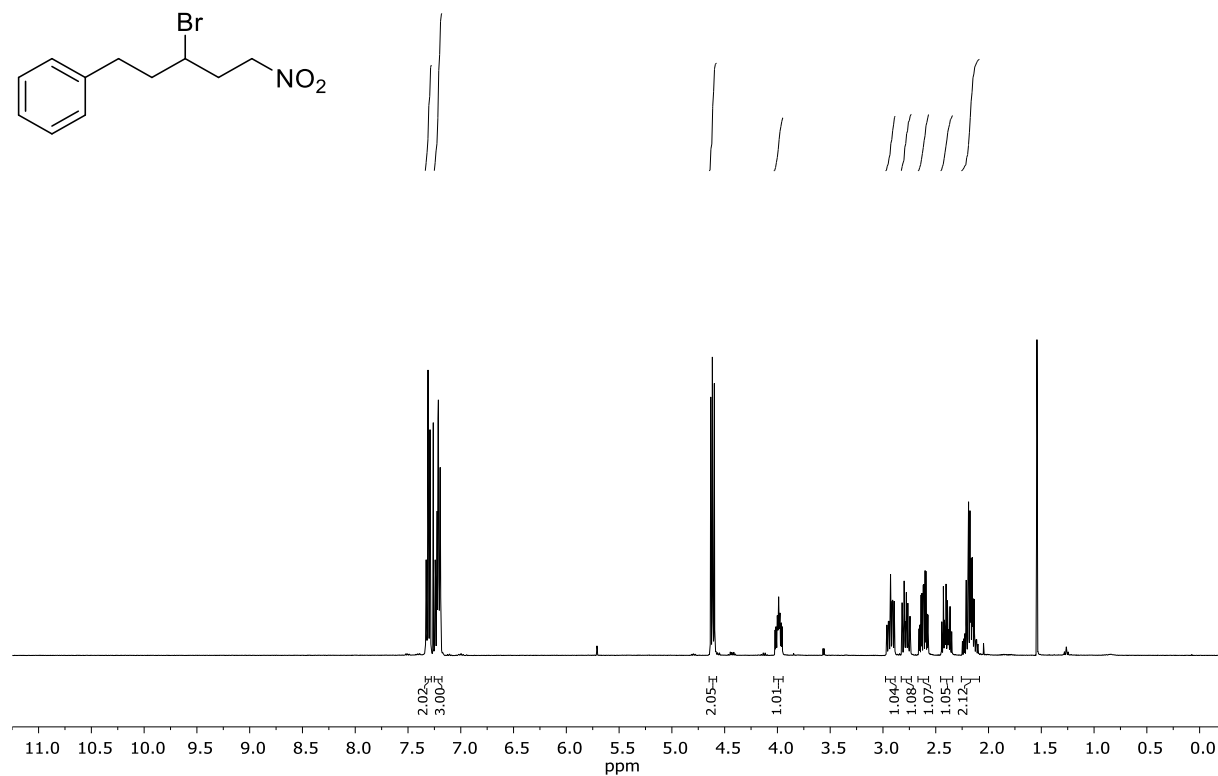
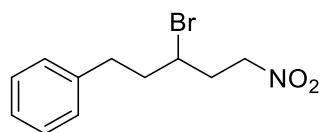
phenyl 2-bromo-4-nitrobutanoate (4ba)



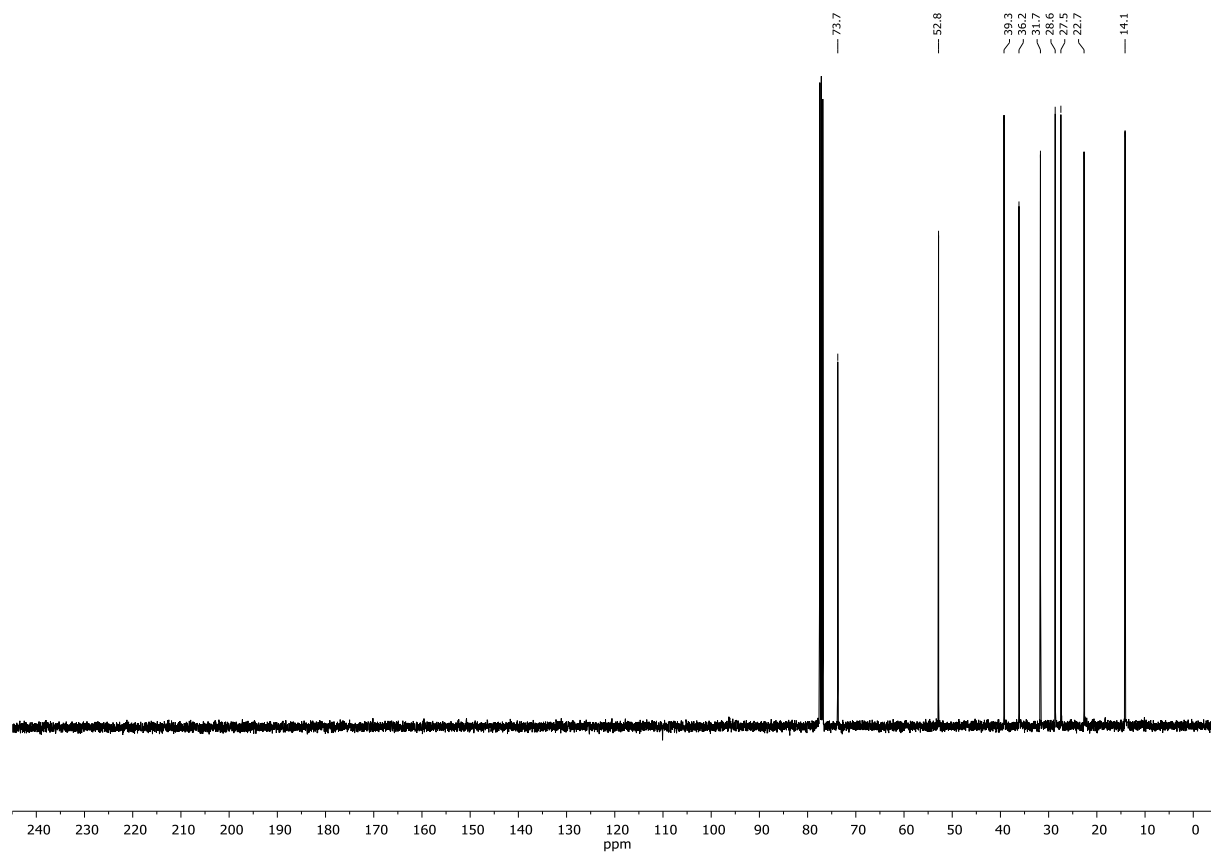
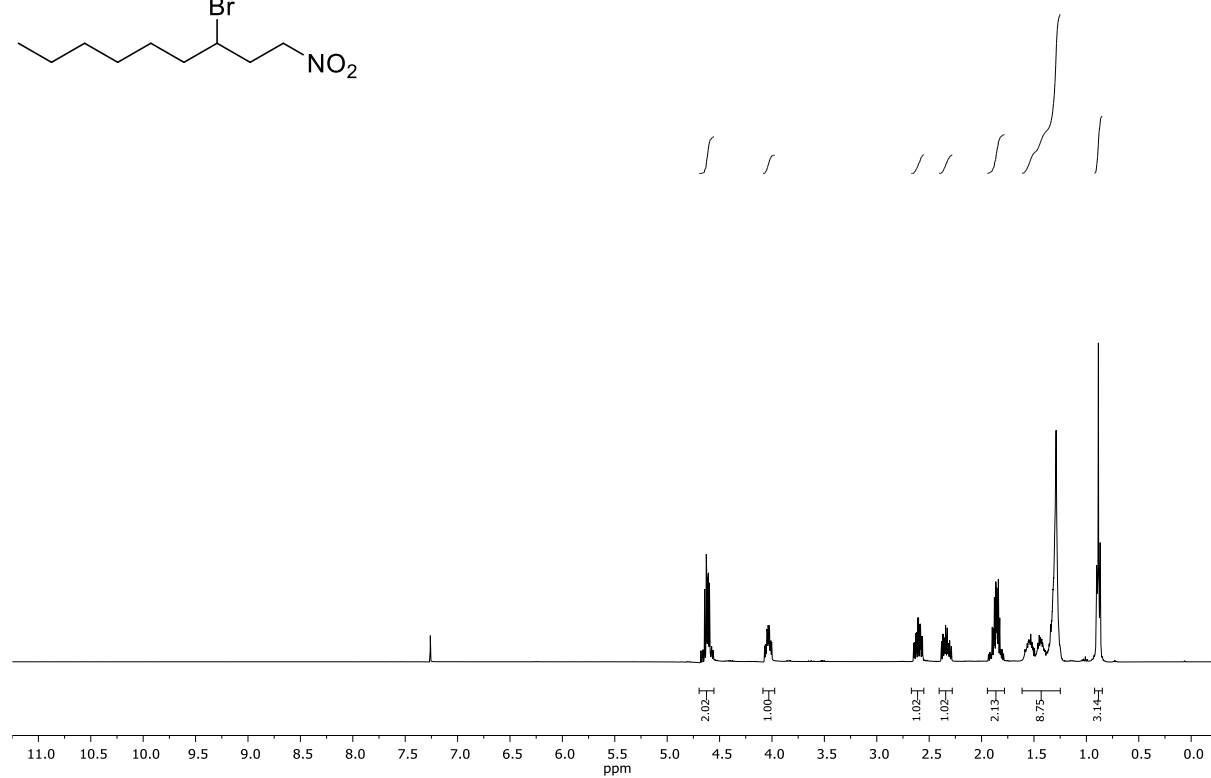
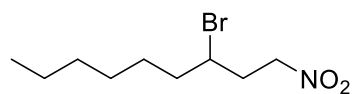
First image: ¹H-NMR; Second image: ¹³C-NMR; NMR solvent: CDCl₃

N-benzyl-2-bromo-4-nitrobutanamide (4bb)

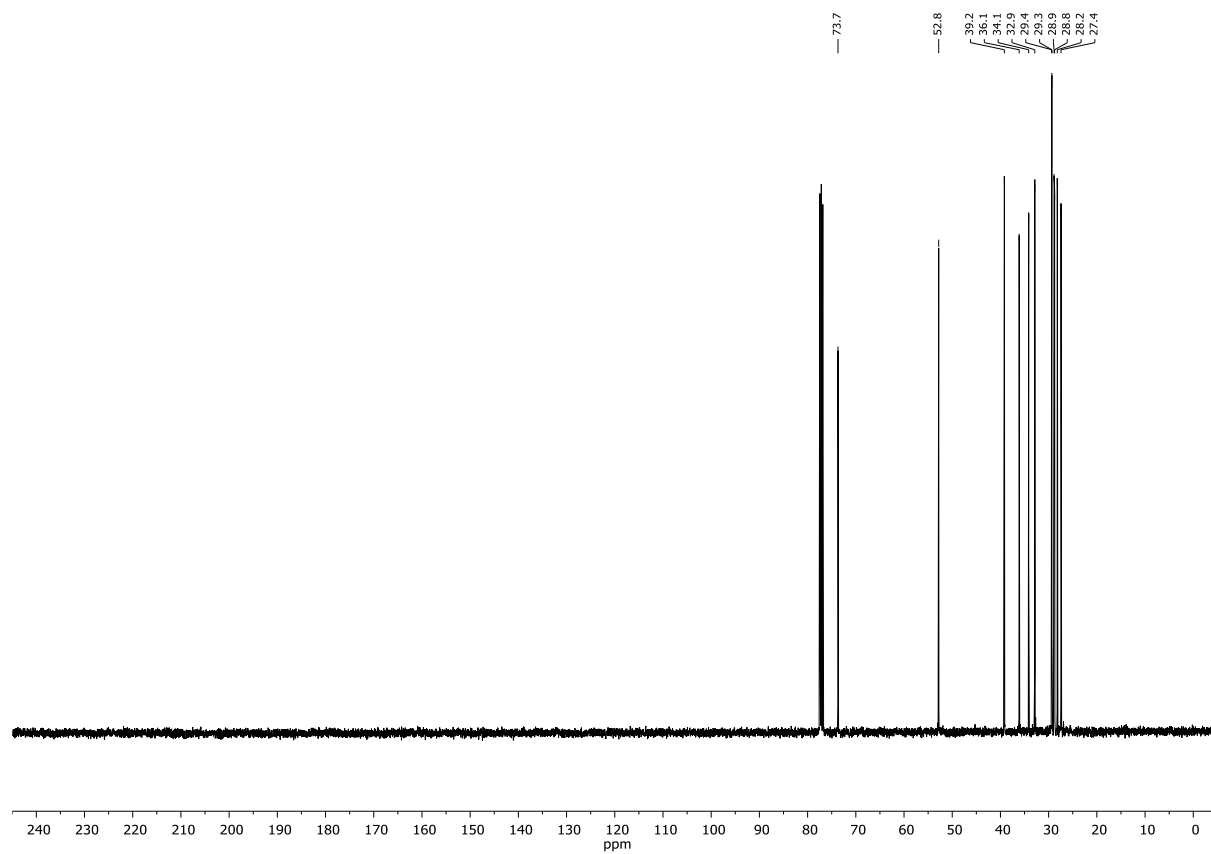
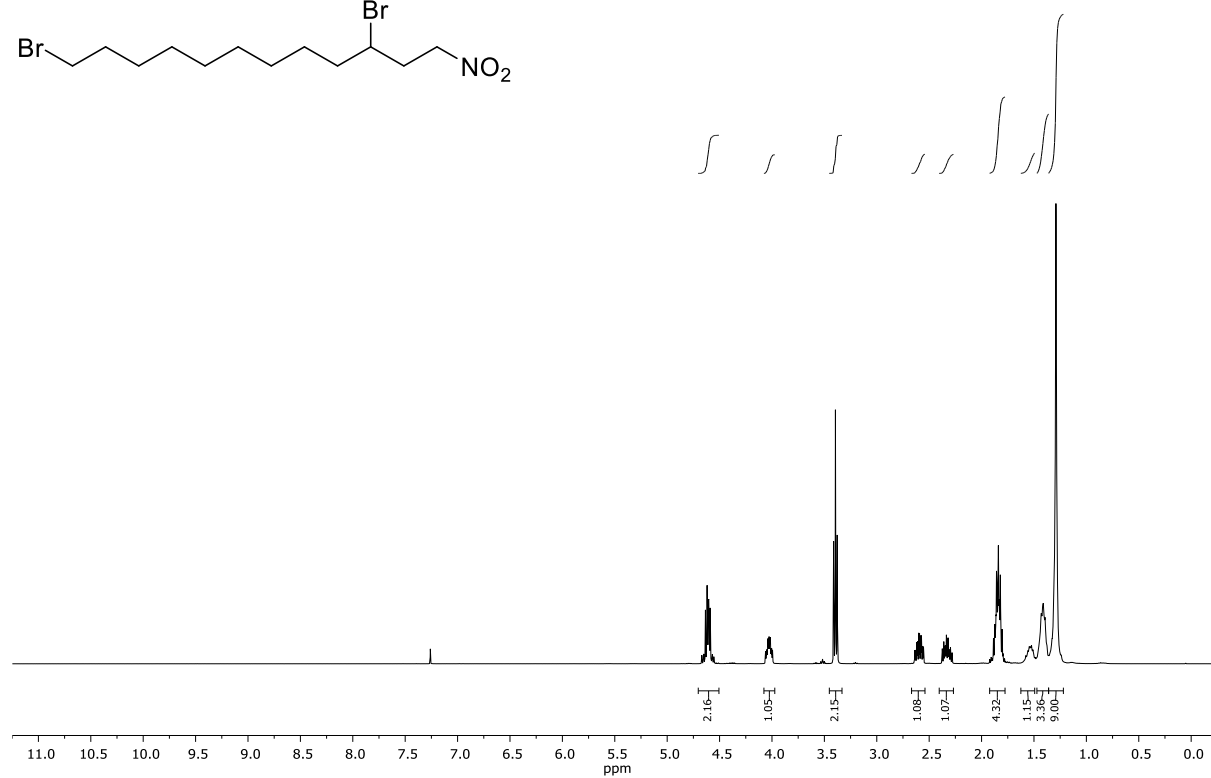
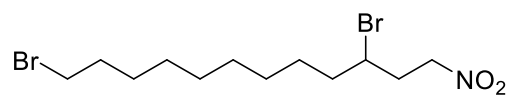
First image: ¹H-NMR; Second image: ¹³C-NMR; NMR solvent: CDCl₃

(3-bromo-5-nitropentyl)benzene (4ca)

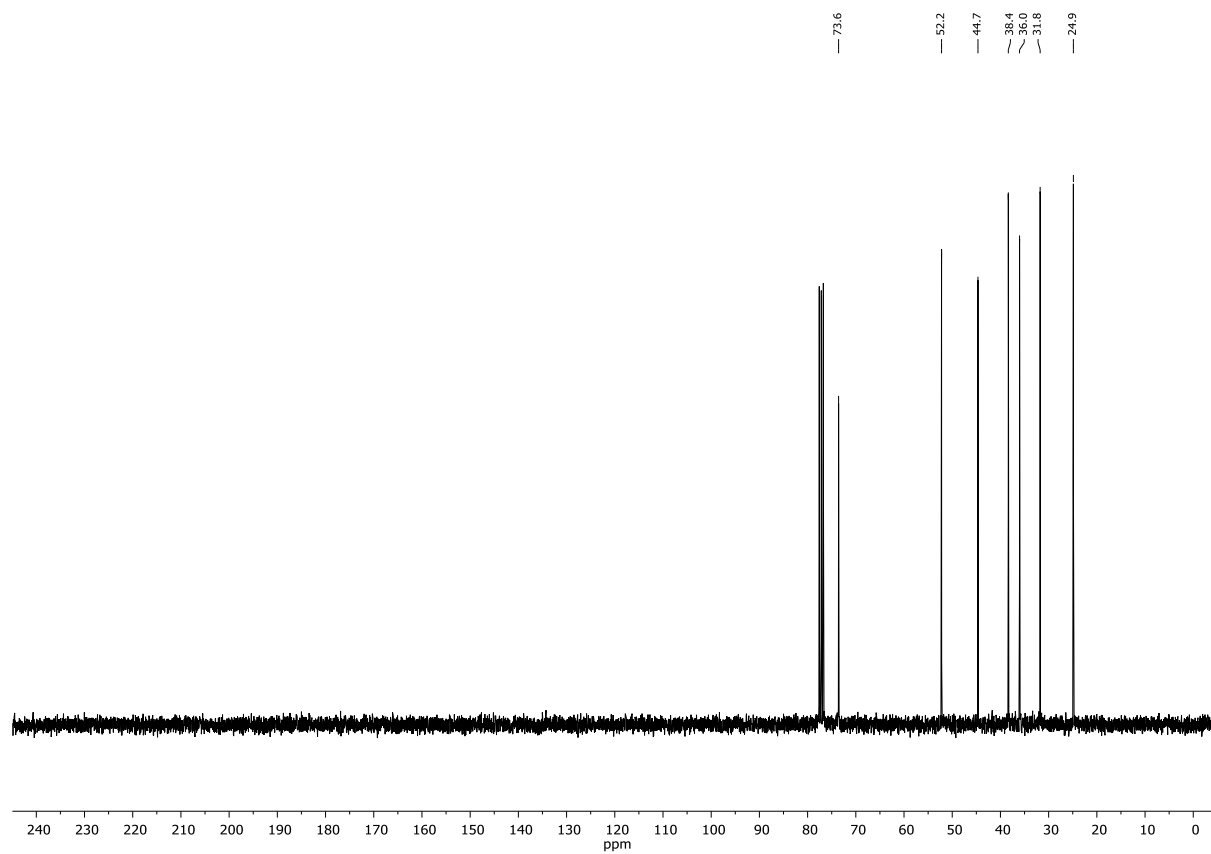
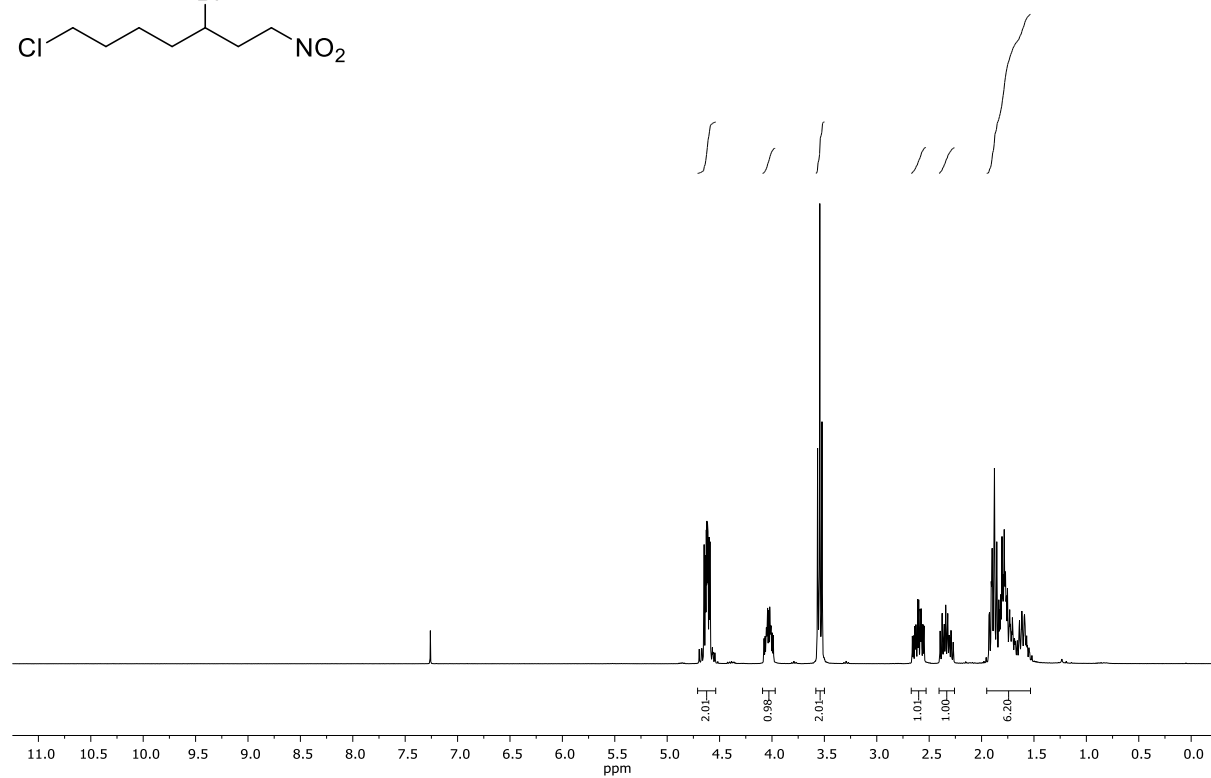
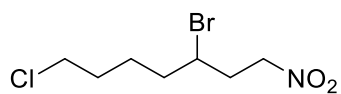
First image: $^1\text{H-NMR}$; Second image: $^{13}\text{C-NMR}$; NMR solvent: CDCl_3

3-bromo-1-nitrononane (4cb)

First image: $^1\text{H-NMR}$; Second image: $^{13}\text{C-NMR}$; NMR solvent: CDCl_3

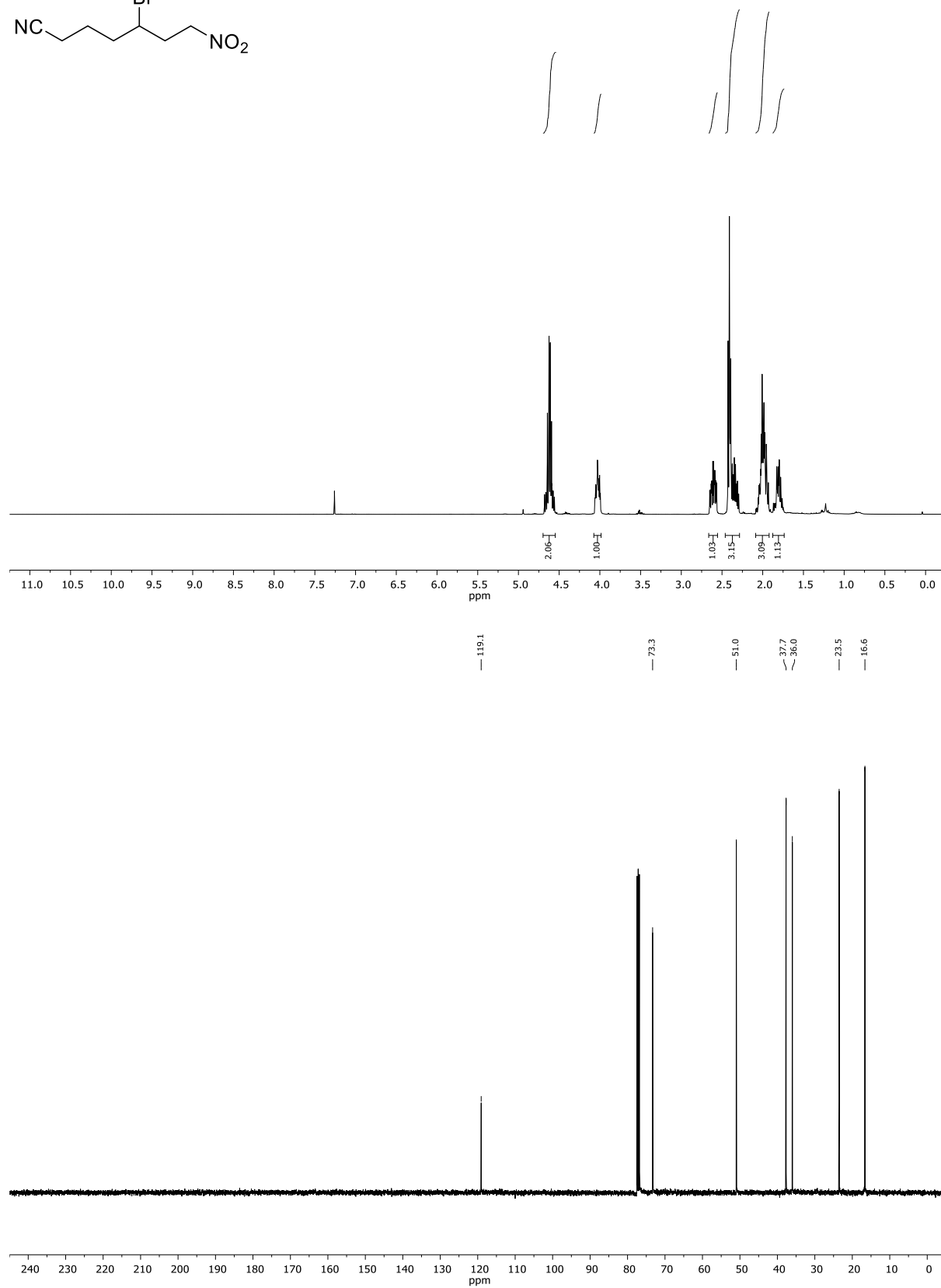
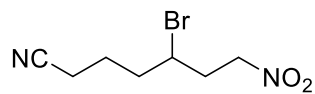
3,12-dibromo-1-nitrododecane (4cd)

First image: $^1\text{H-NMR}$; Second image: $^{13}\text{C-NMR}$; NMR solvent: CDCl_3

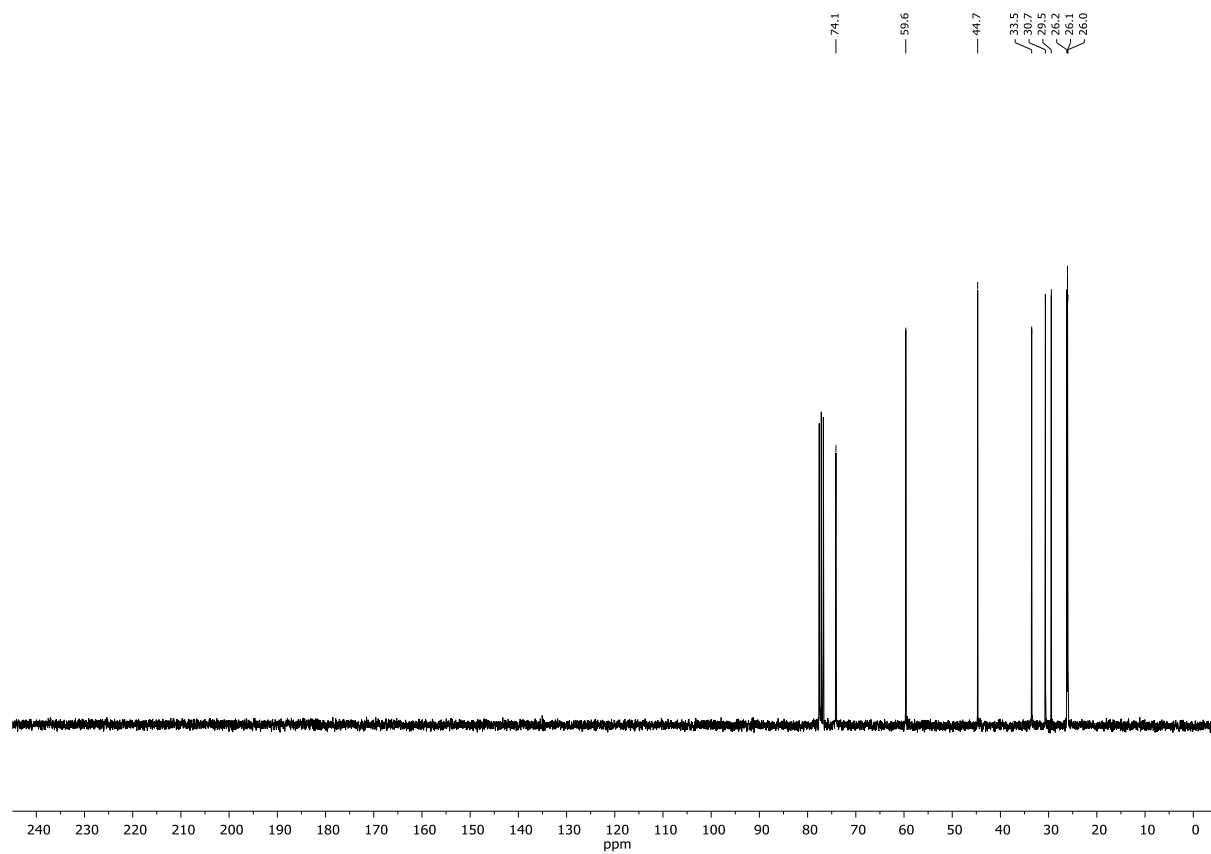
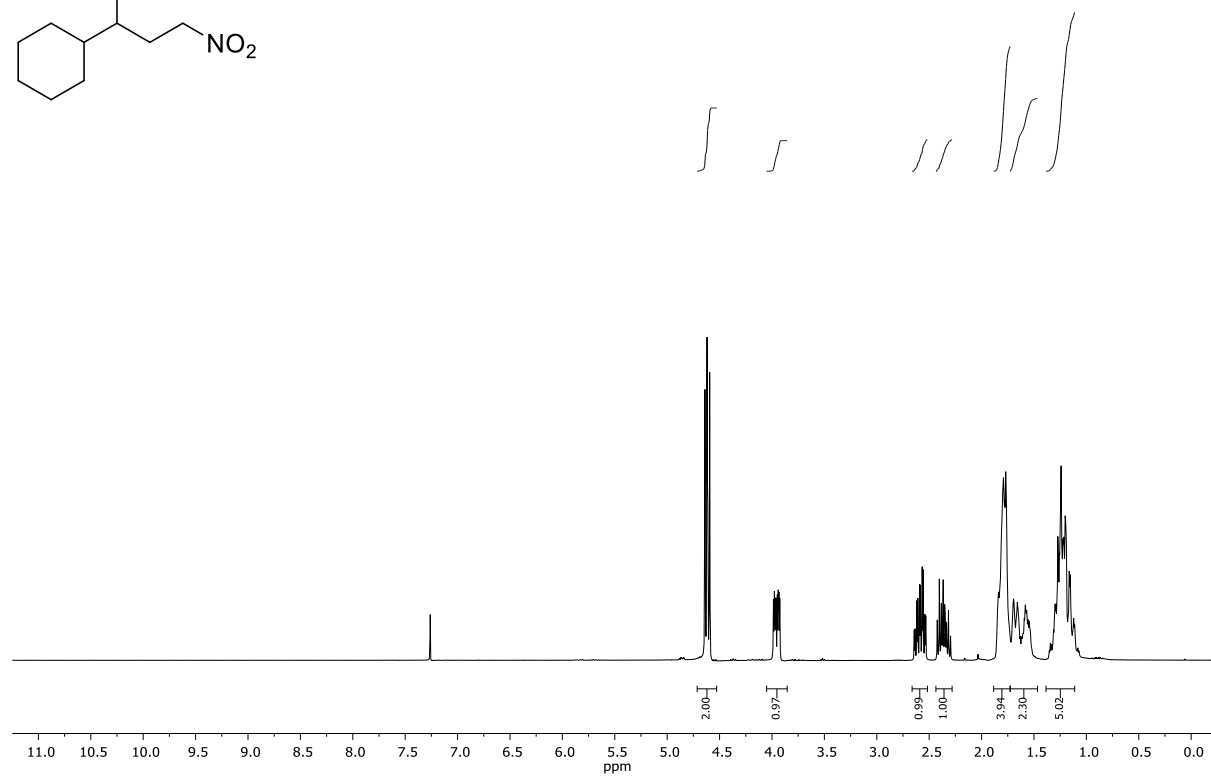
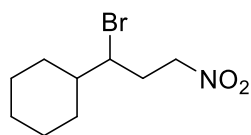
3-bromo-7-chloro-1-nitroheptane (4ce)

First image: $^1\text{H-NMR}$; Second image: $^{13}\text{C-NMR}$; NMR solvent: CDCl_3

5-bromo-7-nitroheptanenitrile (4cf)

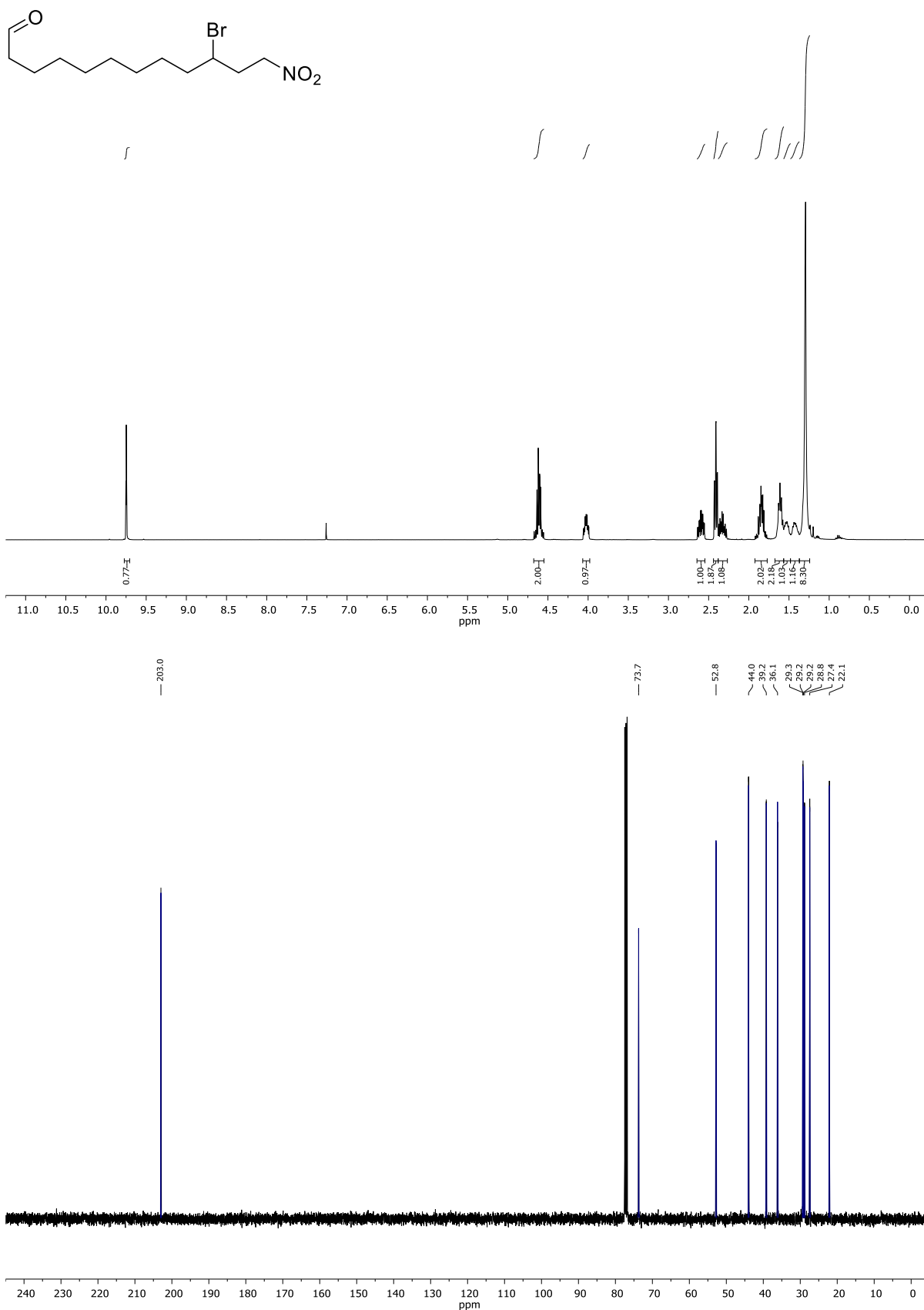


First image: $^1\text{H-NMR}$; Second image: $^{13}\text{C-NMR}$; NMR solvent: CDCl_3

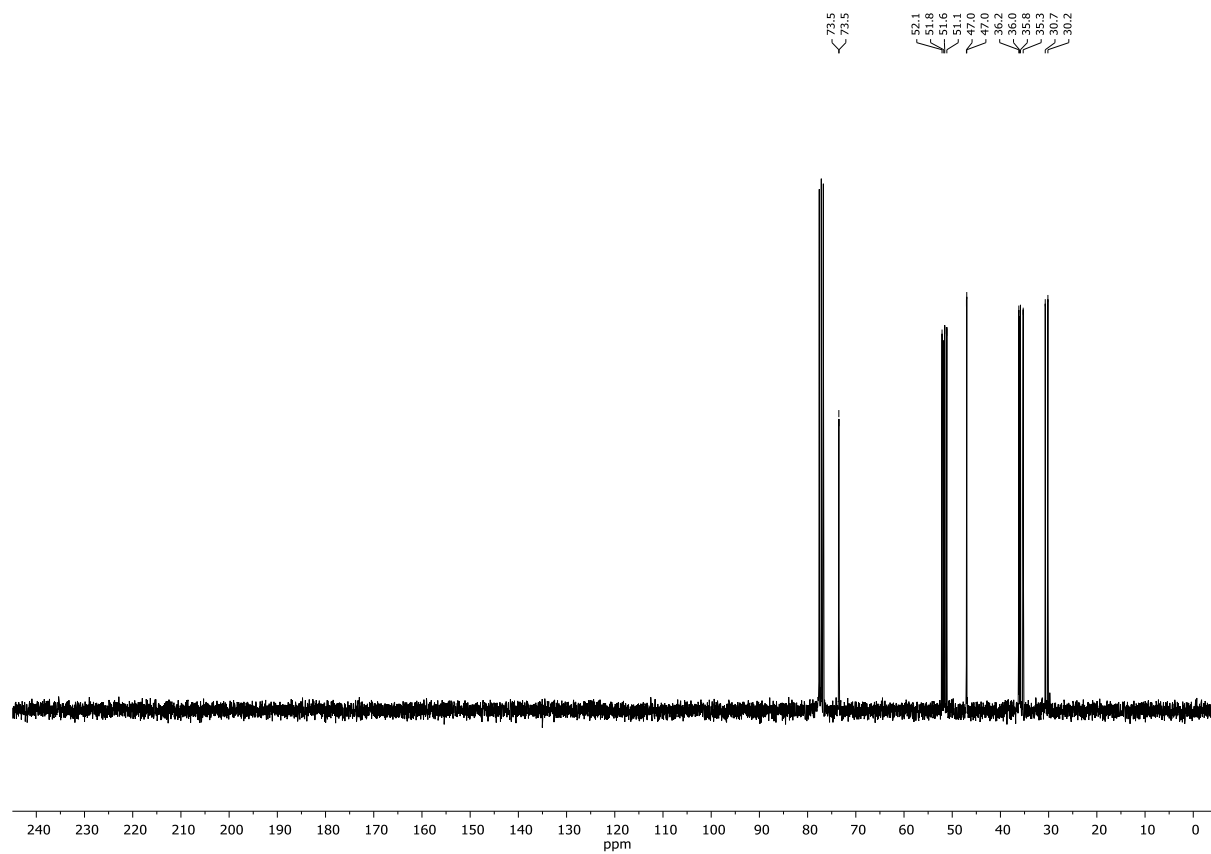
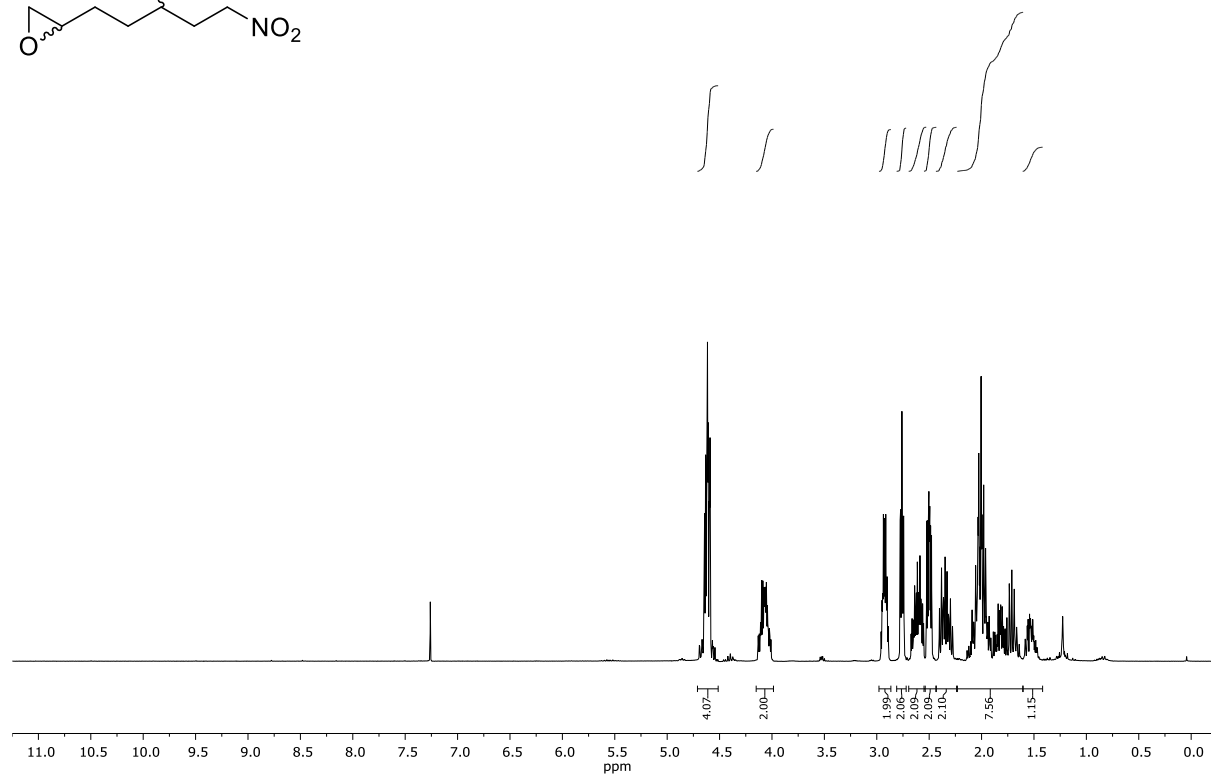
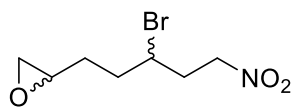
(1-bromo-3-nitropropyl)cyclohexane (4cg)

First image: $^1\text{H-NMR}$; Second image: $^{13}\text{C-NMR}$; NMR solvent: CDCl_3

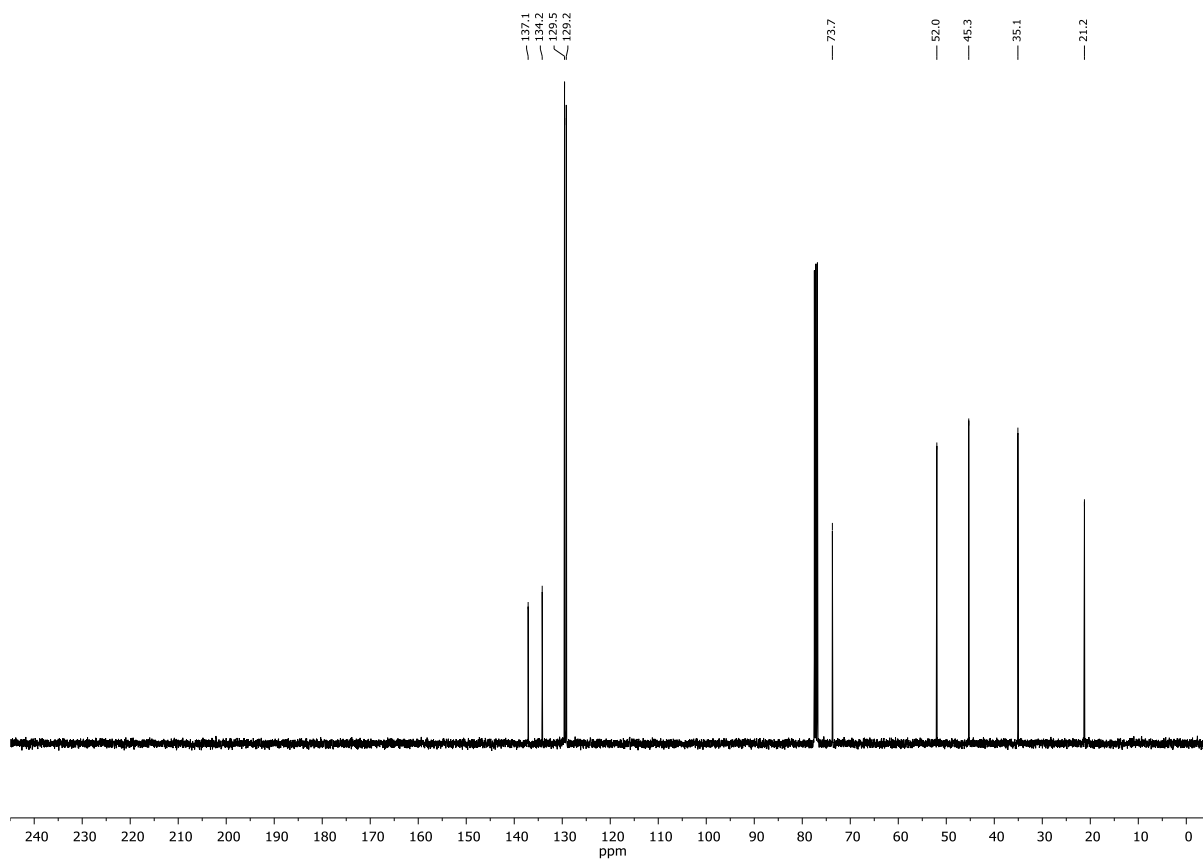
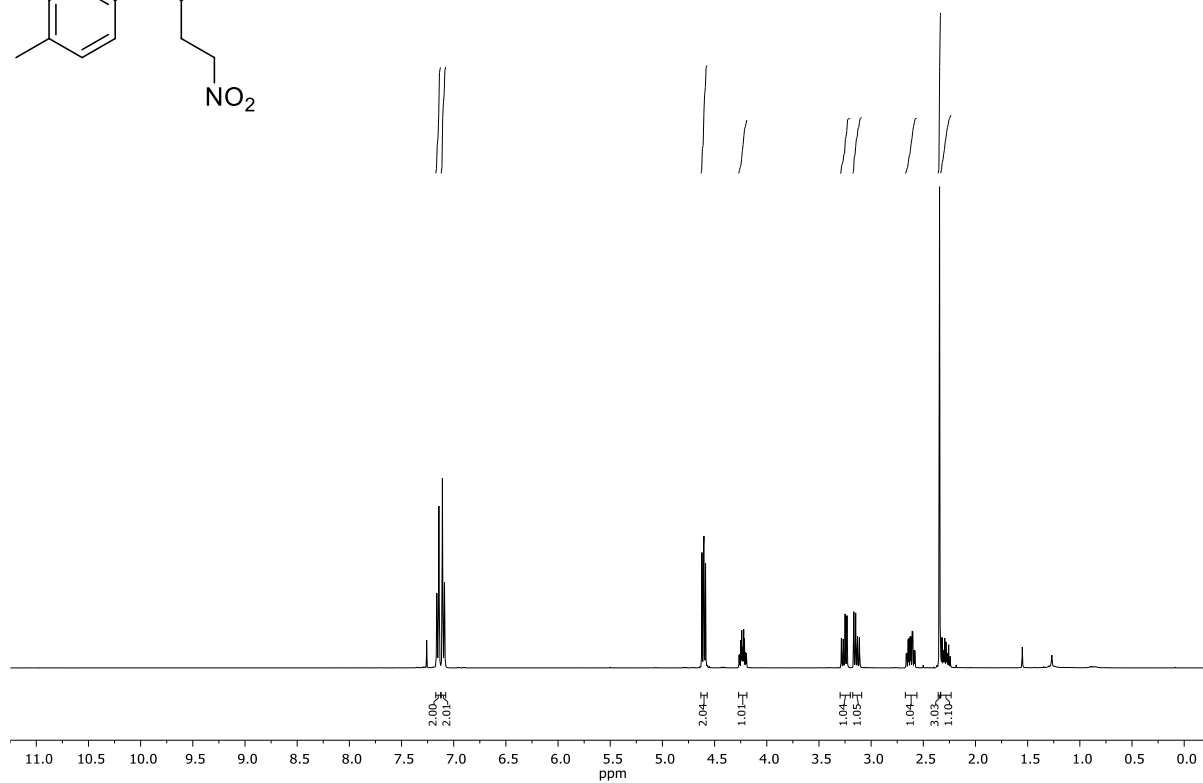
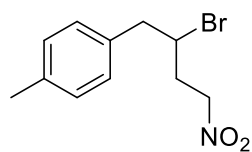
10-bromo-12-nitrododecanal (4ci)



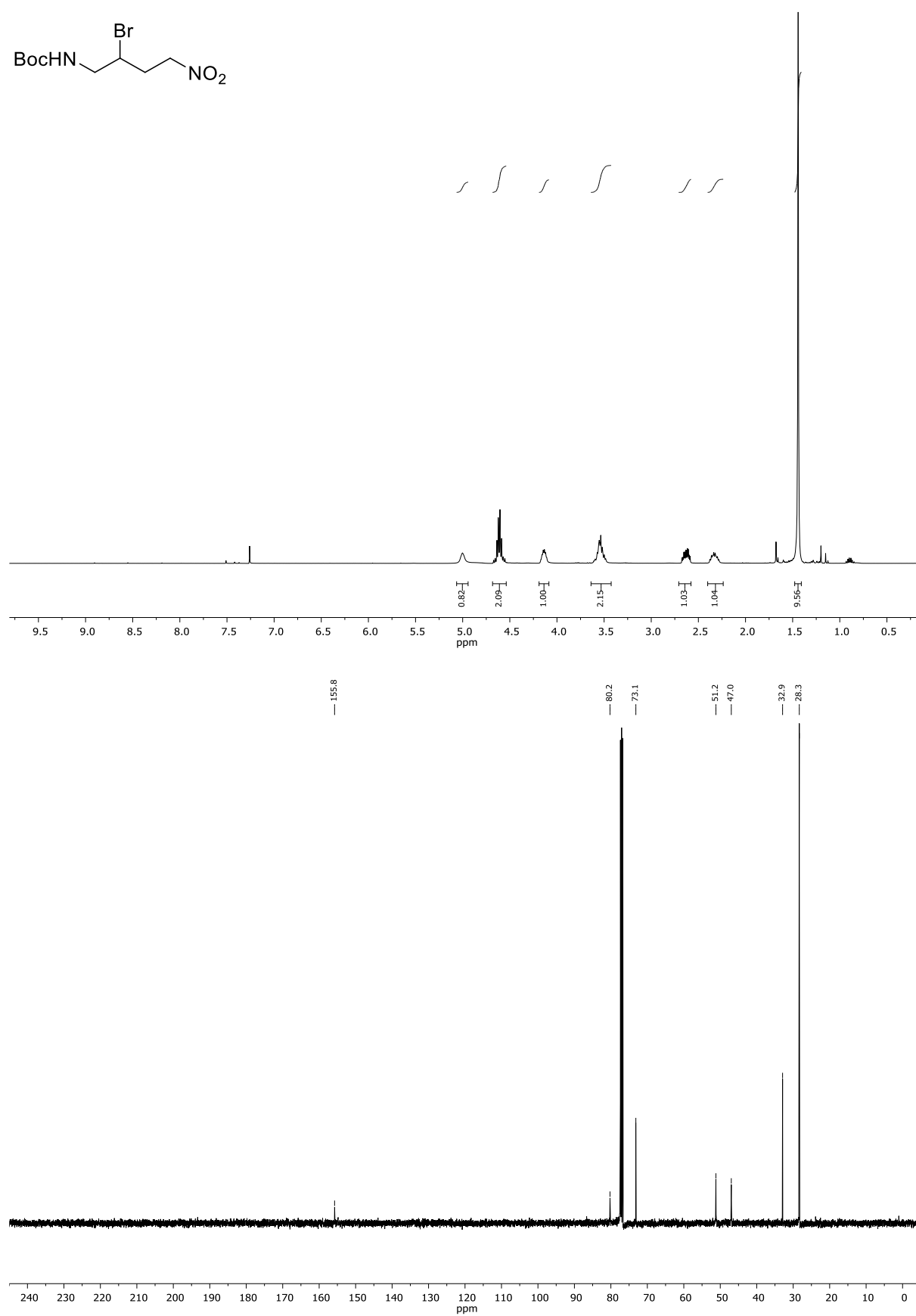
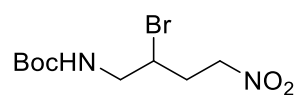
First image: ¹H-NMR; Second image: ¹³C-NMR; NMR solvent: CDCl₃

2-(3-bromo-5-nitropentyl)oxirane (4cj) (d.r. = 54:46)

First image: $^1\text{H-NMR}$; Second image: $^{13}\text{C-NMR}$; NMR solvent: CDCl_3

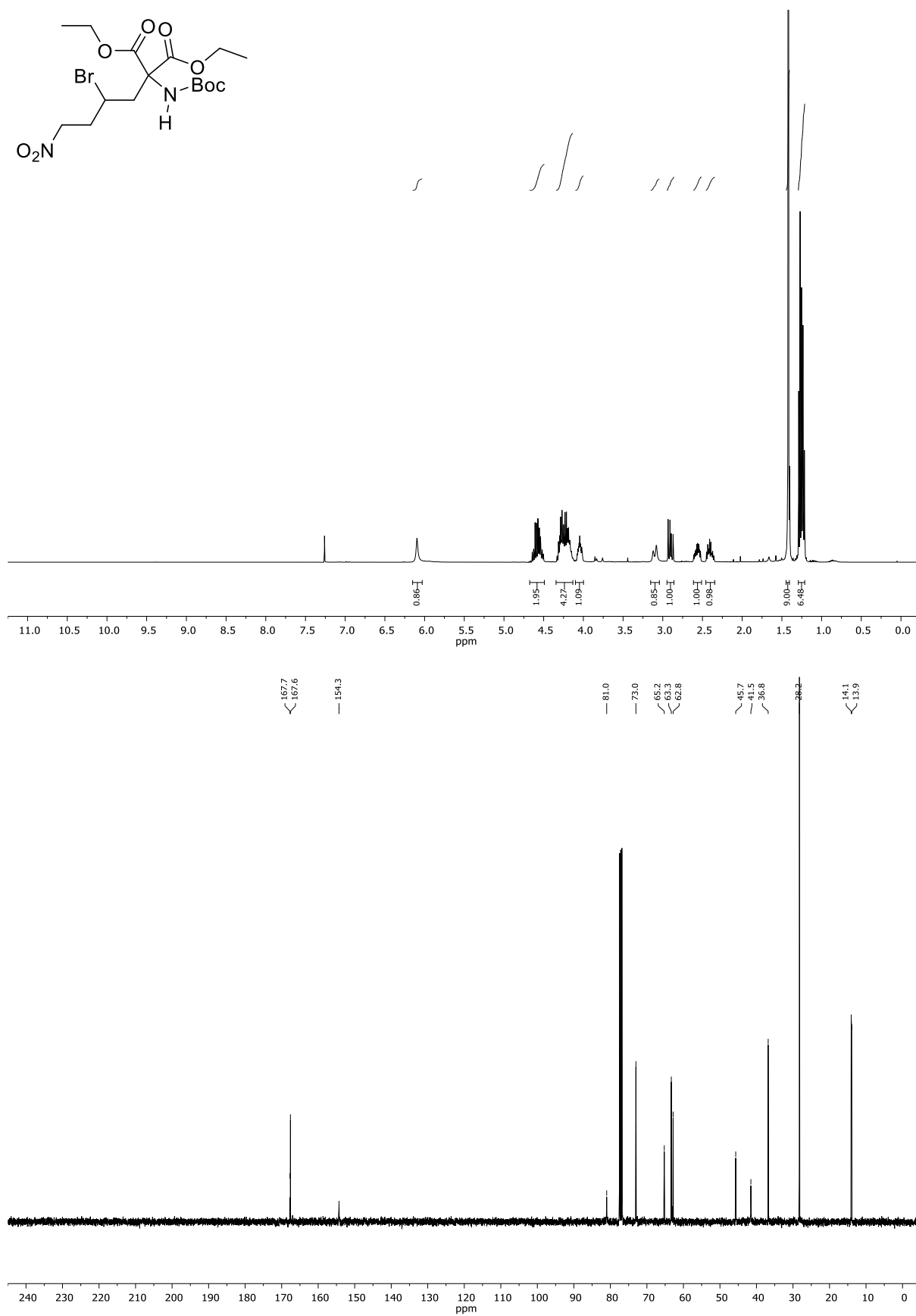
1-(2-bromo-4-nitrobutyl)-4-methylbenzene (4cl)

First image: $^1\text{H-NMR}$; Second image: $^{13}\text{C-NMR}$; NMR solvent: CDCl_3

tert-butyl (2-bromo-4-nitrobutyl)carbamate (4cm)

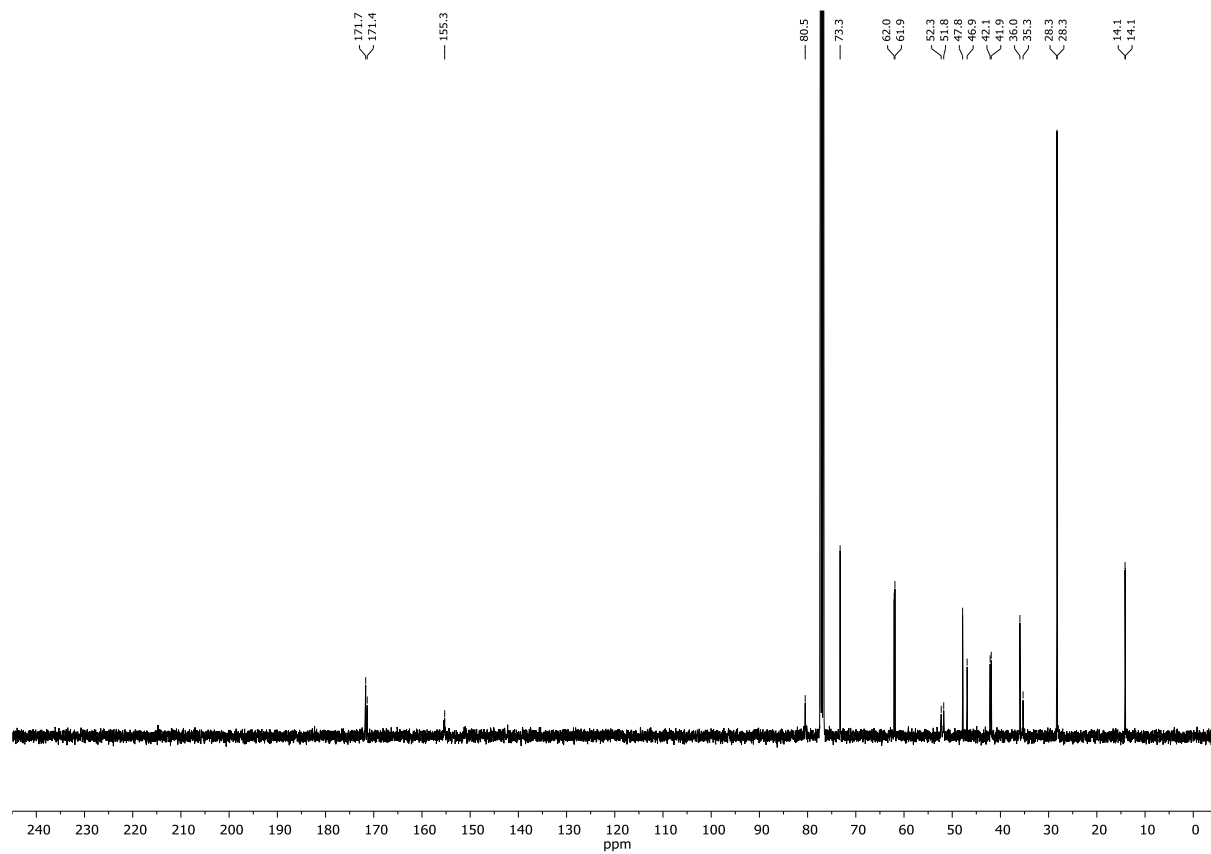
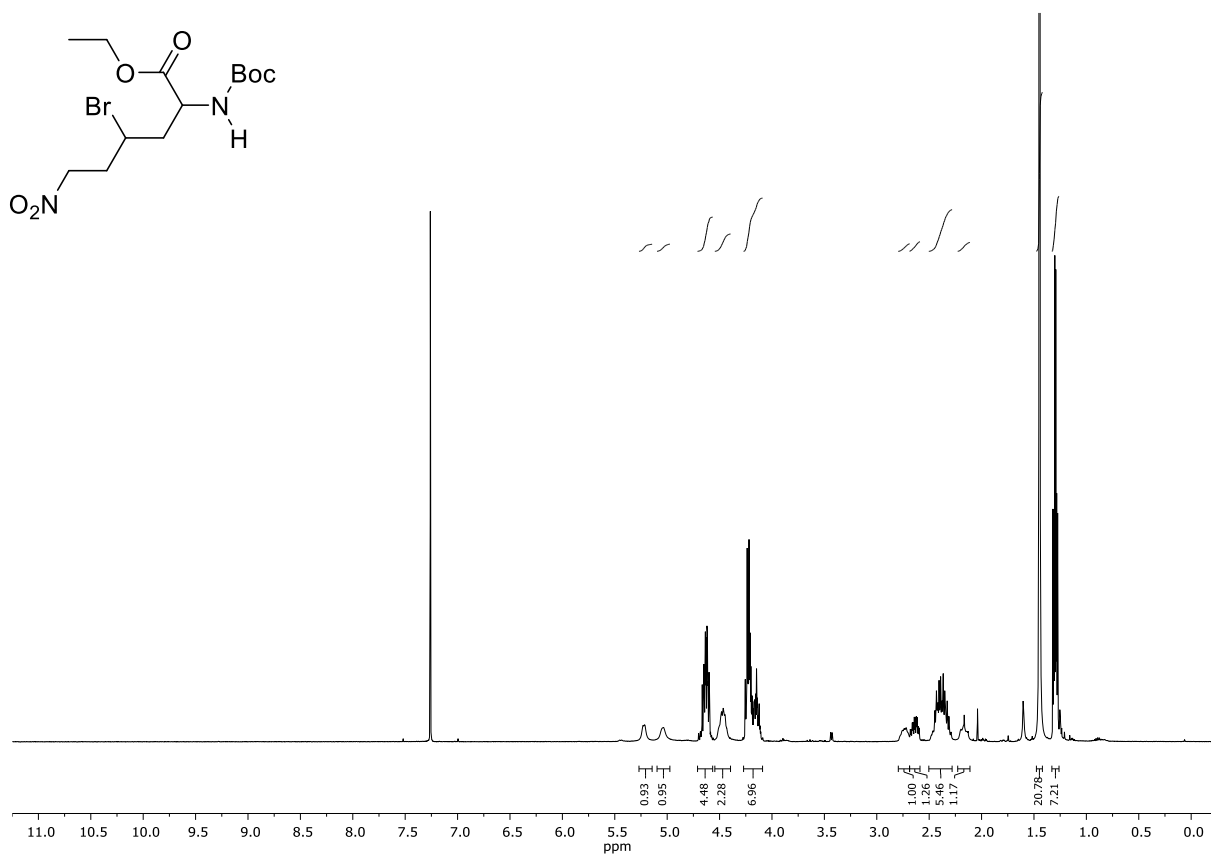
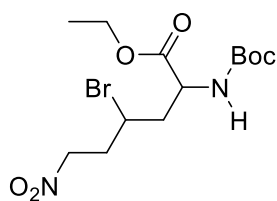
First image: ¹H-NMR; Second image: ¹³C-NMR; NMR solvent: CDCl₃

diethyl 2-(2-bromo-4-nitrobutyl)-2-((tert-butoxycarbonyl)amino)malonate (4co)

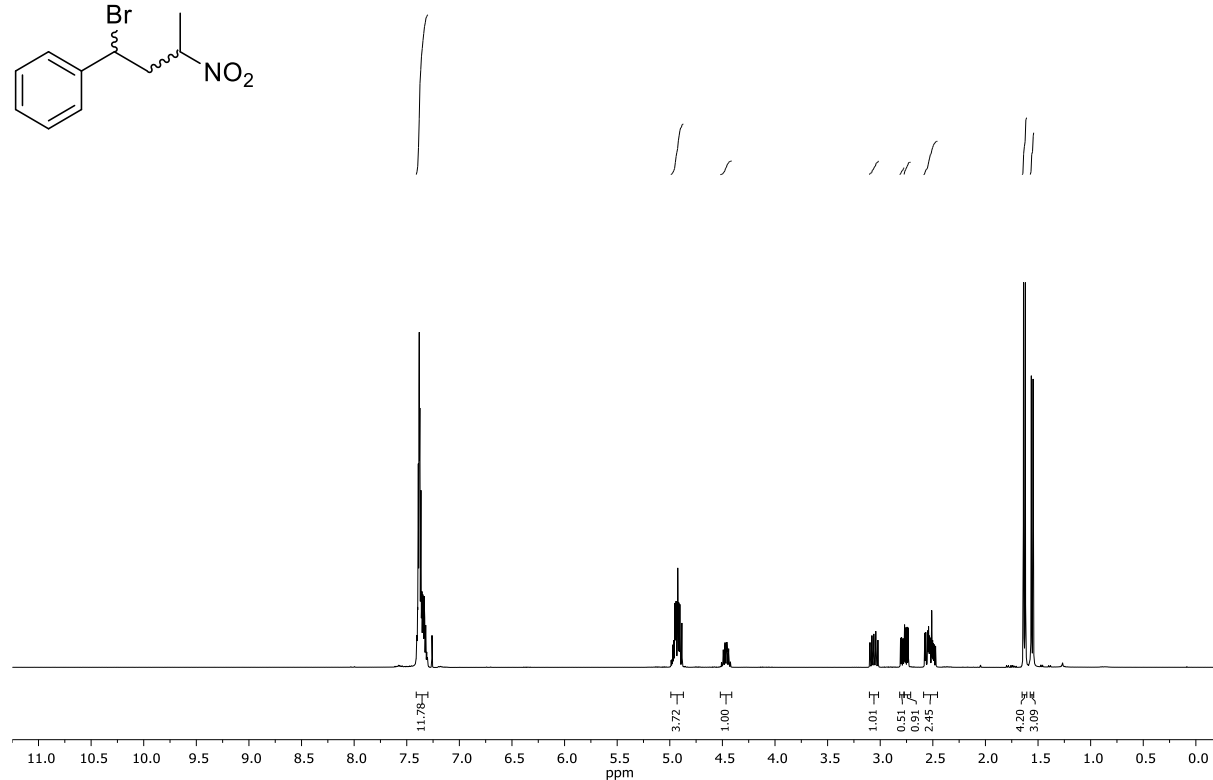
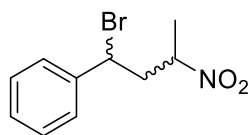


First image: ¹H-NMR; Second image: ¹³C-NMR; NMR solvent: CDCl₃

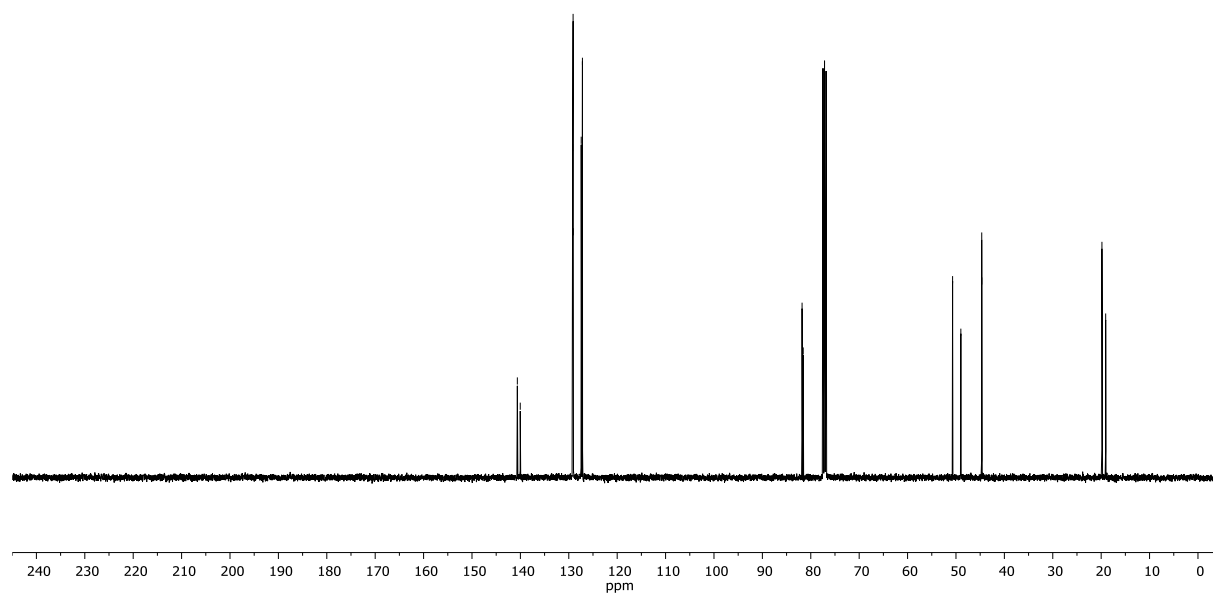
ethyl 4-bromo-2-((tert-butoxycarbonyl)amino)-6-nitrohexanoate (4cp) (d.r. = 56:44)



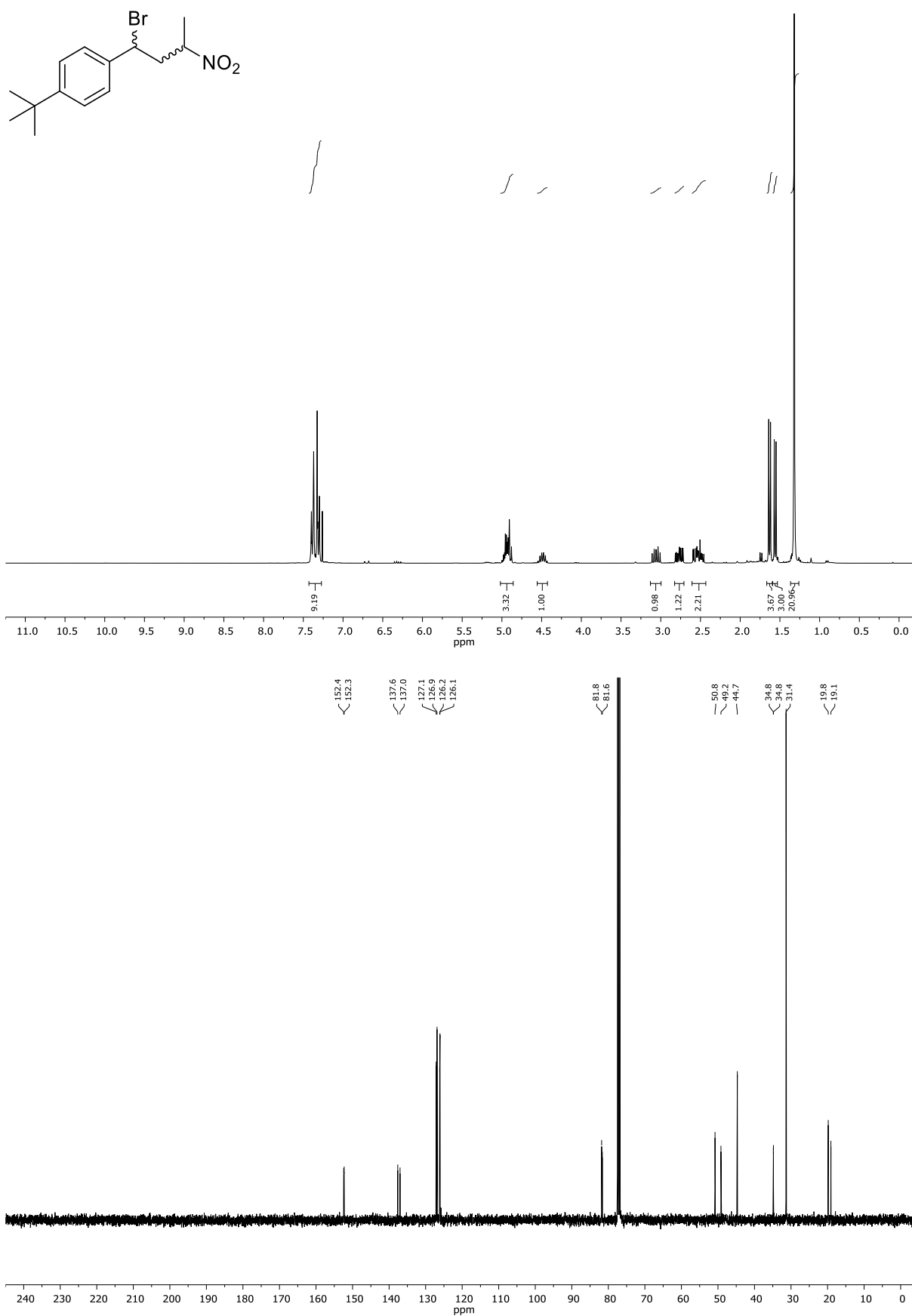
First image: $^1\text{H-NMR}$; Second image: $^{13}\text{C-NMR}$; NMR solvent: CDCl_3

(1-bromo-3-nitrobutyl)benzene (d.r. = 58:42) (4da)

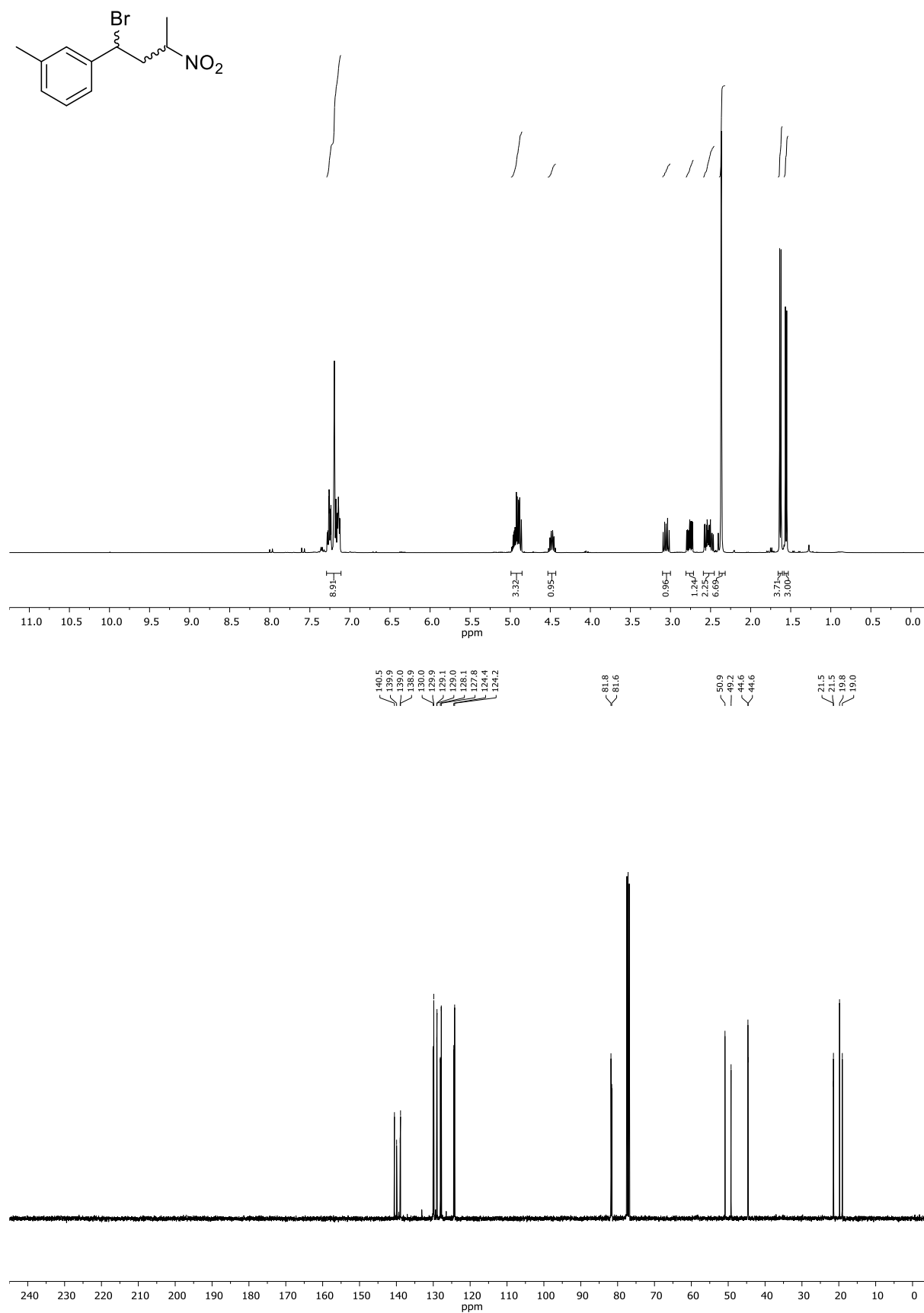
140.6
140.0
128.2
128.2
128.2
128.1
127.4
127.2
81.8
81.6
50.7
49.0
44.7
44.7
19.8
19.1



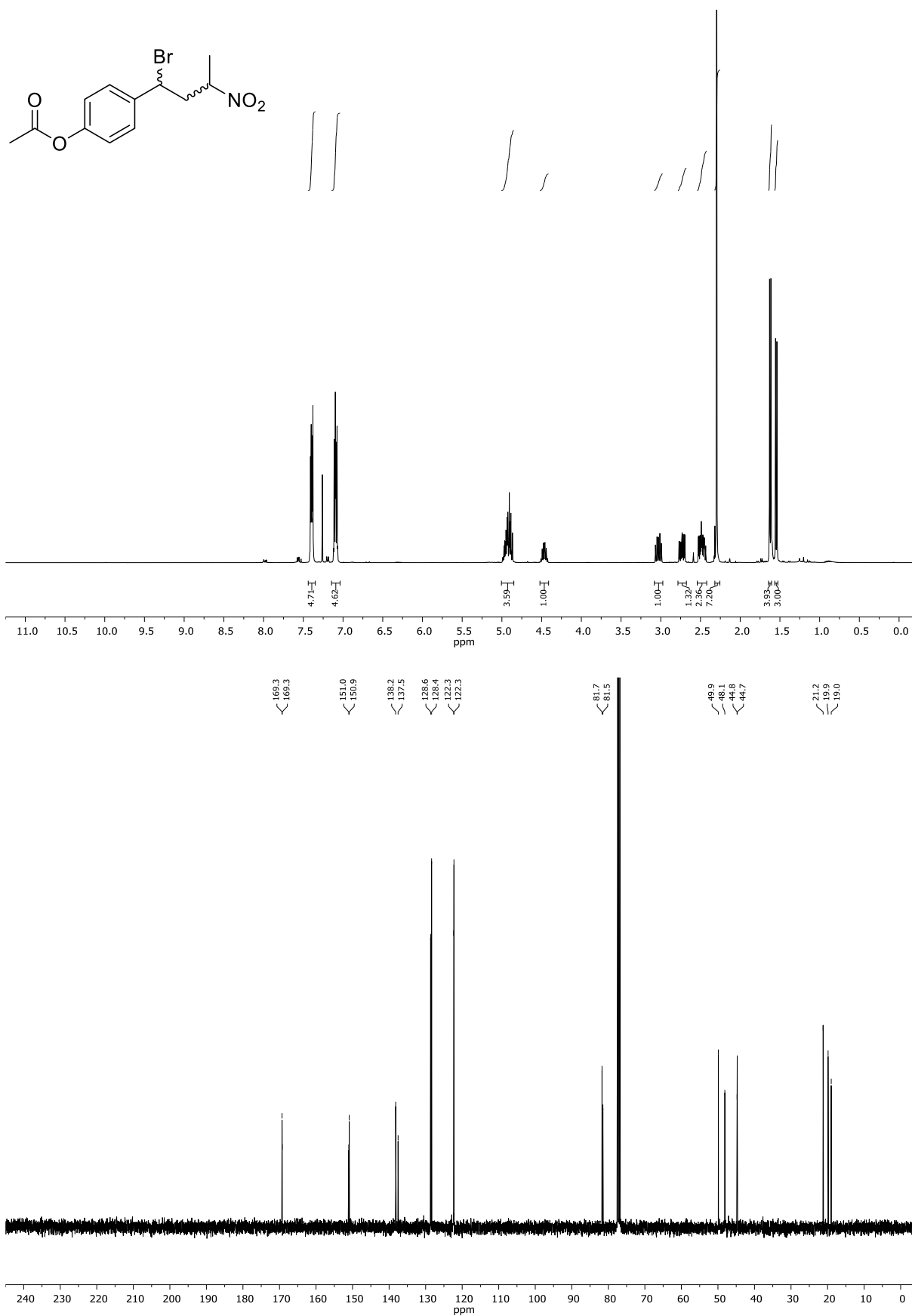
First image: $^1\text{H-NMR}$; Second image: $^{13}\text{C-NMR}$: NMR solvent: CDCl_3

1-(1-bromo-3-nitrobutyl)-4-(tert-butyl)benzene (d.r. = 56:44) (4db)

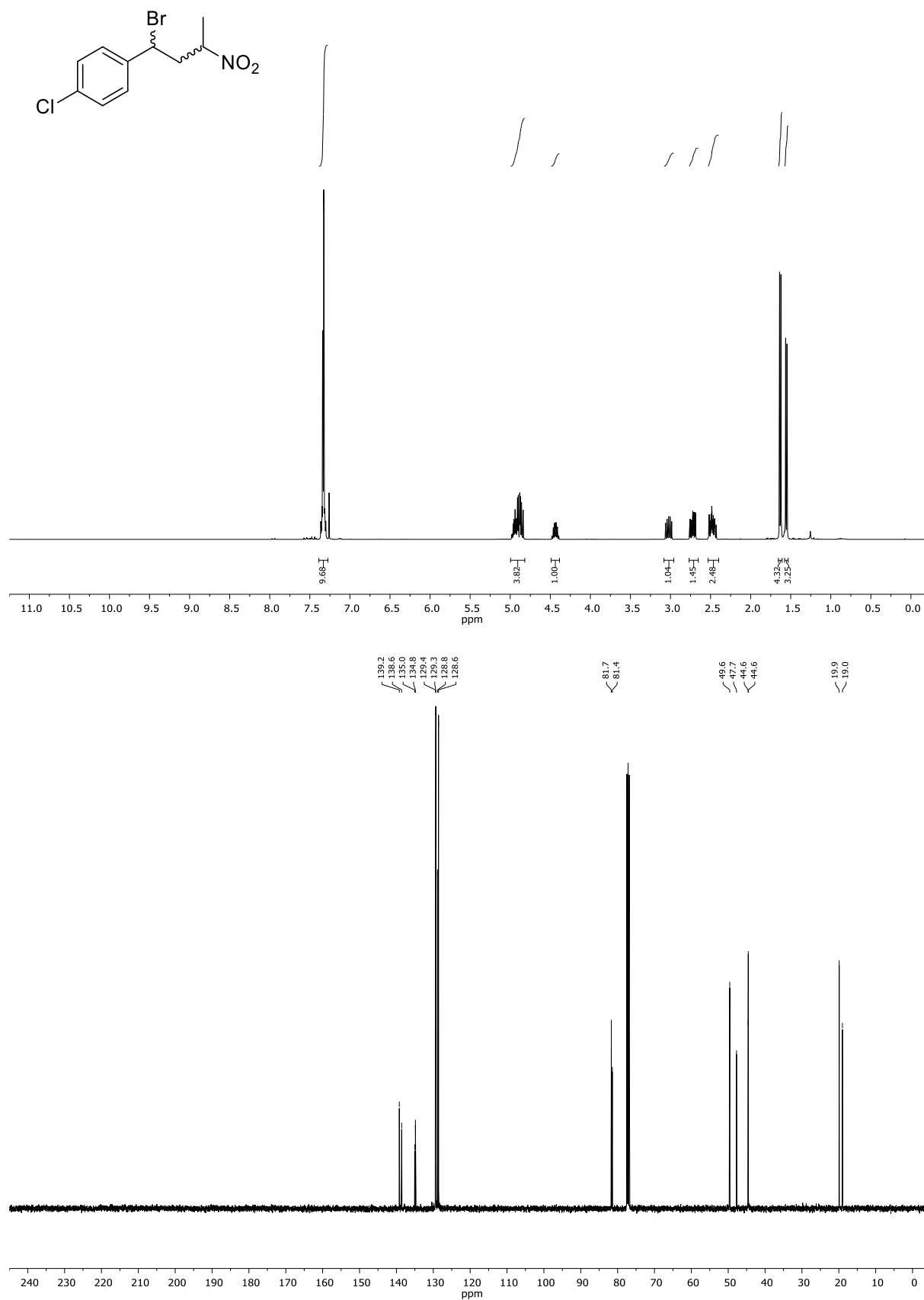
First image: ¹H-NMR; Second image: ¹³C-NMR; NMR solvent: CDCl₃

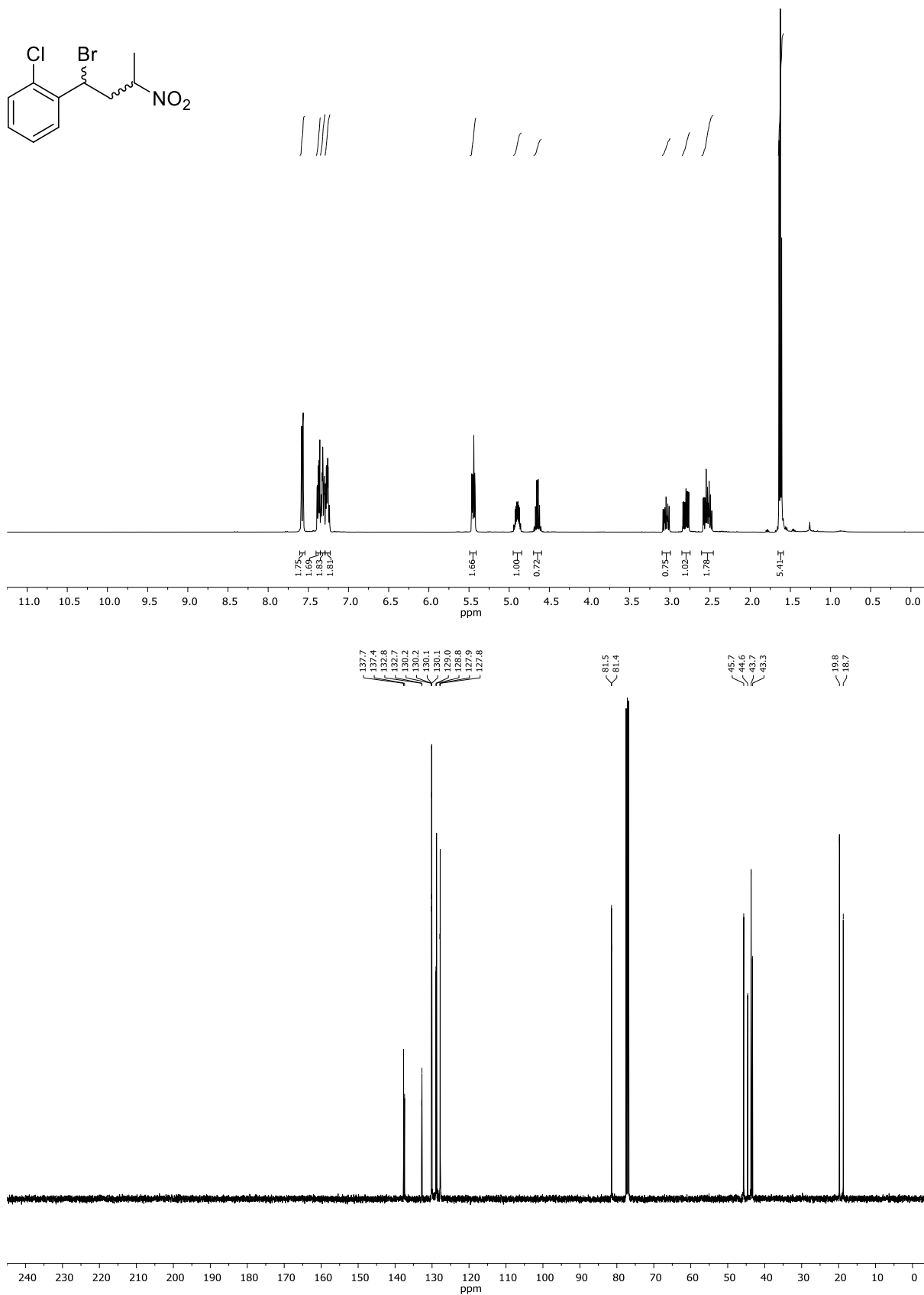
(1-bromo-3-nitrobutyl)-3-methylbenzene (d.r. = 55:45) (4dc)First image: ¹H-NMR; Second image: ¹³C-NMR: NMR solvent: CDCl₃

4-(1-bromo-3-nitrobutyl)phenyl acetate (d.r. = 57:43) (4dd)

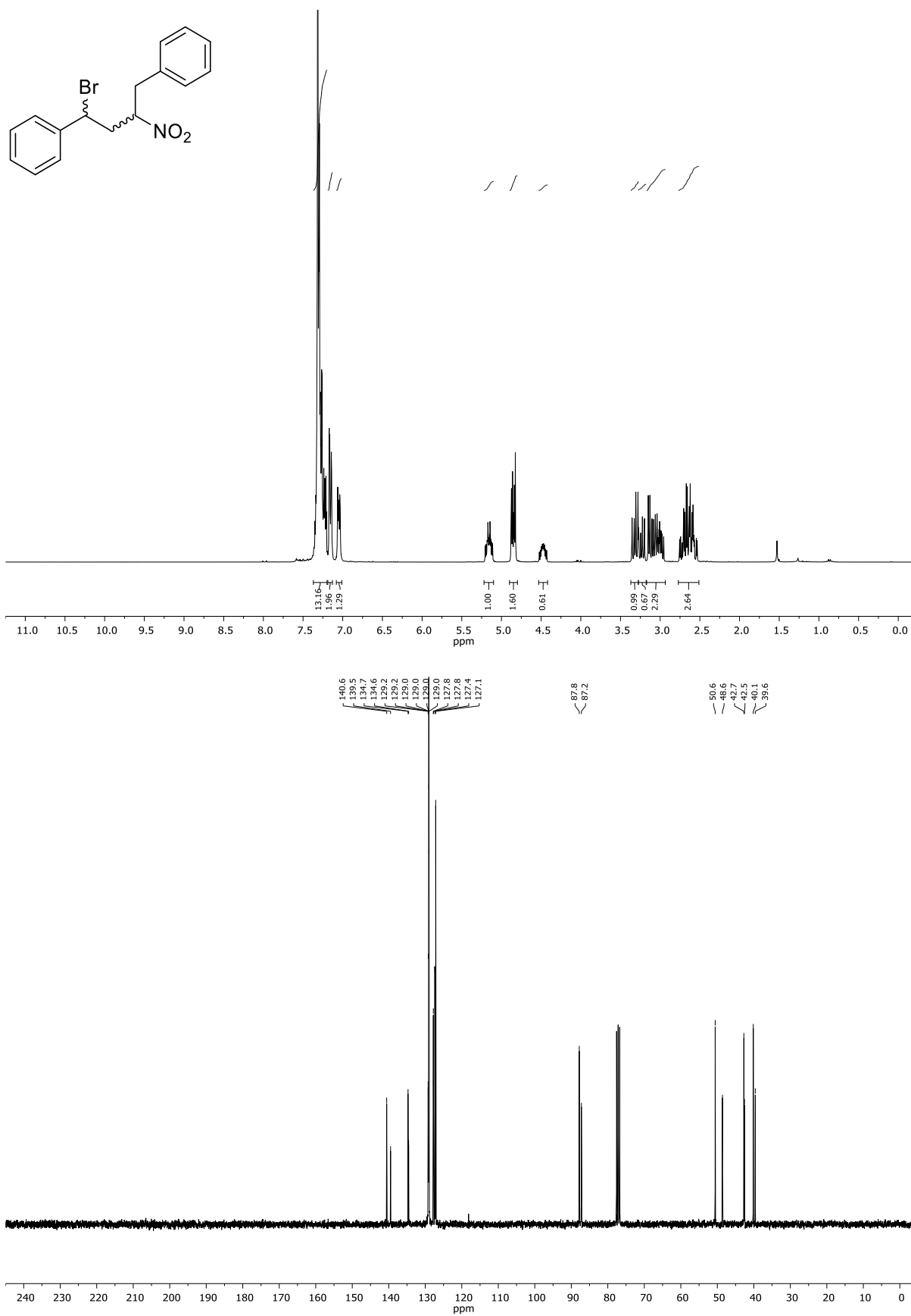


First image: ¹H-NMR; Second image: ¹³C-NMR: NMR solvent: CDCl₃

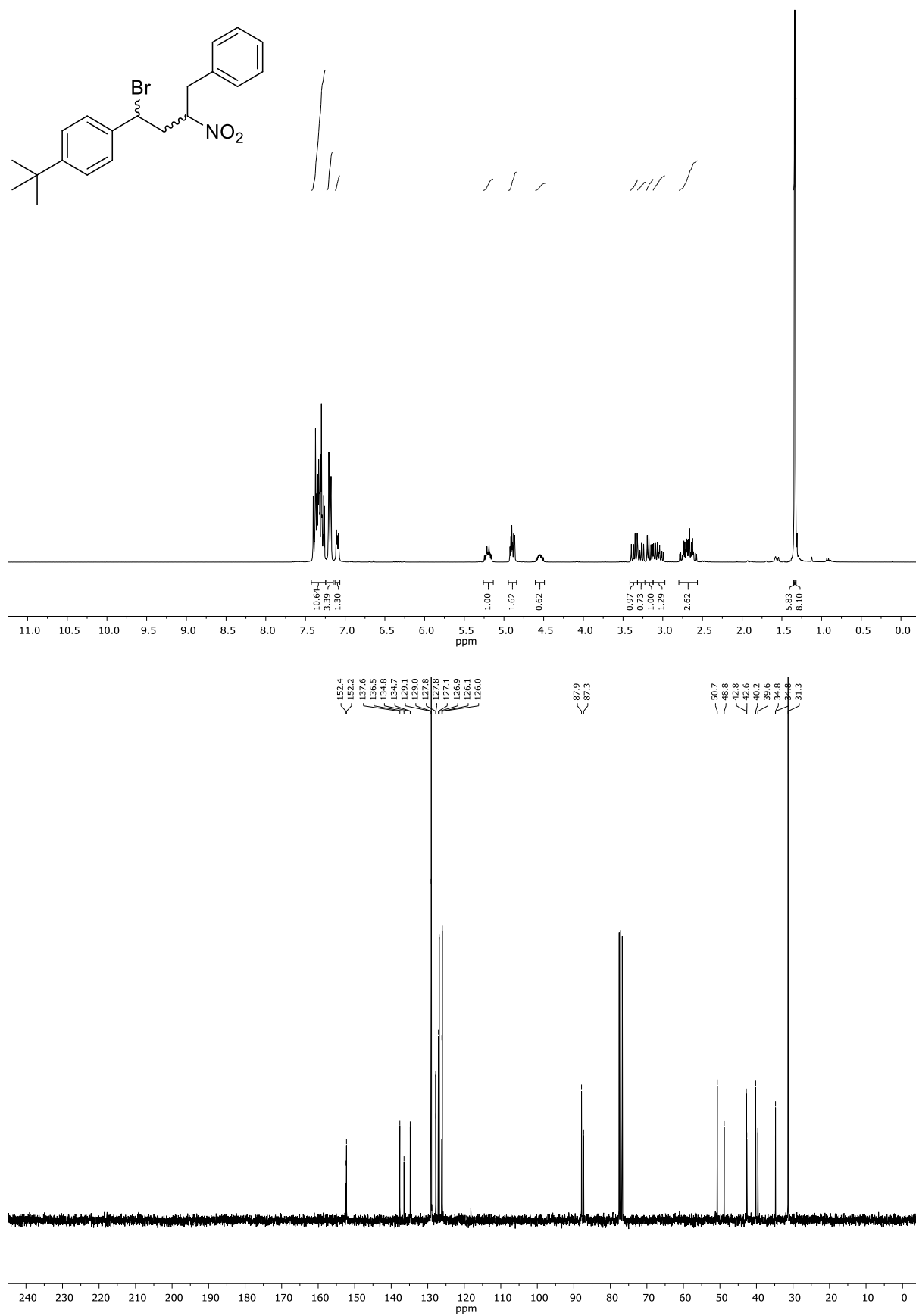
(1-bromo-3-nitrobutyl)-4-chlorobenzene (d.r. = 57:43) (4df)First image: ¹H-NMR; Second image: ¹³C-NMR; NMR solvent: CDCl₃

1-(1-bromo-3-nitrobutyl)-2-chlorobenzene (d.r. = 58:42) (4dg)

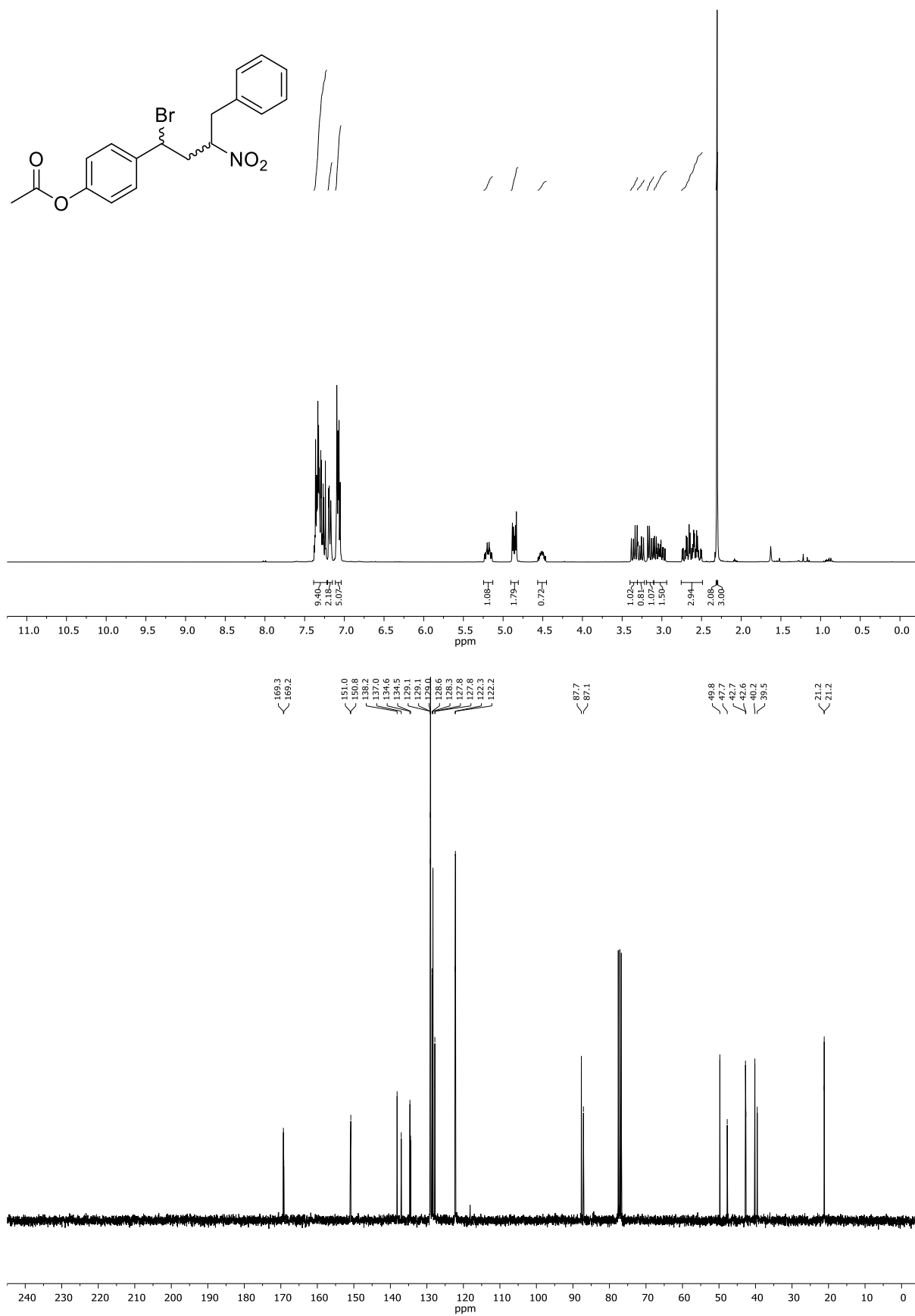
First image: ¹H-NMR; Second image: ¹³C-NMR: NMR solvent: CDCl₃

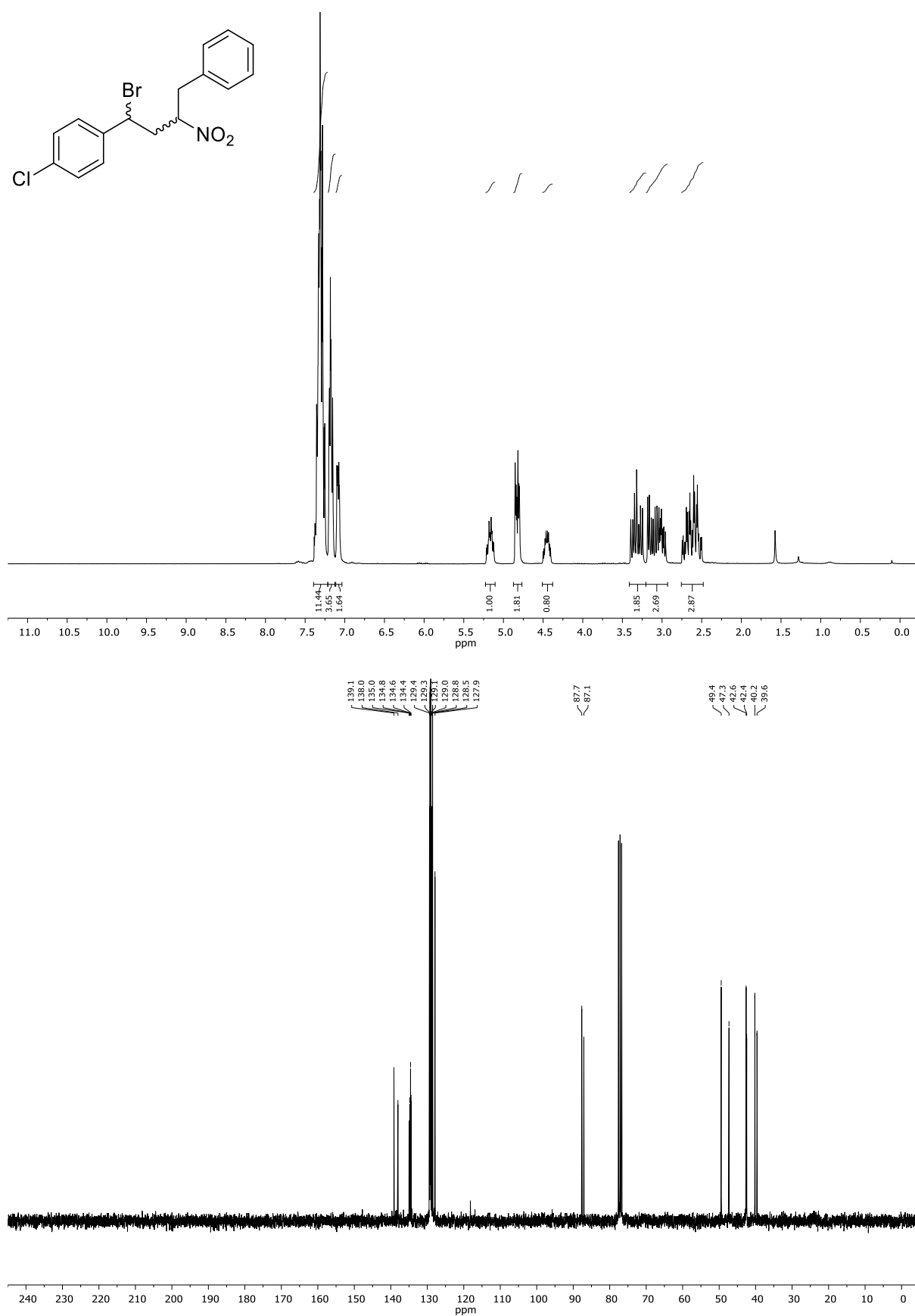
(1-bromo-3-nitrobutane-1,4-diyl)dibenzene (d.r. = 62:38) (4dh)

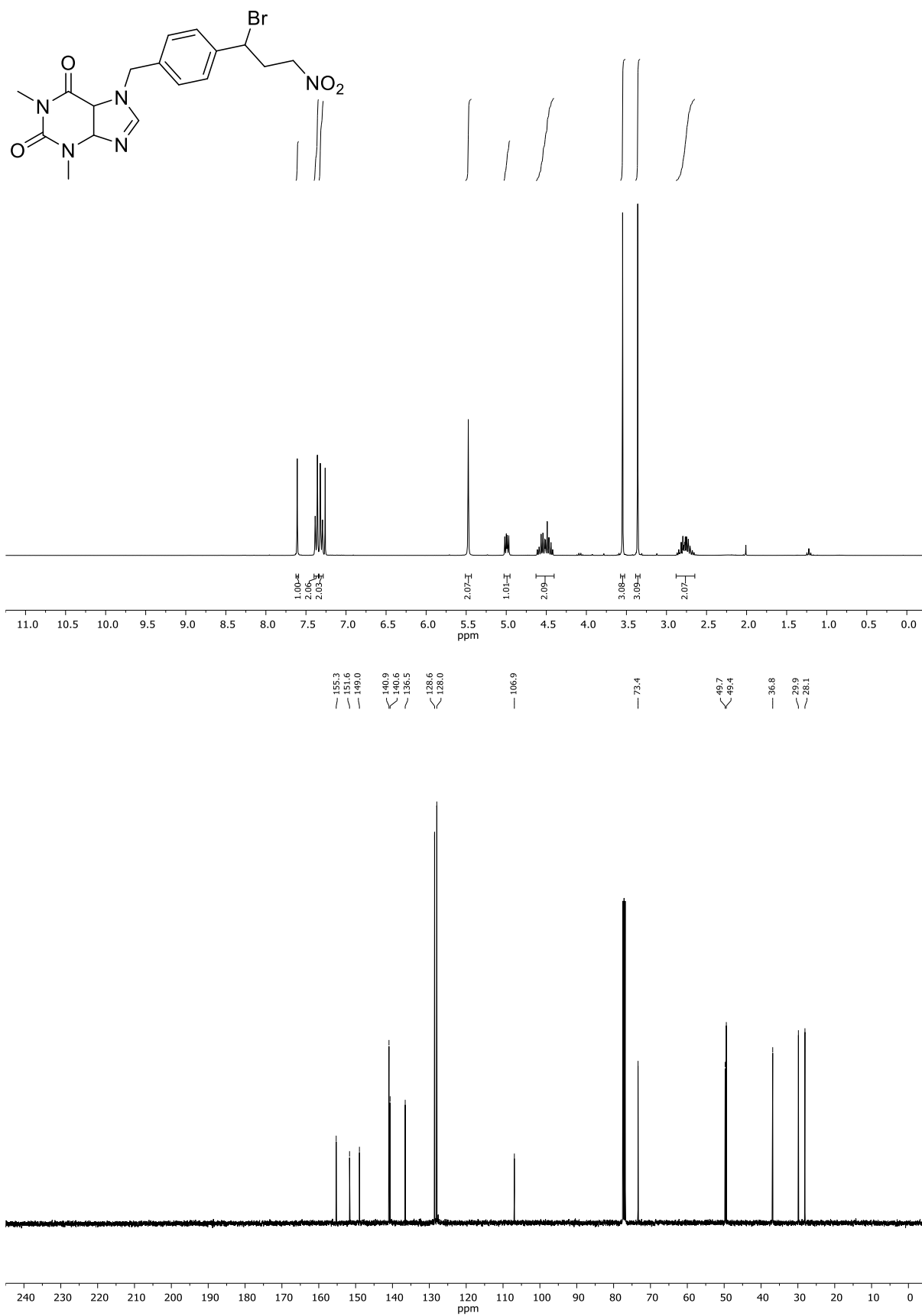
First image: ¹H-NMR; Second image: ¹³C-NMR; NMR solvent: CDCl₃

1-(1-bromo-3-nitro-4-phenylbutyl)-4-(tert-butyl)benzene (d.r. = 62:38) (4di)First image: ¹H-NMR; Second image: ¹³C-NMR; NMR solvent: CDCl₃

4-(1-bromo-3-nitro-4-phenylbutyl)phenyl acetate (d.r. = 60:40) (4dj)

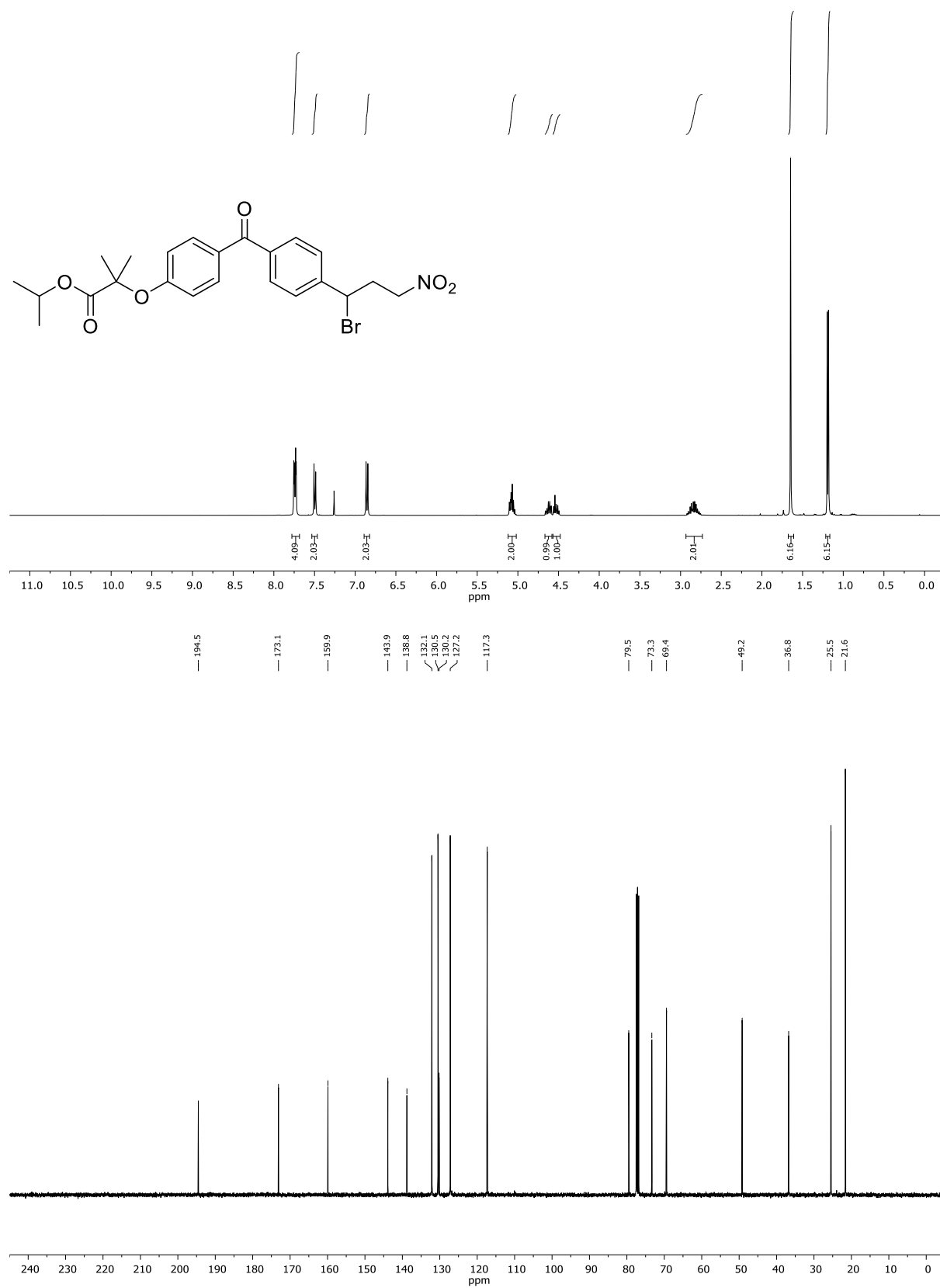
First image: ¹H-NMR; Second image: ¹³C-NMR; NMR solvent: CDCl₃

1-(1-bromo-3-nitro-4-phenylbutyl)-4-chlorobenzene (d.r. = 56:44) (4dl)First image: ¹H-NMR; Second image: ¹³C-NMR; NMR solvent: CDCl₃

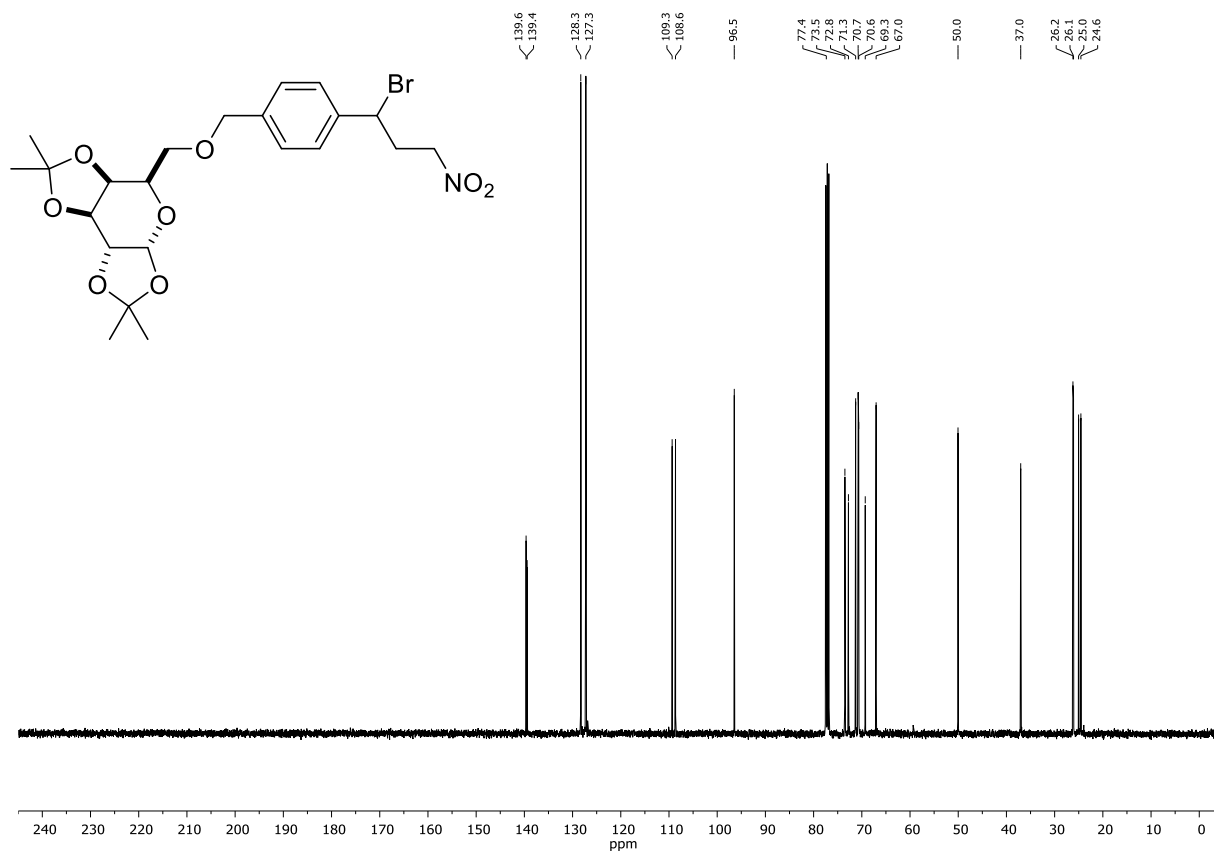
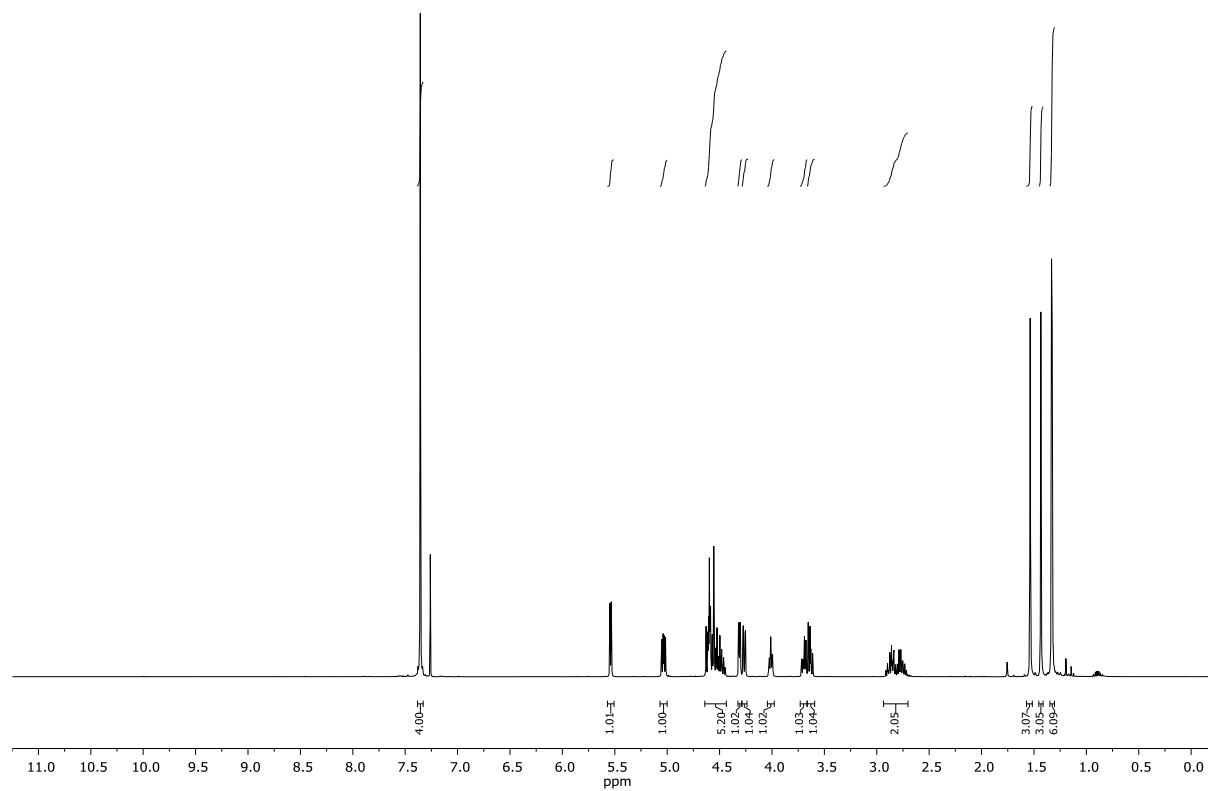
7-(4-(1-bromo-3-nitropropyl)benzyl)-1,3-dimethyl-3,4,5,7-tetrahydro-1H-purine-2,6-dione (4ea)

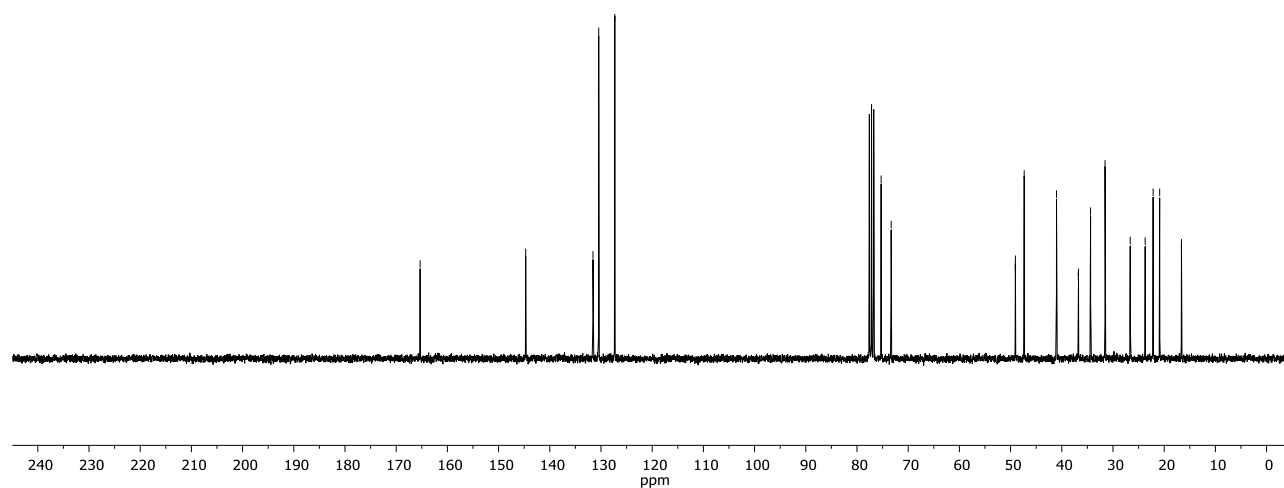
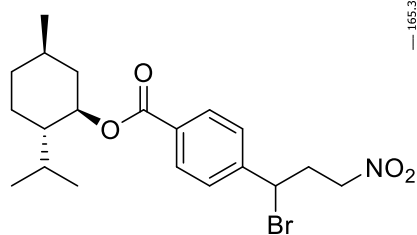
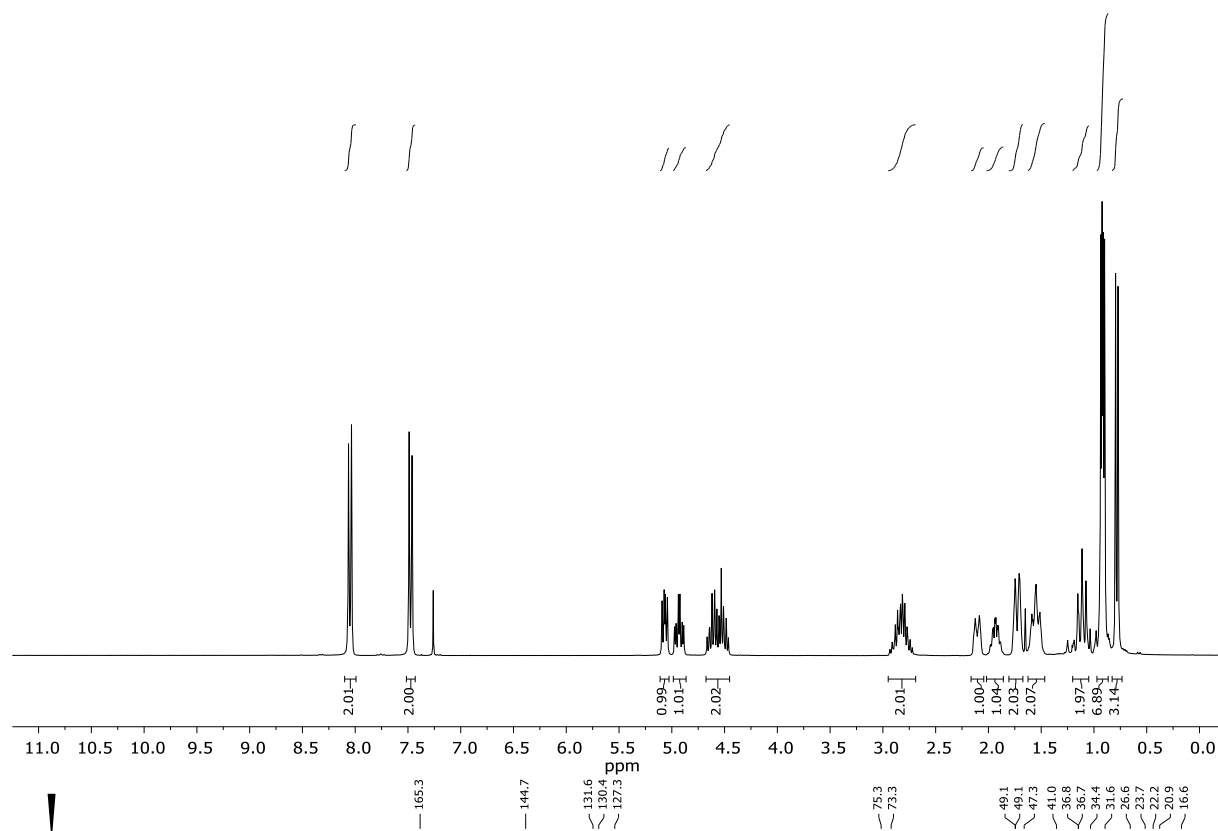
First image: ¹H-NMR; Second image: ¹³C-NMR; NMR solvent: CDCl₃

isopropyl 2-(4-(4-(1-bromo-3-nitropropyl)benzoyl)phenoxy)-2-methylpropanoate (4eb)

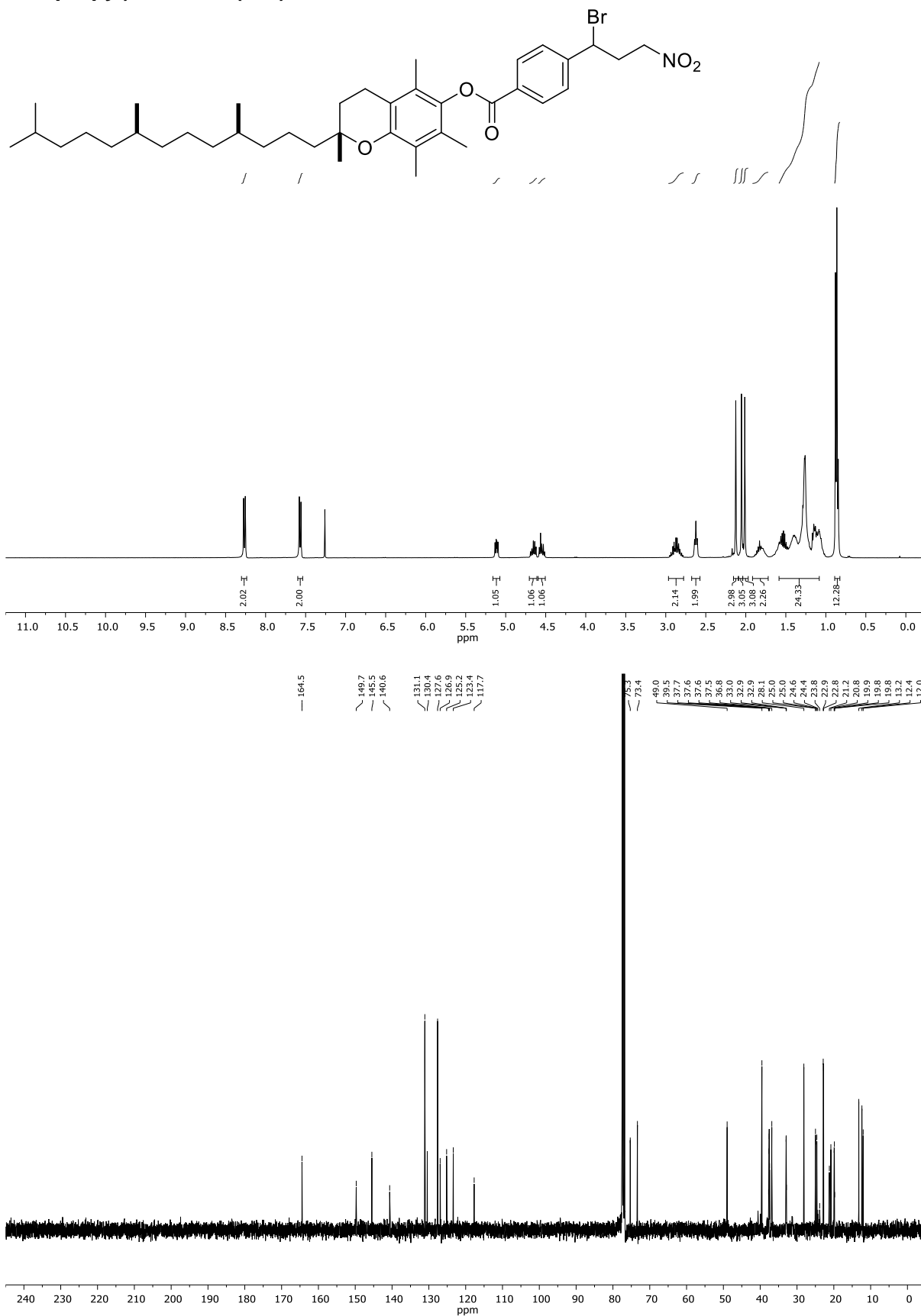


First image: ¹H-NMR; Second image: ¹³C-NMR; NMR solvent: CDCl₃

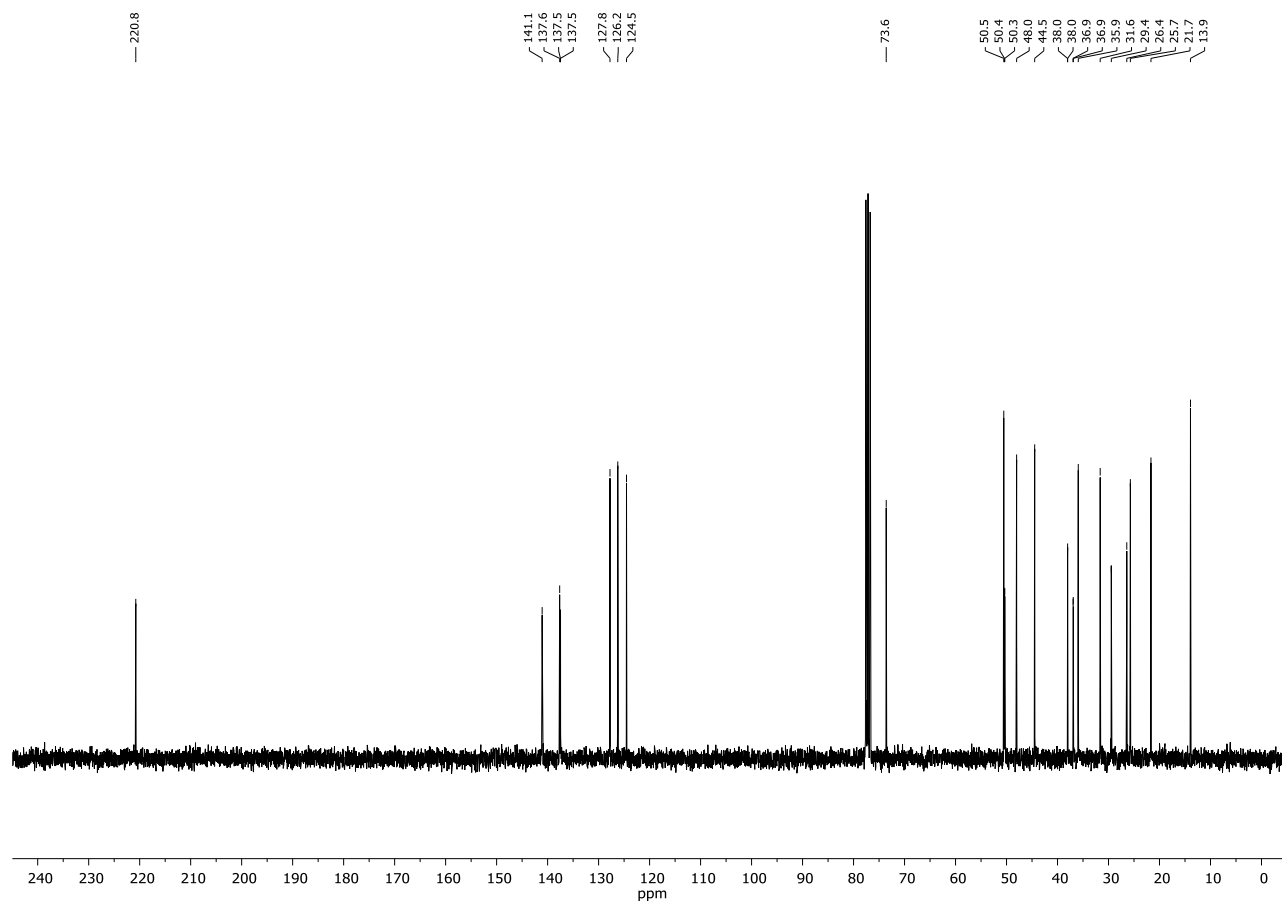
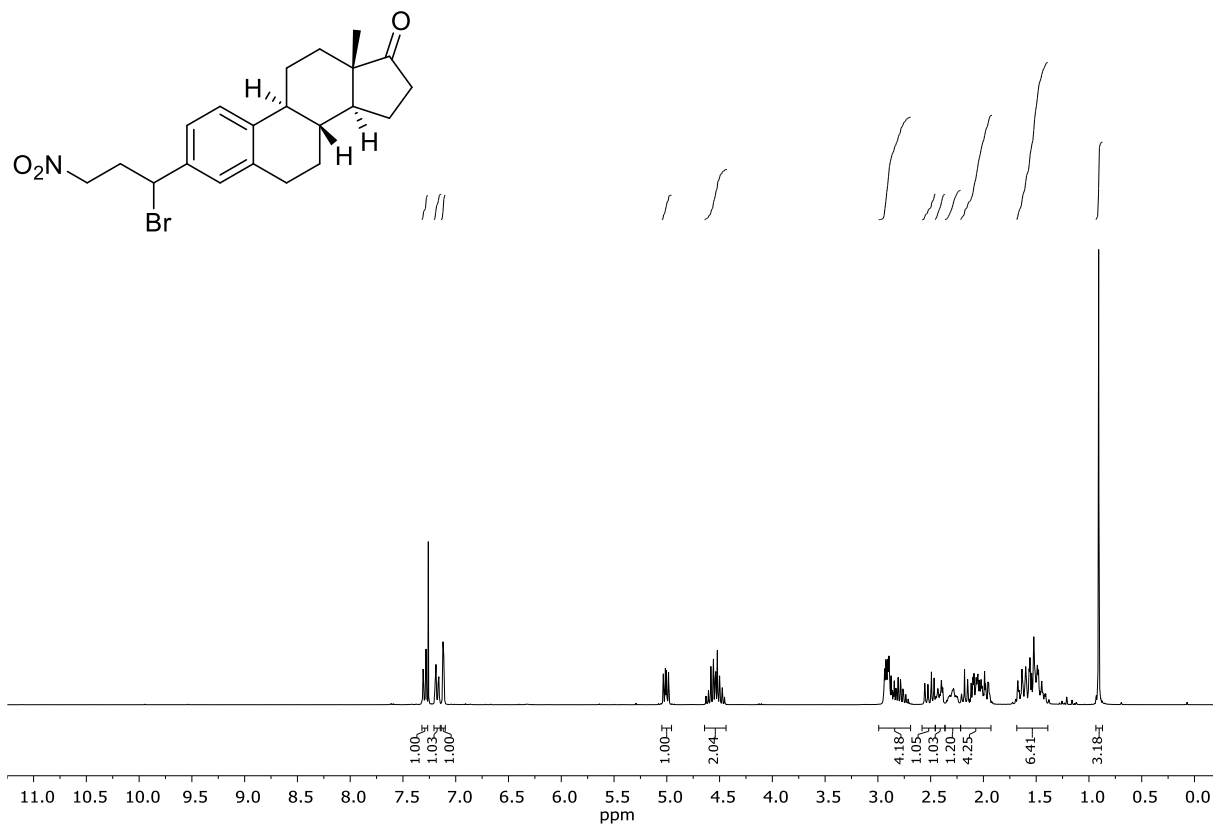
(3aR,5R,5aS,8aS,8bR)-5-(((4-(1-bromo-3-nitropropyl)benzyl)oxy)methyl)-2,2,7,7-tetramethyltetrahydro-5H-bis([1,3]dioxolo)[4,5-b:4',5'-d]pyran (4ec)First image: ¹H-NMR; Second image: ¹³C-NMR; NMR solvent: CDCl₃

(1R,2S,5R)-2-isopropyl-5-methylcyclohexyl 4-(1-bromo-3-nitropropyl)benzoate (4ed)

First image: ¹H-NMR; Second image: ¹³C-NMR; NMR solvent: CDCl₃

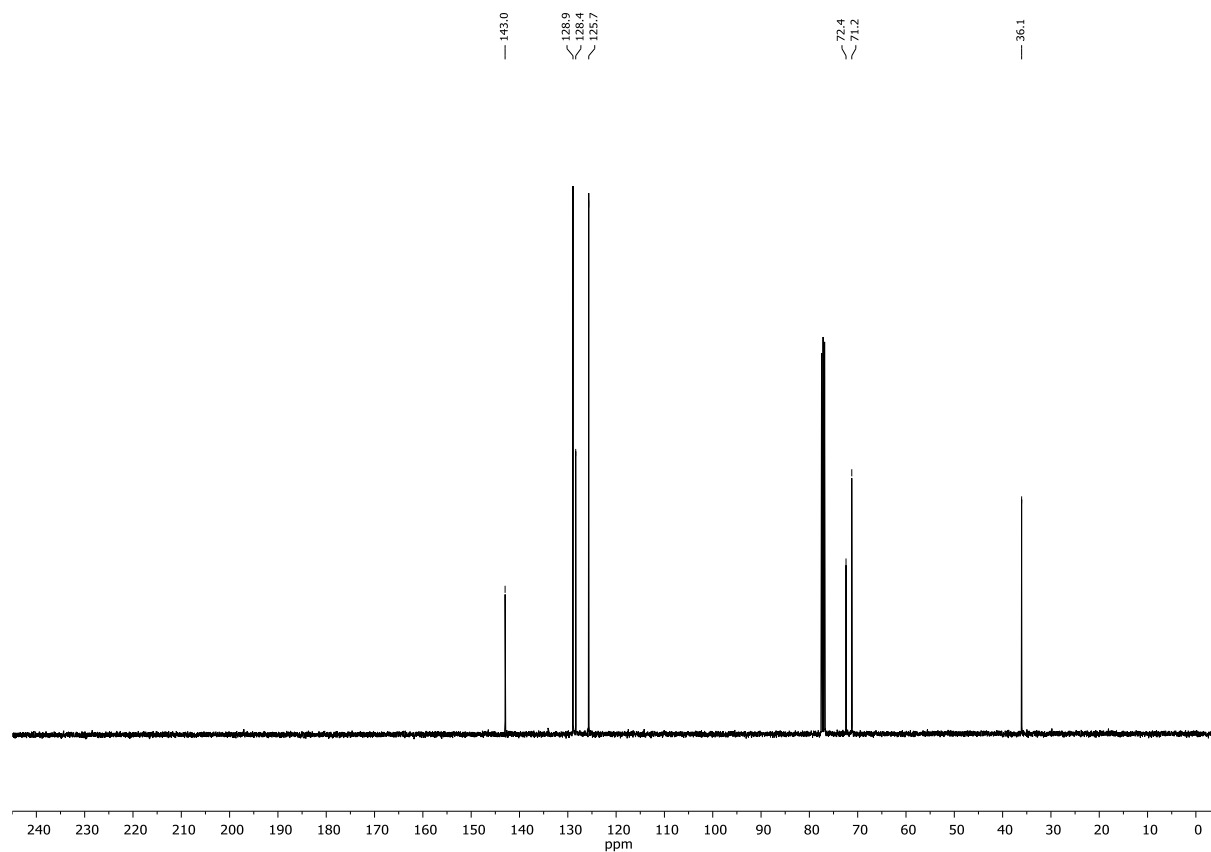
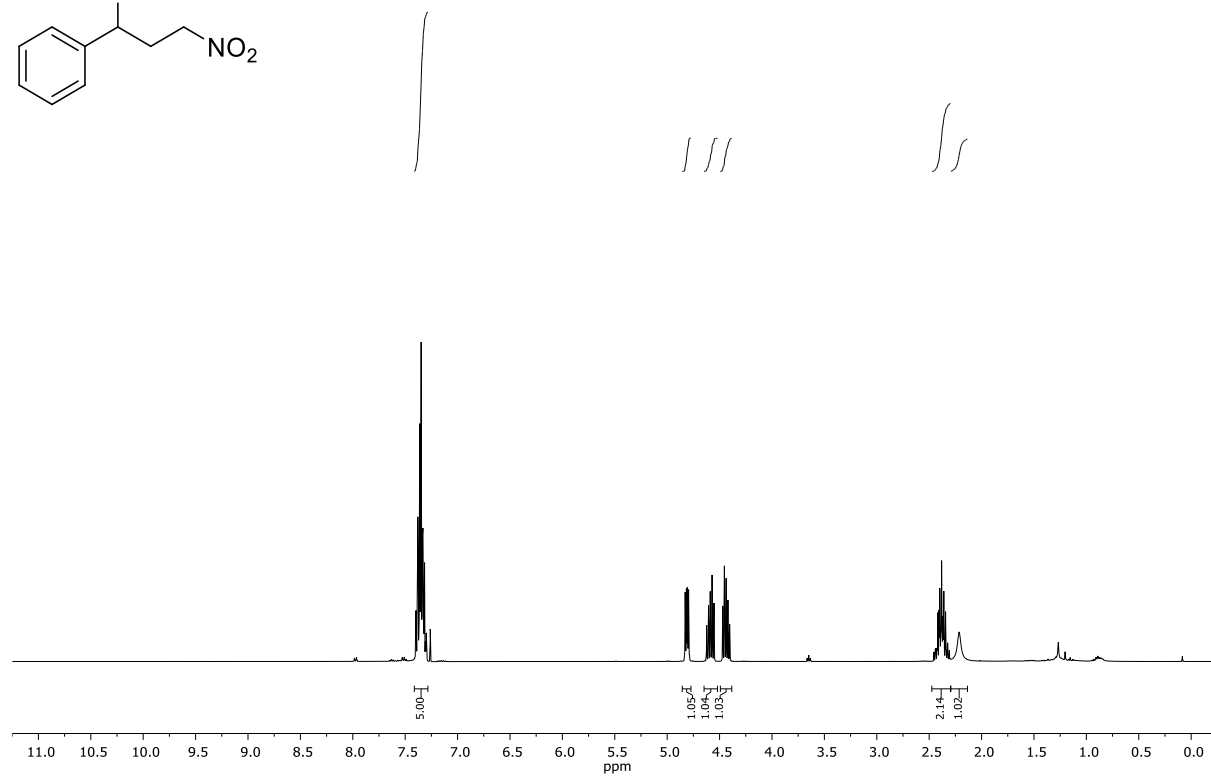
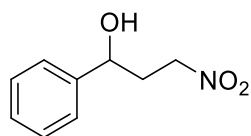
2,5,7,8-tetramethyl-2-((4R,8R)-4,8,12-trimethyltridecyl)chroman-6-yl 4-(1-bromo-3-nitropropyl)benzoate (4ee)

First image: ¹H-NMR; Second image: ¹³C-NMR; NMR solvent: CDCl₃

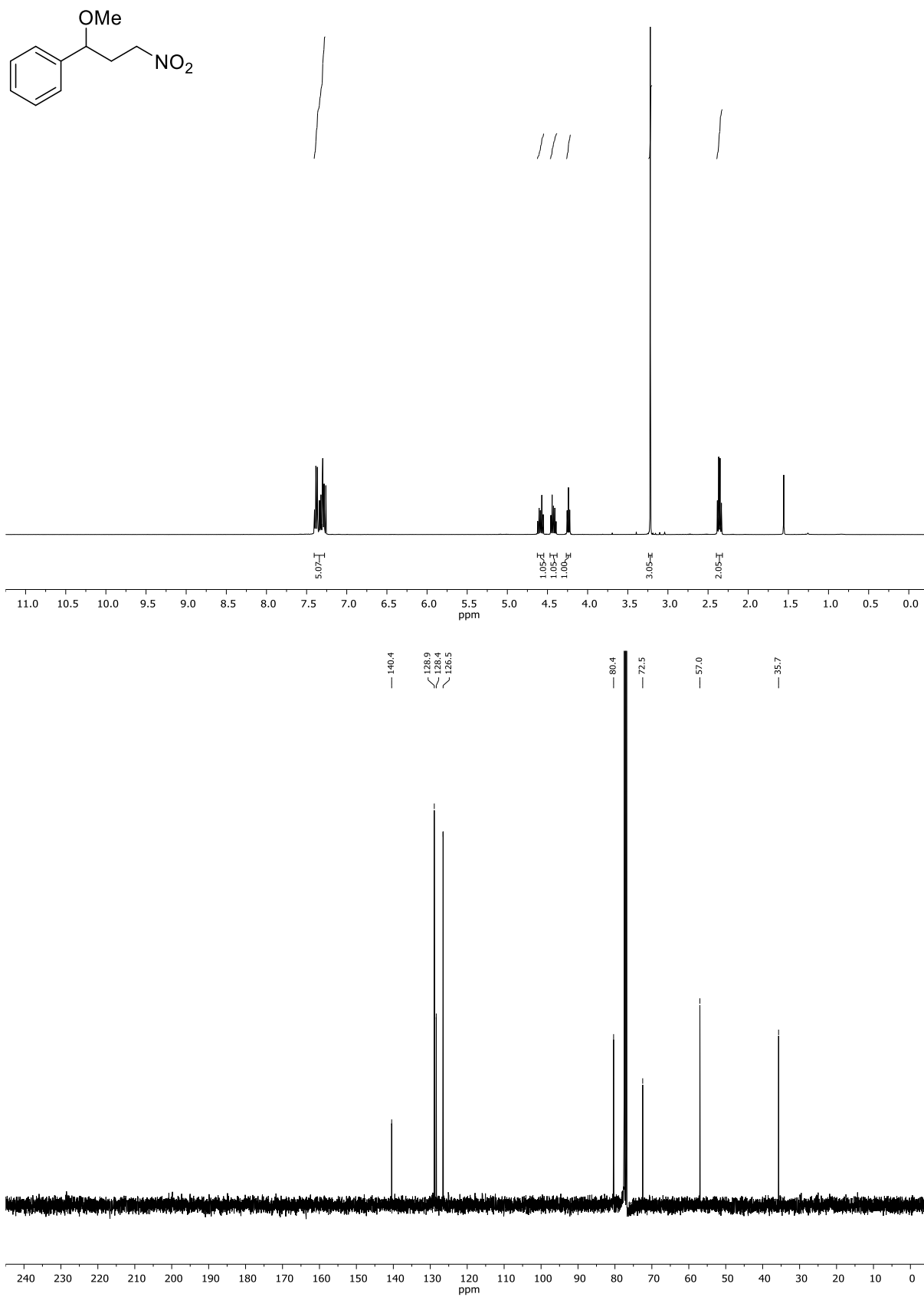
(8R,9S,13S,14S)-3-(1-bromo-3-nitropropyl)-13-methyl-6,7,8,9,11,12,13,14,15,16-decahydro-17H-cyclopenta[a]phenanthren-17-one (4ef)

First image: ¹H-NMR; Second image: ¹³C-NMR; NMR solvent: CDCl₃

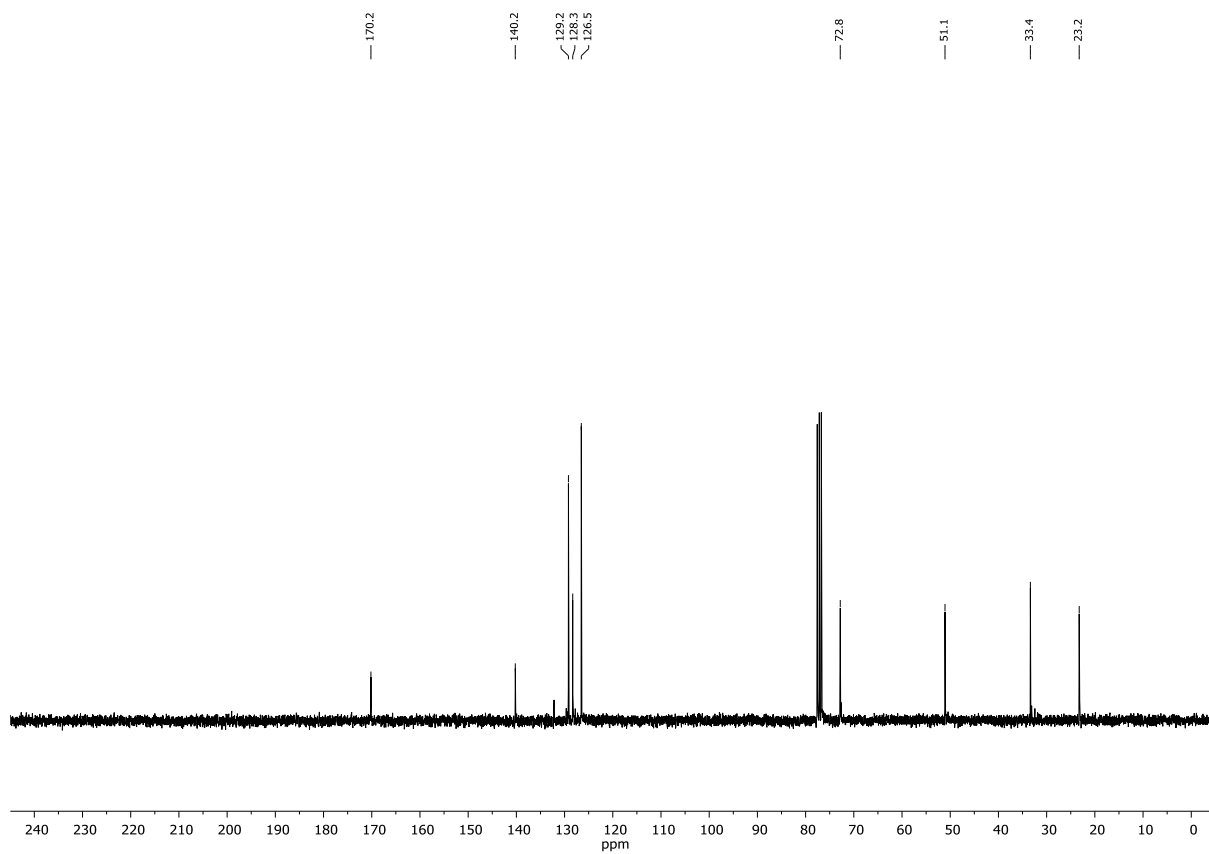
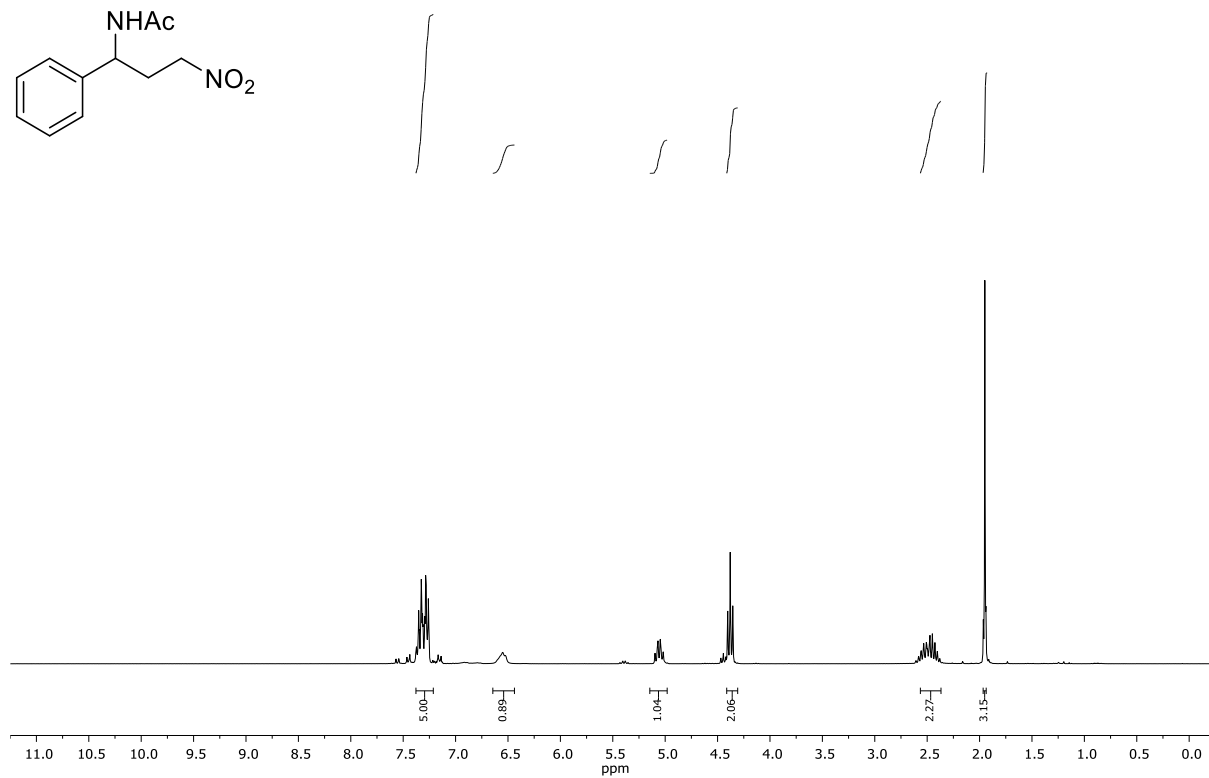
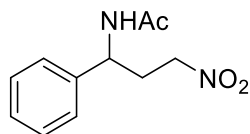
3-nitro-1-phenylpropan-1-ol (5a)



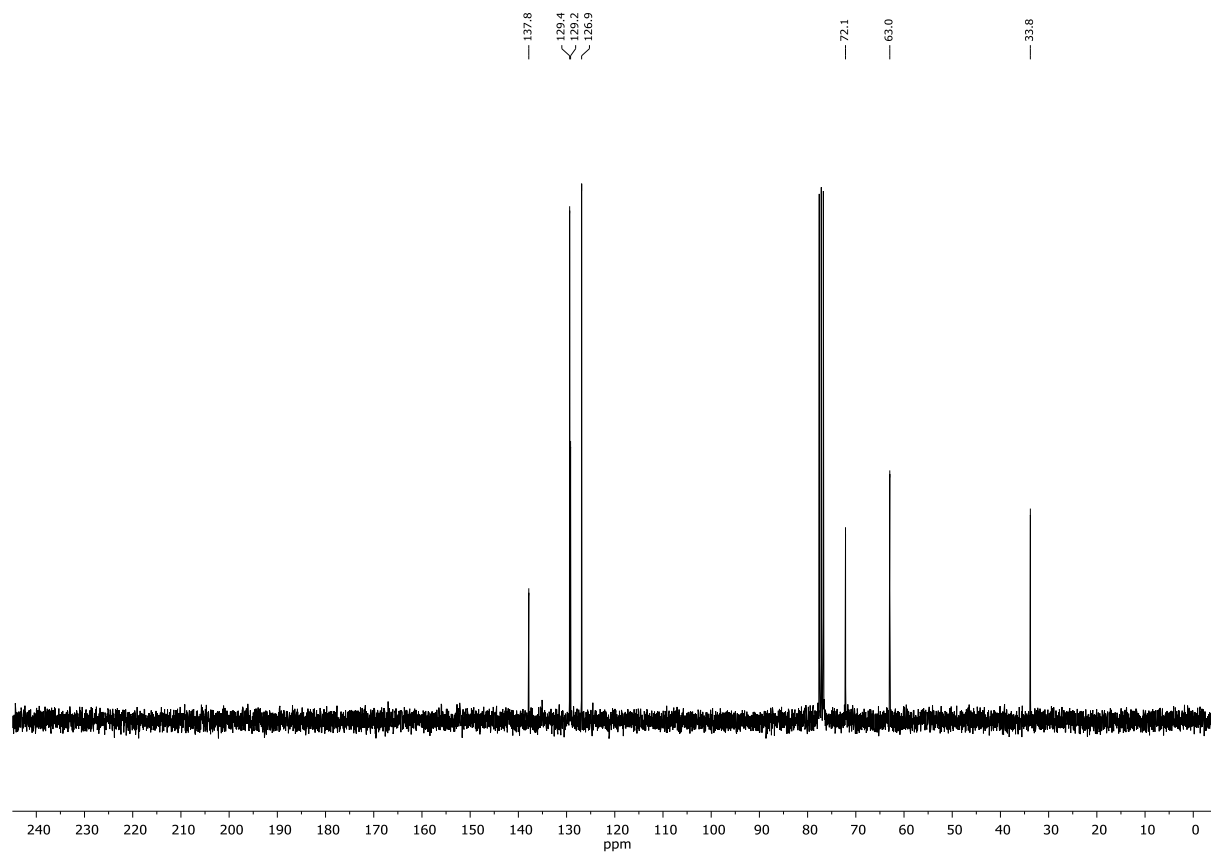
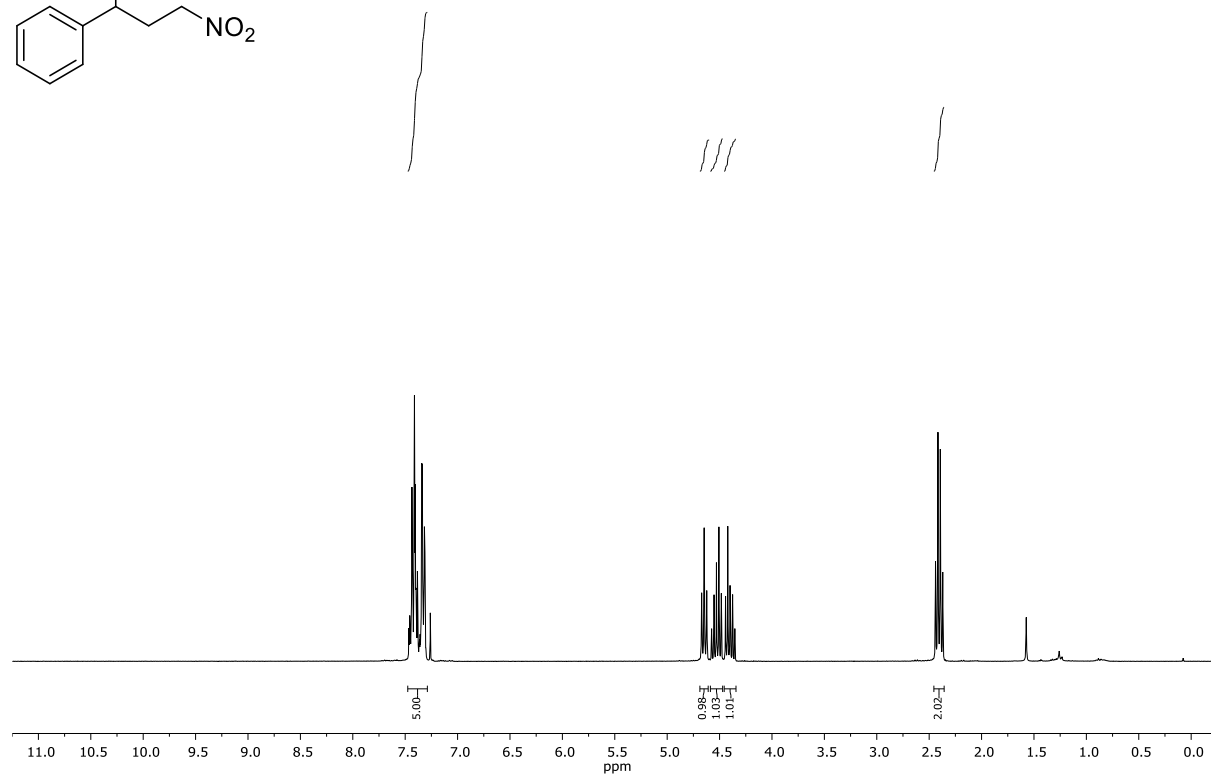
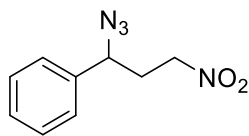
First image: $^1\text{H-NMR}$; Second image: $^{13}\text{C-NMR}$; NMR solvent: CDCl_3

(1-methoxy-3-nitropropyl)benzene (5b)

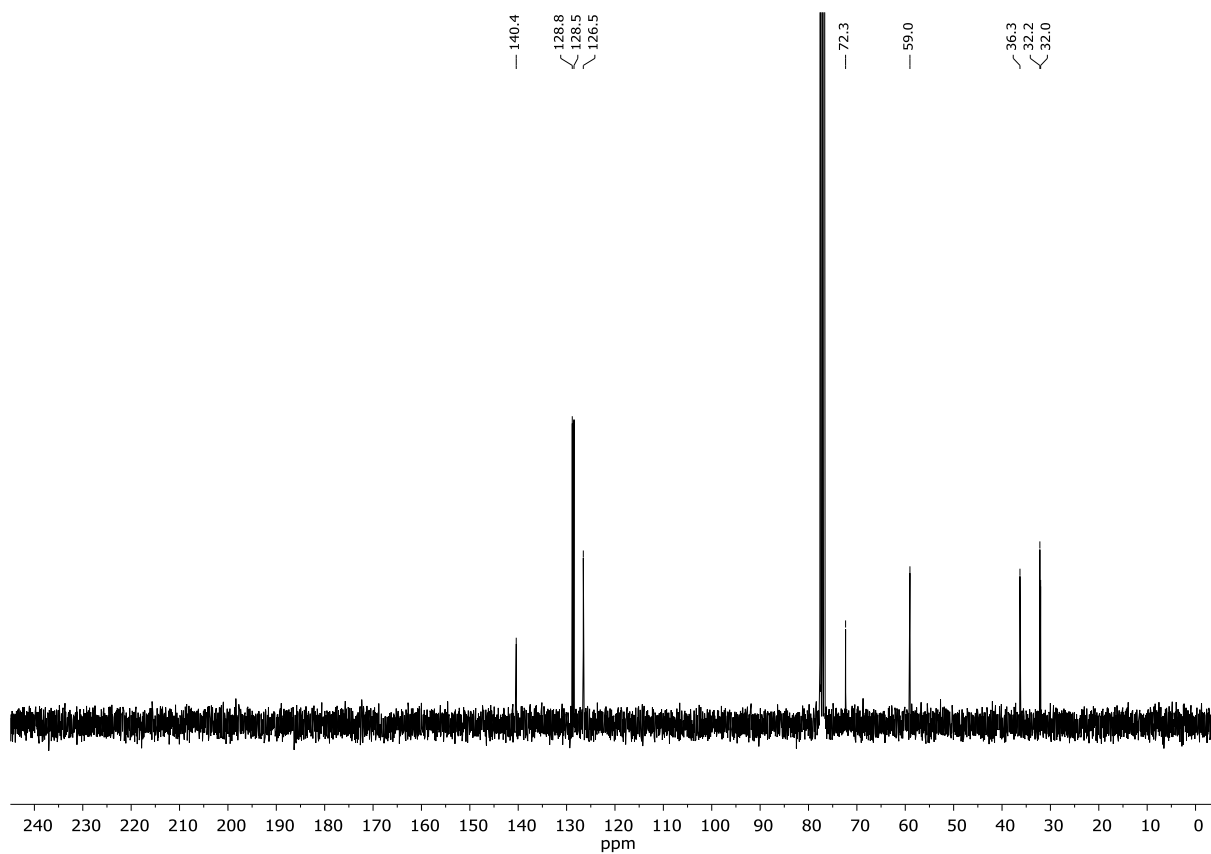
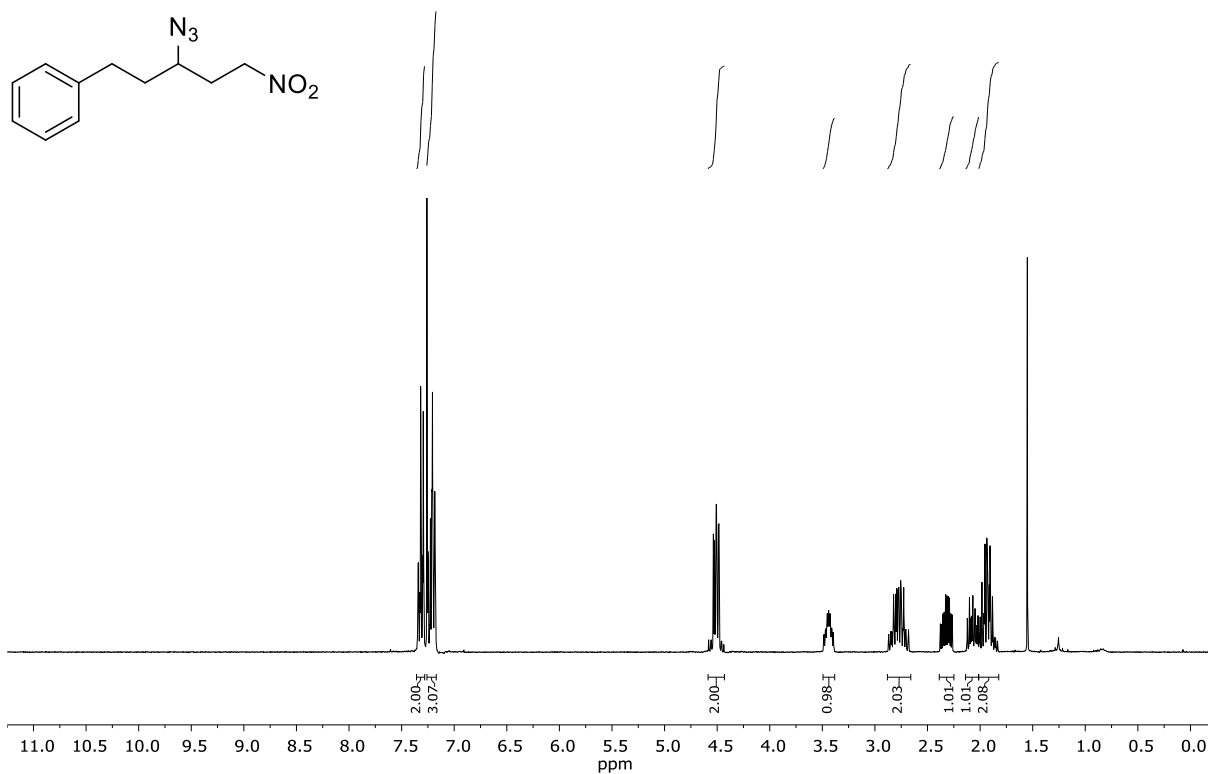
First image: ¹H-NMR; Second image: ¹³C-NMR; NMR solvent: CDCl₃

***N*-(3-nitro-1-phenylpropyl)acetamide (5c)**

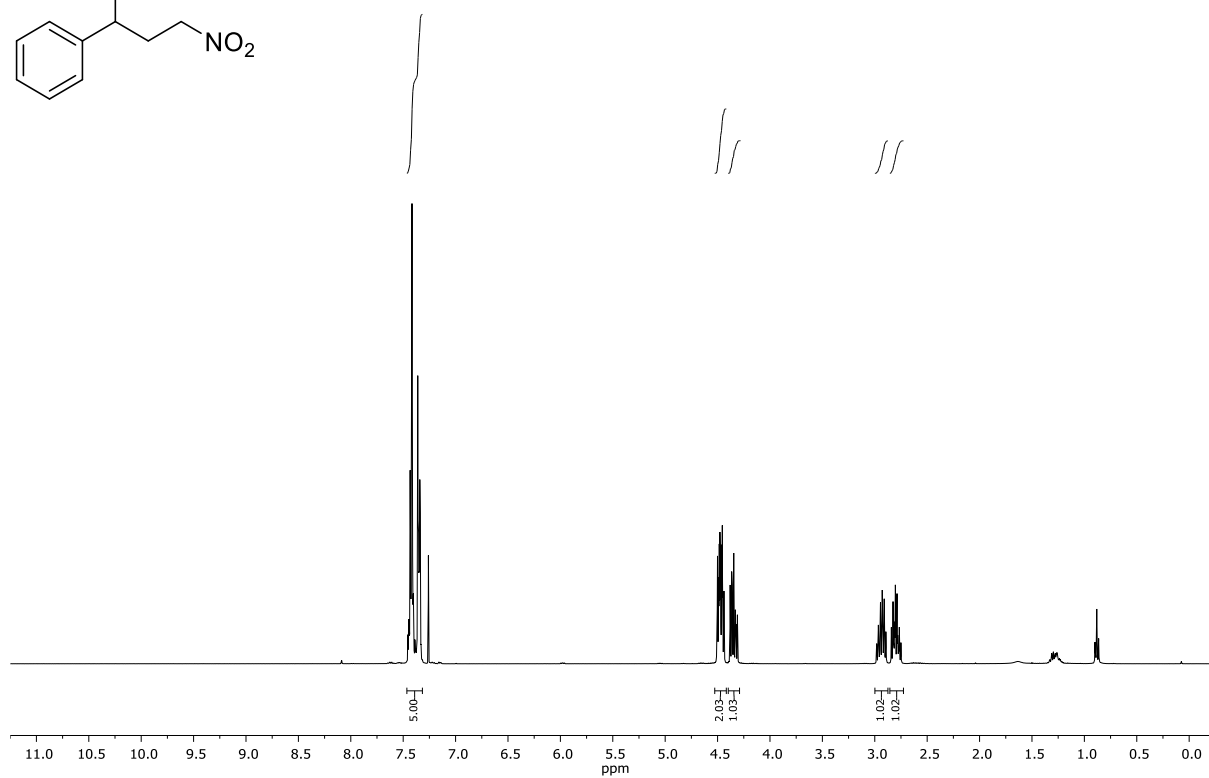
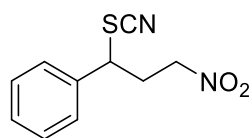
First image: $^1\text{H-NMR}$; Second image: $^{13}\text{C-NMR}$; NMR solvent: CDCl_3

(1-azido-3-nitropropyl)benzene (5d)

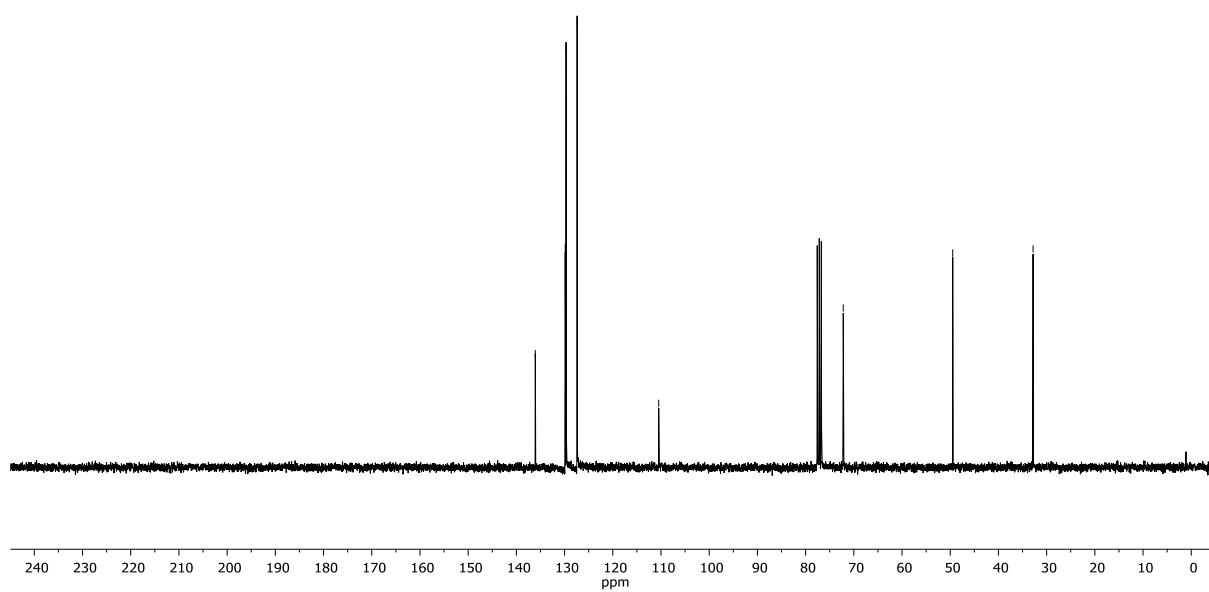
First image: ¹H-NMR; Second image: ¹³C-NMR; NMR solvent: CDCl₃

(3-azido-5-nitropentyl)benzene (5ca)

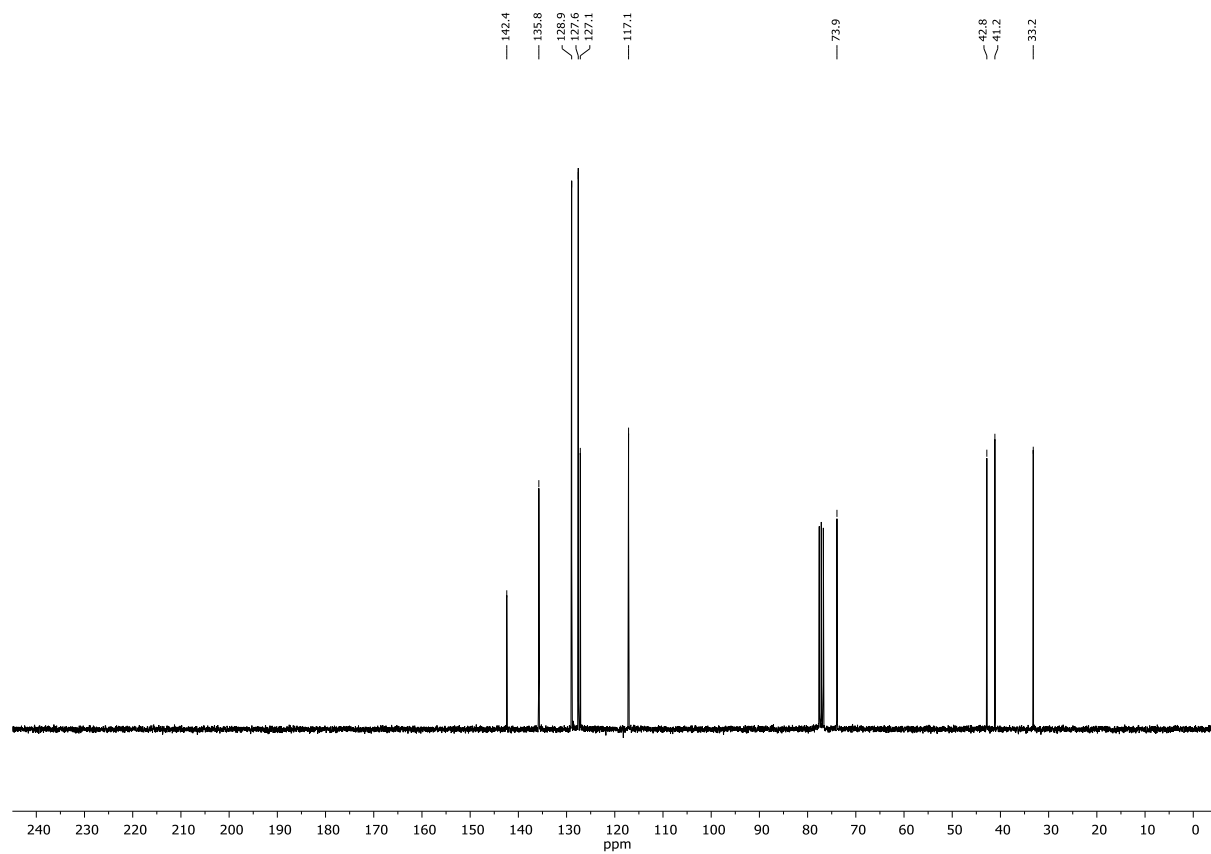
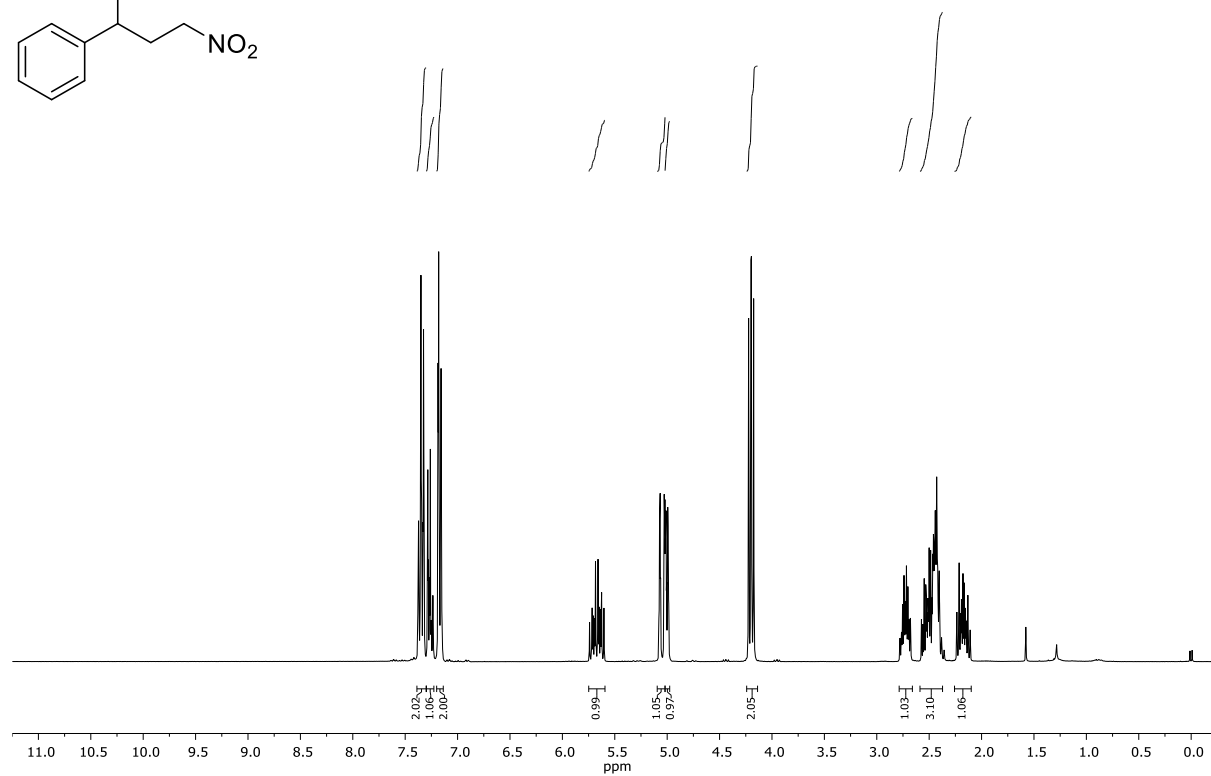
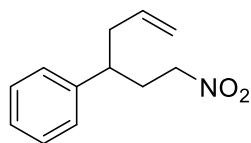
First image: $^1\text{H-NMR}$; Second image: $^{13}\text{C-NMR}$; NMR solvent: CDCl_3

(3-nitro-1-thiocyanatopropyl)benzene (5e)

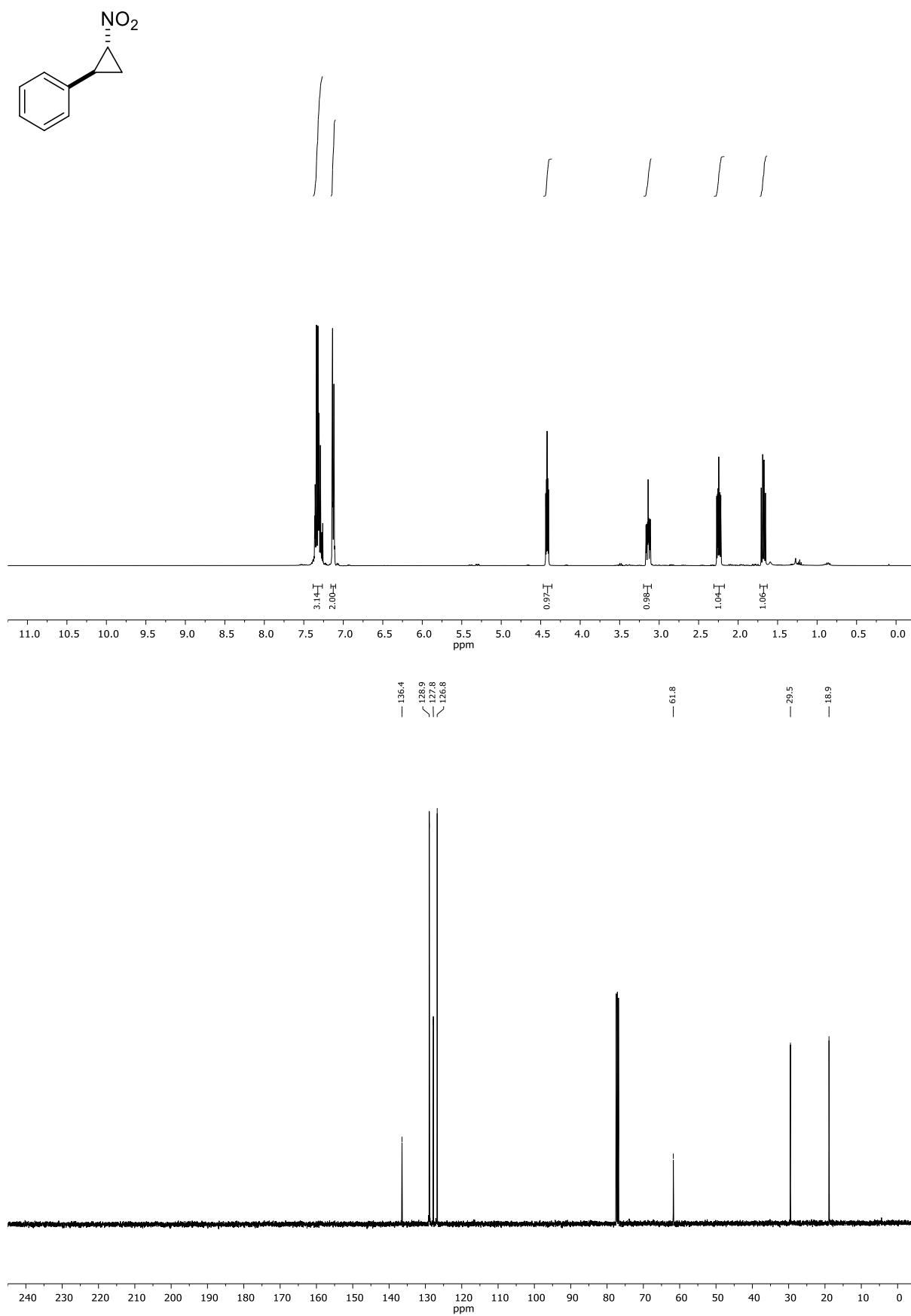
— 136.1
— 129.9
— 129.7
— 127.4
— 110.5
— 72.2
— 49.5
— 32.8



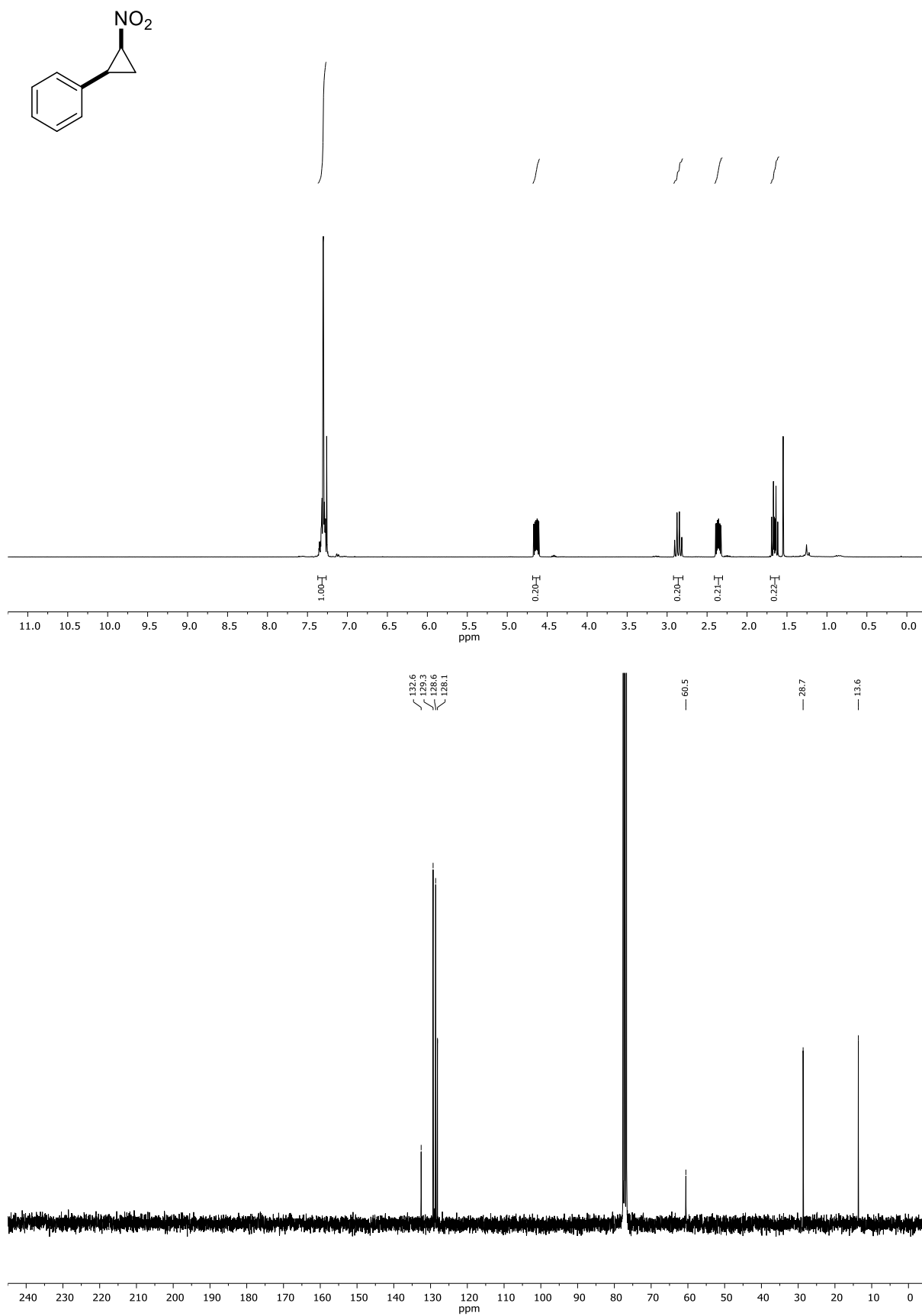
First image: $^1\text{H-NMR}$; Second image: $^{13}\text{C-NMR}$; NMR solvent: CDCl_3

(1-nitrohex-5-en-3-yl)benzene (5f)

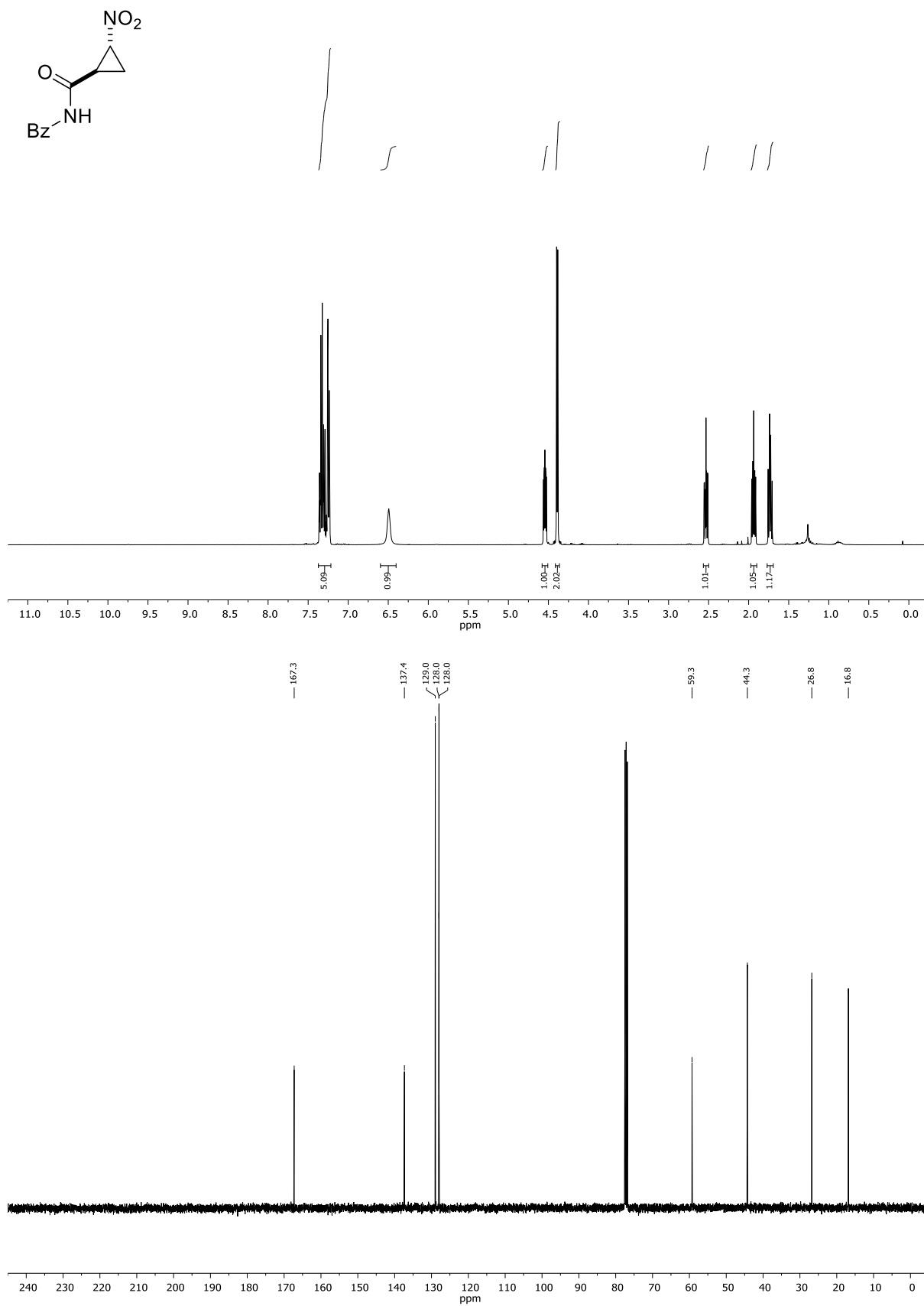
First image: $^1\text{H-NMR}$; Second image: $^{13}\text{C-NMR}$; NMR solvent: CDCl_3

***trans*-((1*S*,2*R*)-2-nitrocyclopropyl)benzene (*trans*-6a)**

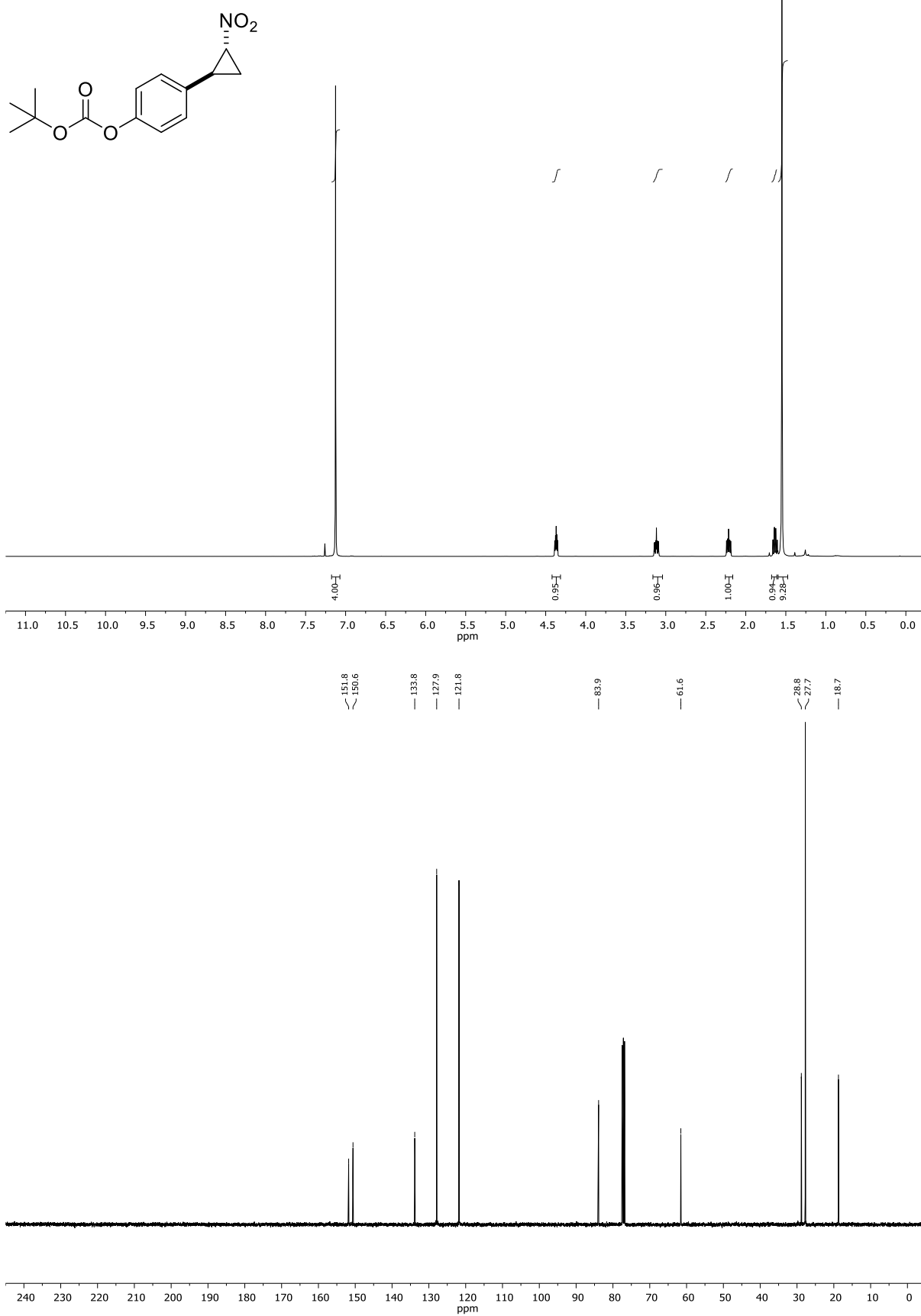
First image: ¹H-NMR; Second image: ¹³C-NMR; NMR solvent: CDCl₃

***cis*-((1*S*,2*R*)-2-nitrocyclopropyl)benzene (*cis*-6a)**

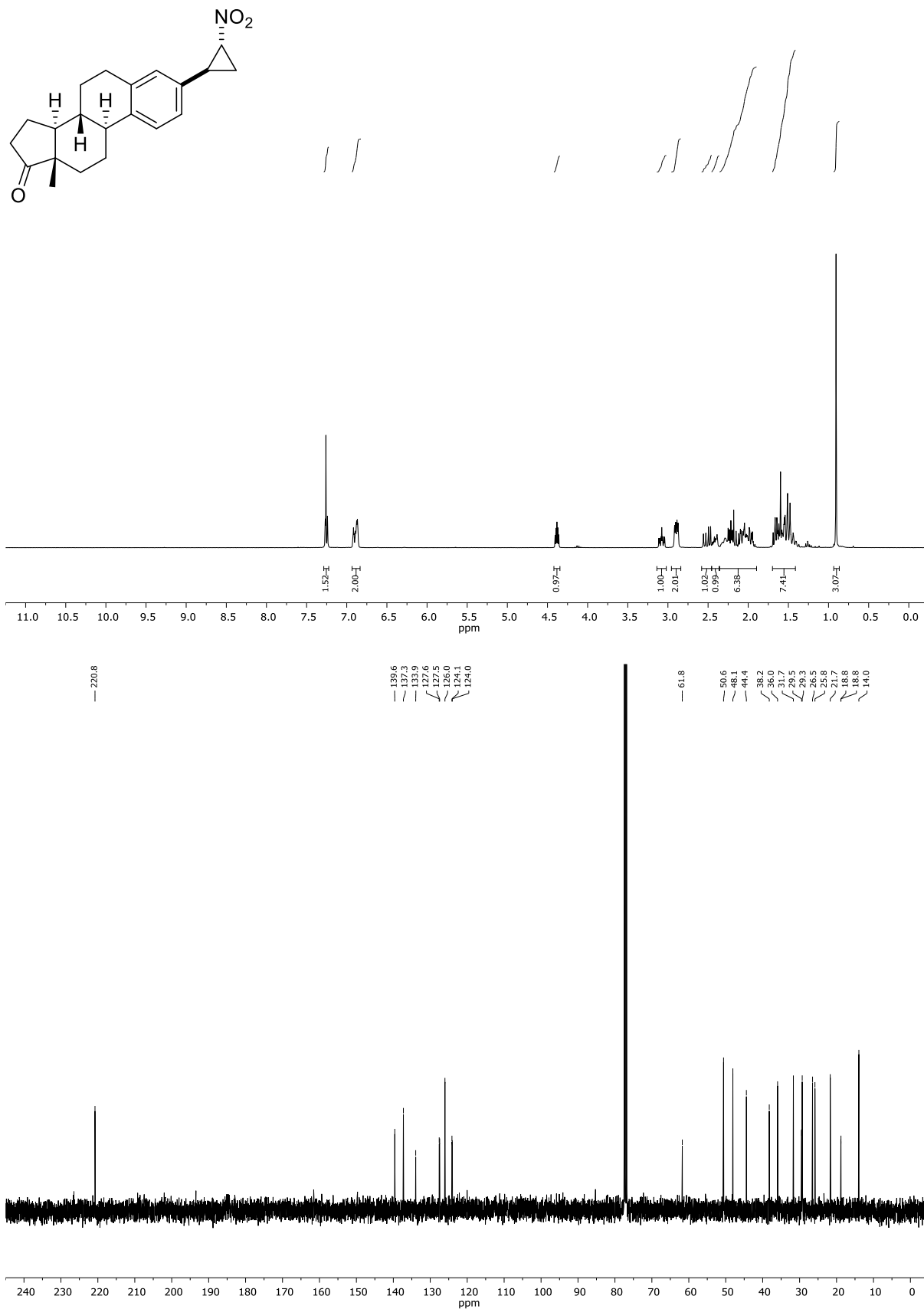
First image: ¹H-NMR; Second image: ¹³C-NMR; NMR solvent: CDCl₃

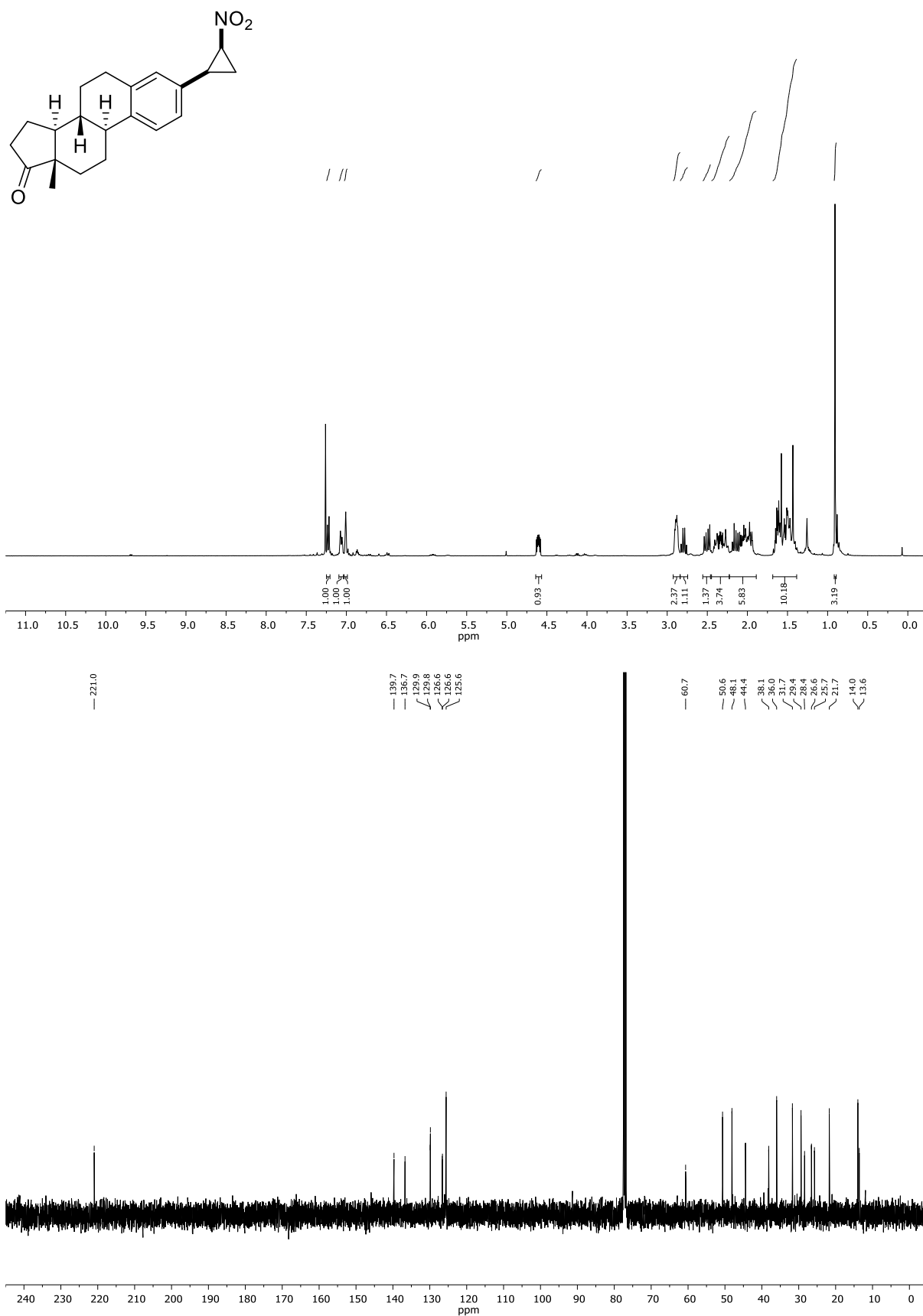
***trans*-N-2-nitrocyclopropane-1-carbonyl)benzamide (trans-6bb)**

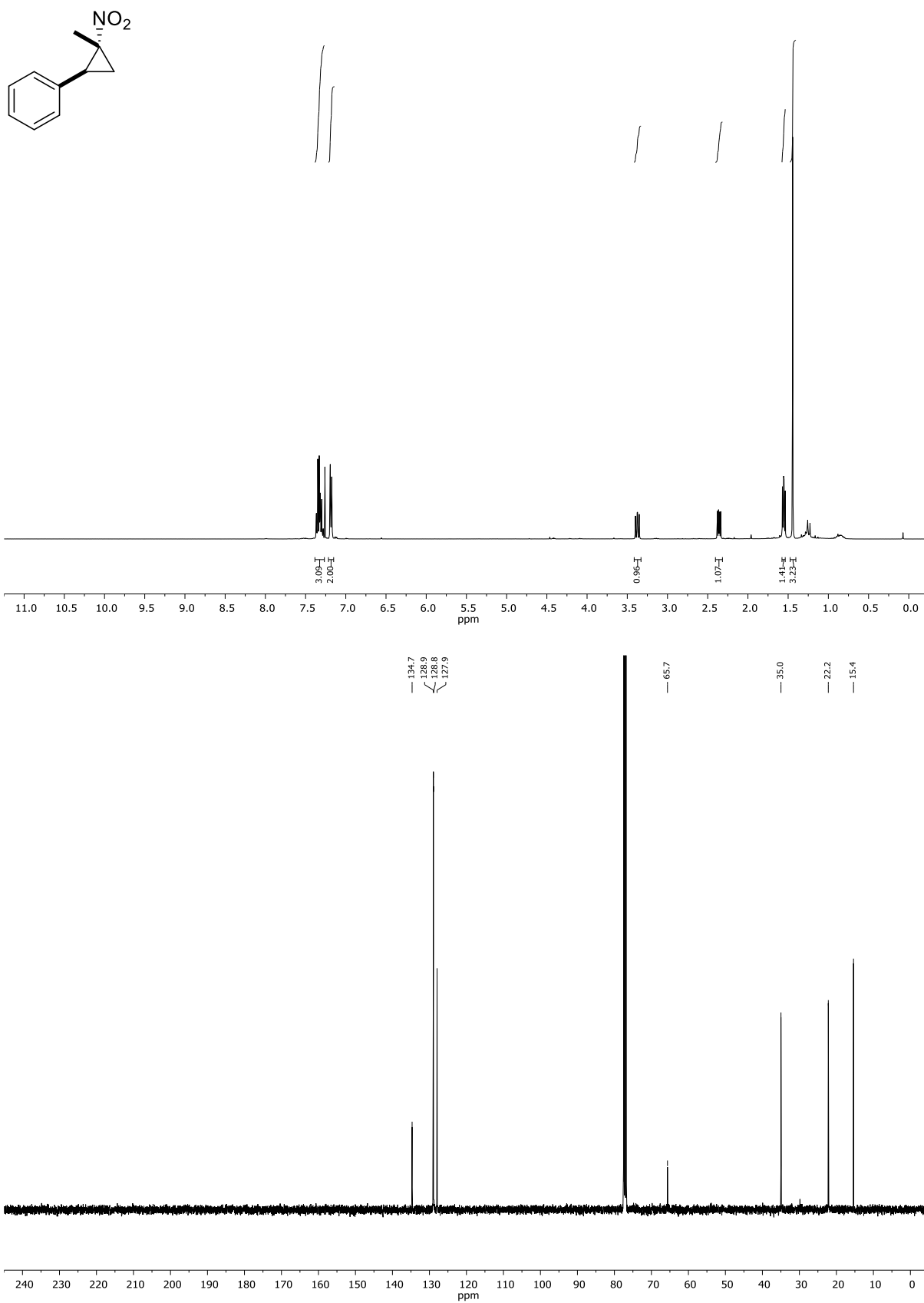
First image: ¹H-NMR; Second image: ¹³C-NMR; NMR solvent: CDCl₃

***trans*-tert-butyl (4-(2-nitrocyclopropyl)phenyl) carbonate (*trans*-6k)**

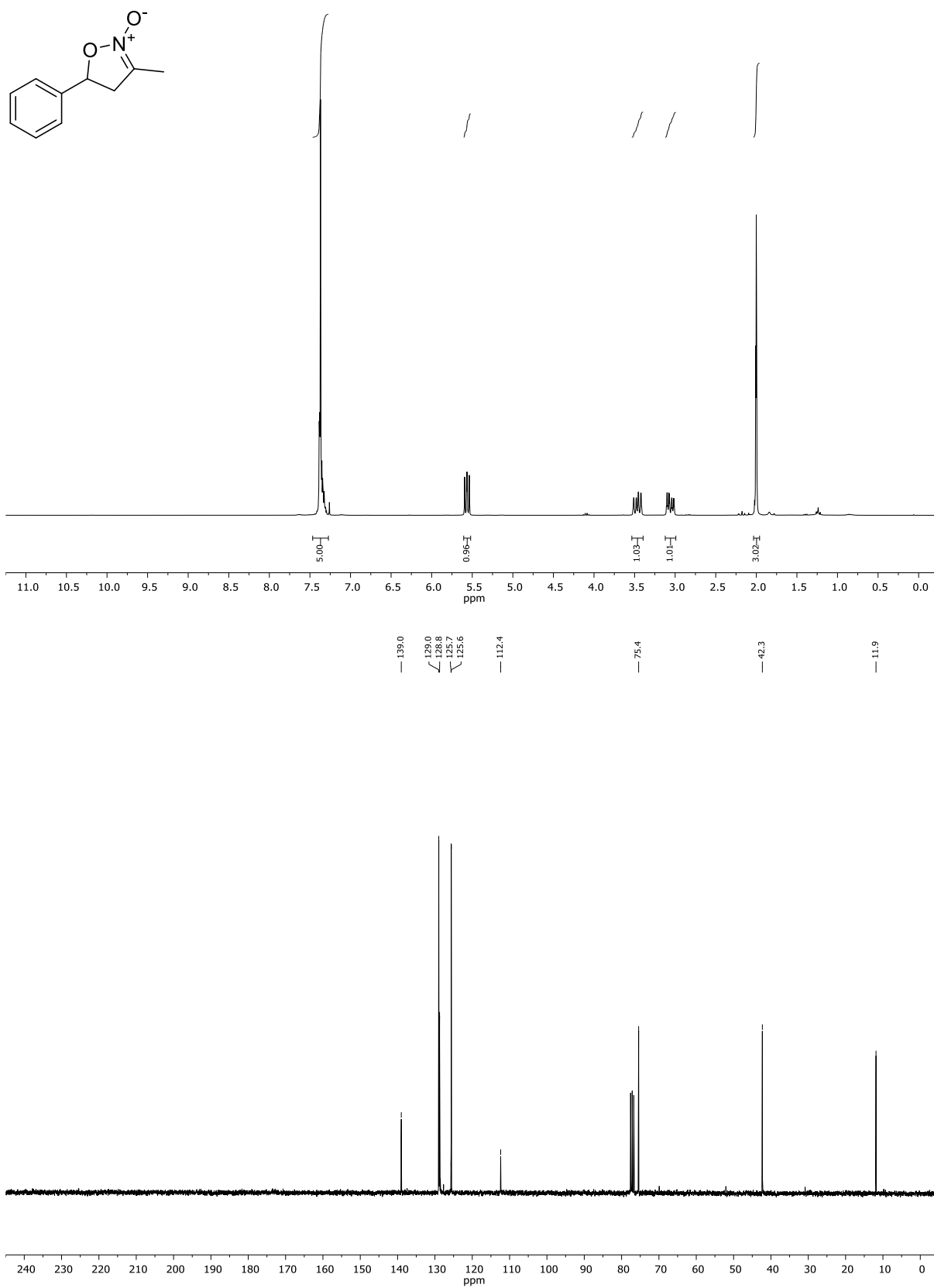
First image: ¹H-NMR; Second image: ¹³C-NMR; NMR solvent: CDCl₃

***trans*-(8*R*,9*S*,13*S*,14*S*)-13-methyl-3-((1*S*,2*R*)-2-nitrocyclopropyl)-6,7,8,9,11,12,13,14,15,16-decahydro-17*H*-cyclopenta[*a*]phenanthren-17-one (*trans*-6ef)**First image: ¹H-NMR; Second image: ¹³C-NMR; NMR solvent: CDCl₃

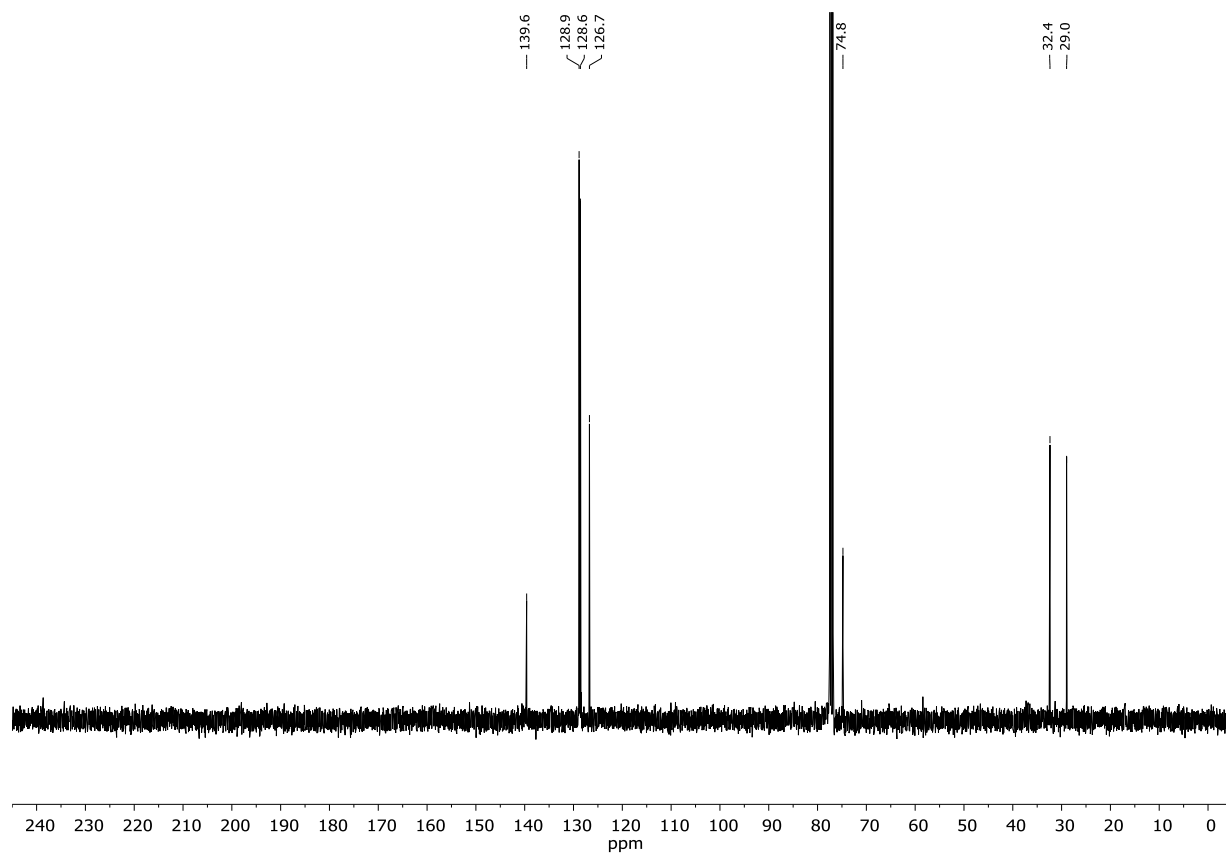
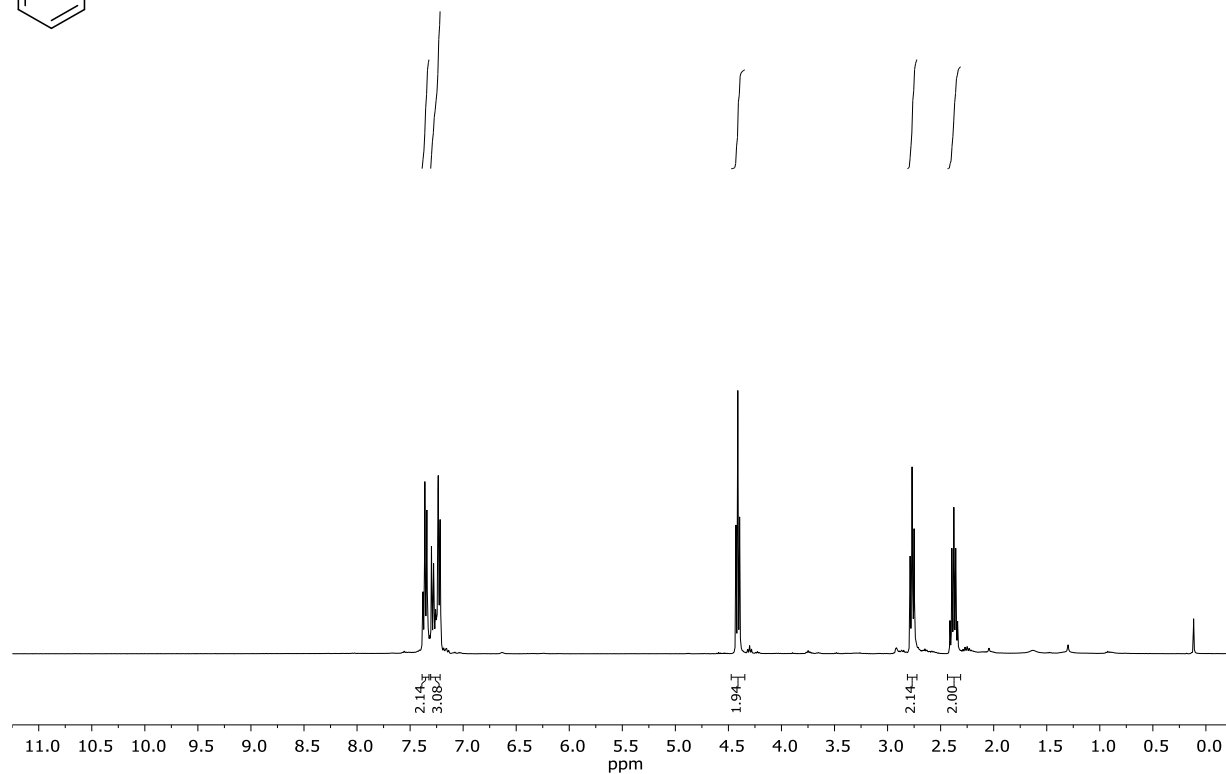
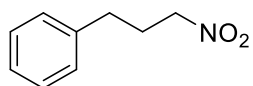
***cis*-(8R,9S,13S,14S)-13-methyl-3-((1S,2R)-2-nitrocyclopropyl)-6,7,8,9,11,12,13,14,15,16-decahydro-17H-cyclopenta[*a*]phenanthren-17-one (*cis*-6ef)**First image: ¹H-NMR; Second image: ¹³C-NMR; NMR solvent: CDCl₃

trans-2-methyl-2-nitrocyclopropyl)benzene (*trans*-6da)

First image: ¹H-NMR; Second image: ¹³C-NMR; NMR solvent: CDCl₃

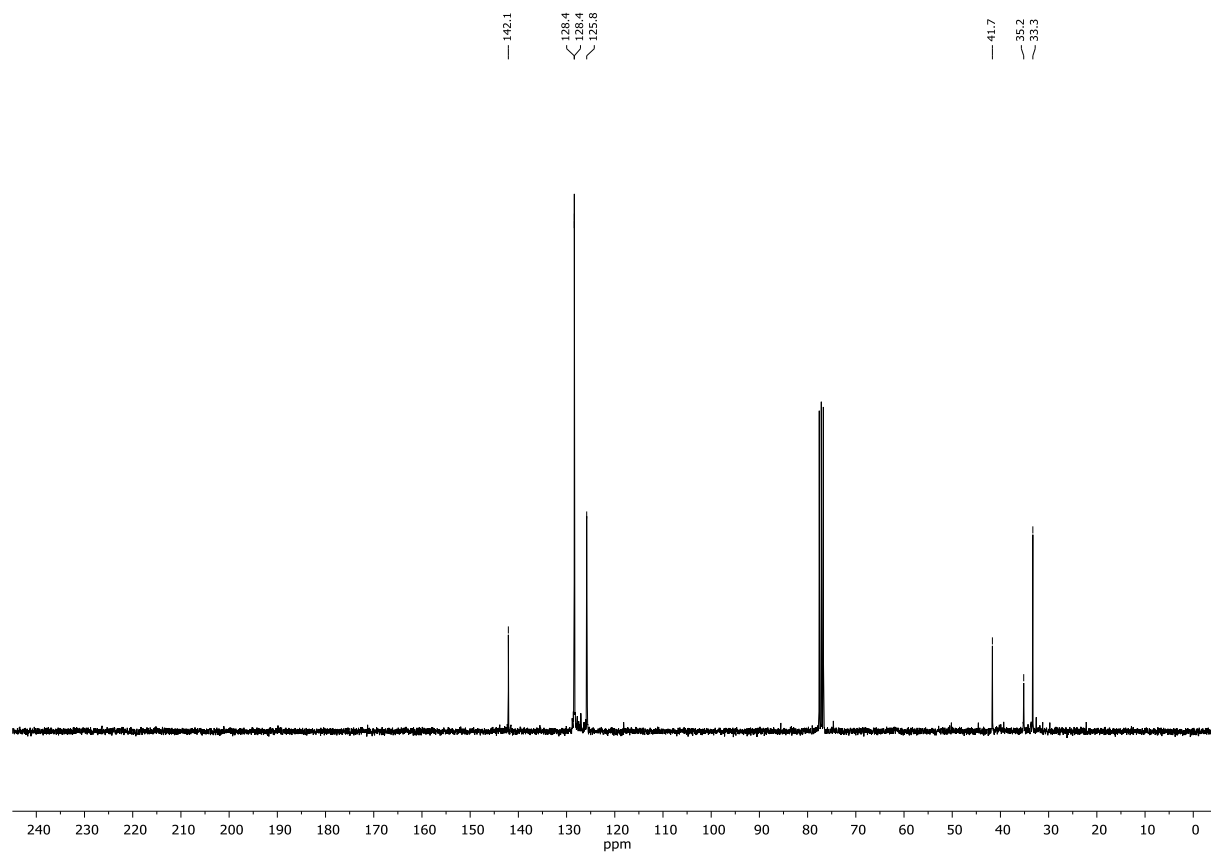
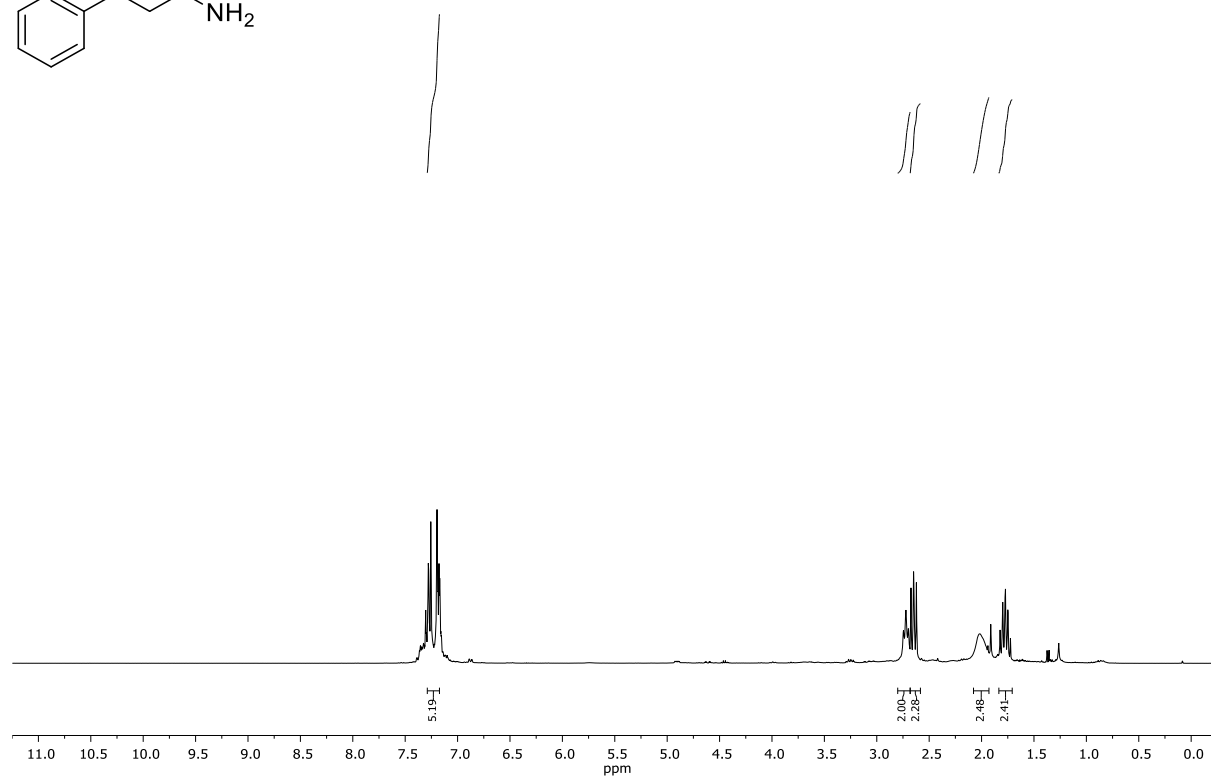
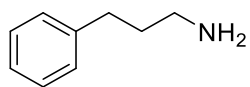
3-methyl-5-phenyl-4,5-dihydroisoxazole 2-oxide (3da)

First image: $^1\text{H-NMR}$; Second image: $^{13}\text{C-NMR}$; NMR solvent: CDCl_3

(3-nitropropyl)benzene (7a)

First image: ¹H-NMR; Second image: ¹³C-NMR; NMR solvent: CDCl₃

3-phenylpropan-1-amine (8a)



First image: ¹H-NMR; Second image: ¹³C-NMR; NMR solvent: CDCl₃

6.4 Crystallographic Data for Chapter 3

Table 2. Crystallographic Data for Chapter 3.

Compound	4i	10
CCDC	2192294	2192295
Formula	C ₁₂ H ₁₈ BrNO ₂ Si	C ₂₈ H ₂₃ Br _{0.59} Cl _{1.41} CuN ₃ O ₂
D _{calc.} / g cm ⁻³	1.423	1.578
μ /mm ⁻¹	4.511	3.983
Formula Weight	316.27	594.33
Colour	clear colorless	clear blue
Shape	plate-shaped	prism-shaped
Size/mm ³	0.22x0.08x0.04	0.33x0.21x0.13
T/K	123.00(10)	123.00(10)
Crystal System	monoclinic	orthorhombic
Space Group	P2 ₁ /c	Pbcn
a/Å	19.8325(4)	24.2587(3)
b/Å	7.91390(10)	14.0308(2)
c/Å	9.6475(2)	14.6985(2)
α /°	90	90
β /°	102.932(2)	90
γ /°	90	90
V/Å ³	1475.79(5)	5002.91(12)
Z	4	8
Z'	1	1
Wavelength/Å	1.54184	1.54184
Radiation type	Cu K α	Cu K α
θ_{\min} /°	2.286	4.723
θ_{\max} /°	74.895	66.895
Measured Refl's.	22933	31203
Indep't Refl's	2964	4437
Refl's I \geq 2 σ (I)	2568	4330
R _{int}	0.0555	0.0502
Parameters	157	330
Restraints	0	0
Largest Peak	0.707	0.706
Deepest Hole	-0.724	-0.559
Goof	1.075	1.074
wR ₂ (all data)	0.1013	0.0962
wR ₂	0.0980	0.0956
R ₁ (all data)	0.0438	0.0358
R ₁	0.0372	0.0350
Solution	Olex2 1.2-alpha	Olex2 1.2-alpha

Chapter 7 Personal Appendix

Curriculum Vitae

Personal Data

Name	Alexander Reichle
Date and place of birth	01.06.1994 in Memmingen, Germany
Nationality	German
Email	alexander.reichle@chemie.uni-regensburg.de

Education

06/2019 – 12/2022	PhD Thesis at the University of Regensburg under the supervision of Prof. Dr. Oliver Reiser “Photocatalysis with Cu(II)- and Cu(I)-complexes: Cu(II)-photocatalyzed Decarboxylative Oxygenation of Carboxylic Acids and Cu(I)-photocatalyzed Bromonitroalkylation of Olefins”
03/2017 – 03/2019	Master of Science, Chemistry at the University of Regensburg Modules: Organic Chemistry, Bioanalytical Chemistry, Biochemistry Master thesis: “Synthesis and Application of Copper(II)-phenanthrolines Towards the Photocatalytic Decarboxylation of Carboxylic Acids” (1.0) M. Sc. (1.0)
09/2016 – 02/2017	Industry internship/ Bachelor thesis at Boehringer Ingelheim RCV GmbH & Co KG in Vienna, Austria Bachelor thesis: “Synthesis of Spiroindolinones and Highly Substituted Quinolinones as Bromodomain Binders”(1.0) B. Sc. (1.3)
08/2013 – 02/2017	Bachelor of Science in pharmaceutical chemistry at the nta Hochschule Isny, Isny im Allgäu
10/2005 – 06/2013	Abitur (A-level) (grade 1.7) Gymnasium Marianum, Buxheim

Awards and Scholarships

03/2020 – 02/2022	Kekulé fellowship for PhD candidates Stiftung Stipendien-Fonds des Verbandes der chemischen Industrie e.V.
05/2017	Graduation award for the best bachelor graduation at the nta Hochschule Isny, Isny im Allgäu.
06/2015 – 02/2017	Scholarship, nta Hochschule Isny.

Scientific Meetings and Congresses

-
- [1] Exploratory Photochemistry: Light Creates Structure, Symposium, Halle, Germany **2021**.
 - [2] Annual Retreat of the CRC 325, Raitenhaslach, Germany **2022**. Oral Presentation: “*Visible Light Mediated Coupling Reactions via Photoexcitation of Cu(I)-Substrate Assemblies*”. Reichle A. and Reiser O.
 - [3] Second Seminar Day of the CRC 325, Regensburg, Germany **2022**.
 - [4] EuChemS Chemistry Congress, Lisbon, Portugal, **2022**.
Poster Presentation: “*Light-Induced Homolysis of Copper(II)-carboxylates*” Reichle A.; Sterzel H.; Kreitmeier P., Fayad R.; Castellano F.N.; Rehbein J. and Reiser O.

List of Publications

-
- [1] Reichle A.; Sterzel H.; Kreitmeier P., Fayad R.; Castellano F.N.; Rehbein J.; Reiser O., “Copper(II)-photocatalyzed decarboxylative oxygenation of carboxylic acids” *Chem. Commun.*, **2022**, 58, 4456-4459. „Advance Article”; DOI:10.1039/D2CC00570K
 - [2] Reichle A.; Koch M.; Sterzel H.; Großkopf L.-J.; Floss J.; Rehbein J.; Reiser O., “Cu(I)-photocatalyzed Bromonitromethylation of Olefins – Evidence for highly efficient inner-sphere pathways” *Angew. Chem. Int. Ed.*, **2023**, e202219086. DOI:10.1002/ange.202219086
 - [3] Reichle A. and Reiser O. “Light-induced homolysis of copper(II)-complexes – a perspective for photocatalysis” *Chem. Sci.*, **2023**, 14, 4449-4462. DOI:10.1039/D3SC00388D
 - [4] Chaibuth P.; Engl S.; Reichle A.; Chainok K.; Sukwattanasinit M.; Reiser O., “In Situ Generated Copper(II)-Quinoline Complexes as Robust and Versatile Photocatalysts for the Chlorosulfonylation of Olefins” *Advan. Synth. Catal.* **2023**, 365, 1-8.

Chapter 8 Acknowledgements

Zunächst möchte ich meinem Doktorvater Prof. Dr. Oliver Reiser für die Aufnahme in seinen Arbeitskreis bedanken. Er hat mir die Möglichkeit eröffnet, auf diesem sehr spannenden Themenfeld, der Photokatalyse mit Kupfer, zu arbeiten. Ich möchte mich ganz herzlich bedanken für die viele Zeit, die er sich allumfassend immer genommen hat. Mit Ihm über chemische Reaktionen und auch die Schwierigkeiten und Stolpersteine, die man im Laufe der Forschungsarbeiten antraf, zu diskutieren hat fundamental zu dieser Arbeit beigetragen. Er hatte immer ein offenes Ohr und half durch sein extrem breit gefächertes Fachwissen mit vielen Ratschlägen in allen Situationen, meinen tiefsten Dank! Danke, dass ich meine eigenen Projekte und Ideen auch verwirklichen konnte.

Mein weiterer Dank gilt besonders Dr. Peter Kreitmeier. In allen Arten von technischen Problemen, z.B. Photoreaktoren, Startmaterialsynthese, Tricks bei der Aufarbeitung und Isolierung von Substanzen *etc.* war er immer bereit, sich Zeit zu nehmen und eine passende Lösung zu erarbeiten. Ebenso ist sein großes Engagement, neue Photoreaktoren zu bauen, um Upscaling-Versuche zu ermöglichen, zu nennen. Danke für alles, Peter!

Ebenso möchte ich hier unsere Techniker aufzählen: Brigitte Eichenseher, Helena Konkel, Klaus Döring, Lucie Reitmeier. Danke, dass Ihr immer unterstützt habt, wo es erforderlich war und auch bei den vielen Dingen, mit denen Ihr unseren Alltag erleichtert habt. Ganz besonders möchte ich mich noch bei Johannes Floß bedanken, der mir immer als guter Freund zur Seite stand. Danke für die vielen schönen Gespräche und Stunden, die wir zusammen im Labor oder der Arbeitskreisküche hatten und für alle Unterstützung in den Projekten, besonders bei der Startmaterialsynthese oder Upscaling-Reaktionen.

Vernetzte Forschung trägt zum Erfolg von Projekten bei, indem alle Puzzleteile zusammengesetzt werden, ergeben sich neue Bilder. Aus diesem Grund gilt mein herzlicher Dank auch in besonderer Weise den Kollaborationspartnern der Rehbein Gruppe, M. Sc. Hannes Sterzel, der die vielen EPR-Messungen, sowie DFT-Berechnungen durchgeführt hat sowie M. Sc. Daniel Schmidhuber. Es hat immer viel Spaß gemacht zusammenzuarbeiten und sich auszutauschen. Auch möchte ich mich an dieser Stelle bei Prof. Dr. Julia Rehbein für die vielen guten Gespräche und Diskussionen im Bezug auf unsere Kollaborationsprojekte bedanken. Ebenso gilt mein Dank der Castellano Gruppe mit Dr. Remi Fayad und Prof. Dr. Felix N. Castellano für die Durchführung der spektroskopischen Untersuchungen im Cu(II)-Projekt.

Des Weiteren möchte ich mich bei unseren Sekretärinnen Michaela Schule, Antje Weigert und Stefanie Berghofer für die Hilfe aller organisatorischer Art bedanken.

Weiterer Dank gilt auch besonders den Mitarbeitern der zentralen Analytik der Universität Regensburg, der Massenspektroskopie durch Josef Kiermeier und Wolfgang Söllner, sowie den Mitarbeitern der Kristallstrukturanalyse, Birgit Hischa, Sabine Stempfhuber, Florian Meurer und Dr. Michael Bodensteiner. Gerne erinnere ich mich an die spannenden Momente bei Kristallmessungen, von denen im Rahmen meiner Forschungsarbeit viele zustande kamen. Ebenso gilt mein Dank den Mitarbeitern der NMR-Abteilung, Fritz Kastner und Tuan-Anh Ngyuen, Anette Schramm und Dr. Ilya Shenderovich.

Ganz besonderer Dank gilt auch allen Ehemaligen des AK Reiser. Besonders möchte ich mich bei meinem Freund Dr. Lukas Traub (durch den ich zum AK Reiser gefunden habe), Dr. Simon Budde, Dr. Natalija Budde, Dr. Sebastian Engl, Dr. Nikolai Wurzer, Dr. Tobias Babl, Dr. Tomislav Krolo, Dr. Peter Ehrnsberger, Dr. Robert Eckl, Dr. Carina Sonnleitner und Dr. Michael Pirtsch und allen anderen bedanken. Ich habe stets die gute familiäre Atmosphäre geschätzt, die am Lehrstuhl durch den guten Umgang miteinander und die gemütlichen Stunden in der AK Küche zu tragen kam.

Ebenso möchte ich mich bei meinen ehemaligen Laborkollegen, M. Sc. Eva Plut, Dr. Peter Ehrnsberger, Dr. Thomas Föll, M. Sc. Kathrin Strunk, M. Sc. Neic Petek, M. Sc. Marco Antonio Henriquez Toro und Dr. Pi Cheng bedanken. Besonders Eva gilt mein großer Dank, ich werde nie die vielen Stunden vergessen, die wir neben herausfordernder Chemie auch gerne mit dem Verzehr der ein- oder anderen Süßigkeit und vielen schönen Gesprächen verbracht haben. Tiefen Dank für die freundschaftliche Atmosphäre und allen Rat!

Besonderer Dank gilt meiner Kollaborationspartnerin M. Sc. Magdalena Koch für die sehr gute Kollaboration bei der Bromonitroalkylierung, zusammen haben wir diesen riesigen Substratscope und die vielen Anwendungen gemeistert.

Bei M. Sc. Hendrik Paps möchte ich mich auch recht herzlich bedanken für die vielen Diskussionen über Kupfer und Photokatalyse. Es hat mir sehr viel Freude bereitet, sich mit Dir täglich auszutauschen.

An dieser Stelle möchte ich mich auch bei M. Sc. Viktor Klöpfer, M. Sc. Anurag-Nitin Chinchole, M. Sc. Youssef Abderrazak, M. Sc. Camillo Verdugo, M. Sc. Prithwa Das, M. Sc. Narender Katta und allen Kupfer-Photochemikern und Kollegen am AK, M. Sc. Lisa Uhlstein, M. Sc. Andreas Ratzenböck, M. Sc. Sebastian Fischer und M. Sc. Anna Rustler für die gute Atmosphäre und schönen Stunden bedanken.

Sehr hilfreich waren auch die Gespräche und Anregungen durch unsere Post Doc's, besonders Dr. Quan-Quing Zhao, Dr. Aditya Bhattacharrya und Dr. Tirtha Mandal. Ich konnte durch Sie immer wieder neue Forschungsansätze und Ideen erschließen, dafür bin ich sehr dankbar. Mit ihrem breiten Fachwissen waren Sie immer gute Ratgeber.

Im Rahmen meiner Forschung hatte ich auch viele Praktikanten und Bacheloranten, die mich im Labor tatkräftig bei der Durchführung von Synthesen/ Photoreaktionen unterstützt haben. Vielen Dank, B. Sc. Lea-Joy Großkopf, B. Sc. Jannes Rückel, B. Sc. Felix Scharff, M. Sc. Lisa Schrag und M. Sc. Franziska Gilch. Ich hoffe, es hat euch ebenso viel Spaß und Freude gemacht, wie mir.

Für die finanzielle Unterstützung während der Forschungsarbeit möchte ich mich bei der Stiftung Stipendien-Fonds des Verbandes der chemischen Industrie e.V. für das Kekulé Promotionsstipendium bedanken und bei dem Graduiertenkolleg CRC325 „Assembly Controlled Chemical Photocatalysis“.

Für das Korrekturlesen meiner Arbeit danke ich herzlichst M. Sc. Magdalena Koch, M. Sc. Viktor Klöpfer, Dr. Lukas Traub, Sandra und Seth Nard sowie meiner Frau Maria Reichle.

Ohne meine Familie wäre diese Arbeit auch nicht möglich gewesen. Meinen Eltern und Großeltern danke ich herzlich für die jahrelange finanzielle Unterstützung und den immerwährenden Rückhalt in allen Situationen und das viele „Aufmuntern“, dass ich immer wieder neue Kraft schöpfen konnte, weiterzumachen.

Ebenso erwähnen möchte ich besonders meine Freunde Daniel Harlander, Alexander Britzl (die vielen schönen Orgelkonzerte) und Josef Spielbichler. Mein tiefer Dank gilt auch meinem ehemaligen Lehrer und Mentor Pater Michael Guggemos, durch den ich zur Chemie fand und ohne den ich diesen Weg wohl nicht gegangen wäre. Ebenso gilt mein herzlicher Dank meinem Freund Pfr. Dr. Martin Schubert und Carina Schinka für die Begeisterung zur Naturwissenschaft.

Für die vielen Spaziergänge, um den Kopf freizubekommen, bedanke ich mich sehr bei meinem Freund Lorenz Gallmeier. Für die lustigen Autofahrten nach Regensburg und die immer guten Gespräche bedanke ich mich herzlich bei meiner guten Freundin Manuela Bockschweiger. Ebenso spreche ich meinen tiefen Dank allen meinen Freunden vom Kirchenchor, Gabriele Schwand, Roswitha Maurer, Renate Friedrich, Hildegard Fichtl, Rudi Feigl, Wolfgang Schäfer, Stefan Unterholzner und Hans Herrmann aus. Die schönen Stunden bei Gesang und unseren Festen haben immer dazu beigetragen, dass ich neue Energie sammeln konnte und mich vom Stress des Alltags und bei schwierigen Situationen erholen konnte.

Ganz zum Schluss bedanke ich mich von Herzen bei meiner Frau Maria. Ohne Dich wäre Vieles nicht möglich gewesen. Danke, dass Du mich immer unterstützt und mir in allen Lebenssituationen beiseite stehst und mit mir dein Leben teilst, ich liebe Dich!

Chapter 9 Declaration/ Eidesstattliche Erklärung

Herewith I declare that this present thesis is a presentation of my original work prepared single-handed. Wherever contributions from others are involved, all of them are marked clearly, with references to the literature, licenses and acknowledgement of collaborative research.

Regensburg, den 06.07.2023

Alexander Reichle